N9114379

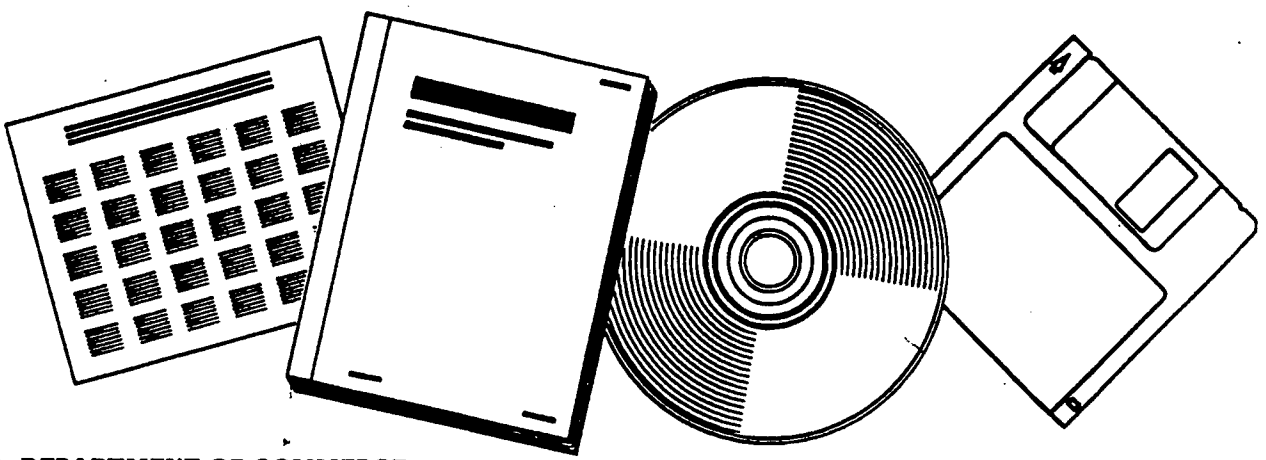
NTIS
Information is our business.

INNOVATIVE LONG WAVELENGTH INFRARED DETECTOR WORKSHOP PROCEEDINGS

JET PROPULSION LABORATORY
PASADENA, CA

DISTRIBUTION STATEMENT A
Approved for public release;
Distribution Unlimited

APR 24



U.S. DEPARTMENT OF COMMERCE
National Technical Information Service

11 6026

19980309 037

DTIC QUALITY INSPECTED 4

Accession Number: 6026

Publication Date: Dec 01, 1995

Title: Innovative Long Wavelength Infrared Detector Workshop Proceedings

Corporate Author Or Publisher: Jet Propulsion Lab, Pasadena, CA

Descriptors, Keywords: Innovative Long Wavelength Infrared Detector Workshop Proceedings

Pages: 00500

Cataloged Date: Mar 11, 1996

Document Type: HC

Number of Copies In Library: 000001

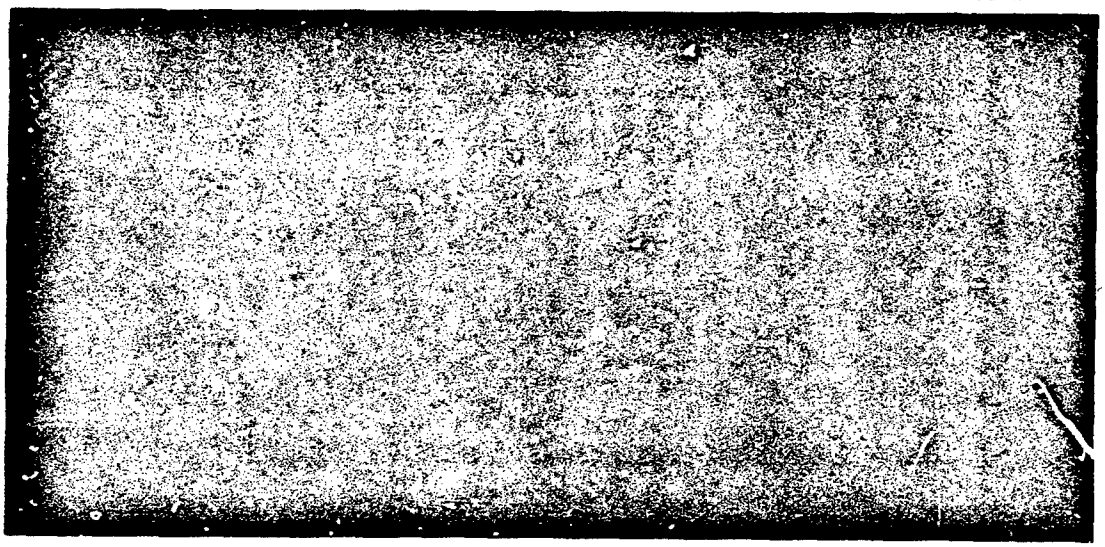
Record ID: 40643

N9114379

Innovative Long Wavelength Infrared Detector Workshop

PROCEEDINGS

April 24-26



(NASA-CR-187433) INNOVATIVE LONG WAVELENGTH INFRARED DETECTOR WORKSHOP PROCEEDINGS (JPL) 498 p CSCL 14B

N91-14379 --THRU-- N91-14411 Unclas G3/19 0317679

Center for Space Microelectronics Technology
Jet Propulsion Laboratory
Pasadena, California

REPRODUCED BY
U.S. DEPARTMENT OF COMMERCE
NATIONAL TECHNICAL
INFORMATION SERVICE
SPRINGFIELD, VA 22161

Innovative Long Wavelength Infrared Detector Workshop

PROCEEDINGS

April 24-26

[redacted]

ORGANIZED BY:

NASA Ames Research Center (ARC)

NASA Langley Research Center (LaRC)

NASA Goddard Space Flight Center (GSFC)

Center for Space Microelectronics Technology (CSMT)
Jet Propulsion Laboratory (JPL), California Institute of Technology

SPONSORED BY:

National Aeronautics and Space Administration
Office of Aeronautics, Exploration and Technology

Strategic Defense Initiative Organization
Innovative Science and Technology Office

U.S. Army Laboratory Command
Army Space Technology and Research Office

Defense Advanced Research Projects Agency

N O T I C E

THIS DOCUMENT HAS BEEN REPRODUCED FROM THE BEST COPY FURNISHED US BY THE SPONSORING AGENCY. ALTHOUGH IT IS RECOGNIZED THAT CERTAIN PORTIONS ARE ILLEGIBLE, IT IS BEING RELEASED IN THE INTEREST OF MAKING AVAILABLE AS MUCH INFORMATION AS POSSIBLE.

This publication was prepared by the Jet Propulsion Laboratory, California Institute of Technology, under a contract with the National Aeronautics and Space Administration.

INNOVATIVE LONG WAVELENGTH INFRARED DETECTOR WORKSHOP

CONFERENCE CHAIRS

F. Allario, LaRC
C.A. Kukkonen, JPL

ORGANIZATION COMMITTEE

R.W. Capps, JPL

R. De Paula, NASA Headquarters

D. Duston, SDIO/IST

F.J. Grunthaner, JPL

D. Jackson, Army/ASTRO

R.A. Lemons, Los Alamos

J. Maserjian, Chair, JPL

C.R. McCreight, ARC

P.B. McLane, JPL

R.R. Nelms, LaRC

A. Pavel, DARPA

V. Sarohia, JPL

B.D. Seery, GSFC

J.R. Swenson, SDIO/SIT

PROGRAM COMMITTEE

K.A. Forrest, GSFC

P.J. Grunthaner, JPL

G.S. Hubbard, ARC

S.A. Lyon, Princeton

T.C. McGill, Caltech

R.E. McMurray, ARC

J.L. Merz, UCSB

W.E. Miller, LaRC

P.S. Peercy, Sandia

D.L. Smith, Los Alamos

D. Spears, MIT/Lincoln

B.A. Wilson, Chair, JPL

M. Wigdor, Nicholas

A. Yariv, Caltech

ABSTRACT

The focus of the workshop was on innovative long wavelength ($\lambda < 17\mu m$) infrared (LWIR) detectors with the potential of meeting future NASA and DoD long-duration space application needs. Requirements are for focal plane arrays which operate near 65K using active refrigeration with mission lifetimes of five to ten years. The workshop addressed innovative concepts, new material systems, novel device physics, and current progress in relation to benchmark technology. It also provided a forum for discussion of performance characterization, producibility, reliability, and fundamental limitations of device physics.

The workshop was attended by a broad cross section of industry, government laboratories and offices, and universities. There were over 170 registered attendees. It covered the status of the incumbent HgCdTe technology, which shows encouraging progress towards LWIR arrays, and provided a snapshot of research and development in several new contender technologies. These contenders span quantum well, heterojunctions, and superlattices in column II-VI, III-V and IV semiconductor materials and promise producible LWIR arrays with the required performance. The workshop also included a session on new innovations for high performance thermal detectors.

PRECEDING PAGE BLANK NOT FILMED

CONTENTS

		Page
SESSION I: Detector Requirements		**1**
I - 1	Sensor Requirements for Earth and Planetary Observations *M.T. Chahine, Jet Propulsion Laboratory*	3
I - 2	SDIO Long Wavelength Infrared Detector Requirements *D. Duston, Strategic Defense Initiative Organization*	33
I - 3	LWIR Detector Requirements for Low-Background Space Applications *F. De Luccia, The Aerospace Corporation*	45
SESSION II: Benchmark Technology Status		**59**
II - 1	Status of LWIR HgCdTe Infrared Detector Technology *M.B. Reine, Loral Infrared & Imaging Systems*	61
II - 2	LWIR HgCdTe - Innovative Detectors in an Incumbent Technology *W.E. Tennant, Rockwell International Science Center*	79
II - 3	HgCdTe for NASA Eos Missions and Detector Uniformity Benchmarks *P.R. Norton, Santa Barbara Research Center*	93
SESSION III: Device Design and Evaluation Issues		**97**
III - 1	Detector Array Evaluation and Figures of Merit *E.L. Dereniak, University of Arizona*	99
III - 2	Issues and Directions in IR Detector Readout Electronics *E.R. Fossum, Columbia University*	117
III - 3	Radiation Response Issues for Infrared Detectors *A.H. Kalma, Mission Research Corporation*	149
SESSION IV: High Performance Thermal Detectors		**159**
IV - 1	Fabrication of Sensitive High T_C Bolometers *M. Nahum, University of California, Berkeley*	161
IV - 2	Pyroelectric Detectors *E. Haller, Lawrence Berkeley Laboratory*	183
IV - 3	A Novel Electron Tunneling Infrared Detector *T.W. Kenny, Jet Propulsion Laboratory*	197
SESSION V: III-V Quantum Well and Heterojunction Detectors		**209**
V - 1	Quantum Well Infrared Photodetectors (QWIP) *B.F. Levine, AT&T Bell Laboratories*	211
V - 2	Photovoltaic Quantum Well Infrared Photodetectors *S.A. Lyon, Princeton University*	231
V - 3	Characteristics of AlGaAs/GaAs Multiple Quantum Well Infrared Detectors *B.K. Janousek, The Aerospace Corporation*	243
V - 4	Resonant Tunneling IR Detectors *J.M. Woodall, IBM*	257
V - 5	Low Dark Current Photovoltaic Multiquantum Well Long Wavelength Infrared Detectors *C.S. Wu, Hughes Aircraft Company*	263

PRECEDING PAGE BLANK NOT FILMED

CONTENTS (Continued)

		Page
V - 6	Fundamental Limits to Performance of Quantum Well Infrared Detectors ..... *A. Yariv, California Institute of Technology*	275
V - 7	New Heterojunction LWIR Detector Options ..... *J. Maserjian, Jet Propulsion Laboratory*	291
SESSION VI: Si-Based Detectors		**303**
VI - 1	Intersubband Absorption in Si_{1-x} Ge_x/Si Superlattices for Long Wavelength Infrared Detectors ..... *Y. Rajakarunanayake, California Institute of Technology*	305
VI-2	Possibilities for LWIR Detectors Using MBE-Grown Si(/$Si_{1-x}Ge_x$) Structures ..... *R.J. Hauenstein, Hughes Research Laboratories*	323
VI-3	Novel $Si_{1-x}Ge_x$/Si Heterojunction Internal Photoemission Long Wavelength Infrared Detectors ..... *T.L. Lin, Jet Propulsion Laboratory*	339
SESSION VII: Alternate II-VI Detectors		**349**
VII-1	MBE HgCdTe Heterostructure Detectors ..... *J.N. Schulman, Hughes Research Laboratories*	351
VII-2	Growth and Properties of Hg-Based Quantum Well Structures and Superlattices ..... *J.F. Schetzina, North Carolina State University*	363
VII-3	HgZnTe-Based Detectors for LWIR NASA Applications ..... *E.A. Patten, Santa Barbara Research Center*	381
SESSION VIII: III-V Superlattice Detectors		**399**
VIII-1	Small Band Gap Superlattices as Intrinsic Long Wavelength Infrared Detector Materials ..... *D.L. Smith, Los Alamos National Laboratory*	401
VIII-2	LWIR Detector Research in InAsSb/InAs ..... *P.S. Peercy, Sandia National Laboratories*	413
VIII-3	InAs/$Ga_{1-x}In_xSb$ Superlattices for Infrared Detector Applications ..... *R.H. Miles, Hughes Research Laboratories*	431
VIII-4	IR Detectors Based on n-i-p-i Superlattices ..... *P.P. Ruden, University of Minnesota*	447
VIII-5	InAs/GaAs and InAs Doping Superlattices ..... *F.J. Grunthaner, Jet Propulsion Laboratory*	463
SESSION IX: New Materials Systems		**479**
IX-1	InAsSbBi, A Direct Band-Gap, III-V, LWIR Material ..... *G.B. Stringfellow, University of Utah*	481
IX-2	AlSb/InAs/AlSb Quantum Wells ..... *H. Kroemer, University of California, Santa Barbara*	495
APPENDIX: Attendance List		**511**

SESSION I: Detector Requirements

I - 1 Sensor Requirements for Earth and Planetary Observations
M.T. Chahine, Jet Propulsion Laboratory

I - 2 SDIO Long Wavelength Infrared Detector Requirements
D. Duston, Strategic Defense Initiative Organization

I - 3 LWIR Detector Requirements for Low-Background Space Applications
F. De Luccia, The Aerospace Corporation

N91
14380
UNCLAS

N91-14380

SENSOR REQUIREMENTS FOR EARTH AND PLANETARY OBSERVATIONS

Moustafa T. Chahine

Chief Scientist
Jet Propulsion Laboratory
California Institute of Technology
Pasadena, CA

ABSTRACT

Future generations of Earth and planetary remote sensing instruments will require extensive developments of new long-wave and very long-wave infrared detectors. The upcoming NASA Earth Observing System (EOS) will carry a suite of instruments to monitor a wide range of atmospheric and surface parameters with an unprecedented degree of accuracy for a period of 10 to 15 years. These instruments will observe Earth over a wide spectral range extending from the visible to nearly 17 micrometers with a moderate to high spectral and spacial resolution. In addition to expected improvements in communication bandwidth and both ground and on-board computing power, these new sensor systems will need large two-dimensional detector arrays. Such arrays exist for visible wavelengths and, to a lesser extent, for short wavelength infrared systems. The most dramatic need is for new LWIR and VLWIR detector technologies that are compatible with area array readout devices and can operate in the temperature range supported by long life, low power refrigerators. A scientific need for radiometric and calibration accuracies approaching 1% translates into a requirement for detectors with excellent linearity, stability and insensitivity to operating conditions and space radiation. Current examples of the kind of scientific missions these new thermal IR detectors would enhance in the future include instruments for Earth science such as AIRS, MODIS, SAFIRE and OVO. Planetary exploration missions such as Cassini also provide examples of instrument concepts that could be enhanced by new IR detector technologies.

PRECEDING PAGE BLANK NOT FILMED

SENSOR REQUIREMENTS FOR EARTH AND PLANETARY EXPLORATION

Moustafa T. Chahine

DETECTOR REQUIREMENTS — GENERAL REMARKS

- PERFORMANCE OF PROPOSED INSTRUMENTS DEPENDS ALMOST ENTIRELY ON DETECTOR PERFORMANCE
- INSTRUMENT PERFORMANCE REQUIREMENTS OFTEN DICTATED BY EXISTING DETECTOR PERFORMANCE DATA
  - NASA FUNDING PROCESS ENSURES THAT PROPOSED DETECTOR PERFORMANCE MUST:
    a, EXIST
    b, BE READILY AVAILABLE, WITH FLIGHT HERITAGE
    c, BE BELIEVED TO SATISFY a, AND b, BY THE COMMUNITY
  - PROPOSED INSTRUMENTS REQUIRING DETECTOR DEVELOPMENT PROGRAMS FARE POORLY AGAINST THOSE THAT DO NOT
- FOR THESE REASONS, REAL DETECTOR REQUIREMENTS ARE OFTEN NOT COMMUNICATED TO THOSE ABLE TO ADDRESS THEM
- THE PRIMARY PURPOSE OF THIS MEETING IS TO ACHIEVE THIS COMMUNICATION.

EARTH OBSERVING SYSTEM (EOS) PAYLOAD

Eos-A	Eos-B
AIRS (JPL) 3-15.4μm	ALT/RA
AMSU	GGI
CERES (LaRC) 0.2-100μm	GLRS
HIRDLS (NCAR/OXFORD) 6-18μm	IPEI
EOSP	LIS
GGI	MLS
HIMSS/MIMR/AMSR	SAFIRE (LaRC) 6.4-125μm
HIRIS	SAGE III
IPEI	SCANSCAT/STIKSCAT
ITIR (JAF) 0.52-11.65μm	SOLSTICE
MISR	SWIRLS (JPL) 7.6-17.2μm
MODIS-N (GSFC) 0.4-14.24μm	TES (JPL) 2.9-17μm
MODIS-T/MERIS	XIE
MOPITT/TRACER	

ORIGINAL PAGE IS OF POOR QUALITY

CRAF PAYLOAD

Acronym	Investigation	PI/Team Leader
ISS	Imaging (Facility)	J. Veverka/Cornell
VIMS 0.35-5.1μm	Visual/Infrared Mapping Spectrometer (Facility)	T. McCord/U of Hawaii
TIREX >5 μm	Thermal Infrared Radiometer Experiment	F. P.J. Valero/NASA Ames
PEN	Penetrator	W. Boynton/U of Arizona
COMA	Cometary Matter Analyzer	J. Kissel/Max Planck Institut
CIDEX	Comet Ice/Dust Experiment	G. Carle/NASA Ames
SEMPA	Scanning Electron Microscope and Particle Analyzer	A. Albee/CIT
CODEM	Comet Dust Environment Monitor	W.M. Alexander/Baylor Univ
NGIMS	Neutral Gas and Ion Mass Spectrometer	H. Niemann/NASA GSFC
CRIMS	Comet Retarding Ion Mass Spectrometer	T. E. Moore/NASA Marshall
SPICE	Suprathermal Plasma Investigation of Cometary Environments	J. L. Burch/SW Research Inst.
MAG	Magnetometer	B. Tsurutani/JPL
CREWE	Coordinated Radio, Electrons, and Waves Experiment	J. D. Scudder/NASA GSFC
RSS	Radio Science (Facility)	D. K. Yeomans/JPL

CASSINI PAYLOAD

Acronym	Investigation	Wavelength/Freq Range
CIRS (GSFC)	Mid & Far IR Spectrometer	7.5-1000μm
HSP	High Speed Photometer	117-180 nm
ISS	Solid State Imaging	0.2-1.1μm
MSAR	Microwave Spectrometer/Radiometer	15-230 GHz
PRWS	Plasma/Radio Wave Spectrometer	5 Hz - 20 MHz
RADR	Radar	14, 30 GHz
RS	Radio Science	3.6-13 cm
UVSI	UV Spectrometer	500-3200 Å
VIMS (JPL)	Visual/Infrared Mapping Spectrometer	0.4-5.2 μm

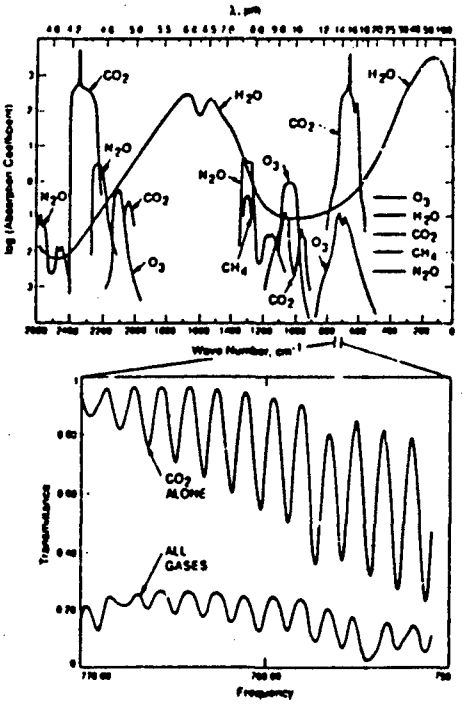
ATMOSPHERIC INFRARED SOUNDER (AIRS)

[Team Leader: Moustafa Chahine, JPL]

AIRS — Atmospheric Infrared Sounder

AIRS is a high spectral-resolution sounder covering the range between 3 and 17 μm with more than 4000 spectral measurements, having a resolving power $\Delta\lambda/\lambda$ = 1/1200. AIRS permits simultaneous determination of a large number of atmospheric and surface parameters including temperature and humidity profiles, ocean and land surface temperature, clouds, O_3, CH_4, and other minor gases. This is accomplished in part through multispectral, narrow bandpass channels which can be selected away from unwanted absorption lines, while taking advantage of the unique spectral properties of several regions such as the high J-lines in the R-branch of the 4.3 μm CO_2 band and the clear super-windows near 3.6 μm.

Infrared Band Absorption of Atmospheric Gases



ORIGINAL PAGE IS
OF POOR QUALITY

AIRS

Global Data Set

AIRS (used with AMSU) provides simultaneous determination of a large number of atmospheric and surface parameters under both day and night conditions:

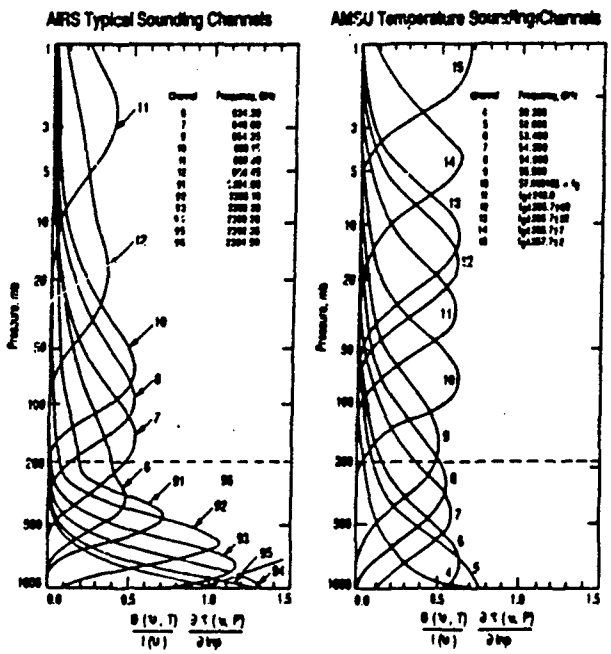
1. Atmospheric temperature profiles with an average accuracy of 1°C and in 1 km thick layers.
2. Relative humidity profiles and total precipitable water vapor
3. Sea surface temperature.
4. Land surface temperature and infrared spectral emissivity.
5. Fractional cloud cover, cloud infrared emissivity, and cloud-top pressure and temperature.
6. Total ozone burden of the atmosphere.
7. Mapping of the distribution of minor atmospheric gases such as methane, carbon monoxide and nitrous oxide.
8. Surface albedo.
9. Snow and ice cover.
10. Outgoing long wave radiation.
11. Precipitation index.

AIRS

Atmospheric Temperature Profile

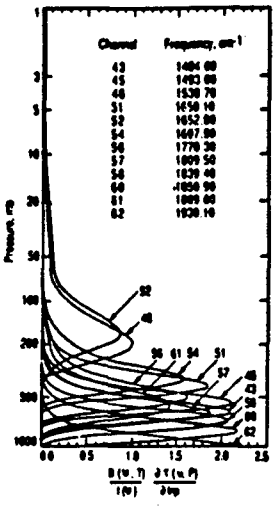
Atmospheric temperature profiles T(p) will be derived with an average accuracy of 1°C in 1 km thick layers. Clear-column temperature profiles will be derived in the presence of multiple cloud layers without requiring any field-of-view (FOV) to be necessarily completely clear. Observations over adjacent FOVs will be used to filter out the effects of clouds on all channels. Improvements in the T(p) are a result of:

- AIRS narrow contribution functions
- Number of available sounding channels
- Minimizing contamination by O_3, H_2O, ...
- Simultaneous determination of the surface temperature, emissivity and reflectivity
- Use of AMSU lower atmosphere sounding channels to filter out the effects of clouds



ORIGINAL PAGE IS
OF POOR QUALITY

Humidity profiles will be derived from channels selected in the 6.3 μm water vapor band and the 11 μm windows which are sensitive to water vapor continuum. The radiance measured in these channels depends on atmosphere and surface temperature and the distribution of humidity in the atmosphere. The 6.3 μm channels are more sensitive to humidity in the middle and upper troposphere, while the narrow bandpass channels in the 11 μm continuum are more sensitive to humidity in the lower troposphere. Determination of surface temperature and spectral emissivity is essential for obtaining accurate low level water vapor distribution.



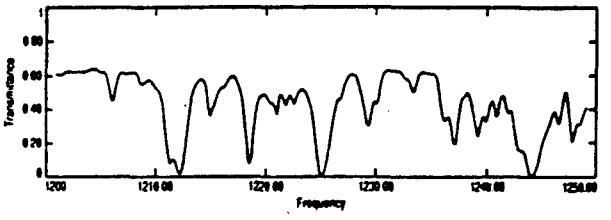


TABLE 1
AIRS FUNCTIONAL PARAMETERS

Design Altitude	705 km
IFOV	1.1°
Cross-track Scan Motion	± 48.95°
Infrared	
Spectral Coverage	3.4 - 17.0 μm
Spectral Resolution	1200
NEΔT	0.2 K
Channels	115 (minimum) 3038 Spectral elements
Visible Light	
Spectral coverage	0.4 - 1.1 μm
Channel wavelengths (tentative)	0.40 - 0.50 μm 0.67 - 0.71 μm 0.70 - 0.80 μm 0.9 - 1.0 μm 0.4 - 1.0 μm
Sensitivity	SNR = 100 at albedo = 0.4 (daytime only)
Data Encoding	12 bits/sample
Number of Samples/Cross-track Scan	89
Mean Data Rate	1.8 Mb/s
Maximum Data Rate	1.8 Mb/s

ORIGINAL PAGE IS
OF POOR QUALITY

TABLE 2
OPTICAL SYSTEM PARAMETERS

IFOV	± 0.52 °	
Visible/near IR system:		
Fore optics:	full aperture	subapertures
Aperture (mm)	10.0	2.0 (5)
EFL (mm)	50	50
Focal Ratio	F/5	F/25
Relay:		
Magnification	4:1	
Final Focal Ratio	F/13.7	
Detector Diam. (mm)	0.5	
IR systems:		
Fore optics:	full aperture	subapertures
Aperture (mm)	121.0 x 5.5	5.5 x 5.5 (8)
EFL (mm)	500	500
Focal Ratio	F/4.1 x F/90.9	F/90.9
Spectrometers:	Short-Wave	Long-Wave
Aperture (mm)	69.3 x 138.6	69.3 x 138.6
Grating Incidence Angle	60 °	60 °
Grating Diffraction Angle	0 °	0 °
Grating Spacing (mm)	0.057	0.127
EFL (mm)	138.6	138.6
Focal Ratio	F/2.0 x F/1.0	F/2.0 x F/1.0
Pixel size (mm)	0.2 x 0.1	0.2 x 0.1

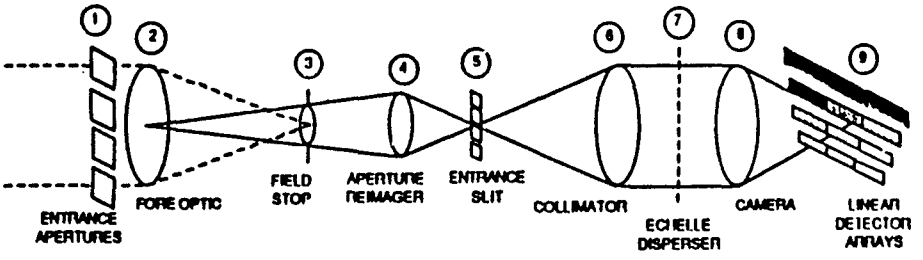
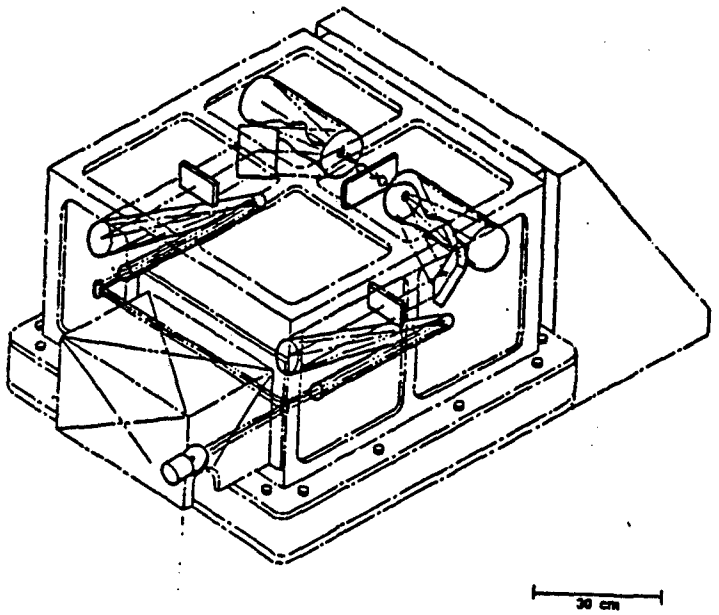


Figure 2

SCHEMATIC MULTI-APERTURE SPECTROMETER DIAGRAM

In the multi-aperture spectrometer, several sub-apertures (1) in a line across the telescope aperture are relayed to the spectrometer slit (5), then dispersed (7) and re-imaged onto a series of linear arrays (9).



AIRS INSTRUMENT DIAGRAM WITH X-RAY

VIEW OF THE TWO SPECTROMETERS

JPL

AIRS DETECTOR TECHNOLOGY REQUIREMENTS / CHALLENGES

ISSUE	REQUIREMENT	CHALLENGE
Photon Flux Range	10^7 - 10^{12} photons/sec/pix	Large dynamic range, low readout noise, storage and speed
Radiometric Performance	BLIP at all flux levels, 1% linearity and calibration accuracy	Low noise detectors, high QE, feedback in cell, radiation tolerance
Wavelength Range	To 15.4 μm extendable to 17 μm	Only single pixels demonstrated in MCT, linear arrays required
Operating Temperature	Compatible with long life coolers, T ≥ 60 K	Not demonstrated, new options needed
Power Dissipation	10 - 50 μW per pixel with readout 0.1 - 0.2 W for full focal plane	Cooler power limitation

MODERATE RESOLUTION IMAGING SPECTROMETER (MODIS-N)

[Team Leader: Vince Salomonson, GSFC]

MODERATE RESOLUTION IMAGING SPECTROMETER
SCIENCE OBJECTIVES

- STUDIES OF SPATIAL AND TEMPORAL VARIABILITY OF OCEANIC SURFACE PROPERTIES WITH SPECIAL EMPHASIS ON OCEAN PRIMARY PRODUCTIVITY
- STUDIES OF THE SPATIAL AND TEMPORAL VARIABILITY IN LAND SURFACE PROPERTIES WITH EMPHASIS ON PROBLEMS SUCH AS DESERTIFICATION, REGIONAL VEGETATION STRESS DUE TO ACID RAIN OR DROUGHT, AND SUCCESSION OR CHANGE IN VEGETATION SPECIES DUE TO DEFORESTATION AND ANTHROPOGENIC EFFECTS
- STUDIES OF TROPOSPHERIC DYNAMICS, CLIMATOLOGY AND CHEMISTRY AS OBTAINED THROUGH OBSERVATIONS OF CLOUD CHARACTERISTICS, AEROSOLS, WATER VAPOR, AND TEMPERATURE (INCLUDING SURFACE TEMPERATURE)

MODERATE RESOLUTION IMAGING SPECTROMETER
INSTRUMENT DESCRIPTION

- SCANNING IMAGING SPECTROMETER
- PIXEL SIZES OF 214 M, 428 M, AND 856 M
- SWATH WIDTH OF 2300 KM
- SPECTRAL RANGE 0.6-15 MICRONS, 36 BANDS
- 200 KG, 8.3 MBPS, 250 W

MODIS-N
SPECTRAL CHANNEL CHARACTERISTICS

No. CHANNELS	λ (μm)	Δλ (nm)	IFOV (meters)	S/N (AT 70° SZA)	NEDT (TYPICAL)	COMMENTS
2	0.6 - 0.9	40 - 50	214	100 - 200		EDGE DETECTION
5	0.4 - 2.1	20 - 50	428	100 - 300		LAND PROCESSES AND CLOUD CHARACTERISTICS
7	0.4 - 0.9	10 - 15	856	500 - 900		OCEAN COLOR
2	0.6 - 0.7	10 - 15	856	1100		FLUORESCENCE
3	0.9 - 1.0	10 - 50	856	60-250		WATER VAPOR
10	3.7 - 8.6	50 - 300	856		0.05K AT 300K	ATMOS. PARAMETERS AND SURFACE TEMPERATURE
7	9.7 - 14.2	300 - 500	856		0.25K AT 250K	CLOUD AND SURFACE TEMPERATURE
36						

MODIS-N
INSTRUMENT SUMMARY

PARAMETERS	DESIGN SPECIFICATIONS OR EXPECTED PERFORMANCE
PLATFORM ALTITUDE	705 km
IFOV (No. OF BANDS AT IFOV)	29 AT 1.21 mrad (856 m) 5 AT 0.607 mrad (428 m) 2 AT 0.303 mrad (214 m)
SWATH	110 deg/2330 km
SPECTRAL BANDS	36 BANDS TOTAL (19/0.4-3.0 µm; 17/3-15 µm)
RADIOMETRIC ACCURACY	5% ABSOLUTE, < 3 µm 1% ABSOLUTE, > 3 µm 2% REFLECTANCE
QUANTIZATION	12 bit
POLARIZATION SENSITIVITY	2% MAX, < 2.2 µm
MODULATION TRANSFER FUNCTION	0.3 AT NYQUIST
S/N PERFORMANCE (70 degree SOLAR ZENITH/OCEANS)	830:1 (443 nm) 745:1 (520 nm) 503:1 (865 nm)
NEDT PERFORMANCE (THERMAL BANDS) AT 300 deg K/WINDOW BANDS	LESS THAN 0.05
SCAN EFFICIENCY	(TO BE DETERMINED)
INTEGRATION TIME	(TO BE DETERMINED)
SIZE (APPROX)	1 x 1.6 x 1 m
WEIGHT	APPROX 200 kg
POWER	250 W
PEAK DATA RATE	15 MBS (DAYTIME)
DUTY CYCLE	100%

MODIS-N
LWIR PARAMETERS

BAND NUMBER	CENTER WVLNGTH (µm)	DELTA WVLNGTH (nm)	TYP. SCENE TEMP (K)	TYP. SPECTRAL RADIANCE (*)	NEDT (K)	NOISE EQUIV. SPECTRAL RADIANCE (*)	REQ. SIGNAL/NOISE RATIO	NOMINAL NEP (W)**	CALCULATED D*
30	9.73	300	250	3.69	0.25	2.19E-02	168	6.04E-11	4.39E+10
31	11.03	500	300	9.55	0.05	7.01E-03	1362	3.22E-11	8.22E+10
32	12.02	500	300	8.94	0.05	6.06E-03	1475	2.79E-11	9.51E+10
33	13.34	300	260	4.52	0.25	1.83E-02	247	5.05E-11	5.25E+10
34	13.64	300	250	3.76	0.25	1.61E-02	234	4.44E-11	5.97E+10
35	13.94	300	240	3.11	0.25	1.41E-02	221	3.89E-11	6.81E+10
36	14.24	300	220	2.08	0.35	1.54E-02	135	4.25E-11	6.24E+10

NOTE:

THE COLUMNS UP TO REQUIRED SIGNAL-TO-NOISE RATIO ARE SPECIFICATION VALUES FROM THE SEPT. 19, 1989 SPECIFICATION CIRCULATED TO INDUSTRY FOR REVIEW. THE CALCULATED D* VALUES DEPEND ON SYSTEM ASSUMPTIONS AND MUST BE ACHIEVED AT FOCAL PLANE TEMPERATURES WARMER THAN 85K.

SYSTEM ASSUMPTIONS ANTICIPATE THE USE OF SHORT LINEAR WHISKBROOM ARRAYS OF LESS THAN 20 DETECTORS.

* WATTS/(cm^2-sr-µm)

** ASSUME:

APERTURE (cm)	20
F-NUMBER =	2.00
TRANSMISSION	0.20
IFOV =	1.21E-03
DET. SIZE (µm) =	4.84E+02
NOISE BW (Hz) =	3000

ORIGINAL PAGE IS
OF POOR QUALITY

TROPOSPHERIC EMISSION SPECTROMETER (TES)

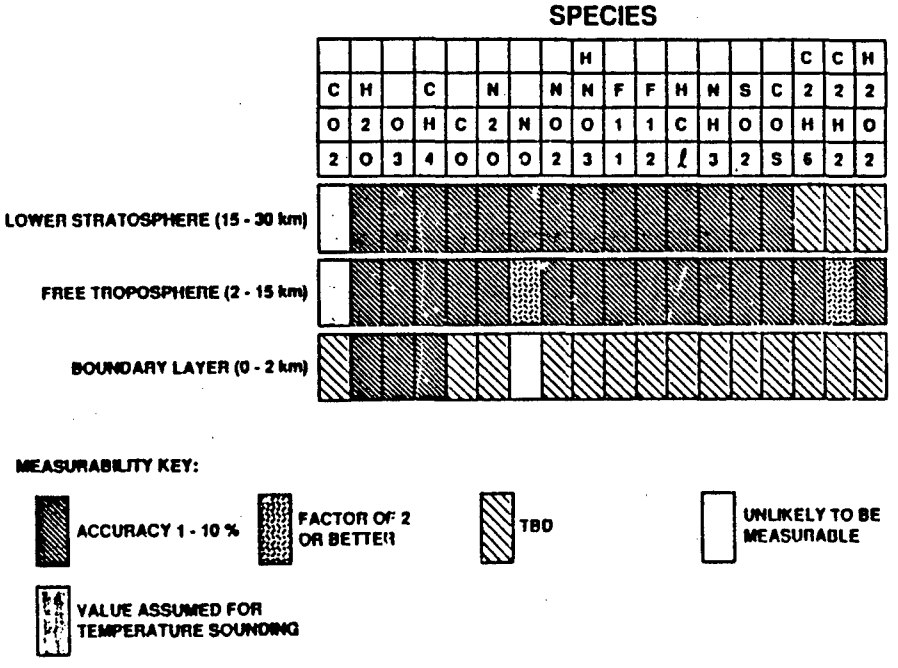
[P.I.: Reinhard Beer, JPL]

TROPOSPHERIC EMISSION SPECTROMETER
SCIENCE OBJECTIVES

- GENERATE VERTICAL CONCENTRATION PROFILES ON A GLOBAL BASIS OF THE FOLLOWING SPECIES WITH SUB-SCALE-HEIGHT RESOLUTION AND 5° LATITUDE SPACING:

Misc.	HO_x	NO_x	Hydrocarbons	SO_x	CFCs
O_3	H_2O	NO	CH_4	SO_2	CF_3Cl
CO	H_2O_2	NO_2	C_2H_6	COS	CF_2Cl_2
(CO_2)		HNO_3	C_2H_2		
N_2O		NH_3			

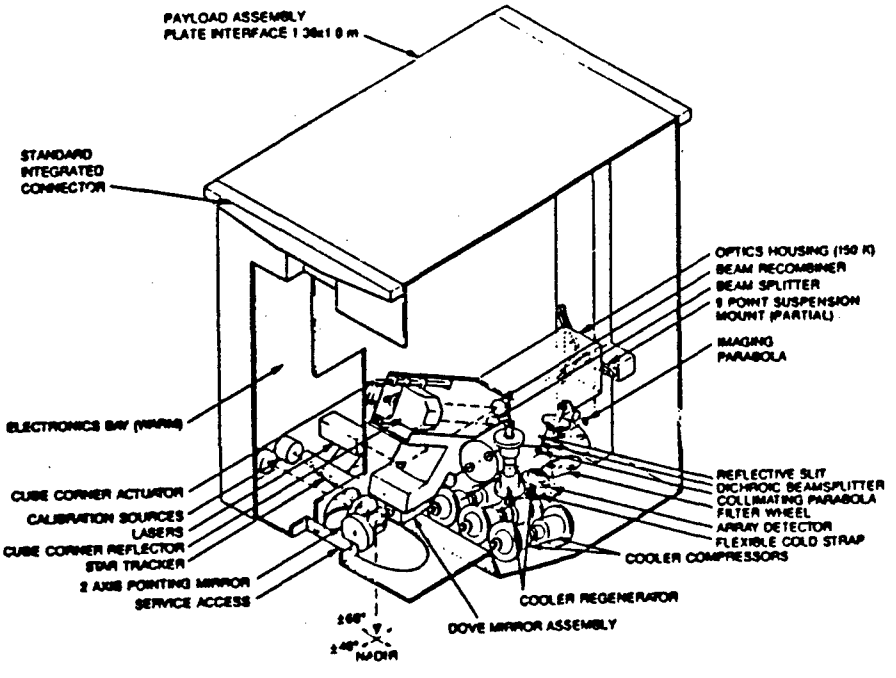
TES: SPECIES DETECTABILITY MATRIX



TROPOSPHERIC EMISSION SPECTROMETER
INSTRUMENT DESCRIPTION

- HIGH SPECTRAL RESOLUTION INFRARED IMAGING FOURIER TRANSFORM SPECTROMETER
- 491 KG, 660 W PEAK POWER
- SPECTRAL COVERAGE 600 TO 3200 CM-1 (2.9 TO 16.6 MICRONS)
- FOUR LINEAR ARRAYS OF 32 DETECTORS, EACH WITH ITS OWN SIGNAL CHAIN, IN CONJUGATE FOCAL PLANES
- ALL DETECTOR ELEMENTS ARE 0.1 MM BY 1.0 MM
- DETECTOR FOV 0.75 X 7.5 MRAD. NADIR PIXEL SUBTENDS 0.5 X 5 KM
- ON-BOARD SOURCES ARE PROVIDED FOR RADIOMETRIC CALIBRATION AND DETECTOR ALIGNMENT

TROPOSPHERIC EMISSION SPECTROMETER
CONCEPTUAL DESIGN



ORIGINAL PAGE IS
OF POOR QUALITY

TROPOSPHERIC EMISSION SPECTROMETER
FOCAL PLANE ARRAY - TECHNICAL SPECIFICATIONS

MATERIAL:	InSb (PV)	HgCdTe (PV)	HgCdTe (PV)	HgCdTe (PC)
WAVEBAND (μm)	2.9-5.6	8.3-12.5	5.3-9.1	11.1-16.7
CUT-OFF FREQ (cm^{-1})	1800-3400	800-1200	1100-1900	600-900
QUANTUM EFFICIENCY	0.6	0.6	0.6	0.8
IMPEDANCE (OHMS)	100 M	10 K	100 K	100
BKGRD FLUX DENSITY ($Ps^{-1}cm^{-1}$)	2.9E11-2.6E14	1.3E14-3.0E15	8.9E12-1.1E15	1.2E15-3.9E15
D* ($cm\ Hz^{1/2}\ W^{-1}$)	>7.0E11	>5.0E11	>6.0E11	>2.0E11
ELECTRICAL BANDWIDTH (kHz)	27	12	14	8.5
OPERATING TEMP (K)	65	65	65	65

THESE DETECTOR REQUIREMENTS ARE COMPATIBLE
WITH DETECTOR MATERIAL CURRENTLY BEING PRODUCED

TROPOSPHERIC EMISSION SPECTROMETER
PERFORMANCE ESTIMATES

FREQ. RANGE cm^{-1}	WAVELENGTH microns	NADIR SNR (2 sec scan)	LIMB SNR (8 sec scan)
600 - 900	11.1 - 16.7	500 - 600	200 - 300
800 - 1200	8.3 - 12.5	400 - 500	100 - 200
1100 - 1900	5.3 - 9.1	100 - 600	40 - 300
1900 - 3450(N)	2.9 - 5.6	30 - 150	na
1800 - 2450(L)	4.1 - 5.6	na	20 - 40

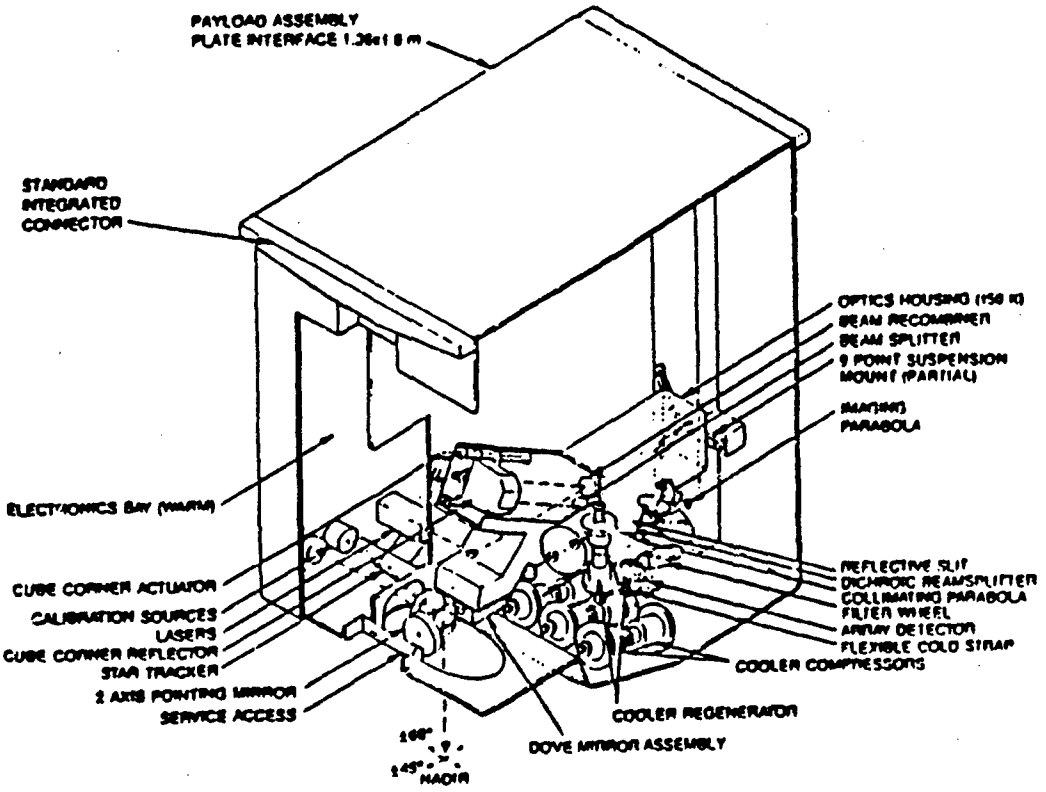
SPECTROSCOPY OF THE ATMOSPHERE USING FAR INFRARED EMISSION (SAFIRE)

[P.I.: Jim Russell, LaRC]

- SCIENTIFIC GOAL
  - To improve understanding of the middle atmosphere ozone distribution by conducting and analyzing global-scale measurements of important chemical, radiative, and dynamical processes, including coupling among processes and atmospheric regions.

- SCIENTIFIC OBJECTIVES
  - Study key processes in the O_y, HO_y, NO_y, ClO_y, and BrO_y chemical families
  - Study polar night chemistry
  - Conduct non-LTE investigations
  - Investigate diurnal change processes (OH, HO_2, NO_2, N_2O_5, O_3)
  - Conduct dynamics studies and study coupling between chemistry and dynamics
  - Investigate lower stratosphere phenomena (e.g. polar night O_3 depletion)

TROPOSPHERIC EMISSION SPECTROMETER
CONCEPTUAL DESIGN



TROPOSPHERIC EMISSION SPECTROMETER

FOCAL PLANE ARRAY - TECHNICAL SPECIFICATIONS

MATERIAL:	InSb (PV)	HgCdTe (PV)	HgCdTe (PV)	HgCdTe (PC)
WAVEBAND (μm)	2.9-5.6	8.3-12.5	5.3-9.1	11.1-16.7
CUT-OFF FREQ (cm^{-1})	1800-3400	800-1200	1100-1900	600-900
QUANTUM EFFICIENCY	0.6	0.6	0.6	0.8
IMPEDANCE (OHMS)	100 M	10 K	100 K	100
BKGRD FLUX DENSITY ($Ps^{-1}cm^{-1}$)	2.9E11-2.6E14	1.3E14-3.0E15	8.9E12-1.1E15	1.2E15-3.9E15
D* ($cm\ Hz^{1/2}\ W^{-1}$)	>7.0E11	>5.0E11	>6.0E11	>2.0E11
ELECTRICAL BANDWIDTH (kHz)	27	12	14	8.5
OPERATING TEMP (K)	65	65	65	65

THESE DETECTOR REQUIREMENTS ARE COMPATIBLE
WITH DETECTOR MATERIAL CURRENTLY BEING PRODUCED

TROPOSPHERIC EMISSION SPECTROMETER
PERFORMANCE ESTIMATES

FREQ. RANGE cm^{-1}	WAVELENGTH microns	NADIR SNR (2 sec scan)	LIMB SNR (8 sec scan)
600 - 900	11.1 - 16.7	500 - 600	200 - 300
800 - 1200	8.3 - 12.5	400 - 500	100 - 200
1100 - 1900	5.3 - 9.1	100 - 600	40 - 300
1800 - 3450(N)	2.9 - 5.6	30 - 150	na
1800 - 2450(L)	4.1 - 5.6	na	20 - 40

ORBITAL VOLCANOLOGICAL OBSERVATIONS (OVO)

[P.I.: Dave Pieri, JPL]

ORBITAL VOLCANOLOGICAL OBSERVATIONS
SCIENCE GOALS

- IMPROVED UNDERSTANDING OF ERUPTION MECHANISMS
- IMPROVED DETERMINATION OF THE NATURE AND AMOUNT OF VOLCANIC CONTRIBUTIONS TO THE GLOBAL ENVIRONMENT
- IMPROVED UNDERSTANDING OF HOW THE PRODUCTS OF VOLCANIC ERUPTIONS INTERACT WITH THE ENVIRONMENT TO PRODUCE SIGNIFICANT GLOBAL CHANGES

ORBITAL VOLCANOLOGICAL OBSERVATIONS
MEASUREMENT OBJECTIVES

- MULTISPECTRAL THERMAL IR MAPPING OF VOLCANIC LITHOLOGIES
- BRIGHTNESS TEMPERATURE AND HEAT SOURCE DISTRIBUTION MAPS OF ACTIVE VOLCANIC FEATURES (E.G. LAVA FLOWS, SUMMIT CRATERS, LAVA TUBE SYSTEMS, FUMAROLES, HOT WATER LAKES, HOT WATER OCEANIC PLUMES)
- BRIGHTNESS TEMPERATURE MAPS OF ERUPTION COLUMNS AND DISPERSED VOLCANIC PLUMES
- MULTISPECTRAL DETECTION AND MAPPING OF AIRBORNE ASH PLUMES IN THE PRESENCE OF METEOROLOGICAL CLOUDS
- DETERMINATION OF COMPOSITION AND VOLUME OF SUBAERIAL GLOBAL VOLCANIC GAS BUDGET OVER TIME

ORBITAL VOLCANOLOGICAL OBSERVATIONS
DATA PRODUCTS

- THERMAL MAPS OF SOLID PRODUCTS OF VOLCANIC ERUPTIONS ON THE GROUND
- MULTISPECTRAL MAPPING IMAGES OF THE SURFACE OF VOLCANOES
- 2-D THERMAL MAPS OF AIRBORNE PLUMES
- 3-D THERMAL PROFILES OF ERUPTION PLUMES

ORBITAL VOLCANOLOGICAL OBSERVATIONS
INFRARED DETECTOR REQUIREMENTS

- 1.0-2.5 μm, 5-10 CHANNELS FOR HIGH TEMPERATURE THERMAL RADIOMETRY, GAS AND AEROSOL MEASUREMENTS
- 2.5-5.0 μm, 5 CHANNELS FOR LOWER TEMPERATURE RADIOMETRY, GEOLOGICAL MAPPING, GAS AND AEROSOL MEASUREMENTS
- 8-12 μm, 10+ CHANNELS FOR MULTISPECTRAL MAPPING, LOWEST TEMPERATURE THERMAL RADIOMETRY, ATMOSPHERIC MEASUREMENTS AND CORRECTIONS
- IMAGING CAPABILITY REQUIRED, $\geq$ 25 km SWATH, $\leq$100 m SPATIAL SAMPLING
- LOW TEMP RADIOMETRY REQUIRES ~0.3K NedT MEASUREMENT CAPABILITY
- MASS CONSIDERATIONS ARGUE FOR DEVELOPMENT OF DETECTORS WITH REDUCED COOLING REQUIREMENTS

MULTISPECTRAL THERMAL IMAGER (MSTI)

[P.I.: Tim Schofield, JPL]

MULTISPECTRAL THERMAL IMAGER
SCIENCE OBJECTIVES AND KEY MEASUREMENTS

- **UNDERSTAND THE INTERPLAY BETWEEN RADIATIVE, DYNAMICAL AND PHOTOCHEMICAL PROCESSES IN THE ATMOSPHERES OF SATURN, TITAN AND JUPITER**
  - **OBTAIN MEASUREMENTS OF THE 3-D DISTRIBUTION OF TEMPERATURE, DYNAMICAL FIELDS, KEY SPECIES CONCENTRATIONS AND AEROSOL EXTINCTION IN THESE ATMOSPHERES WITH COMPREHENSIVE COVERAGE AND RESOLUTION, BOTH SPATIALLY AND TEMPORALLY**
- **DEVELOP A DESCRIPTION OF THE PHYSICAL AND COMPOSITIONAL UNITS OF THE SATELLITES AND RINGS**

  OBTAIN COMPREHENSIVE MULTISPECTRAL MEASUREMENTS OF BRIGHTNESS TEMPERATURE AND ALBEDO

MULTI-SPECTRAL THERMAL IMAGER (MSTI)
CONCEPTUAL INSTRUMENT SPECIFICATIONS

INSTRUMENT PARAMETER	VALUE/COMMENTS
INSTRUMENT TYPE	MULTI-SPECTRAL THERMAL IMAGER
MEASUREMENT TECHNIQUES	GAS CORRELATION AND FILTER RADIOMETRY
SPECTRAL CHANNELS AND RANGE	8 CHANNELS, 8-14 μm 7 CHANNELS, 15-100 μm 1 CHANNEL, 0.3-3.0 μm
TELESCOPE APERTURE	NARROW ANGLE, 16 cm WIDE ANGLE, 4 cm
NARROW ANGLE FOV	ARRAY, 1.15° x 1.15°
WIDE ANGLE FOV	ARRAY, 4.58° x 4.58 °
MID-IR DETECTOR	64 x 64 PV HgCdTe ARRAY, 70K
FAR-IR AND SOLAR DETECTOR	64 x 64 BOLOMETER ARRAY, 180K
DATA RATE	1.5 kbps, APOCHRONE 3.0 kbps, FAR ENCOUNTER 6.0 kbps, NEAR ENCOUNTER
INSTRUMENT DATA BUFFER	2 MBytes
SPACECRAFT POINTING PITCH, ROLL, AND YAW	CONTROL, 2 mrad KNOWLEDGE, 1 mrad STABILITY, 100 μrad - 2 seconds STABILITY, 300 μrad - 30 seconds
MASS GOAL	23 kg
POWER GOAL	19 WATTS (AVERAGE)

ORIGINAL PAGE IS
OF POOR QUALITY

MULTI-SPECTRAL THERMAL IMAGER (MSTI)
CHANNEL SPECTRAL CHARACTERISTICS AND MEASUREMENT FUNCTIONS

CHANNEL (1)	BANDPASS cm^{-1}	BAND CENTER, μm	CHANNEL TYPE (2)	MEASUREMENT FUNCTION
FILTER WHEEL A - MID INFRARED, 70 K HgCdTe DETECTOR ARRAY, 64 x 64 PIXELS				
A1	1240 - 1290	7.9	0.5 cm CELL, 300 mbar CH_4	STRATOSPHERIC TEMPERATURE
A2	1240 - 1290	7.9	1.5 cm CELL, 300 mbar CH_4	
A3	805 - 845	12.1	0.5 cm CELL, 300 mbar C_2H_6	ETHANE CONCENTRATION
A4	805 - 845	12.1	1.5 cm CELL, 300 mbar C_2H_6	
A5	730 - 760	13.4	0.5 cm CELL, 150 mbar C_2H_2	ACETYLENE CONCENTRATION
A6	730 - 760	13.4	1.5 cm CELL, 150 mbar C_2H_2	
A7	920 - 1050	10.2	BANDPASS FILTER	PHOSPHINE
A8	1120 - 1180	8.7	BANDPASS FILTER	AMMONIA ICE
FILTER WHEEL B - FAR INFRARED, 180 K BOLOMETRIC DETECTOR ARRAY, 64 x 64 PIXELS				
B1	570 - 630	16.7	BANDPASS FILTER	TROPOSPHERIC TEMPERATURE ORTHO-PARA HYDROGEN RATIO AEROSOL DISTRIBUTION
B2	470 - 510	20.4	BANDPASS FILTER	
B3	350 - 390	27.0	BANDPASS FILTER	
B4	210 - 250	43.5	BANDPASS FILTER	
B5	170 - 210	52.6	BANDPASS FILTER	
B6	80 - 140	90.1	BANDPASS FILTER	
B7	OPEN	-	OPEN	ENERGY BALANCE
B8	3333 - 33333	0.54	LONGWAVE BLOCKER	

(1). IMAGING IS PERFORMED IN ALL SPECTRAL CHANNELS.
(2). CHANNELS A1 - A6 PERFORM GAS CORRELATION RADIOMETRY USING BANDPASS FILTERS AND CELLS CONTAINING THE GAS INDICATED TO OBTAIN HIGH ENERGY GRASP, SPECTRAL DISCRIMINATION, AND SPECIES SELECTIVITY. CHANNELS A7, A8, AND B1 - B8 BANDPASS FILTERS ONLY.

MULTISPECTRAL THERMAL IMAGER (MSTI)
LWIR FOCAL PLANE ARRAY REQUIREMENTS

- **D^* (cm $hz^{1/2}$ w^{-1})**

  GOAL: ≥2.0E+11 (8μm), ≥2.0E+10 (13.5μm), ≥1.0E+09 (100μm)
  REQ: ≥1.0E+11 (8μm), ≥1.0E+10 (13.5μm), ≥1.0E+10 (100μm)

- **CURRENT PV-HgCdTe TECHNOLOGY CAN MEET THE D^* REQUIREMENTS, BUT CANNOT MEET THE GOALS AT BOTH 8 AND 13.5 μm SIMULTANEOUSLY**

COMPOSITE INFRARED SPECTROMETER (CIRS)

[P.I.: Virgil Kunde, GSFC]

COMPOSITE INFRARED SPECTROMETER
SCIENCE OBJECTIVES

- DETERMINE THE TROPOSPHERIC AND STRATOSPHERIC TEMPERATURE AND AEROSOL STRUCTURE OF SATURN AND TITAN
- DETERMINE THE MIXING RATIOS AND SPATIAL DISTRIBUTIONS OF TRACE GASES IN BOTH ATMOSPHERES
  - MANY ORGANIC MOLECULES FOR TITAN
  - PH_3 AND NH_3 FOR SATURN
- CONSTRAIN THE PROPERTIES OF NH_3 ICE CLOUDS IN SATURN'S ATMOSPHERE
- DETERMINE THE BULK COMPOSITION OF SATURN'S ATMOSPHERE
- DETERMINE SURFACE TEMPERATURE PROPERTIES OF THE SMALLER ICY SATELLITES AND THE EMISSIVITY OF THE RINGS

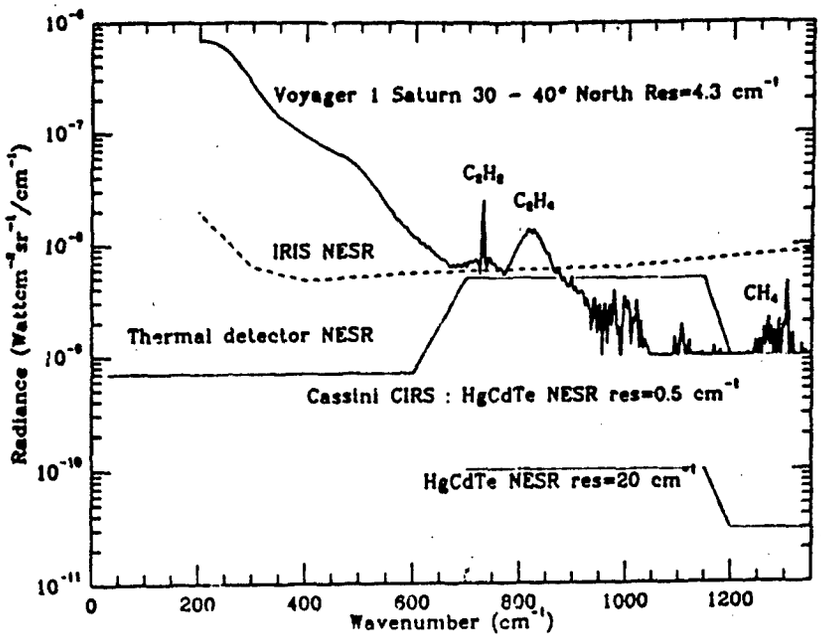


Figure B6 CIRS sensitivity for Saturn.

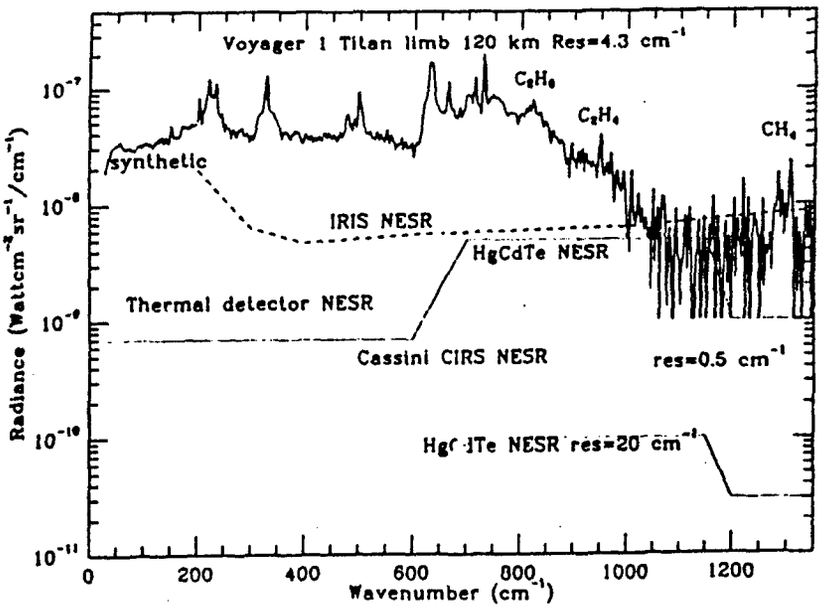


Figure B7 CIRS sensitivity for Titan.

ORIGINAL PAGE IS
OF POOR QUALITY

COMPOSITE INFRARED SPECTROMETER
INSTRUMENT CHARACTERISTICS

- DUAL INTERFEROMETER CONFIGURATION SHARING A 50 CM CASSEGRAIN TELESCOPE
- SPECTRAL RANGE 7.5-1000 μm
- SPECTRAL RESOLUTION 0.25 cm^{-1} UNAPODIZED
- INDIVIDUAL DETECTOR FIELD-OF-VIEW .25° (FAR-IR); .0057° (MID-IR)
- FAR-IR INTERFEROMETER EMPLOYS A 1x5 ARRAY USING EITHER THERMOPILES OR PYROELECTRICS
- MID-IR INTERFEROMETER EMPLOYS TWO 1 x 43 HgCdTe ARRAYS, COOLED TO 70-90K

POLARIZING FTS (CIRS)

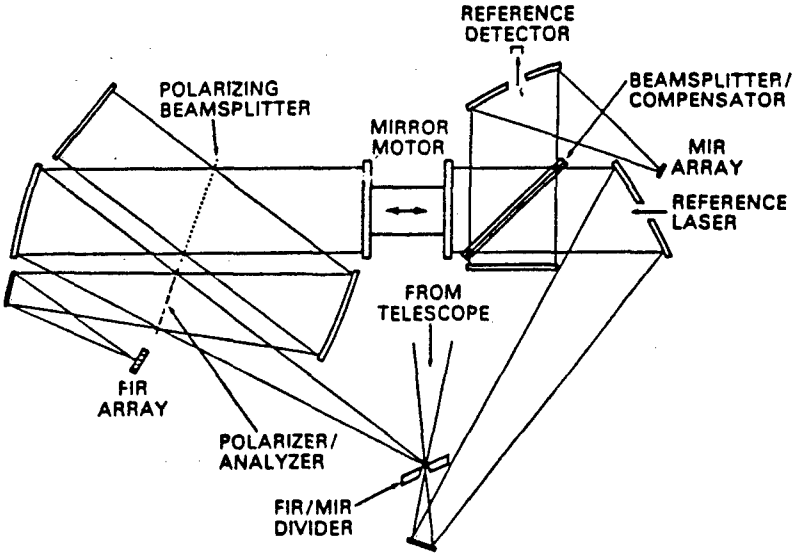


Figure B8 Optical schematic for CIRS.

COMPOSITE INFRARED SPECTROMETER
FOCAL PLANE PARAMETERS

	#1	#2	#3
SPECTRAL RANGE (cm^{-1})	10-700	700-1200	1200-1400
DETECTORS	THERMOPILE (1x5)	HgCdTe (1x43)	HgCdTe (1x43)
PIXEL FOV (mrad)	4.3x12.9	0.1x0.3	0.1x0.3
PIXEL AΩ (cm^2-sr)	1.1×10^{-1}	6.1×10^{-6}	6.1×10^{-6}
NEP (W $Hz^{-1/2}$)	2×10^{-11}	8×10^{-14}	2×10^{-14}
NESR (W · $cm^{-2}sr^{-1}/cm^{-1}$)	7×10^{-10}	5×10^{-9}	1×10^{-9}
TEMPERATURE (K)	170	90	90

GENERAL AREAS FOR EXPERIMENT ENHANCEMENT

- ALL THE PROPOSED EXPERIMENTS WOULD BE ENHANCED BY ONE OR MORE OF THE FOLLOWING IMPROVEMENTS.
  - IMPROVED DETECTOR PERFORMANCE, GIVING:
    - SAME INSTRUMENT PERFORMANCE AT HIGHER DETECTOR TEMPERATURES.
    - IMPROVED PERFORMANCE AT THE SAME DETECTOR TEMPERATURE
  - LOWER INSTRUMENT AND DETECTOR OPERATING TEMPERATURES, GIVING:
    - IMPROVED PERFORMANCE WITH EXISTING DETECTORS
  - IMPROVED DETECTOR PERFORMANCE PLUS LOWER OPERATING TEMPERATURES
- IMPROVED COOLING IS EXPENSIVE IN MASS AND POWER
- IMPROVED DETECTOR PERFORMANCE IS EXPENSIVE IN UP FRONT DEVELOPMENT COSTS

SAFIRE MEASUREMENT OBJECTIVES

- **Conduct global-scale, simultaneous, vertical profile measurements of temperature and key Oy, HOy, NOy, ClOy, and BrOy constituents, including the following:**

O_3, O_3^{50}, $O(^3P)$; OH, HO_2, H_2O_2, H_2O, HDO, CH_4; NO_2, HNO_3, N_2O_5; HCl, HOCl; HBr and HF

Oy HOy NOy ClOy

- **Conduct measurements (e.g. T, O_3, CH_4, and H_2O) that can be used to derive and study dynamical quantities such as geopotential height, potential vorticity, winds, and Eliassen Palm flux**

- **Employ a 3 km IFOV in the far IR and 1.5 km in the mid IR**

- **Provide scan mode flexibility to enhance science return**
  - Chemistry mode, 10-110 km vertical scan, 1.5 km sampling interval, 5° of latitude
  - Polar chemistry mode, 10-106 km, 3 km, 2.5°
  - Dynamics mode, 10-100 km, 0.75 km, 1.25°
  - Thermospheric mode, 84-180 km, 3 km, 5°

SAFIRE Experiment Measurement Objectives

Parameters Measured[1]	Spectral Range (cm^{-1})	Alt. Range (km)	IFOV[2] (km)	Horizontal Resolution[2]		Temporal Resolution (sec.)[4]	Lat. Cov. (deg.)	Estimated Precision[5]	
				Lat. (deg.)	Long. (deg.)			% (1σ)	Vertical Range (km)
O_3	82 - 84.4; 926 - 1141	10 - 100	1.5 - 3	1 - 5	25	18 - 72	8° - 86°N	5	10 - 70
$O(^3P)$	157 - 159	90 - 180	3	2.5 - 5		36 - 72		15	110-180
OH	82 - 84.4; 117.8 - 119.6	20 - 90	3	2.5 - 5		36 - 72		7	30 - 75
HO_2	93.8 - 96; 111.0 - 112.6	20 - 75	3	2.5 - 5		36 - 72		7	30 - 60
H_2O_2	93.8 - 96	20 - 50	3	2.5 - 5		36 - 72		7	30 - 45
H_2O	157 - 159	10 - 100	3	2.5 - 5		36 - 72		5	20 - 80
HDO	93.8 - 96	10 - 60	3	2.5 - 5		36-72		7	20 - 50
CH_4	1335 - 1365	10 - 65	1.5	1 - 5		18 - 72		7	15 - 55
NO_2	1560 - 1630	15 - 60	1.5	1 - 5		18 - 72		5	20 - 55
HNO_3	850 - 920	10 - 45	1.5	1 - 5		18 - 72		7	15 - 40
N_2O_5	310 - 390; 1230 - 1260	10 - 45	1.5 - 3	1 - 5		18 - 72		10	20 - 40
HCl	82 - 84.4	10 - 65	3	2.5 - 5		36 - 72		5	25 - 55
HOCl	98.5 - 100; 117.8-119.6	20 - 45	3	2.5 - 5		36 - 72		7	35 - 40
HBr	98.5 - 100	15 - 40	3	2.5 - 5		36 - 72		10	25 - 35
HF	82 - 84.4	40 - 60	3	2.5 - 5		36 - 72		15	40 - 60
Temp.	630 - 670; 580 - 760	10 - 110	1.5	1 - 5		18 - 72		<0.5K	16 - 65
Pressure	630 - 670; 580 - 760	10 - 110	1.5	1 - 5		18 - 72		<2	16 - 70
O_2	82 - 120	10 - 80	3	1 - 5		36 - 72		<2	10 - 65
$O_3(v_2)$	82-84.4	20-50	↓	2.5-5	↓	↓	↓	10°	20-40
$O_3(v_{1,3})$	82-84.4	20-35	↓	2.5-5	↓	↓	↓	15°	20-30
^{18}OOO	82-84.4	20-40	↓	2.5-5	↓	↓	↓	15°	20-35

SAFIRE Experiment Measurement Objectives (Con't)

Parameters Measured[1]	Spectral Range (cm^{-1})	Alt. Range (km)	IFOV[2] (km)	Horizontal Resolution[3]		Temporal Resolution (sec.)[4]	Lat. Cov. (deg.)	Estimated Precision[5]	
				Lat. (deg.)	Long. (deg.)			% (1σ)	Vertical Range (km)
$O^{18}OO$	82-84.4	20-35	3	2.5-5	25	36-72	86°S - 86°N	15°	20-30
^{17}OOO	117.8-119.8	20-40	↓	↓	↓	↓	↓	15°	20-35
$O^{17}OO$	82-84.4	20-35						40°	20-30
$H_2{}^{18}O$	93.8-96, 117.8-119.8	20-60						10°	20-50
$H_2{}^{17}O$	99.2-101.4, 117.8-119.8	20-50						10°	20-40
HCN	82-84	25-35						35°	25-30
N_2O	1230-1280	20-40	1.5	1-5				15°	20-35

[6]These are estimated precisions based on spectral features and absorption strengths. Retrieval simulations have not been performed.

[1]Does not include derived quantities such as winds, potential vorticity, and others.

[2]Vertical resolution is estimated to be 4 km.

[3] Latitudinal resolution is determined by vertical profile skew or ground-track motion during the measurement time. Longitudinal resolution is determined by the orbital spacing. The horizontal FOV width is ≈ 0.1°.

[4]Obeervations are made continuously with a vertical profile scan time of 72 sec in the chemistry and thermospheric modes, 36 sec in the polar chemistry mode, and 18 sec in the dynamics mode.

[5]Precision is the 1σ uncertainty determined from simulation set of 5 retrievals, except for HDO which is for a single retreival only.

SAFIRE INSTRUMENT PARAMETERS

- **Mass** — 304 kg
- **Power (watts)** — Average--304, Peak--350, Standby--175
- **Data Rate** — 9 mbs (FTS), 9 kbs (Radiometer)
- **Envelope** — 1.5m(L) x 1.5m(W) x 1.5m(H)
- **Limb View Direction** — Elevation 14° to 27° depression angle
  Azimuth + 10° Forward
  - 170° Aft

SAFIRE MID-IR DETECTOR REQUIREMENTS

CHANNEL	FREQUENCY (cm^{-1})	DYNAMIC RANGE (E+03)	D* REQUIRED (E+10 cm $(Hz/W)^{1/2}$)
1	630-670	7	1.4
2	580-760	28	1.5
3	850-920	7	1.5
4	1335-1365	1	1.4
5	1560-1630	1	1.4
6	926-1141	15	1.6
7	1230-1260	1	1.5

CONFIGURATION: 15 x 7 Array
ELEMENT SIZE: 0.2 x 0.3 mm

SAFIRE FAR-IR REQUIREMENTS

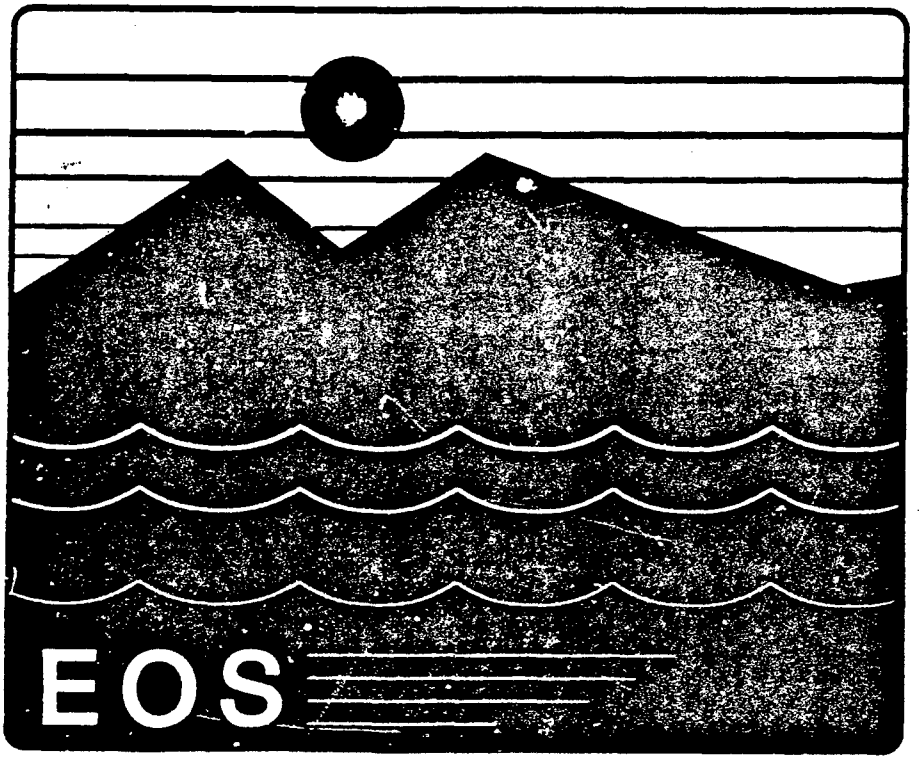
CHANNEL	FREQUENCY (cm^{-1})	NO. OF DETECTORS	TYPE	NEP (W $Hz^{-1/2}$) x E-15
1	82-85	8	Ge:Ga	1
2	94-96	8	Ge:Ga	1
3	98-100	8	Ge:Ga	1
4	111-113	8	Ge:Ga	1
5	118-120	8	Ge:Ga	1
6A	157-160	4	Ge:Ga	1
6B	310-390	4	Ge:Be	10

CONFIGURATION: (3) 2 x 8 ARRAYS
ELECTRONICS: TIA-JFET 10 kHz BANDWIDTH
BLIP-LIMITED PERFORMANCE (10^{10} ph/sec-typical)
DETECTORS TO BE PROVIDED BY FRANCE

1990 REFERENCE HANDBOOK

Goddard Space Flight Center

NASA



Earth Observing System

ORIGINAL PAGE IS
OF POOR QUALITY

N91
14381
UNCLAS

N91-14381

SDIO Long Wavelength Infrared Detector Requirements

Dr. Dwight Duston
Director, Innovative Science and Technology
Strategic Defense Initiative Organization
Washington, DC

The Strategic Defense Initiative Organization has a significant requirement for infrard sensors for surveillance, tracking and discrimination of objects in space. Projected SDIO needs cover the range from short wavelengths out to 30 μm. Large arrays are required, and producibility and cost are major factors. The SDIO is pursuing several approaches including innovative concepts based on semiconductors and superconductors.

PRECEDING PAGE BLANK NOT FILMED

SDIO INFRARED TECHNOLOGY EFFORTS

LT COL HILMER SWENSON
SENSORS AND INTERCEPTORS DIRECTORATE

MARCH 13, 1990

AGENDA (U)

UNCLASSIFIED

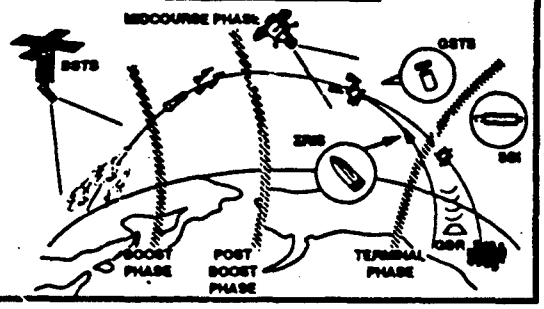
UNCLASSIFIED

- SCOPE OF SDIO IR SENSOR TECHNOLOGY DEVELOPMENT
- TECHNOLOGY THRUSTS
  - — OPTICS TECHNOLOGY
  - — FOCAL PLANE TECHNOLOGY
  - — CRYO COOLERS
  - — SIGNAL PROCESSORS
  - — INTEGRATED SENSORS
- SUMMARY

SCOPE OF SDIO IR SENSOR TECHNOLOGY (U) (U)

UNCLASSIFIED

SDI MISSION AREAS



UNCLASSIFIED

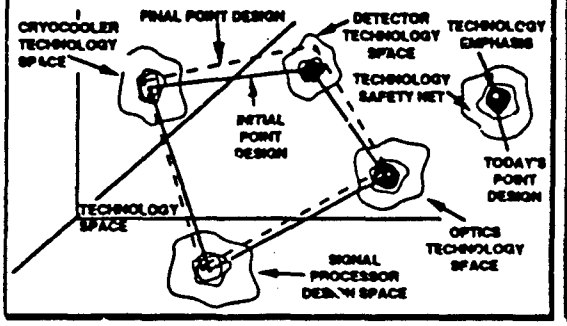
PROJECT 5 MISSION

- DEVELOP IR TECHNOLOGY NECESSARY TO SUPPORT SDI SURVEILLANCE AND WEAPON SYSTEM SENSORS FOR PHASE I
- ADVANCE THE STATE OF ART FOR IR SENSORS

AGENTS
SAT 9.1 USASOC DONALD PARKER (205)896-3788
SAT 18 AFSTC CAPT MICHAEL DEVINE (505)846-8964
SAT 18 AFSTC LT. JEFF BRUNING (505)846-4964

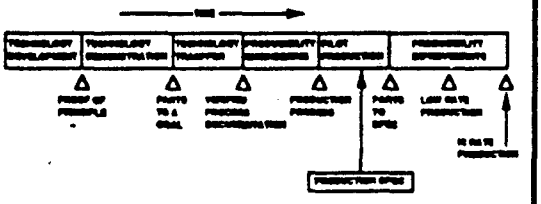
UNCLASSIFIED

PROJECT PHILOSOPHY



UNCLASSIFIED

TECHNOLOGY MATURITY



UNCLASSIFIED

CRYOCOOLERS (U)

UNCLASSIFIED

DRIVERS

- HIGH RELIABILITY
- EXTEND ON-ORBIT LIFETIME
- HIGH EFFICIENCY
- LOW WEIGHT
- ACCUMULATE OPERATING HISTORY
- REDUCE COST

UNCLASSIFIED

CURRENT APPROACH

- TURBO-BRAYTON(3-STAGE)
- ROTARY RECIPROCATING REFIGERATOR (R-3 STAGE)
- 2-STAGE LIFE TESTING
- DEVELOP THERMAL INTEGRATION TECHNOLOGIES
  (HEAT PIPE, THERMAL SWITCH)

UNCLASSIFIED

NEW TECHNOLOGY

- MAGNETIC COOLING
- SORPTION COMPRESSION
- MIXED GAS QUICK COOLDOWN J-T
- PULSE TUBES
- ACOUSTIC DRIVERS

UNCLASSIFIED

NEEDS

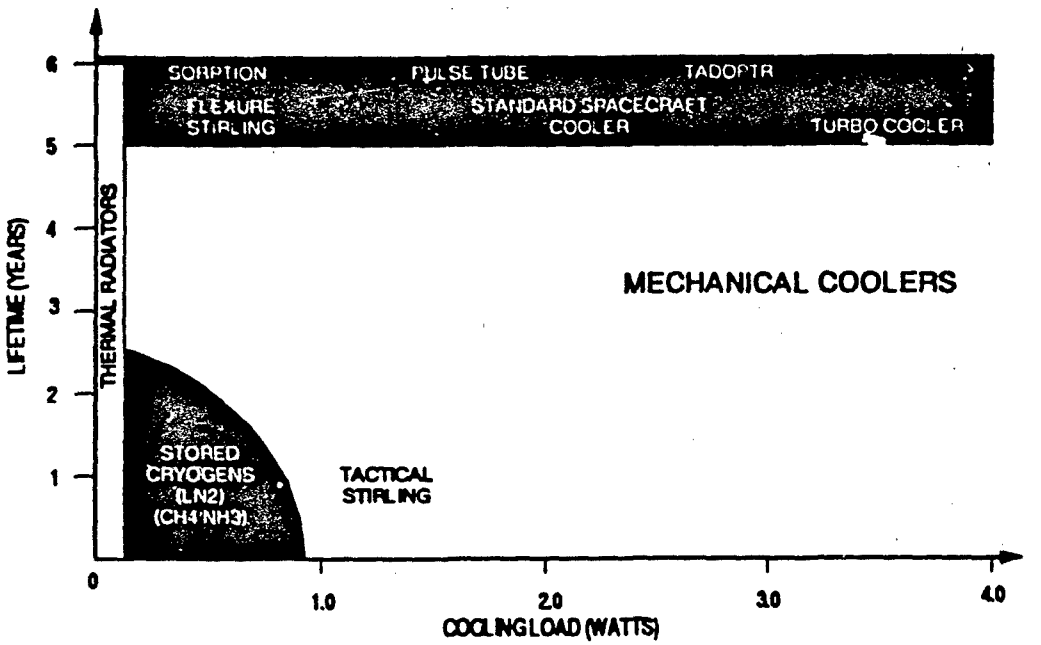
- HARDENED FLIGHT CONTROL ELECTRONICS
- REDUCED WEIGHT HIGH EFFECTIVENESS HEAT EXCHANGERS
- MODULAR/SCALEABLE CRYOCOOLERS
- SOLID STATE CONCEPTS

ORIGINAL PAGE IS
OF POOR QUALITY

CRYOGENIC TECHNOLOGY PARAMETERS

ASSUME COOLING TEMPERATURE 65-80K

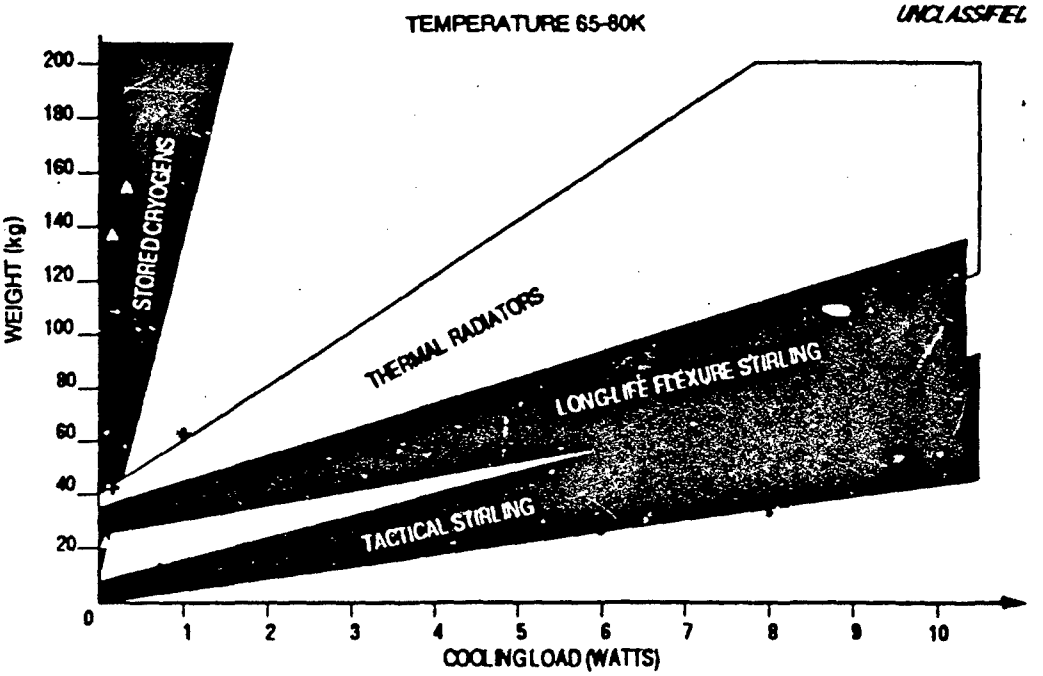
UNCLASSIFIED



CRYOGENIC SYSTEM WEIGHT

TEMPERATURE 65-80K

UNCLASSIFIED



FOCAL PLANE ARRAY TECHNOLOGY (U)

UNCLASSIFIED

UNCLASSIFIED

DRIVERS	DRIVING SYSTEM
• YIELD/COST/ PRODUCIBILITY	KEW,GSTS
• RADIATION HARDNESS	KEW, SSTS
• OPERATING TEMPERATURE	SSTS
• HYBRID PERFORMANCE	SPIRIT III , SSTS, GSTS
• D*	SSTS, GSTS
• CUTOFF WAVELENGTH	SSTS, GSTS
• UNIFORMITY	SPIRIT III, GSTS,
• CROSSTALK	SPIRIT III, SSTS, GSTS

UNCLASSIFIED

CURRENT APPROACH

- MANTECH
  - MWIR PILOT LINE DEMO FOR BOOST PHASE APPLICATION
- HYWAYS
  - IBC HYBRID DEVELOPMENT FOR SSTS, GSTS
  - ADVANCED HYBRID DEVELOPMENT
  - PILOT LINE DEMO
- SLIM
  - LWIR HgCdTe FOR KEW & SSTS BACKUP
- HARDENED InSe TECHNOLOGY FOR SCANNERS

UNCLASSIFIED

NEW TECHNOLOGY

- INTRINSIC EVENT DISCRIMINATOR
- SOLID STATE PHOTOMULTIPLIER
- Ge CTIA
- GaAs MUX FOR HgCdTe
- HIGH OPERATING TEMPERATURE DETECTORS
- HIGH TEMPERATURE SUPERCONDUCTORS
- STRAINED LAYER SUPERLATTICE
- VLWIR HgCdTe – HIT DETECTORS, SOFRADIR
- LWIR Hg CdTe TECHNOLOGY
- HgCdTe PASSIVATION TECHNOLOGY

UNCLASSIFIED

NEEDS

- MODULES
- NOISE MODELS FOR HYBRID INTEGRATION
- LARGER SUBSTRATES
- AUTOMATED TESTING FACILITY
- TRAINING FOR TEST FACILITY PERSONNEL
- INTEGRATED FOCAL PLANE TECHNOLOGY

IRFPA DESIGN DRIVERS (U)

UNCLASSIFIED

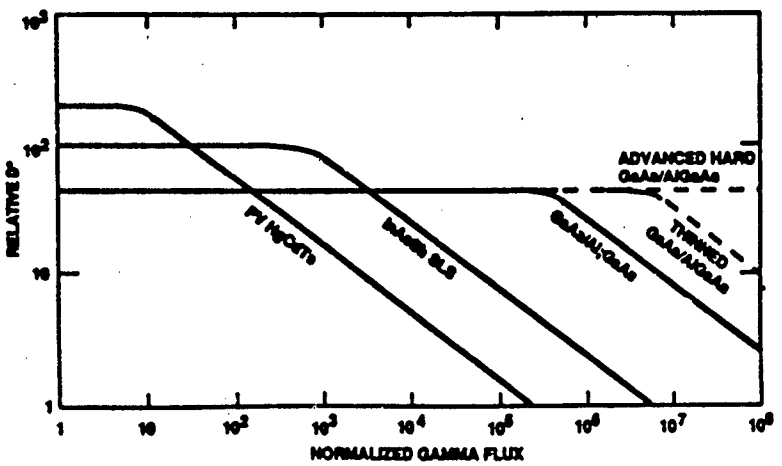
UNCLASSIFIED

- LOW TEMPERATURE TARGETS
- LOW BACKGROUNDS
- HIGH TOTAL DOSE ENVIRONMENT
- 3 COLORS REQUIRED FOR DISCRIMINATION
- LARGE FOV – HIGH SCAN RATES
  - SHORT INTEGRATION TIMES
  - HIGH DATA RATES FOR ANALOG SIGNAL PROCESSOR
- LARGE NUMBERS OF TARGETS/DECOYS
- HIGH THROUGHPUT REQUIREMENTS FOR OBJECT DEPENDENT PROCESSORS

ORIGINAL PAGE IS
OF POOR QUALITY

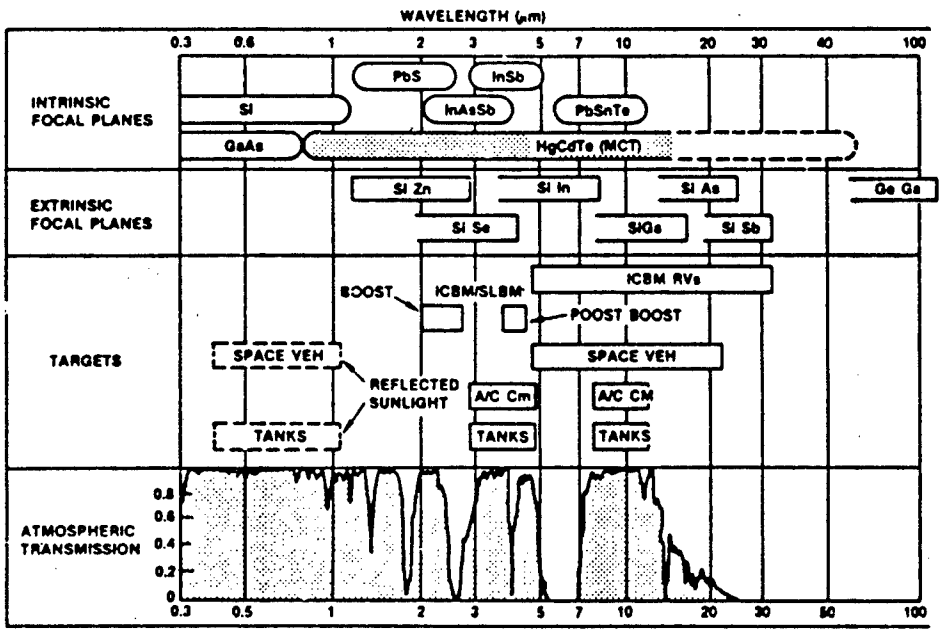
RELATIVE HARDNESS

UNCLASSIFIED
HSH1690605A



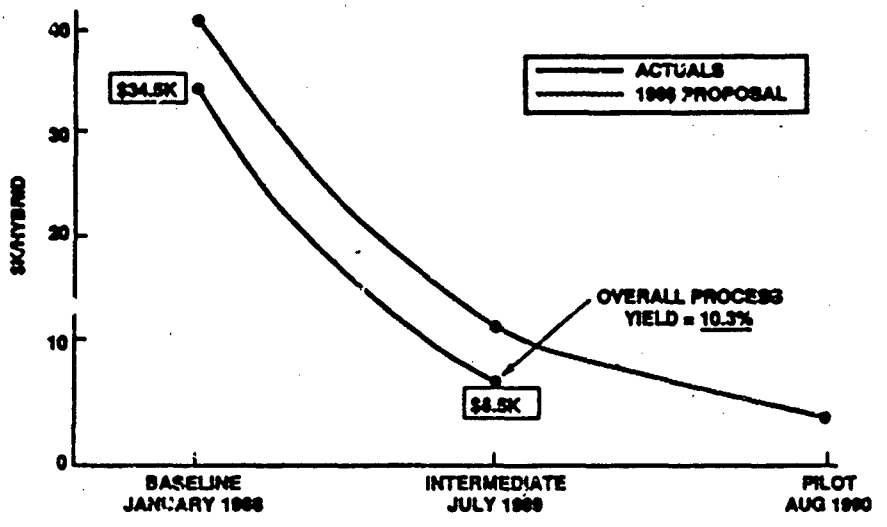
MATERIALS/APPLICATIONS MATCH-UPS (U)

UNCLASSIFIED



UNCLASSIFIED

80% COST REDUCTION DEMONSTRATED WITH INTERMEDIATE RUN



MANTECH STATUS (U)

UNCLASSIFIED

	CONFIGURATION	YIELD	YIELD GOAL	COST/HYBRID	COST GOAL
• ORIGINAL					
— ROCKWELL (HYBRIDS)	32x8	0.2	—	$100 K	—
— SBRC (DETECTOR ARRAYS)	32x8	0.2	—	$200 K	—
• BASELINE RESULTS					
— ROCKWELL (HYBRIDS)	32x64	1.35%	0.4%	$34 K (100% TEST)	$20/CHANNEL
— SBRC (DETECTOR ARRAYS)	128x128	3.5%	0.4%	$15 K (SAMPLE TEST)	$20/CHANNEL
• INTERMEDIATE RESULTS					
— ROCKWELL • YIELD 2X BASELINE	32x64	10.3%	1.5%	$8.5 K	$5/CHANNEL ($3.16 ACHIEVED)
— SBRC • YIELD/PERFORMANCE IMPROVEMENTS • CdTe PASSIVATION	128x128	35% PRO-JECTED	1.5%	$4.6 K (SAMPLE TEST)	$5/CHANNEL ($0.28 PROJECTED WITH SAMPLE TESTING)

OF PIXELS WORKING MADE UNDER MANTECH = >3M

OF PIXELS REQUIRED BY END OF CONTRACT = ~2M

ISSUES REMAINING AFTER MWIR HgCdTe MANTECH (U)

UNCLASSIFIED

ISSUE	NEED TO BE ADDRESSED BY
• HARDNESS	TECHNOLOGY PROGRAM MANTECH REVISITED
• PRODUCIBILITY OF NUCLEAR HARD ARRAYS	
• INTERGRATION OF ARRAYS	TECHNOLOGY OR PRIMES
• UNIFORMITY	TECHNOLOGY DEVELOPMENT
• SUSTAINING MARKET PLACE	TATICAL?
• TRUE HANDOFF TO PRODUCTION WITH LESS TOUCH LABOR	DPESO/DSTAR
• THIRST FOR HIGHER PERFORMANCE AT LOWER COST	TECHNOLOGY MATERIALS/ DSTAR LABOR
• RADIOMETRY PERFORMANCE	TECHNOLOGY
• READOUTS	TECHNOLOGY



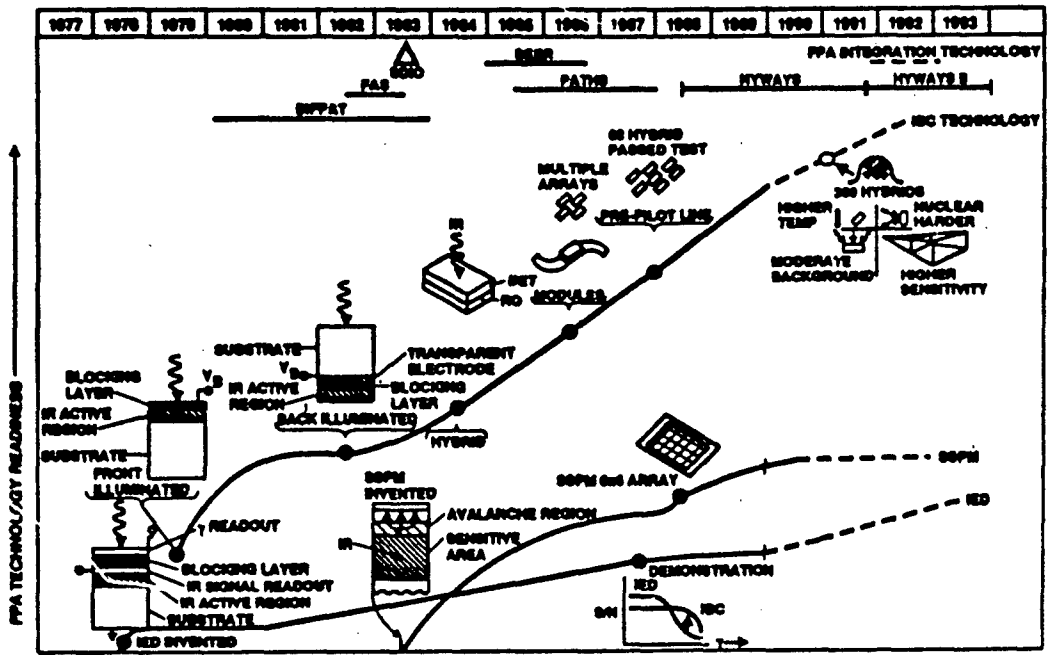
BENEFITS OF IBC DETECTORS (U)

UNCLASSIFIED

- RADIATION HARDNESS
- RESPONSE LINEARITY
- FREQUENCY OF RESPONSE
- UNIFORMITY OF RESPONSE
- PREDICTABLE BEHAVIOR
- HIGH RESPONSIVITY
- RELATIVELY HIGH PIXEL YIELD

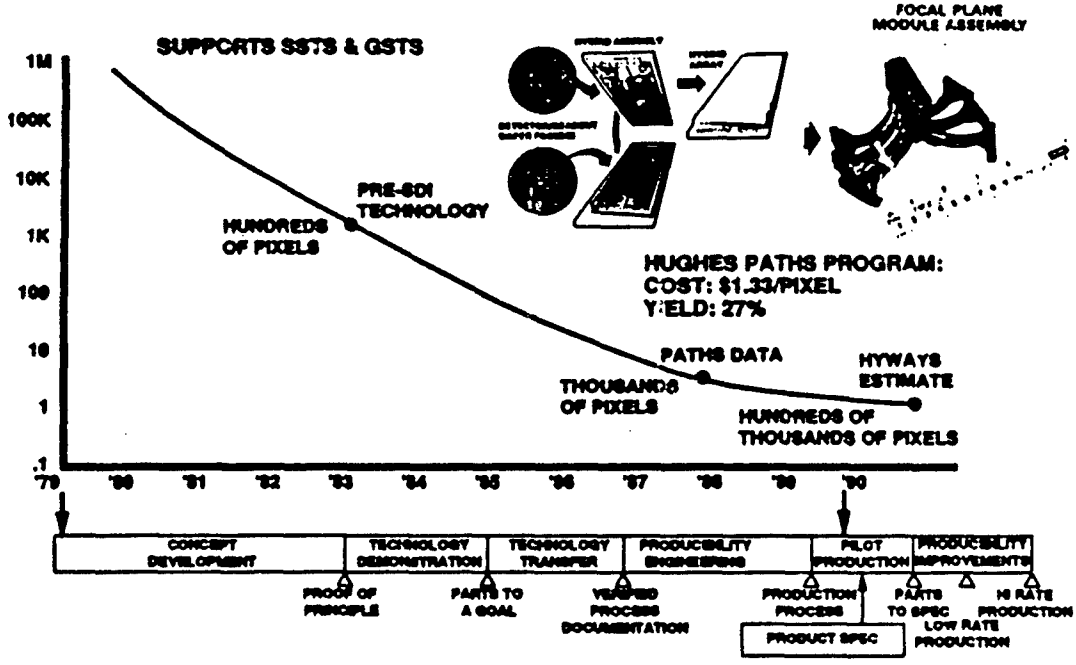
IBC FOCAL PLANE DEVELOPMENT (U)

UNCLASSIFIED



VLWIR TECHNOLOGY NEARS PILOT PRODUCTION (U)

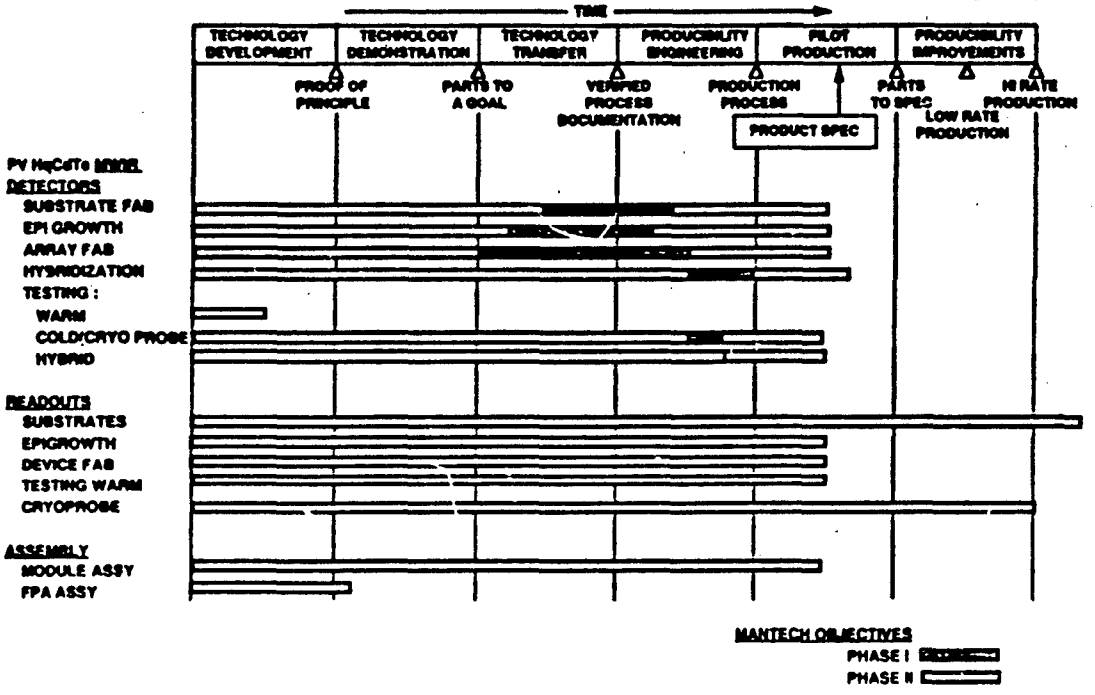
UNCLASSIFIED

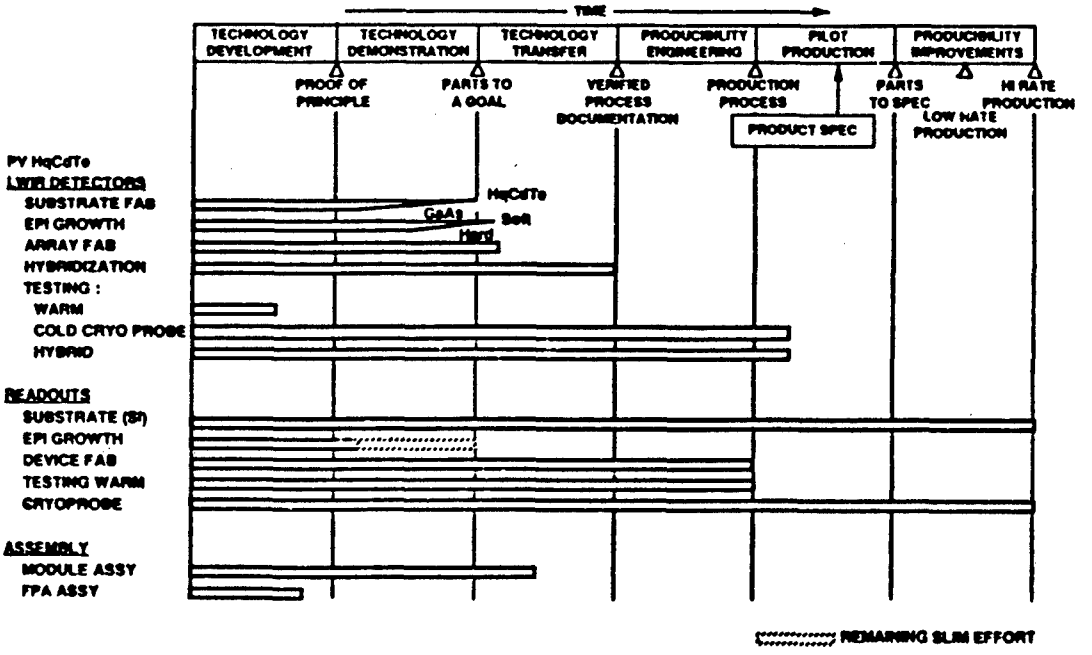


ORIGINAL PAGE IS
OF POOR QUALITY

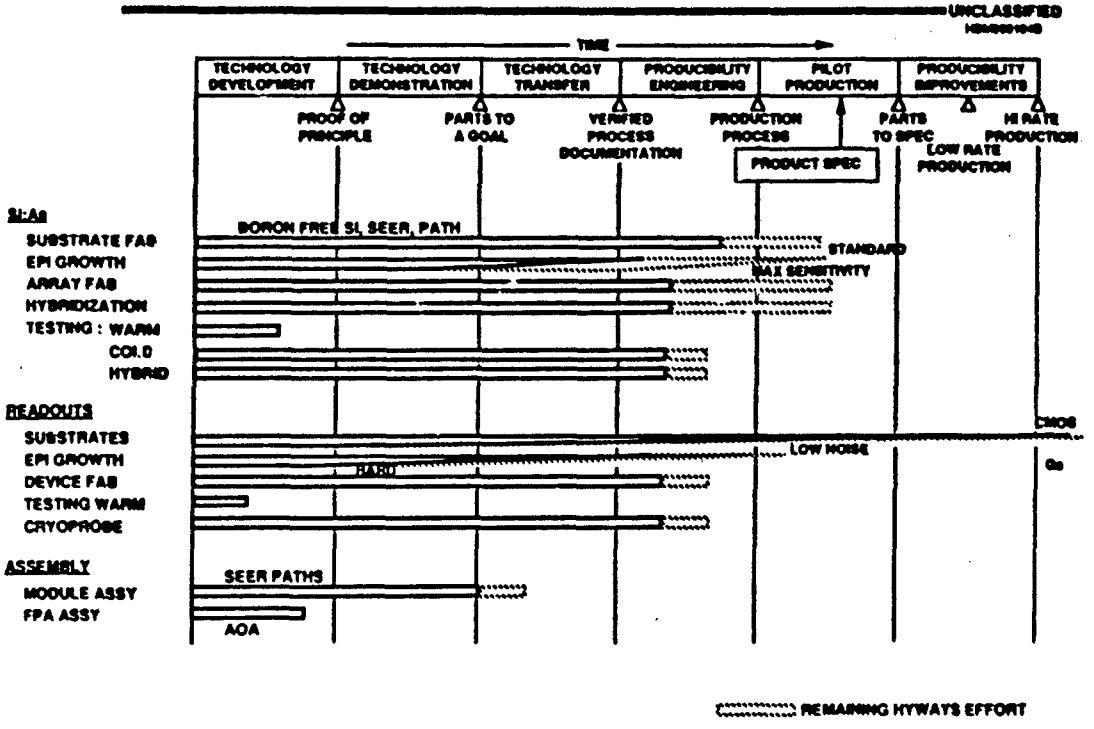
IR SENSOR COMPONENTS STATUS ON TECHNOLOGY CYCLE MODEL(U)

UNCLASSIFIED





IR SENSOR COMPONENTS STATUS ON TECHNOLOGY CYCLE MODEL(U)



FUTURE PLANS (U)

UNCLASSIFIED

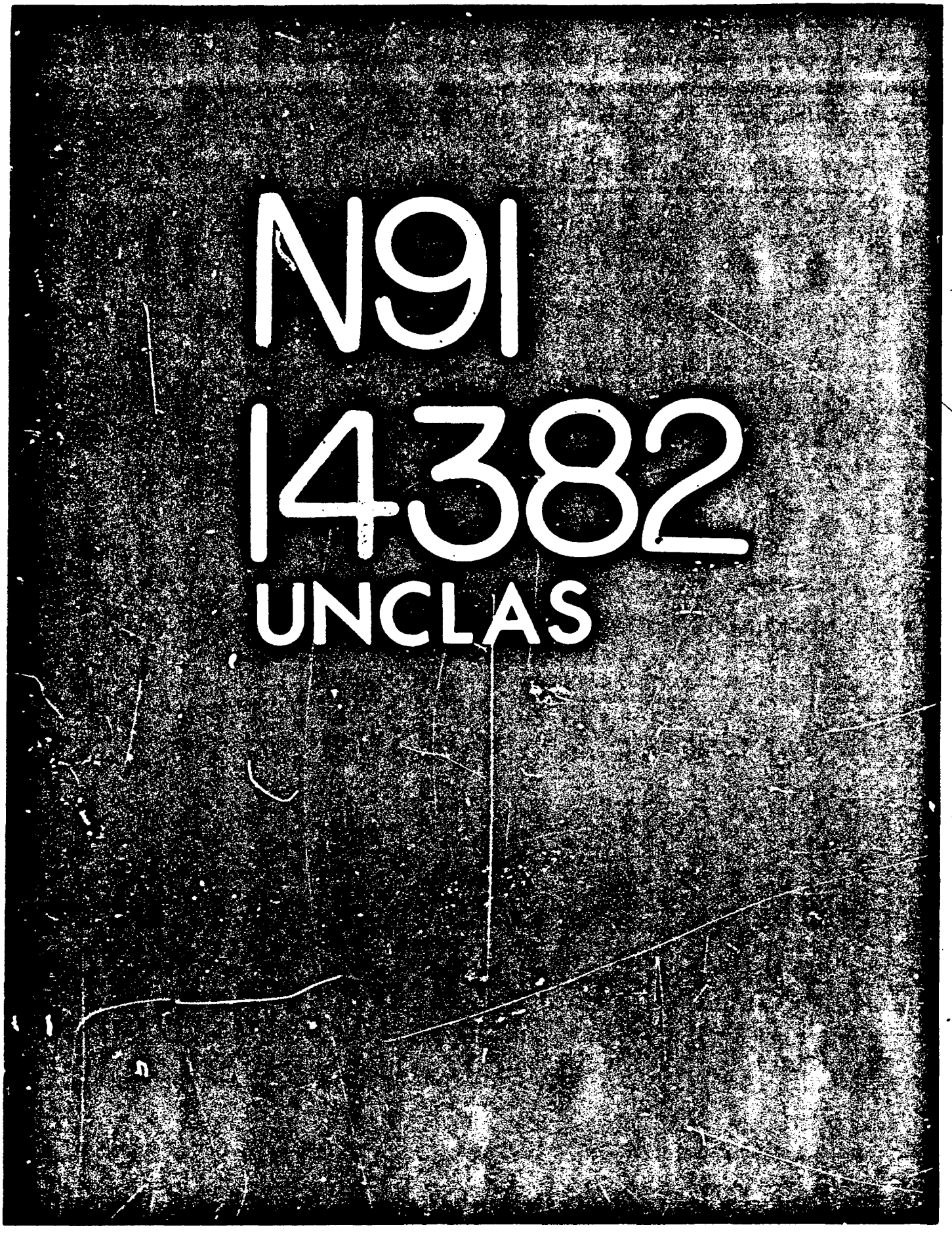
- NEAR TERM
  - HYWAYS - ADVANCED HYBRIDS FOR ENHANCED RADIATION TOLERANCE, HIGHER SENSITIVITY, LOWER NOISE
  - HYWAYS - ENHANCED PRODUCTION RATES
  - DECISION ON CONTINUATION OF SI:Ga
- MID-TERM
  - IED PERFORMANCE IMPROVEMENTS
  - EXTENDED WAVELENGTH RESPONSE
  - MICROLENSES
  - APPLICATION OF IBC TECHNOLOGY TO INTERCEPTOR REQUIREMENTS
  - HIGHER OPERATING TEMPERATURE
- FAR TERM
  - EXPLORE IBC CONCEPT IN OTHER MATERIALS AND DEVICES
  - ADDRESS IED/SSPM PRODUCIBILITY

ORIGINAL PAGE IS
OF POOR QUALITY

CONCLUSION

UNCLASSIFIED

- TECHNOLOGY PROGRAMS ARE PLANNED TO ENCOMPASS SYSTEM NEEDS FOR DETECTOR/READOUT PERFORMANCE AND AVAILABILITY
- TECHNOLOGY PROGRAMS OR SYSTEM PROGRAMS MUST ADDRESS FPA INTEGRATION ISSUES
- HARDNESS IS THE LAGGING TECHNOLOGY
- HARDNESS IS SUFFICIENT FOR SPACE DEMO PROGRAM


N91
14382
UNCLAS

I-3

N91-14382

LWIR Detector Requirements for Low-Background Space Applications

Frank J. De Luccia
The Aerospace Corporation
P.O Box 92957
Los Angeles, CA 90009

Detection of "cold" bodies (200 - 300 K) against space backgrounds has many important applications, both military and non-military. The detector performance and design characteristics required to support low-background applications are discussed, with particular emphasis on those characteristics required for space surveillance. The status of existing detector technologies under active development for these applications is also discussed. In order to play a role in future systems, new, potentially competing detector technologies such as multiple quantum well detectors must not only meet system-derived requirements, but also offer distinct performance or other advantages over these incumbent technologies.

LWIR DETECTOR REQUIREMENTS FOR LOW-BACKGROUND SPACE APPLICATIONS

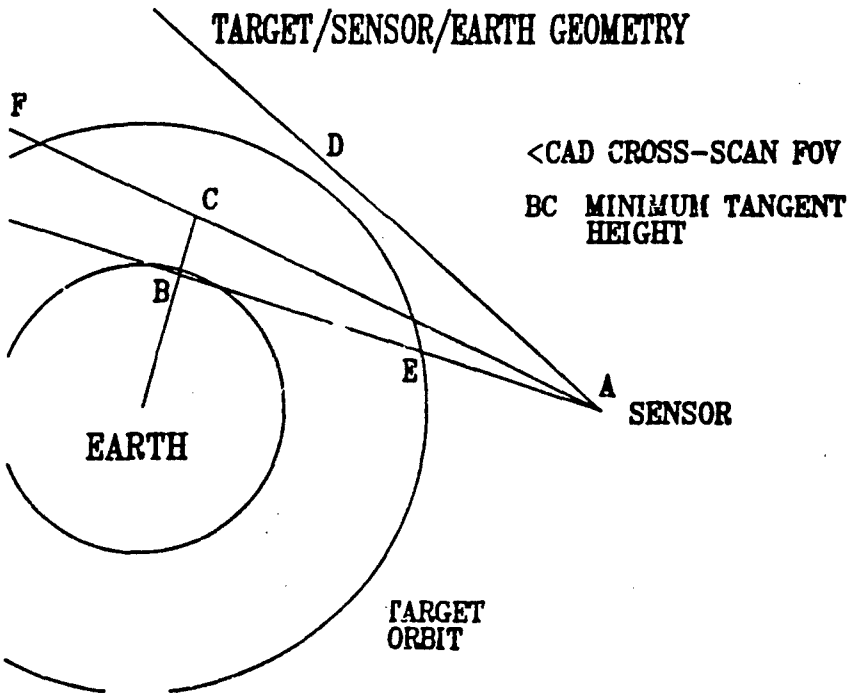
FRANK J. DE LUCCIA
THE AEROSPACE CORPORATION

TOPICS

- APPLICATIONS OVERVIEW
  - OBJECTS OF INTEREST
  - BACKGROUNDS
  - RADIATION ENVIRONMENT
  - SENSORS
- DETECTOR REQUIREMENTS
- APPLICABLE DETECTOR TECHNOLOGIES
  - STATE OF THE ART
  - TECHNOLOGY DEVELOPMENT DIRECTIONS
- REQUIREMENTS FOR NEW, COMPETING DETECTOR TECHNOLOGIES

LOW-BACKGROUND LWIR APPLICATIONS

- STRATEGIC DEFENSE
  - SURVEILLANCE, ACQUISITION, TRACKING, DISCRIMINATION, AND KILL ASSESSMENT ("SATKA")
  - WEAPON SYSTEM SUPPORT (FIRE CONTROL, HOMING, ETC.)
- OTHER MILITARY APPLICATIONS
  - RESIDENT SPACE OBJECT SURVEILLANCE
  - DETECTION OF NEWLY LAUNCHED OBJECTS
  - TREATY MONITORING
- NON-MILITARY APPLICATIONS
  - INFRARED ASTRONOMY
  - NEAR-EARTH PHENOMENOLOGY
  - SPACE "JUNK" DETECTION AND TRACKING



OBJECTS OF INTEREST

- EMISSIVITY-AREA PRODUCTS:

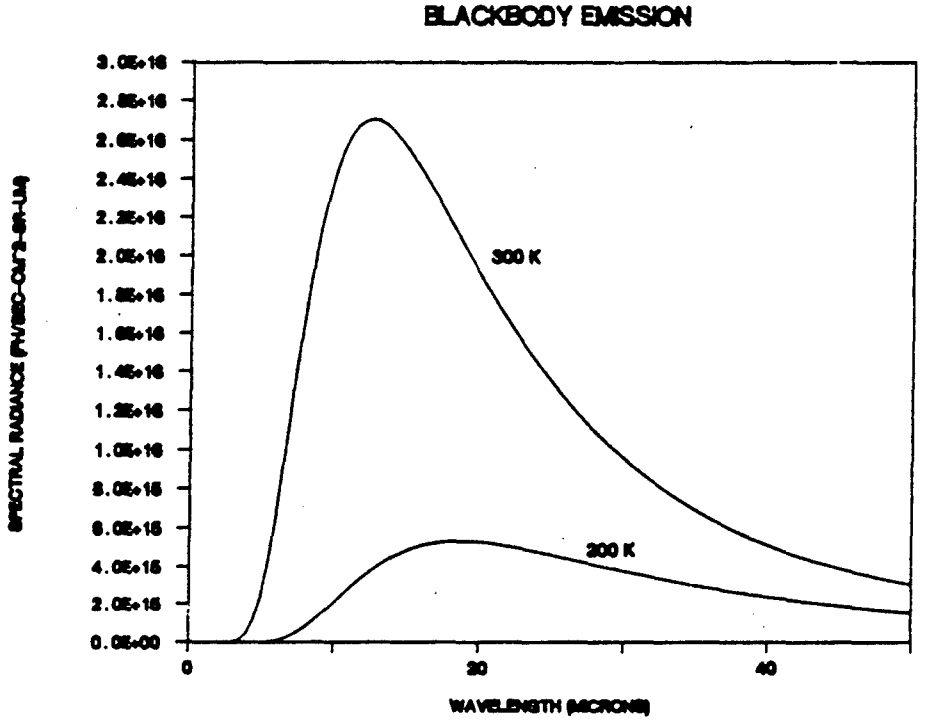
  0.1 - 10 M^2

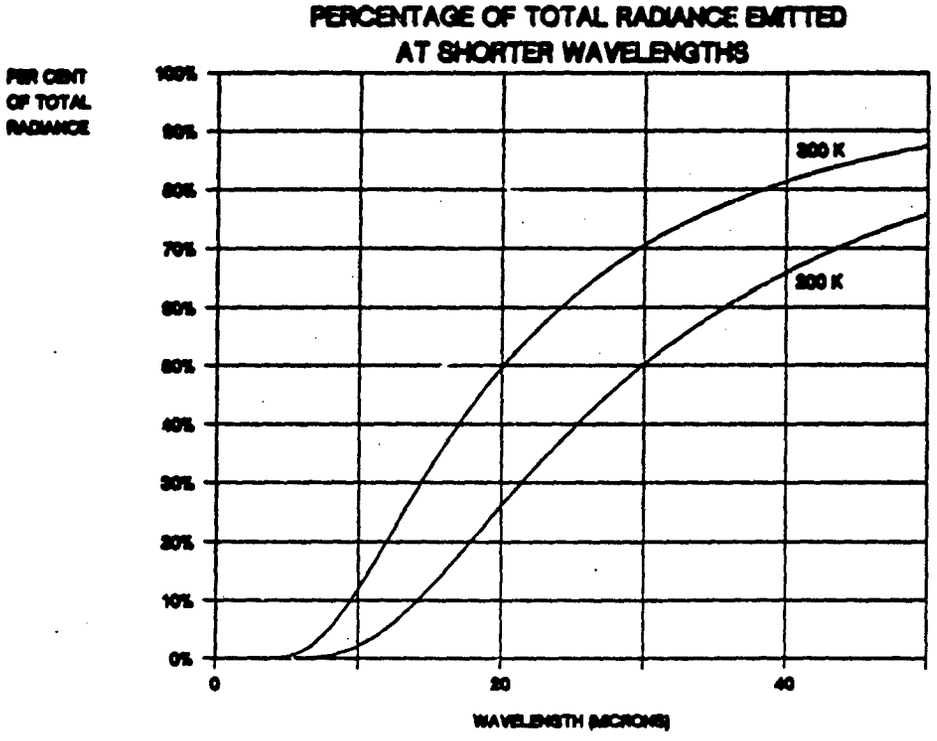
- TEMPERATURE:

  200 - 300 K

- RANGES:

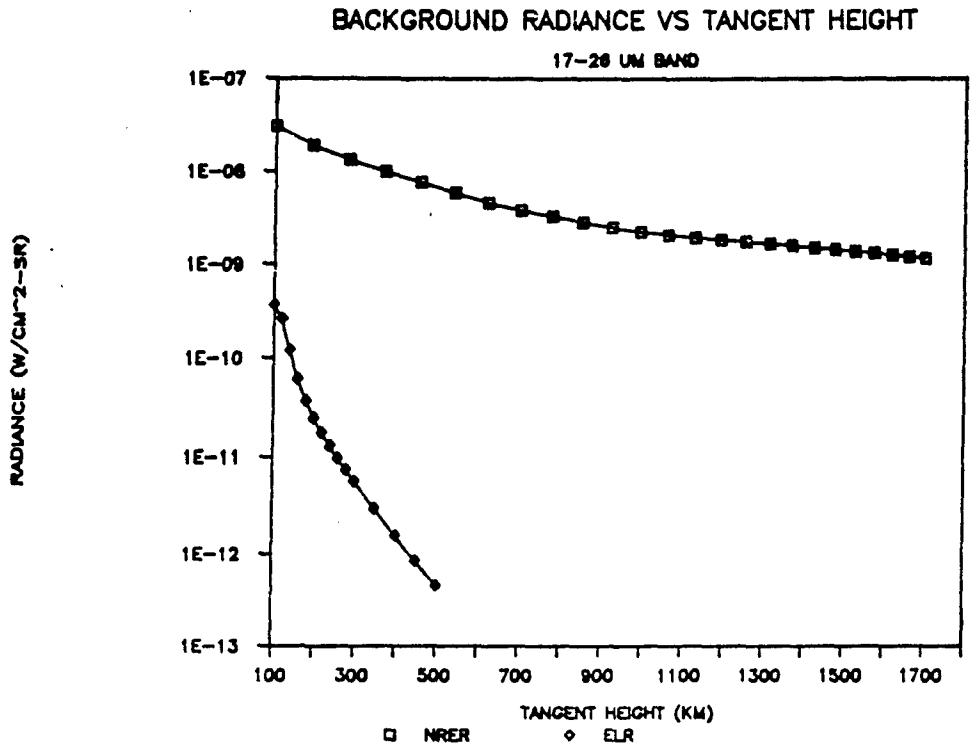
  1000 - 8000 KM

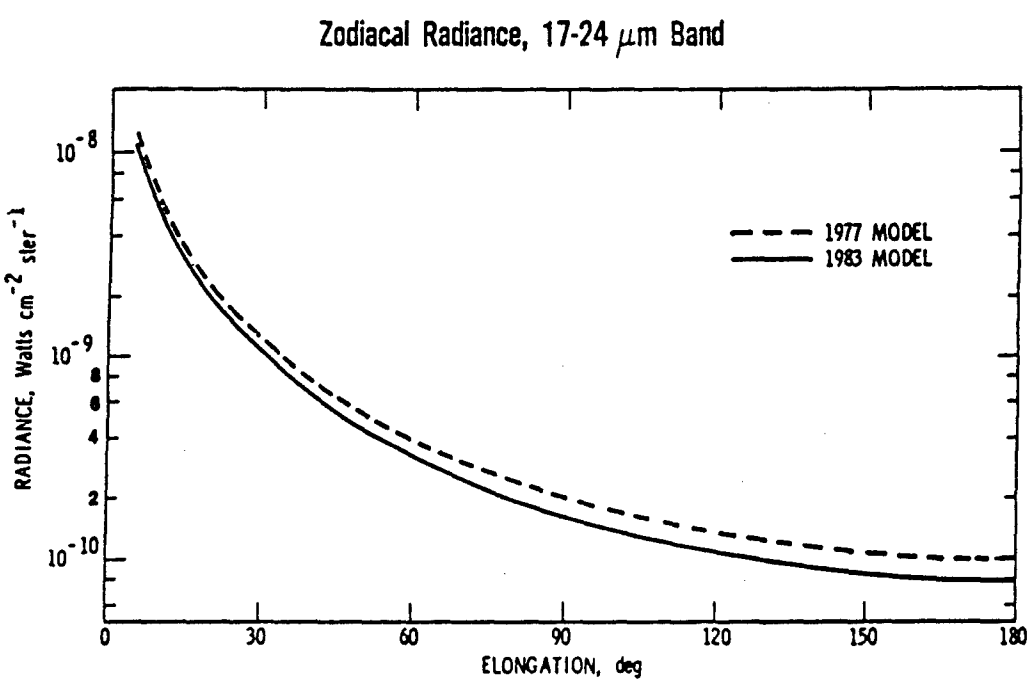




IR BACKGROUNDS

- SPACE BACKGROUNDS
  - EARTH LIMB ("ELR")
  - ZODIACAL
  - CELESTIAL
  - NON-REJECTED EARTH RADIANCE ("NRER")
  - ENHANCED (NATURAL AND NUCLEAR)
- FOR TANGENT HEIGHTS › 100 KM AND REALISTIC ASSUMPTIONS ABOUT THE LEVEL OF LIKELY OPTICS CONTAMINATION, NRER WILL BE THE DOMINANT NON-ENHANCED BACKGROUND FOR NEAR-EARTH LINES OF SIGHT

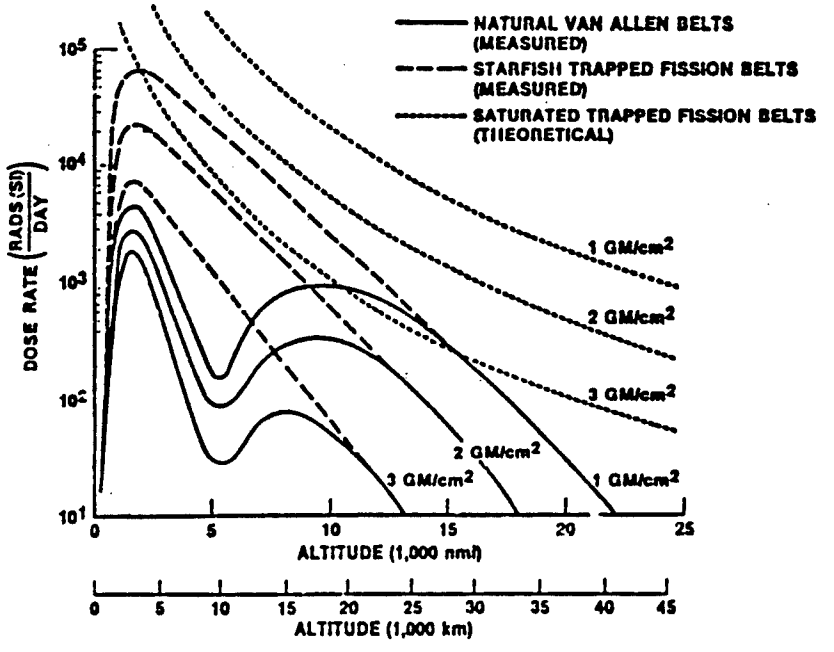

BACKGROUND RADIANCE VS TANGENT HEIGHT
17-26 UM BAND
RADIANCE (W/CM^2-SR)
1E-07
1E-08
1E-09
1E-10
1E-11
1E-12
1E-13
100
300
500
700
900
1100
1300
1500
1700
TANGENT HEIGHT (KM)
NRER
ELR


Zodiacal Radiance, 17-24 μm Band
RADIANCE, Watts cm^-2 ster^-1
10^-8
10^-9
8
6
4
2
10^-10
1977 MODEL
1983 MODEL
0
30
60
90
120
150
180
ELONGATION, deg

RADIATION ENVIRONMENT

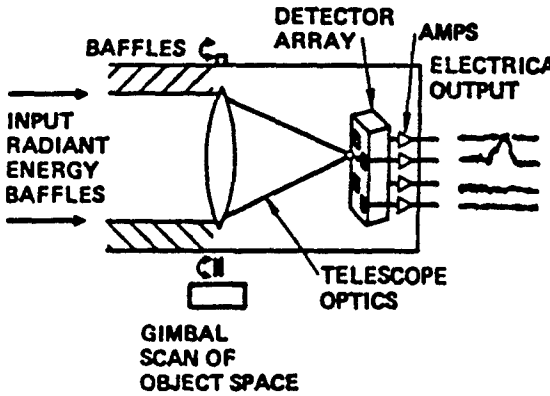
- **NATURAL ENVIRONMENT**
  - WORST CASE DOSE RATE AT FPA, ASSUMING 0.5 INCH ALUMINUM SHIELDING:
    0.02 RAD(SI)/SEC (5×10^7 GAMMAS/CM^2-SEC)
  - WORST CASE TOTAL DOSE AFTER 5 YEARS ON ORBIT:
    3×10^6 RAD(SI)
- **ENHANCED NUCLEAR ENVIRONMENT**
  - TRANSIENT DOSE RATE DUE TO NUCLEAR DETONATIONS CAN BE ORDERS OF MAGNITUDE HIGHER
  - SUSTAINED DOSE RATE DUE TO SATURATED BELT CONDITION CAN BE 1 RAD(SI)/SEC, WORST CASE
  - WORST CASE TOTAL DOSE DUE TO SATURATED BELTS:
    $> 10^7$ ACCUMULATED OVER 10–300 DAYS

EARTH'S VAN ALLEN BELTS VERSUS ALTITUDE AT 0°



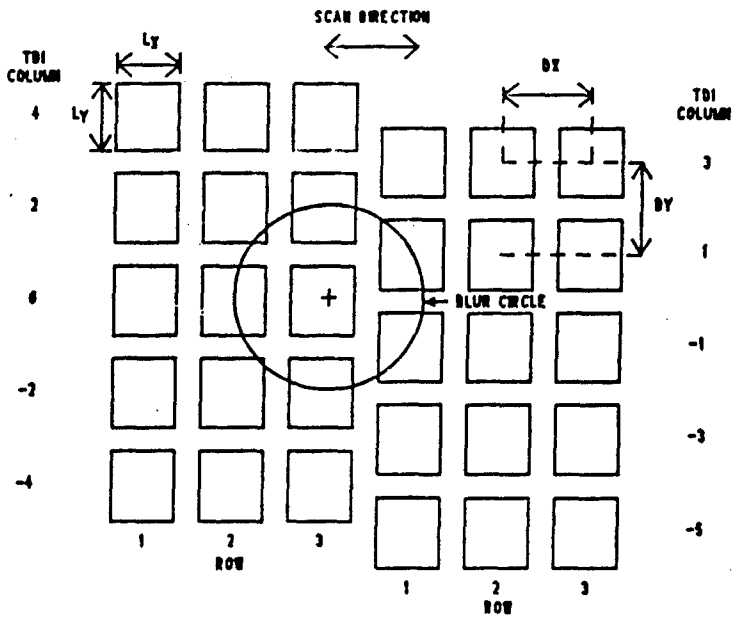
ORIGINAL PAGE IS
OF POOR QUALITY

SENSOR SYSTEM OPERATION



- BAFFLES REJECT OFF-AXIS RADIATION
- OPTICS FOCUS TARGET AND BACKGROUND ENERGY
- GIMBAL SCANS SCENE ACROSS DETECTORS
- DETECTORS CONVERT PHOTON SCENE TO ELECTRICAL SIGNAL

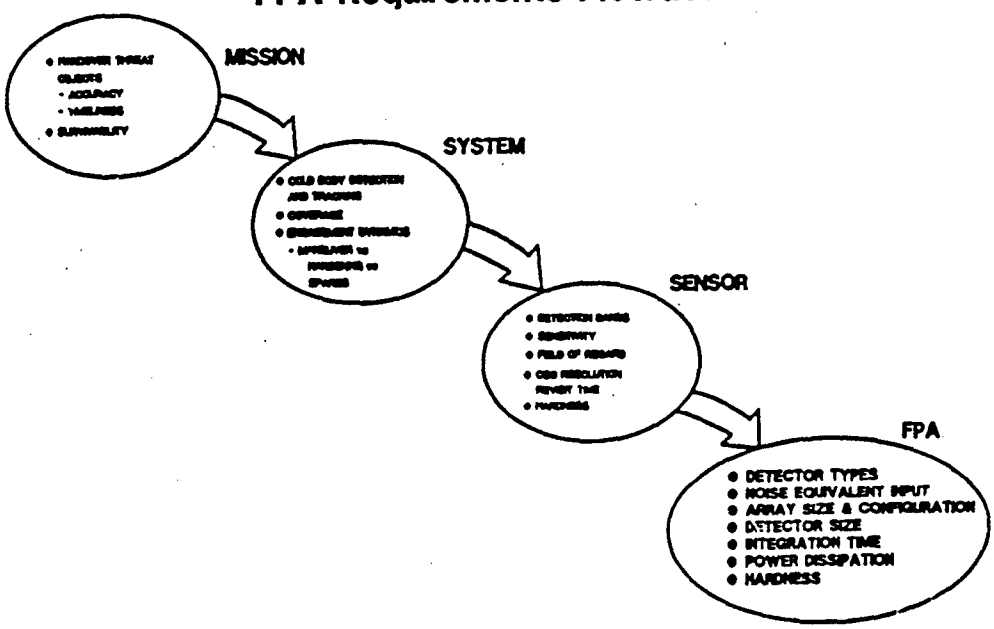
SAMPLE FPA DESIGN CONFIGURATION
THREE TDI STAGES, TWO STAGGERED SUBARRAYS



SIGNAL PROCESSING CHAIN

- Detector Bias/ Photocurrent Integration
- Charge-to-Voltage Conversion/ Buffer Amplifier
- First Stage Multiplexing
- Analog-to-Digital Conversion
- Gain & Offset Correction
- TDI
- BG Subtraction/ Clutter Suppression
- Matched Filtering/ Centroiding/ Track Formation ...

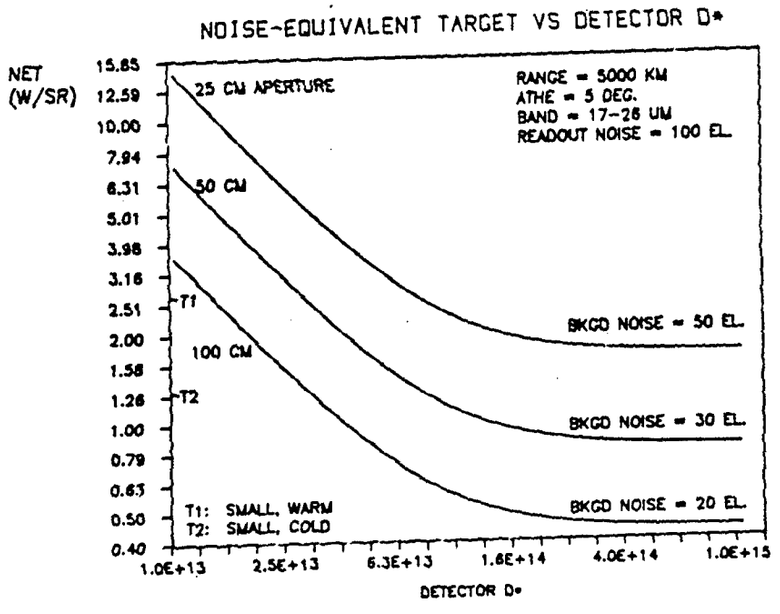
FPA Requirements Flowdown

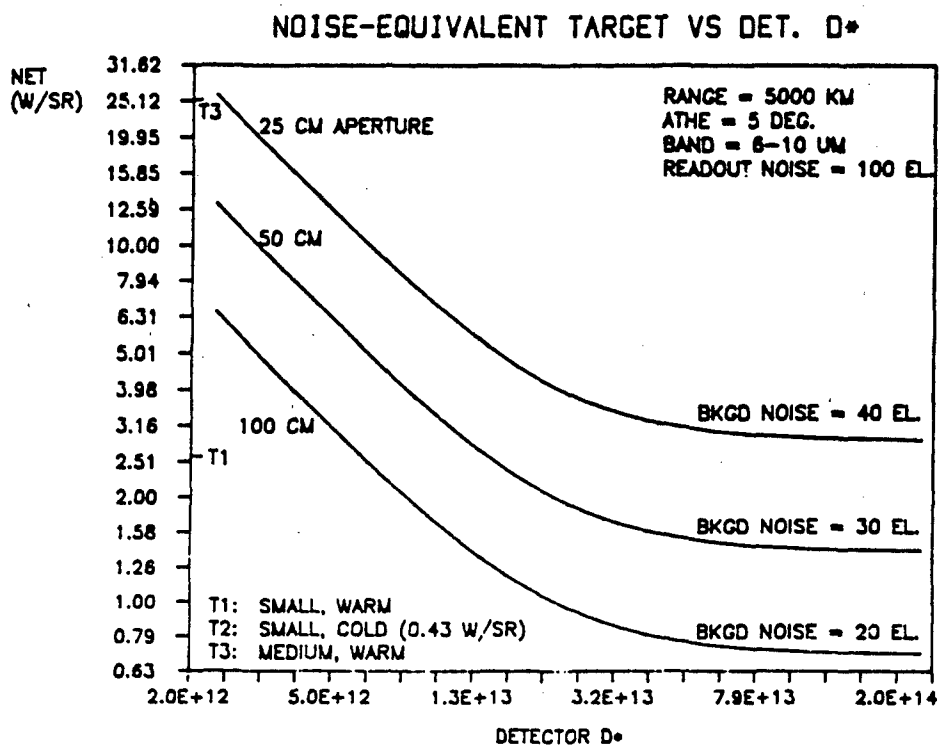


ORIGINAL PAGE IS
OF POOR QUALITY

SENSOR PERFORMANCE LIMITED BY NOISE

- **DETECTOR NOISE**
  - MAY BE REDUCED BY COOLING
- **READOUT NOISE**
  - DEPENDS STRONGLY ON COUPLING CIRCUIT DESIGN AND DEVICE CHARACTERISTICS
- **IR BACKGROUND NOISE**
  - RANDOM FLUCTUATIONS OF IN-FOV SOURCES
    - FUNDAMENTAL LIMIT ON SENSOR PERFORMANCE DUE TO NIMBUS VIEWING NEAR EARTH, ZODIACAL RADIANCE VIEWING AWAY FROM EARTH
  - SPATIAL STRUCTURE ("CLUTTER")
  - OPTICS THERMAL EMISSION
    - CAN BE RENDERED NEGLIGIBLE BY COOLING





KEY DETECTOR REQUIREMENTS FOR LOW-BACKGROUND SPACE APPLICATIONS

- **SPECTRAL COVERAGE:**

  SIGNIFICANT BROAD-BAND RESPONSE WITHIN 6–30 UM REGION, E.G., QUANTUM EFFICIENCY > 40% OVER A 5 UM SUB-BAND

- **SENSITIVITY:**

  D* > 1E14 CM-HZ /W AT 20 UM

  D* > 5E13 CM-HZ /W AT 10 UM

- **FREQUENCY RESPONSE:**

  BANDPASS > 10 KHZ, NO ANOMALIES

- **DYNAMIC RANGE:**

  LINEAR RESPONSE FROM NOISE LEVEL TO 1E4 TIMES THE NOISE LEVEL

KEY DETECTOR REQUIREMENTS FOR LOW-BACKGROUND SPACE APPLICATIONS (CONT.)

- POWER DISSIPATION:

  POWER DISSIPATED ON FPA < 10 UW/DETECTOR

- RADIATION HARDNESS:

  TOTAL DOSE HARDNESS > 100 RAD(Si)

  EFFECTIVE GAMMA AREA < 1E-6 CM (100 UM DET.)

- PIXEL SIZE:

  50-150 UM (SQUARE)

- CONFIGURATION:

  TWO-DIMENSIONAL MOSAIC ARRAYS, E.G., 10-20 X 50 DETECTORS PER CHIP

APPLICABLE TECHNOLOGIES

- DETECTORS

	SPECTRAL CUTOFF (UM)	OPERATING TEMPERATURE (K)
StAs BC	28	12
StGa BC	17	18
PV HgCdTe	10	40

- READOUTS

  - MATERIALS: SILICON, GERMANIUM, GaAs

  - VERY LOW NOISE, RADIATION HARD DEVICES ARE UNDER DEVELOPMENT

TECHNOLOGY ASSESSMENT

- StAs BC
  - MEETS PERFORMANCE REQUIREMENTS
  - LOW OPERATING TEMPERATURE REQUIRES ADVANCED 3-STAGE CRYOCOOLERS FOR SPACE-BASED SYSTEMS
  - PRODUCIBILITY DEMONSTRATION PLANNED
- StGa BC
  - REQUIRES DEVELOPMENT
  - OPERATING TEMPERATURE NOT HIGH ENOUGH TO ALLEVIA TE CRYOCOOLER PROBLEM (3 STAGES STILL REQUIRED)
- LWIR PV HgCdTe
  - INDIVIDUAL DETECTORS WITHIN ARRAYS MEET REQUIREM ENTS
  - OPERATING TEMPERATURE COULD BE SUPPORTED BY A 3- STAGE COOLER
  - SEVERE NON-UNIFORMITY PROBLEM
  - UNSUITABLE FOR SOME STRATEGIC DEFENSE SURVEILLNA NCE MISSIONS
    - TRACKING COLD TARGETS
    - DISCRIMINATION

TECHNOLOGY DEVELOPMENT DIRECTIONS

- GREATER SENSITIVITY
  - ULTRA-LOW NOISE READOUTS
  - IMPROVED RoA UNIFORMITY OF HgCdTe DETECTORS
- GREATER TOTAL DOSE HARDNESS
  - ULTRA-RAD HARD READOUTS
  - IMPROVED HARDNESS OF HgCdTe DETECTORS
- GREATER OPERABILITY IN GAMMA ENVIRONMENTS
  - DEVELOPMENT OF "INTRINSIC EVENT DISCRIMINATION" (IED) CONCEPTS
- GREATER PRODUCIBILITY
  - PILOT LINE DEMONSTRATION FOR StAs BC HYBRIDS IS PLANNED

REQUIREMENTS FOR NEW, COMPETING TECHNOLOGIES

ASSUMPTION: NEW TECHNOLOGY HAS PERFORMANCE EQUIVALENT TO OR SUPERIOR TO THAT OF THE INCUMBENT TECHNOLOGY WITH WHICH IT COMPETES

SPECTRAL BAND: 6 - N UM	OPERATING TEMPERATURE ‹ 25 K	OPERATING TEMPERATURE › 25 K
N = 10	R [redacted] NOT COMPETITIVE WITH EITHER HgCdTe OR StAs.	G [redacted] COMPETITIVE WITH HgCdTe, ESPECIALLY IF HARDER OR MORE UNIFORM.
N = 25	G [redacted] COMPETITIVE WITH StAs, ESPECIALLY IF OPERABILITY IN A GAMMA ENVIRONMENT IS SUPERIOR.	B [redacted] COULD DISPLACE StAs— ONLY A 2-STAGE COOLER REQUIRED.
N = 30	G [redacted] COULD DISPLACE StAs IN APPLICATIONS REQUIRING VERY COLD BODY DETECTION.	B [redacted] COULD DISPLACE StAs. ADDITIONAL SPECTRAL COVERAGE MAY BE USEFUL.

[redacted] = LITTLE OR NO UTILITY (R) [redacted] = MODERATE UTILITY (G) [redacted] = GREAT UTILITY (B)

SUMMARY

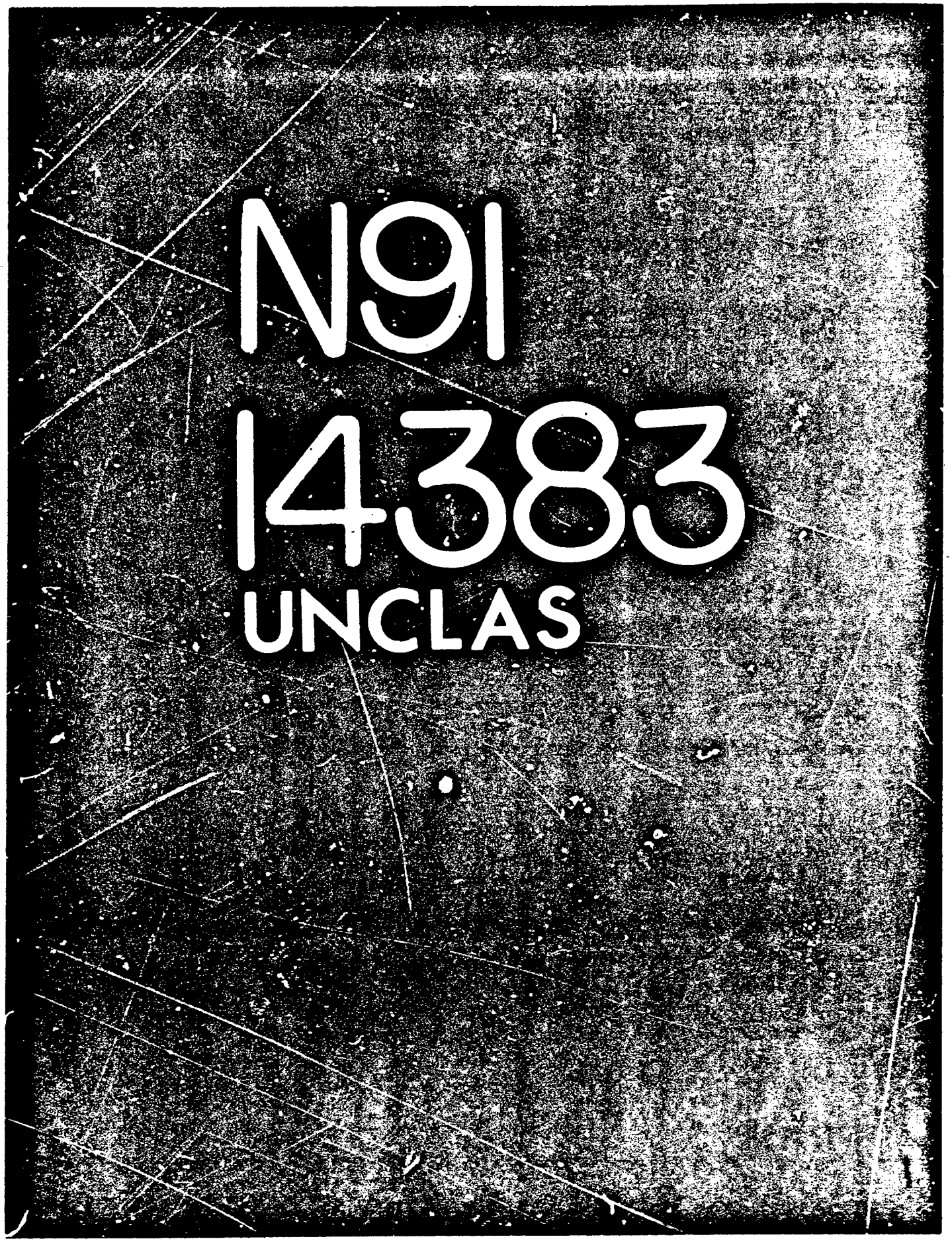
- DETECTOR SENSITIVITY REQUIREMENTS FOR LOW BACKGROUND SPACE APPLICATIONS ARE STRINGENT AND ARE DRIVEN BY:
  - STRESSING MISSIONS, E.G., DIM TARGETS, LONG RANGES
  - LOW BACKGROUND NOISE LIMIT
  - AVAILABILITY OF LOW NOISE READOUTS
- DETECTOR RADIATION HARDNESS REQUIREMENTS ARE ALSO STRINGENT:
  - SPACE BASING MAKES HIGH TOTAL DOSE HARDNESS ESSENTIAL
  - STRATEGIC DEFENSE SURVIVAL AND OPERABILITY REQUIREMENTS ARE EXTREMELY STRESSING
- NEW TECHNOLOGIES SUCH AS MQW DETECTORS CAN COMPETE WITH THE BETTER DEVELOPED EXISTING TECHNOLOGIES ONLY IF THEY:
  - MEET PERFORMANCE REQUIREMENTS
  - OFFER A SUBSTANTIAL ADVANTAGE OVER AN EXISTING TECHNOLOGY
    - HIGHER OPERATING TEMPERATURES (› 25 K) WITH SPECTRAL COVERAGE TO 25–30 UM
    - HIGHER PERFORMANCE OR PRODUCIBILITY THAN HgCdTe WITH COMPARABLE SPECTRAL COVERAGE AT A COMPARABLE OPERATING TEMPERATURE

SESSION II: Benchmark Technology Status

II - 1 Status of LWIR HgCdTe Infrared Detector Technology
M.B. Reine, Loral Infrared & Imaging Systems

II - 2 LWIR HgCdTe - Innovative Detectors in an Incumbent Technology
W.E. Tennant, Rockwell International Science Center

II - 3 HgCdTe for NASA Eos Missions and Detector Uniformity Benchmarks
P.R. Norton, Santa Barbara Research Center


N91
14383
UNCLAS

N91-14383

Status of LWIR HgCdTe Infrared Detector Technology

M.B. Reine

Loral Infrared & Imaging Systems
Two Forbes Road
Lexington, Massachusetts 02173-7393

Since its first synthesis in 1959, the HgCdTe semiconductor alloy system has proven to be a remarkably versatile intrinsic infrared detector material. A wide variety of high performance HgCdTe infrared detectors have been demonstrated and developed, including photoconductors, homojunction and heterojunction photodiodes, and metal-insulator-semiconductor photovoltaic devices. Controlled variations in HgCdTe alloy composition have enabled cutoff wavelengths to be tailored over the 2-25 μm wavelength region.

The success that HgCdTe has achieved is rooted in a unique set of semiconductor properties that make it a nearly ideal infrared detector material. Its large optical absorption coefficient enables (internal) quantum efficiencies approaching 100% to be achieved in devices that are 12-15 μm thick. Long carrier lifetimes allow the highest operating temperatures for achieving a given detectivity at a given cutoff wavelength.

This paper will review the status of LWIR HgCdTe detector technology for wavelengths between 8 and 17 μm, for application in NASA and DoD focal plane arrays (FPAs) operating at temperatures near 65 K with mission lifetimes of 5 to 10 years.

Linear arrays of LWIR HgCdTe photoconductors have been in production for the past ten years for DoD applications such as scanning thermal imaging systems and missile seekers. These arrays contain as many as 180 elements, operate at 77 K and cover the 8 to 12 μm wavelength region, which corresponds to a $Hg_{1-x}Cd_xTe$ alloy composition of x=0.21. These arrays are usually fabricated from bulk-grown n-type HgCdTe crystals having donor concentrations of 2-5 E14 cm^{-3}. Detector sensitivity is typically background limited, with detectivities of 0.6-1.5E11 cm-$Hz^{1/2}$/W. Device resistances are typically 40 ohms per square at 77 K, with dc power dissipations of 0.1-0.5 mW. The total U.S. industry capacity for these units is about 2500-3000 deliveries per month.

LWIR HgCdTe photoconductors represent a mature established technology that will continue to play an important role in NASA and DoD applications that require relatively small numbers of elements (less than several hundred) which do not require a multiplexer on the focal plane. For example, Loral provided a large-area HgCdTe photoconductor with a detectivity of 3E10 cm-$Hz^{1/2}$/W at 16 μm for the ATMOS interferometer.

Advanced DoD and NASA applications require orders of magnitude more detectors in a focal plane array. For these applications, HgCdTe photovoltaic (PV) devices are the detectors of choice because their higher impedance enables them to match into low-noise silicon CMOS input amplifiers. NxM arrays of HgCdTe photovoltaic detectors on IR-transparent substrates are bump interconnected to matching NxM arrays of input circuits on silicon CMOS multiplexer chips to form large focal

PRECEDING PAGE BLANK NOT FILMED

plane arrays. LWIR FPAs for scanning applications are typically 128 to 256 elements long, with 4, 8 or 16 elements in the scan direction for signal-to-noise enhancement, and have pixel sizes on the order of 50 μm x 50 μm. LWIR staring FPAs typically have 64x64 or 128x128 formats, with unit cells usually less than 50 μm x 50μm.

These advanced LWIR FPAs place stringent performance requirements on the HgCdTe photovoltaic detector arrays in terms of zero-bias impedance, reverse-bias impedance and leakage current, quantum efficiency, fill factor, crosstalk, 1/f noise, uniformity of response and reliability.

Initial LWIR HgCdTe photovoltaic detectors were planar n-on-p devices made by mercury-diffusion and ion implantation. More recently, substantial improvements in device performance have been achieved with the use of a double-layer P-on-n LPE heterojunction photodiodes grown onto CdTe substrates. These LPE heterojunctions have demonstrated performance which approaches the theoretical limit set by n-side diffusion current at temperatures of 80 to 70 K over the 10-19 μm range.

Major improvements have been made over the years in HgCdTe materials technology. At Loral, uniformity of alloy composition in both bulk-grown and LPE HgCdTe is such that variations in detector cutoff wavelength are less than $\pm 1\%$ over the 2-12 μm range.

In this paper, the performance requirements that today's advanced LWIR focal plane arrays place on the HgCdTe photovoltaic detector array will be summarized. The theoretical performance limits for intrinsic LWIR HgCdTe detectors will be reviewed as functions of cutoff wavelength and operating temperature. The status of LWIR HgCdTe photovoltaic detectors will be reviewed and compared to the FPA requirements and to the theoretical limits. Emphasis will be placed on recent data for two-layer HgCdTe LPE heterojunction photodiodes grown at Loral with cutoff wavelengths ranging between 10 and 19 μm at temperatures of 70 - 80 K. Development trends in LWIR HgCdTe detector technology will be outlined, and conclusions will be drawn about the ability for photovoltaic HgCdTe detector arrays to satisfy a wide variety of advanced focal plane array applications.

LORAL
Infrared & Imaging Systems

Status of LWIR HgCdTe Infrared Detector Technology

M.B. Reine

Loral Infrared & Imaging Systems
Lexington, Massachusetts 02173-7393

Innovative Long Wavelength Infrared Detector Workshop

April 24 - 26, 1990

Jet Propulsion Laboratory
California Institute of Technology
Pasadena, California 91109

Status of LWIR HgCdTe Detector Technology

EMPHASIS

- Wavelength: 10 to 17 μm
- Operating temperature: 60 K to 65 K
- Future NASA and DoD long-duration space applications

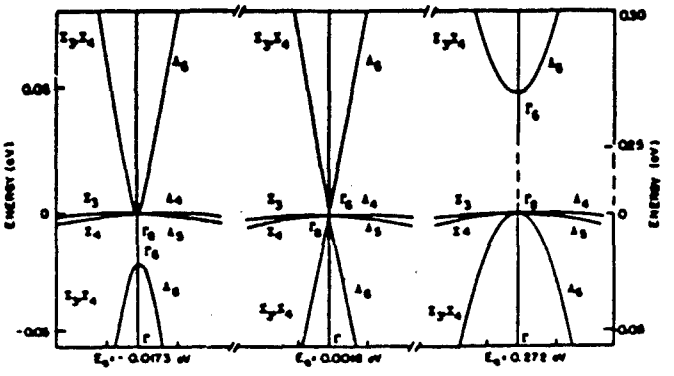
TOPICS:

1. HgCdTe material properties for infrared detectors
   - Uniformity of $Hg_{1-x}Cd_xTe$ alloy composition
2. Theoretical limits to HgCdTe detector performance and operating temperature
   - Thermal g-r noise
   - Background g-r noise
3. Detector requirements for advanced focal plane arrays
4. Status of HgCdTe infrared detectors:
   - Photoconductors
   - Photodiodes
5. Development trends in HgCdTe materials and devices

LORAL Infrared & Imaging Systems

Success of HgCdTe as an Infrared Detector Material Is Due to Its Energy Band Structure

- Adjustable energy band gap covers the 1-25 μm IR region
- Direct interband transitions give quantum efficiencies approaching 100% for 15 μm thick devices
- Intrinsic recombination mechanisms give long carrier lifetimes and high operating temperatures



The $Hg_{1-x}Cd_xTe$ Semiconductor Alloy System Possesses Many Desirable Properties for an Infrared Detector Material

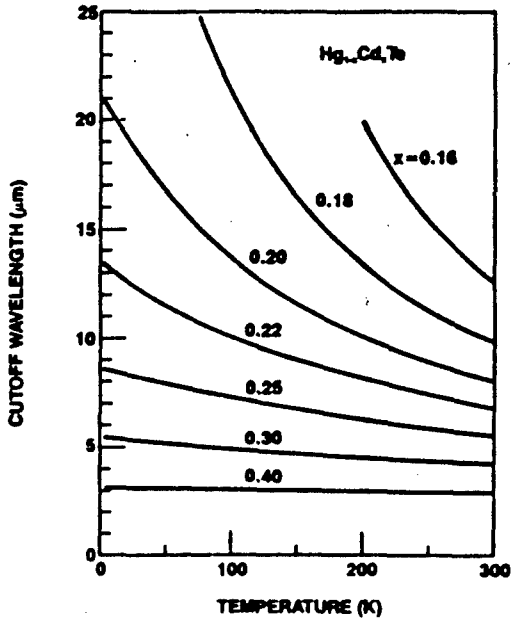
- Continuously adjustable energy gap from -0.3 eV to 1.6 eV
- Large absorption coefficient for high quantum efficiency
- Small lattice mismatch: 0.3% between HgTe and CdTe
- Amphoteric (can be made n-type or p-type):
  - Foreign atom donors and acceptors
  - Native defect acceptors
- Large electron-to-hole mobility ratio (400 for x=0.2 at 77K)
- Electrical purity levels of less than 1E14 cm^{-3}
- Surfaces are compatible with many passivation approaches:
  - ZnS, SiO_2
  - Native (anodic) oxide, sulphide or fluoride
  - Wide-gap HgCdTe

LORAL
Infrared & Imaging Systems

The $Hg_{1-x}Cd_xTe$ Semiconductor Alloy System Possesses Many Desirable Properties for an Infrared Detector Material (continued)

- Long minority carrier lifetimes:
  - p-type: Shockley-Read, Auger 7
  - n-type: Auger 1, Shockley-Read
- Favorable thermal expansion coefficient:
  - Good match to silicon
  - Excellent match to GaAs, sapphire
- Low dielectric constant for low junction capacitance
- Compatible with many advanced crystal growth techniques:
  - Bulk: Honeywell's DME; THM
  - LPE: from Hg-rich and Te-rich solutions
  - VPE: MOCVD, MBE

Detector Cutoff Wavelength for $Hg_{1-x}Cd_xTe$ Devices



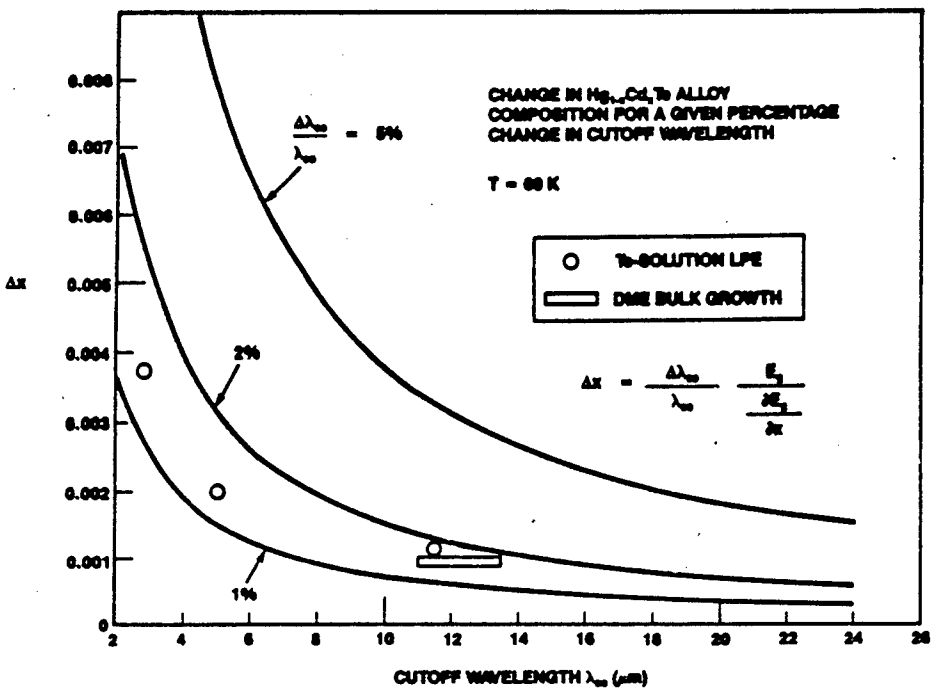
$$\lambda_{co}\,(\mu m) = \frac{1.24}{E_g(eV)}$$

$E_g(x,T)$ from:

Hansen, Schmit, Casselman
J. Appl. Phys. 53, 7099 (1982).

LORAL
Infrared & Imaging Systems

Today's $Hg_{1-x}Cd_xTe$ has Excellent Uniformity of Alloy Composition



HgCdTe Device Technology

PHOTOCONDUCTORS

- n-type and p-type
- Signal PRocessing In The Element (SPRITE)
- Photo-JFET structures with gain enhancement

PHOTODIODES

- Homojunctions: n-on-p and p-on-n
- Heterojunctions: N-on-p and P-on-n
- Avalanche photodiode for 1.3 to 1.6 μm

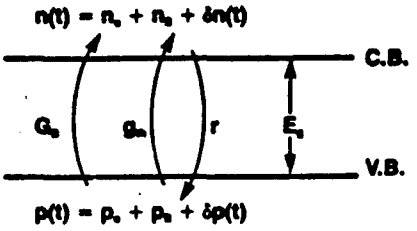
PHOTOCAPACITORS

- n-channel and p-channel Charge Coupled Devices
- Charge Imaging Matrix

OTHER

- n-channel Insulated-Gate Field Effect Transistors
- Spin-flip Raman laser

Noise in A Two-Level Detector



$n_o = p_o = G_n \tau$

$\frac{1}{\tau} = \frac{\partial}{\partial n}(r-g)$

$\delta n(t) = \delta p(t)$

g-r Theorem (Burgess, 1954):

$$\overline{\delta n(t)^2} = \frac{1}{Ad}\left[g_{th} + G_n \right] \tau$$

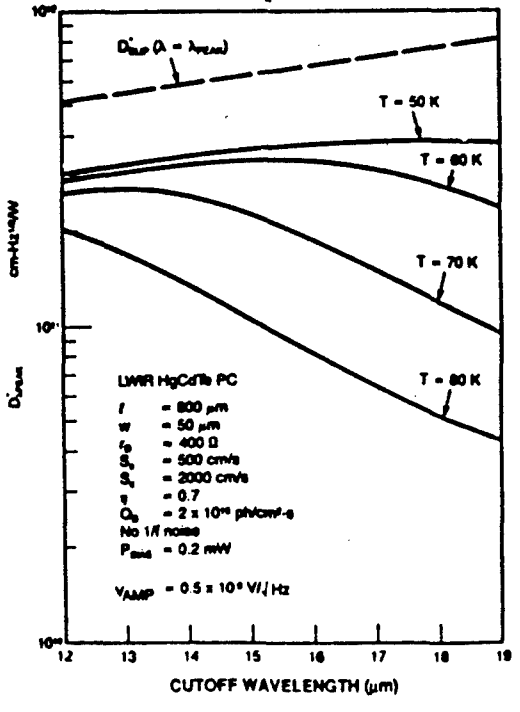
$$= \frac{1}{Ad}\left[\frac{n_o p_o}{n_o + p_o} \frac{1}{\tau} + \frac{\eta G_n}{d} \right] \tau$$

$$= \frac{1}{Ad}\left[\frac{n_i^2}{n_o \tau} + \frac{\eta G_n}{d} \right] \tau$$

$n_o p_o = n_i^2(Eg,T)$

for $n_o >> p_o$

LWIR PC HgCdTe Sensitivity vs Temperature

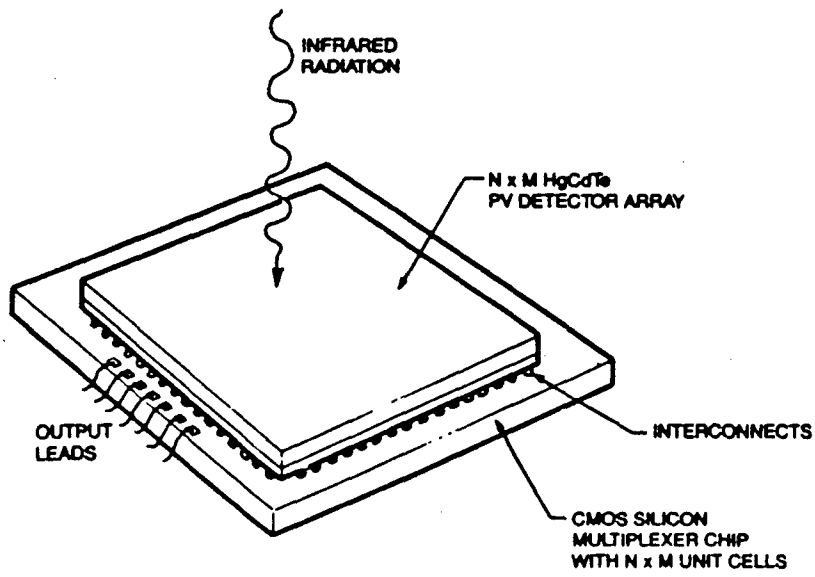


LORAL
Infrared & Imaging Systems

LWIR PC HgCdTe Status

- Transit-limited response times of 0.5 μsec
- Photoconductive gain = 200
- DC bias power = 0.1-0.3 mW
- 60-180 element linear arrays in full production (capacity: 600 units/month):
  - T = 77 K
  - λ_{peak} = 11.8 μm
  - λ_{co} = 13.0 μm
  - D_λ^* = 6 x 10^{10} - 1.4 x 10^{11} cm-$Hz^{1/2}$/W (BLIP for Q_s = 0.3 - 1 x 10^{17} ph/cm^2-s)
  - 1/f noise knee frequencies less than 50 - 100 Hz
  - Area = 50 μm x 50 μm
- DME bulk-grown $Hg_{1-x}Cd_xTe$ material:
  - x - uniformity: $\Delta x = \pm 0.0005 \rightarrow \Delta\lambda_{co}$ (77 K, 12.5 μm) = $\pm$ 0.1 μm
  - Electrical purity: 1 x 10^{14} cm^{-3}
- Passivation by anodic oxide surface accumulation:
  - Surface recombination velocity < 500 cm/s
  - Shunt resistance = 70 Ω/□

Generalized Backside-Illuminated HgCdTe Focal Plane Array



LORAL
Infrared & Imaging Systems

The Photon Detection Process in LWIR Focal Plane Arrays

1. Photoexcitation of electrons or electron-hole pairs
2. Transport and recombination of photoexcited carriers:
   drift, diffusion, charge separation
3. Interaction with the external "input" circuit
4. Signal conditioning within each unit cell:
   amplification, integration, filtering, sampling
5. Multiplexing
6. Signal processing with uncooled electronics off the focal plane:
   nonuniformity compensation, sub-frame integration

Detector Requirements for LWIR Focal Plane Arrays

1. Cutoff Wavelength:	Today: 10.5 - 12.0 μm Desired: out to 19 μm (e.g., AIRS)
2. Operating Temperature:	60-80 K (always as high as possible)
3. Detectivity:	Usually BLIP: 1E11 cm-Hz$^{1/2}$/W
4. Impedance:	High; 10 to 20 times larger than for BLIP
5. Quantum Efficiency:	> 70%
6. Active Area:	35 μm x 35 μm to 100 μm x 100 μm
7. 1/f Noise:	Critical for staring FPAs (BW=0.1 - 10 Hz)
8. Uniformity:	
cutoff wavelength:	± 0.1 - 0.2 μm
quantum efficiency:	± 10%
impedance:	depends on input circuit design

LORAL
Infrared & Imaging Systems

Detector Requirements for LWIR Focal Plane Arrays (Continued)

9. Bias Voltage:	-10 mV to -40 mV for direct injection 0 ± 0.5 mV with active offset control
10. Crosstalk:	< 2 - 3%
11. Fill Factor:	> 80% for staring FPAs
12. Linearity:	± 2%
13. Dynamic Range:	1E4-1E5
14. Frequency Response:	Not an issue
15. Environmental Stability:	Thermal cycling; shock; vibration
16. Radiation Hardness:	Total dose; various particles

Simplified Input Coupling Model for Hybrid FPA

$$D^* = \frac{q\eta\lambda}{hc}\sqrt{A}\left(\underbrace{2q^2\ \eta\phi A}_{\text{BACKGROUND NOISE}} + \underbrace{\frac{4kT}{R}}_{\text{DETECTOR JOHNSON NOISE}} + \underbrace{\frac{e_n^2}{R^2}}_{\text{INPUT NOISE}}\right)^{-1/2}$$

e_n = amplifier (or input gate) noise voltage

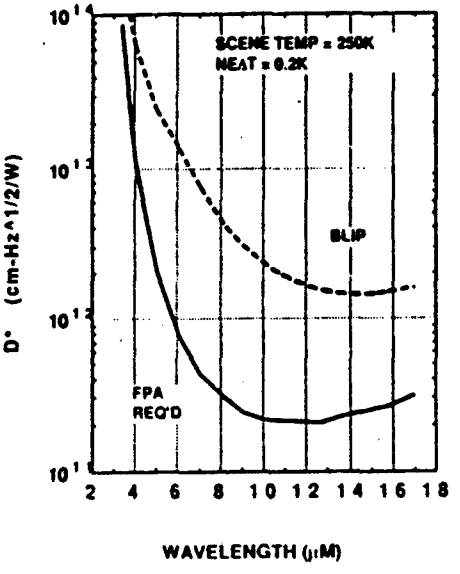
A = detector area

R = detector zero bias resistance

(Assumes coupling efficiency ≈ 1.0)

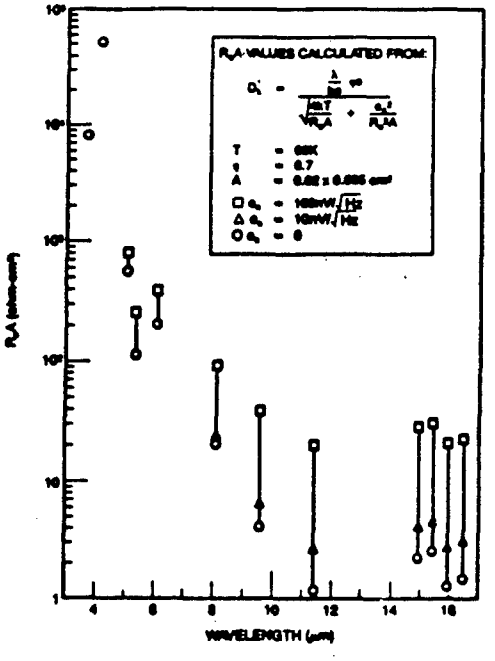
Key Focal Plane Requirements for AIRS Instrument

FPA SENSITIVITY REQUIREMENTS



- Configuration
  - Multiple linear arrays
  - 8 SWIR Bands: 3.4 to 8.0 μm
  - 8 LWIR Bands: 8.0 to 15.4 μm (17.0 μm Goal)
- Pixel Size: 200 μm x 100 μm
- Total Pixel Count: 3950
- Background Flux Density: ≤ 2E15 ph/cm²-s (LWIR)
- Minimum Operating Temp: 60 K
- Thermal Heat Load ≤ 500 mW
- Outages ≤ 2%
- Reliability ≥ 0.99 at 5 years
- Total Dose ≤ 2E4 rads (Si)
- Technology Cutoff: 1992 1st Instrument

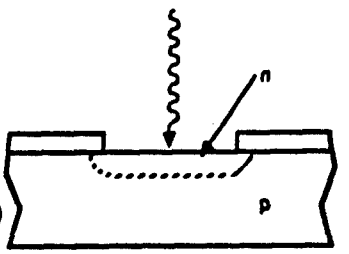
REQUIRED R_oA PRODUCTS FOR AIRS PV DETECTORS

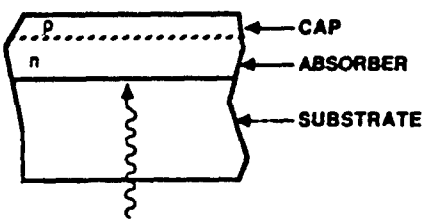


ORIGINAL PAGE IS
OF POOR QUALITY

P-N Junction Formation in HgCdTe

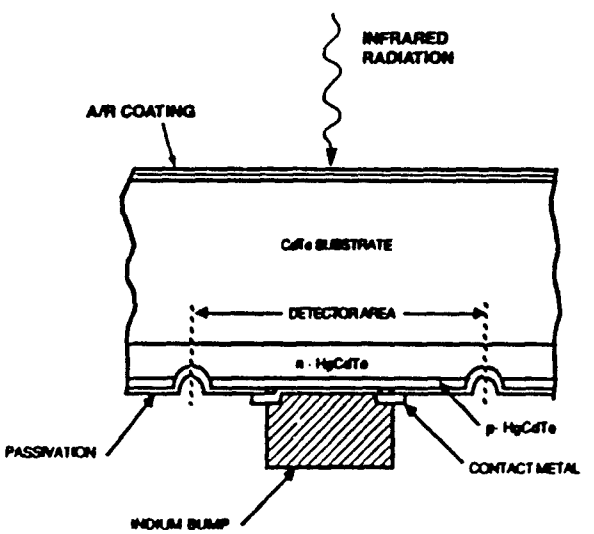
1968	Hg-Diffused n^--on-p • Hg-vacancy acceptors
1975	Ion-implanted n^+-on-p (n^+-n^--on-p) • implant damage • native & foreign acceptors
1982	LPE grown heterojunctions • N-on-p • P-on-n
1987	Acceptor-diffused p-on-n • diffusion sources: ion implant Hg-solution
1990	MOCVD grown heterojunctions





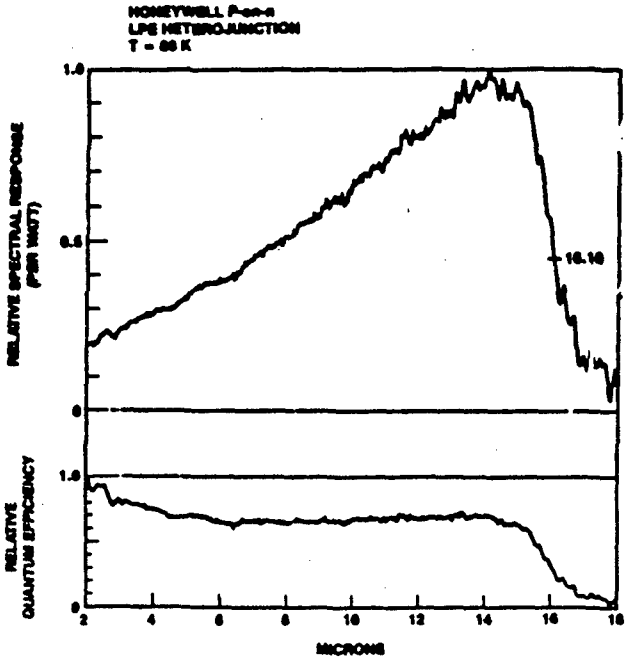
BACKSIDE-ILLUMINATED P-on-n LPE HgCdTe
HETEROJUNCTION PHOTODIODES



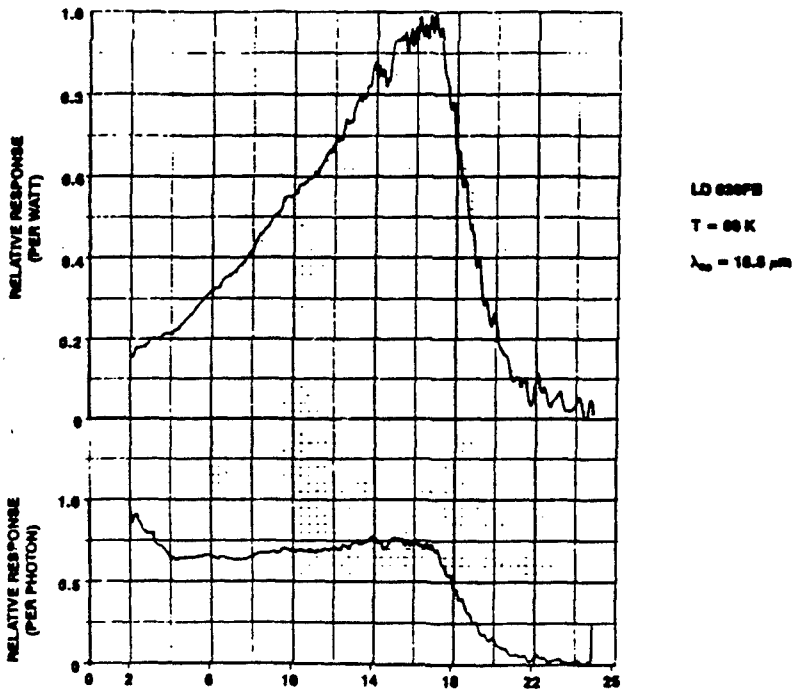


LORAL
Infrared & Imaging Systems

VLWIR P-on-n LPE HgCdTe Heterojunction Film Grown at Loral



VLWIR P-on-n LPE HgCdTe Heterojunction Film Grown at Loral



LORAL
Infrared & Imaging Systems

Dark Current Mechanisms in LWIR HgCdTe p-n Junction Photodiodes

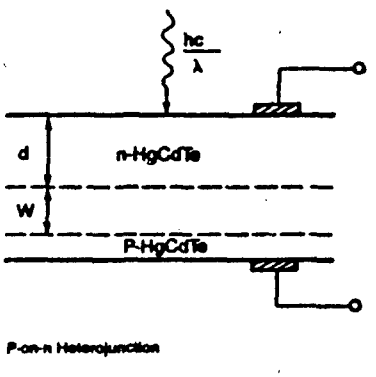
I. INTRINSIC MECHANISMS

- Diffusion Current (Thermally Generated Current)
  - n-side
  - p-side
- Band-to-Band Tunneling current (Zener Tunneling)
  - Can be eliminated near zero bias by low doping

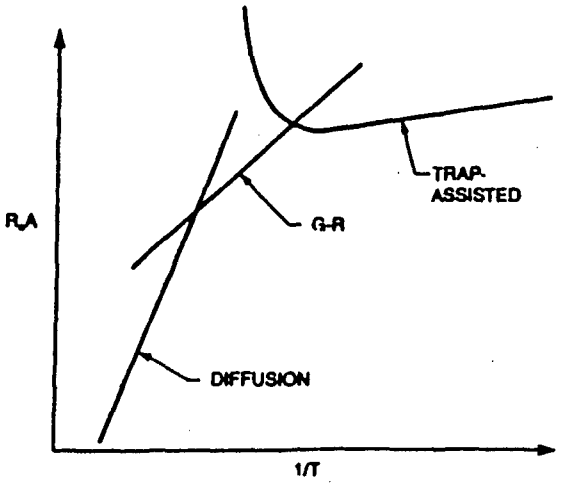
II. DEFECT-MEDIATED MECHANISMS

- Generation-Recombination (g-r) current
- Trap-Assisted Tunneling Current
- Defects may be at surface or within bulk

Dark Current Mechanisms in HgCdTe p-n Junction Photodiodes



P-on-n Heterojunction



DIFFUSION CURRENT:

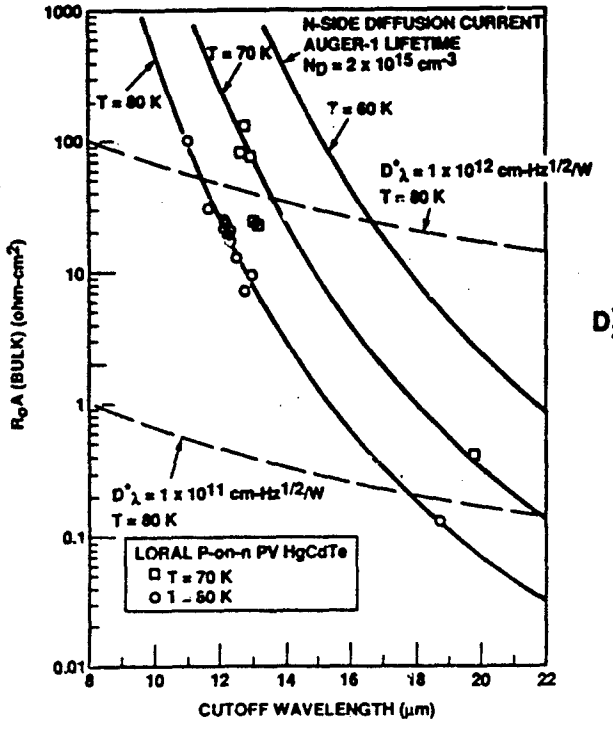
$$\frac{1}{R_0A} = \frac{e^2 n_i^2}{kT n_a \tau} d$$

G-R CURRENT:

$$\frac{1}{R_0A} = \frac{e}{V_{bi}} \frac{n_i}{\tau_o} W$$

LORAL

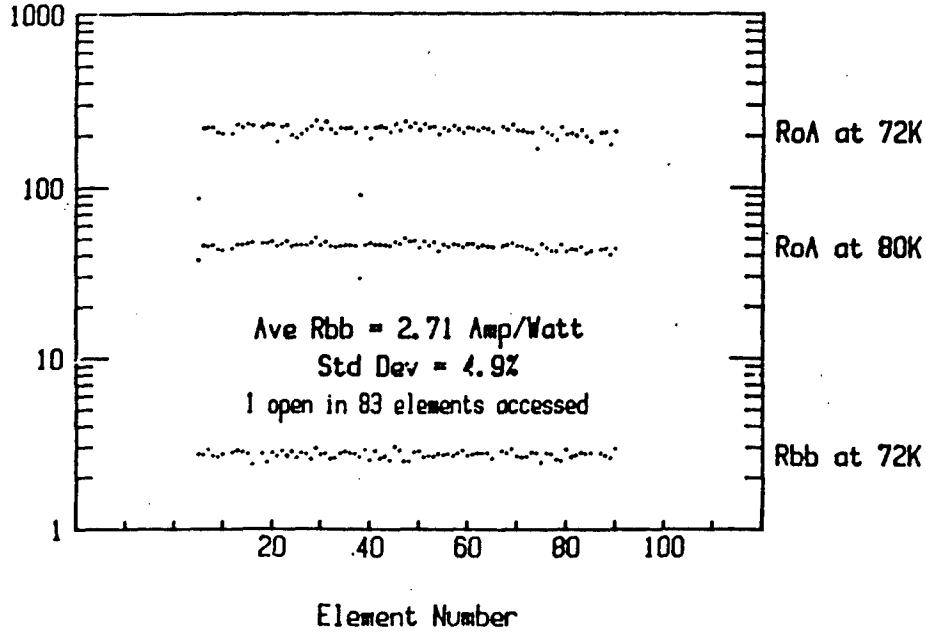
LWIR LPE P-on-n HgCdTe Photodiodes Grown at Loral



D^*_λ Limited by thermal noise:

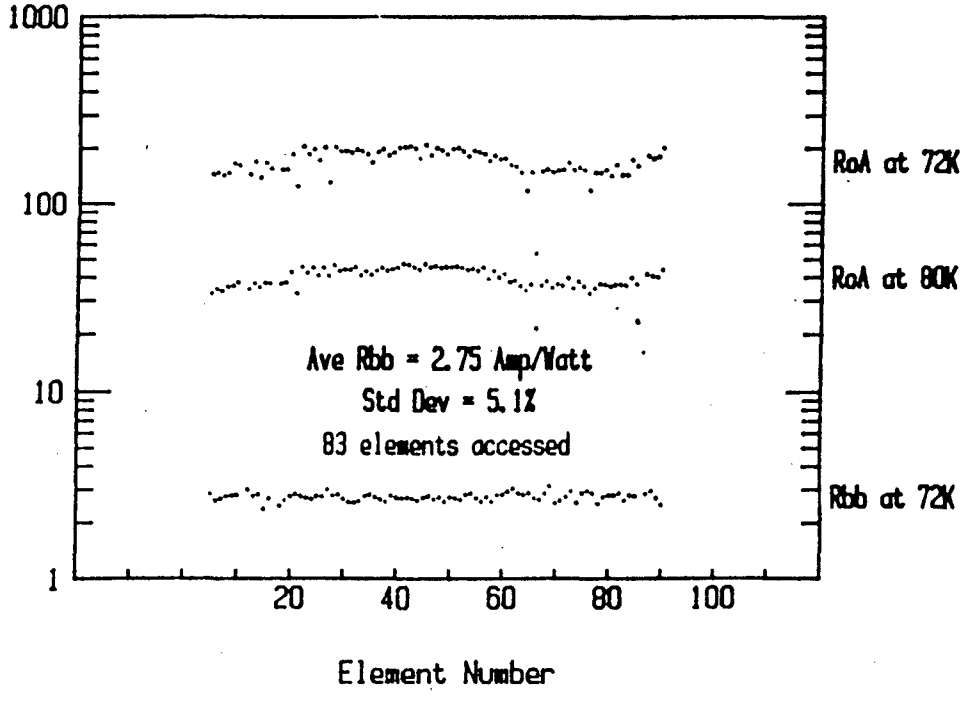
$$D^*_\lambda = \frac{\lambda}{hc}\,\eta e \sqrt{\frac{R_oA}{4\,kT}}$$

Bilinear Array ER02C2
10.58 μm at 72 K

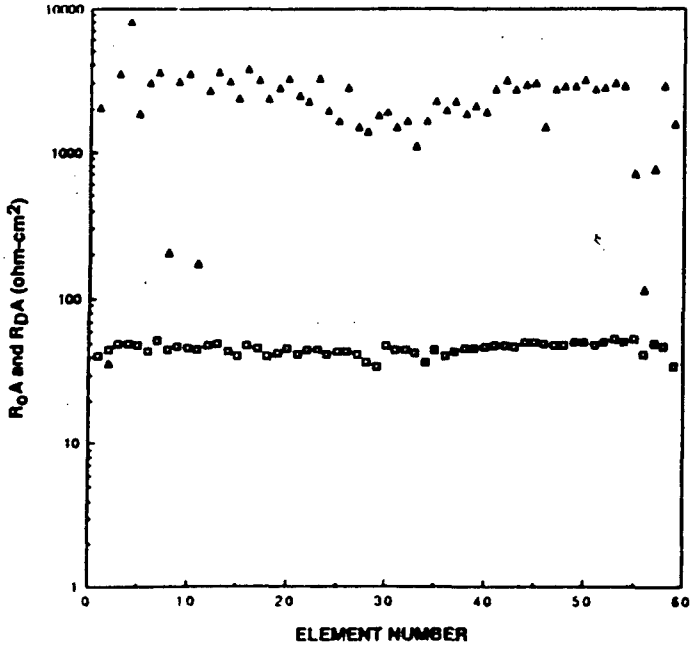


LORAL
Infrared & Imaging Systems

Bilinear Array ER02D4
10.68 μm at 72 K



LWIR P-on-n HgCdTe PV Array



T = 70 K

λ_{CO} = 11.6 μm

Δ -40 mV reverse bias

0 zero bias voltage

LORAL Infrared & Imaging Systems

Trends in HgCdTe Materials Growth

1. LOWER GROWTH TEMPERATURE AND LAYERED GROWTH:

Temperature	Technique	
700 °C	Bulk crystal growth: • Solid state recrystallization • Honeywell's DME • Traveling heater method	PC
400 °C - 500 °C	Liquid Phase Epitaxy • Te-Rich • Hg-Rich	PV
150 °C - 300 °C	MOCVD	PV
120 °C - 195 °C	MBE	PV

2. FOREIGN SUBSTRATES:

CdTe — CdTeSe — Sapphire — GaAs — GaAs on Si
CdZnTe

Conclusions

1. HgCdTe has nearly ideal semiconductor properties for LWIR detection
2. Alloy composition uniformity of today's bulk-grown and LPE HgCdTe is more than adequate
3. LWIR HgCdTe P-on-n LPE heterojunction photodiode performance is at the limit set by n-side diffusion current for Auger-1 lifetime for T > 70 K
4. Continued development of HgCdTe material and device technology will:
   a. Improve performance:
      - Reduced leakage current and 1/f noise
      - Longer cutoff wavelengths
   b. Increase producibility:
      - Low-cost large-area substrates
      - Improved screening techniques for material and arrays
   c. Enable in situ VPE growth of advanced device structures:
      - p-n homojunctions and heterojunctions
      - Wide-gap passivation
      - Low-resistivity contact layers

N91
14384
UNCLAS

N91-14384

LWIR HgCdTe - INNOVATIVE DETECTORS IN AN INCUMBENT TECHNOLOGY

W. E. TENNANT

Rockwell International
Science Center
Thousand Oaks, California

ABSTRACT

HgCdTe is the current material of choice for high performance imagers operating at relatively high temperatures. Its lack of technological maturity compared with silicon and wide-band gap III-V compounds is more than offset by its outstanding IR sensitivity and by the relatively benign effect of its materials defects. This latter property has allowed non-equilibrium growth techniques (MOCVD and MBE) to produce device quality LWIR HgCdTe even on common substrates like GaAs and GaAs/Si. Detector performance in these exotic materials structures is comparable in many ways with devices in equilibrium-grown material. Lifetimes are similar. RoA values at 77K as high as several hundred have been seen in HgCdTe/GaAs/Si with 9.5 μm cut-off wavelength. HgCdTe/GaAs layers with ~15 μm cut-off wavelengths have given average 77K R_0As of >2. Hybrid focal plane arrays have been evaluated with excellent operability.

PRECEDING PAGE BLANK NOT FILMED

LWIR HgCdTe - INNOVATIVE DETECTORS IN AN INCUMBENT TECHNOLOGY

WILLIAM E. TENNANT

APRIL 24, 1990



Rockwell International
Science Center
1049 Camino Dos Rios
Thousand Oaks, CA 91360

OVERVIEW

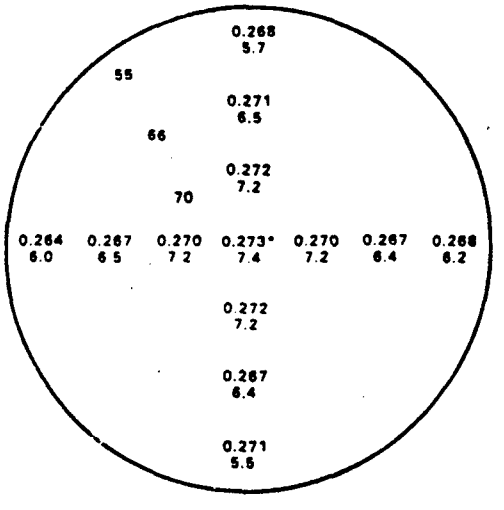
- PACE BACKGROUND AND MATERIALS
- TEST DIODE PERFORMANCE AND TECHOLOLGY LIMITS
- PRELIMINARY LWIR ARRAY DATA
- DIRECTIONS AND CONCLUSIONS



DEFINITIONS

- **CONVENTIONAL TECHNOLOGY**
  - -- MCT GROWN BY LIQUID PHASE EPITAXY ON CdTe OR SIMILAR COMPOUND
- **PACE (PRODUCIBLE ALTERNATIVE TO CdTe FOR EPITAXY)**
  - -- ROCKWELL APPROACH TO OVERCOME MCT PRODUCIBILITY ISSUES
  - -- **PACE-1:** MCT GROWN BY LIQUID PHASE EPITAXY ON VAPOR PHASE EPITAXIAL CdTe/SAPPHIRE -- SUITABLE FOR SWIR (1-3 MICRONS) AND MWIR (3-5+) MICRONS
  - -- **PACE-2:** MCT GROWN BY VAPOR PHASE EPITAXY ON GaAs (OR EVENTUALLY SI) -- SUITABLE FOR ALL IR WAVELENGTHS

PACE-2 HAS BETTER COMPOSITIONAL UNIFORMITY THAN LPE



3" DIA GaAs WAFER

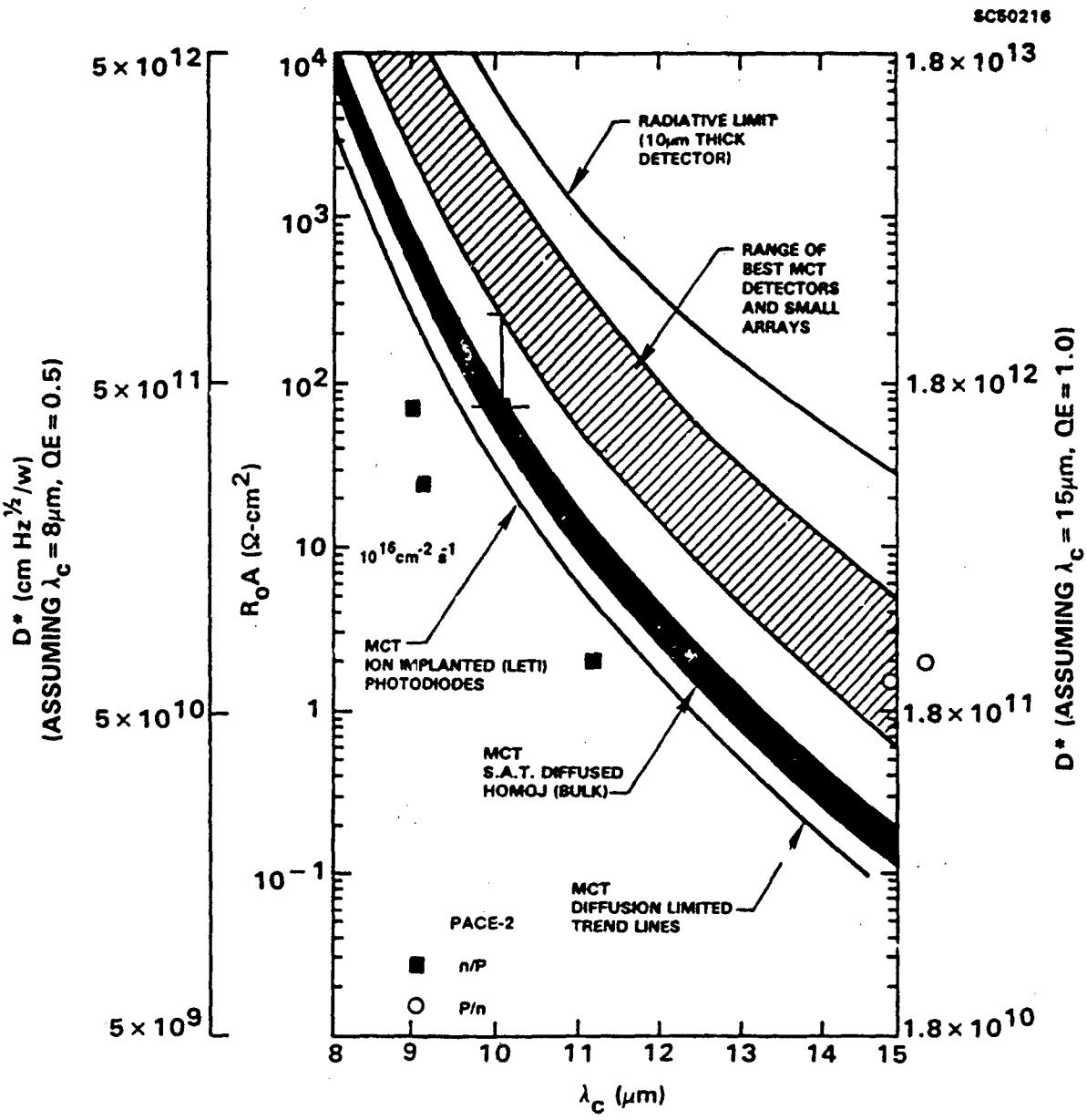
$\max \frac{\Delta x}{\bar{x}} = 3.3\%$, $\max \frac{\Delta \bar{d}}{\bar{d}} = 29\%$ OVER 3" DIA

$\max \frac{\Delta x}{\bar{x}} = 2.2\%$, $\max \frac{\Delta d}{\bar{d}} = 17\%$ OVER 2" DIA

LEGEND
- * – COMPOSITION, X VALUE
- – THICKNESS, μm
- – CRYSTALLINITY, ARC-SEC

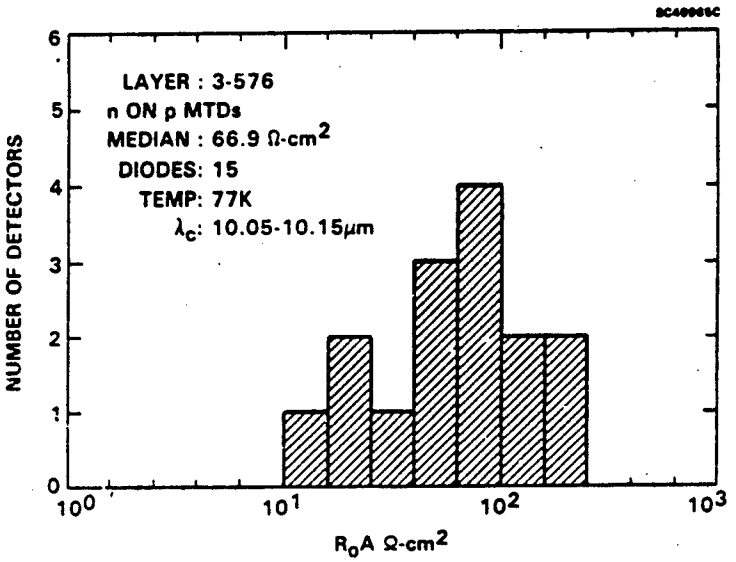
Rockwell International
Science Center

LWIR TACTICAL MCT DETECTOR PERFORMANCE

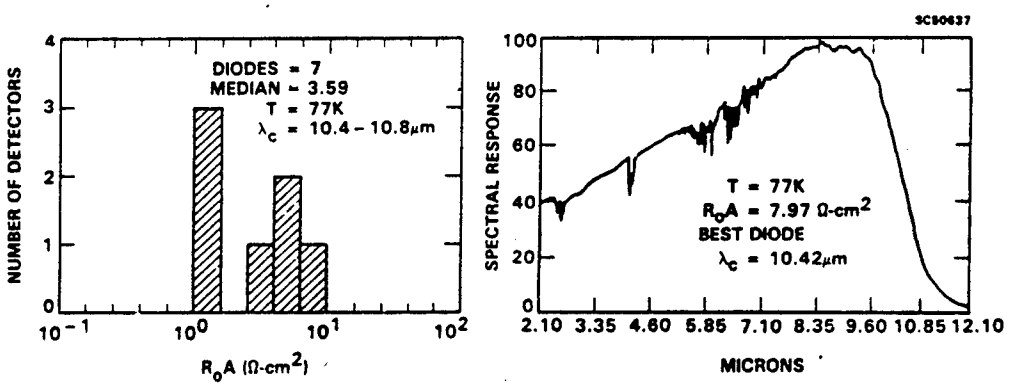


Rockwell International
Science Center

n^+/p TEST DIODES IN HgCdTe/GaAs (PACE-2)



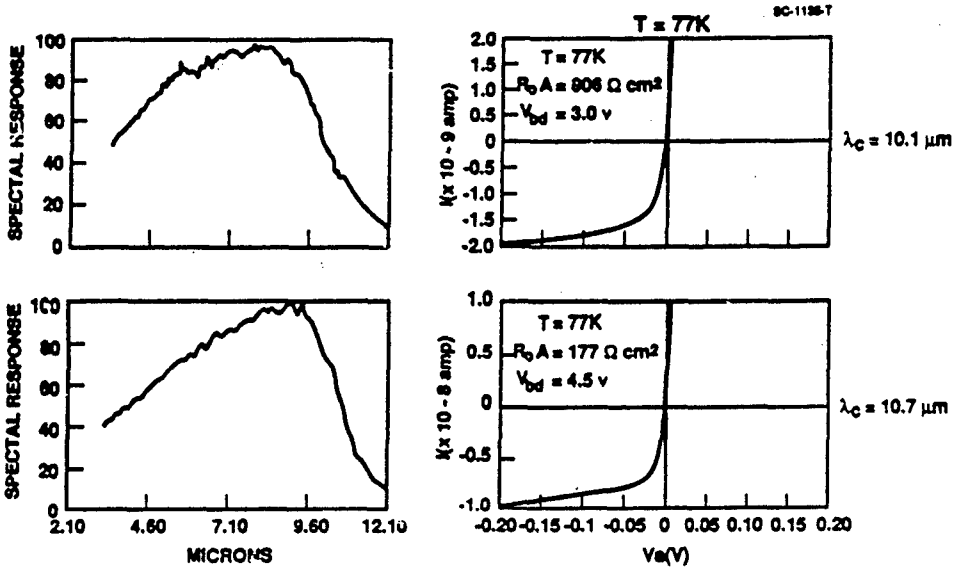
MTD DATA FOR 3-623 BASELINE LAYER n ON p DEVICES, ION IMPLANTED



Rockwell International
Science Center

ORIGINAL PAGE IS
OF POOR QUALITY

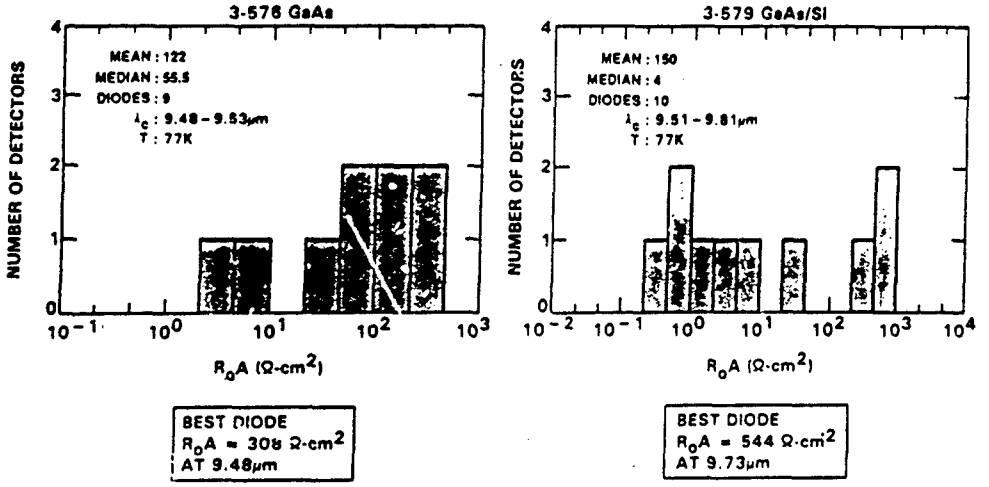
LWIR HgCdTe/Pace-2 p/n Devices Show Higher Performance Than LPE Devices



- ARSENIC IMPLANATATION
- OMVPE HgCdTe ON GaAs

RECENT p ON n MTD PERFORMANCE CONFIRM EARLIER RESULTS

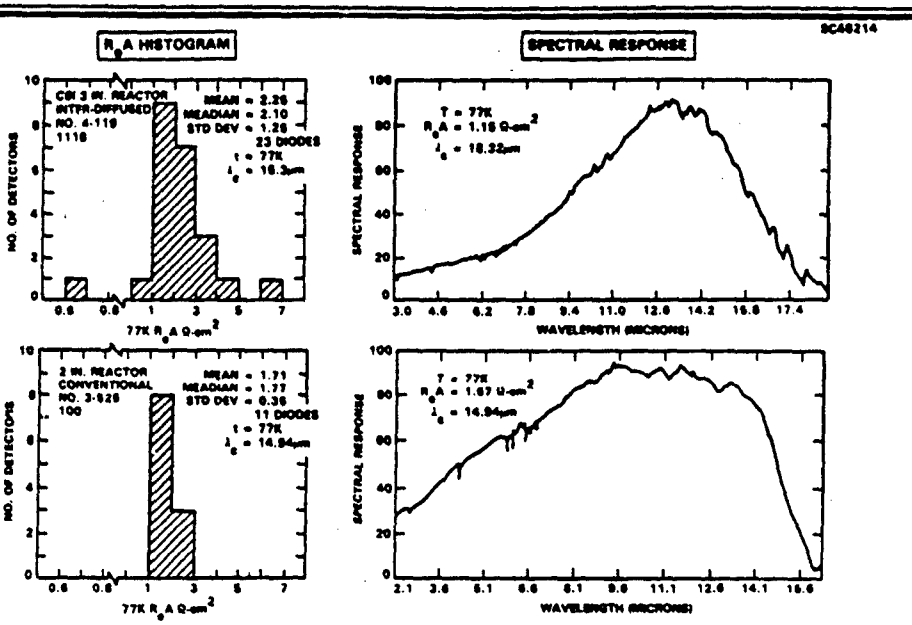
ARSENIC IMPLANT/DIFFUSION IN DOUBLE LAYER HETEROSTRUCTURE



- n ON p DIODES HAVE BETTER UNIFORMITY

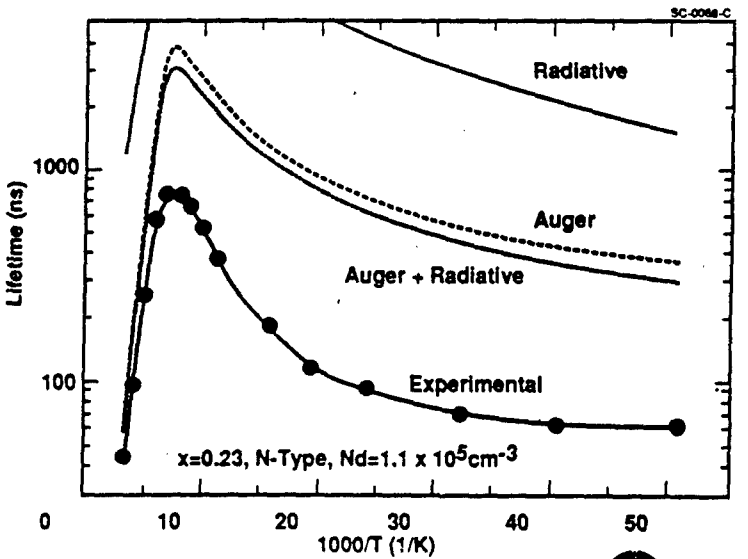
Rockwell International
Science Center

EXCELLENT DIODE PERFORMANCE IN VLWIR MOCVD MCT/GaAs p ON n DIODES



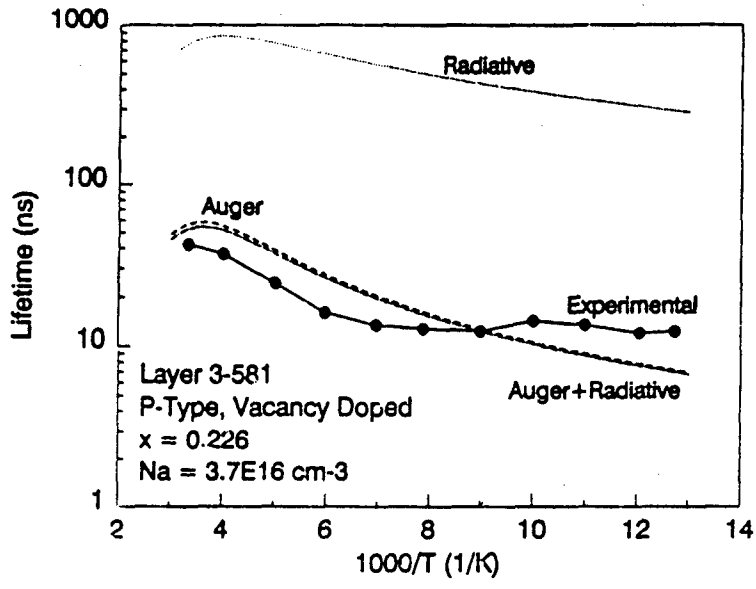
Minority Carrier Lifetime

4-334, N-Type, Undoped, x=0.235, Nd=1.1 x 10^{15}cm^{-3}

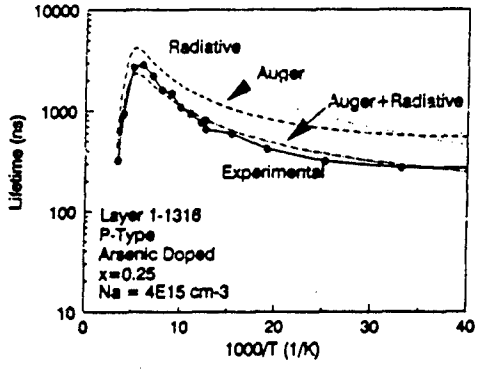


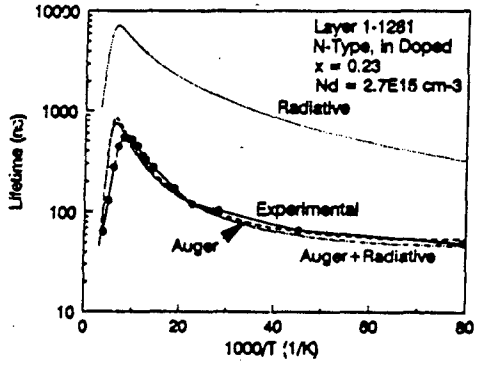
Rockwell International
Science Center

LIFETIMES IN SOME VACANCY DOPED PACE-2 APPROXIMATE THEORY



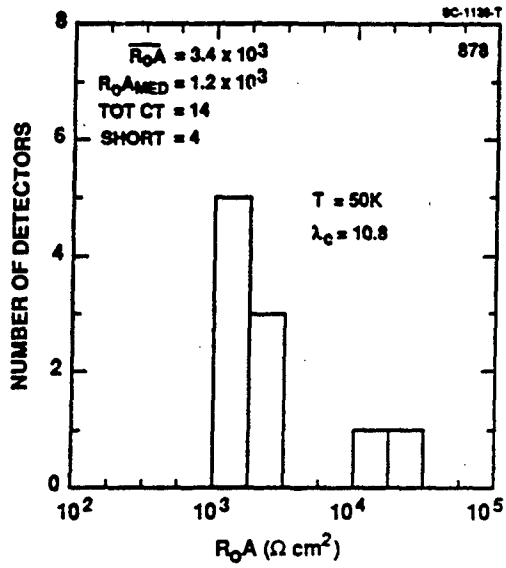
BEST IMPURITY DOPED PACE-2 SAMPLES SHOW THEORETICAL LIFETIMES



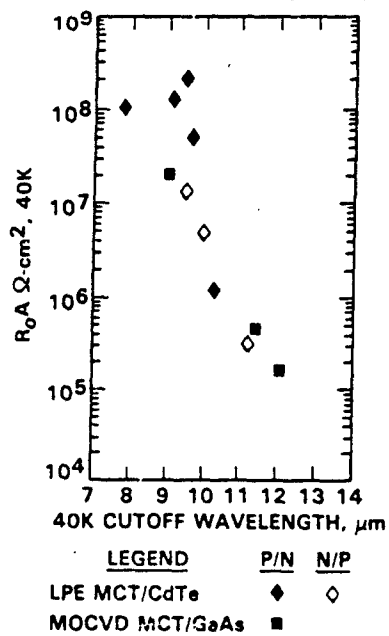


Rockwell International
Science Center

Performance of an LWIR MCT/GaAs Array at 50K



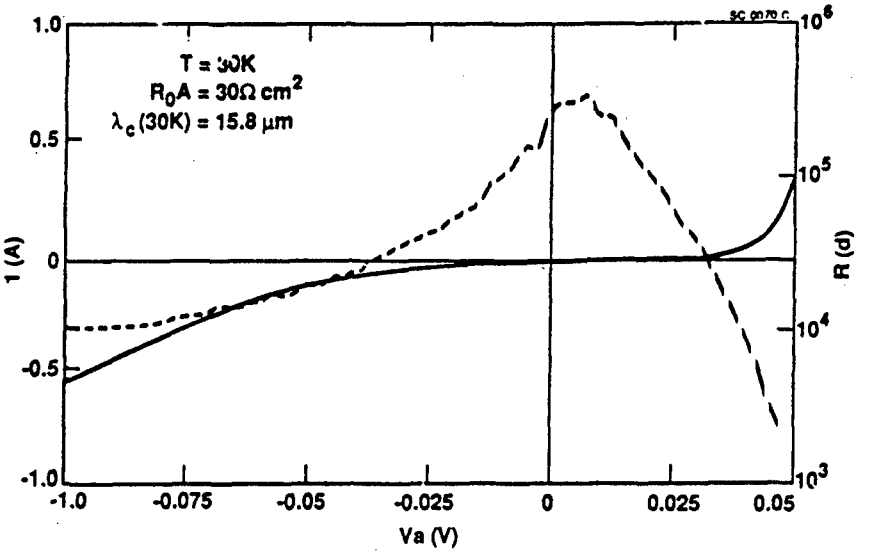
LWIR MOCVD HgCdTe/GaAs DIODES BEST PERFORMANCE IS AT TOP LPE LEVELS FOR 77 AND 40K



Rockwell International Science Center

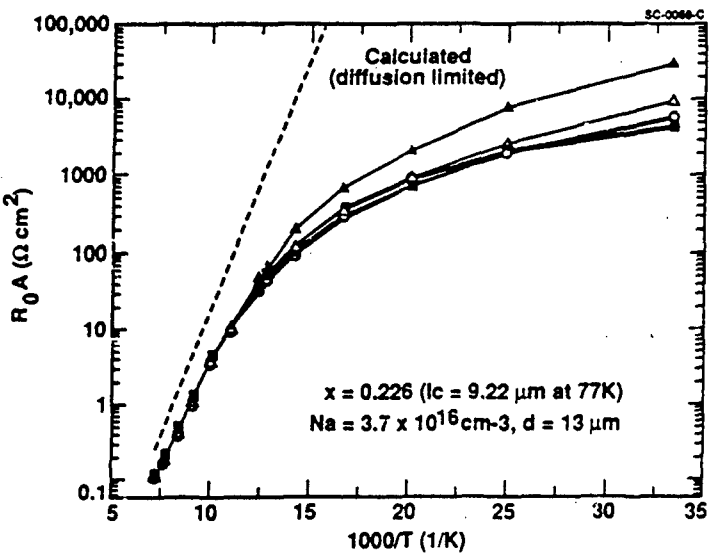
ORIGINAL PAGE IS OF POOR QUALITY

VLWIR I-V Characteristics for MOCVD Grown MCT/GaAs Detector



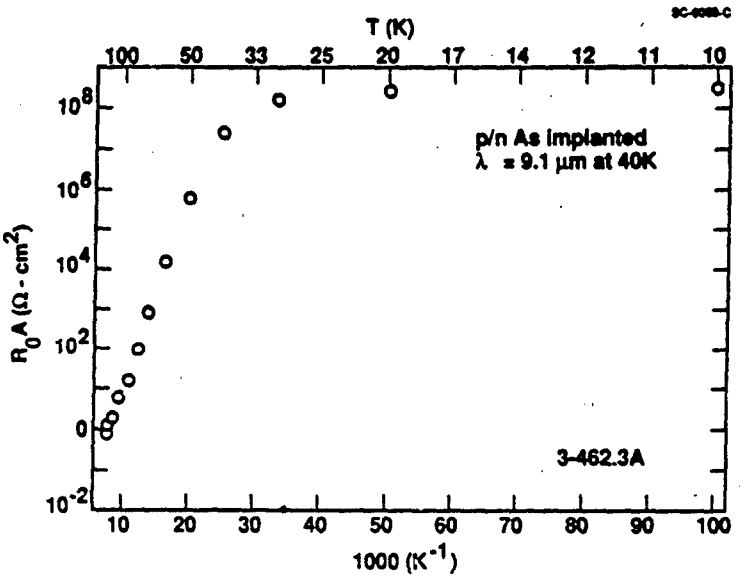
R_0A vs 1/T

Layer 3-581, L-134, Planar Ion Implanted

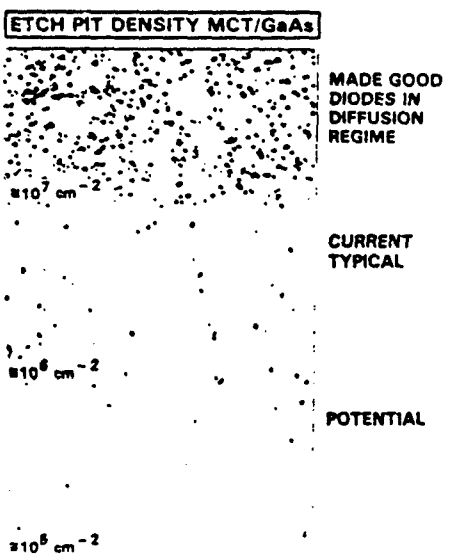


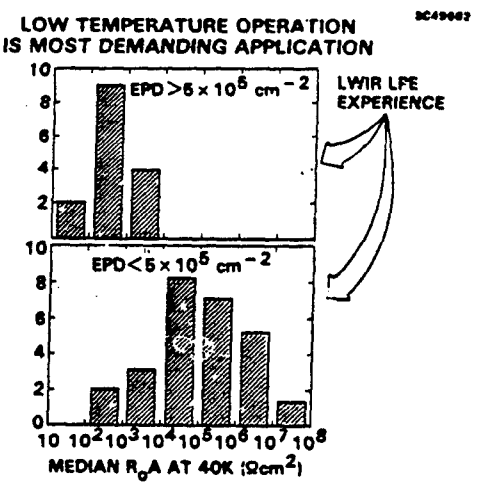
Rockwell International
Science Center

Temperature Dependence of the R_0A Product of a P/N Diode Fabricated from PACE-2 Material



STRATEGIC APPLICATIONS REQUIRE CONTROL OF DISLOCATION DENSITY



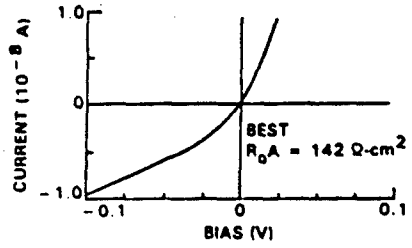


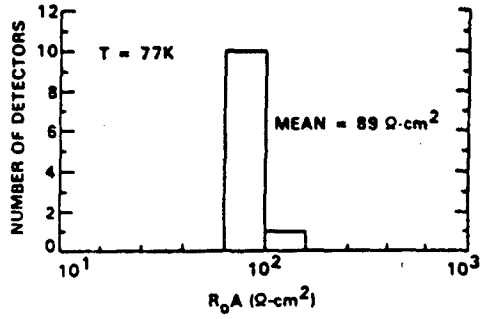
λ_c > 9.1-10.3µm AT 40K FOR 38 LAYERS

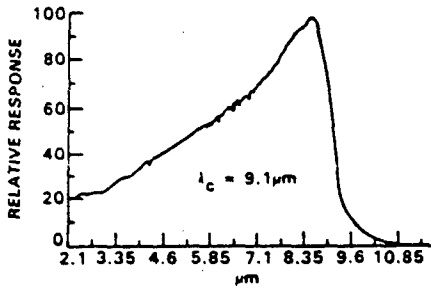
Rockwell International
Science Center

SAMPLE DIODES FROM PACE II 128 x 128 WAFER (ROCKWELL IR&D)

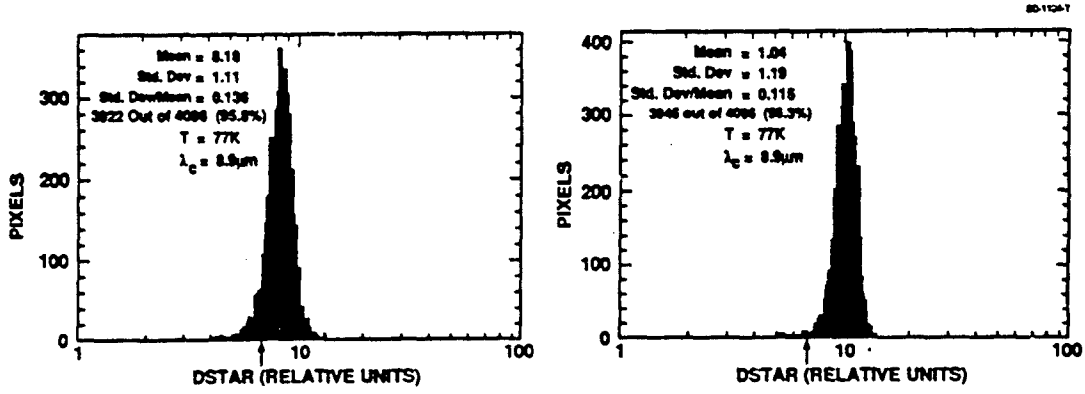
FULL PLANAR PROCESS: n/p, B-IMPLANTED, ZnS/SiO_2 PASSIVATED







Pace-2 Shows D* Uniformity and Operability of LWIR Hybrid



Rockwell International
Science Center

C-2

ORIGINAL PAGE IS
OF POOR QUALITY

CONCLUSIONS

- MCT HAS DEMONSTRATED THE HIGHEST PERFORMANCE OF ANY INTRINSIC AT ALL IR WAVELENGTHS
- NOVEL, ALTERNATIVE-SUBSTRATE, VPE APPROACHES CAN MEET PROGRAM GOALS WHILE ENHANCING PRODUCIBILITY AND MAKING POSSIBLE ADVANCED ARCHITECTURES
- THE PRESENT LIMITATIONS OF THE TECHNOLOGY ARE NOT FUNDAMENTAL BUT DUE TO IMMATURITY
- WE EXPECT LWIR/PACE-2 (GaAs)OR 3 (SI) TO FOLLOW A SIMILAR PATH TO PRODUCIBILITY AS THAT OF MWIR PACE-1 WHICH HAS RESULTED IN THE LARGEST (256X256) INSTRINSIC IR FPA TO DATE



Rockwell International
Science Center



N91
14385
UNCLAS

II-3 N91-14385

HgCdTe for NASA Eos Missions and Detector Uniformity Benchmarks

Paul R. Norton
Santa Barbara Research Center
Goleta, CA 93117

Important NASA Eos missions (AIRS and MODIS-N) which require detector spectral response in the range of 14 to 17 μm at medium background flux levels and operation in the range of temperatures between 65 to 95 K will be flown beginning in the next few years. Currently, a prime candidate detector technology for these missions is trapping-mode photoconductive HgCdTe devices. These devices can be tailored to the exact cutoff wavelengths required by those missions, and thus offer the performance advantages of an *intrinsic* detector which is ideally matched to the mission wavelength.

Under the long wavelength-background-temperature conditions of these Eos missions, any detector will at best be thermal generation-recombination noise limited. Photoconductive devices are generally preferred under these circumstances, since at elevated temperatures their performance degrades with n_i while for photovoltaic detectors performance degrades as n_i^2 (n_i is the *intrinsic* carrier concentration which is a function of alloy composition and temperature, but not doping).

Very high performance trapping-mode photoconductive HgCdTe detectors have been developed which can be reproducibly fabricated. Detectivity (D*) at 80K and 16 μm cutoff wavelength in excess of 10^{11} Jones has been measured for these devices. Power dissipation is at least two orders of magnitude less than conventional HgCdTe photoconductors - on the order of 0.12 W/cm^2 compared with 12 W/cm^2.

Eos missions define *thermal noise limited conditions* for the long wavelength operating bands. Trapping-mode photoconductive HgCdTe detectors are linear under such conditions and responsivity is independent of background flux. At lower temperatures or high flux conditions in which background flux limits detector performance, trapping-mode detectors have a responsivity which varies with background flux. Internal

PRECEDING PAGE BLANK NOT FILMED

calibration must be provided for radiometric measurements under the latter conditions (not an Eos mission concern).

Liquid phase epitaxy is used to grow these HgCdTe device structures. This technique has been shown to give control of the cutoff wavelength on the order of 16±1 μm or less, both from run to run and across wafer dimensions of several centimeters on a side. Responsivity uniformity of linear arrays (300 elements with areas of $\sim 2.5 \times 10^{-5}$ cm^2 and 100 μm center-to-center spacings) of trapping-mode detectors with 12 μm cutoff have shown typcal uniformities of 5-10% one-sigma standard deviation measured at 80 K and 5×10^{16} photons/cm^2/sec background flux. Measurements of PV detector responsivity uniformity shows that uniformity scales as $1/\sqrt{A}$ and can be attributed to ±1mm variations in detector area. Thus, larger area HgCdTe detectors are anticipated to be more uniform.

II - 3

HgCdTe for NASA Eos Missions and Detector Uniformity Benchmarks

P. R. Norton, Santa Barbara Research Center

Hard copies of visuals not available for publication due to ITAR restrictions.

SESSION III: Device Design and Evaluation Issues

III - 1 Detector Array Evaluation and Figures of Merit
E.L. Dereniak, University of Arizona

III - 2 Issues and Directions in IR Detector Readout Electronics
E.R. Fossum, Columbia University

III - 3 Radiation Response Issues for Infrared Detectors
A.H. Kalma, Mission Research Corporation

PRECEDING PAGE BLANK NOT FILMED

N91
14386
UNCLAS

III-1

N91-14386

Detector Array Evaluation and Figures of Merit

Eustace L. Dereniak
Optical Sciences Center
University of Arizona

This presentation will review the commonly used methods to evaluate the performance of a two-dimensional focal-plane array using charge transfer devices. Two figures of merit that attempt to combine quantum efficiency, read noise and dark-current generation into a single parameter are discussed. The figures of merit are suggested as possible alternatives to the D*.

PRECEDING PAGE BLANK NOT FILMED

DETECTOR ARRAY EVALUATION AND FIGURES OF MERIT

STATE OF CONFUSION

- WHAT WE GET FROM MANUFACTURER
- WHAT WE WANT
- WHAT WE TEST FOR

EUSTACE L. DERENIAK

OPTICAL SCIENCES CENTER
UNIVERSITY OF ARIZONA

(602) 621-1019

GENERIC PARAMETERS QUOTED FROM MANUFACTURER

- SIZE AND # OF PIXELS
- D*
- D* HISTOGRAM
- READ NOISE HISTOGRAM
- DARK CURRENT HISTOGRAM
- SATURATION LEVEL
- RESPONSIVITY MAP

D* PROBLEMS

- SMALL AREA DETECTORS (D* = CONSTANT)
- SPATIAL VARIATIONS ACROSS ARRAY
- RADIANT "POWER" DEPENDENT FOR PHOTODETECTOR
- D*(f) - NO 1/f CHARACTERISTIC (I.e., 0.5 Hz)

  SPECIFICATION OF CHOPPER FREQ.
- WAVELENGTH SPECIFICATION

PARAMETERS WANTED BY USER

- SPATIAL AVERAGED QUANTUM EFF. vs WAVELENGTH
- CONVERSION GAIN
- SPATIAL AVERAGED DARK CURRENT vs INTEGRATION TIME FOR OPERATING TEMPERATURE
- READ NOISE
- DEFECTIVE PIXEL MAP
- DYNAMIC RANGE
- CROSSTALK
- FILL FACTOR (DETECTOR AREA)
- SATURATION LEVEL

TEST/DATA COLLECTED

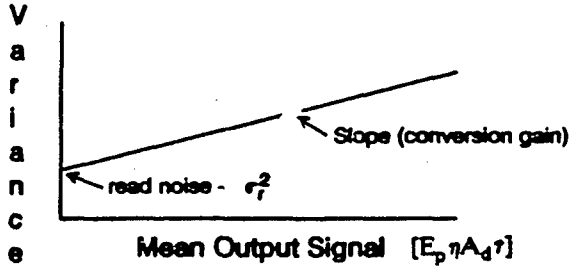
- o MEAN VARIANCE CURVE - σ_r
- o DARK CURRENT GENERATION - Dg
- o SIGNAL MEASURE FOR Q.E. OVER SPECTRAL BAND - η
- o EFFECTIVE DETECTOR AREA - Ad

PLOT SPATIAL MAPS OF:

- DARK CURRENT
- QUANTUM EFFICIENCY
- DEAD PIXELS

MEAN - VARIANCE CURVE

PLOT OF VARIANCE (NOISE^2) VERSUS
THE MEAN IRRADIANCE (FLAT FIELD) ACROSS ARRAY



$$\sigma^2 = \sigma_r^2 + E_p \eta A_d \tau \text{ (electrons)}$$

COMPUTER PROCESSING

Ep∝ADU (ANALOG - DIGITAL UNITS IN COMPUTER)
SO UNITS CAN BE RELATED BETWEEN ADU'S AND
FLAT FIELD IRRADIANCE.

MEAN - VARIANCE IN PRACTICE

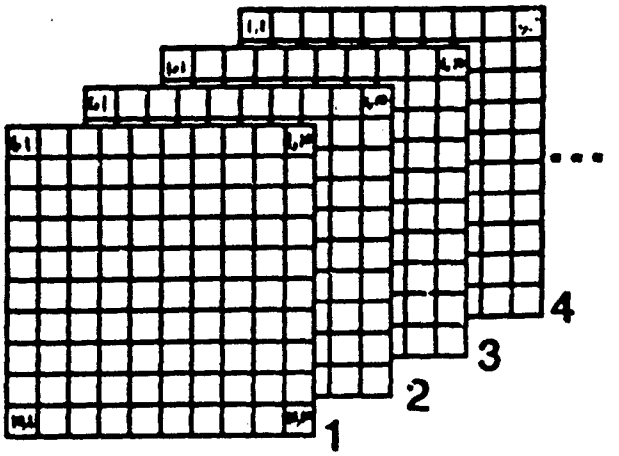
- TWO WAYS TO CHANGE MEAN IRRADIANCE ON ARRAY
  - VARY INTEGRATION TIME
  - VARY BLACKBODY TEMPERATURE, OR RANGE

[NOT NECESSARILY EQUIVALENT]

IMPORTANCE OF DARK CURRENT

WILL PHOTONS BE DETECTED IN INTEGRATION TIME,
OR WILL DARK GENERATED ELECTRONS DOMINATE
FOR PARTICULAR APPLICATION?

DARK CURRENT TESTS



FOR VARIOUS INTEGRATION TIMES; ONE TAKES SEVERAL (i.e. 25) FRAMES OF DATA;

A. $\tau \cong 1$ ms (SHORTEST POSSIBLE)

$$\overline{P_{ij}} = \frac{1}{25}\sum_{K=1}^{25} P_{ij}(K) \quad ; \quad K \text{ is Time Index}$$

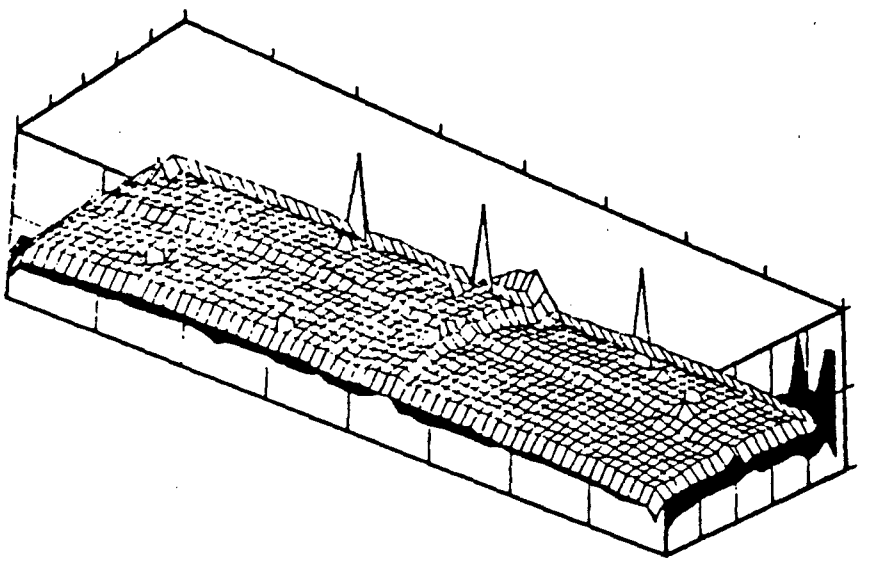
$F_\tau = \{\overline{P}_{11}, \overline{P}_{12}, \overline{P}_{13} \ldots \overline{P}_{ij}\}$ Average Dark Frame

B. $\tau >> 1$ ms

(REPEAT)
FIND THE DARK FRAME VALUE FOR SEVERAL INTEGRATION TIMES

DARK FRAME ANALYSIS

- LOCATE A WELL BEHAVED REGION
- READ NOISE VALUE IS FOUND @ SHORT INTEGRATION TIMES

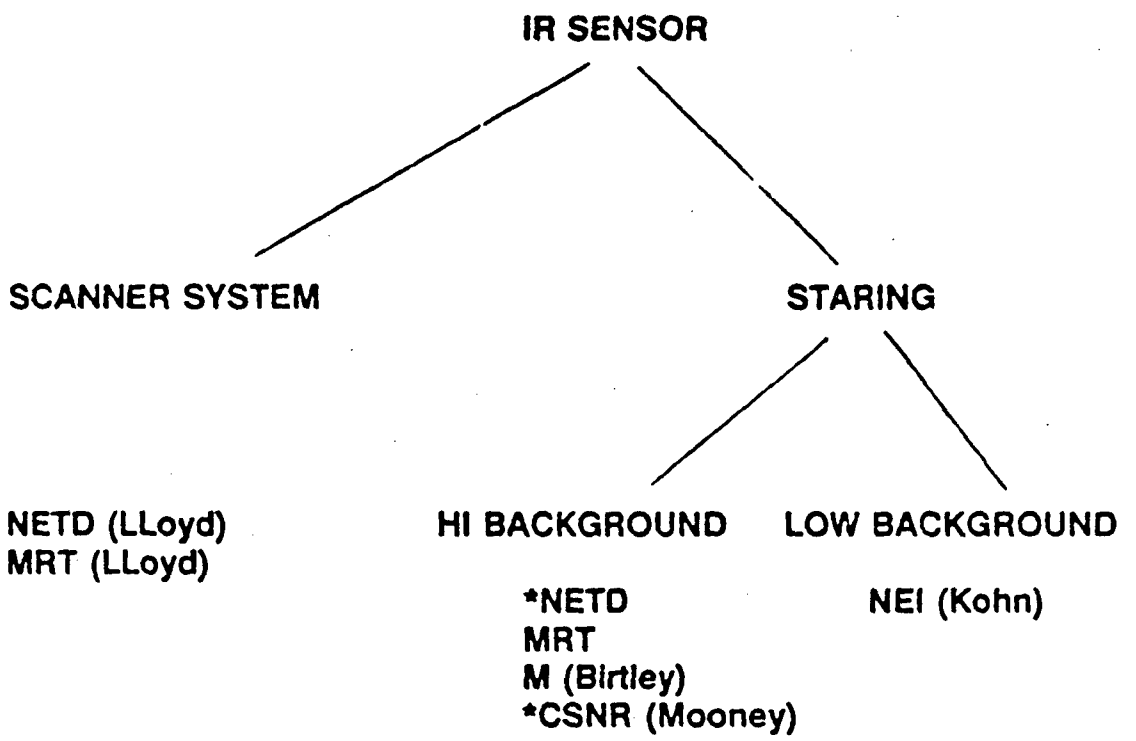


DARK CURRENT GENERATION RATE
Dg (# OF e^- /SEC-PIXEL)

INCLUDES OTHER SOURCES

- LIGHT LEAKS
- "SELF-EMISSION" OF ELECTRICAL COMPONENTS

FIGURES OF MERIT



ARRAY TESTING AND FIGURE OF MERIT ARE APPLICATION DEPENDENT

* RELATED

NON-UNIFORMITY DEFINITION

$$U(Ep) = \frac{\text{r.m.s. SPATIAL VARIATION IN ARRAY OUTPUT}}{\text{SPATIALLY AVERAGED ARRAY OUTPUT}}$$

$$= \frac{\sigma_{\bar{P}_{ij}}}{\langle \bar{P} \rangle}$$

SPATIAL AVERAGE

$$\langle \bar{P} \rangle = \frac{1}{NM} \sum_{i}^{N} \sum_{j}^{M} \bar{P}_{ij}$$

SPATIAL VARIANCE

$$\sigma^2_{\bar{P}_{ij}} = \frac{1}{NM} \sum_{i}^{N} \sum_{j}^{M} [\bar{P}_{ij} - \langle \bar{P} \rangle]^2$$

- U (Ep) CAN BE IMPROVED THROUGH USE OF A NON-UNIFORMITY CORRECTOR
- U (Ep) IS TYPICALLY REDUCED TO ZERO AT SYSTEM CALIBRATION POINTS.

ARRAY FIGURE OF MERIT

- 2-D* IS A D* PLUS THE RANDOM CONTRIBUTION OF NON-UNIFORMITY, READ NOISE, AND DARK CURRENT
- A MODIFIED D* CALLED 2-D* MAY BE USED IN LLOYDS NETD EXPRESSION TO YIELD CSNR

$$2\text{-}D^* = \frac{\lambda}{hc} \sqrt{\frac{\eta}{2\left[E_p + \frac{\sigma_r^2}{A_d \eta \tau} + E_p^2 A_d \eta \tau U^2 + \frac{D_g}{A_d \eta}\right]}}$$

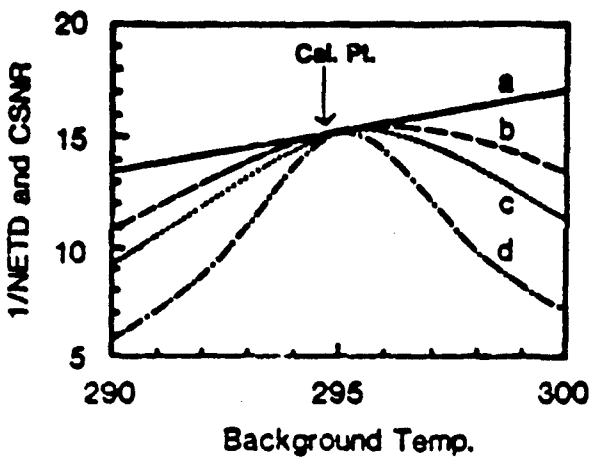
- PHOTON SHOT NOISE - Ep
- READ NOISE - σ_r
- SPATIAL PATTERN - u
- DARK CURRENT GENERATION (ZERO) - Dg

HIGH BACKGROUND CONTRAST SIGNAL-TO-NOISE RATIO (CSNR)

$$CSNR = \frac{\partial[E_p \eta A_d \tau]/\partial T}{[E_p \eta A_d \tau + \sigma_r^2 + E_p^2 \eta^2 A_d^2 U^2 \tau^2]^{1/2}}$$

Ep	=	PHOTON IRRADIANCE (P/s-cm^2)
η	=	QUANTUM EFF.
Ad	=	PIXEL AREA
τ	=	INTEGRATION TIME
σ_r	=	READ NOISE
U	=	RMS NON-UNIFORMITY
T	=	TEMPERATURE

CSNR vs BACKGROUND TEMPERATURE FOR VARIOUS AMOUNTS OF RESIDUAL NON-UNIFORMITY



a. NO NON-UNIFORMITY; CSNR = 1/NETD

b. u = 1%

c. > b

d. > c

UNIFORMITY CORRECTION IS LIMITED BY QUANTIZATION NOISE OF A/D CONVERTER

ARRAY TESTING IS APPLICATION DEPENDENT
THEREFORE, FIGURES OF MERITS VARY

- HIGH BACKGROUND SENSOR SYSTEM

  NETD - NOISE EQUIV. TEMP. DIFFERENCE

  MRT - MINIMUM RESOLVABLE TEMPERATURE

  CSNR - CONTRAST SIGNAL-TO-NOISE RATIO

- LOW BACKGROUND SENSOR SYSTEM

  NEI - NOISE EQUIV. IRRADIANCE [PHOTONS/SEC-CM ^{2}]

  DQE - DETECTIVE QUANTUM EFFICIENCY

Detective Quantum Efficiency - DQE (single detector)

$$DQE \equiv \frac{(S/N)^2_{meas}}{(S/N)^2_{in}} \qquad \text{iff BLIP; } \eta$$

Apply to a 2-dimensional array

$$(S/N)_{in} = \sqrt{E_p A_d \tau}$$

$$(S/N)_{meas} = \frac{E_p A_d \tau \eta}{[E_p A_d \eta \tau + \sigma_r^2 + (E_p A_d \eta \tau U)^2 + D_g \tau]^{1/2}}$$

↑ shot ↑ read ↑ uniformity ↑ dark generation

2-Dimensional DQE

$$2\text{-}DQE = \frac{(S/N)^2_{meas}}{(S/N)^2_{in}} = \frac{1}{\frac{1}{\eta} + \frac{\sigma_r^2}{E_p A_d \eta^2 \tau} + E_p A_d \tau U^2 + \frac{D_g}{E_p A_d \eta^2}}$$

iff E_p is large enough to produce shot noise,
or U, σ_r, and D_g are small,
DQE is equal to quantum efficiency.

SAMPLE CALCULATION

$$\eta = 0.6$$

$$N_{full} = 10^6$$

$$A_d = (50\ \mu m)^2$$

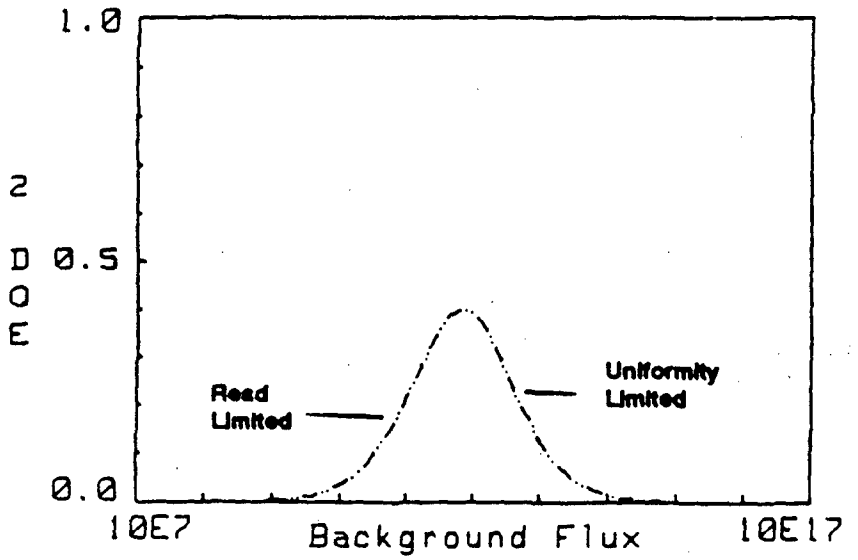
$$\tau = 0.001\ sec$$

$$\sigma_r = 50\ e^-$$

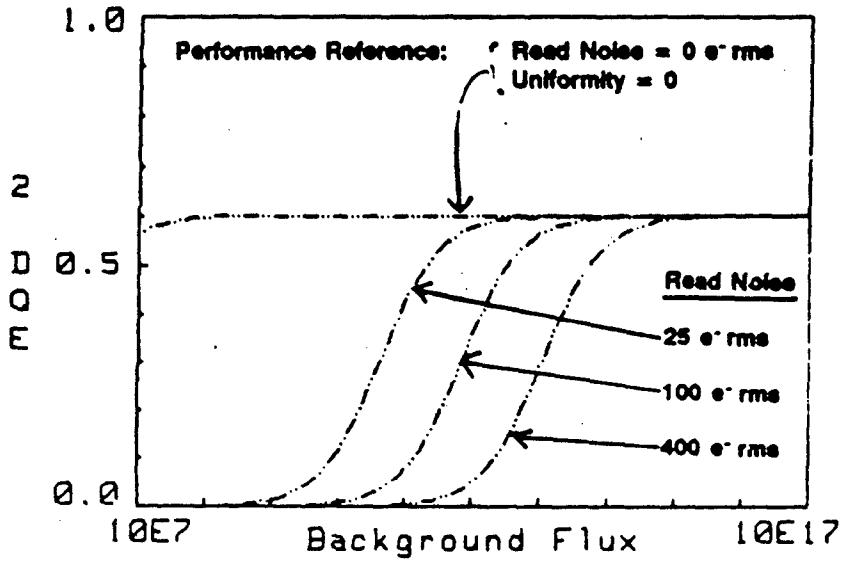
$$D_g = 10\dot{e}/sec\text{-}pixel$$

$$U = 0.005$$

$$2 - DQE = 1/\left(\frac{1}{0.6} + \frac{2.79(10^{11})}{E_p} + E_p\ 6.25(10^{-13}) + \frac{1.11(10^6)}{E_p}\right)$$



READ NOISE INFLUENCE



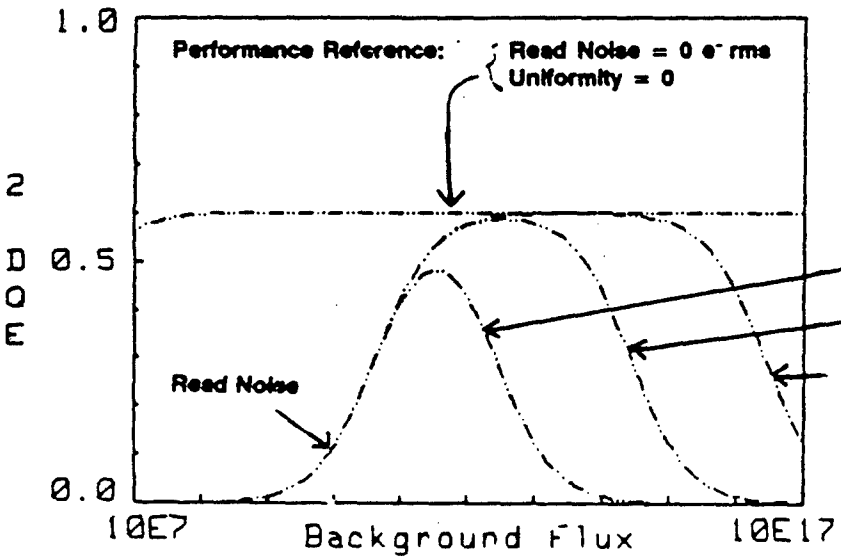
η = .60

τ = .001 sec

Ad = $(50\mu m)^2$

Dg = $10e^-$ /sec-pixel

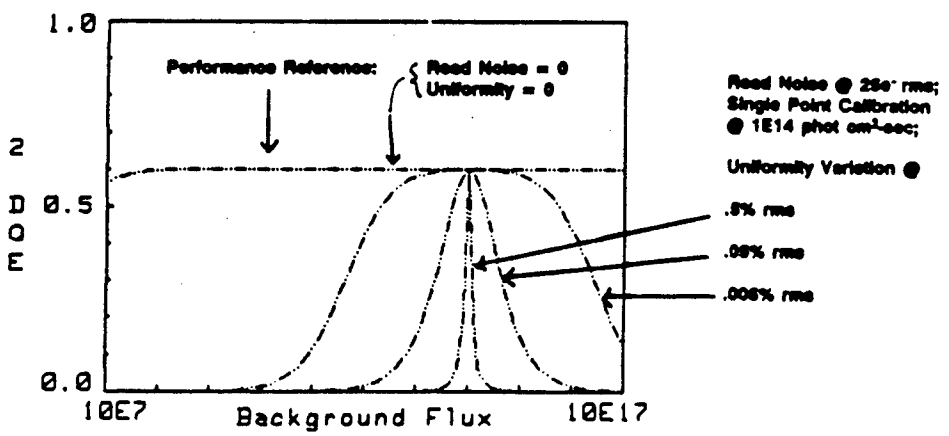
NON-UNIFORMITY INFLUENCE



WHERE DOES SPATIAL NON-UNIFORMITY COME FROM

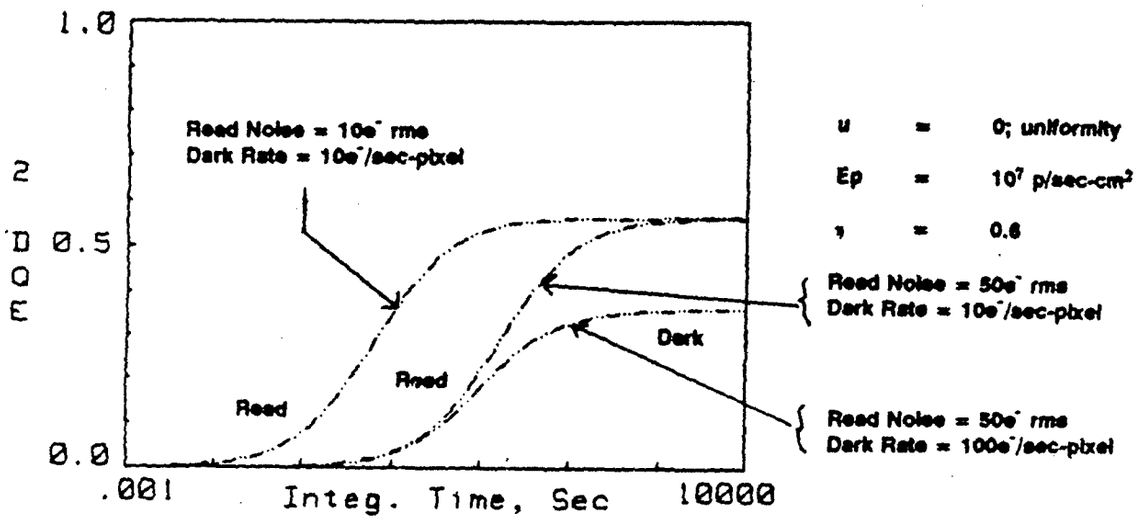
- VARIATIONS IN DARK CURRENT DENSITY
- VARIATIONS IN DETECTOR ACTIVE AREA
- VARIATIONS IN THE ABSOLUTE VALUE, OR IN SOME CASES, VARIATIONS IN THE SPECTRAL SHAPE, OF THE QUANTUM EFFICIENCY CURVE.
- VARIATIONS IN THE DETECTOR-TO-DETECTOR NON-LINEARITY OF RESPONSE
- VARIATIONS IN THE 1/f NOISE ASSOCIATED WITH EACH DETECTOR OR OTHER UNIT-CELL ELECTRONICS.

FLAT FIELD CALIBRATION EFFECTS



DARK CURRENT EFFECTS

$$2 - DQE = \frac{1}{\frac{1}{0.6} + \frac{27.7}{\tau} + 1.1(10^{-3})D_g}$$



DARK CURRENT SIMPLY LIMITS THE MAXIMUM DETECTIVE QUANTUM EFFICIENCY

- GOOD (τ) DQE REQUIRES "LOW" READ NOISE AND "LOW" DARK CURRENT

CONCLUSIONS

TESTS ON ARRAYS

- MEAN VARIANCE
- DARK CURRENT GENERATION FRAMES
- SIGNAL MEASUREMENTS FOR Q.E. VALUES
- EFFECTIVE DETECTOR AREA

FIGURES OF MERITS FOR FPA

- 2-D* (CSNR - CONTRAST SIGNAL TO NOISE) RATIO
  - GOOD FOR HIGH BACKGROUNDS AND CALIBRATION ONCE AN HOUR
- DQE (DETECTIVE QUANTUM EFFICIENCY)
  - GOOD FOR LOW BACKGROUNDS
  - COMBINES READ NOISE, DARK CURRENT, QUANTUM EFFICIENCY AND NON-UNIFORMITY INTO ONE PARAMETER

N91
14387
UNCLAS

III-2

N91-14387

ISSUES AND DIRECTIONS IN IR DETECTOR READOUT ELECTRONICS

Eric R. Fossum
Department of Electrical Engineering
Columbia University
New York, NY 10027

Abstract

An introduction to the major issues encountered in the read out of imaging detector arrays in the infrared will be presented. These include circuit issues such as multiplexing, buffering, and noise, as well as materials issues.

Future directions in infrared readout electronics will also be discussed. These include on-chip signal processing and advanced hybridization schemes. Finally, recent work at Columbia on 2DEG-CCDs for IR detector multiplexing will be described.

Issues in FPA Readout Electronics

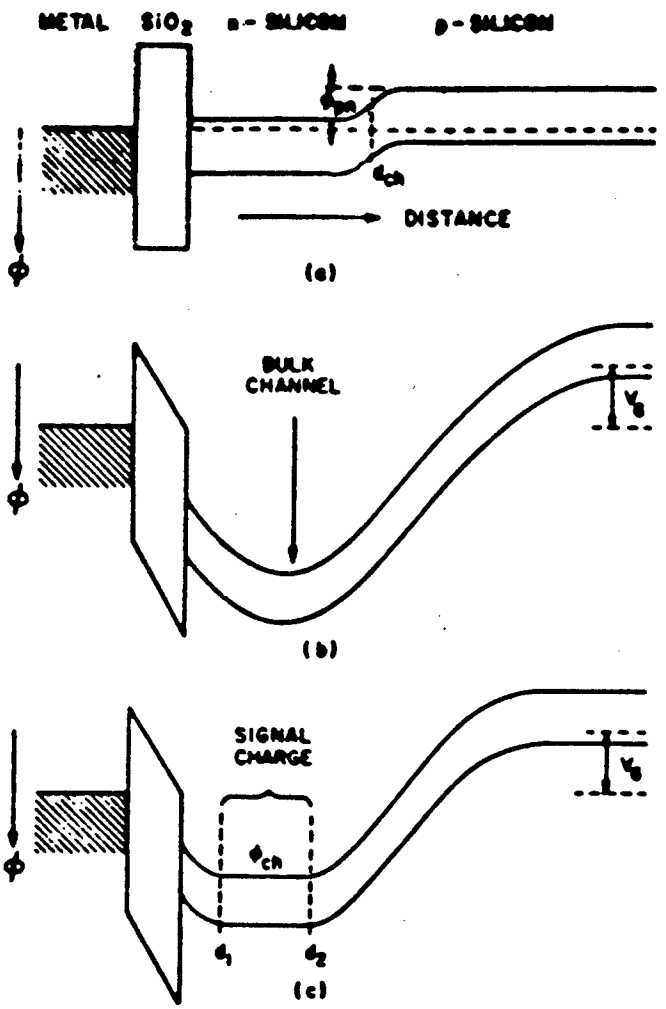
Eric R. Fossum
Dept. of Electrical Engineering
Columbia University
NY NY 10027

ERF

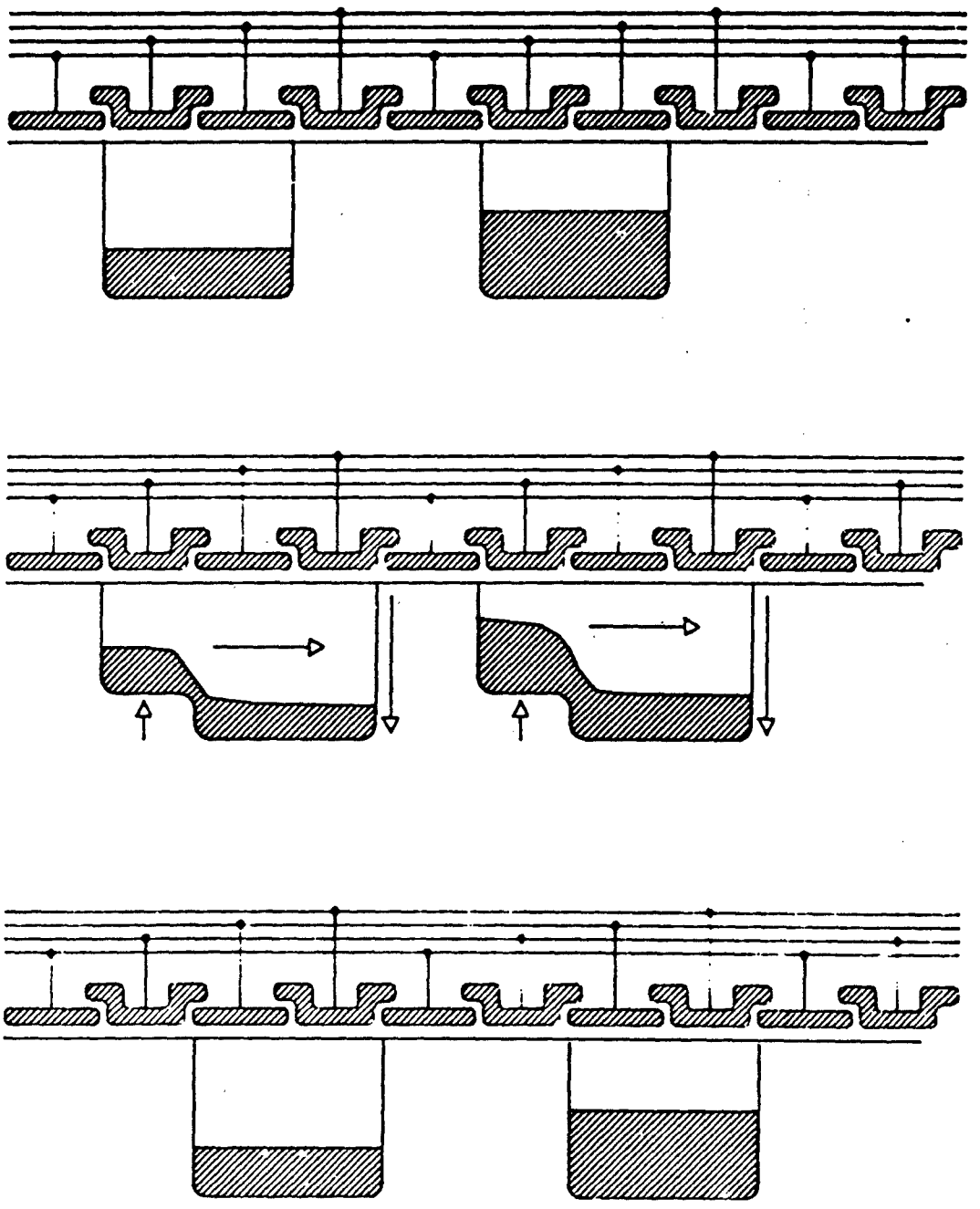
Outline

1. Present Imager Readout Architectures
2. Special Problems in LWIR Readout
3. GaAs CCD Readout
4. On-chip Signal Processing

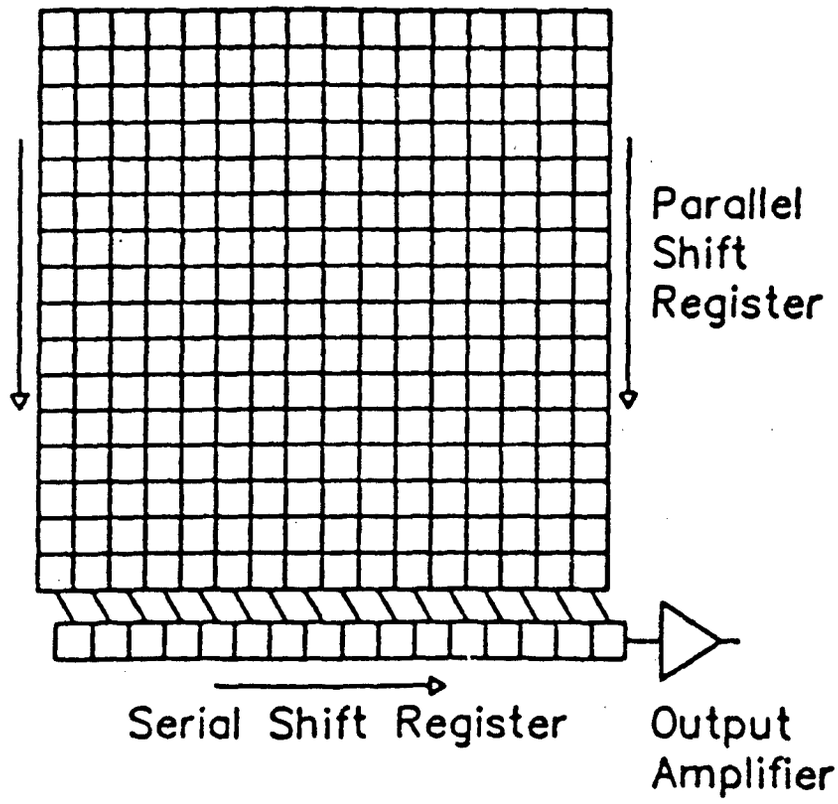
ERF


METAL
SiO_2
n - SILICON
p - SILICON
ϕ_{ch}
DISTANCE
(a)
BULK CHANNEL
V_B
(b)
SIGNAL CHARGE
V_B
ϕ_{ch}
q_1
q_2
(c)

4-PHASE CHARGE TRANSFER



Schematic illustration of a charge-coupled device (CCD) imager read-out structure.

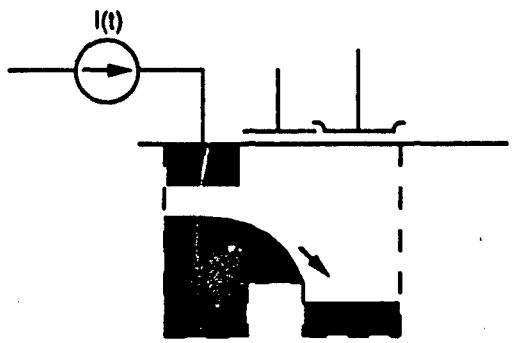


COMMERCIALLY-AVAILABLE CCDS

MANUFACTURER	DEVICE	FORMAT	STRUCTURE	PIXEL SIZE, μm	DIMENSIONS, mm	GATES/PIXEL	
EG&G Reticon (US)	RA0256B	256x256	Full Frame	40x40	10.2x10.2	4	
Fairchild (US)	CCD222	488x380	Interline	30x18	8.8x11.4	2	
Photometrics (US)		516x516	Full Frame	20x20	10.3x10.3	4	
Tektronix (US)	TK512M	512x512	Full Frame	27x27	13.8x13.8	3	Thinned
	TK2048M	2048x2048	Full Frame	27x27	55.3x55.3	3	Thinned, Develop.
Videk (US)	Megaplus	1320x1035	Full Frame	6.8x6.8	9.0x7.0	2	
Amperex (Holland)	NKA1010	604x294	Frame Transfer	10x15.6		4/3	
Dalsa (Canada)	IA-D1-0256	256x256	Frame Transfer	16x16	4.1x4.1		
Eng. Elec. Valve (UK)	P-86131	576x385	Full Frame	22x22	12.8x8.5		
Sanyo (Japan)		572x485					
		640x480					
Texas Inst. (Japan)	T1241	754x488	Frame Transfer	11.5x27		1	
	TC215	1024x1024	Full Frame	12x12	12.3x12.3	1	
	TC217	1134x486	Frame Transfer	7.8x13.6		1	
Thomson CSF (France)	TNX31156	1024x1024	Full Frame	19x19	19.5x19.5	4	Develop.
	TNX7863	576x384	Full Frame	23x23		4	
Toshiba (Japan)		1920x1036					

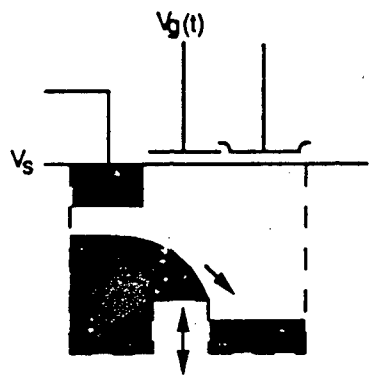
INTEGRATING INPUTS

1. DIRECT INJECTION



$$Q_{sig} = \int_T I(t)dt$$

2. GATE MODULATION



$$Q_{sig} = \int_T I(V_g(t))dt$$

COULD BE SUBTHRESHOLD
OR WEAK INVERSION
OR INVERSION

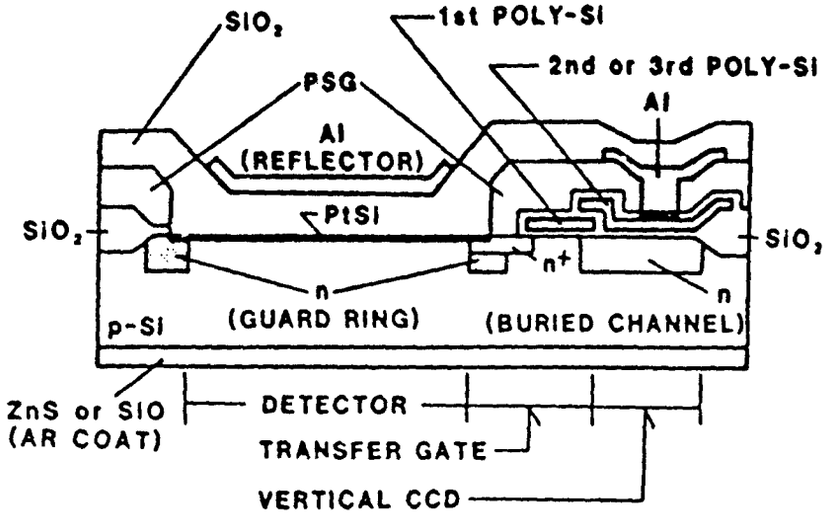


Fig. 5. Pixel cross section of 256 × 256 element IR-CCD image sensor.

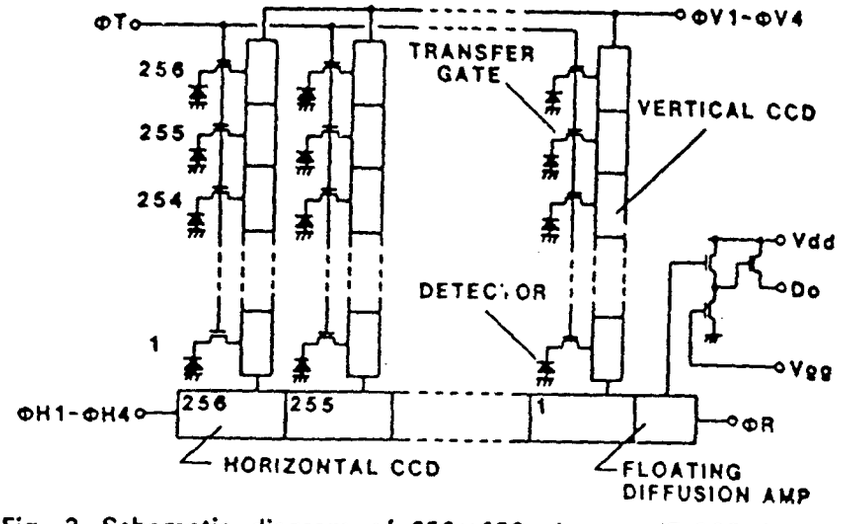


Fig. 3. Schematic diagram of 256 × 256 element IR-CCD image sensor.

Kimata, et al. Opt. Eng 26(3) 211 (1987).

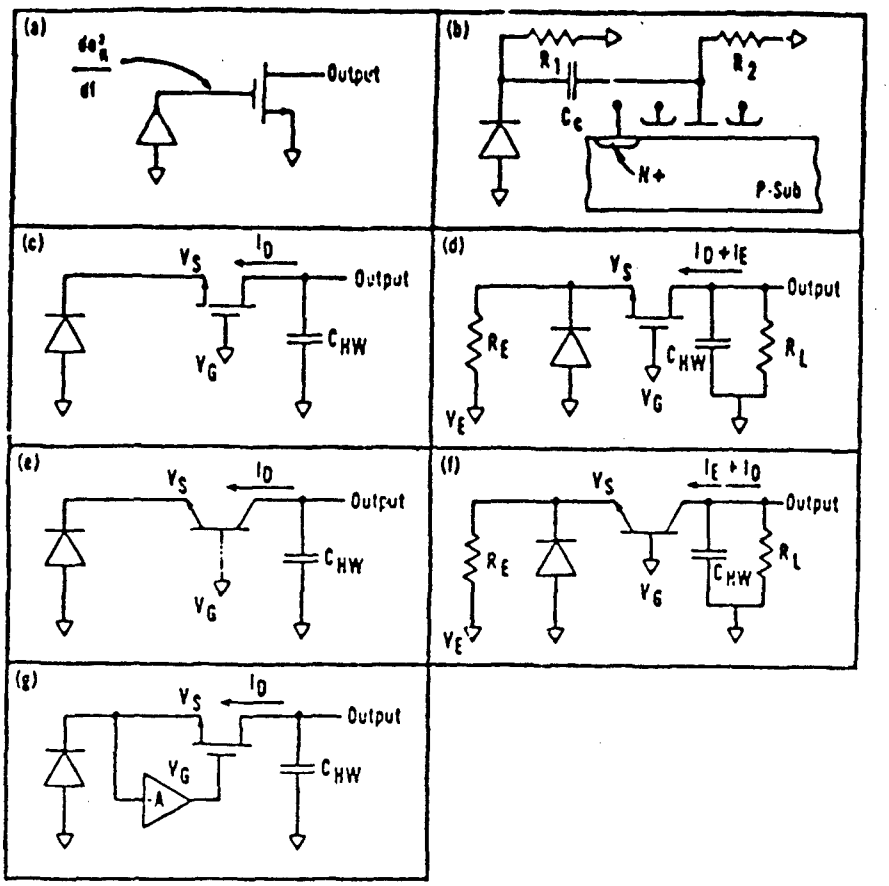
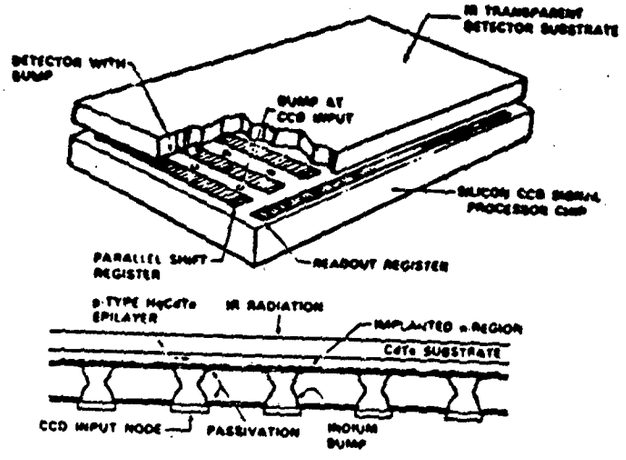


Fig. 2. Various detector readout structures: (a) gate readout (GRO); (b) gate-coupled readout (GCRO) to CCD; (c) direct-injection (DI) current readout; (d) direct-injection ancillary current (DIAC) readout; (e) direct-injection bipolar (DIB) current readout; (f) direct-injection bipolar ancillary current (DIBAC) readout; (g) buffered direct-injection (BDI) current readout.

Bluzer and Jensen Opt. Eng. 26(3) 241 (1987).



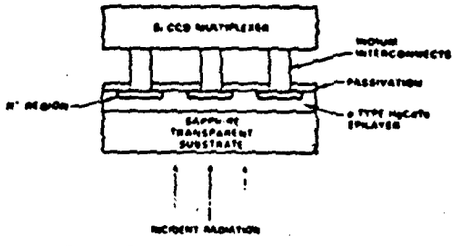


Fig. 8. Backside-illuminated hybrid FPA.

VURAL

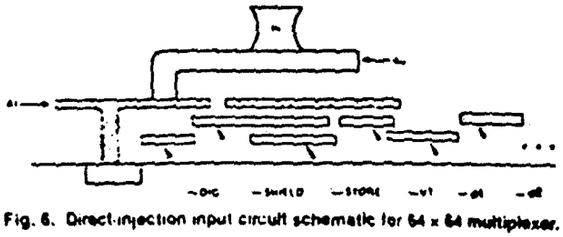
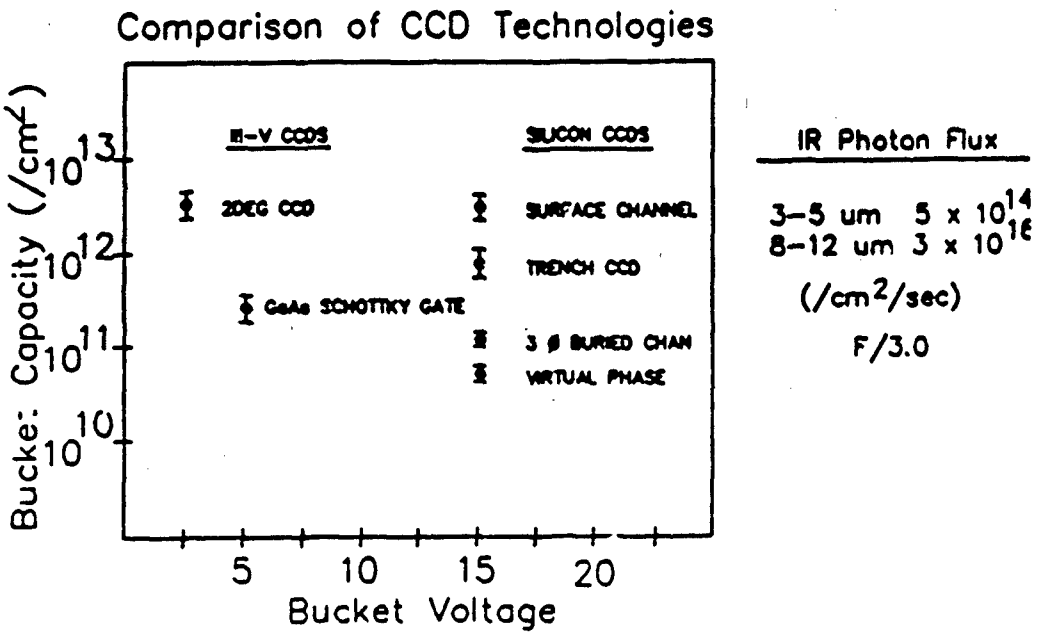
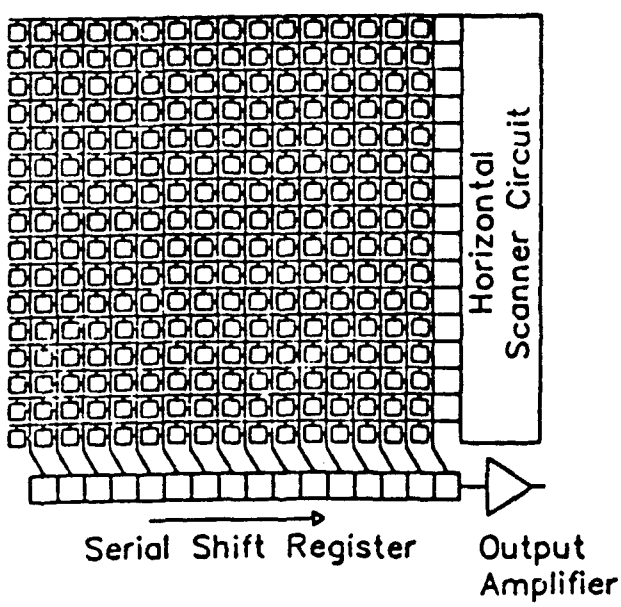


Fig. 6. Direct-injection input circuit schematic for 64 x 64 multiplexer.



Schematic illustration of a MOS-CCD imager read-out structure.



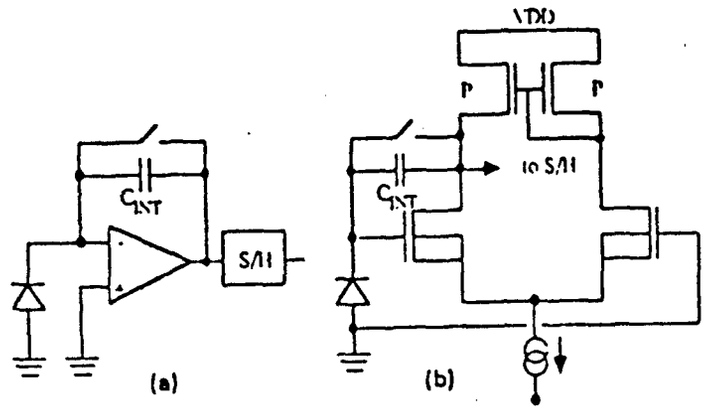


Fig. 5. Reset integrator input circuit: (a) functional block diagram, (b) MOSFET implementation.

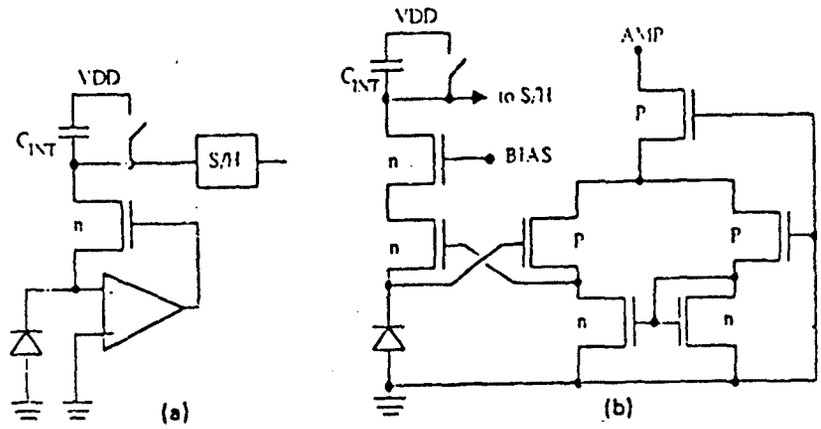


Fig. 6. Buffered common gate input circuit: (a) functional block diagram, (b) MOSFET implementation.

Lockwood and Parrish, Opt. Eng 26(3) 228 (1987).

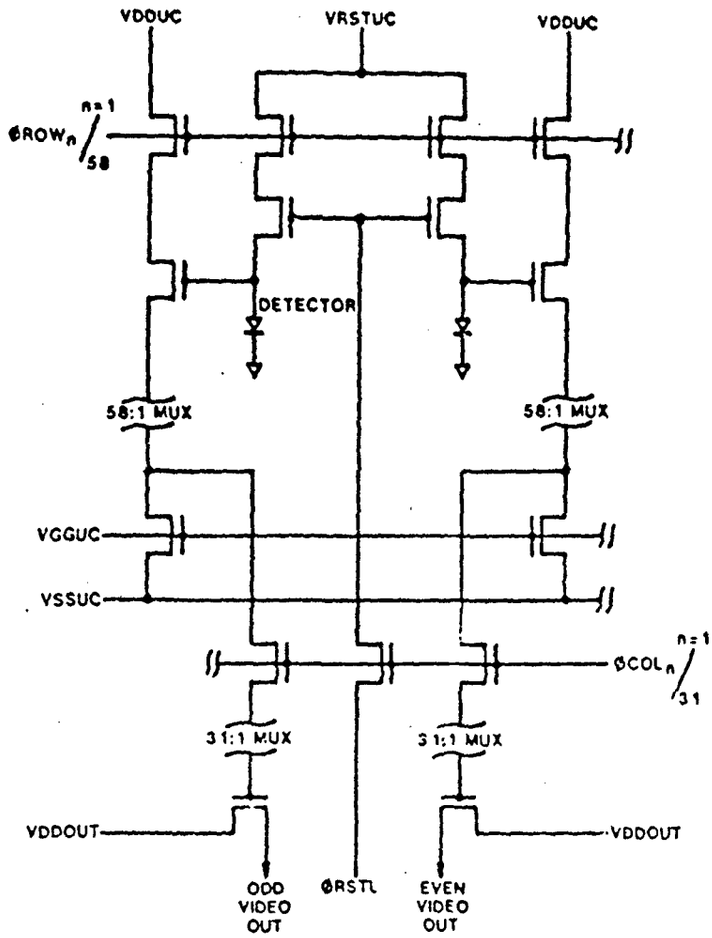


Fig. 2. Simplified schematic of the direct readout circuit used for this array.

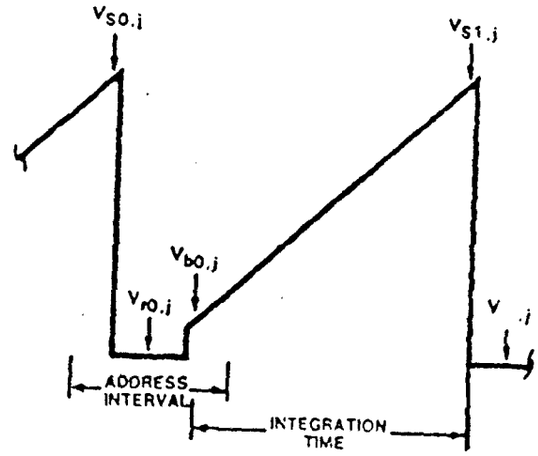


Fig. 5. Representation of the voltage across a single pixel during an integration interval at the detector node.

Fowler et al. Opt. Eng. 26(3) 232 (1987).

ORIGINAL PAGE IS OF POOR QUALITY

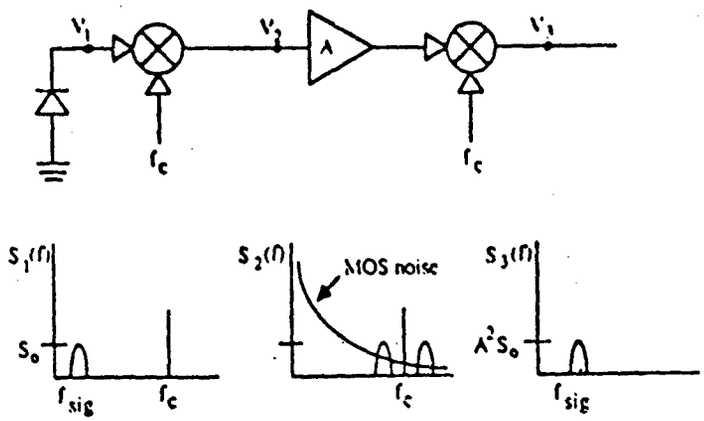


Fig. 8. Carrier modulation scheme used to upconvert detect signals to higher frequencies where MOSFET noise is low.

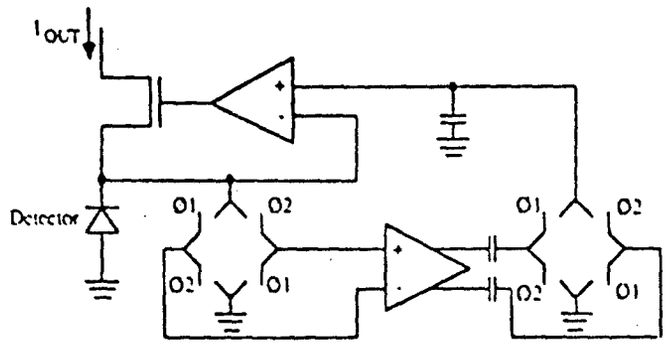


Fig. 9. Buffered common gate readout input circuit using chopp stabilization to reduce detector bias offsets and amplifier 1/f noi

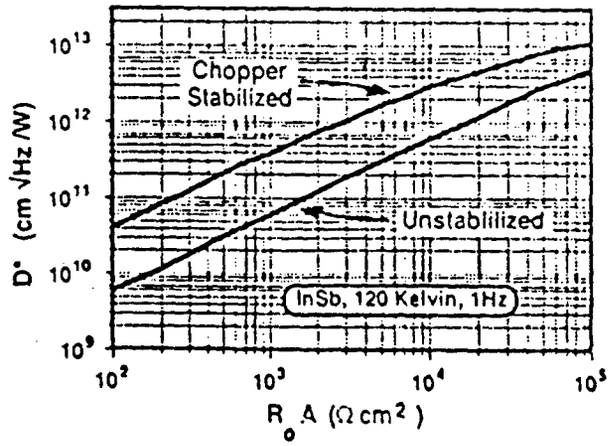


Fig. 10. Projected chopper-stabilized InSb focal plane perfc mance.

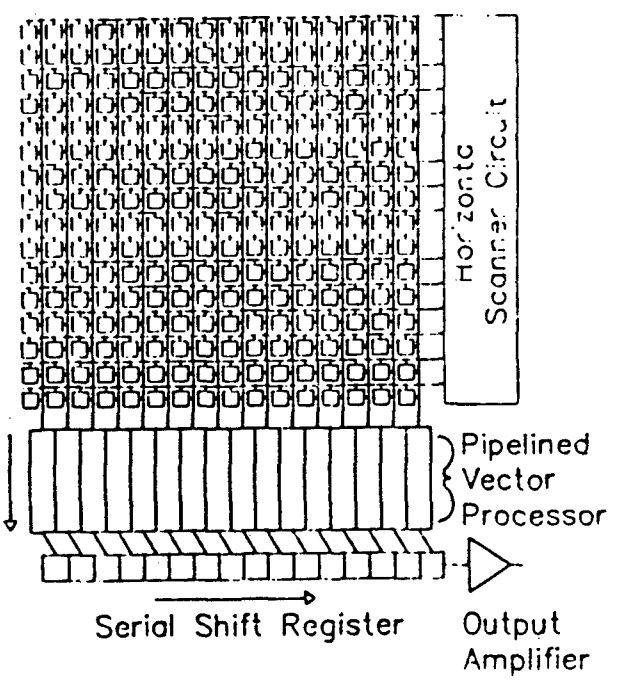
Lockwood and Parrish, Opt. Eng 26(3) 228 (1987).

IMAGE ACQUISITION

+ IMAGE PROCESSING

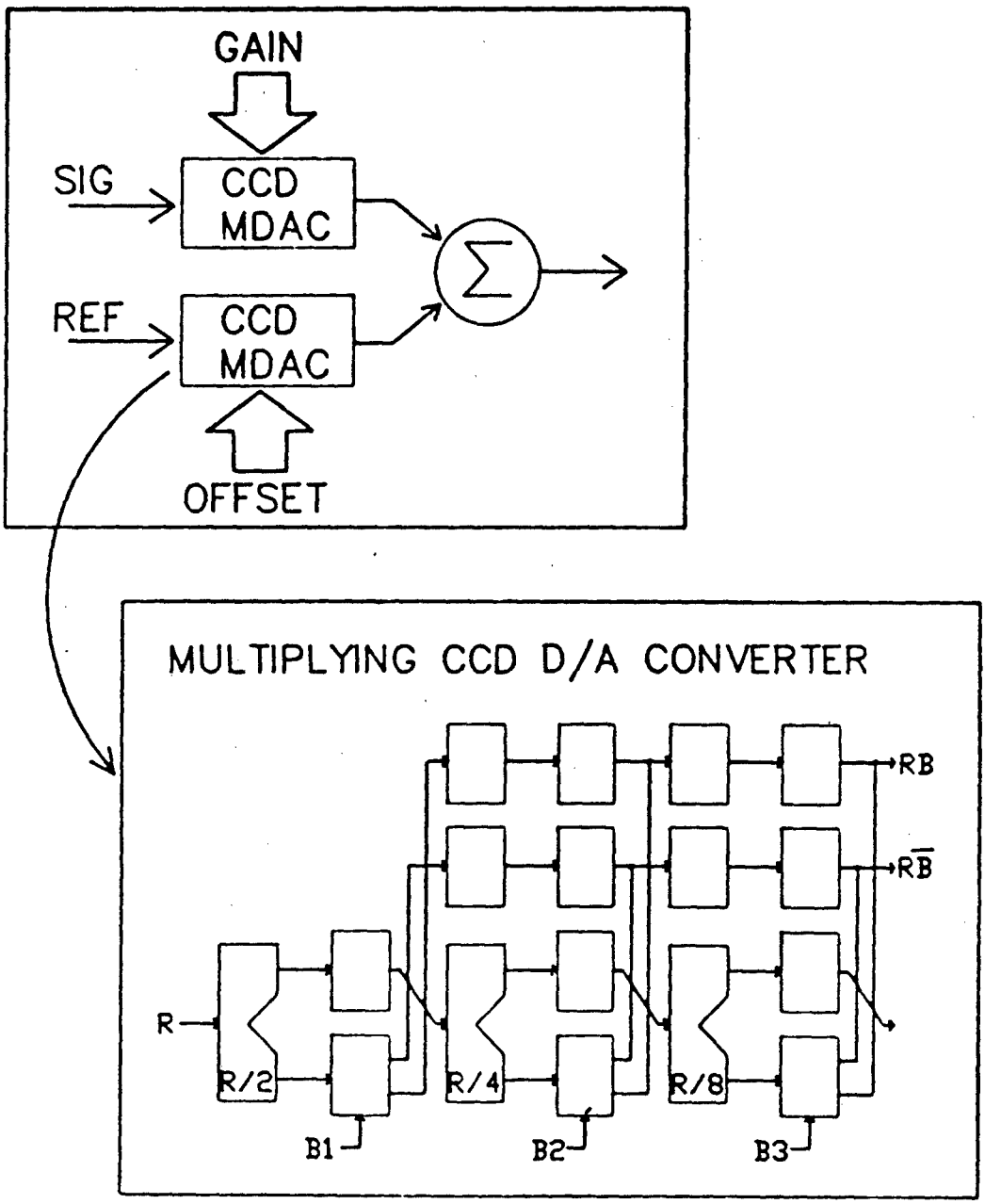
FOCAL PLANE IMAGE PROCESSING

WHY	WHY NOT
NOISE	YIELD
DISTORTION	CHIP SIZE
POWER	COOLING
SIZE	NON-UNIFORMITY CORRECTION
RELIABILITY	
COST	



ORIGINAL PAGE IS
OF POOR QUALITY

NON-UNIFORMITY CORRECTION



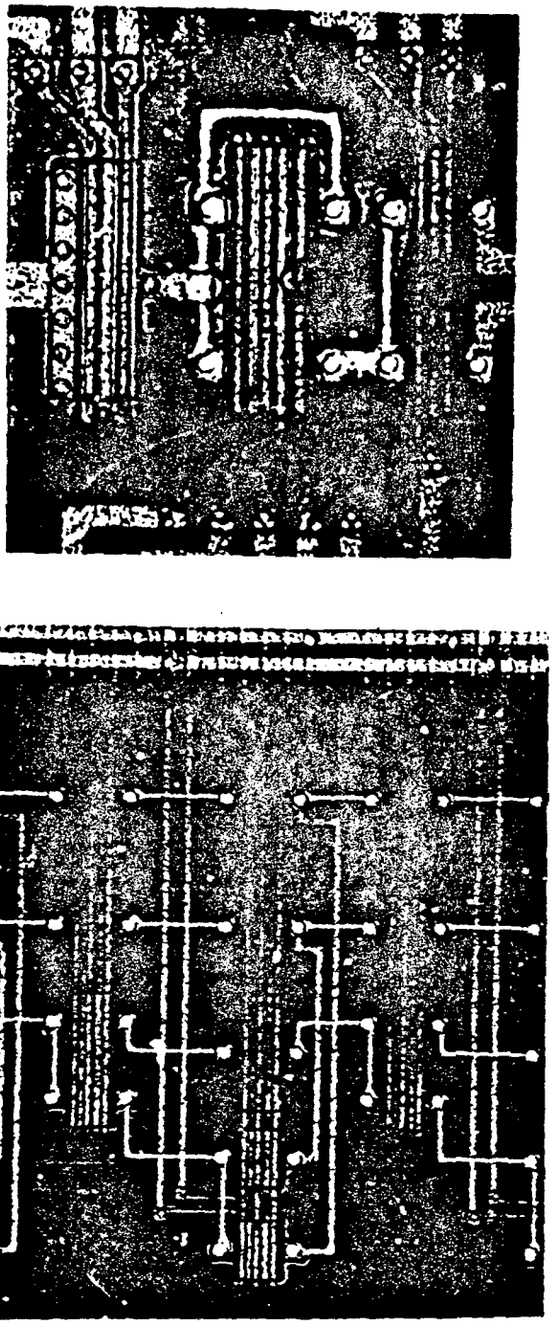


Fig. 2. Photograph of (a) serial recursive circuit and (b) single stage of pipeline circuit.

ORIGINAL PAGE IS
OF POOR QUALITY

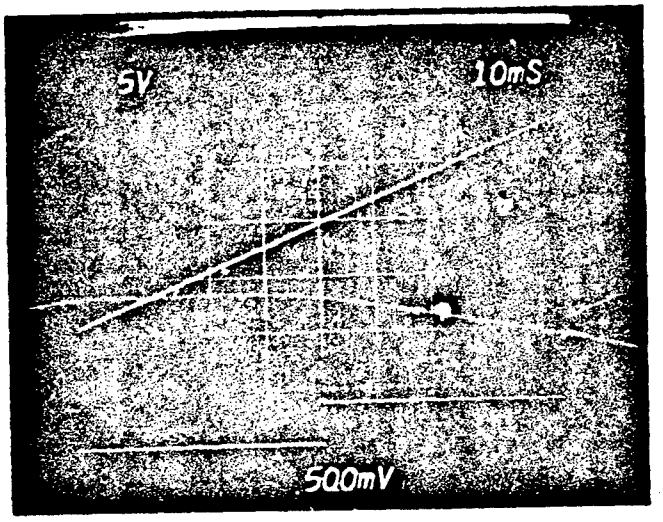


Fig. 3. Oscilloscope photograph showing analog output of pipeline programmable gain control circuit in response to a digital ramp (upper trace) and MSB of digital control word (lower trace).

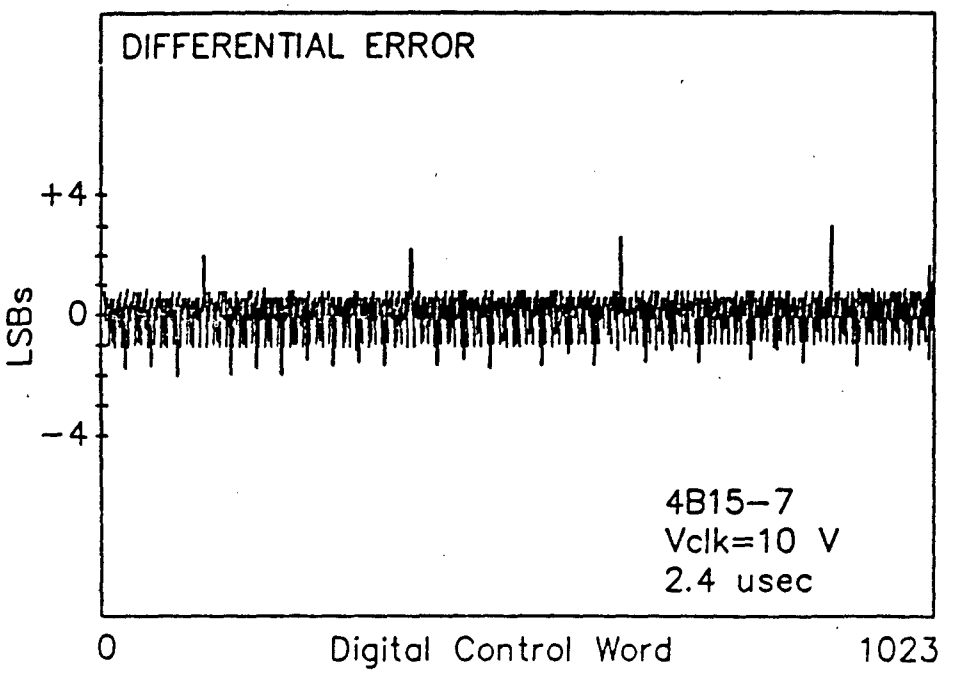


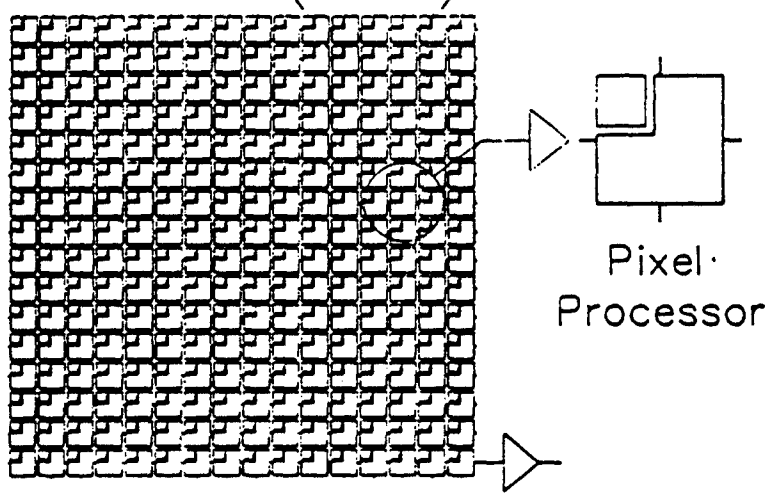
Fig. 4. Differential linearity error of pipeline circuit. Note that 1 LSB tic mark corresponds to 1/1024 of full scale.

CCD Programmable Gain Control Circuit

Performance Summary

	Pipeline	Serial
Technology	3 μ m CCD	3 μ m CCD
Circuit Size	0.4 mm^2	0.013 mm^2
Resolution	10 bits	variable
Integral Linearity	8 bits	6 bits
Differential Linearity	8 bits	6 bits
Clock Voltage	10 volts	10 volts
Bucket Cap. (electrons)	$5x10^6$	$5x10^6$
Power (10^3 conv/sec)	2 μ W	2 μ W
Max. Conversion Rate	$>8x10^6$/sec	$>0.5x10^6$/sec

Spatially Parallel Architecture (SIMD)



ORIGINAL PAGE IS
OF POOR QUALITY

FPA CCC POWER CONSIDERATIONS

TO TRANSFER 1 BUCKET (HALF FULL) $\Delta V = 10$ VOLTS

ENERGY = 8 pJ

ARRAY WITH 1500 PEs OPERATING IN PARALLEL

12 nJ

SAY EACH INSTRUCTION REQUIRES 10 TRANSFERS,
SAY 100 INSTRUCTIONS PER PIXEL TO PREPROCESS

12 μJ PER FRAME

SAY 1000 Hz FRAME RATE*

12 mW CHIP DISSIPATION

ADD IN DRIVERS, PARASITICS, MULTIPLY BY 2

25 mW

FOR 1 kHz REAL TIME PREPROCESSED IMAGERY

* AT 100 nsec/TRANSFER, CAN OPERATE AT 1MHz INSTRUCTION RATE, OR 10 kHz FRAME RATE POSSIBLE

NOISE CONSIDERATIONS

SAY BIAS = 10 V ⟶ 8 VOLT BUCKET

~250,000,000 ELECTRONS/HOLES

SAY WANT 8-BIT EQUIVALENT ACCURACY W/ SNR = 4 ON LSB

⟶ MAXIMUM NOISE ~ 250,000 CARRIERS

NOISE SOURCES:

1) CAPACITIVELY COUPLED CIRCUITS

$$n_{RMS} = \frac{(kTC)^{1/2}}{q} \leq 1000 \text{ CARRIERS}$$

2) TRANSFER

$$n_{RMS} = (2\,E\,R)^{1/2} \leq 5000 \text{ CARRIERS}$$

E: 0.05 FULL

3) INTERFACE

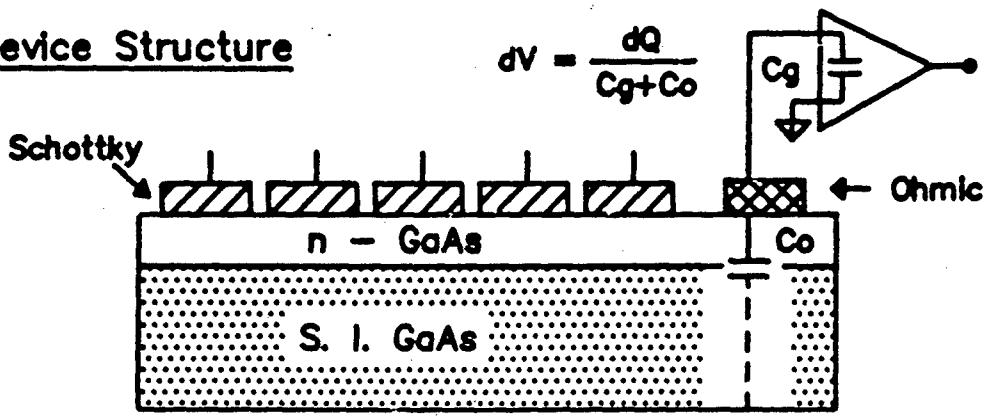
$$(1.4\,kTD_{IT}A_E)^{1/2} \leq 200 \text{ CARRIERS}$$

CCC PROGRAM, SAY 50 TRANSFERS AND 10 FILL & SPILLS

⟶ RMS 35,000 CARRIERS

WHY GaAs CCDs ?

Device Structure



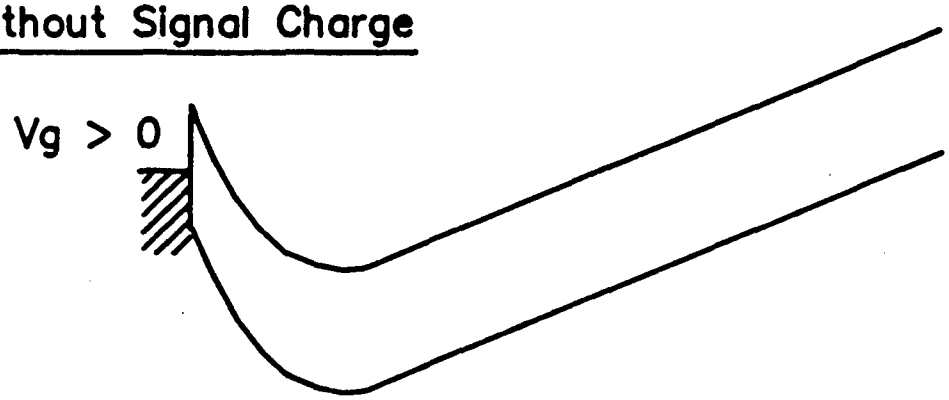
Features

- High Electron Mobility
  - High Transfer Speed
  - High f_t Transistors
- Wide Bandgap
  - Radiation Hard
  - Low Noise
- Semi–Insulating Substrate
  - Low Parasitic Capacitance
  - Mesa Isolation
- Compatibility with III–V Detectors

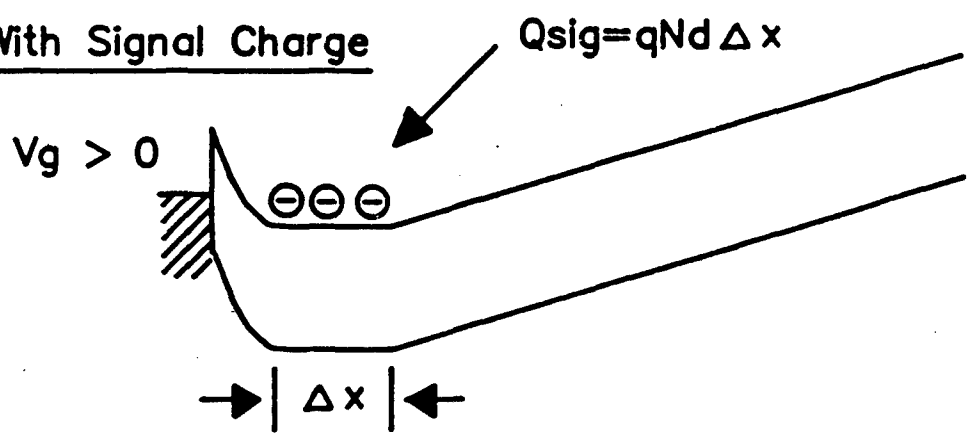
BAND DIAGRAM OF GaAs CCD



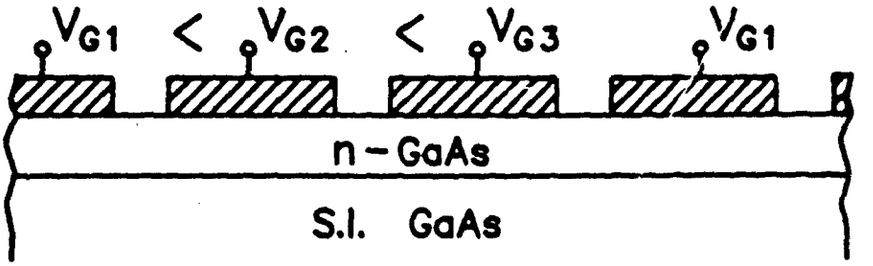
Without Signal Charge

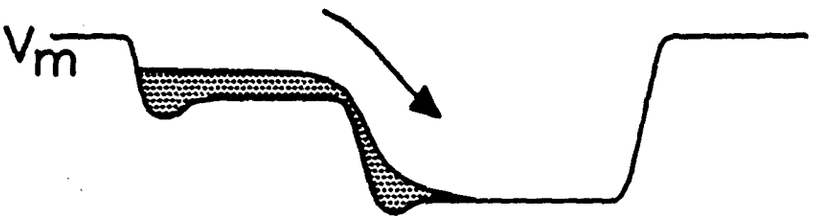


With Signal Charge

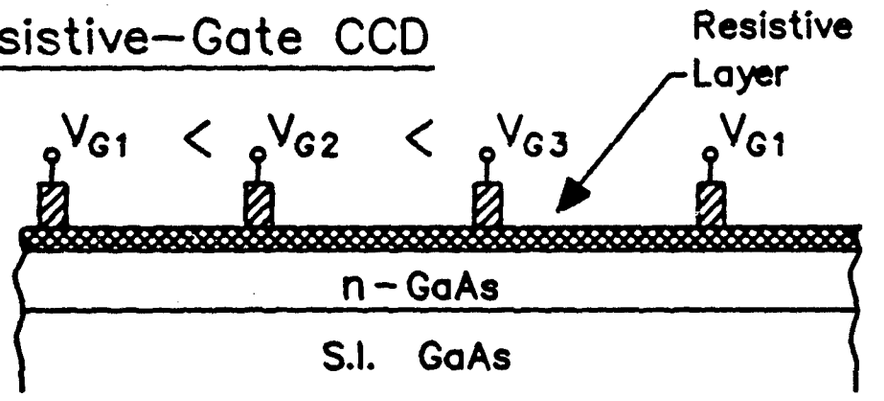


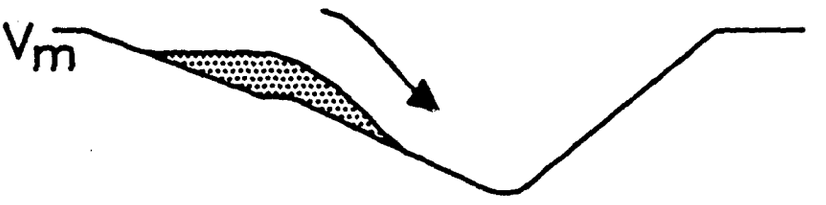
Capacitive-Gate CCD



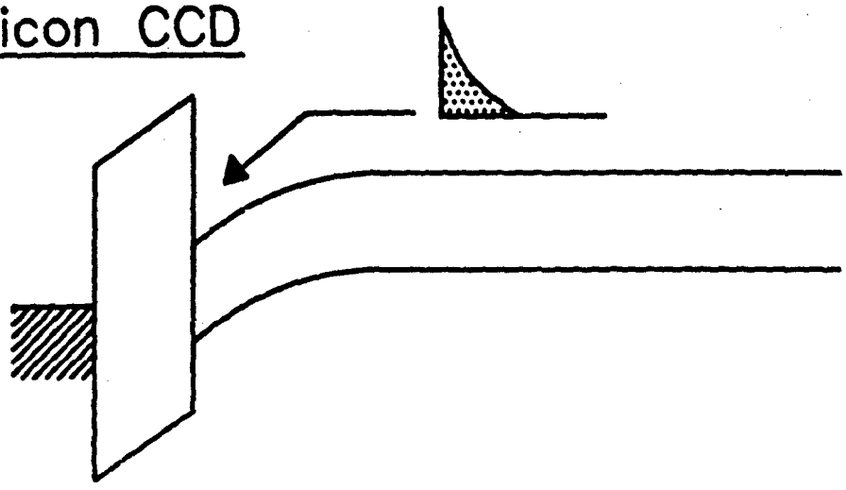


Resistive-Gate CCD



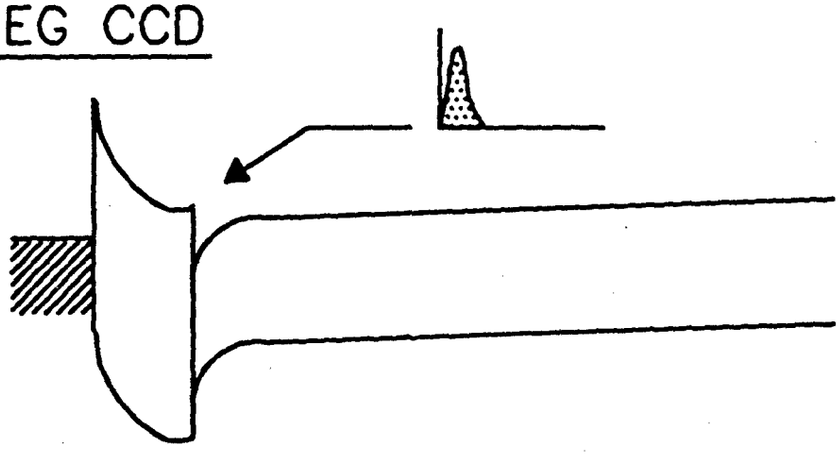


Silicon CCD



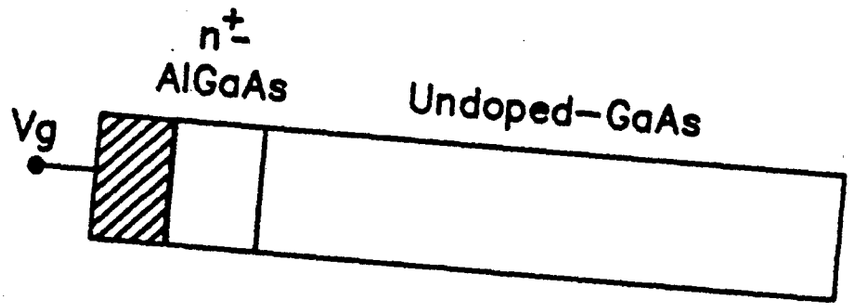
SiO_2 p–Type Silicon

2DEG CCD

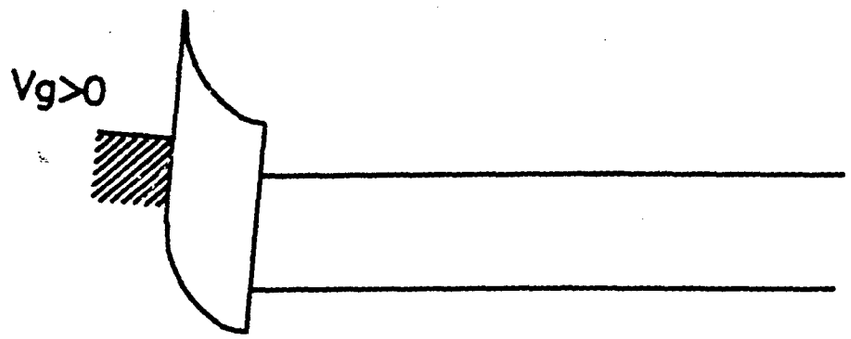


AlGaAs S. I. GaAs

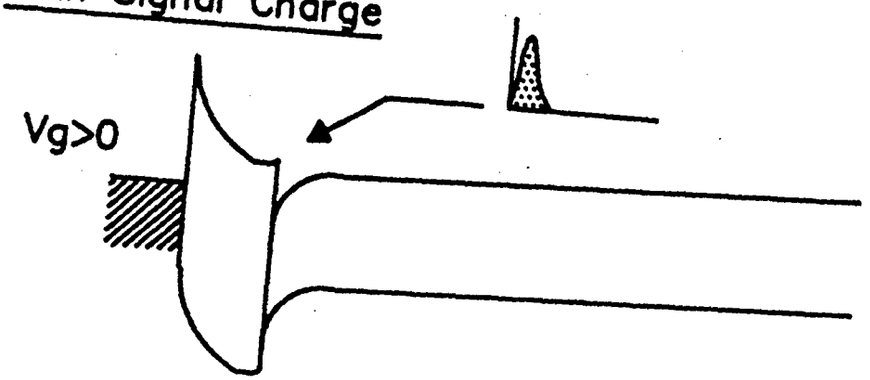
BAND DIAGRAM OF 2DEG CCD



Without Signal Charge

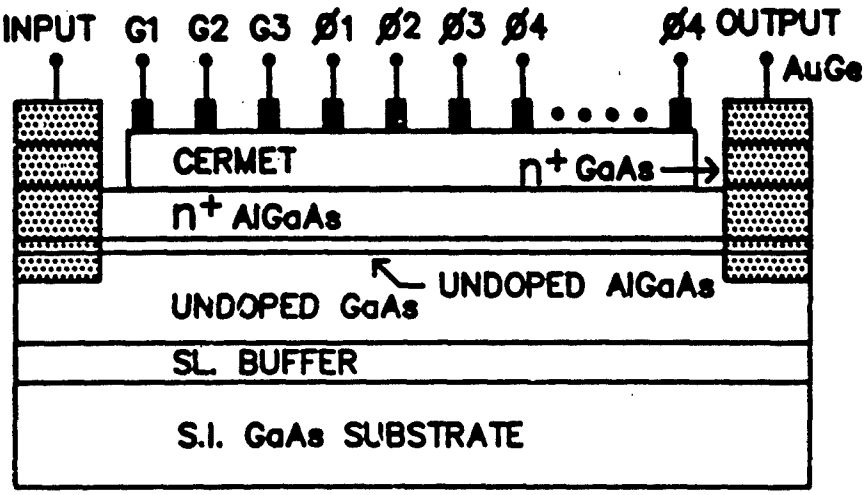


With Signal Charge



2DEG RGCCD

Device Structure



Features

- High Electron Mobility

  High Transfer Speed

  High Performance 2DEGFET
- Large Dynamic Range

  $n_s > 1 \times 10^{12} /cm^2$
- High Sensitivity Input
- Enhanced

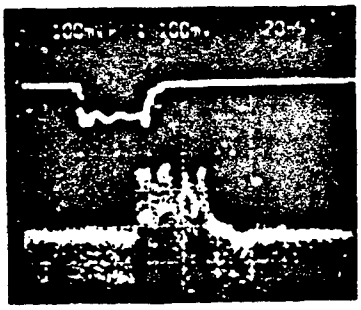
  Low Temperature Performance

OPERATION OF 2DEG RGCCDs

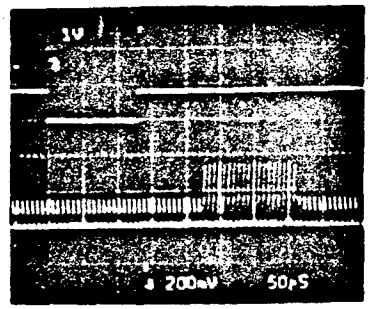
Room Temperature

4 Phase Clocking, 32 Stages (128 Transfers)

1 um Electrode Width, 4 um Spacing, 100 um Channel Width



Uniform-Doped 2DEG RGCCD
CTE = 0.999 At 1 GHz



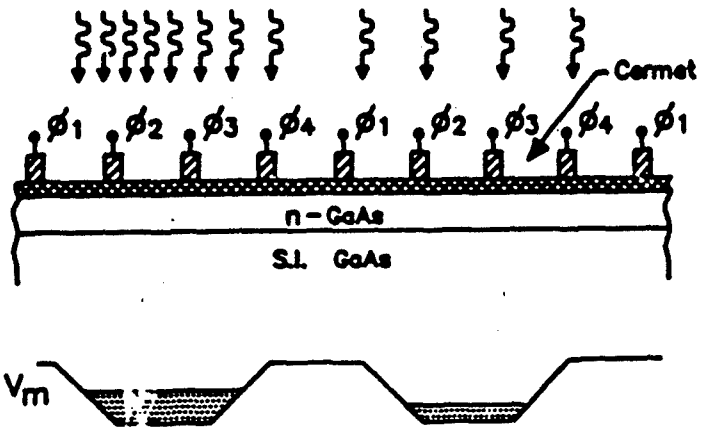
Planar-Doped 2DEG RGCCD
CTE > 0.999 At 133 KHz

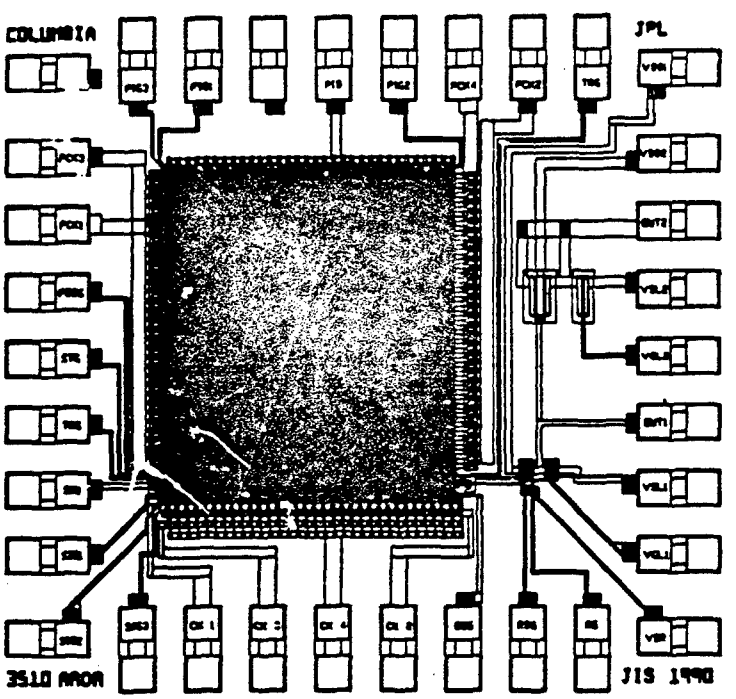
Advances in 2DEG CCDs

Year	Group	Channel Layer Material	Gate Structure	Gap Size	Gate Length x Width (um)	Clock Frequency	CTE	Test Conditions
1982	Rockwell	AlGaAs /GaAs	Capacitive	2	40 x 400	< 83 KHz	0.98	300 K
1983	Rockwell	AlGaAs /GaAs	Capacitive	1	5 x	< 83 KHz	< 0.9	300 K
							0.989	77 K
1990	Columbia	AlGaAs /GaAs	Resistive	N/A	5 x 100	13 MHz – 1 GHz	0.999	300 K
1990	Columbia	AlGaAs /GaAs (δ-Doped)	Resistive	N/A	5 x 100	130 KHz – 1 GHz	> 0.999	300 K
1990	Columbia	InAlAs / InGaAs (δ-Doped)	Resistive	N/A	5 x 100			

ORIGINAL PAGE IS
OF POOR QUALITY

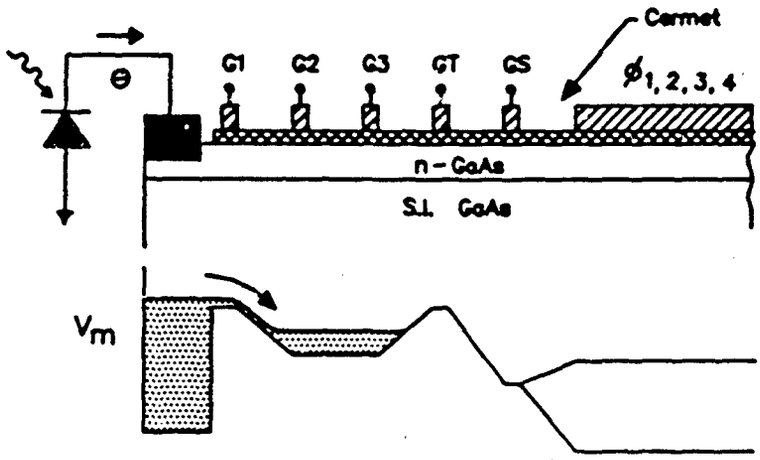
DIRECT DETECTION





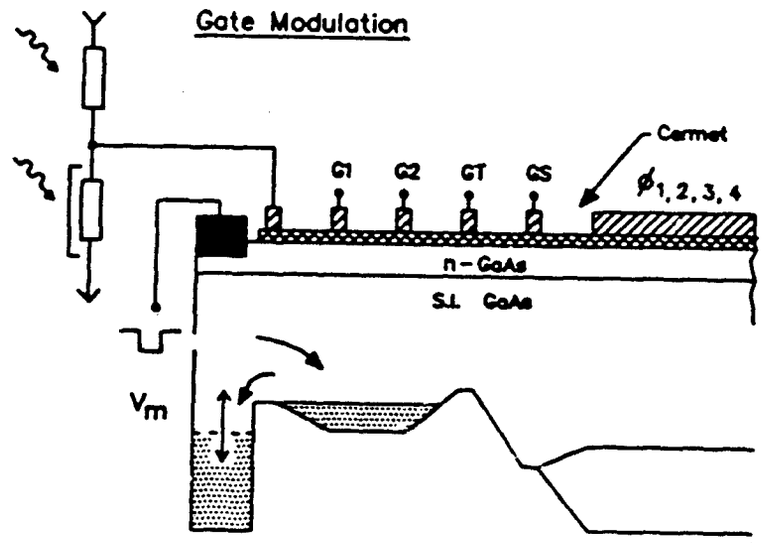
INDIRECT DETECTION

Direct Injection



INDIRECT DETECTION

Gate Modulation



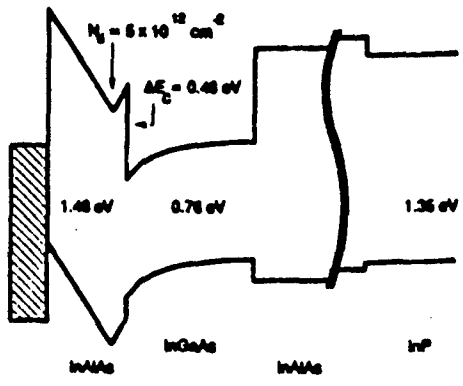
GaAs CCD MULTIPLEXER DESIGN

- Linear Arrays (32 Stages, RGCCD, CGCCD)
  - Direct Detection
  - Indirect Detection
    - Direct Injection
    - Gate modulation
- 2-D Arrays (32x32, RGCCD)
  - Direct Detection

RESEARCH ISSUES

- Leakage Current Reduction
  - Transport Mechanisms
  - Materials Quality
  - Structure
- Dynamic Range
  - Pinch Off Voltage
  - Leakage Current
- New Material System (InAlAs/InGaAs)
  - Higher Electron Mobility
  - Larger Dynamic Range

Planar-Doped In Al As / In Ga As RGCCD



- High Mobility ($\approx$20,000 $\frac{cm^2}{Vs}$ at 77 K)
- Large Sheet Carrier Density
- SWIR Direct Detection
- Compatible with Fiber-optic Integration

Present and Future Issues in Readout Electronics

Hybridization Technology
- center-to-center spacing
- array size
- buttability
- reliability

Multiplexer Material
- thermal match
- low 1/f noise devices

On-Chip Signal Processing
- random event correction
- detector non-uniformity correction
- image processing
- signature recognition

4/13/90 DWF

N91
14388
UNCLAS

N91-14388

Abstract

RADIATION RESPONSE ISSUES FOR INFRARED DETECTORS

Arne H. Kalma
MISSION RESEARCH CORPORATION
4935 North 30th Street
Colorado Springs, Colorado

One important issue facing space systems is survivability and operability in radiation environments. All space systems will be subject to the natural space environment, and most DoD and SDI systems must also be concerned with the much higher radiation environments produced by nuclear weapons. As a result, survivability and operability are necessary requirements that must be met by any space system.

Historically, infrared detectors (which are the key component in sensor subsystems) have been very vulnerable to nuclear radiation exposure. Most semiconductor components are subject to a variety of radiation-induced degradation mechanisms, and infrared detectors are no exception. In addition, high-quality infrared detectors are extremely sensitive detectors of optical photons, but this also makes them very sensitive to gamma photons, electrons, and protons.

Although some infrared detector technologies are less vulnerable to nuclear radiation than others, and hardening approaches have been developed for some of the technologies, there is no realistic expectation that the vulnerability problem will be completely eliminated for any infrared detector technology. Therefore, it is necessary to understand the vulnerability issues presented by nuclear radiation exposure, so that ones that impact sensor performance can be addressed.

In this paper, we will describe the most important radiation response issues for infrared detectors. In general, the two key degradation mechanisms in infrared detectors are the noise produced by exposure to a flux of ionizing particles (e.g.; trapped electrons and protons, debris gammas and electrons, radioactive decay of neutron-activated materials) and permanent damage produced by exposure to total dose. Total-dose-induced damage is most often the result of charge trapping in insulators or at interfaces. Exposure to short pulses of ionization (e.g.; prompt x-rays or gammas, delayed gammas) will cause detector upset. However, this upset is not important to a sensor unless the recovery time is too long. A few detector technologies are vulnerable to neutron-induced displacement damage, but fortunately most are not.

PRECEDING PAGE BLANK NOT FILMED

We will discuss the radiation responses of various infrared detector technologies, emphasizing where possible the responses of the newer technologies that are the subject of the Workshop. Because of the newness of most of these technologies, much of this will be analytical projections of the radiation response. In some cases, we will not even be able to accomplish the analytical predictions because of a lack of sufficient information about the use of the technology as an infrared detector. We will compare the responses of the newer technologies with those of the mainstream technologies of PV HgCdTe and IBC Si:As. One important reason for this comparison is to note where some of the newer technologies have the potential to provide significantly improved radiation hardness compared with that of the mainstream technologies, and thus to provide greater motivation for the pursuit of these technologies.

RADIATION RESPONSE ISSUES FOR INFRARED DETECTORS

PRESENTED AT:
INNOVATIVE LWIR DETECTOR WORKSHOP
JET PROPULSION LABORATORY

24-26 APRIL 1990

PRESENTED BY:
ARNE H. KALMA
MISSION RESEARCH CORPORATION
4935 N. 30TH STREET
COLORADO SPRINGS, COLORADO 80919

CONTRACT NO. F29601-88-C-0026
SUBCONTRACT NO. S-CUBED 1761/63003
MRC CONTRACT 86196

RADIATION HARDNESS IS A BASIC REQUIREMENT, NOT AN ADD-ON, FOR SPACE SYSTEMS

- NATURAL SPACE RADIATION ENVIRONMENT EXISTS AT ALL TIMES
  - NATURAL RADIATION ENVIRONMENT AROUND EARTH MAY BE RELATIVELY BENIGN, BUT LONG-DURATION MISSIONS CAN ACCUMULATE HIGH DOSE
  - NASA MISSIONS TO OUTER PLANETS CAN ENCOUNTER RADIATION ENVIRONMENTS MUCH HIGHER THAN EARTH'S
- SDI AND DoD SYSTEMS MUST SURVIVE THE NUCLEAR-ENHANCED ENVIRONMENTS
- IR DETECTORS WILL HAVE TO BE HARD, OR THEY WILL NOT BE USED FOR SPACE APPLICATIONS, PARTICULARLY IN THE SDS
  - ONE SHOULD NO LONGER ASSUME THAT ONE CAN DEVELOP A COMPONENT OR SUBSYSTEM, AND THEN THINK ABOUT HARDENING
- HARDENING MUST BE CONSIDERED FROM THE BEGINNING

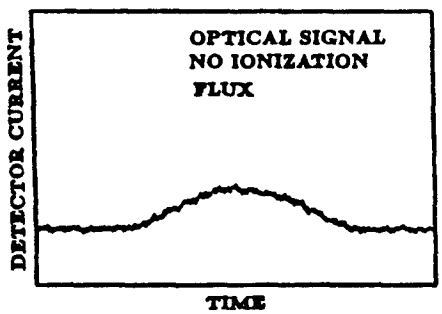


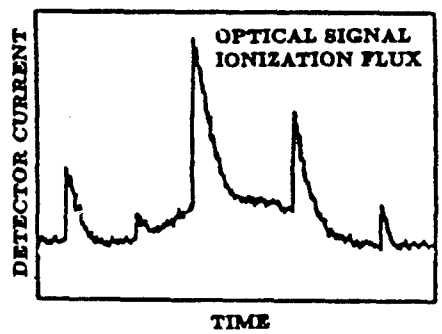
Mission Research Corporation

THERE ARE SEVERAL RADIATION HARDNESS ISSUES THAT ARE IMPORTANT

- OPERABILITY DURING EXPOSURE TO A FLUX OF IONIZING PARTICLES
  - TRAPPED ELECTRONS OR PROTONS, DEBRIS GAMMAS OR ELECTRONS, DECAY OF ACTIVATED MATERIALS, ETC.
- SURVIVABILITY FOLLOWING TOTAL-DOSE EXPOSURE
  - TRAPPED ELECTRONS OR PROTONS, PROMPT X-RAYS OR GAMMAS, DELAYED OR SECONDARY GAMMAS, ETC.
- UPSET/RECOVERY WHEN EXPOSED TO PROMPT PULSE
- SURVIVABILITY FOLLOWING NEUTRON EXPOSURE
- ISSUES THAT ARE MORE SYSTEM-RELATED WILL NOT BE DISCUSSED
  - OPERABILITY IN THE PRESENCE OF NUCLEAR-INDUCED OPTICAL CLUTTER
  - RECOOLING FOLLOWING NUCLEAR-INDUCED HEATING
  - SGEMP/IEMP

OPERABILITY IN A GAMMA-FLUX ENVIRONMENT REMAINS A KEY ISSUE FOR INFRARED SENSORS

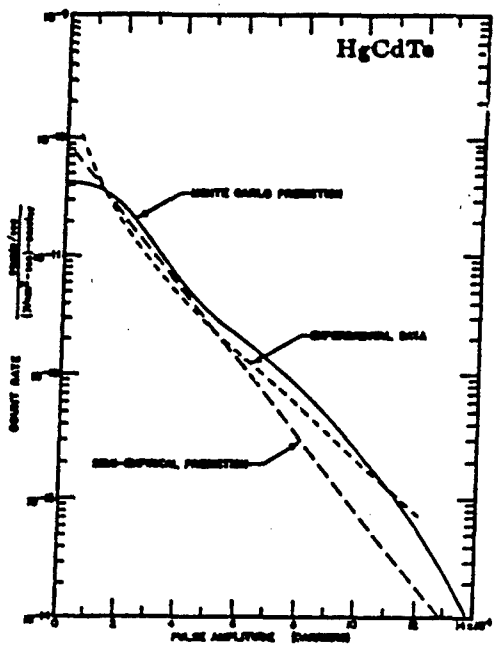




- DETECTORS ARE SO SENSITIVE THAT CHARGE DEPOSITED BY A SINGLE IONIZING PARTICLE CAN COMPLETELY MASK THE OPTICAL SIGNAL
- DETECTORS ARE RELATIVELY LARGE, SO EVENT RATES ARE HIGH
  - ALL PIXELS CAN BE CONTAMINATED AT RELATIVELY LOW FLUX

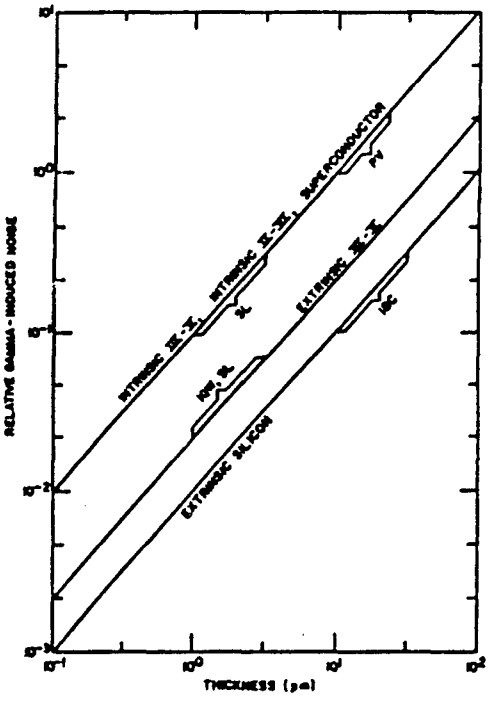
Mission Research Corporation

IONIZATION-INDUCED PULSES IN LWIR DETECTORS ARE PARTICULARLY LARGE



- DETECTORS ARE VERY SENSITIVE ANALOG DEVICES
- PULSES PRODUCED BY IONIZING PARTICLES CAN COMPLETELY MASK OPTICAL SIGNALS
  - $< n > \approx (E/L) \cdot < x > / \epsilon_p$
  - $R \approx \mu L < A_p > \gamma$
  - $i_n \approx 2e < n > (R(\Delta f))^{\frac{1}{2}}$
- EFFECT IS TRANSIENT, AND OCCURS ONLY WHEN DETECTORS ARE EXPOSED TO FLUX

SELECTION OF DETECTOR TECHNOLOGY CAN IMPACT OPERABILITY IN IONIZING-FLUX ENVIRONMENT

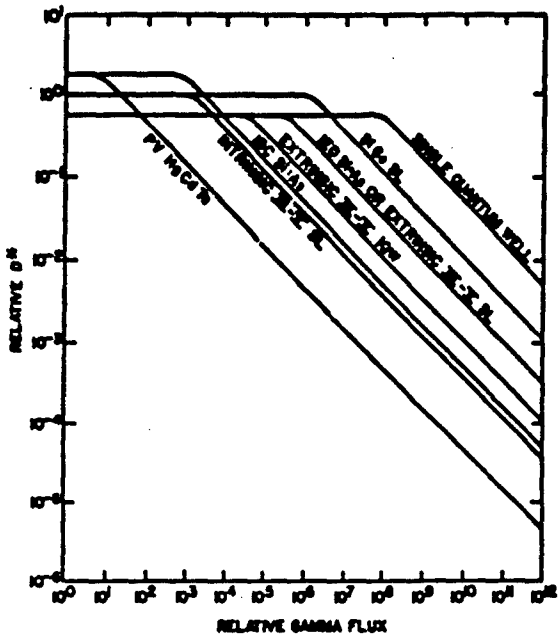


- HIGHER α FOR THINNER DETECTORS
- EXTRINSIC DETECTORS FOR HIGHER ϵ_p
  - ADVANCED HARDENING CONCEPTS ARE MORE LIKELY FOR EXTRINSIC DETECTORS

Mission Research Corporation

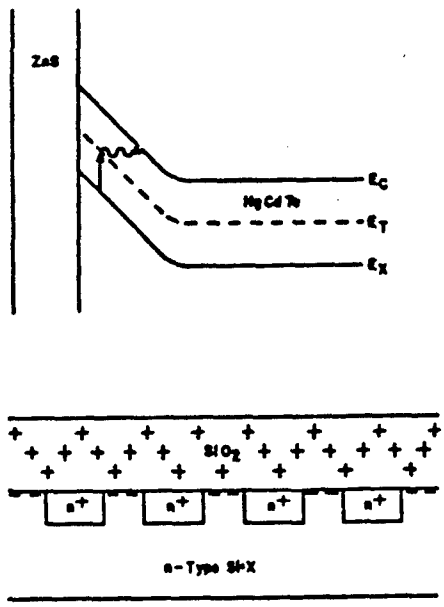
ORIGINAL PAGE IS OF POOR QUALITY

MANY OF THESE INNOVATIVE DETECTOR CONCEPTS GIVE PROMISE OF IMPROVED HARDNESS TO IONIZING PARTICLE FLUX



- PRIMARY ADVANCE IS DETECTOR THINNESS
- MOST OF CURVES BASED ON ANALYTICAL PREDICTIONS
- GaAs/AlGaAs QUANTUM WELL CURVE BASED ON EXPERIMENTAL DATA

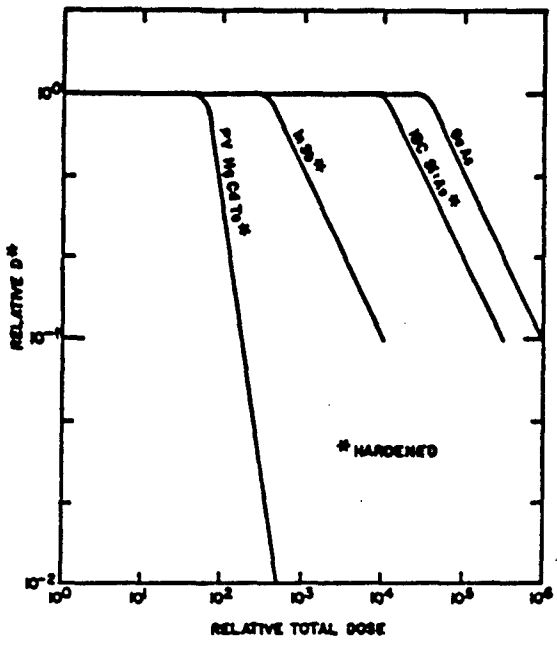
SURVIVABILITY FOLLOWING TOTAL-DOSE EXPOSURE IS ALSO AN IMPORTANT ISSUE



- DAMAGE MECHANISM IS TRAPPING OF RADIATION-INDUCED CHARGE IN INSULATORS OR AT INTERFACES
  - DAMAGE IS PERMANENT
- NARROW-BANDGAP SEMICONDUCTORS ARE PARTICULARLY VULNERABLE TO TUNNELING EFFECTS
- HIGH IMPEDANCE DEVICES ARE PARTICULARLY VULNERABLE TO SURFACE LEAKAGE

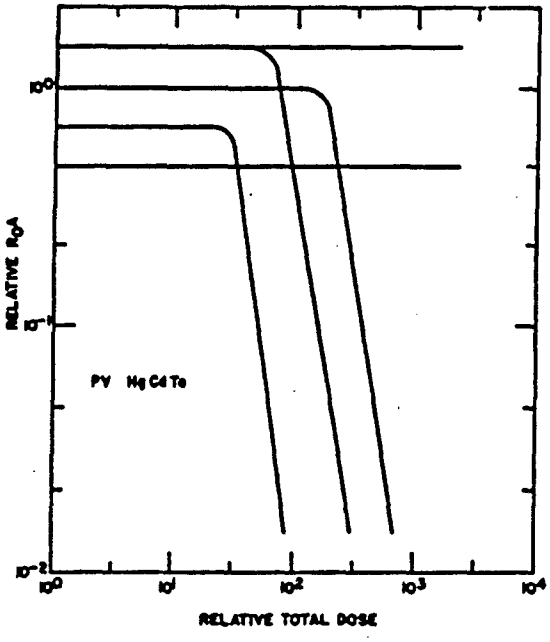
Mission Research Corporation

DETERMINING TOTAL-DOSE HARDNESS OF ANY TECHNOLOGY USUALLY ACCOMPLISHED ONLY BY EXPERIMENT



- MOST SEMICONDUCTOR TECHNOLOGIES WITH INSULATORS ARE VULNERABLE TO TOTAL DOSE
  - INCLUDES Si, Ge, AND MOST III-Vs
  - PINNED SURFACE POTENTIAL MAKES GaAs AN EXCEPTION
- HARDENING APPROACHES CAN BE DEVELOPED
  - TUNNELING MAKES PROBLEM MORE DIFFICULT FOR NARROW BANDGAP MATERIALS

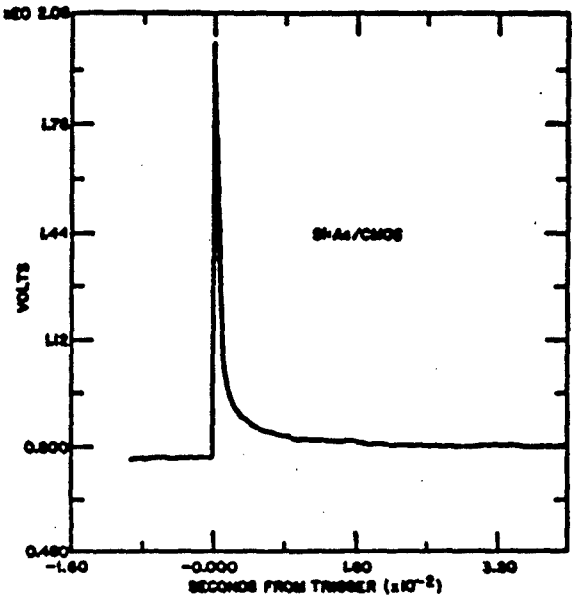
HARDENING OF HgCdTe AGAINST TOTAL-DOSE EXPOSURE HAS PROVEN TO BE PARTICULARLY DIFFICULT



- DAMAGE MECHANISM NOT WELL UNDERSTOOD
  - ANY OF SEVERAL DIFFERENT MECHANISMS CAN DOMINATE OBSERVED DAMAGE
- STANDARD HARDENING APPROACHES HAVE NOT BEEN EFFECTIVE
- HARDNESS HAS NOT BEEN REPEATABLE
  - VARIATION IN HARDNESS OFTEN OBSERVED IN SAME ARRAY
- ONE QUESTION IS WHETHER SIMILAR PROBLEMS WILL BE ENCOUNTERED FOR ANY NARROW-BANDGAP SEMICONDUCTOR

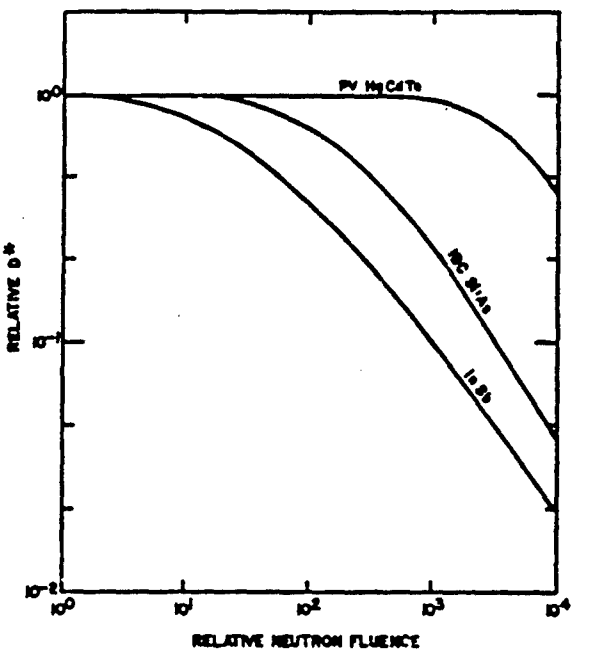
Mission Research Corporation

RECOVERY TIME IS KEY ISSUE FOR PROMPT-PULSE EXPOSURE



- UPSET THRESHOLD IS SO LOW THAT UPSET IS SURE TO OCCUR
  - ISSUE IS RELATIVELY INDEPENDENT OF DETECTOR TECHNOLOGY
  - SYSTEMS MUST BE DESIGNED TO IGNORE THIS UPSET
- RECOVERY, ESPECIALLY IN MULTI-BURST ENVIRONMENT, IS KEY
- READOUT OFTEN GOVERNS RECOVERY OF FPA, BUT DETECTOR RECOVERY MUST BE CONSIDERED
  - RECOVERY AT CRYOGENIC TEMPERATURE CAN BE LONG

MOST DETECTOR TECHNOLOGIES ARE RELATIVELY HARD TO NEUTRON EXPOSURE



- PERMANENT DEGRADATION PRODUCED BY NEUTRON-INDUCED DISPLACEMENTS
- Si:X AND InSb ARE EXCEPTIONS
- ANALYTICALLY PREDICTING THE NEUTRON RESPONSE OF A NEW TECHNOLOGY IS DIFFICULT

Mission Research Corporation

SUMMARY

- RADIATION HARDNESS IS ONE OF THE BASIC REQUIREMENTS FOR LWIR DETECTOR TECHNOLOGIES DEVELOPED FOR SPACE APPLICATIONS
- IONIZING-PARTICLE-FLUX AND TOTAL-DOSE HARDNESS ARE THE MOST IMPORTANT OPERABILITY/SURVIVABILITY ISSUES
  - THESE ISSUES EXIST FOR BOTH NATURAL-SPACE AND NUCLEAR-WEAPON-ENHANCED ENVIRONMENTS
- RECOVERY FOLLOWING PROMPT-PULSE EXPOSURE AND SURVIVABILITY FOLLOWING NEUTRON EXPOSURE ARE SECONDARY ISSUES FOR MOST DETECTOR TECHNOLOGIES
  - RECOVERY TIME IN MULTI-BURST ENVIRONMENT CAN BE IMPORTANT
  - THESE ISSUES ONLY EXIST FOR NUCLEAR-WEAPON-ENHANCED ENVIRONMENTS
- MANY OF THE PROPOSED INNOVATIVE TECHNOLOGIES HAVE POTENTIAL HARDNESS ADVANTAGES OVER THE EXISTING MAINSTREAM TECHNOLOGIES OF HgCdTe AND IBC Si:As



Mission Research Corporation

SESSION IV: High Performance Thermal Detectors

IV - 1 Fabrication of Sensitive High TCBolometers
M. Nahum, University of California, Berkeley

IV - 2 Pyroelectric Detectors
E. Haller, Lawrence Berkeley Laboratory

IV - 3 A Novel Electron Tunneling Infrared Detector
T.W. Kenny, Jet Propulsion Laboratory

PRECEDING PAGE BLANK NOT FILMED

N91
14389
UNCLAS

N91-14389

FABRICATION OF SENSITIVE HIGH T_c BOLOMETERS*

M. Nahum, S. Verghese, Qing Hu†, and P.L. Richards
Department of Physics, University of California,
and Materials and Chemical Sciences Division,
Lawrence Berkeley Laboratory, Berkeley, CA 94720

K. Char, N. Newman, and S.A. Sachtjen
Conductus Inc., Sunnyvale, CA

The rapid change of resistance with temperature of high quality films of high T_c superconductors can be used to make resistance thermometers with very low temperature noise. Measurements on c-axis YBCO films have given a spectral intensity of temperature noise less than $4x10^{-8}$ K/Hz$^{1/2}$ at 10 Hz. Consequently, the opportunity exists to make useful bolometric infrared detectors that operate near 90 K which can be cooled with liquid nitrogen. This talk will summarize the fabrication and measurement of two bolometer architectures. The first is a conventional bolometer which consists of a 3000 Å thick YBCO film deposited *in situ* by laser ablation on top of a 500 Å thick $SrTiO_3$ buffer layer on a {1012} Al_2O_3 substrate. The sample was lapped to 20 μm thickness and diced into 1x1 mm^2 bolometer chips. Gold black smoke was used as the radiation absorber. The voltage noise was less than the amplifier noise when the film was current biased. Optical measurements gave an NEP of $5x10^{-11}$ W/Hz$^{1/2}$ at 10 Hz. The second architecture is that of an antenna-coupled microbolometer which consists of a small (5x10 μm^2) YBCO film deposited directly on a bulk substrate with a low thermal conductance (YSZ) and an impedance matched planar lithographed spiral or log-periodic antenna. This structure is produced by standard photolithographic techniques. Measurements gave an electrical NEP of $4.7x10^{-12}$ W/Hz$^{1/2}$ at 10 kHz. Measurements of the optical efficiency are in progress. The measured performance of both bolometers will be compared to other detectors operating at or above liquid nitrogen temperatures so as to identify potential applications.

* Supported in part by the Director, Office of Energy Research, Office of Basic Energy Sciences, Materials Sciences Division of the U.S. Department of Energy under contract No. DE-AC03-76SF00098, and by the Department of Defense.
† Present address: Department of Electrical Engineering and Computer Science and Research Laboratory of Electronics, MIT.

PRECEDING PAGE BLANK NOT FILMED

Fabrication of Sensitive High Tc Bolometers

M. Nahum

Dept. of Physics, University of California, Berkeley
and Materials and Chemical Sciences Division,
Lawrence Berkeley Laboratory

Berkeley

Qing Hu (MIT)
M. Nahum
P. L. Richards
S. Verghese

Conductus Inc., Sunnyvale, CA

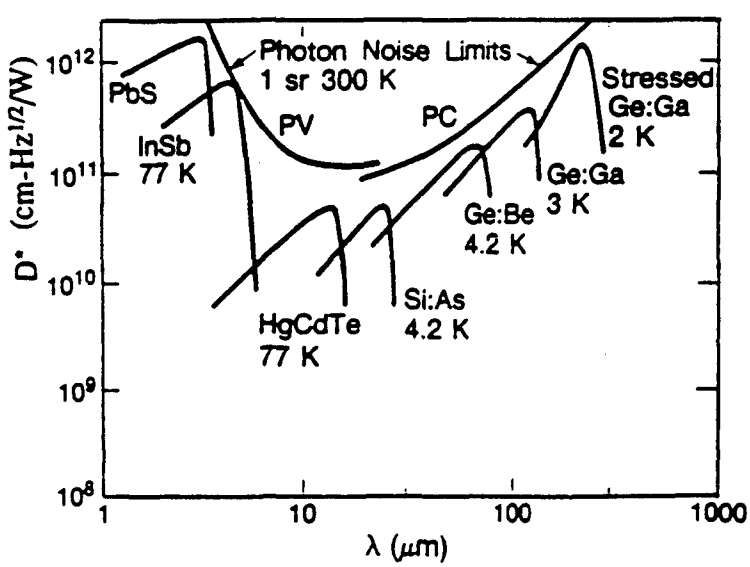
K. Char
N. Newman
S. A. Sachtjen

Outline

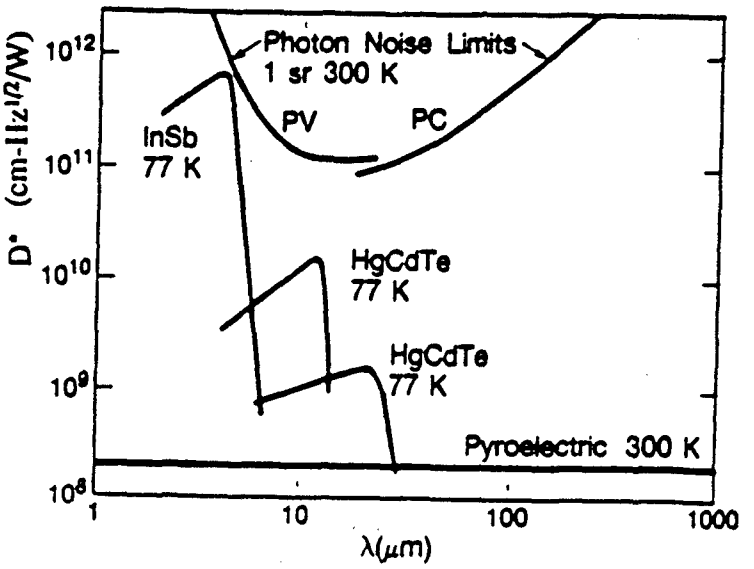
- Motivation and applications
- Conventional composite bolometer
- Microbolometer
- Conclusions

High background applications

Performance ($D^* = AREA^{1/2}/NEP$) of commercial photon detectors viewing 300K source.

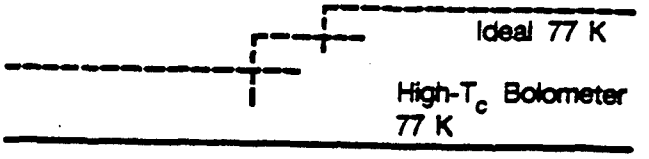


Performance available at or above 77K



Applications above 77K:

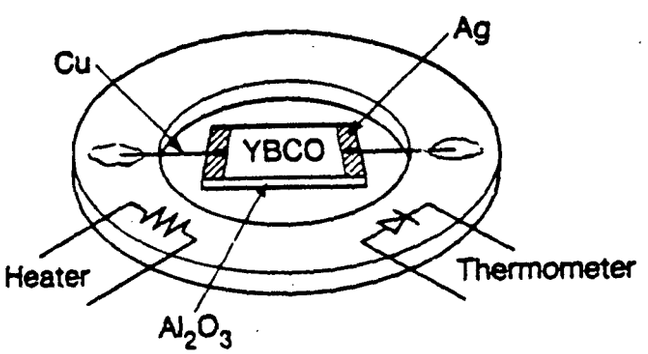
- Laboratory IR spectrometers
- Earth observations from space

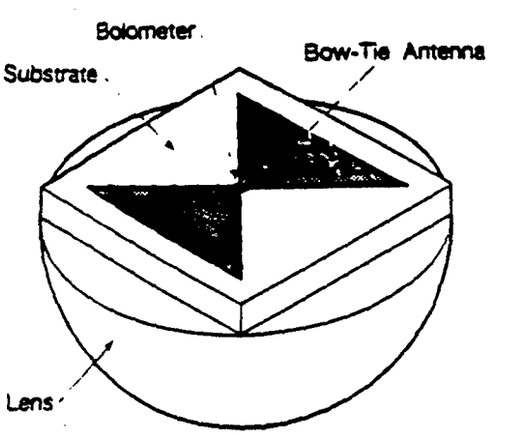


P. L. Richards et al, *Appl. Phys. Lett.* 54, 283 (1989).

Elements of high Tc infrared bolometers

	Conventional Bolometer	Microbolometer
Substrate	sapphire	yttria stabilized zirconia (YSZ)
Radiation absorber	gold black Bi film	antenna-coupled YBCO
Thermometer R(T)	YBCO	YBCO
Thermal conductance G	Cu leads	thermal spreading resistance





The high T_c conventional bolometer

- Easy to make one that "works".
- Hard to get useful sensitivity.
- Good ones can be made now.
- Materials needs very specific.
- Low-noise and high $\frac{1}{R}\frac{dR}{dT}$.
- Proper optimization.

Fabrication

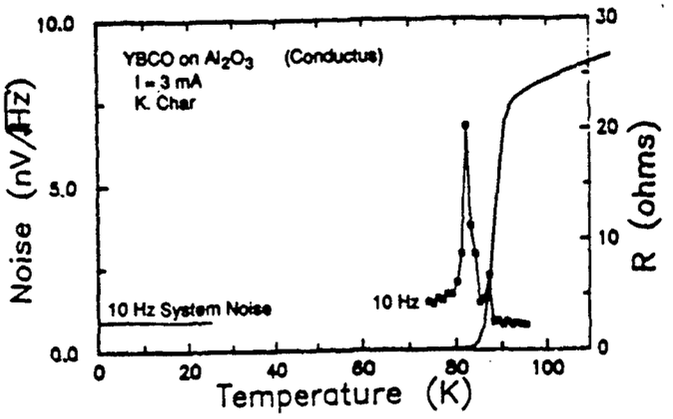
- Substrate 1X1 mm^2, 20 μm thick, { $1\bar{1}02$ } sapphire.
  - Low specific heat
  - Strong
  - YBCO compatible
- Laser ablate 3000 Å YBCO on a 500 Å $SrTiO_3$ buffer layer on 6X6X0.5 mm^3 sapphire.
- Sputter clean YBCO surface and sputter deposit Ag electrical contacts.
- Polish and dice.

Sensitivity ⇒ YBCO film quality

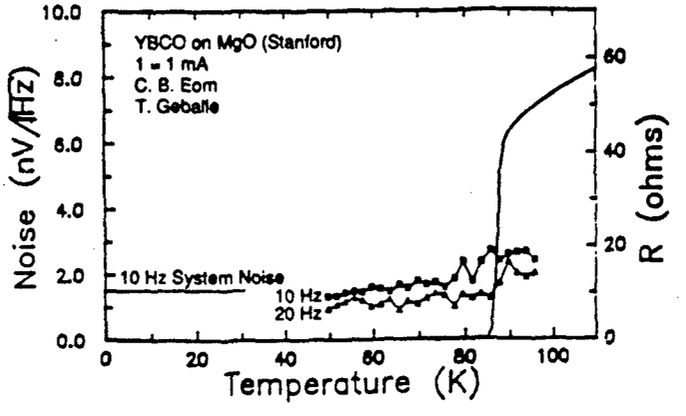
high $\frac{1}{R}\frac{dR}{dT}$, low noise

- Laser ablating YBCO on sapphire gives sharp resistive transitions (K. Char et al, *Appl. Phys. Lett.*, 56. 785 (1990)).

- But there is excess voltage noise near T_c under current bias in these films.



- Using the 500Å $SrTiO_3$ buffer layer ⇒ reduced voltage noise.



Bolometer optimization

Given: $\frac{1}{R}\frac{dR}{dT}$, C -- heat capacity

Pick:
- I -- current bias
- R -- operating resistance
- G -- thermal conductance
- ω -- chopping frequency

$$NEP = \left(4kT^2G + \frac{4kTR + V_{amp}^2 + V_{1/f}^2}{|S|^2} \right)^{1/2}$$

$$S = I \frac{dR(T)}{dT} |G + i\omega C|^{-1} , \qquad I^2R < 0.3G\delta T \text{ for stability .}$$

δT -- transition width

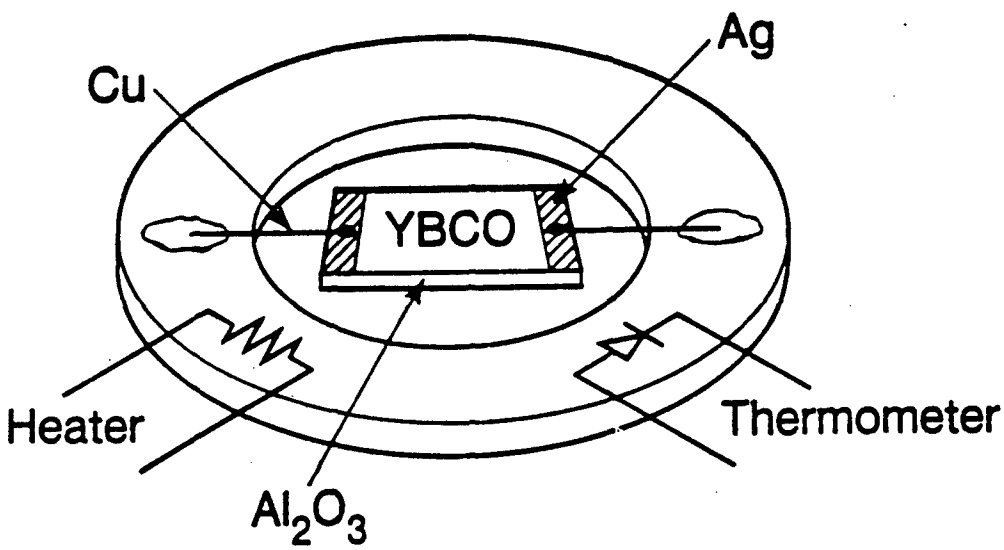
For a sapphire bolometer:

$\omega/2\pi = 10$ Hz 1X1X0.02 mm^3 sapphire

$\delta T = 0.5$ K NEP $\leq 10^{-11}$ W/Hz$^{1/2}$

PRECEDING PAGE BLANK NOT FILMED

Measurements

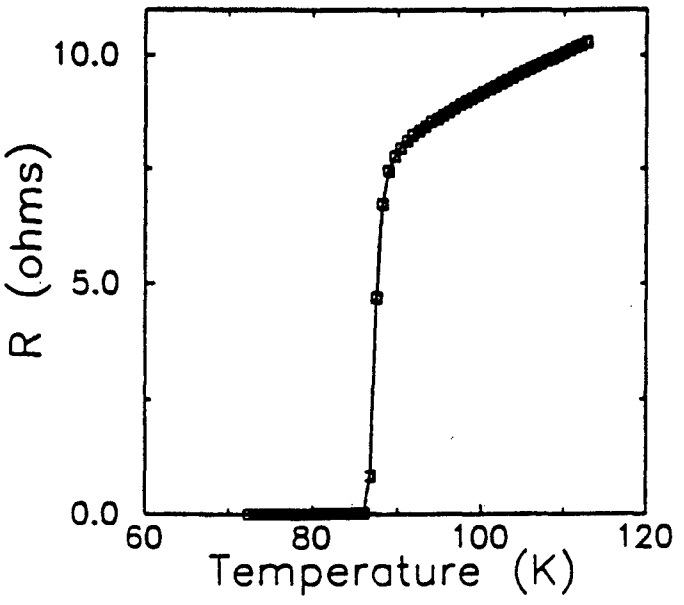


Typical Size 1×1 mm

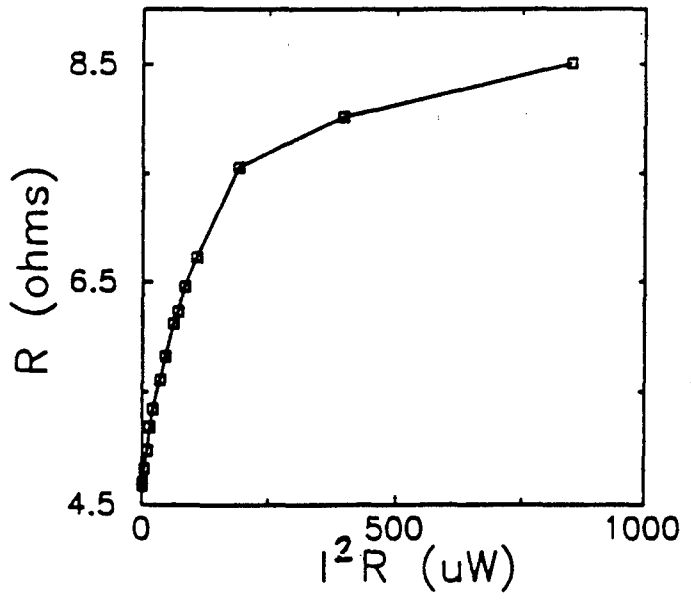
- R(T) and load curve ⇒ $S_{electrical}$ = 26 V/W , 10 Hz
- Chopped He-Ne laser ⇒ $S_{optical}$ = 22 V/W , 10 Hz
- At present, noise is amplifier limited ⇒ NEP = 5×10^{-11} W/$Hz^{1/2}$, 10 Hz

Electrical measurements

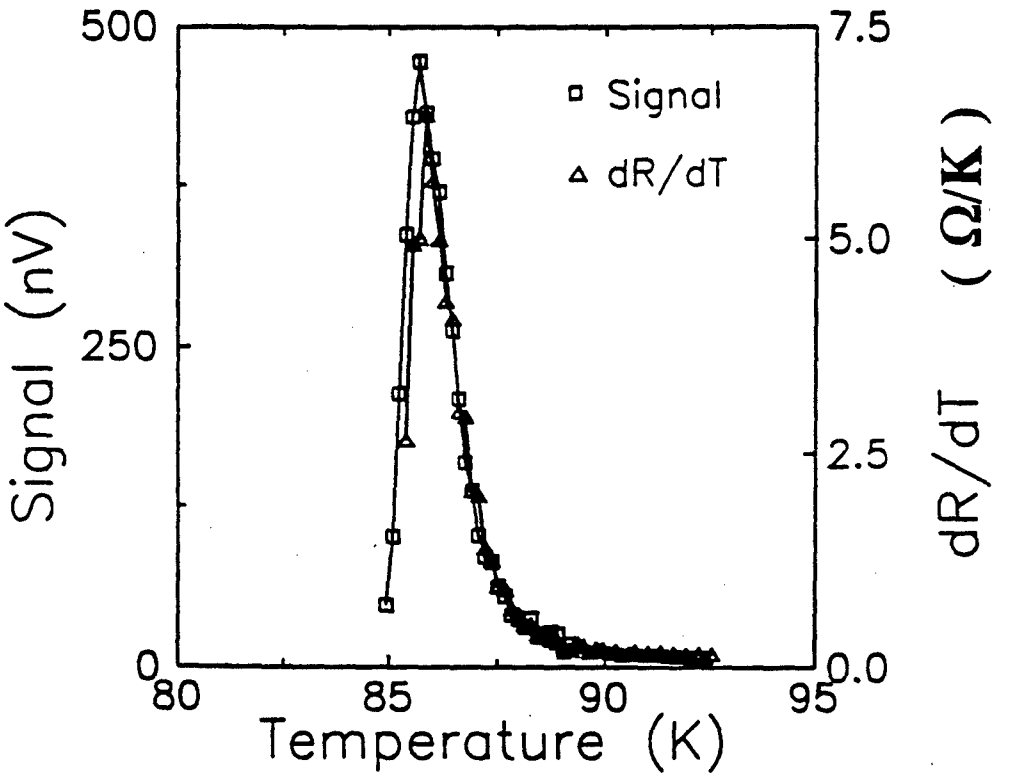
Bolometer R(T)

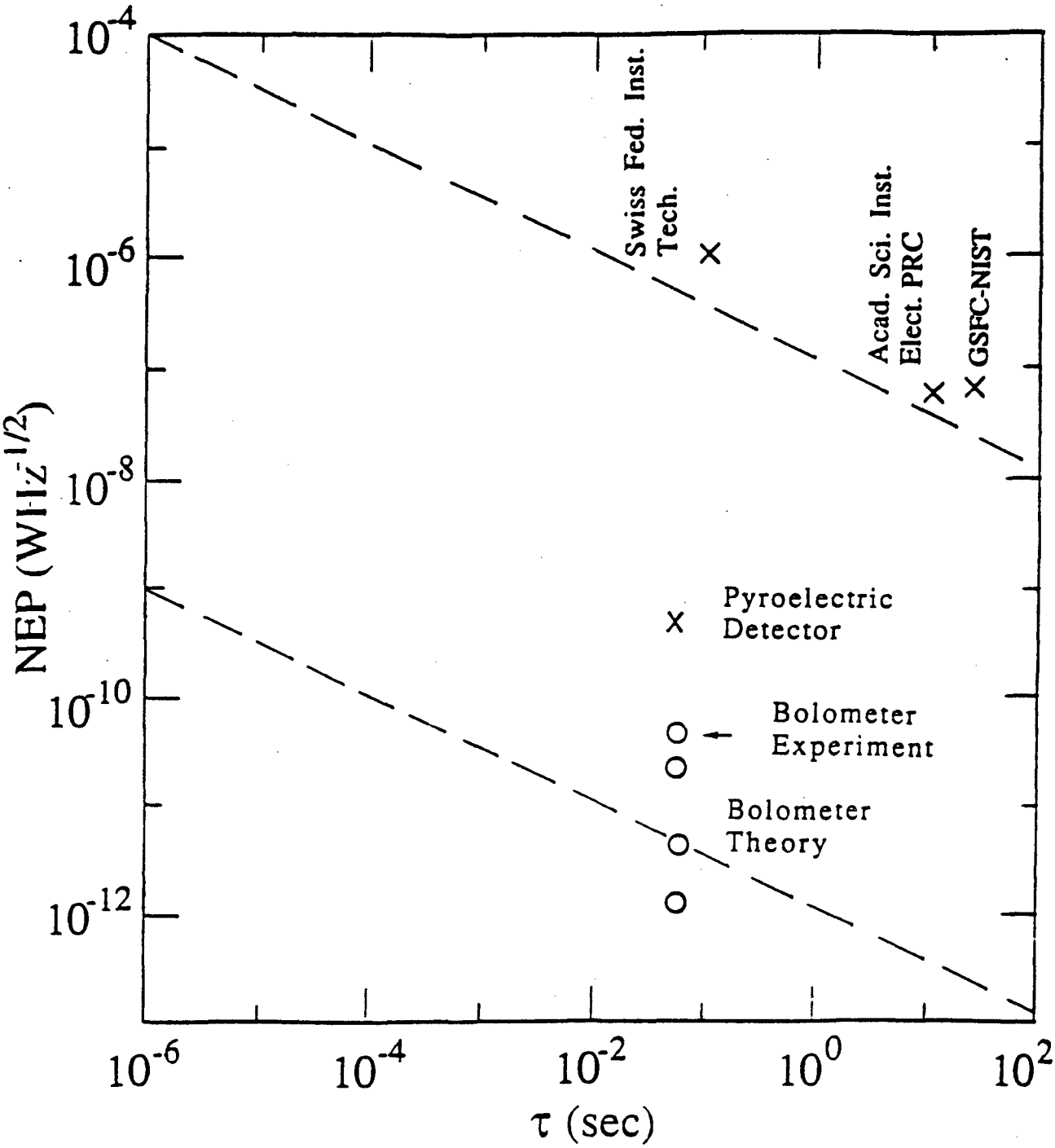


Load Curve



Optical response




10^{-4}
10^{-6}
10^{-8}
10^{-10}
10^{-12}
NEP ($W Hz^{-1/2}$)
10^{-6}
10^{-4}
10^{-2}
10^{0}
10^{2}
τ (sec)
Swiss Fed. Inst. Tech.
Acad. Sci. Inst. Elect. PRC
GSFC-NIST
Pyroelectric Detector
Bolometer Experiment
Bolometer Theory

XBL 903-5434

High Tc Microbolometer

Sensitive and fast

- Small area ($A \approx 5\ \mu m^2$)
- Deposited directly on thick substrate
- Only small volume of substrate contributes thermally ($V \approx 10\ \mu m^3$)
- NEP α $A^{1/4}$
- Response time α A
- Couple directly $\lambda < 2\ \mu m$
- Couple with antenna $\lambda > 100\ \mu m$
- Array compatible fabrication

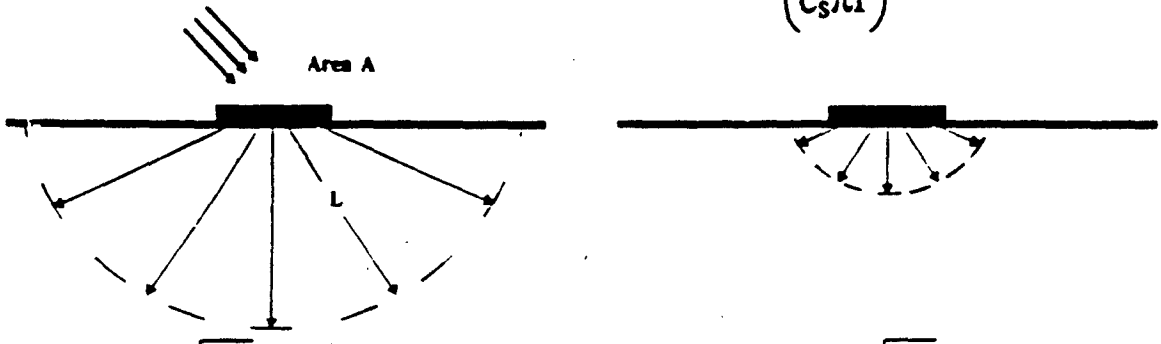
Qing Hu and P. L. Richards, *Appl. Phys. Lett.* **55**, 2444 (1989).

Idea from: Hwang, Schwarz, Rutledge
Neikirk, Lam, Rutledge
Rutledge, Neikirk, Kasilingam

Microbolometer thermal response

$NEP = (4kT^2G(f))^{1/2}$, $G(f) = ?$

Diffusion length $L = \left(\frac{\kappa_s}{c_s \pi f}\right)^{1/2}$



$L > \sqrt{A}$

$G = \sqrt{2\pi A}\,\kappa_s$

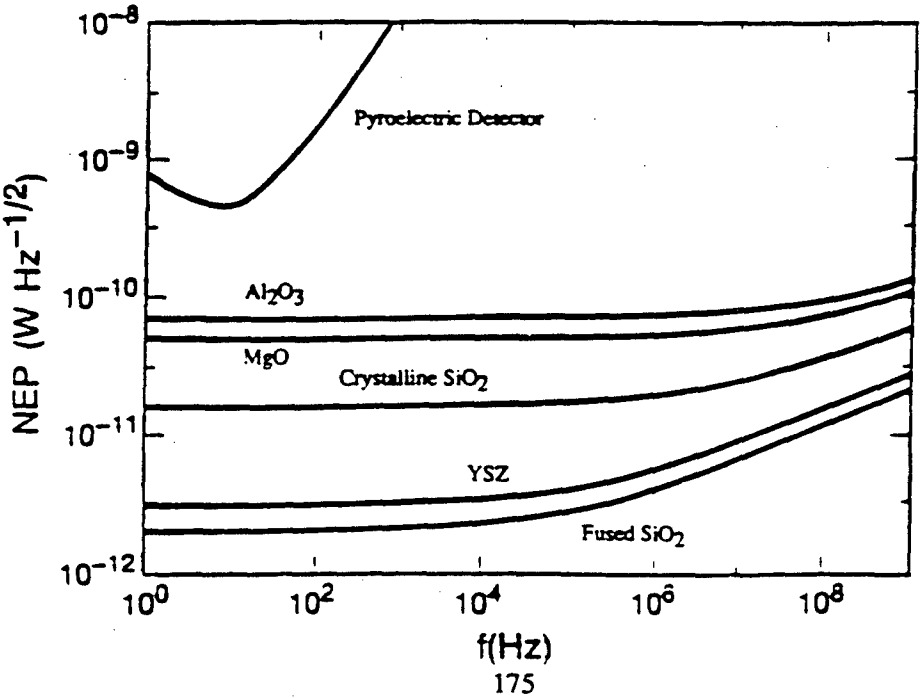
$NEP \alpha A^{1/4}$

$L < \sqrt{A}$

$G = \sqrt{2\pi}\,A(\kappa_s c_s f)^{1/2}$

$NEP \alpha A^{1/2} f^{1/4}$

Calculated NEP (Area = 1X5 μm^2)



How to couple long wavelengths into a small bolometer?

- Antenna-coupled microbolometer
- Self complementary planar antenna
  - Real antenna impedance
  - Broadband response $\lambda > 100\ \mu m$
- Single mode throughput $A\Omega = \lambda^2$



Log-Periodic Antenna



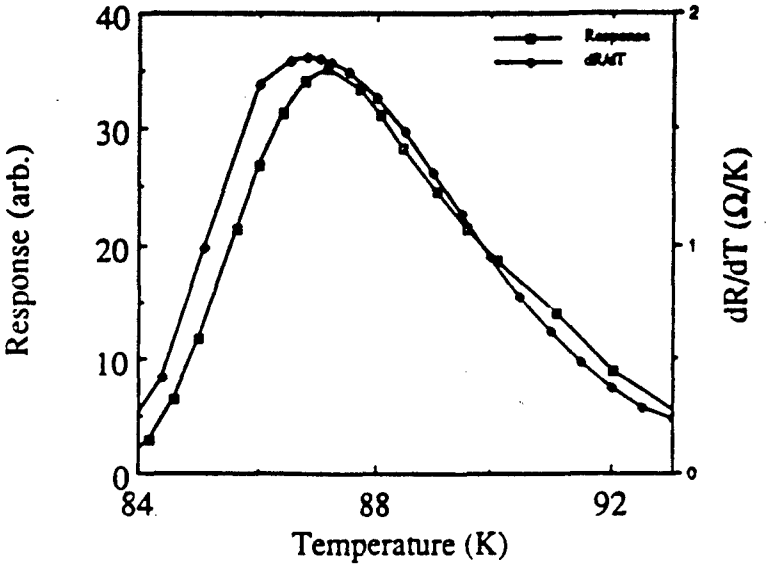
Spiral Antenna

Fabrication of microbolometer

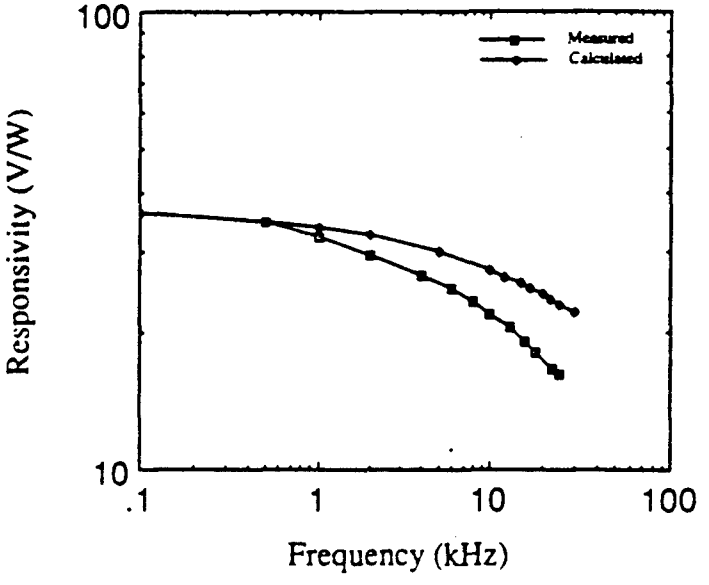
- Single target sputtered 3000 Å YBCO on YSZ.
- Pattern YBCO into 5 μm wide strips in acid etch.
- Sputter clean YBCO surface and sputter deposit Ag.
- Wet etch Ag antenna pattern.
- Oxygen anneal 500° C for 1 hr.

Optical response of microbolometer

I=500 μA, f=2 kHz

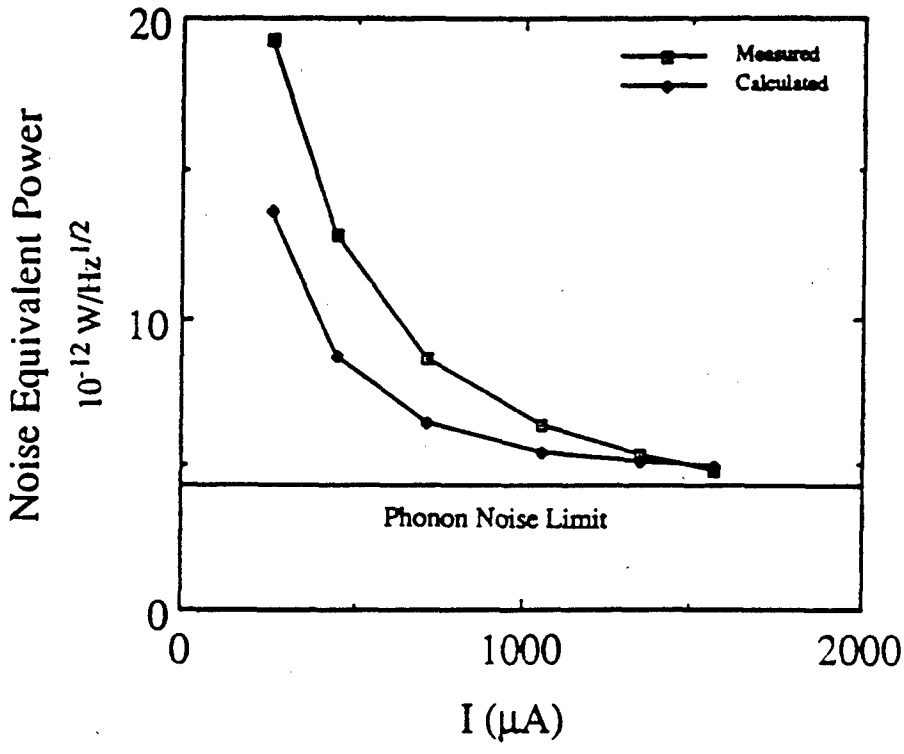


I=500 μA, T=87.2 K

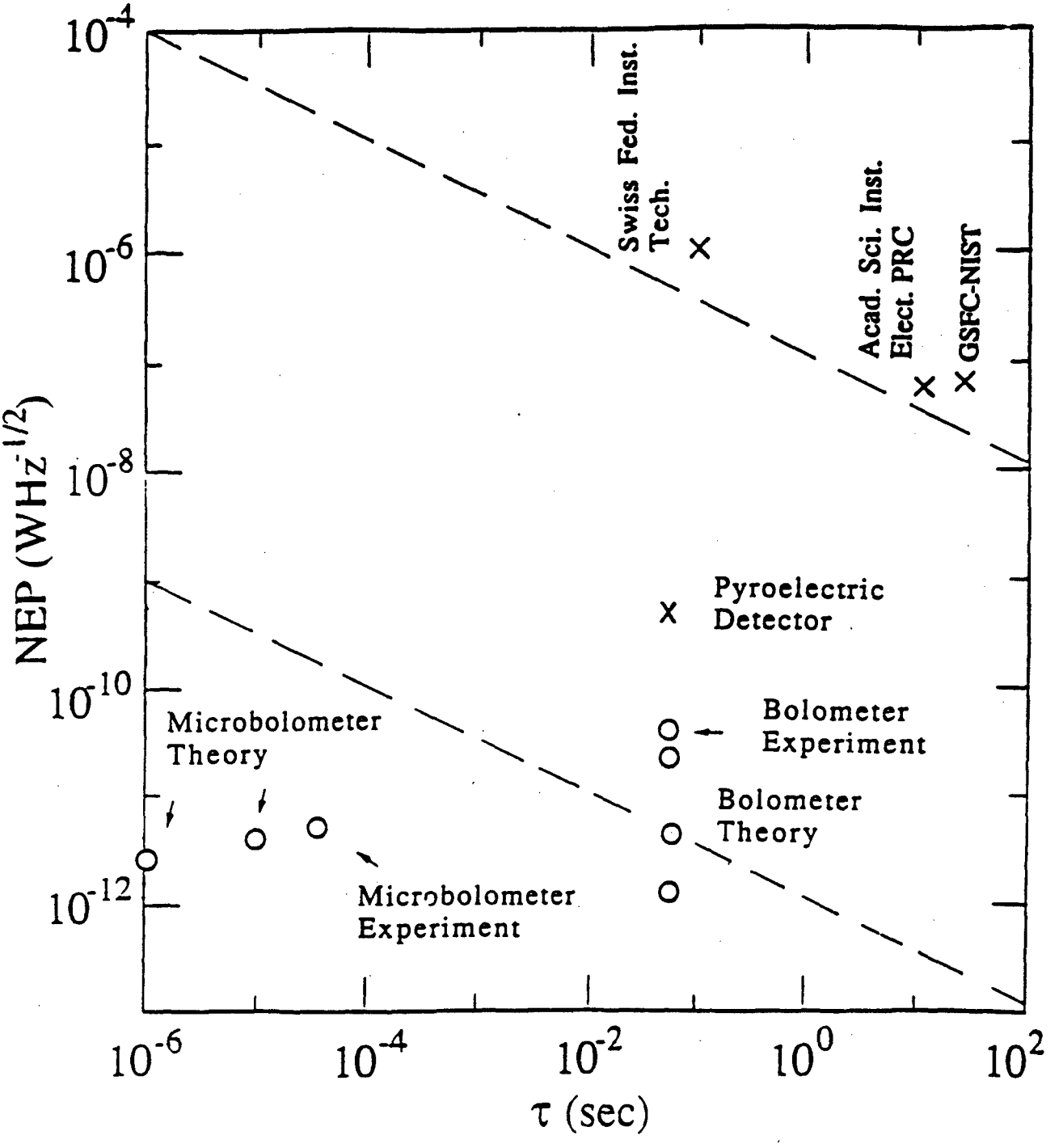


Electrical NEP of microbolometer

T=88.3 K, f=10 kHz



- Electrical NEP is G-noise limited.
- R = 6Ω ⇒ transformer - coupled.
- Optical efficiency measurements in progress.


10^{-4}
10^{-6}
10^{-8}
10^{-10}
10^{-12}
NEP ($WHz^{-1/2}$)
Swiss Fed. Inst. Tech.
Acad. Sci. Inst. Elect. PRC
GSFC-NIST
Pyroelectric Detector
Bolometer Experiment
Bolometer Theory
Microbolometer Theory
Microbolometer Experiment
10^{-6}
10^{-4}
10^{-2}
10^{0}
10^{2}
τ (sec)

XBL 903-5434

Conclusions

- High T_c bolometers have a future for applications where cooling is limited.
- Best opportunities are for $\lambda \geq 15$ μm.
- Require highest materials quality on the "right" substrates.
- We have made conventional bolometers and microbolometers with performance approaching theoretical predictions.

N91
14390
UNCLAS

N91-14390

PYROELECTRIC DETECTORS

Eugene E. Haller, J. Beeman and W.L. Hansen

Lawrence Berkeley Laboratory and University of California at Berkeley
1 Cyclotron Road, Berkeley, California 94720

and

G. Scott Hubbard and R.E. McMurray, Jr.

NASA Ames Research Center, Moffett Field, Califonia 94035

The multi-agency, long-term Global Change programs, and specifically NASA's Earth Observing system, will require some new and advanced photon detector technology which must be specifically tailored for long-term stability, broad spectral range, cooling constraints, and other parameters. Whereas MCT and GaAs alloy based photovoltaic detectors and detector arrays reach most impressive results to wavelengths as long as 12 μm when cooled to below 70 K, other materials, such as ferroelectrics and pyroelectrics, appear to offer special opportunities beyond 12 μm and above 70 K. These materials have found very broad use in a wide variety of room temperature applications. Little is known about these classes of materials at sub-room temperatures and no photon detector results have been reported. From the limited information available we conclude that the room temperature values of $D^* \gtrsim 10^9$ cm $Hz^{1/2}/W$ may be improved by one to two orders of magnitude upon cooling to temperatures around 70 K Improvements of up to one order of magnitude appear feasible for temperatures achievable by passive cooling.

The flat detector response over a wavelength range reaching from the visible to beyond 50 μm, which is an intrinsic advantage of bolometric devices, makes for easy calibration. The fact that these materials have not been developed for reduced temperature applications makes ferro- and pyroelectric materials most attractive candidates for serious exploration.

PRECEDING PAGE BLANK NOT FILMED

PYROELECTRIC MATERIALS AND DETECTORS

Eugene E. Haller, J. Beeman and W.L. Hansen
Lawrence Berkeley Laboratory
and University of California at Berkeley
1 Cyclotron Road, Berkeley, CA 94720

and

G. Scott Hubbard and R.E. McMurray, Jr.
NASA Ames Research Center
Moffett Field, CA 94025

Contents

- **Introduction**
- **Thermal Detectors**
- **Pyroelectric Devices**
  - **Operation below T_c**
  - **Operation above T_c with an applied DC bias**
- **Materials Properties**
- **Summary**

PRECEDING PAGE BLANK NOT FILMED

INTRODUCTION

- Global Change programs, including NASA's Earth Observing System (EOS) require a variety of detectors which can:
  - cover a broad spectral range from the visible to the LWIR and beyond
  - operate at temperatures ≥ 65 K in actively cooled instruments
  - operate at temperatures ≥ 120 K in passively cooled instruments
  - have long term stability
  - utilize simple and reliable calibration procedures
  - be integrated into imaging arrays
- Thermal detectors, including bolometers and pyroelectric detectors, fulfill a large number of the above requirements
- Operation of thermal detectors in the above given temperature ranges has not been explored in detail

THERMAL DETECTORS

- **Basic parameters and equations:**

  - Heat capacity $H = dE/dT$ $(J\ K^{-1})$

  - Heat conductance $G = dP/dT$ $(W\ K^{-1})$

    with E = total energy
    P = power
    T = temperature

  - Thermal circuit:

$$\eta P = H\frac{d\theta}{dt} + G\theta$$

with η = quantum efficiency (fraction of incident power absorbed by detector)

θ = average temperature rise of the detector i.e. $T_D = T_O + \theta$

t = time

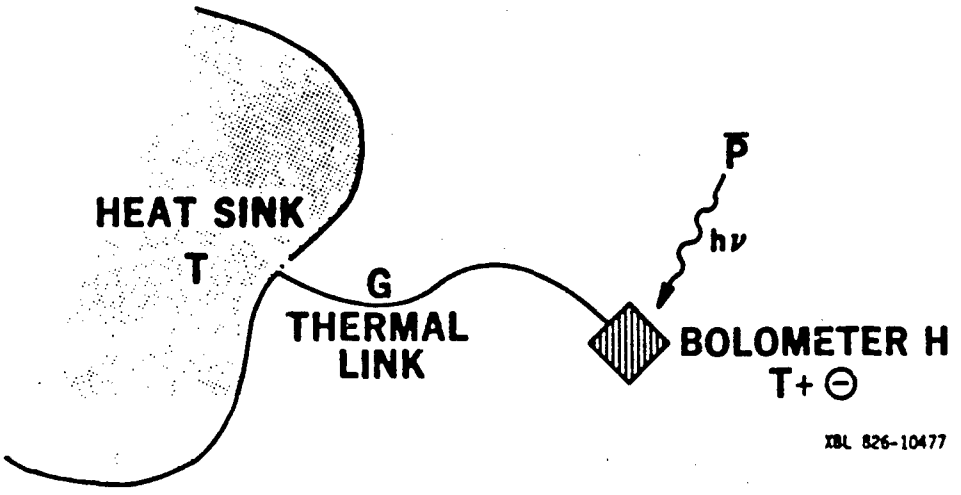
for a radiation source with

$$P = P_o + P_\omega e^{i\omega t}$$

one finds:

$$\theta_\omega = \eta P_\omega \left(G^2 + \omega^2 H^2\right)^{-1/2}$$

$$\varphi = \tan^{-1}\left(\omega H / G\right)$$



- thermal time constant

  $\tau_T = H/G$

- minimum value of G:

  $G_{min} = G_{radiative} = 4\,A\eta\,\sigma\,T^3$

  with A = detector area
  σ = Stefan-Boltzmann constant
  (= 5.67×10^{-12} W cm^{-2} K^{-4})

- **Background limited performance:**

  - Power fluctuation through thermal link:

    $\Delta W_T = (4kT^2G)^{1/2}$

  - Minimum detectable signal power P_N:

    $\eta P_N = \Delta W_T = (16A\,\eta\,\sigma\,kT^5G)^{1/2}$

    or $P_N = (16A\,\sigma\,kT^5/\eta)^{1/2}$

    $P_N = (16A\,\sigma\,kT^5)^{1/2} = 5\times10^{-10}$ W (at T=300 K)

    (for 1 Hz bandwidth, A = 1 cm^2,
    2π field of view and η = 1)

    P_N (T=200 K) = 2×10^{-11}W

    P_N (T=100 K) = 3.5×10^{-12}W

    (equivalent to $D^* = 2.86\times10^{11}$cm $\sqrt{Hz}$ W^{-1})

PYROELECTRIC DEVICES

- **Pyroelectric devices are thermal detectors**
- **No fundamental limits for wavelength of photons to be detected**
- **Flat wavelength response makes for easy calibration**

- **Figures of merit:**
  - Pyroelectric coefficient:

    $p = dP_s/dT$

    P_s = spontaneous polarization
  - pyroelectric current

    $I_p = Ap\ dT/dt$

    with:

    c = volume specific heat

    d = thickness of the detector
  - current responsivity:

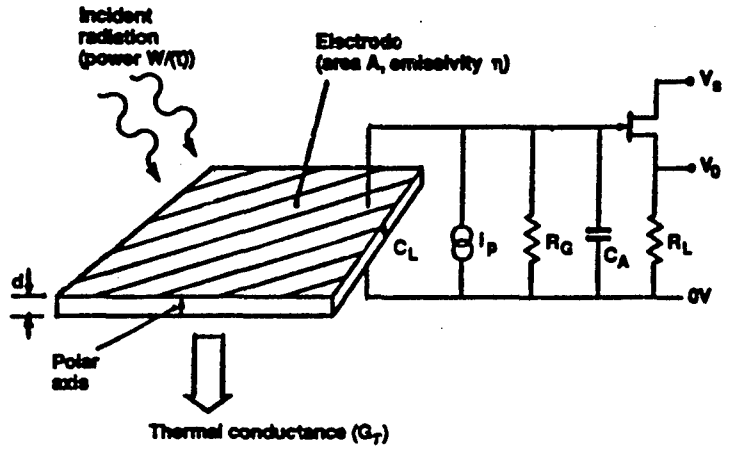
$$R_I = \frac{I_p}{P_\omega} = \frac{\eta p A \omega}{G\left(1+\omega^2\tau_T^2\right)^{1/2}}$$

at low frequencies $\left(\omega << \tau_T^{-1}\right)$

$$R_I \propto \omega$$

at high frequencies $\left(\omega >> \tau_T^{-1}\right)$

$$R_I = \frac{\eta p A}{H} = \frac{\eta p}{c d}$$



Schematic diagram of a pyroelectric radiation detector.

(From R. W. Whatmore, Rep. Prog. Phys. 49, 1335 (1986), Fig. 5)

- voltage responsivity:

$$R_v = \frac{I_p}{Y P_\omega} = \frac{R \eta p A \omega}{G\left(1+\omega^2\tau_T^2\right)^{1/2}\left(1+\omega^2\tau_E^2\right)^{1/2}}$$

with $Y = R^{-1} + i\omega C$; R = total input resistance, C = total input capacitance, $\tau_E = R C$

- at high frequencies $\left(\omega >> \tau_T^{-1}, \tau_E^{-1}\right)$:

$$R_v = \frac{\eta p}{c \varepsilon \varepsilon_0 A \omega}$$

Pyroelectric material figure of merit:

$$F_v = p/c\varepsilon\varepsilon_0$$

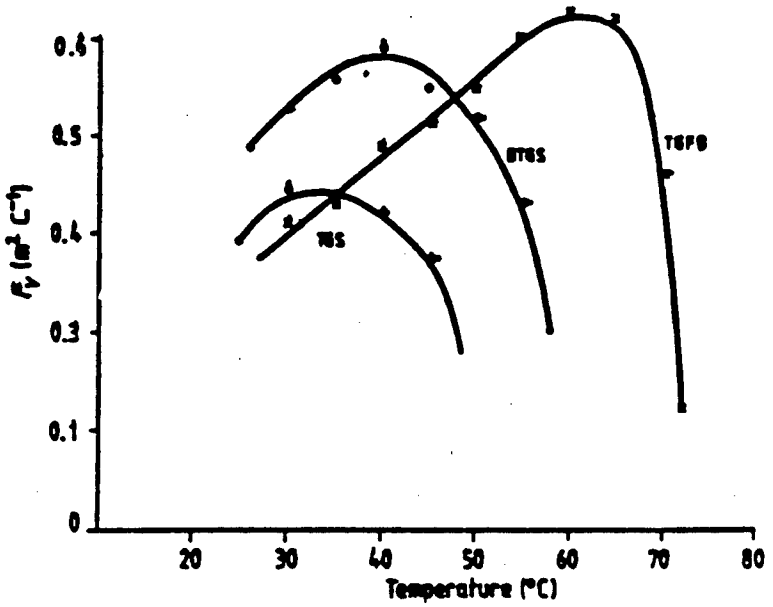
(The larger F_v, the closer we can approach D_{BLIP})

Pyroelectrics have a relative dielectric constant ε which is temperature dependent. With a DC electric field E applied one finds:

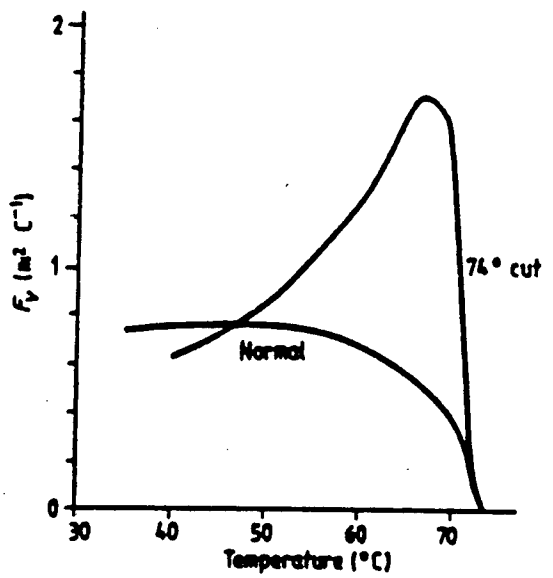
$$p = \left.\frac{dD}{dT}\right|_E = \left.\frac{dP_s}{dT}\right|_E + \left.\frac{d\varepsilon}{dT}\right|_E E$$

Of special interest are ferroelectrics operated above T_c. Dielectric losses approach zero in this range.

C-3



Temperature dependence of the merit figure F_v for some members of the TGS family.



Temperature dependence of F_v in DTGFB at a normal cut and in a cut perpendicular to a direction that forms an angle of 74° with the pyroelectric axis (after Shaulov 1981).

(after R.W. Whatmore, Rep. Prog.Phys. 49, 1335 (1986), Figs. 15 (upper) and Fig. 16 (lower))

MATERIALS PROPERTIES

- **Triglycine sulphate family (TGS) at room temperature:**

  p: 5.5 – 7.0 ($\times 10^{-4} Cm^{-2} K^{-1}$)

  ε: 30 – 60

  dielectric loss tangent at 1 kHz: 0.02 (typical)

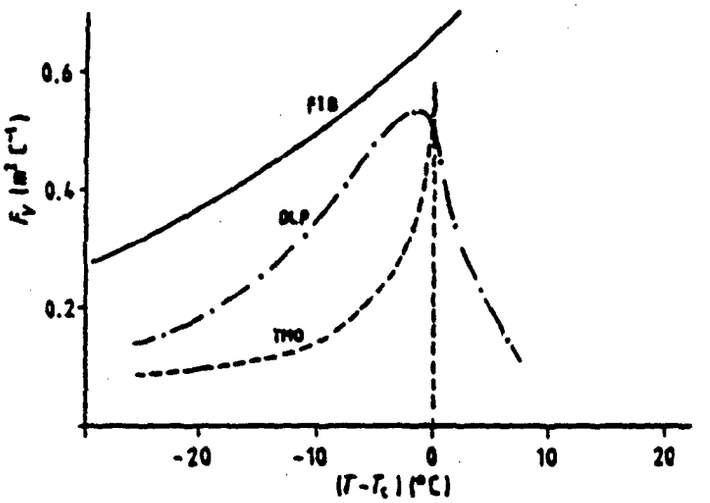
  c: 2.5×10^{6} J $cm^{-3} K^{-1}$

  F_v: 0.4 – 0.6 $m^2 C^{-1}$

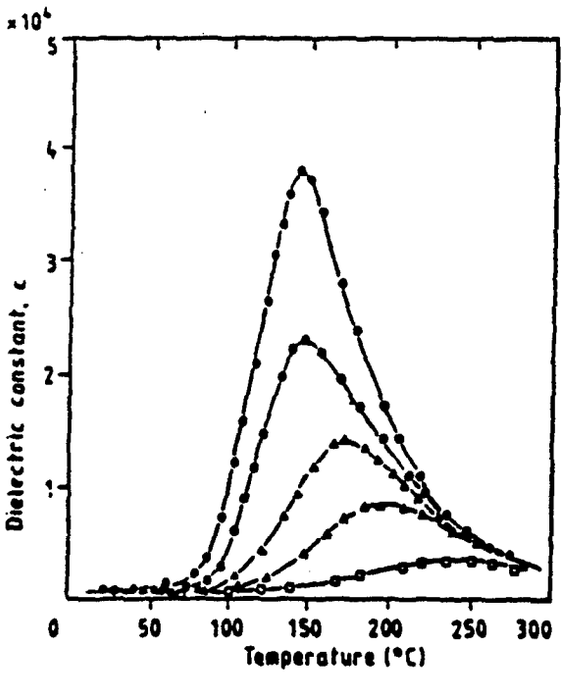
  – **for room temperature application the TGS family offers the best set of materials properties**

- **Polar materials at 25°C**

	Fv: ($m^2 C^{-1}$)
Polyvinilidyne fluoride (PVDF)	0.1
Li TaO_3	0.17
$Sr_xBa_{1-x}Nb_2O_6$ ($0.25 < x < 0.75$)	0.07
Lead zirconates (PZ)	0.06
Improper ferroelectrics	≤ 0.5



Temperature dependence of F_V in selected improper ferroelectrics (after Shaulov *et al* 1980).



Effect of DC bias on dielectric constant as a function of temperature in $Pb(Zn_{1/3}Nb_{2/3})O_3$ (after Yokomizo *et al* 1970). ●, zero bias; ○, 3 kV cm^{-1}; ▲, 7 kV cm^{-1}; △, 11 kV cm^{-1}; □, 25 kV cm^{-1}.

(after R.W. Whatmore, Rep. Prog. Phys. 49, 1335 (1986), Fig. 22 (upper) and Fig. 23 (lower))

- **Pyroelectrics under DC bias**
  - above T_c we find:

    $$p = \left.\frac{d\varepsilon}{dT}\right]_E E$$

  - T_c can be engineered through alloy formation:

    e.g. $\alpha\ Ta_x\ Nb_{1-x}\ O$

  - at temperatures near the zero field T_c, both

    $\frac{dP_s}{dT}$ and $\frac{d\varepsilon}{dT}$ increase with the applied DC

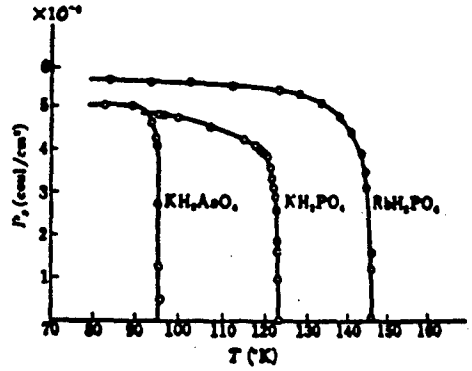
  - dielectric losses above T_c vanish

- **Pyro and Ferroelectric Materials with $100\ K < T_c < 200\ K$**
  - KDP (Potassium dihydrogen phosphate) family:

    T_c depends on the specific chemical composition

  - KTN (Potassium tantalum niobium oxide) family:

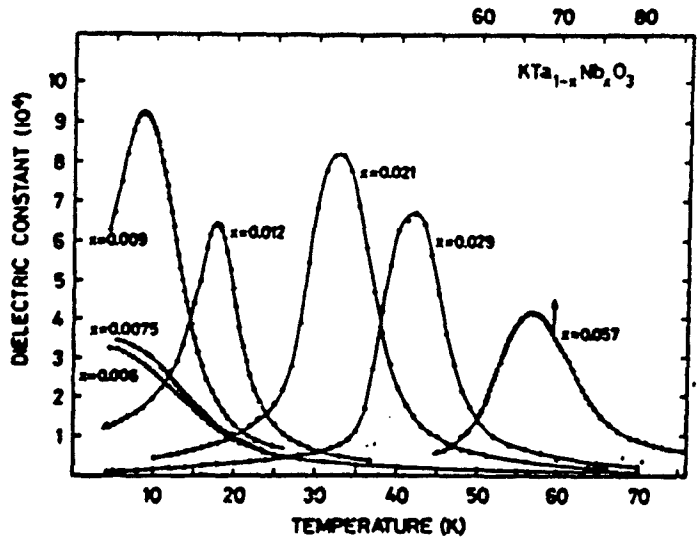
    T_c can be adjusted to any given temperature between 0 and 500 K by alloying. This materials system is fully miscible.



Temperature dependences of the spontaneous polarization of KH_2PO_4 type ferroelectrics.

(From T. Mitsui et al., "An Introduction to the Physics of Ferroelectrics", Gordon and Breach 1984)

D. RYTZ, A. CHÂTELAIN, AND U. T. HÖCHLI



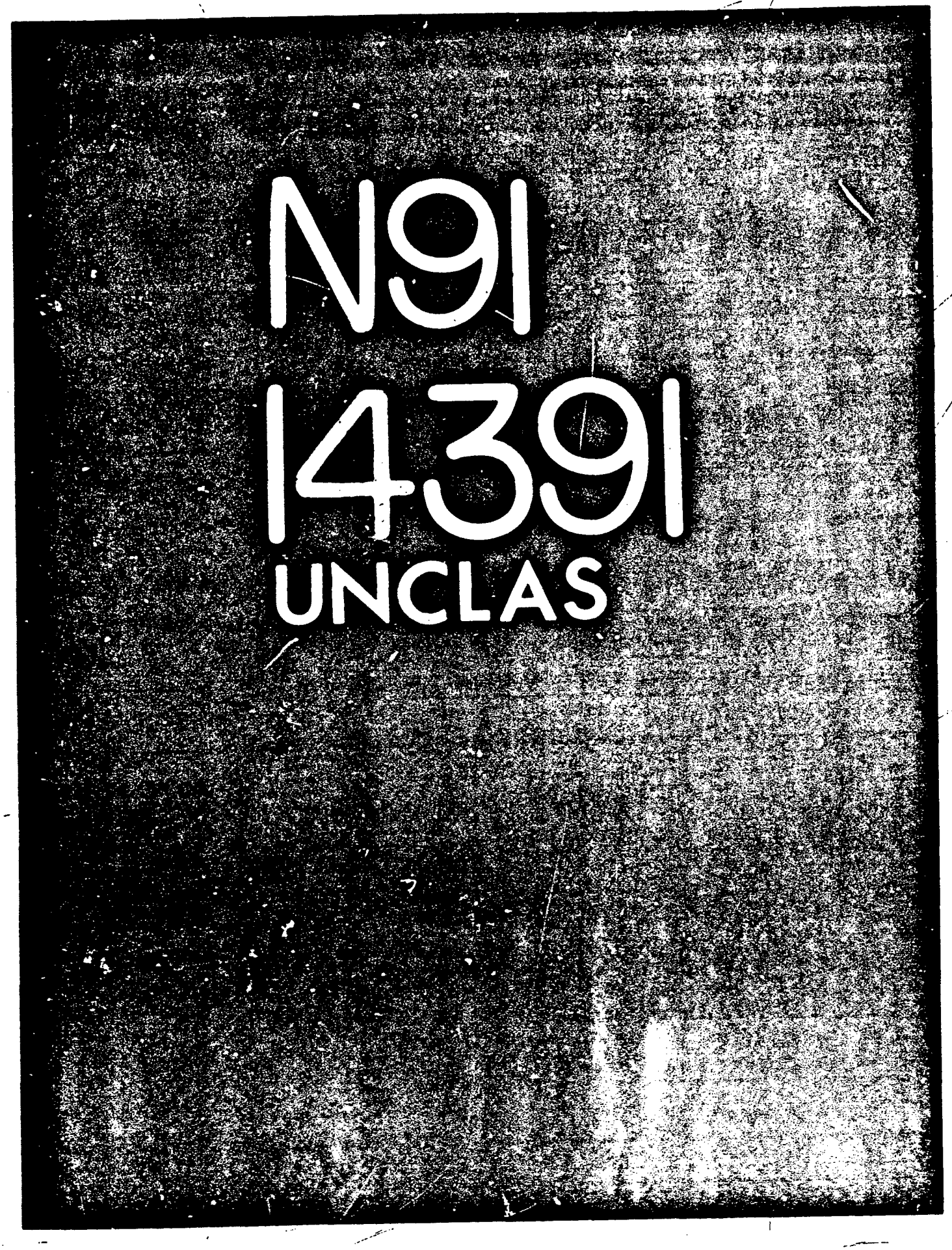
Temperature dependence of the static dielectric constant ϵ with concentration x as a parameter. The data were obtained by a conventional bridge technique at 1 kHz. The temperature was changed at a rate of no more than 0.5 K/min. Note the change on the temperature scale for $x=0.057$.

(From D. Rytz et al., Phys. Rev. B27, 6830 (1983), Fig. 3)

SUMMARY

- **Bolometric detection has specific advantages such as:**
  - **response to photon power unlimited by the photon wavelength**
  - **ease of calibration**
- **Background limited D^* (100 K)**

  $= 2.86 \times 10^{11}$ cm $\sqrt{Hz}$ W^{-1}; this appears sufficient for a number of remote sensing applications, possibly including EOS LWIR focal plane arrays
- **Passively cooled systems can make use of pyro- and ferroelectrics**
- **The critical temperature of pyroelectrics near which highest performance is achieved, can be engineered through alloying**
- **Low temperature pyro- and ferroelectrics offer great potential for exploratory research**


N91
14391
UNCLAS

N91-14391

A novel electron tunneling infrared detector

T.W. Kenny, S.B. Waltman, J.K. Reynolds, and W.J. Kaiser
Center for Space Microelectronics Technology
Jet Propulsion Laboratory
California Institute of Technology
Pasadena, CA 91109

All thermal detectors of infrared radiation include the following components: An absorber of infrared radiation converts the incoming photons to heat, producing a temperature rise in the detector. A thermo-electric transducer converts the change in the temperature of the detector to an electrical signal. The detector is connected to a temperature reference by a finite thermal conductance, G. Given the efficiency of the infrared absorber, the temperature coefficient of the thermo-electric transducer, the thermal conductance to the temperature reference and the heat capacity of the detector, the performance of the device may be fully characterized. Useful thermal detectors require the existence of sensitive thermo-electric transducers that operate at the required temperature with low heat capacity. If the sensitivity of the transducer is high enough, the performance of the detector is limited by thermal fluctuations, for which the Noise Equivalent Power (NEP) is given by $\sqrt{4kT^2G}$.

The pneumatic infrared detector, originally developed by Golay in the late 1940s, uses the thermal expansion of one cm^3 of xenon at room temperature to detect the heat deposited by infrared radiation. This detector was limited by thermal fluctuations within a 10 Hz bandwidth, but suffered from long thermal time constants and a fragile structure. Nevertheless, it represents the most sensitive room temperature detector currently available in the LWIR. Fabrication of this type of detector on smaller scales has been limited by the lack of a suitably sensitive transducer.

We have designed a detector based on this principle, but which is constructed entirely from micromachined silicon, and uses a vacuum tunneling transducer to detect the expansion of the trapped gas. Because this detector is fabricated using micromachining techniques, miniaturization and integration into one and two-dimensional arrays is feasible. The extreme sensitivity of vacuum tunneling to changes in electrode separation will allow a prototype of this detector to operate in the limit of thermal fluctuations over a 10 kHz bandwidth. A calculation of the predicted response and noise of the prototype is

presented within the general formalism of thermal detectors. Although the prototype electron tunneling infrared detector has not been designed to optimize the sensitivity, it should feature an NEP as low as 6×10^{-11} W/$\sqrt{\text{Hz}}$ for a 1 mm^2 active area while operating at room temperature. Some design changes that will allow reductions in the NEP by as much as another order of magnitude for a 1 mm^2 area will be discussed. The dependence of the characteristics upon the area of the detector will also be discussed.

At present, most of the components of the prototype have been fabricated and tested independently. In particular, a characterization of the micromachined electron tunneling transducer has been carried out. The measured noise in the tunnel current is within a decade of the limit imposed by shot noise, and well below the requirements for the operation of an infrared detector with the predicted sensitivity. Assembly and characterization of the prototype infrared detector will be carried out promptly.

The work described in this paper was performed by the Center for Space Microelectronics Technology, Jet Propulsion Laboratory, California Institute of Technology and was sponsored by the Defense Advanced Research Projects Agency/Information Science and Technology Office and the Strategic Defense Initiative Organization/Innovative Science and Technology Office through agreements with the National Aeronautics and Space Administration (NASA).

A Novel Electron Tunneling Infrared Detector

T.W. Kenny, S. B. Waltman, J.K. Reynolds, and W.J. Kaiser

Center for Space Microelectronics Technology
Jet Propulsion Laboratory
California Institute of Technology
Pasadena, CA 91109

- **General Considerations**
- **Electron Tunneling Thermo-electric Transducer**
- **Design and Analysis**
- **Conclusions**

Research Supported by DARPA and SDIO/IST

IR Detector Classification

Quantum Detectors

- Incoming photons are converted to excited carriers in a semiconducting structure.
- The carriers propagate ballistically over barriers in the band structure and are counted. The barriers block the thermally generated carriers.

Thermal Detectors

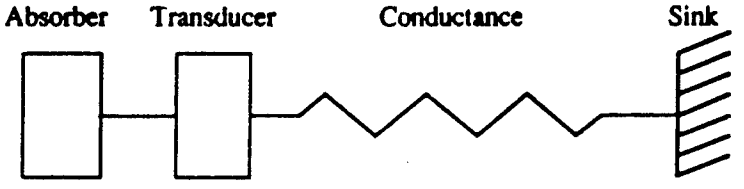
- Incoming photons are converted to heat.
- The heat is detected by a change in temperature of a thermally sensitive element.

Thermal Infrared Detector Requirements

- Infrared Absorber
  Converts incoming radiation to heat.
  Should have low heat capacity and high efficiency.

- Thermo-Electric Transducer
  Converts change in temperature to electrical signal.
  Should have low heat capacity and high conversion coefficient.

- Thermal Conductance
  Connects detector to temperature reference.
  Usually used to provide mechanical support and electrical contact.



Existing Thermal Detectors

- Bolometers
  Use temperature-dependent resistance of semiconductor or superconductor as thermo-electric transducer.
  Limited by availability of large resistance variations.
  State of the art detector for $\lambda > 100\ \mu m$.

- Pyroelectrics and Thermoelectrics
  Use temperature-dependent potential which occurs due to pyroelectric or thermoelectric effect.
  Difficult to fabricate with low heat capacity and thermal conductance.
  Most convenient technology for room-temperature detection in the LWIR.

- Pneumatics
  Use thermal expansion of gas at STP coupled with mechano-electrical transducer. Requires production of thin, flexible membrane.
  Small detectors limited by transducer sensitivity.
  Most sensitive room-temperature detector in the LWIR.

Improving the Pneumatic Infrared Detector

Use silicon micromachining to fabricate sensor components.

- Photolithographic techniques allow μm-scale precision.
- Use single crystals of silicon as raw material.
- Free-standing silicon oxy-nitride membranes may be used.
- Miniaturization of sensor components to less than 100 μm.
- Eventual integration of sensor and electronics possible.

Problem:

As the area of the pneumatic detector is reduced, the capacitive transducer becomes less sensitive.

Solution:

Find a more sensitive transducer technology.

Electron Tunneling

- In the early 1980 s, Binnig and Rohrer at IBM invented a new technique, Scanning Tunneling Microscopy (STM), for studying the structure of surfaces with atomic-scale resolution.

- In STM, a 'Tip' is positioned several Angstroms above the surface of interest. With the application of a voltage bias between the tip and the surface, a small tunneling current is observed.

- According to Quantum Mechanics, the probability for tunneling of individual electrons across the barrier depends exponentially on the thickness of the barrier, which is the separation between the electrodes in this case.

- For the conditions common to STM experiments, the tunnel current varies by an order of magnitude for each Å change in the electrode separation.

- This extreme sensitivity to changes in separation could be useful in an electro-mechanical transducer.

Transducer Sensitivity Comparison

Capacitive Motion Transducer

- Active area : 10 μm x 10 μm
- Voltage : 1 Volt
- Frequency : 200 kHz

Separation : 1 μm
Capacitance : 0.88 fF
Current : 1.1 nA

1 % change in current represents a 90 Å change in separation.

Electron Tunneling Motion Transducer

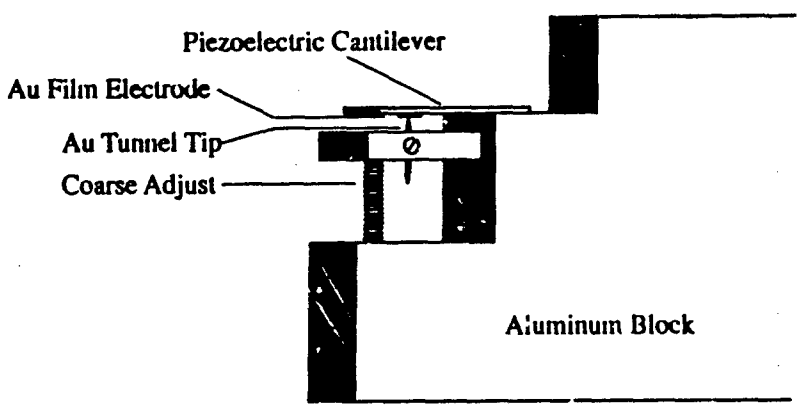
- Active area : 10 Å x 10 Å
- Voltage : 100 mV
- Frequency : 10 Hz - 10 kHz

Separation : 5 Å
Current : 1 nA

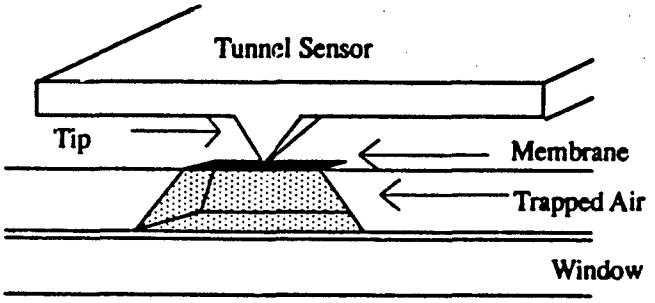
1 % change in current represents a 0.004 Å change in separation.

Prototype Tunnel Sensor

- Piezoelectric Bimorph as actuator.
- Rigid mechanical structure.



Design of the Micromachined Infrared Tunnel Sensor



- Air-filled cavity bounded on one side by 0.5 μm silicon oxy-nitride membrane.
- 80 Å Au film used as IR Absorber and tunneling electrode.
- Folded silicon cantilever spring with integral tip.
- Electrostatic deflection used to control electrode separation.

Design Parameters for the Prototype Infrared Tunnel Sensor

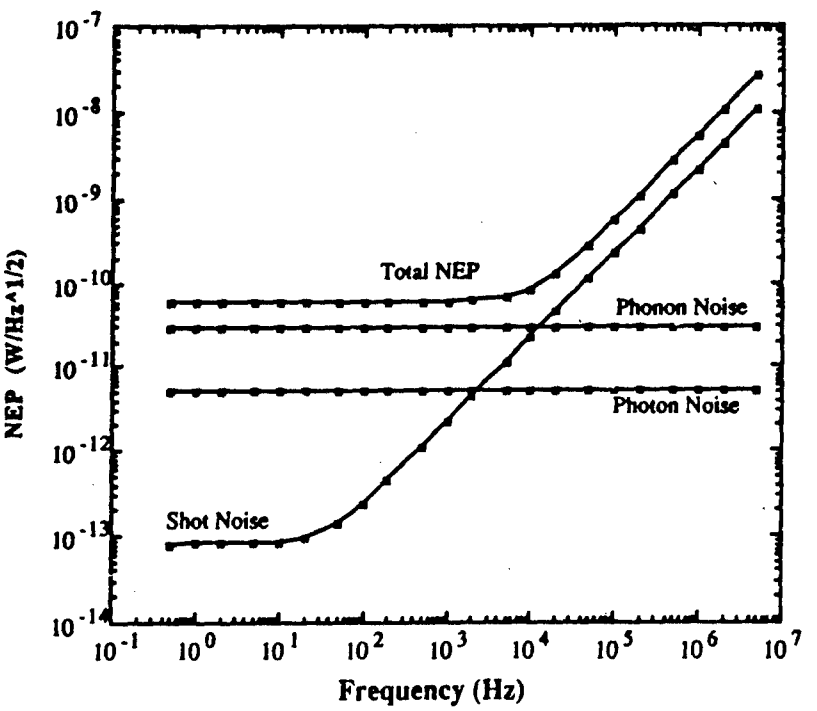
Area	$A = 10^{-2}$	cm^2
Thermal conductance between membrane and surroundings : Dominated by air in cavity	$G = 2 \times 10^{-4}$	W/K
Heat capacity of membrane and gas : Dominated by membrane	$C = 8 \times 10^{-7}$	J/K
Time constant (C/G) :	$\tau = 4 \times 10^{-3}$	s
Response coefficient of thermo-electric transducer : $\alpha = \frac{1}{I}\frac{\partial I}{\partial z}\frac{\partial z}{\partial T}$	$\alpha = 2.3 \times 10^{4}$	/K
Detector responsivity : $S = \frac{I\,\alpha}{(G^2 + (\omega C)^2)^{1/2}}$	$S = 0.38$	A/W

Fundamental Noise in the Tunnel IR Detector

$$(NEP)^2 = \underbrace{4k_BT^2G}_{\text{phonon}} + \underbrace{16A\sigma k_BT^5}_{\text{photon}} + \underbrace{\frac{2eI(G^2+(\omega C)^2)}{I^2\alpha^2}}_{\text{electron}} + \underbrace{\frac{I_n^2(G^2+(\omega C)^2)}{\omega I^2\alpha^2}}_{\text{amplifier}}$$

- Since α is very large in this detector, the electron and amplifier noise terms are only important for frequencies $\omega >> 1/\tau$.
- At low frequencies, the phonon noise dominates. Improvements can only be obtained through reductions in G
- The prototype Tunnel IR Detector is expected to have NEP of 6×10^{-11} W/$\sqrt{\text{Hz}}$ at frequencies below 10 kHz.

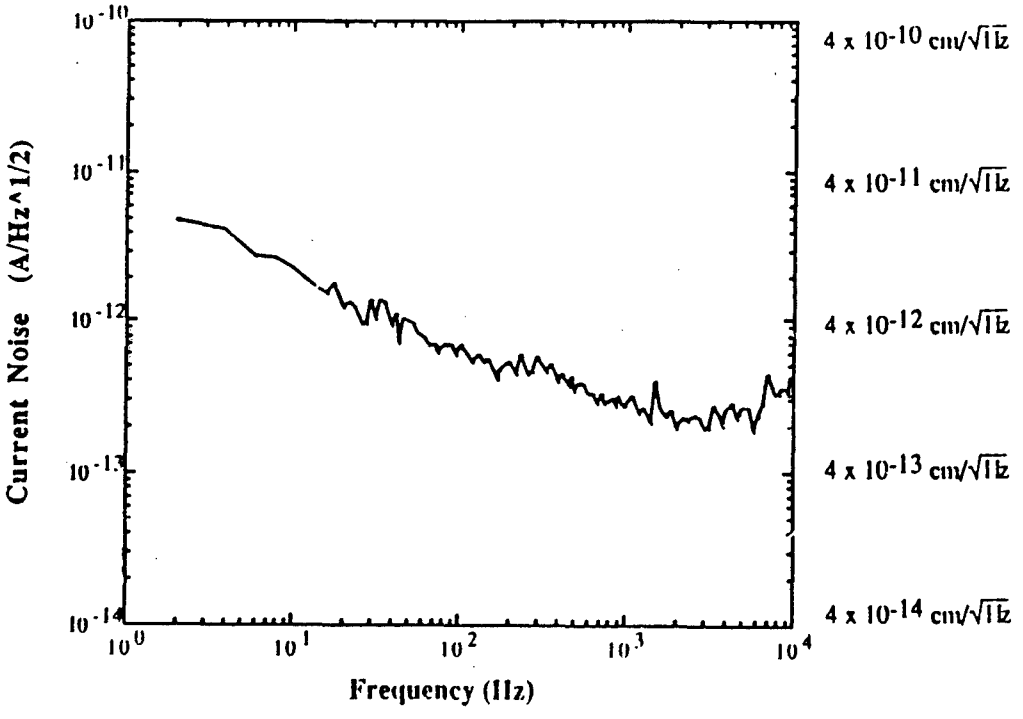
Calculated Contributions to the NEP



Sensor Construction : Present Status

Micromachined Springs	Fabricated
Micromachined Tips	Fabricated
Free-Standing Silicon Oxy-Nitride Membrane	Fabricated
Metallization	Complete
Transducer Characterization	Almost Complete
Infrared Sensor Assembly	Next
Sensor Characterization	

Measured Current Noise



Speculations

The NEP of the Tunneling IR Detector can be improved by reducing the thermal conductance to the heat sink as follows:

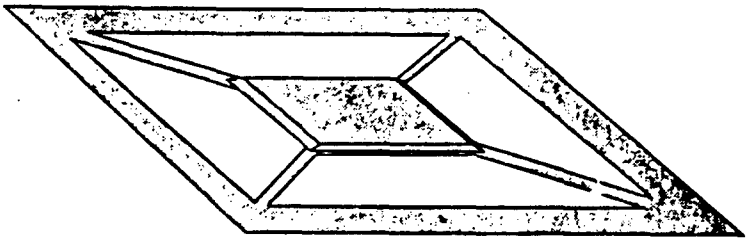
- Replace the air in the cavity with Xenon.
- Increase thickness of cavity to 400 μm
- Reduce the cavity area to 500 μm x 500 μm.

Combined effect is to reduce NEP by a factor of approximately 6.

Further reductions in the NEP of the prototype IR Tunnel Sensor are constrained by the thermal contact to the walls of the cavity, which act as a heat sink.

By vacuum-encapsulating a 'bag' of gas, the thermal conductance may be reduced much further. Improvements in the NEP of more than an order of magnitude are likely.

Vacuum-Encapsulated IR Sensor



- Air-filled silicon oxy-nitride balloon supported by silicon oxy-nitride ribbons.
- Au film on balloon for IR absorption and tunneling electrode.
- Active area = 50 mm x 50 mm.
- Thermal conductance to heat sink limited by ribbons : G = 16 nW/K
- Predicted NEP is limited by background fluctuations (BLIP Limit)

Conclusions

- We have designed a device based on the Pneumatic Infrared detector, but which is constructed entirely from micromachined silicon and uses a vacuum tunnel sensor to detect the expansion of the trapped gas.
- A calculation of the performance of this device, which is based only on thermal physics and the known characteristics of tunneling has been carried out.
- The performance of the prototype is expected to meet or exceed that of all room temperature detectors which operate in the I.WIR.
- Fabrication and characterization of the components of the detector is under way.
- Simple modifications to the design of the prototype can improve its NEP by a factor of 6. More complicated modifications can lead to more substantial improvements in the NEP.

SESSION V: III-V Quantum Well and Heterojunction Detectors

V - 1 Quantum Well Infrared Photodetectors (QWIP)
B.F. Levine, AT&T Bell Laboratories

V - 2 Photovoltaic Quantum Well Infrared Detectors
S.A. Lyon, Princeton University

V - 3 Characteristics of AlGaAs/GaAs Multiple Quantum Well Infrared Detectors
B.K. Janousek, The Aerospace Corporation

V - 4 Resonant Tunneling IR Detectors
J.M. Woodall, IBM

V - 5 Low Dark Current Photovoltaic Multiquantum Well Long Wavelength Infrared Detectors
C.S. Wu, Hughes Aircraft Company

V - 6 Fundamental Limits to Performance of Quantum Well Infrared Detectors
A. Yariv, California Institute of Technology

V - 7 New Heterojunction LWIR Detector Options
J. Maserijian, Jet Propulsion Laboratory

PRECEDING PAGE BLANK NOT FILMED

N91
14392
UNCLAS

N91-14392

Quantum Well Infrared Photodetectors (QWIP)

B. F. Levine
AT&T Bell Laboratories
Murray Hill, NJ 07974

There has been a lot of interest in III-V long wavelength detectors in the λ = 8 - 12 μm spectral range as alternatives to HgCdTe.[1-6] Recently high performance quantum well infrared photodetectors (QWIP) have been demonstrated. They have a responsivity of R = 1.2 A/W, and a detectivity $D^*_\lambda = 2x10^{10}$ cm $Hz^{1/2}$ / W at 68 K for a QWIP with a cutoff wavelength of λ_c = 10.7 μm and a R = 1.0 A/W, and $D^*_\lambda = 2x10^{10}$ cm $Hz^{1/2}$ / W at T = 77 K for λ_c = 8.4 μm. These detectors consist of 50 periods of MBE grown layers doped n = $1x10^{18}$ cm^{-3} having GaAs quantum well widths of 40 Å and barrier widths of 500 Å of $Al_xGa_{1-x}As$.

Due to the well-established GaAs growth and processing techniques these detectors have the potential for large, highly uniform, low cost, high performance arrays as well as monolithic integration with GaAs electronics, high speed and radiation hardness.

Our latest results on the transport physics, device performance and arrays will be discussed.

1. J.S. Smith, L.C. Chiu, S. Margalit, A. Yariv, and A.Y. Cho, J. Vac. Sci. Technol. *B1*, 376 (1983).

2. D.D. Coon and R.P.G. Karunasini, Appl. Phys. Lett. *45*, 649 (1984).

3. K. W. Goossen, S. A. Lyon, and K. Aiavi, Appl. Phys. Lett. *52*, 1701 (1988).

4. A. Kastalsky, T. Duffield, S. J. Allen, and J. Harbison, Appl. Phys. Lett. *52*, 1320 (1988).

5. S. R. Kurtz, L. R. Dawson, T. E. Zipperian, and R. D. Whaley, Jr., IEEE Electron. Dev. Lett. *11*, 54 (1989).

6. B. F. Levine, C. G. Bethea, G. Hasnain, V. O. Shen, E. Pelve, R. R. Abbott, and S. J. Hsieh, Appl. Phys. Lett. *56*, 851 (1990).

PRECEDING PAGE BLANK NOT FILMED

Quantum Well Infrared Photodetectors
QWIP

Research	Development
B. F. Levine	P. J. Anthony
C. G. Bethea	W. A. Gault
S. D. Gunapala	J. W. Stayt
R. J. Malik	K. G. Glogovsky
G. Hasnain	R. A. Morgan
	Y. M. Wong
Government Systems	M. T. Asom
	S. J. Hsieh
C. L. Allyn	R. M. Braun
V. O. Shen	

LWIR GaAs Quantum Well Detectors

Esaki, Sakaki

Smith, Chiu, Margalit, Yariv, Cho

Coon, Karunasiri

Goosen, Lyon

Capasso, Mohammed, Cho

Kastalsky, Duffield, Allen, Harbison

Janousek, Daugherty, Bloss, Rosenbluth, O'Loughlin, Kauter, DeLuccia, Perry

Woodall

Wu, Sato, Wen

Maserjian

Döhler

Mii, Karunasiri, Wang, Bai

Abstreiter et al.

MATERIAL FOR 10 μm DETECTORS

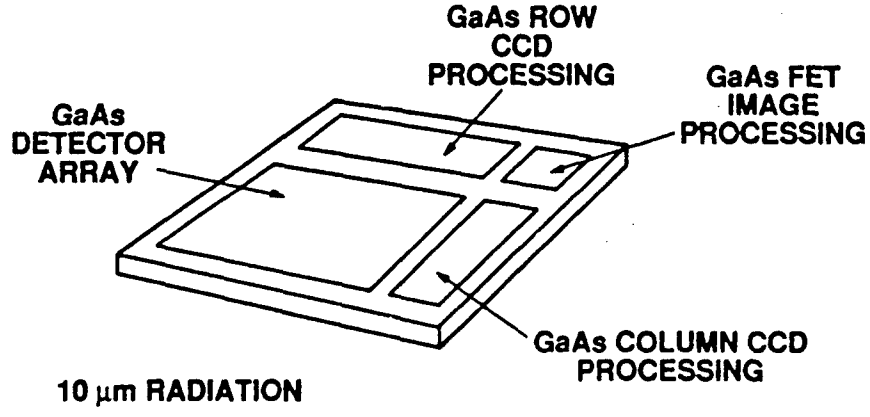
HgCdTe DETECTORS

- DIFFICULT GROWTH AND PROCESSING TECHNOLOGY
- POOR UNIFORMITY OF ARRAYS
- LOW QUALITY CdTe SUBSTRATES

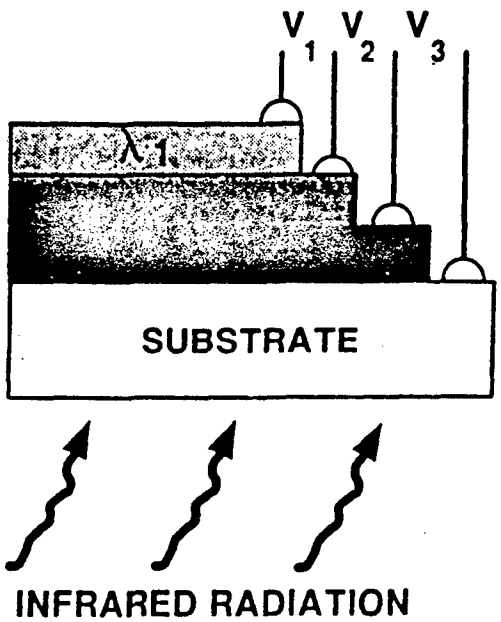
GaAs DOPED QUANTUM WELL DETECTORS

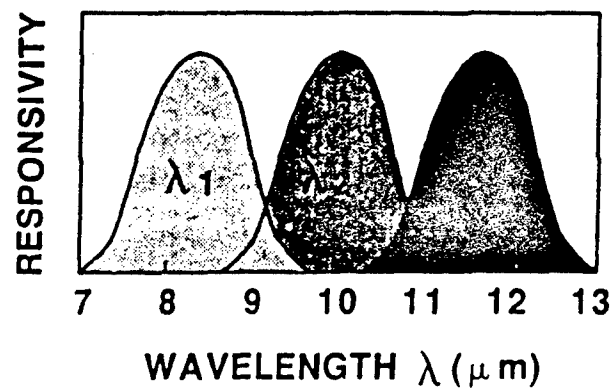
- PERFORMANCE COMPARABLE TO HgCdTe
- MATURE GROWTH AND PROCESSING TECHNOLOGY
- EXCELLENT 3" GaAs SUBSTRATES
- MONOLITHIC INTEGRATION WITH GaAs ELECTRONICS

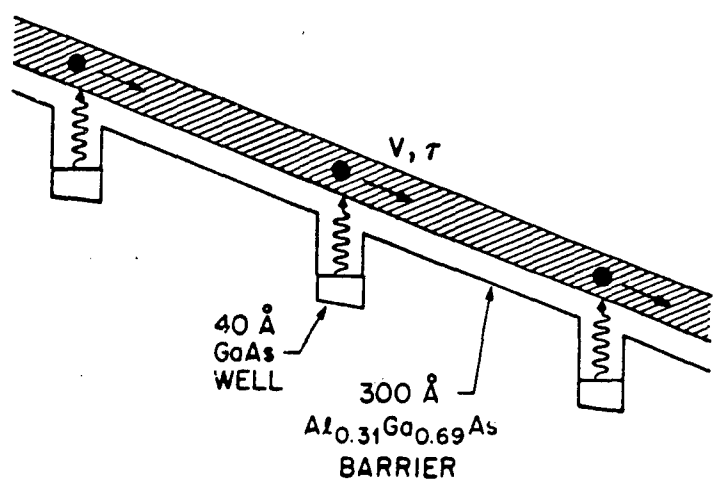
MONOLITHICALLY INTEGRATED GaAs QUANTUM WELL DETECTOR ARRAY AND IMAGE PROCESSING ELECTRONICS

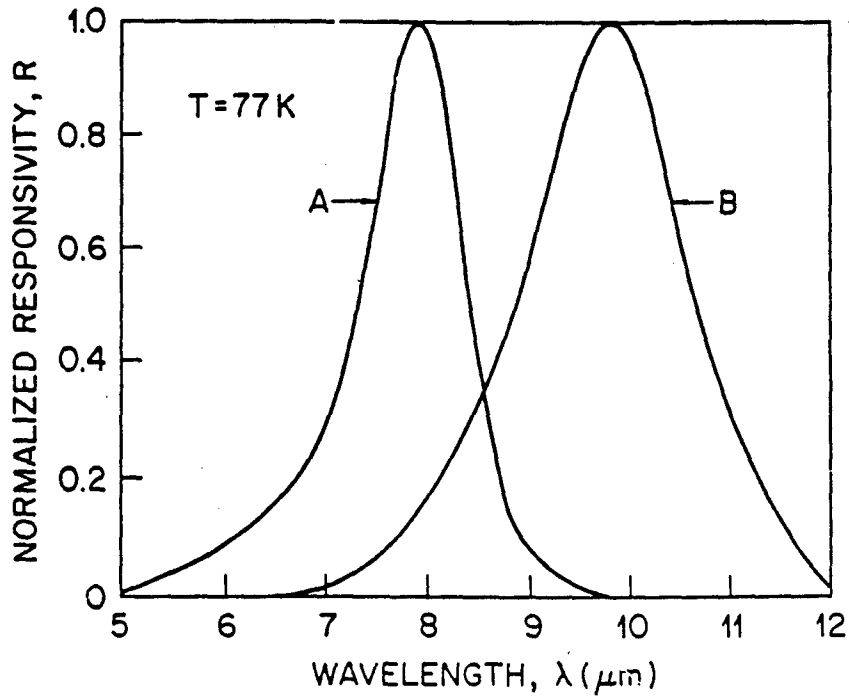


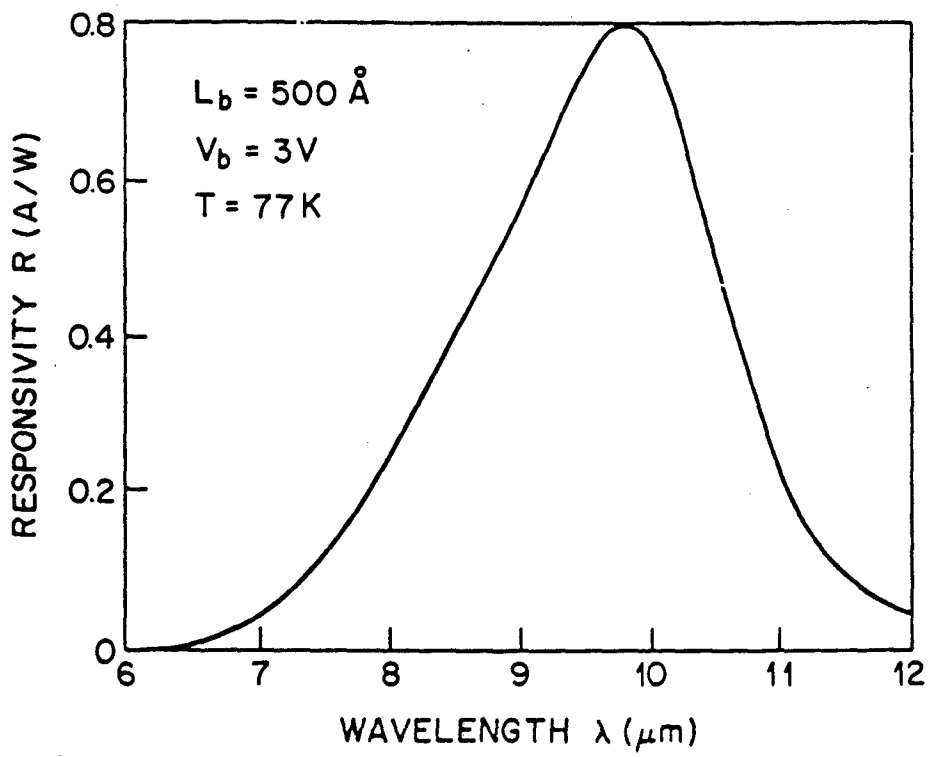
VERTICALLY INTEGRATED GaAs QUANTUM WELL INFRARED SPECTROMETER

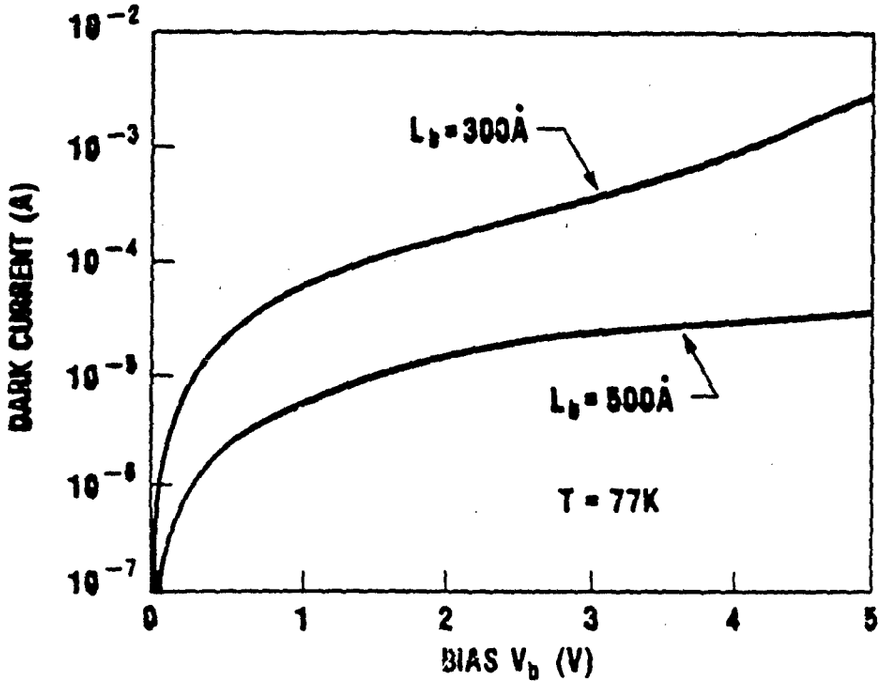







T=77K
A
B
NORMALIZED RESPONSIVITY, R
1.0
0.8
0.6
0.4
0.2
0
5
6
7
8
9
10
11
12
WAVELENGTH, λ (μm)


L_b = 500 Å
V_b = 3V
T = 77K
RESPONSIVITY R (A/W)
0.8
0.6
0.4
0.2
0
6
7
8
9
10
11
12
WAVELENGTH λ (μm)



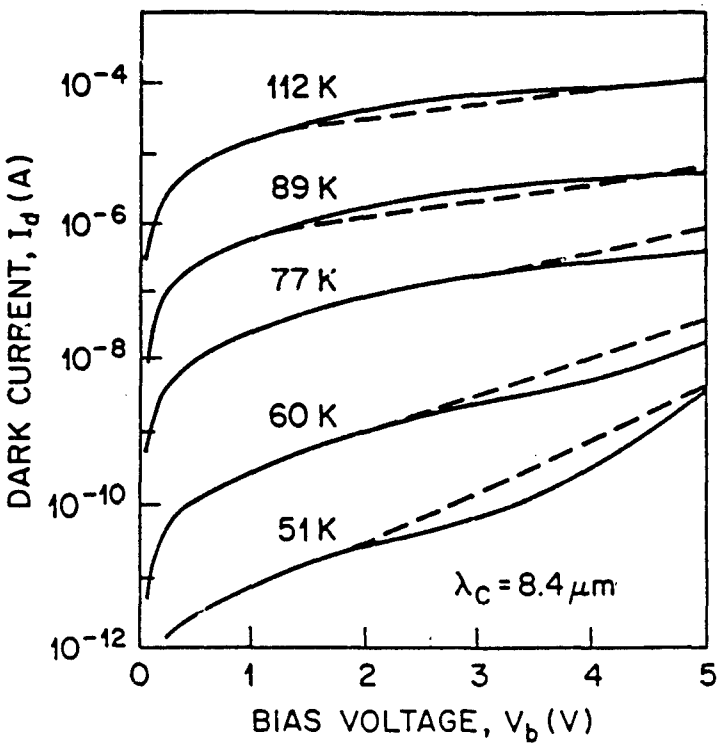
DARK CURRENT CALCULATION

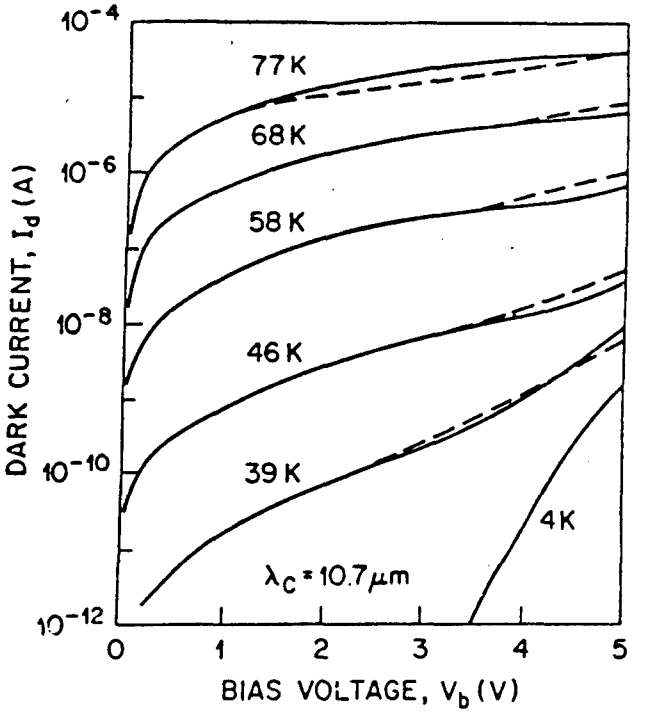
$$n(V) = \frac{m^*}{\pi\hbar^2 Lp} \int_{E_a}^{\infty} f(E)T(E)dE$$

$E > E_b$ Thermionic

$E < E_b$ Tunneling

$$I_D = nevA$$


DARK CURRENT, I_d (A)
10^{-4}
10^{-6}
10^{-8}
10^{-10}
10^{-12}
112 K
89 K
77 K
60 K
51 K
$\lambda_c = 8.4\,\mu m$
0
1
2
3
4
5
BIAS VOLTAGE, V_b (V)


DARK CURRENT, I_d (A)
10^{-4}
10^{-6}
10^{-8}
10^{-10}
10^{-12}
77 K
68 K
58 K
46 K
39 K
4K
$\lambda_c = 10.7\,\mu m$
0
1
2
3
4
5
BIAS VOLTAGE, V_b (V)

$$\lambda_c = 10.7\ \mu m$$

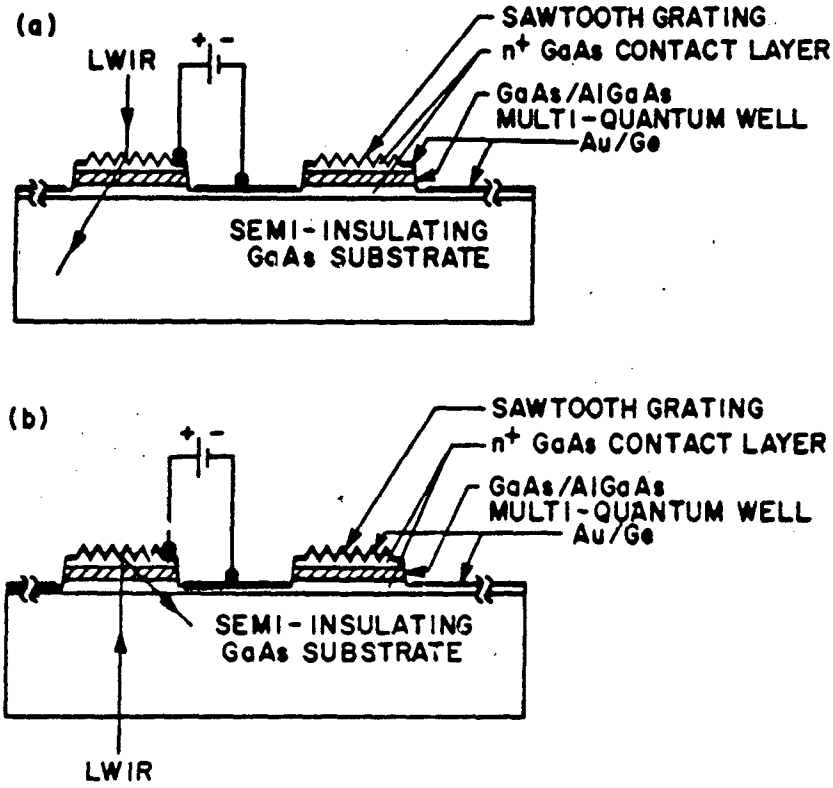
$$D^* = 1 \times 10^{10}\ cm\sqrt{Hz}/W$$

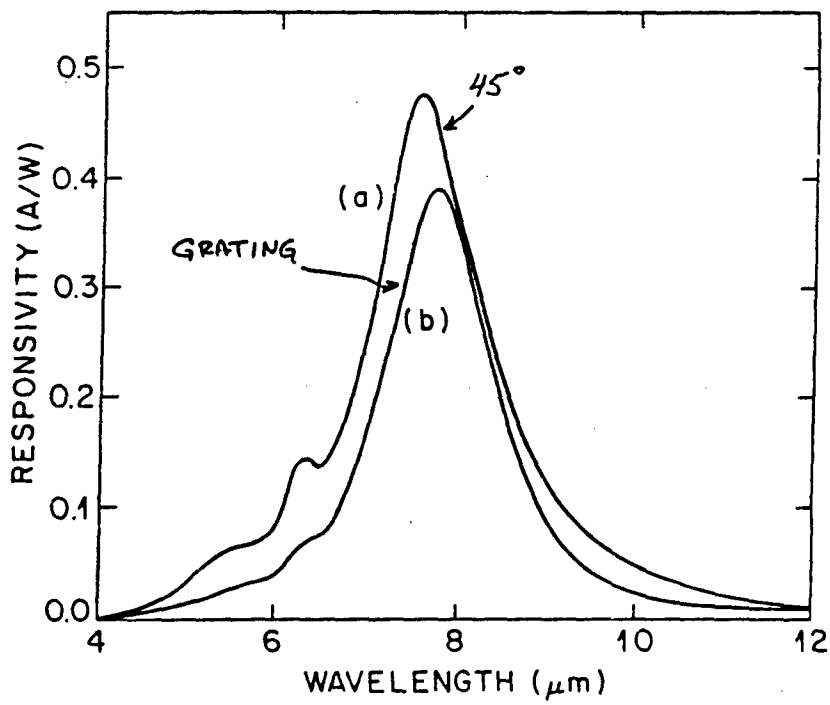
$$T = 68\ K$$

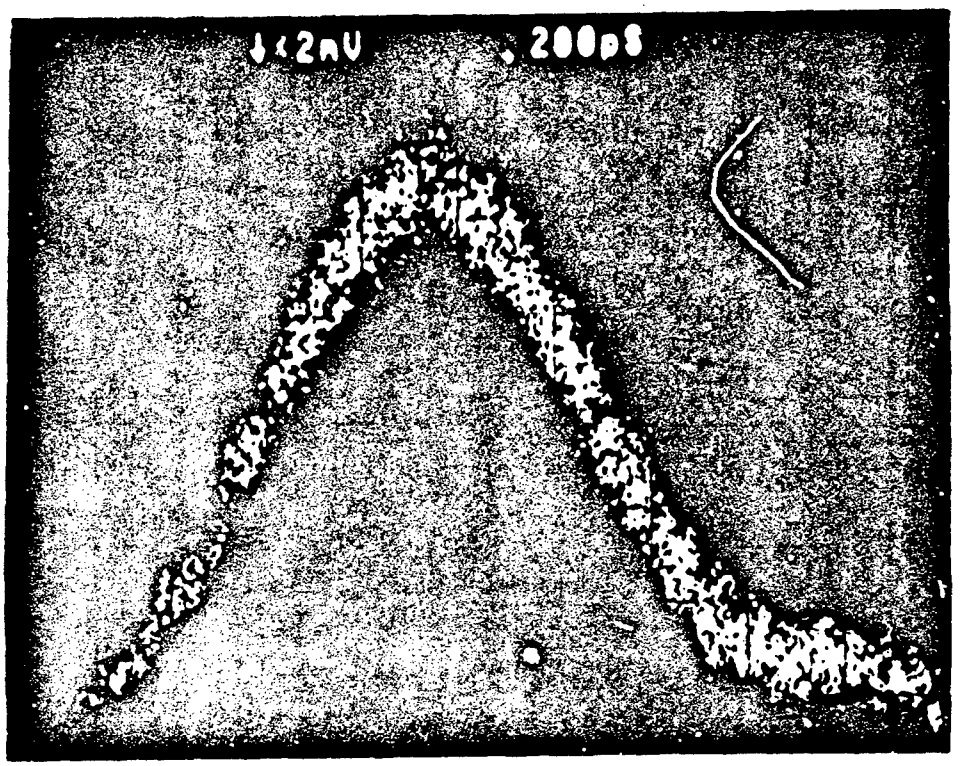
$$\lambda_c = 10\ \mu m$$

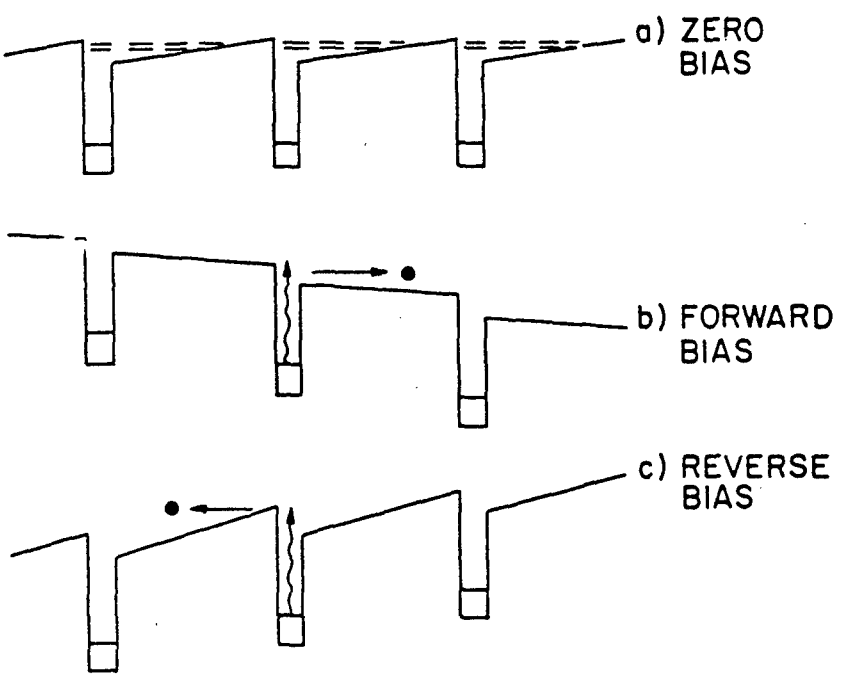
$$D^*(\text{theory}) > 10^{10}\ cm\sqrt{Hz}/W$$

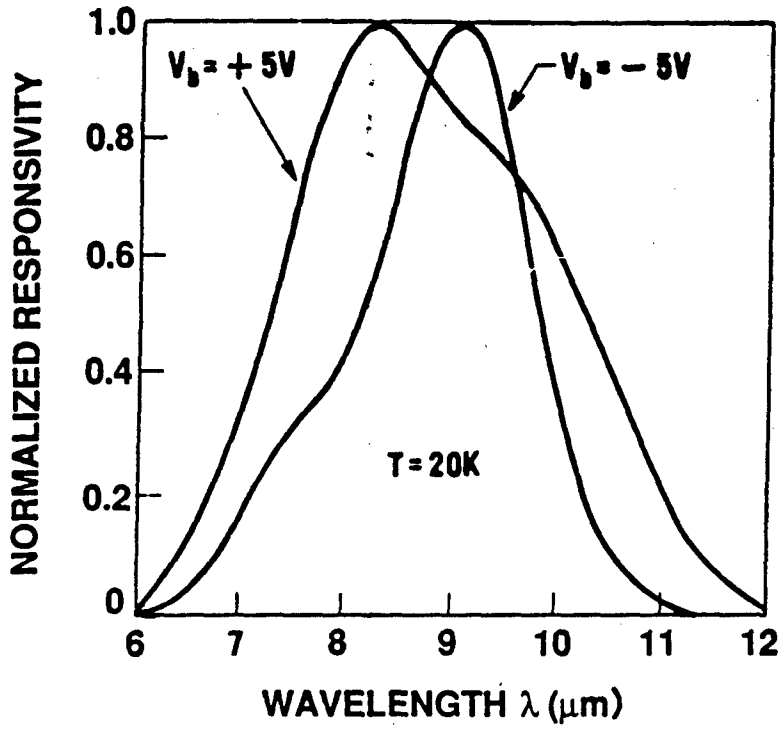
$$T = 77\ K$$

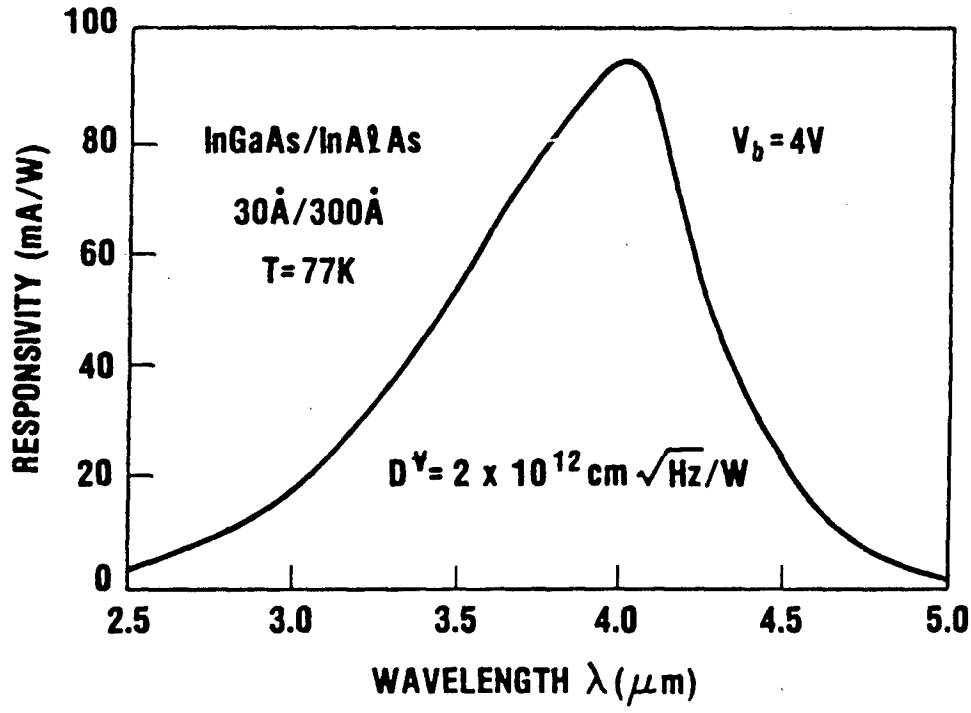

(a)
LWIR
+
-
SAWTOOTH GRATING
n+ GaAs CONTACT LAYER
GaAs/AlGaAs
MULTI-QUANTUM WELL
Au/Ge
SEMI-INSULATING
GaAs SUBSTRATE
(b)
+
-
SAWTOOTH GRATING
n+ GaAs CONTACT LAYER
GaAs/AlGaAs
MULTI-QUANTUM WELL
Au/Ge
SEMI-INSULATING
GaAs SUBSTRATE
LWIR

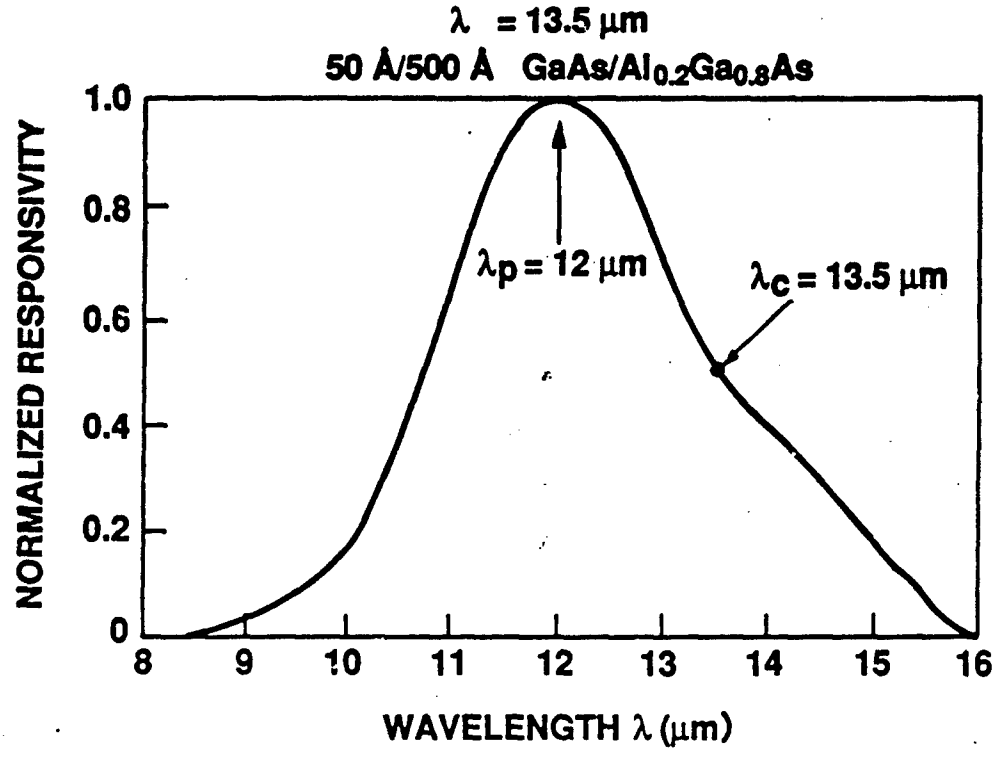

RESPONSIVITY (A/W)
0.0
0.1
0.2
0.3
0.4
0.5
4
6
8
10
12
WAVELENGTH (μm)
45°
(a)
GRATING
(b)


2mV
200pS


a) ZERO BIAS
b) FORWARD BIAS
c) REVERSE BIAS

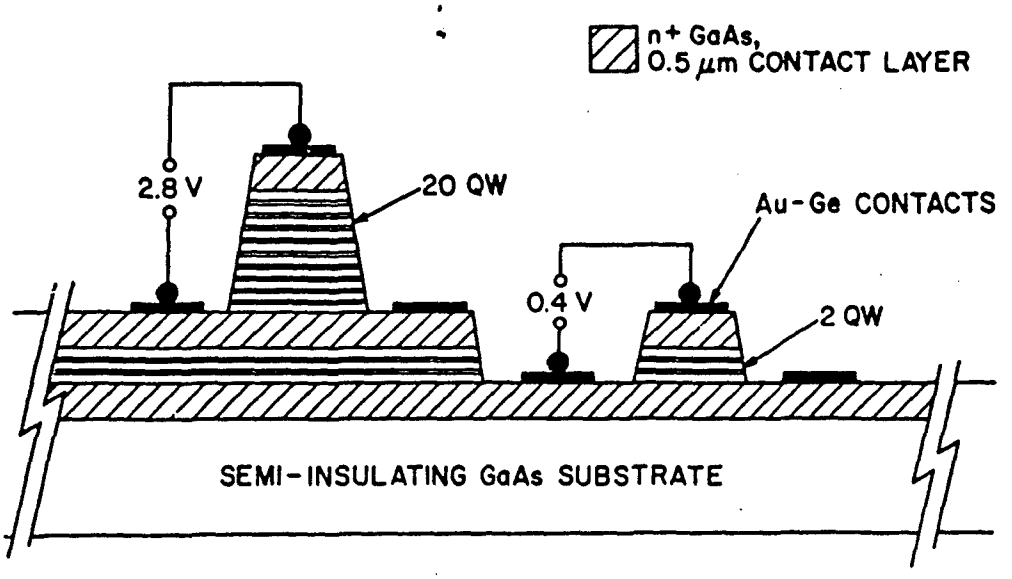

NORMALIZED RESPONSIVITY
1.0
0.8
0.6
0.4
0.2
0
$V_b = +5V$
$V_b = -5V$
T = 20K
6
7
8
9
10
11
12
WAVELENGTH λ (μm)

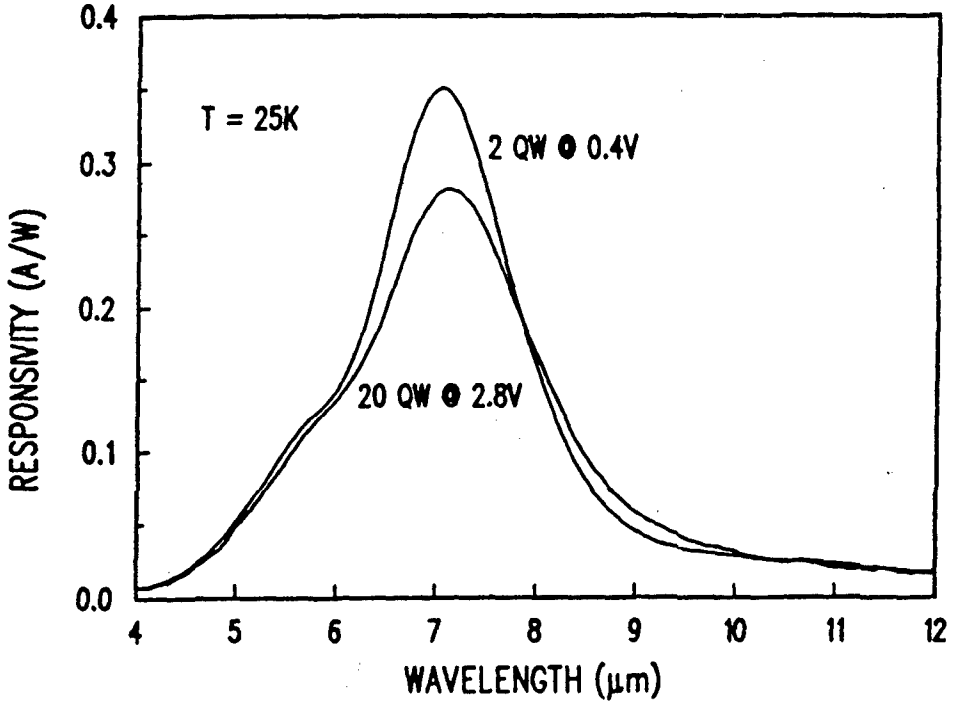

RESPONSIVITY (mA/W)
100
80
60
40
20
0
InGaAs/InAlAs
30Å/300Å
T = 77K
$V_b = 4V$
$D^* = 2 \times 10^{12}$ cm $\sqrt{Hz}/W$
2.5
3.0
3.5
4.0
4.5
5.0
WAVELENGTH λ (μm)

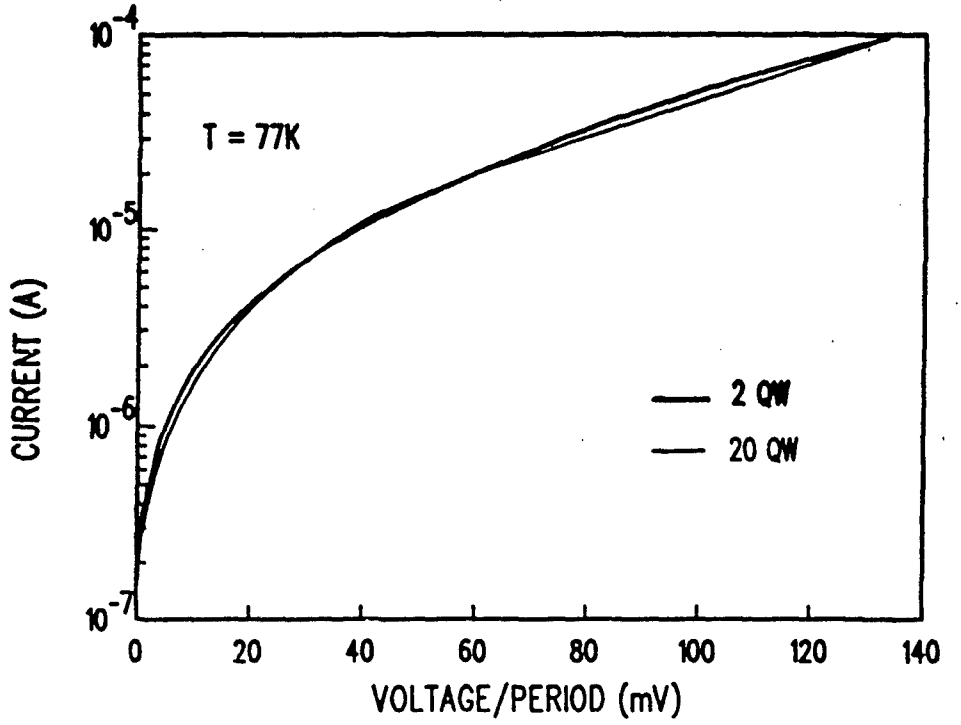


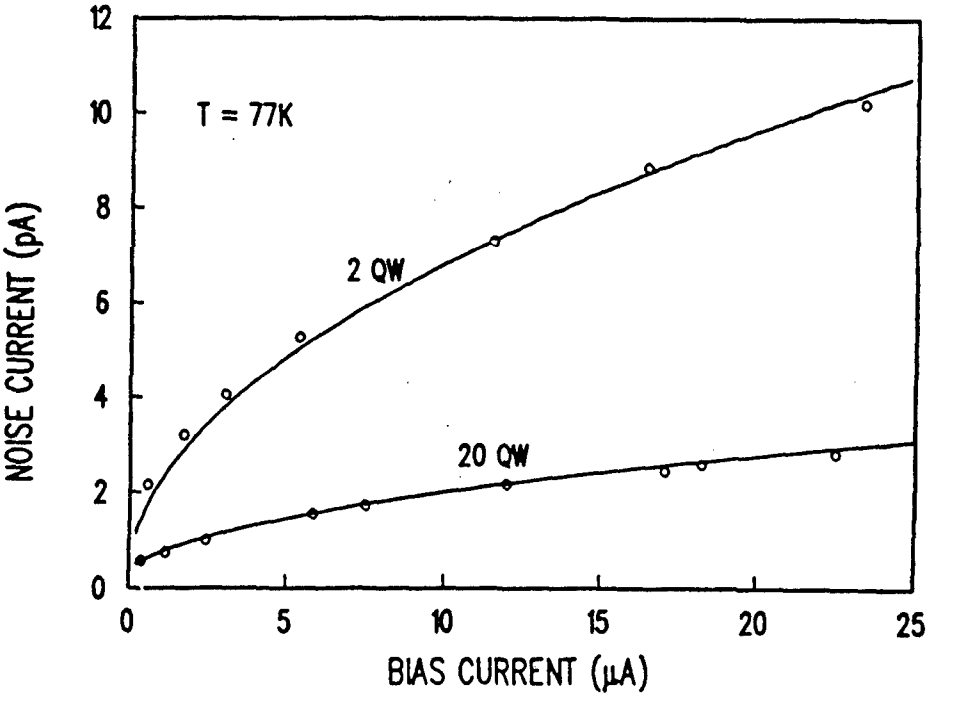
Optical Gain

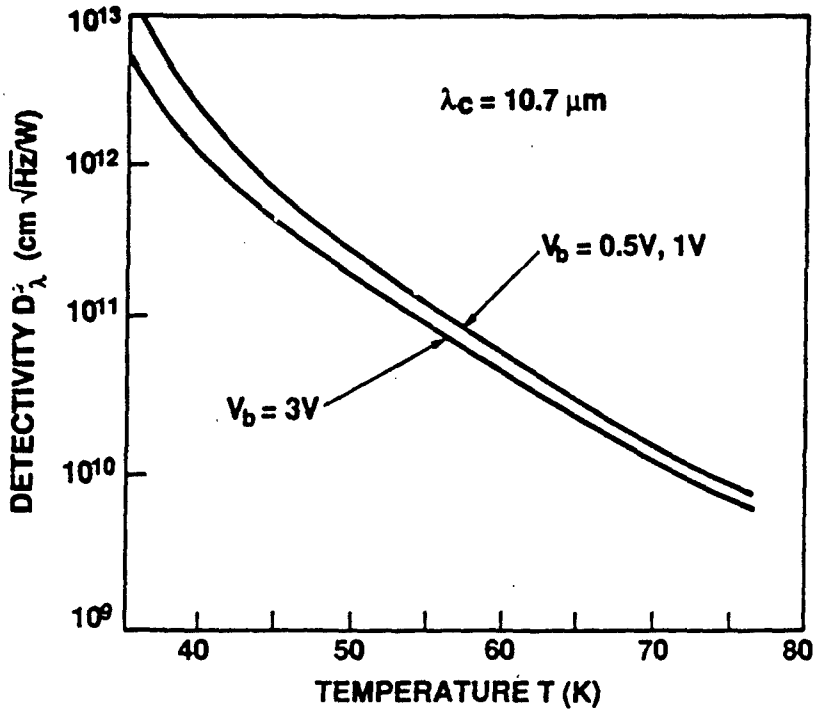
$$g = \frac{\tau_L}{\tau_T} = \frac{L}{\ell}$$


n+ GaAs,
0.5 μm CONTACT LAYER
2.8 V
20 QW
Au-Ge CONTACTS
0.4 V
2 QW
SEMI-INSULATING GaAs SUBSTRATE


T = 25K
2 QW @ 0.4V
20 QW @ 2.8V
RESPONSIVITY (A/W)
0.0
0.1
0.2
0.3
0.4
4
5
6
7
8
9
10
11
12
WAVELENGTH (μm)


T = 77K
CURRENT (A)
10^{-4}
10^{-5}
10^{-6}
10^{-7}
2 QW
20 QW
0
20
40
60
80
100
120
140
VOLTAGE/PERIOD (mV)


T = 77K
NOISE CURRENT (pA)
12
10
8
6
4
2
0
2 QW
20 QW
0
5
10
15
20
25
BIAS CURRENT (μA)



NOISE EQUIVALENT TEMPERATURE CHANGE

$$NE\Delta T = \frac{(A\Delta f)^{1/2}}{D^*_B(dP_B/dT)\sin^2(\theta/2)}$$

$$A = (50\ \mu m)^2$$

$$\Delta f = 60\ Hz$$

$$f/2\ \text{optics}\ (\theta/2 = 14^\circ)$$

$$D^* = 1\times10^{10}\,cm\sqrt{Hz}/W$$

$$NE\Delta T = 0.01\ K$$

ARRAY NONUNIFORMITY

To Obtain Background Limited Array Performance

$$U < \frac{1}{\sqrt{N}}$$

U = uniformity

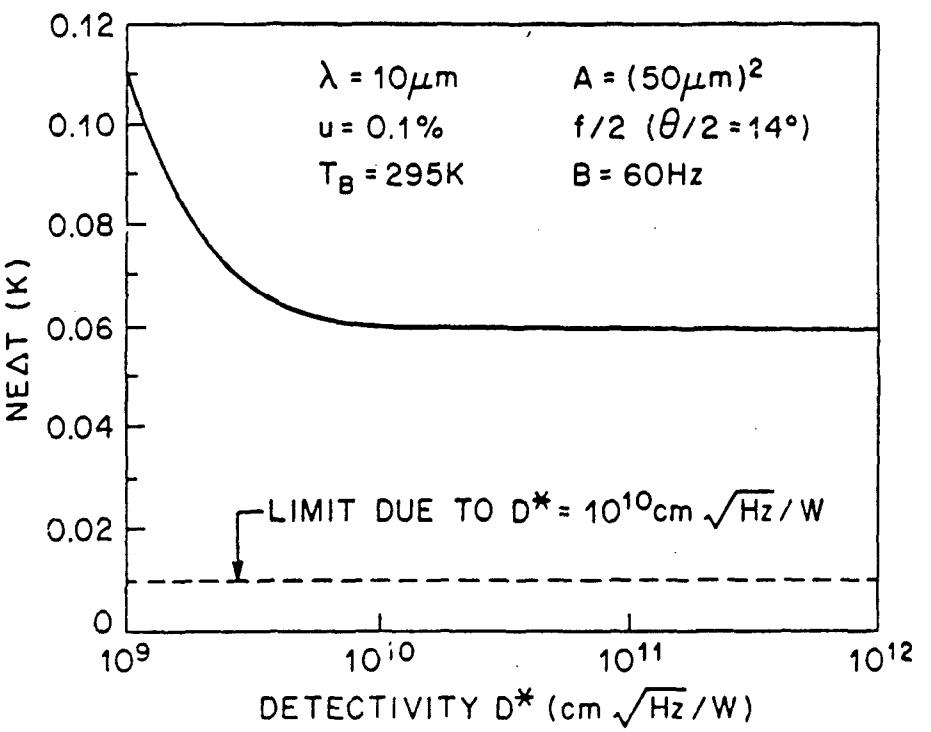
N = number of photoelectrons

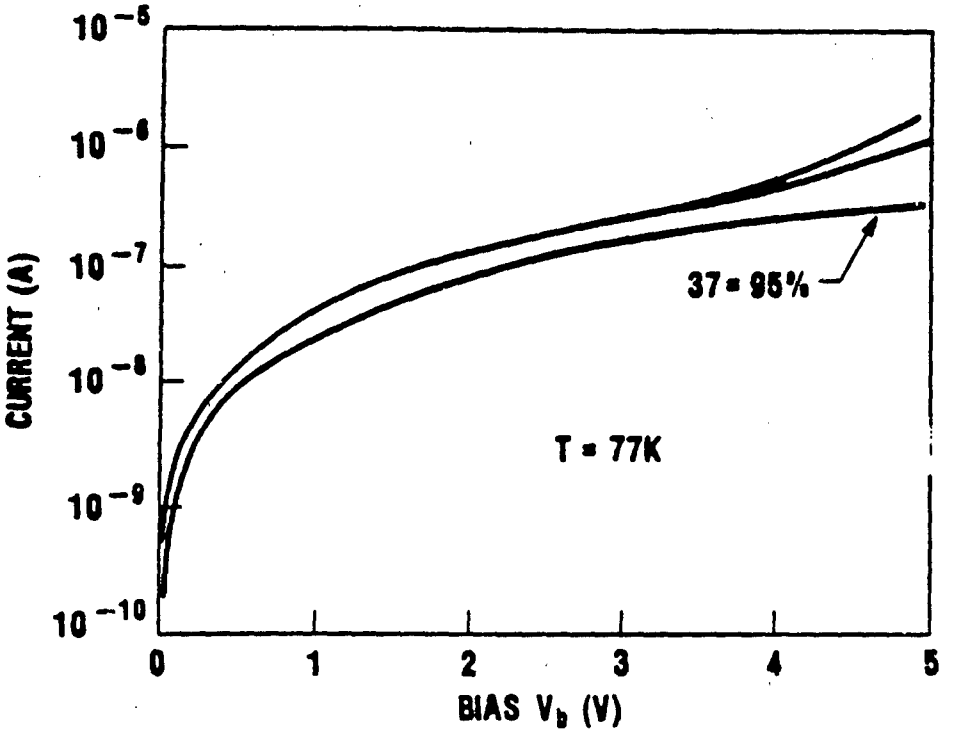
$N = 10^6 \Rightarrow U < 0.1\%$

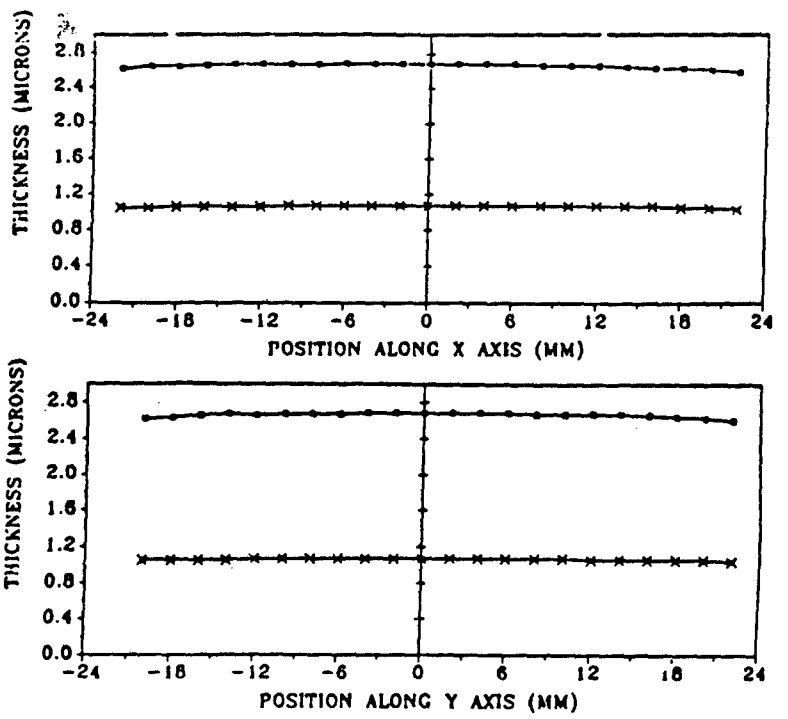
$$(NE\Delta T)_U = \frac{T_B^2 \lambda U}{1.44}$$

$T_B = 295$ K, $\lambda = 10\ \mu$m, $U = 0.1\%$

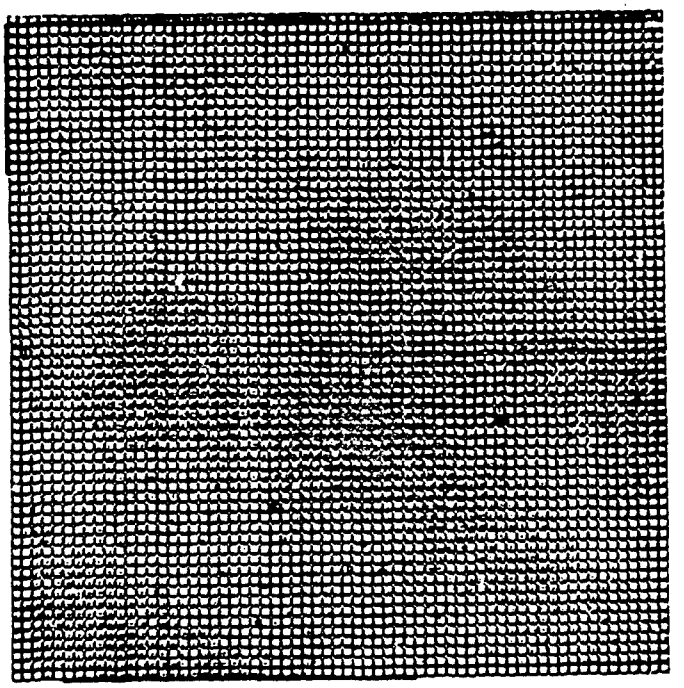
$(NE\Delta T)_U = 0.06$ K

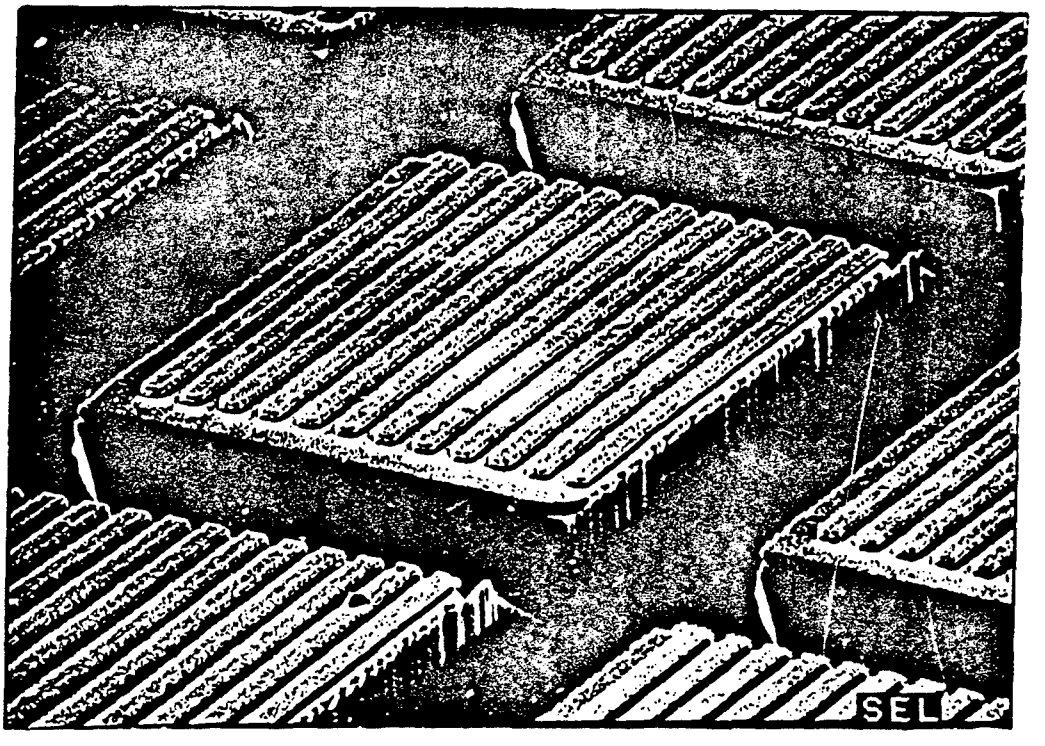



CURRENT (A)
10^{-5}
10^{-6}
10^{-7}
10^{-8}
10^{-9}
10^{-10}
37 = 95%
T = 77K
0
1
2
3
4
5
BIAS V_b (V)


THICKNESS (MICRONS)
2.8
2.4
2.0
1.6
1.2
0.8
0.4
0.0
-24
-18
-12
-6
0
6
12
18
24
POSITION ALONG X AXIS (MM)
THICKNESS (MICRONS)
POSITION ALONG Y AXIS (MM)

64 X 64 ARRAY 50 μm PIXELS





ORIGINAL PACE IS
OF POOR QUALITY

Conclusions

- Demonstrated detectors having $\lambda_c = 4-13.5\ \mu m$
- Spectral width $\Delta\nu/\nu = 13\% - 36\%$
- $D^*_{BB} = 1\times10^{10} cm\sqrt{Hz}/W \quad T = 68\ K \quad \lambda_c = 10.7\ \mu m$
- $D^*_{BB} = 3\times10^{10} cm\sqrt{Hz}/W \quad T = 77\ K \quad \lambda_c = 8.4\ \mu m$
- $D^*_{BB} = 1\times10^{13} cm\sqrt{Hz}/W \quad T < 40\ K \quad \lambda_c = 10.7\ \mu m$
- D^* sufficiently large (arrays uniformity limited)
- Calculated dark current (thermionic, tunneling)
- Hot electron continuum transport resonances
- High speed $\tau < 200$ psec
- Optical gain
- Graded barrier tunable spectral response
- Demonstrated grating detectors
- High uniformity
- Large arrays
- Camera demonstration

N91
14393
UNCLAS

N91-14393

Photovoltaic Quantum Well Infrared Photodetectors

S.A. Lyon
Department of Electrical Engineering
Princeton University
Princeton, NJ 08544

Quantum well infrared photodetectors are a promising new approach to long-wavelength infrared detector arrays. Both single-well photovoltaic and multiple-well photoconductive devices have been demonstrated. I will discuss noise considerations as they apply to photovoltaic devices, grating coupling of the infrared light into QWIPs, and recently demonstrated electrically tunable detectors. The use of "light trapping" to enhance the quantum efficiency and reduce cross-talk in an array will also be addressed.

PRECEDING PAGE BLANK NOT FILMED

LONG WAVELENGTH QUANTUM WELL DETECTORS

(Quantum Well Infrared Photodetectors)
= QWIP's

S. A. Lyon

Electrical Engineering, Princeton

Theory & Measurements

Keith Goossen – now at AT&T Bell Labs

Sanjay Parihar – Princeton

Materials

Kambiz Alavi (Siemens) – now at U. of Texas

Mike Santos & Mansour Shayegan – Princeton

I. Background on IR detectors and Quantum Wells

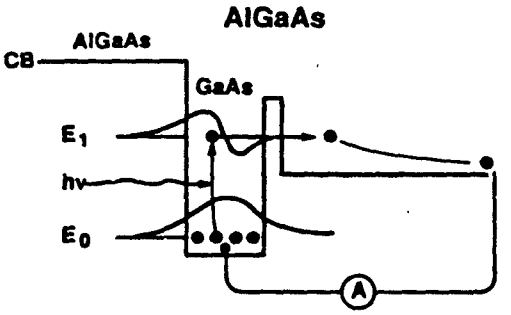
II. Single Well detectors

III. Grating enhanced detectors

VI. Voltage Tunable Detectors

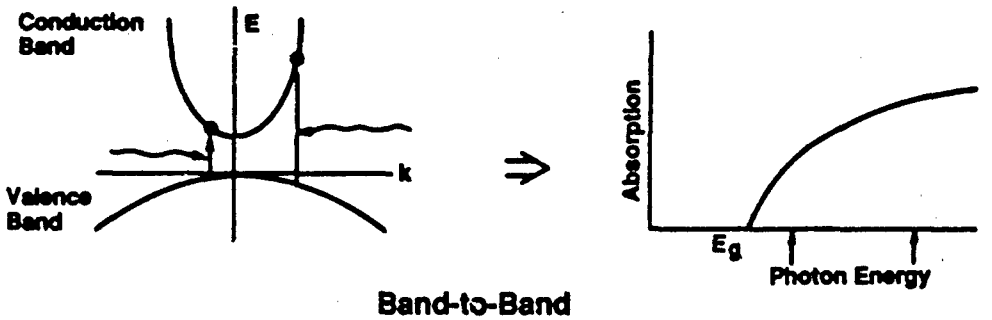
V. Summary

QUANTUM WELL DETECTOR

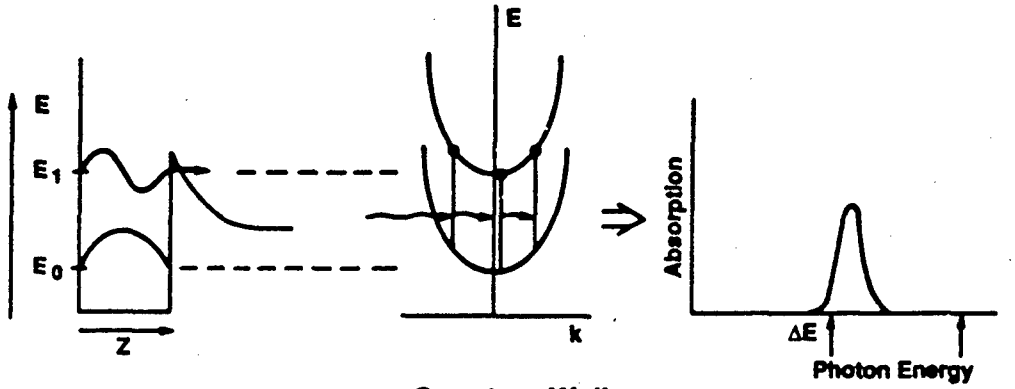


Advantages:
- — Easily change structure for different wavelengths
- — Long wavelength sensitivity with simple materials
- — Voltage tunable

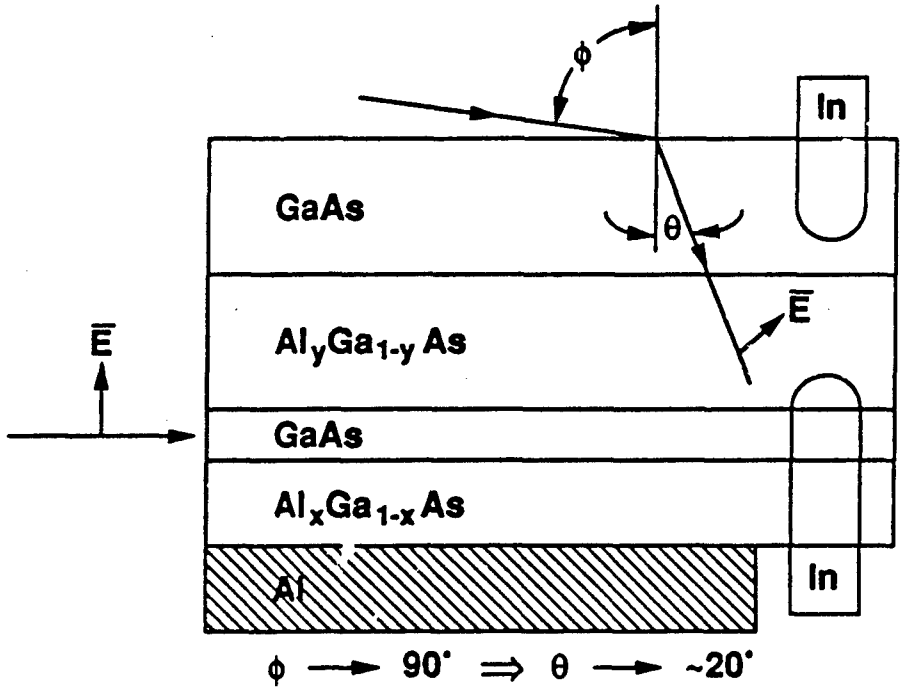
Problems:
- — Not many electrons ⇒ low quantum efficiency
- — Short relaxation time (intersubband scattering)
  ⇒ high dark current

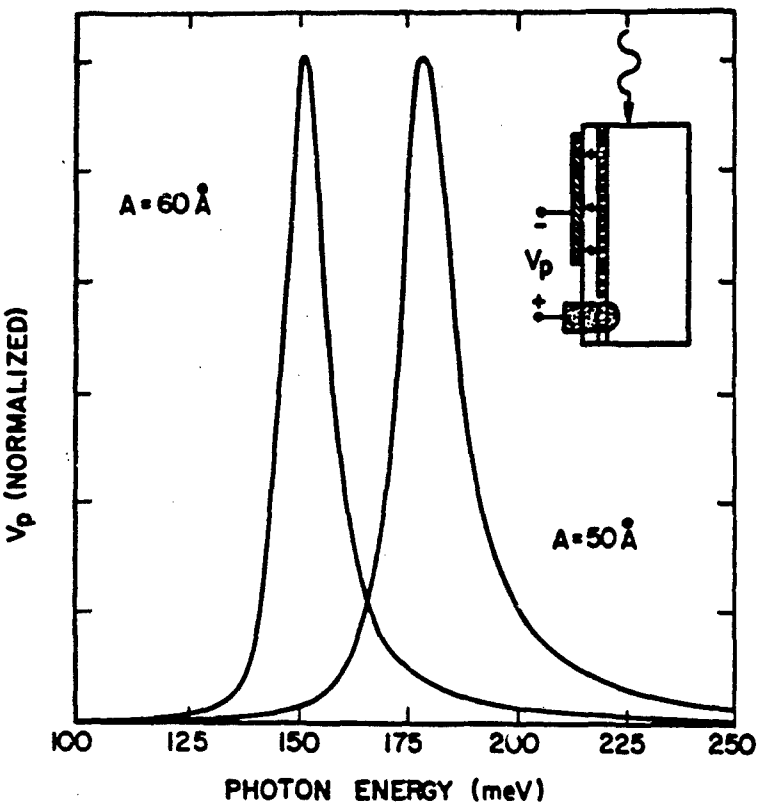


Band-to-Band



Quantum Well
(intersuband)

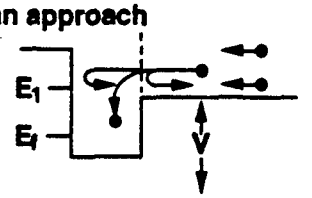




DARK CURRENT (IDEAL)

Use Richardson -Dushman approach

1. **Find the rate of electron capture by the well in thermal equilibrium**



2. **This will also be the emission rate ⇒ dark current under small biases**
3. **Assume relaxction time of 1 ps**

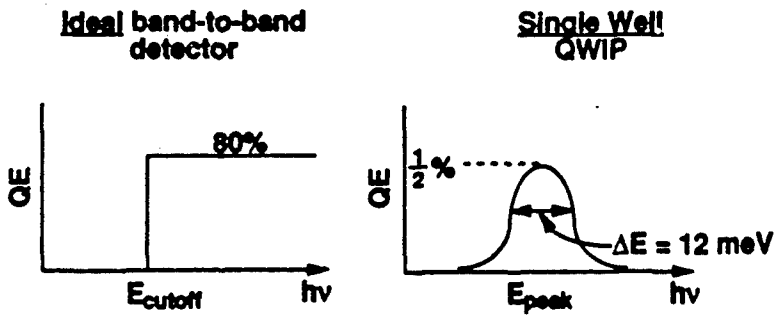
* **Unlike usual assumption for a metal:**
- **Capture probability < 1**
- **Capture probability depends on energy**

Dark current ~100x less for QW than metal

Work function ~ ($E_1 - E_f$) not ($V - E_f$)

STARING ARRAY COMPARISON

50 X 50 μm Pixel F2 Optics
30 ms frame (integration) time
$T_{Detector}$ = 80K $T_{Background}$ = 300K
10 μm



	τ - Auger Limited (Parameters for HgCdTe)	τ - Intersubband Scattering lps
Signal (e^-/cm^2-sec)	3×10^{16}	3×10^{13}
Dark Current (e^-/cm^2-sec)	1.0×10^{14}	1.5×10^{15}
Signal/Noise	1.2×10^5	1×10^3 (NETD = 0.1K)

IMPROVING QUANTUM EFFICIENCY

1. Multiple Wells

   Absorption ∝ # wells

   Dark Noise ∝ $\sqrt{\#\text{wells}}$ (ideal)

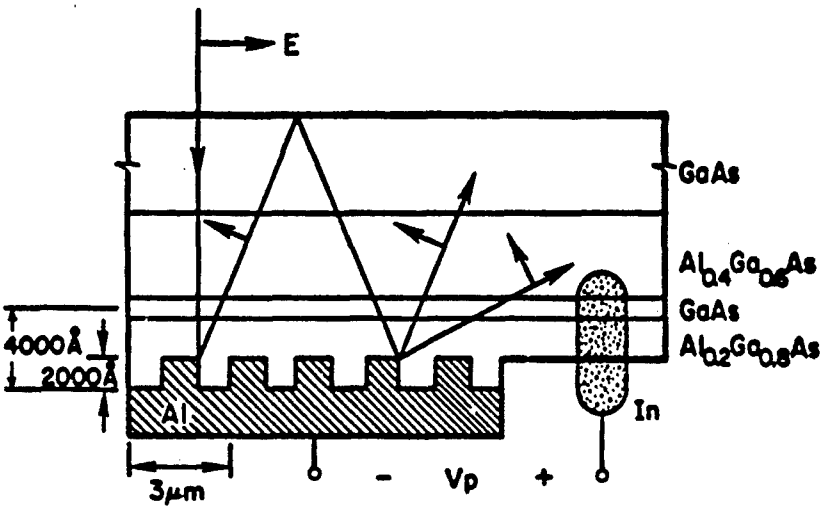
   ∴ $D^* \propto \sqrt{\#\text{wells}}$

2. "Light Trapping"

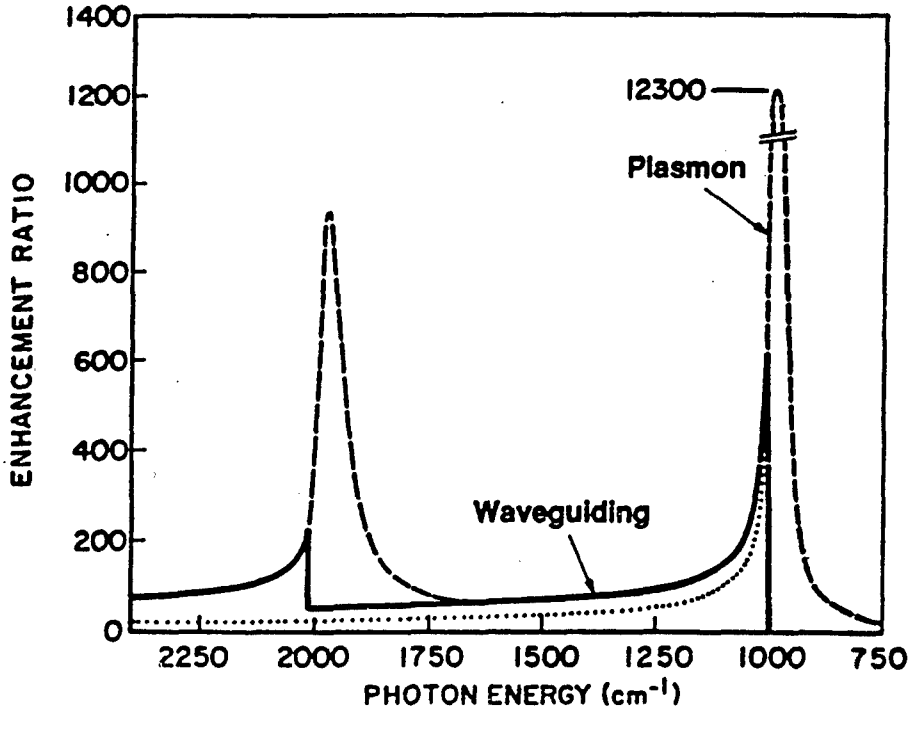
   Surface Plasmons on gratings

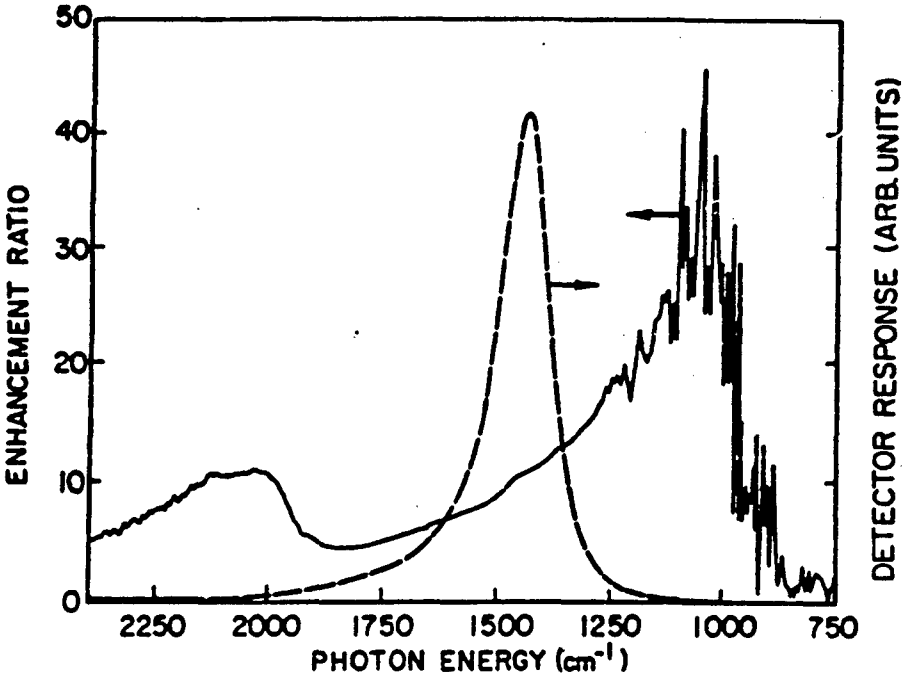
   Waveguiding in GaAs

WAVEGUIDING

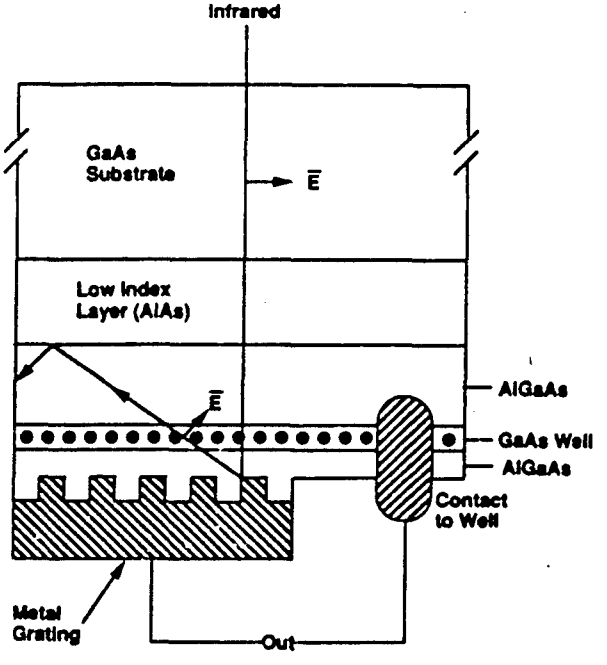


K. W. Goossen, S. A. Lyon, and K. Alavi
Appl. Phys. Lett. 53, 1027 (1988)

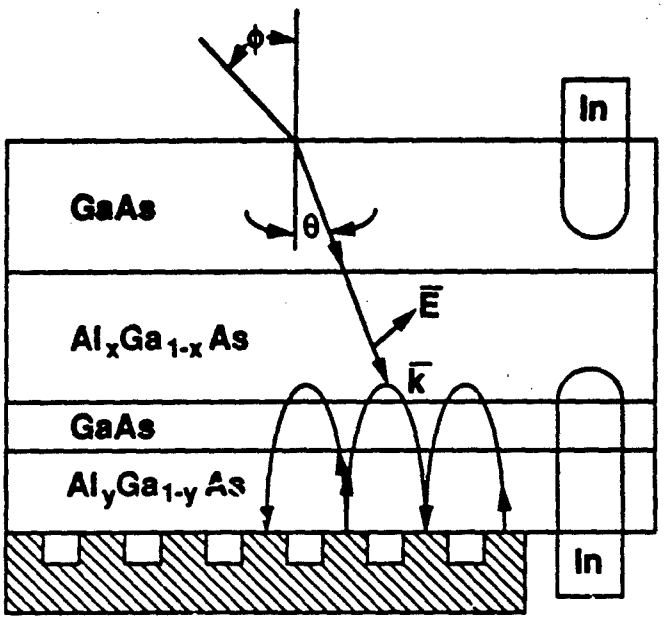




WAVEGUIDING

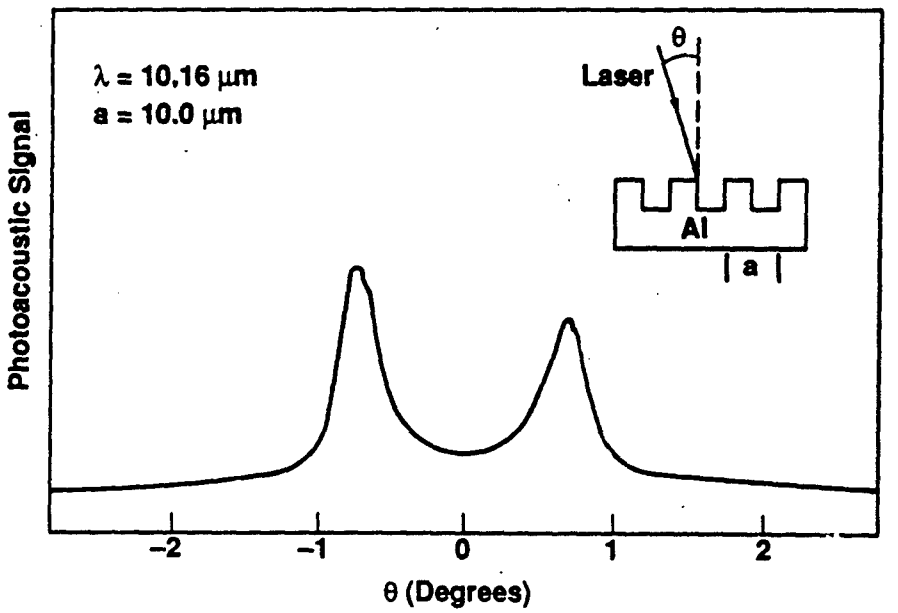


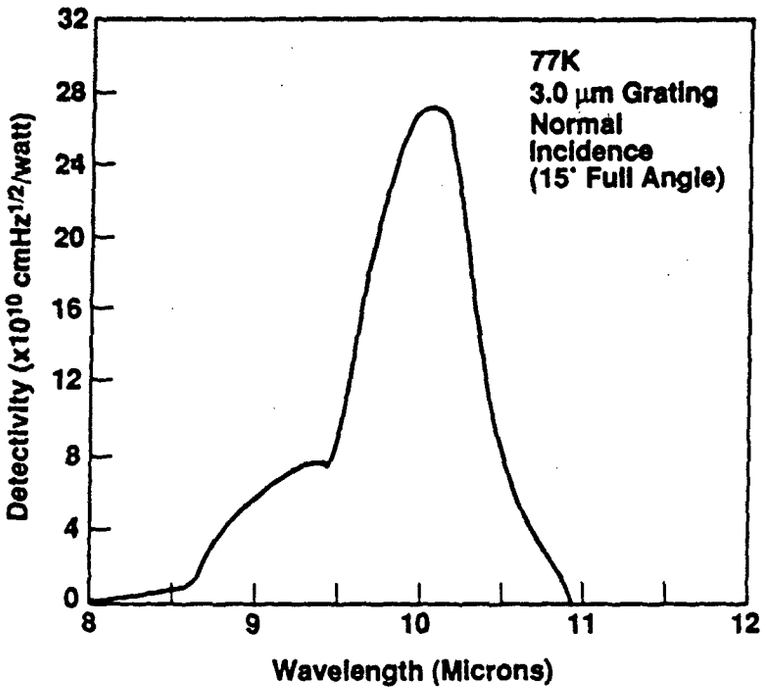
PLASMON ENHANCEMENT



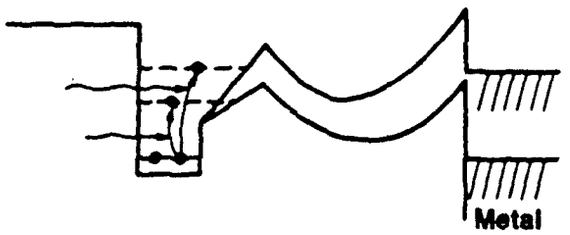
K. W. Goossen and S. A. Lyon
Appl. Phys. Lett. 47, 1257 (1985)

SURFACE PLASMON EXCITATION

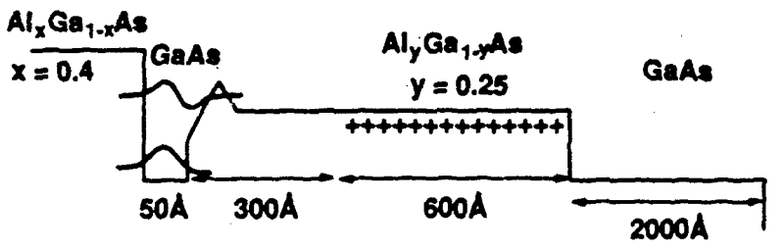




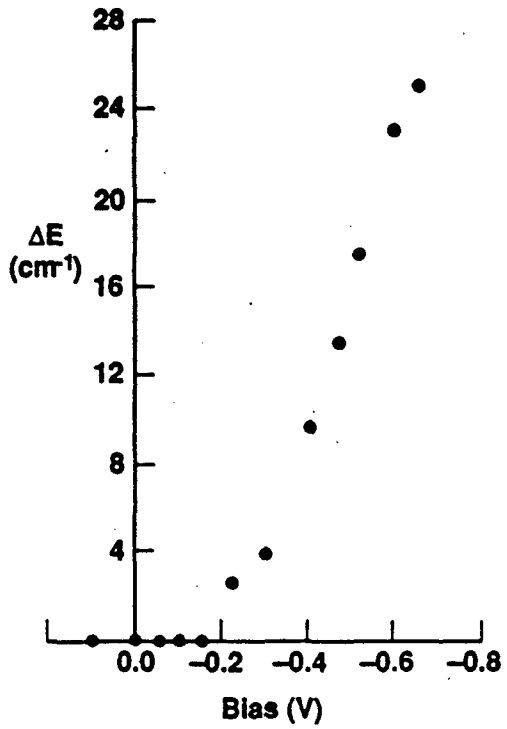
TUNABLE DETECTOR



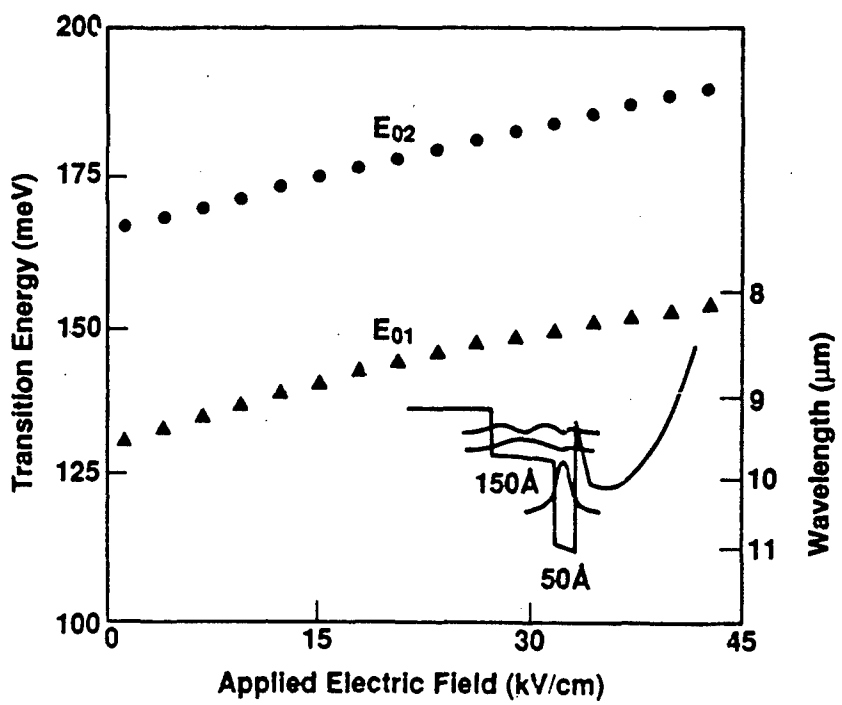
Actual Sample
(Santos & Shayegan)



ENERGY SHIFT VS BIAS FOR GRADED WELL



S. A. Lyon, MSS-4 (July 1989).
S. R. Parihar, S. A. Lyon, M. Santos and M. Shayegan Appl. Phys. Lett. 55, 2417 (1989)



CONCLUSIONS

1. Single-well QWIP's work as expected
   - — Quantum Efficiency (~1/2 – 1%)
   - — Dark Current
2. Incorporation of a diffraction grating allows operation at normal incidence
3. As a single element detector QWIP's cannot compete with photoconductive HgCdTe
4. Single-well QWIP's can compete in a staring array
5. Waveguiding shows promise for enhancing quantum efficiency without the noise penalty of multiple wells
6. Voltage tunable detectors have been demonstrated
   - — Similar structures expected to show large optical nonlinearities

N91
14394
UNCLAS

N91-14394

Characteristics of AlGaAs/GaAs Multiple Quantum Well Infrared Detectors

Bruce K. Janousek, Mary L. Rosenbluth, Michael J. O'Loughlin,
Walter L. Bloss, Frank J. De Luccia, Helmut Kanter, L. Elaine Perry,
and Michael J. Daugherty

The Aerospace Corporation, P.O. Box 92957, Los Angeles, CA 90009

We have fabricated and characterized several AlGaAs/GaAs multiple quantum well infrared detectors to evaluate the ultimate performance of these devices for low infrared background applications. The detectors were designed to have a single bound state in the quantum well and the first excited state in the continuum above the AlGaAs conduction band edge. The difference in energy between the two levels, as determined by the quantum well width and aluminum mole fraction in the barrier, was chosen such that peak absorption would occur near 8 μm. The initial structures studied comprised 50 periods with 40 Å well widths and 300 Å $Al_{0.28}Ga_{0.72}As$ barriers. The performance of these detectors can be summarized as follows:

1). Low dark current densities at 6K which are very sensitive to the device peak absorption wavelength (8.9 μm ⇒ 1E-06 A/cm^2 ; 7.5 μm ⇒ 3E-08 A/cm^2).

2). Dark current activation energies (135-150 meV) in good agreement with the predicted quantum well transition energies.

3). Measured noise which is <u>less than</u> the predicted shot noise on the device dark current.

4). The absence of 1/f noise at frequencies down to 20 Hz.

5). Peak responsivities of approximately 0.3 A/W (uncorrected for reflection losses).

6). Peak detectivities in excess of 10^{12} cm√Hz/W at 6K.

7). Constant detectivity over the temperature range from 6K to approximately 50K.

To better interpret these results and design optimized detectors, we have modeled both the detector noise and tunneling currents. The noise model correctly predicts that multiple quantum well detectors will, indeed, exhibit noise lower than full shot noise. The tunneling current model predicts the dark current versus bias for any choice of design parameters in a multiple quantum well detector. This model predicts a substantially reduced dark current (x 10^{-4}) for samples with 400 Å barriers.

To evaluate structures with thicker barriers, we have fabricated and characterized detectors with 400 Å and 500 Å barriers; a comparison of detector dark currents is shown in Fig. 1. These results are consistent with the predictions of our dark current model. Since the responsivity for these samples (0.3 A/W) is not compromised by the additional barrier width, these new devices have a significantly higher detectivity, as shown in Fig. 2 for the 400 Å barrier sample where detectivities in excess of 10^{13} cm√Hz/W have been measured at temperatures above 30K. The behavior of this device as a function of temperature indicates that tunneling currents are no longer limiting the low-temperature performance of this device.

PRECEDING PAGE BLANK NOT FILMED

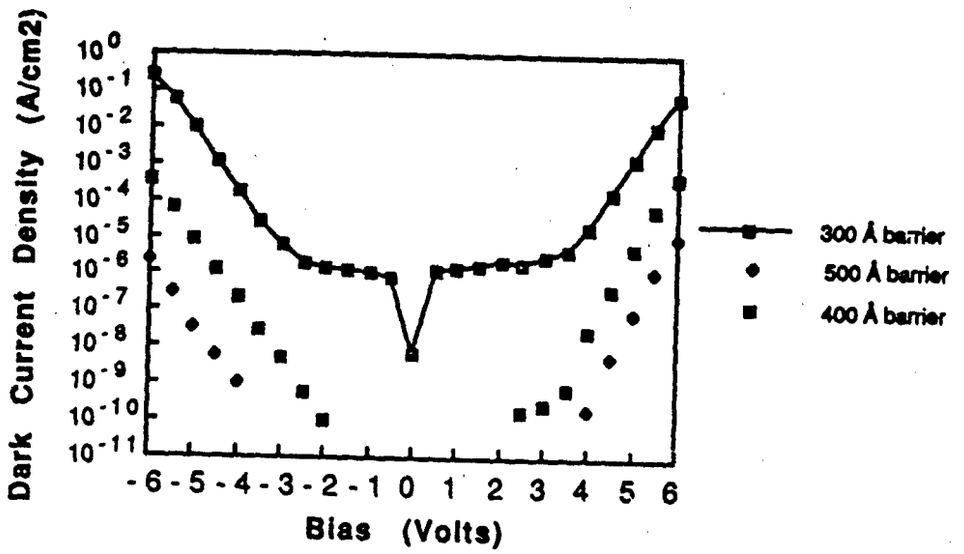


Fig. 1. Dark current density vs. bias at 6K for samples with 300Å, 400Å, and 500Å barriers.

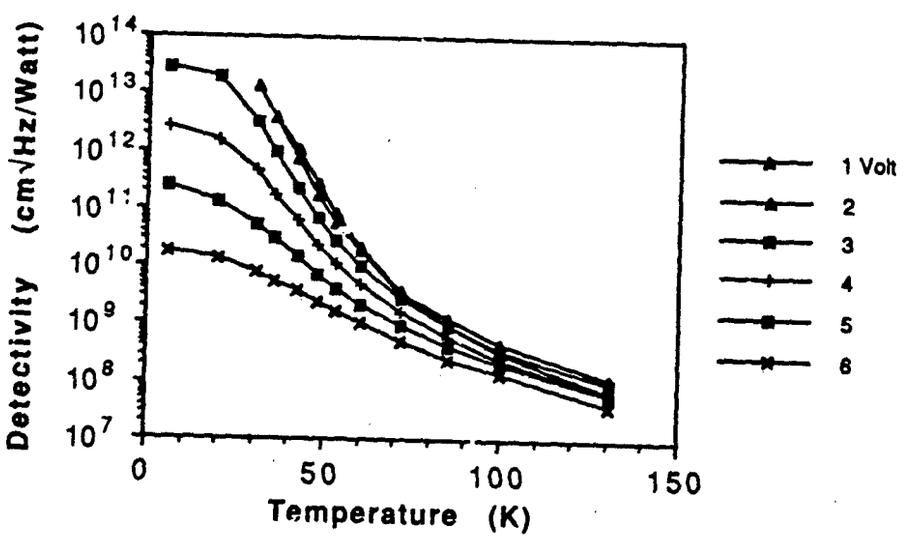


Fig. 2. Detectivity vs. temperature for 400Å barrier sample.

Characteristics of AlGaAs/GaAs Multiple Quantum Well Infrared Detectors

B. Janousek, W. Bloss, M. Rosenbluth, M. O'Loughlin, H. Kanter,
F. DeLuccia, L.E. Perry, and M. Daugherty

The Aerospace Corporation

Outline:

- Motivation
- Materials Preparation/Characterization
- Device Fabrication
- Detector Performance/Modeling Results
  - Noise, dark current models
  - Performance vs. barrier width
- Summary/Conclusions

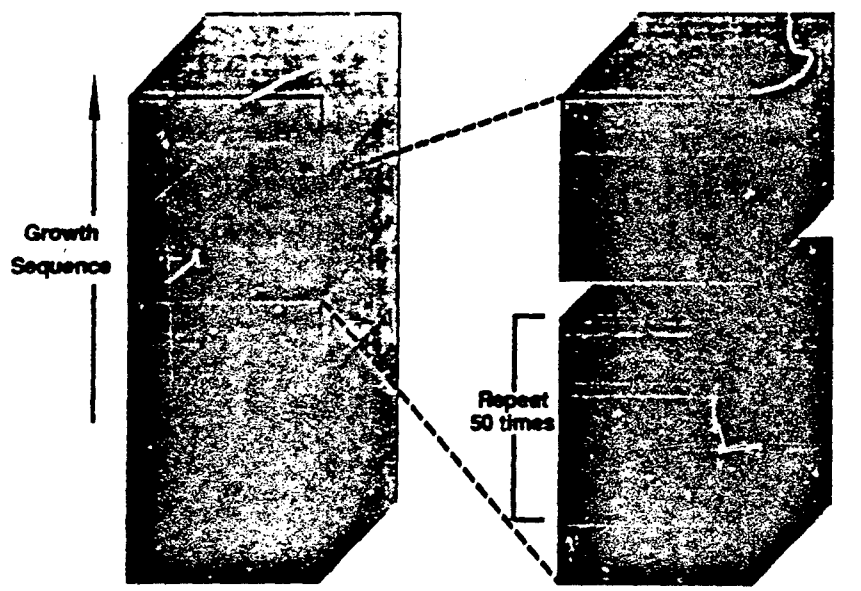
Background/Motivation

- Aerospace role in IR detector development
- VG Semicon MBE machine operational January, 1989
- Are AlGaAs/GaAs quantum well IR detectors appropriate for low infrared background applications?
- What is the ultimate performance of these devices?

Approach

- Two wafers comprise the initial focus of this study:
  - Nominal structure: 40Å GaAs wells/300Å AlGaAs barriers (x=0.28) - 50 periods
  - Excited state in continuum above AlGaAs conduction band edge.
  - Predict ~ 8μm peak responsivity
    - Reproduce AT&T results?
    - Low-background, low temperature performance?
    - Noise sources?
- Additional structures grown to suppress device tunneling currents
  - 300Å, 400Å, 500Å barrier samples

Quantum Well Detector Growth



Electronics Research Laboratory
THE AEROSPACE CORPORATION

FTIR Absorption Spectra of IR Quantum Well Samples

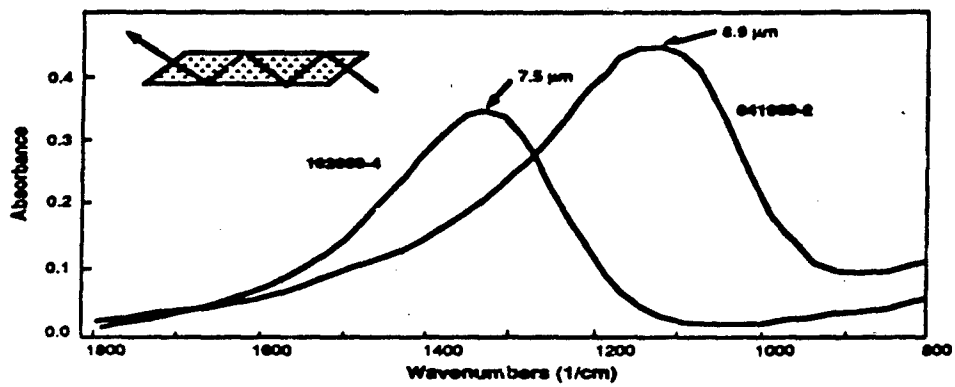
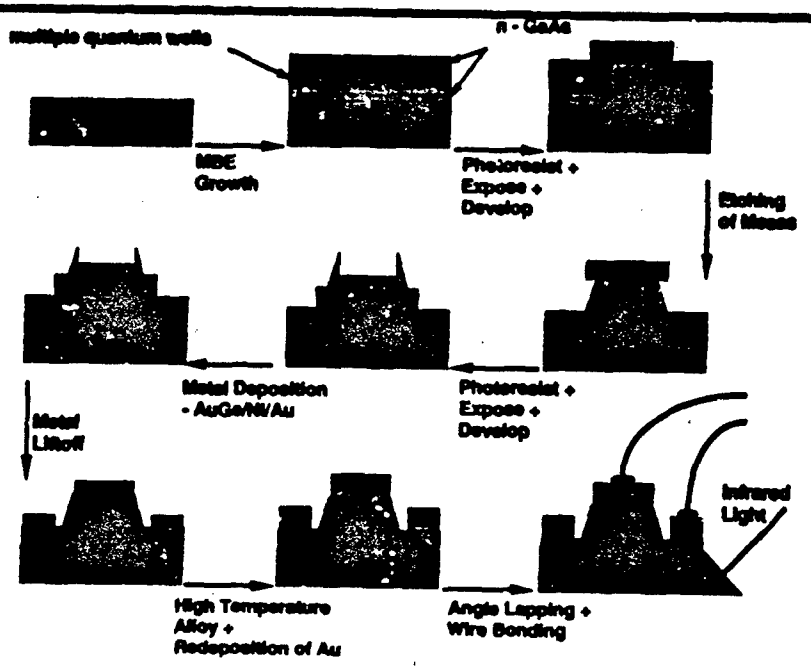


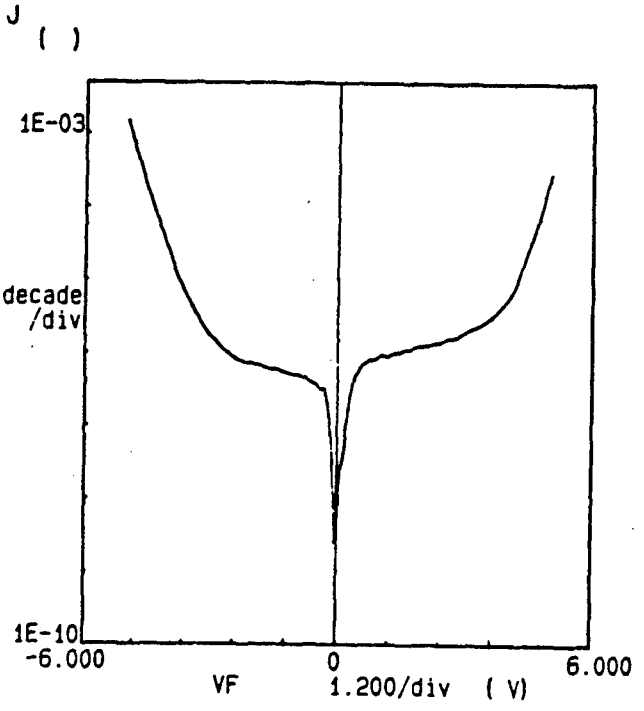
Table of Measured Material Parameters

	041989-2	102089-4	010890-2	010890-4
Peak Wavelength (FTIR)	8.9μm	7.5μm	8.5μm	8.3μm
Superlattice Period (x-ray)		346Å	528Å	432Å
Superlattice Period (TEM)	320Å			
Al Mole Fraction (x-ray)		.35	.31	.31
Al Mole Fraction (Modulation Spectroscopy)	.29	.33		

IR Detector Fabrication

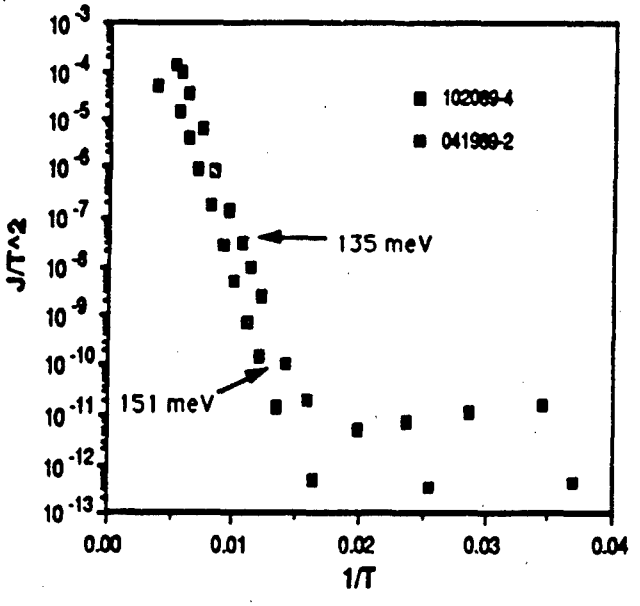


****** GRAPHICS PLOT ******
041989-2 5K

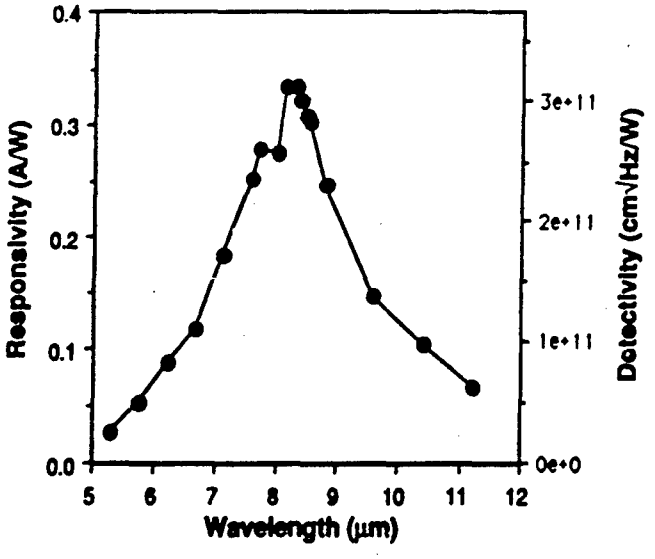


Electronics Research Laboratory
THE AEROSPACE CORPORATION

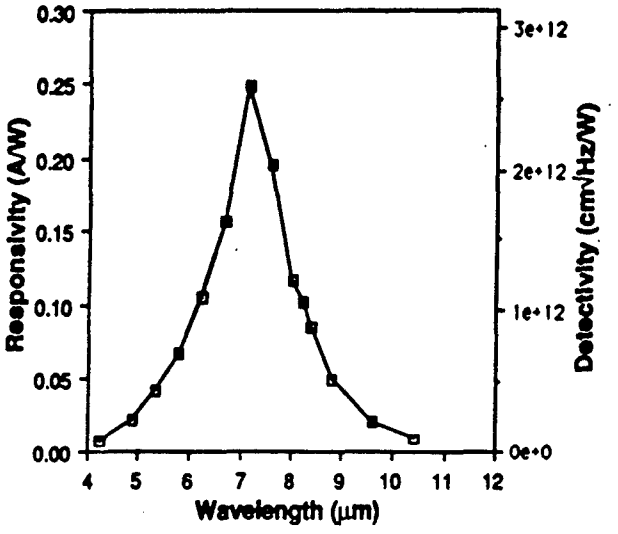
Arrhenius Plots of Detector Dark Current



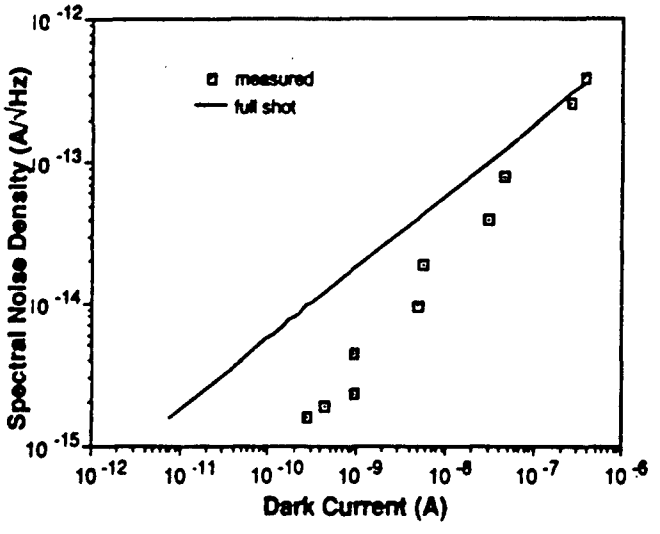
R and D* vs. Wavelength (6K) - Sample 041989-2



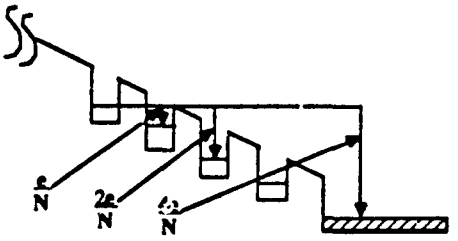
R and D* vs. Wavelength (6K) - Sample 10[illegible]89-4



Spectral Noise Density vs. Dark Current (7K) - Sample 041989-2



Noise Model

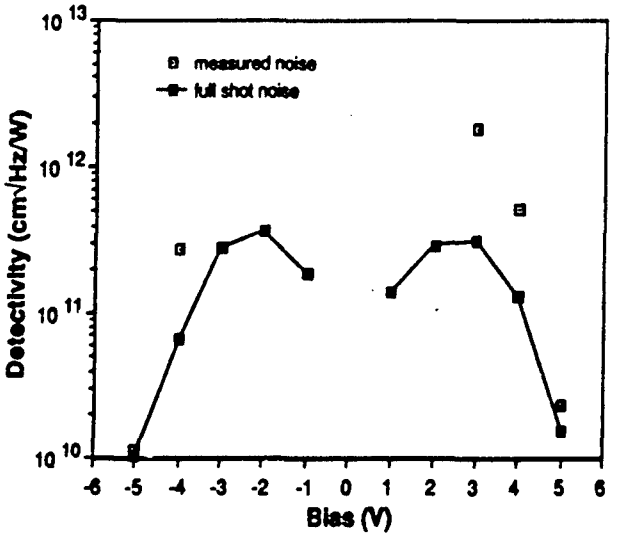


- tunneling events are independent
- governed by Poisson statistics

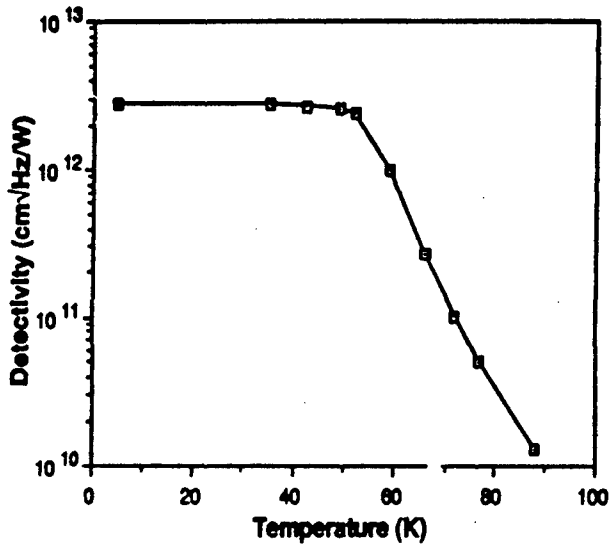
- Input parameters:
  - Fraction of total tunneling current from an internal well that is emitted to the continuum
  - Hot electron mean free path
  - Number of periods

- Key Results:
  - Quantum well detectors are predicted to exhibit noise lower than full shot noise.

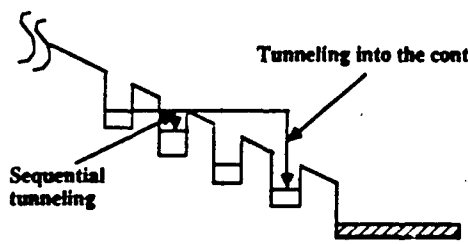
IR Quantum Well Detectivity (7K) - Sample 041989-2



Detectivity vs. Temperature - Sample 102089-4



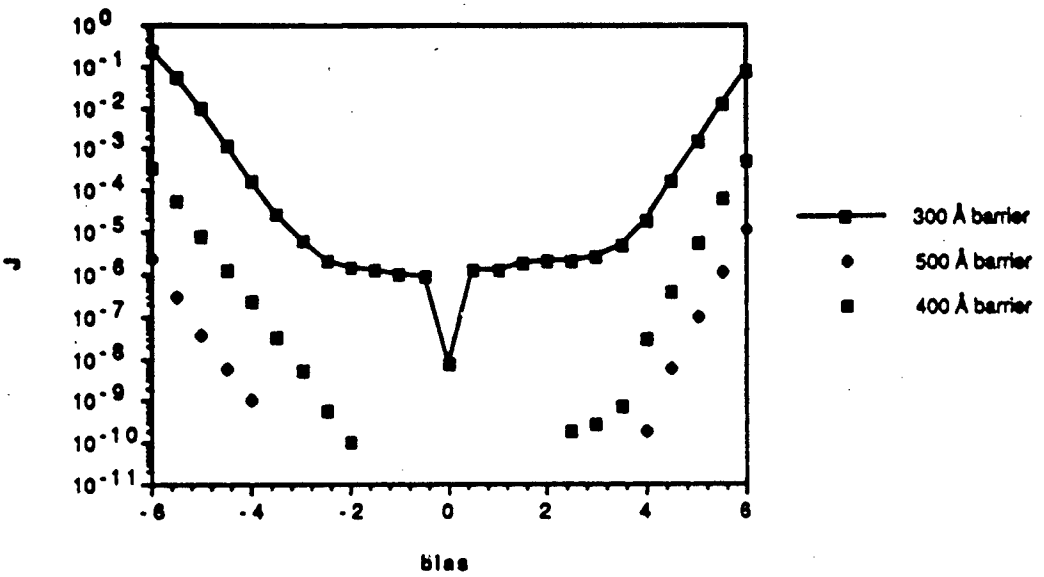
Tunneling Dark Current Model



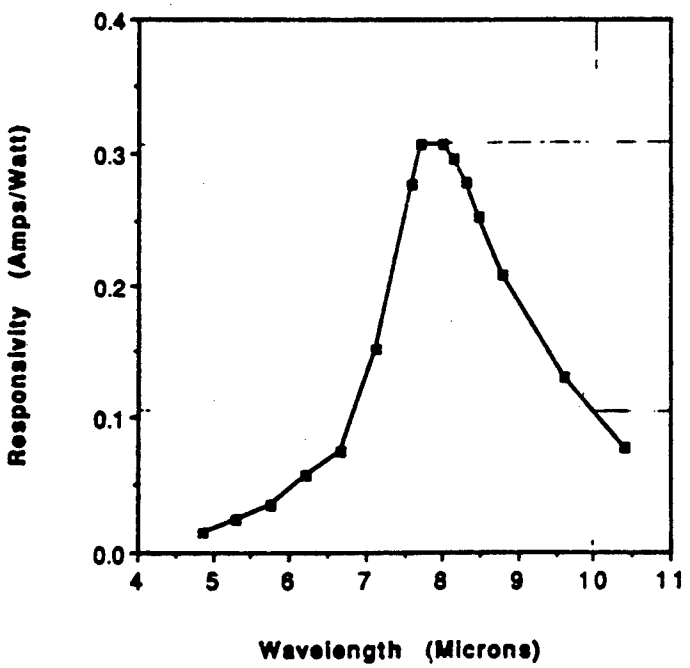
- Dark current vs. bias for any choice of detector design parameters.

- Approach: Nodal analysis in which analogs of Kirchhoff's current and voltage laws are applied
  - Net current into each internal well (node) is zero
  - Applied bias is the sum of the potential drops across barriers
  - Charge distribution in internal wells, cathode, and anode adjusted until Kirchhoff's laws are satisfied
- Results:
  - Model-generated I-V curves similar to experimental curves
  - Predict substantially reduced dark current $(x10^{-4})$ for detector with 400Å barriers

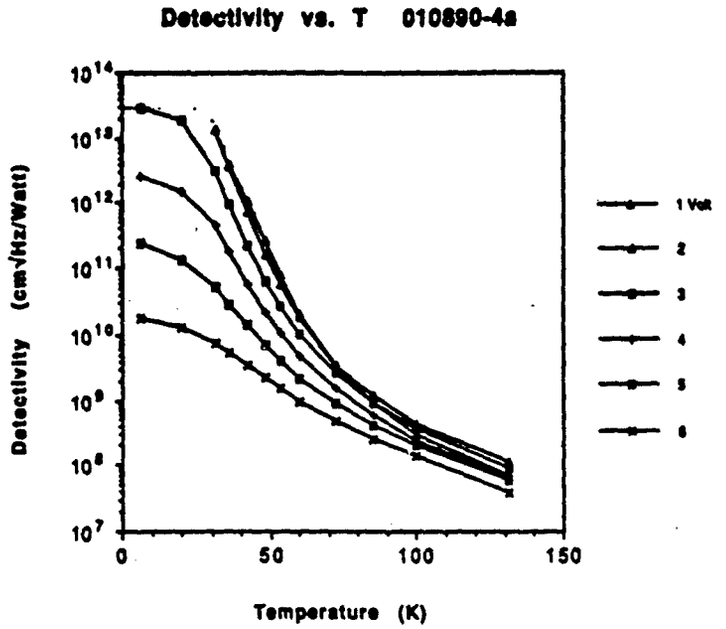
Dark Current Density vs. Applied Bias

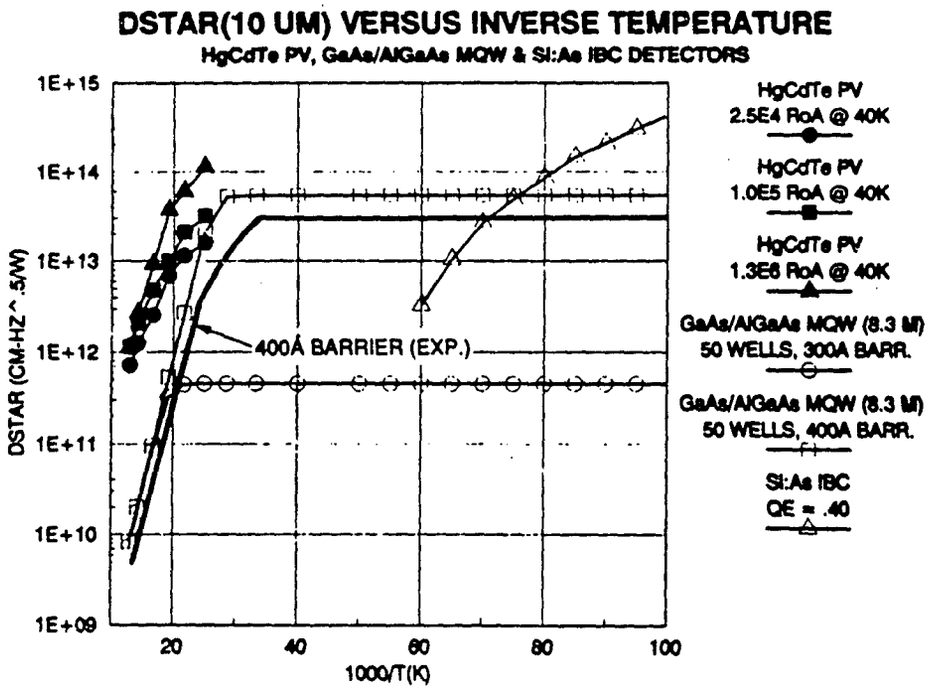


R vs. Wavelength 010890-4a 6K; V = 5 Volts



$$\frac{R_{10\,\mu m}}{R_{peak}} = \frac{0.11}{0.31} = 0.36$$


Detectivity vs. T 010890-4a
Detectivity (cm-√Hz/Watt)
Temperature (K)
1 Volt
2
3
4
5
6


DSTAR(10 UM) VERSUS INVERSE TEMPERATURE
HgCdTe PV, GaAs/AlGaAs MQW & SI:As IBC DETECTORS
DSTAR (CM-HZ^.5/W)
1000/T(K)
400Å BARRIER (EXP.)
HgCdTe PV
2.5E4 RoA @ 40K
HgCdTe PV
1.0E5 RoA @ 40K
HgCdTe PV
1.3E6 RoA @ 40K
GaAs/AlGaAs MQW (8.3 M)
50 WELLS, 300A BARR.
GaAs/AlGaAs MQW (8.3 M)
50 WELLS, 400A BARR.
SI:As IBC
QE = .40

Summary/Conclusions

- High detectivity quantum well IR detectors have been demonstrated
  - $D^* = 1E13$ $cm\sqrt{Hz}/W$ at 10 μm and 20K
- Devices show excellent reproducibility, uniformity, and radiation hardness
  - Simple physical models correctly predict device performance
- Progress in the development of LWIR quantum well detectors has been very rapid, particularly given the small investment made to date
- Future efforts: Increase the device quantum efficiency and develop array concepts



N91
14395
UNCLAS

N91-14395

Resonant Tunneling IR Detectors

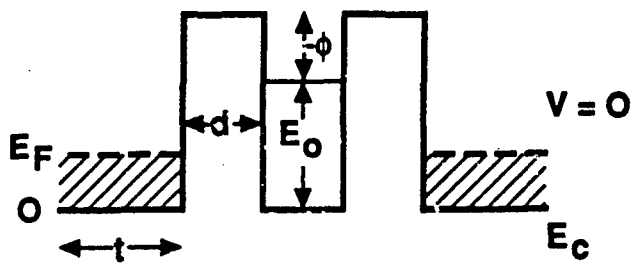
Jerry M. Woodall and T. P. Smith, III
IBM Thomas J. Watson Research Center
P. O. Box 218
Yorktown Heights, NY 10598

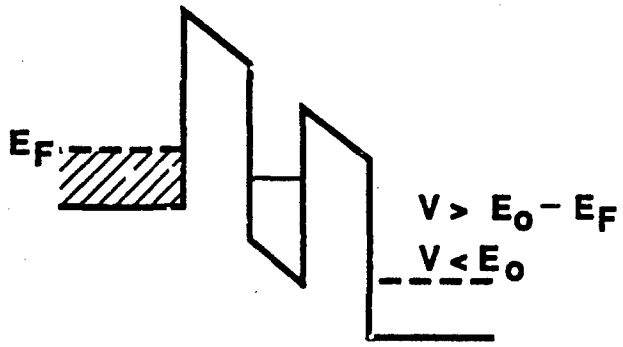
We propose a novel semiconductor heterojunction photodetector which would have a very low dark current and would be voltage tunable. A schematic diagram of the device and its band structure are shown in Figure 1. The two crucial components of the device are a cathode (InGaAs) whose condition band edge is below the conduction band edge of the quantum wells and a resonant tunneling filter (GaAs-AlGaAs). In a standard resonant tunneling device the electrodes are made of the same material as the quantum wells, and this device becomes highly conducting when the quantum levels in the wells are aligned with the Fermi level in the negatively biased electrode. In contrast, our device is essentially non-conducting under the same bias conditions. This is because the Fermi Level of the cathode (InGaAs) is still well below the quantum levels to that no resonant transport occurs and the barriers (AlGaAs) effectively block current flow through the device. However, if light with the same photon energy as the conduction-band discontinuity between the cathode and the quantum wells, E_{c3}-E_{c1} is shone on the sample, free carriers will excited to an energy corresponding to the lowest quantum level in the well closest to the cathode ($h\nu + E_{c1}=E_o$). These electrons will resonantly tunnel through the quantum wells and be collected as a photocurrent in the anode (GaAs). To improve the quantum efficiency, the cathode (InGaAs) should be very heavily doped and capped with a highly reflective metal ohmic contact. The thickness of the device should be tailored to optimize thin film interference effects and afford the maximum absorption of light.

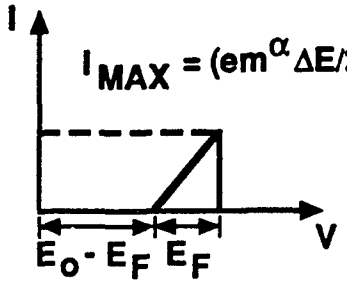
Because the device relies on resonant tunneling, its response should be very fast, and the small voltages needed to change the responsivity should allow for very high frequency modulation of the photocurrent. In addition, the device is tuned to a specific photon energy so that it can be designed to detect a fairly narrow range of wavelengths. This selectivity is important for reducing the photocurrent due to spurious light sources. Although we have cited the use of InGaAs, GaAs, and AlGaAs by way of example this device can be fabricated from a number of materials depending on the detector characteristics one desires. Also, the resonant tunneling filter may comprise any number of quantum wells to obtain the appropriate operating voltage so long as the filter region is not so thick that it significantly reduces the photocurrent when the electron energy is resonant with the levels in the wells.

PRECEDING PAGE BLANK NOT FILMED

RESONANT TUNNELING





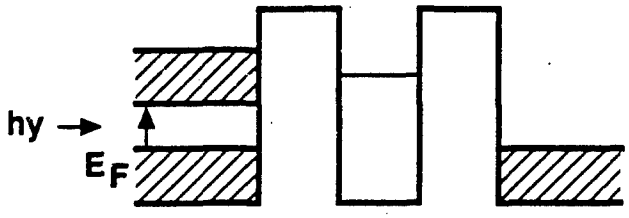


$$I_{MAX} = (em^{\alpha} \Delta E / 2\pi h^3) E_F$$

ΔE is resonance width

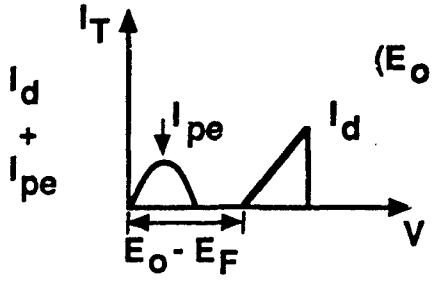
- ↑ as d ↓
- as ϕ_{eff} ↓
- as m^{α} ↓

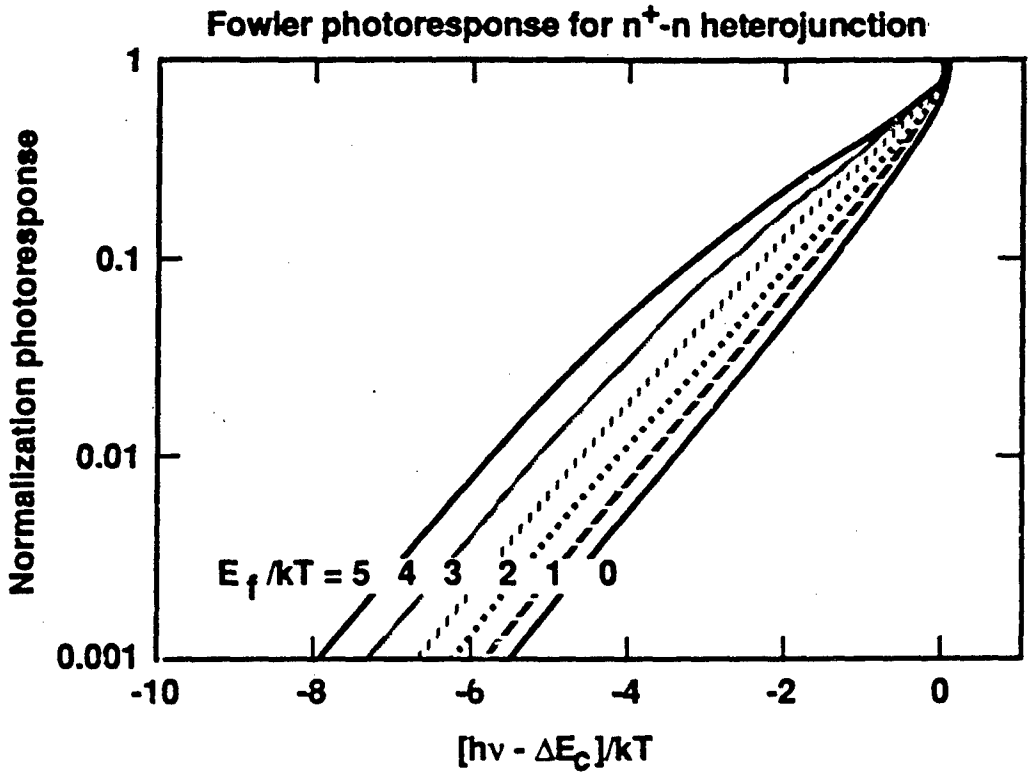
PHOTOEXCITED RESONANT TUNNELING



$I_{pe\ MAX}$ When $h\nu = E_o$

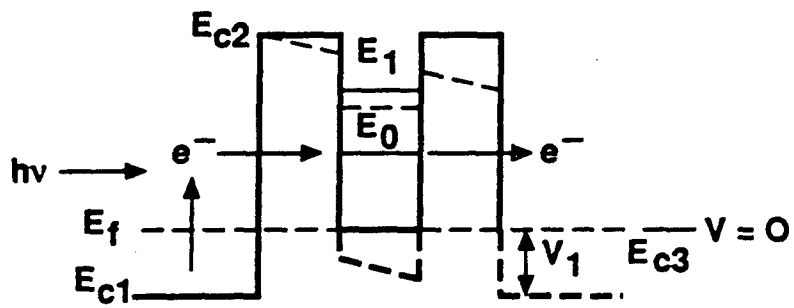
Photocurrent when $(E_o - E_F) \leq h\nu \leq E_o$





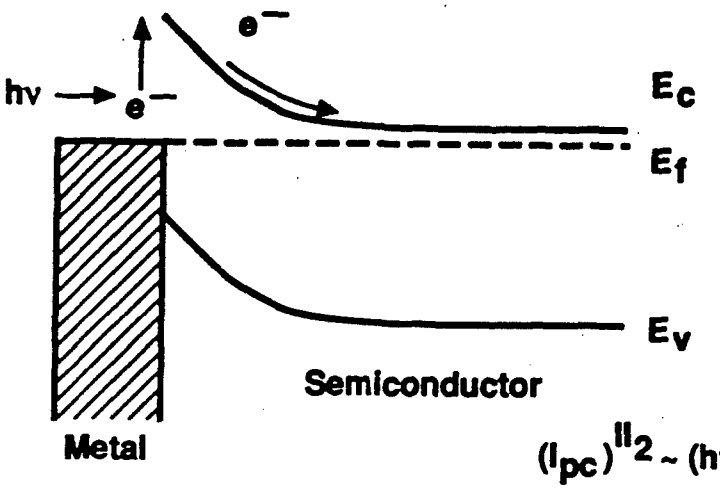
$$R \propto A^* T^{3/2} \int_{\frac{\Delta E_c - h\nu}{kT}}^{\infty} y^{-1/2} \ln\left[1 + \exp\left[\frac{E_f}{kT} - y\right]\right] dy$$

RESONANT TUNNELING IR-PHOTODETECTOR

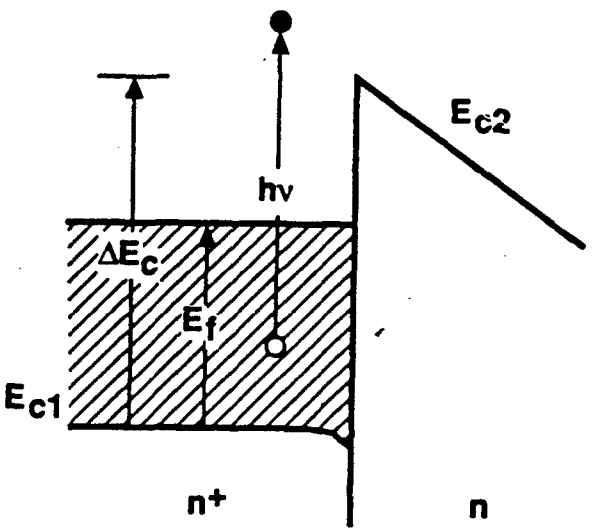


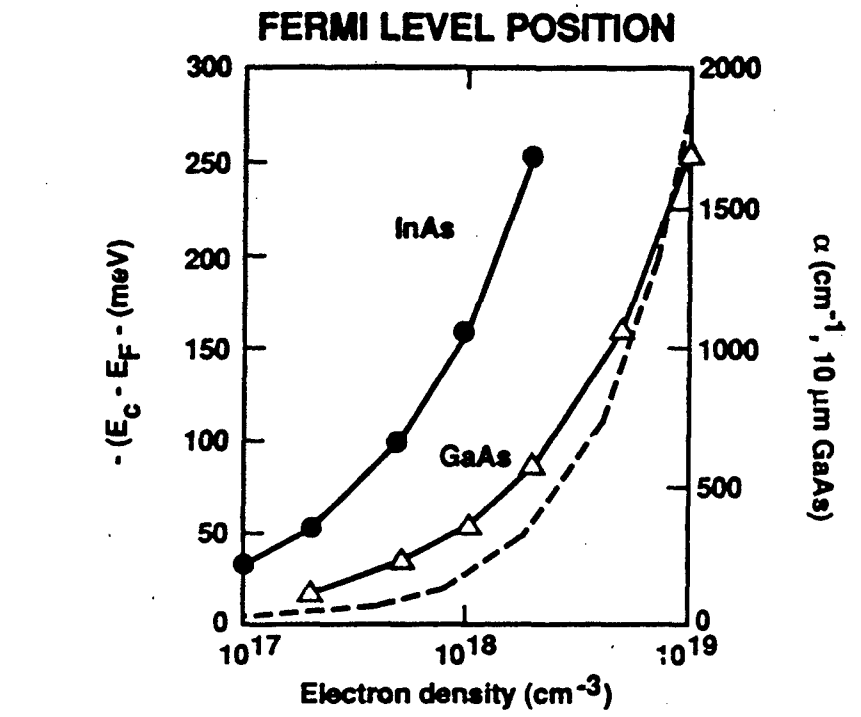
- High IR absorption
- Low dark current

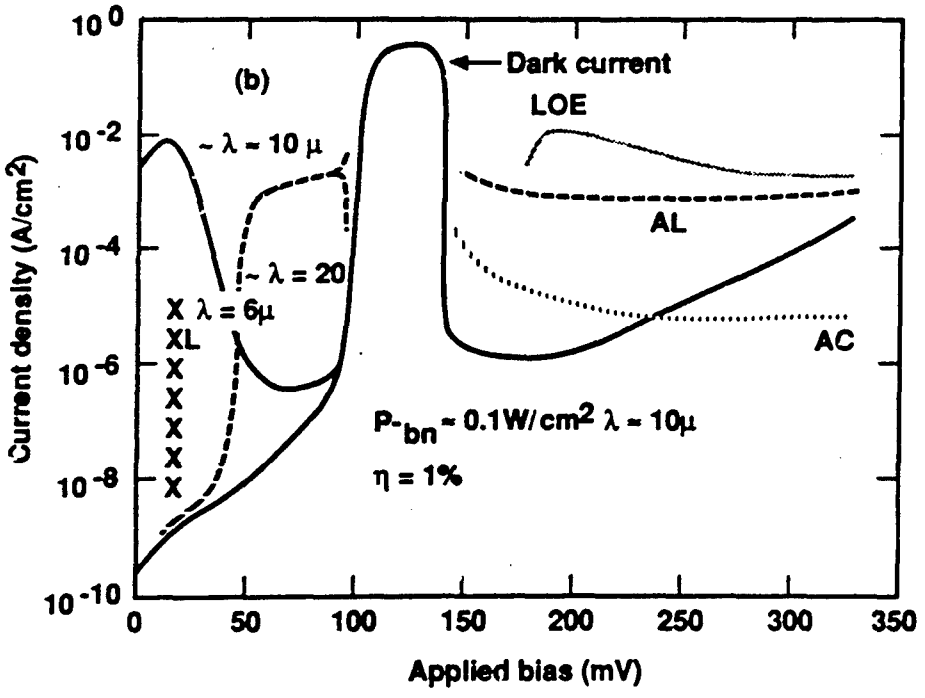
SCHOTTKY BARRIER
INTERNAL PHOTOEMISSION DEVICE

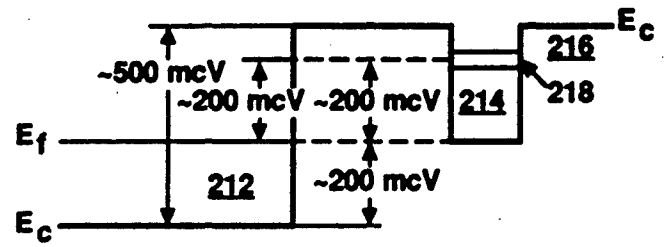


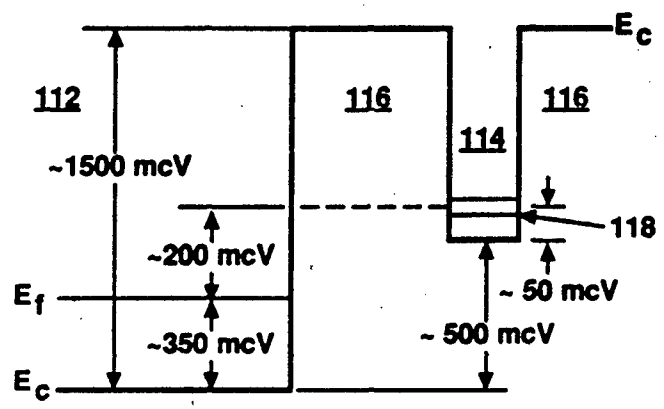
- IR Photon excites e⁻ over barrier
- High dark current – barrier ~ h ν
- Low quantum efficiency
- ϕ_{bn} = 0.8 → -0.2 for GaInAs

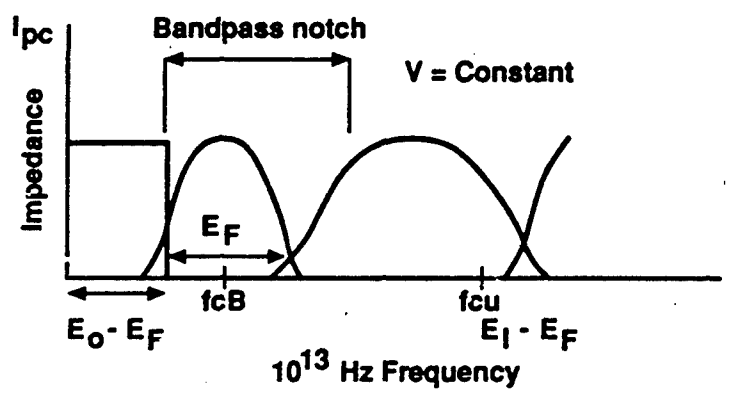


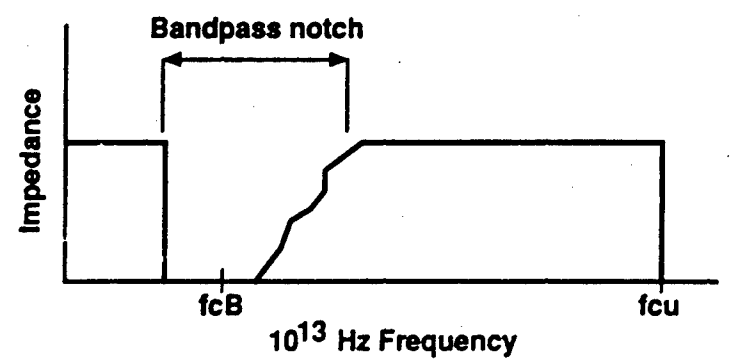

FERMI LEVEL POSITION
300
250
200
150
100
50
0
2000
1500
1000
500
0
InAs
GaAs
$-(E_c - E_F)$ - (meV)
α (cm^{-1}, 10 μm GaAs)
10^{17}
10^{18}
10^{19}
Electron density (cm^{-3})


(b)
Dark current
LOE
AL
AC
~ λ = 10 μ
~ λ = 20
X λ = 6μ
XL
X
X
X
X
X
P_{bn} ~ 0.1W/cm^2 λ ~ 10μ
η = 1%
Current density (A/cm^2)
10^0
10^{-2}
10^{-4}
10^{-6}
10^{-8}
10^{-10}
0
50
100
150
200
250
300
350
Applied bias (mV)


E_c
216
~500 mcV
~200 mcV
~200 mcV
214
218
E_f
212
~200 mcV
E_c


E_c
112
116
116
114
~1500 mcV
118
~200 mcV
~ 50 mcV
E_f
~350 mcV
~ 500 mcV
E_c


I_{pc}
Bandpass notch
V = Constant
Impedance
E_F
fcB
fcu
$E_o - E_F$
$E_l - E_F$
10^{13} Hz Frequency


Bandpass notch
Impedance
fcB
fcu
10^{13} Hz Frequency

N91
14396
UNCLAS

N91-14396

LOW DARK CURRENT PHOTOVOLTAIC MULTIQUANTUM WELL LONG WAVELENGTH INFRARED DETECTORS

C.S. WU, C.P. WEN, R.N. SATO and M. HU

HUGHES AIRCRAFT COMPANY

We have, for the first time, demonstrated photovoltaic detection for an multiple quantum well (MQW) detector. With a blocking layer, the MQW detector exhibits Schottky I-V characteristics with extremely low dark current and excellent ideality factor. The dark current is 5×10^{-14} A for an 100x100 um^2 10 um detector at 40 K, 8-9 orders of magnitude lower than that of a similar 10 um MQW detector without blocking layer. The ideality factor is ~1.01-1.05 at T=40-80 K. The measured barrier height is consistent with the energy difference between first excited states and ground states, or the peak of spectral response. We also, for the first time, report the measured effective Richardson constant (A**) for the GaAs/AlGaAs heterojunction using this blocking layer structure. The A** is low ~2.3 $A/cm^2/K^2$.

GaAs-BASED MULTIQUANTUM WELL LONG WAVELENGTH INFRARED DETECTOR

C. S. WU, C. P. WEN, R. N. SATO
HUGHES AIRCRAFT COMPANY

CONTRIBUTORS

(HUGHES)	(UCSD)	(NOSC)
M. HU	C. W. TU	L. FLESNER
LE PHAM	J. ZHANG	J. MERRIAM
P. S. NAYAR		



GaAs MQW SL DETECTOR OUTLINE

HUGHES

- ADVANTAGES
- CONVENTIONAL VS HUGHES MQW
- MQW DETECTOR DESIGN
- TEST RESULTS
  - -LOW DARK CURRENT OPERATION
  - -PHOTOVOLTAIC DETECTION
- SUMMARY

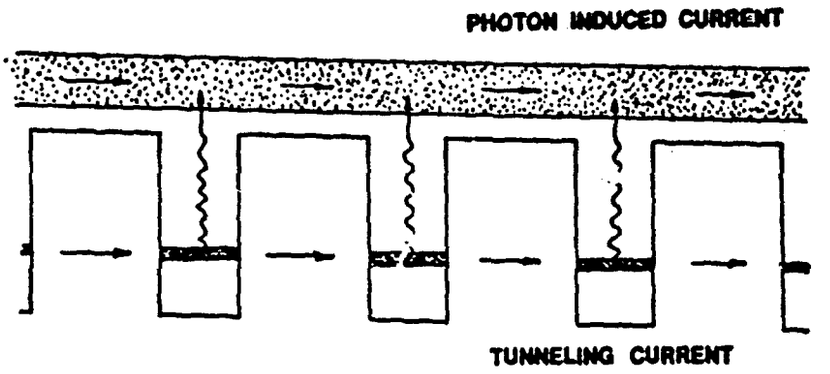
ADVANTAGES OF MQW SUPERLATTICE LWIR DETECTOR

HUGHES

- BUILT-IN FILTER CHARACTERISTICS
- DESIGN FLEXIBILITY IN SPECTRAL RESPONSE
- RADIATION HARDNESS POTENTIAL
- POTENTIALLY EXCELLENT UNIFORMITY FROM PIXEL TO PIXEL
- COMPATIBLE WITH STANDARD GaAs IC PROCESSING TECHNOLOGY

MULTIPLE QUANTUM WELL DETECTOR OPERATION

HUGHES

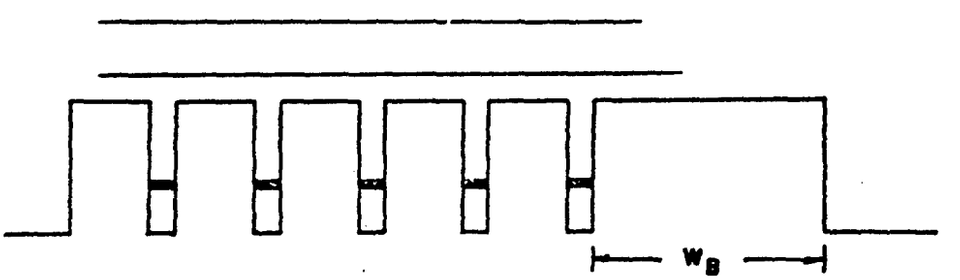


$I_{TOT} = I_{PH} + I_{TUN}$

DESIGN FLEXIBILITY

MQW DETECTOR WITH TUNNELING CURRENT BLOCKING LAYER

HUGHES



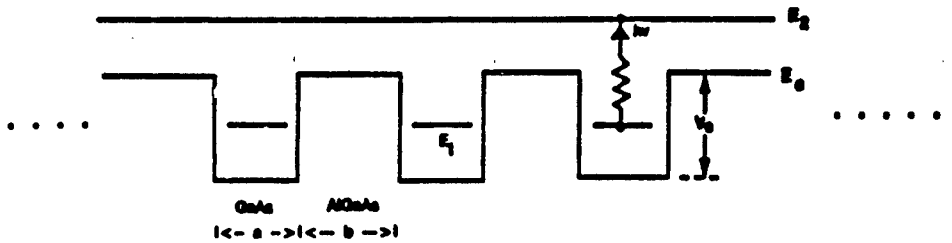
$I_{TUN} \sim \exp(-2KW_B)$

BLOCKING LAYER RESULTS IN LOW DETECTOR DARK CURRENT, IMPROVED SNR AND REDUCED PRIME POWER CONSUMPTION

DETECTOR PERFORMANCE SIMULATION - MQW PARAMETER DEFINITION

HUGHES

A PERIODIC POTENTIAL WITH RECTANGULAR SECTIONS
(PERIOD LENGTH = a + b)



SCHRODINGER EQUATION FOR KRONIG-PENNEY POTENTIAL:

$$-\frac{\hbar^2}{2M^*}\frac{d^2\psi(x)}{dx^2} + V(x)\psi(x) = E\psi(x)$$ (two unknowns: $\psi(x)$ (wave function) and E (electron energy))

where $V(x)$ and $\psi(x)$ satisfy

PERIODICITY CONDITIONS:
$V(x) = V(x+a+b)$ and
$\psi(x+a+b) = e^{ik}\psi(x)$ (e^{ik}: real)

therefore

MQW IR DETECTOR DESIGN CONSIDERATIONS

HUGHES

* SPECTRAL RESPONSE
  - WELL WIDTH, BARRIER HEIGHT, BARRIER THICKNESS
* ACTIVE REGION THICKNESS
  - CARRIER DENSITY, BARRIER THICKNESS
* CARRIER MEAN FREE PATH
  - MOBILITY, BIAS CONDITION, CARRIER LIFE TIME
* DARK CURRENT
  - BARRIER THICKNESS, BARRIER HEIGHT
  - BLOCKING LAYER (THICKNESS, HEIGHT)

GaAs/AlGaAs MQW DETECTOR ARRAYS DESIGN

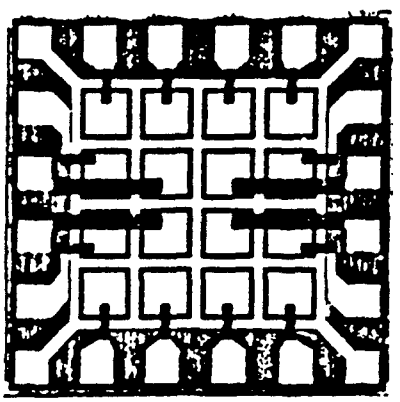
HUGHES

* DESIGNED FOR $\lambda_{\sim}$ 10 MICRONS
* BLOCKING LAYER FOR LOW DARK CURRENT
  - -LOW BACKGROUND OPERATION
* 4 X 4 ARRAYS
  - -100μM X 100μM DETECTORS
  - - 40μM X 40μM DETECTORS
* THIN DETECTOR STRUCTURE TO ENHANCE RADIATION HARDNESS
* STANDARD GaAs IC PRODUCTION LINE FABRICATION TECHNOLOGY

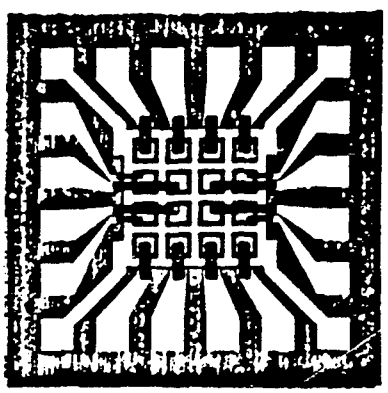
4 x 4 PHOTO DETECTOR ARRAYS

HUGHES

DETECTOR SIZE 100 x 100 uM

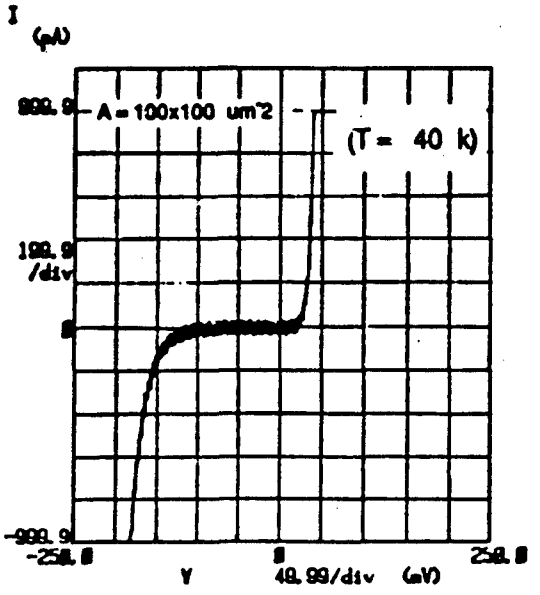


40 x 40 uM



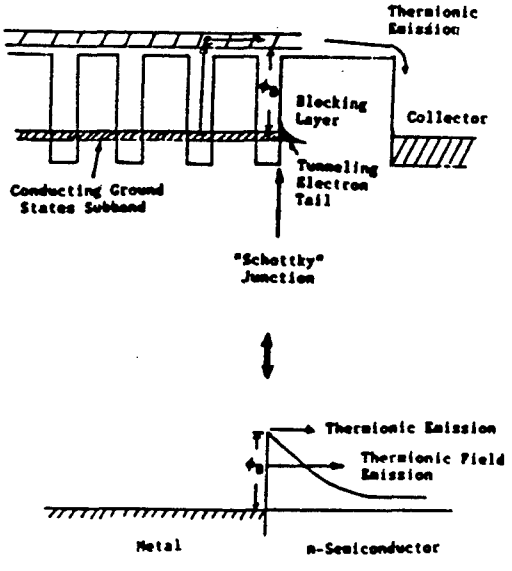
DARK I-V CHARACTERISTICS

HUGHES



MQW SL DETECTOR STRUCTURE WITH BLOCKING LAYER - QUANTUM WELL " SCHOTTKY " JUNCTION

HUGHES



- PHOTOVOLTAIC DETECTION LIKE PtSi DETECTOR
- LOW DARK CURRENT & HIGH RoA (NO THERMIONIC FIELD EMISSION)
- SELECTIVE SPECTRAL RESPONSE (ADJUSTABLE "Φ_B")

SCHOTTKY DIODE'S EQUATION

HUGHES

$$J = J_S(e^{qV/nkT} - 1)$$

$$J_S = A^{**}T^2 \exp\left(-\frac{q\phi_B}{kT}\right)$$

ϕ_B Schottky barrier height

A^{**} effective Richardson constant

n ideality factor

MEASUREMENT OF SCHOTTKY BARRIER HEIGHT, IDEALITY FACTOR & RICHARDSON CONSTANT

HUGHES

(A) $\ln I_F$ versus V_F ——> solve for n & ϕ_B

$$\ln I_F = \ln I_S + \frac{qV_F}{nkT}$$

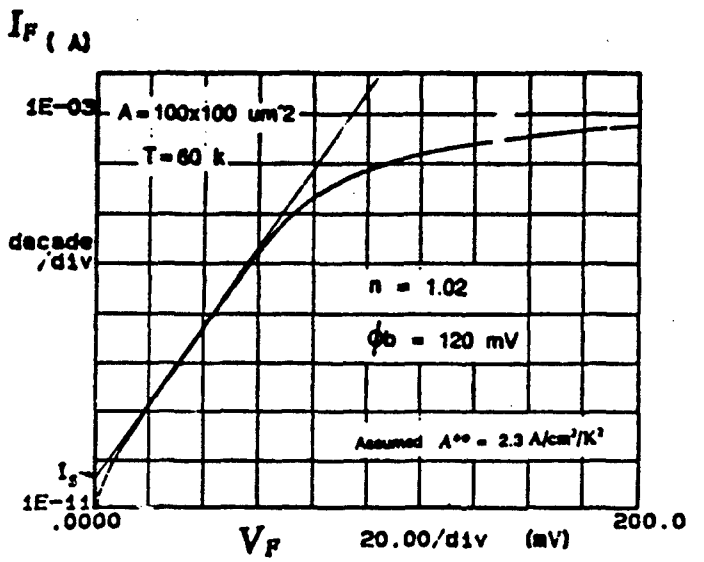
(B) $\ln(I_F/T^2)$ versus $1/T$ (ACTIVATION ENERGY PLOT)

——> solve for ϕ_B & A^{**}

$$\ln(I_F/T^2) = \ln(A\,A^{**}) - q(\phi_B - V_F)/kT$$

FORWARD DARK I-V CHARACTERISTICS

HUGHES

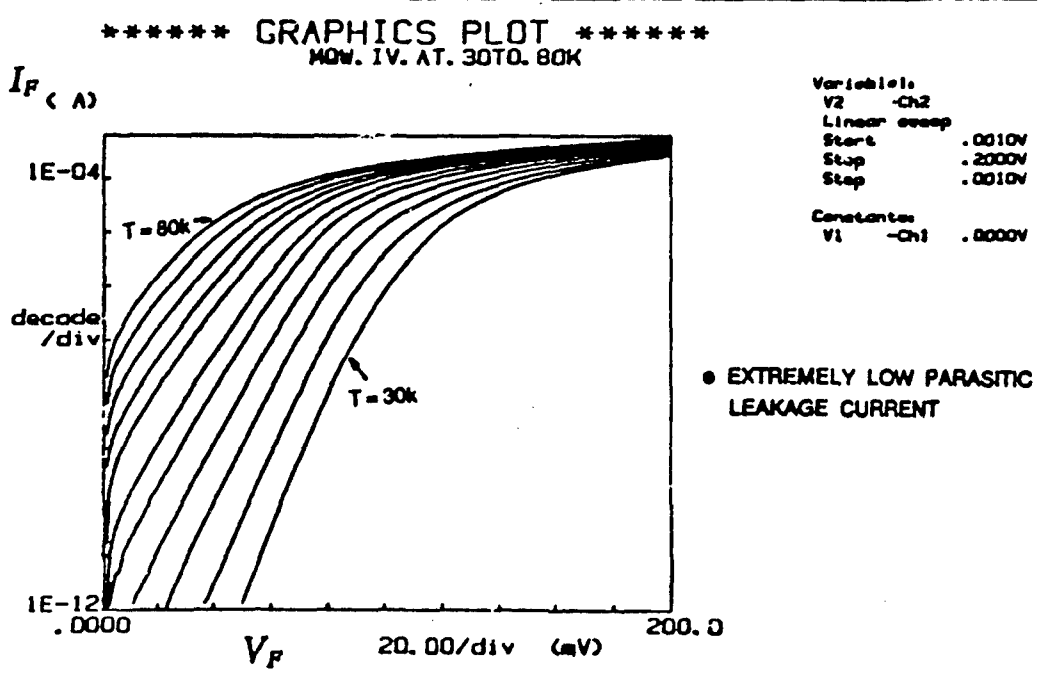


$$n = \frac{q}{kT}\frac{\partial V}{\partial(\ln J)}$$

$$\phi_B = \frac{kT}{q}\ln\left(\frac{A^{**}T^2}{J_s}\right)$$

FORWARD I-V CHARACTERISTICS AT T = 30 TO 80 K

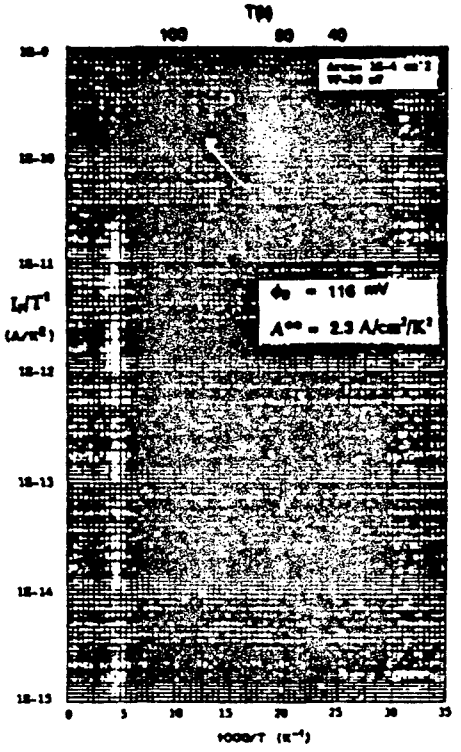
HUGHES



- EXTREMELY LOW PARASITIC LEAKAGE CURRENT

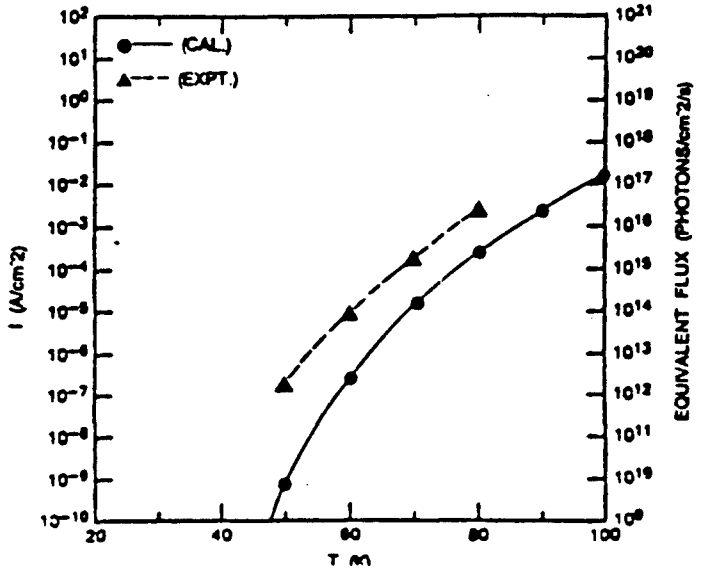
SCHOTTKY BARRIER HEIGHT AND RICHARDSON CONSTANT OBTAINED FROM ACTIVATION ENERGY PLOT

HUGHES



DARK CURRENT VS TEMPERATURE FOR 10 um PHOTOVOLTAIC MQW DETECTOR

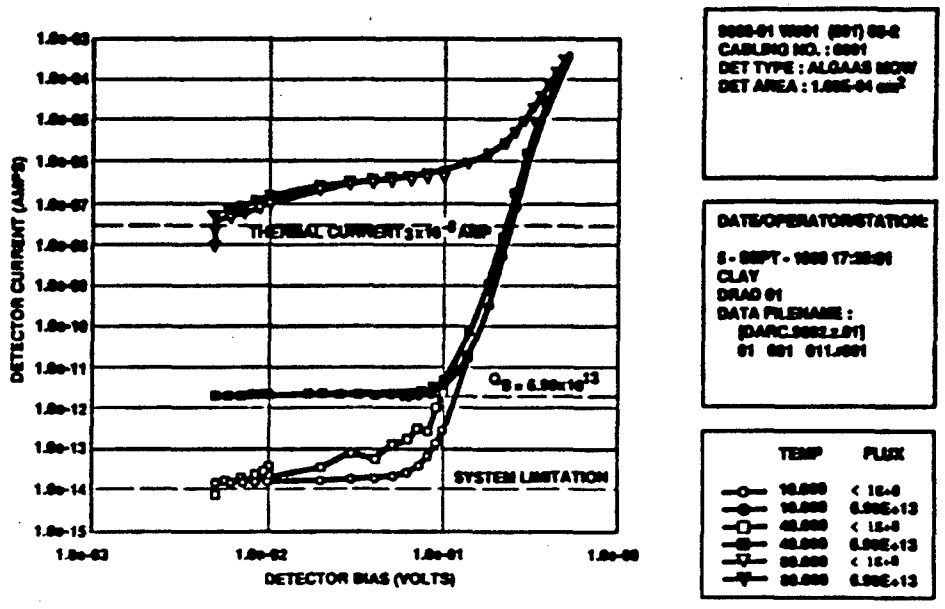
HUGHES



ORIGINAL PAGE IS
OF POOR QUALITY

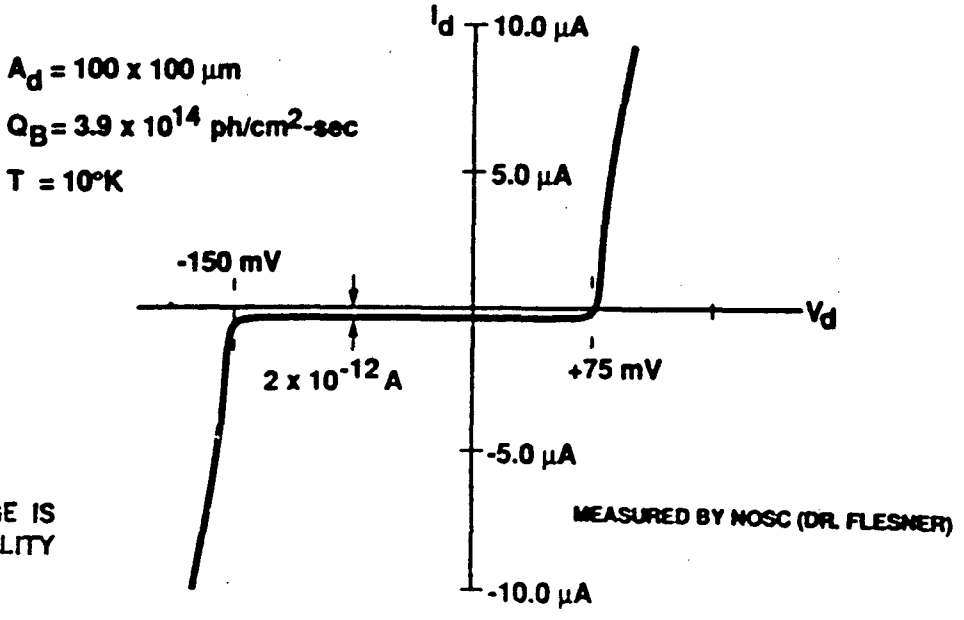
GaAs Based MQW IR Detector Dark Current Characterization

HUGHES



GaAs/AlGaAs MQW IR DETECTOR PHOTOVOLTAIC IR DETECTION I - V CURVE

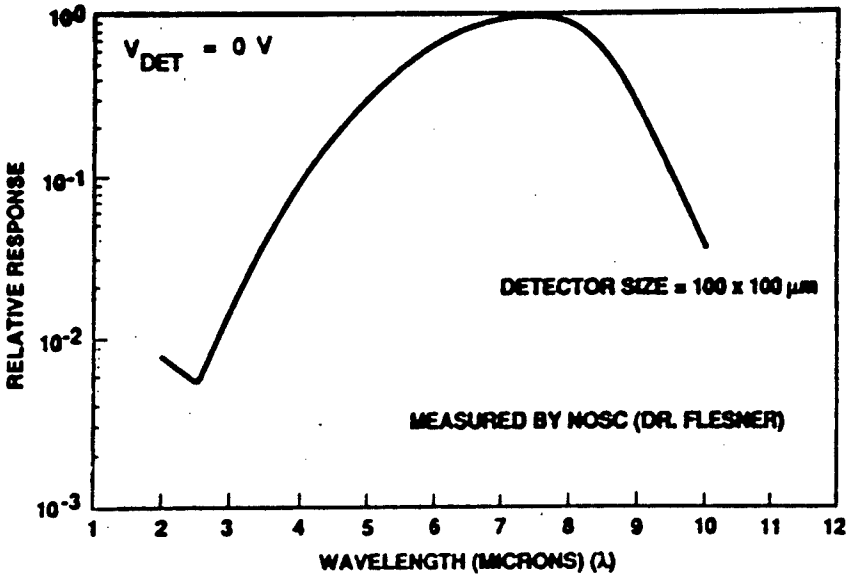
HUGHES



ORIGINAL PAGE IS
OF POOR QUALITY

GaAs/AlGaAs MQW IR DETECTOR NORMALIZED SPECTRAL RESPONSE T = 10° K $Q_B = 3.9 \times 10^{14}$

HUGHES



SUMMARY

HUGHES

- GaAs MQW LW IR DETECTORS DEMONSTRATED
  - -LOW DARK CURRENT
  - -POTENTIAL LOW NOISE
  - -PHOTOVOLTAIC DETECTION (LOW DETECTOR BIAS REQUIRED)
  - -POTENTIAL RADIATION HARDNESS
  - -EXCELLENT DESIGN FLEXIBILITY
    - PEAK PHOTO RESPONSE BANDWIDTH
- GaAs IC PRODUCTION TECHNOLOGY COMPATIBLE
  - -MATURED TECHNOLOGY
  - -HIGH YIELD, GOOD UNIFORMITY


N91
14397
UNCLAS

N91-14397

Fundamental Limits to Performance of Quantum Well Infrared Detectors

Amnon Yariv
California Institute of Technology
Pasadena, California 91125

ABSTRACT

Radiometric, density of states (material), and thermal considerations are used to obtain the figure of merit of the quantum-well GaAs/GaAlAs infrared detctors described by Smith et. al[1]. The results are compared with HgCdTe, the present industry standard, as well as with recent experiments at other laboratories.

(1) J.S. Smith, L.C. Chiu, S. Margalit, A. Yariv and A.Y. Cho, J. Vac. Sci. Tech. B, 376 (1986).

Fundamental Limits to Quantum Well Infrared Detectors

Amnon Yariv
California Institute of Technology

Michael Kinch
Texas Instruments

S. Borenstain
Jet Propulsion Laboratory

I. Gravé
California Institute of Technology

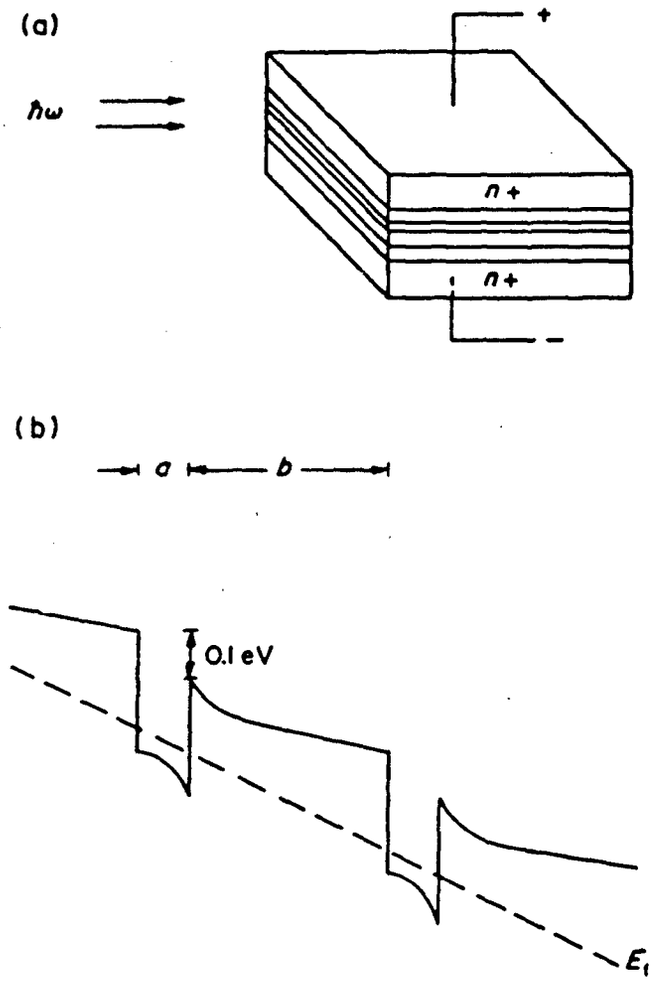
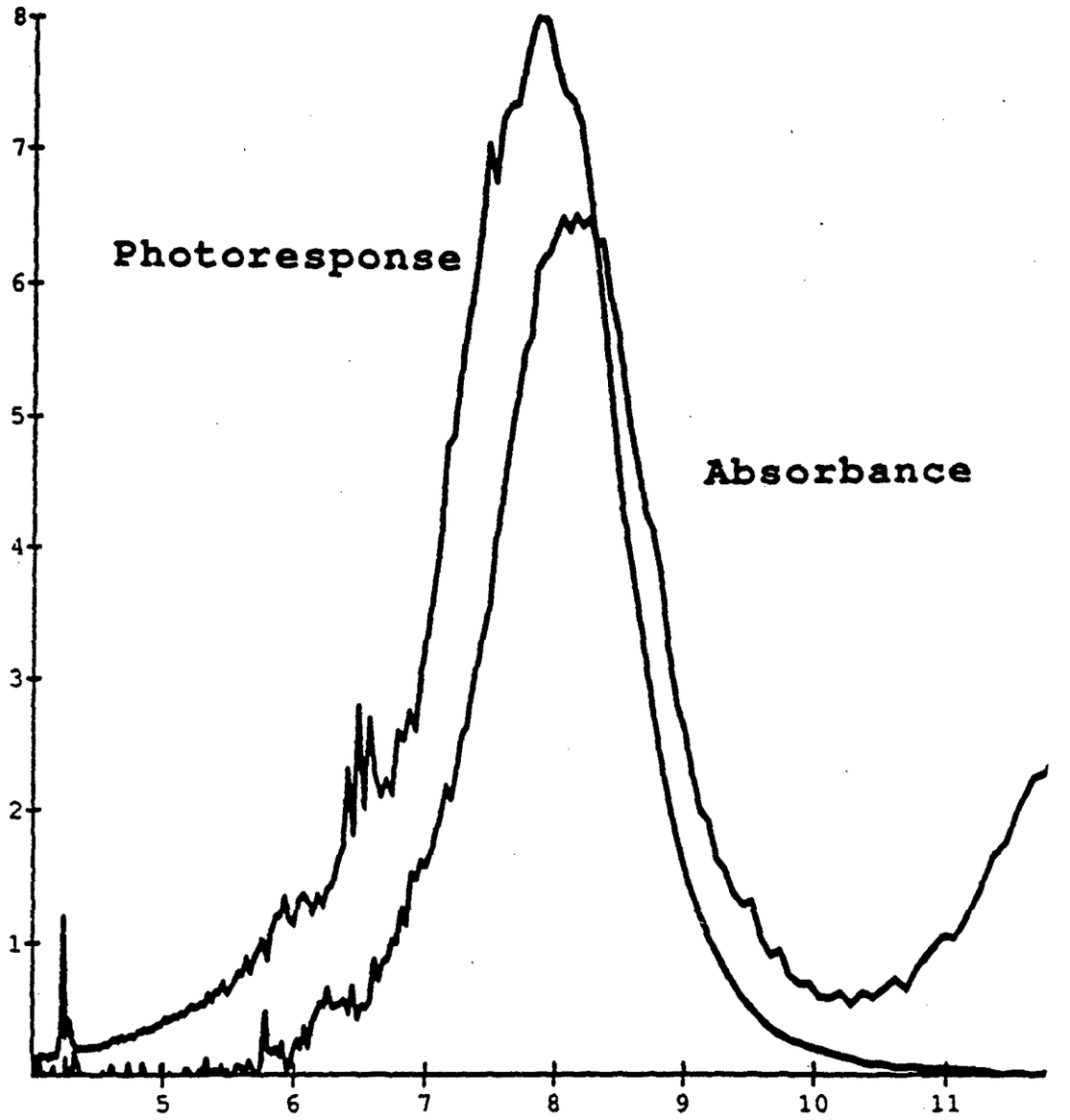


Fig. 3. (a) A schematic drawing of the proposed detector.
(b) Band diagram of the proposed structure.

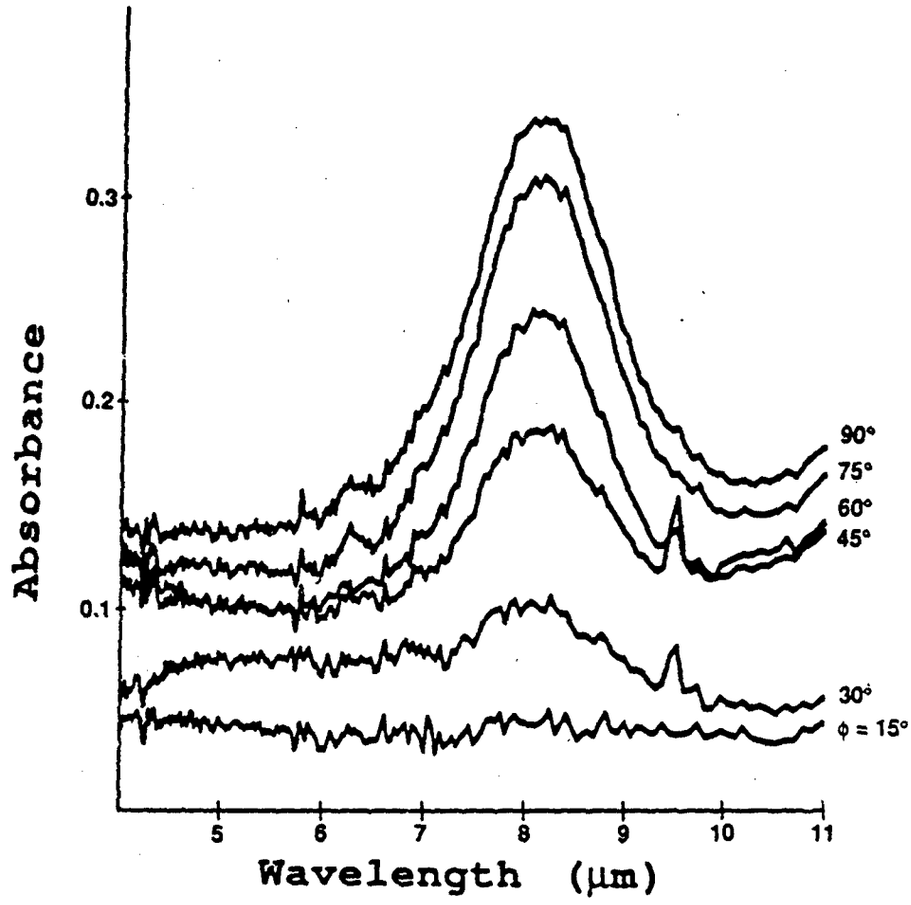
(Smith et. al., Infrared Phys., Vol 23, p. 93, 1983)

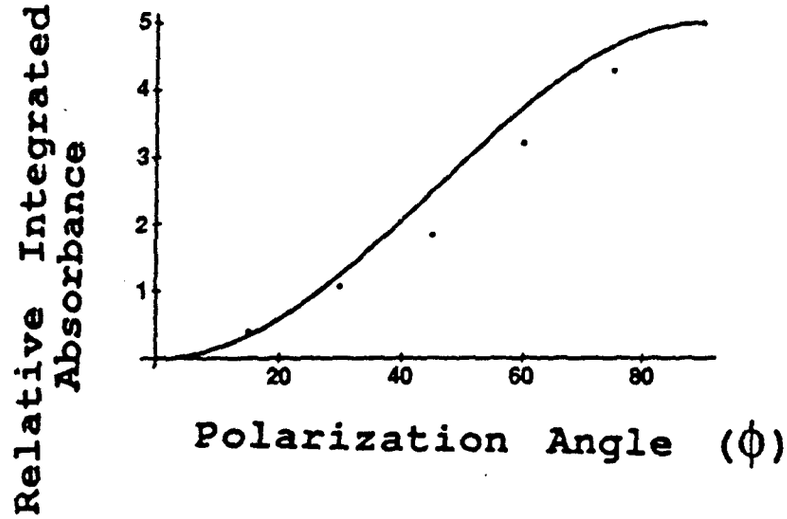


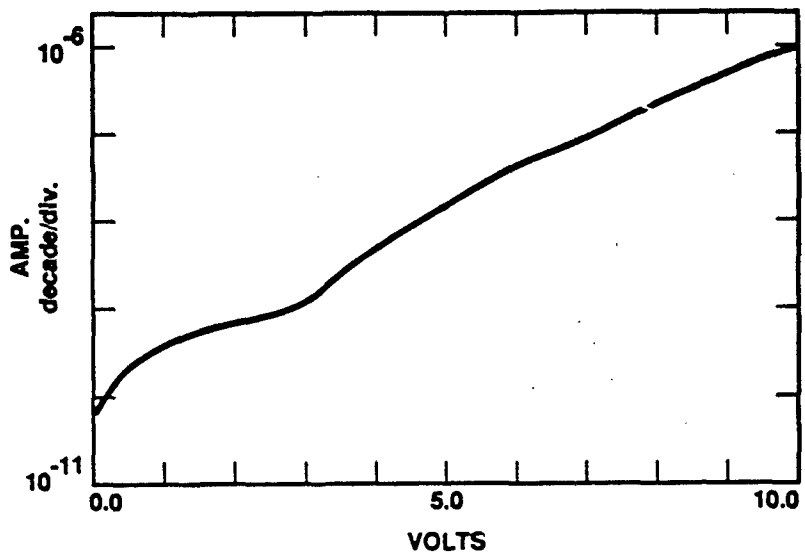
λ_{PEAK} = 8.00 μm

$\frac{\Delta\lambda}{\lambda}$ = 20%

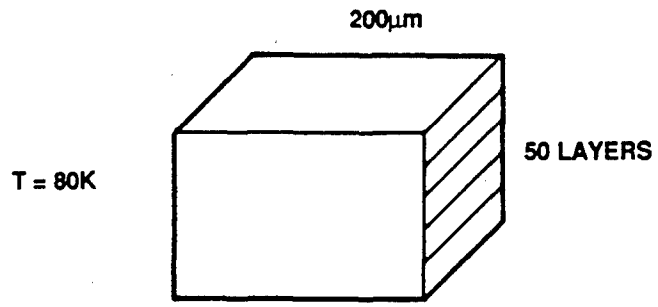
#1045
L = 300 Å
d = 50 Å
50 periods
Ga .76 AL .24 As


Absorbance
0.3
0.2
0.1
90°
75°
60°
45°
30°
ϕ = 15°
5
6
7
8
9
10
11
Wavelength (μm)


Relative Integrated Absorbance
5
4
3
2
1
20
40
60
80
Polarization Angle (ϕ)



DARK CURRENT OF GaAs/GaAlAs MQW DETECTOR AT 77K

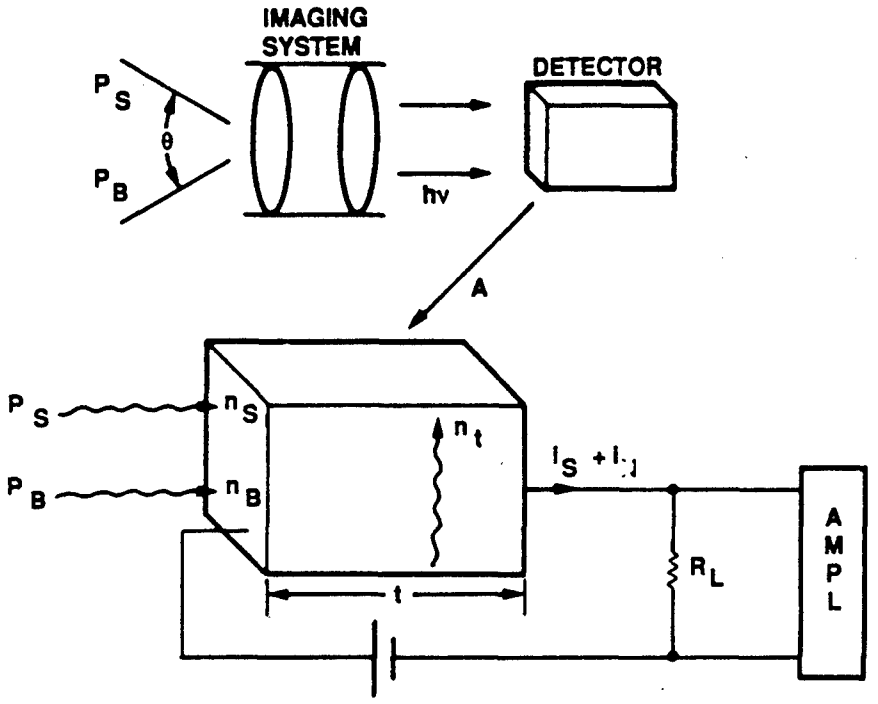


$V_B = 0$ $I_d \sim 10^{-11}$ A

$V_B = 10V$ $I_d \sim 10^{-6}$ A

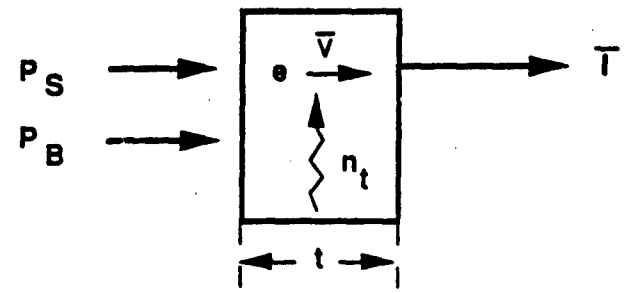
$V_B = 5V$

$I_d \sim 10^{-9}$ A



Configuration

NOISE PHYSICS — P.C. DETC.



$$\bar{I} = (n_B + n_t)\, e \bar{V} A$$

$$\boxed{\bar{i}_N^2 = 4e\bar{I}\,\frac{\tau_o}{\tau_d}\,\Delta\nu} \qquad \frac{\tau_o}{\tau_d} \equiv g \quad \tau_d \equiv \frac{t}{V} = \text{DRIFT TIME}$$

GENERATION-RECOMBINATION NOISE

$$= 4e\,(n_B + n_t)\, e\bar{V}A \left(\frac{\tau_o}{\tau_d}\right) \Delta\nu$$

$$n_B = \frac{(P_B/A)\,\eta\tau_o}{h\nu t} = \frac{2\pi h\nu^3 \Delta\nu (\mathrm{Sin}^2\theta/2)}{c^2\,(e^{h\nu/kT_B} - 1)} \left(\frac{\eta\tau_o}{h\nu t}\right)$$

NEED TO COOL TILL

$$n_t \lesssim n_B \qquad \underline{\text{BLIP}}$$

BLIP AND D^*_B

ASSUME $n_t < n_B$ (BLIP)

$$\bar{i}^2_{NB} = 4e\,(n_B\, e\bar{v}A)\,\frac{\tau_o}{\tau_d}\,\Delta\nu, \quad \tau_d = \frac{t}{\bar{v}}$$

$$= \frac{4e^2\, P_B \eta \Delta\nu}{h\nu}\left(\frac{\tau_o}{\tau_d}\right)^2, \qquad n_B = \left(\frac{P_B\, \eta \tau_o}{Ah\nu t}\right)$$

$$\bar{i}^2_s = \left(\frac{\eta P_s\, e}{h\nu}\right)^2 \left(\frac{\tau_o}{\tau_d}\right)^2$$

DEFINE: NEP = VALUE OF P_s WHICH MAKES

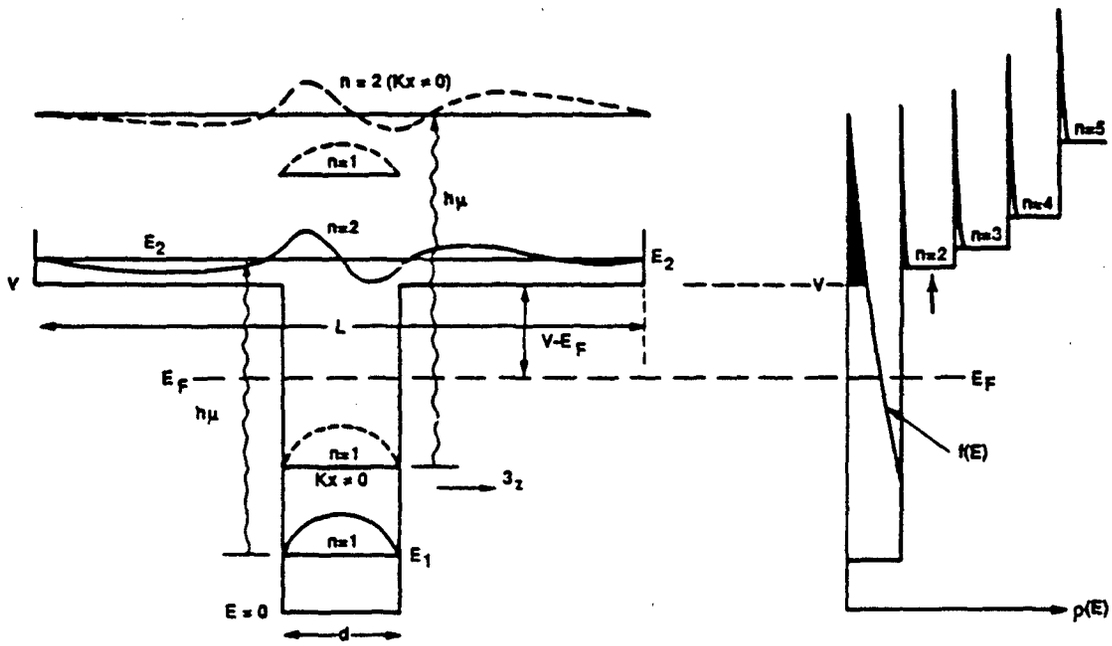
$$\bar{i}^2_s = \bar{i}^2_{NB}$$

$$NEP = \frac{2\sqrt{A\Delta\nu(P_B/A)}}{\eta}$$

$$D^*_B \equiv \frac{\sqrt{A\Delta\nu}}{NEP} = \frac{1}{2}\sqrt{\frac{\eta}{h\nu(P_B/A)}}$$

REMINDER:

TO OBTAIN D^*_B MUST COOL SO $n_t < n_B$.
SO NEED TO FIND DEPENDENCE OF n_t ON T.



$$n_t = \frac{m^*}{\pi\hbar^2 L} \int_V^\infty \left\{ \left| + \ln\left[L\left(\frac{2m^*(E-V)}{\pi^2\hbar^2} \right)^{1/2} \right] \right| \right\} \times \frac{dE}{e^{(E-E_F)/kT} + 1}$$

$$n_t = n_0 \left(\frac{d}{L}\right) \frac{kT}{E_F} \exp\left[-(V - E_F)/kT\right]$$

C. 4

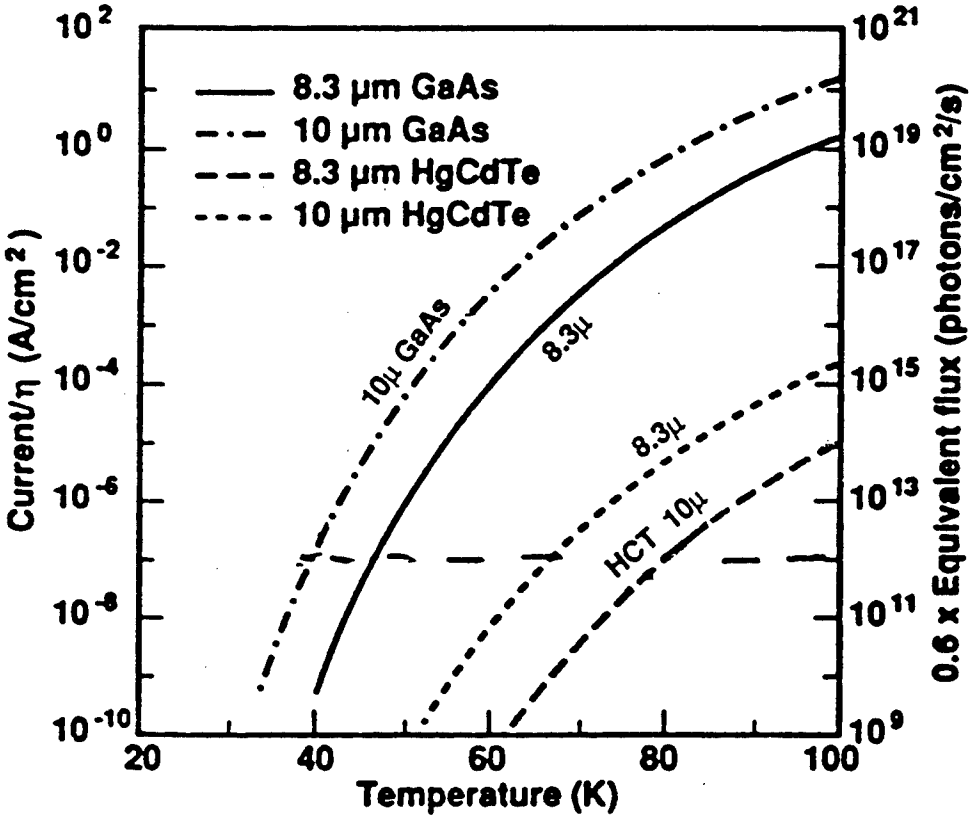
SUMMARY

$$D_B^* = \frac{1}{2}\sqrt{\frac{\eta}{h\nu(P_B/A)}}$$

$n_t < n_B$ FOR BLIP i.e.

$$n_o \frac{kT}{E_F} \frac{d}{L} e^{-(V - E_F)/kT}_{\text{BLIP}} \lesssim \frac{P_B \eta \tau_o}{Ah\nu t}$$

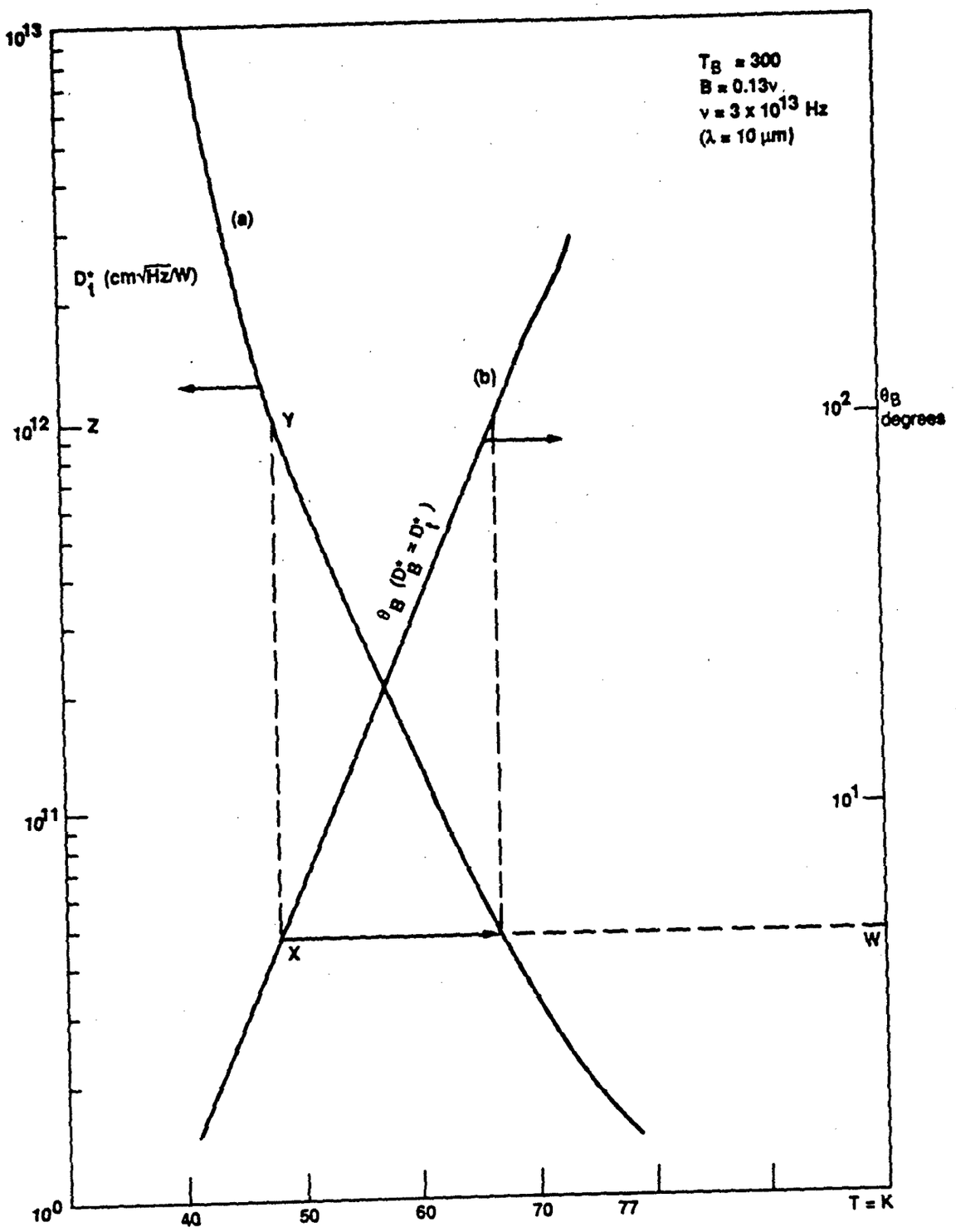
$\Rightarrow$ IF $\tau_o \uparrow$ T $\uparrow$
Q. WELL $\tau \sim 10^{-11}$ s
HCT $\tau \sim 10^{-6}$ s

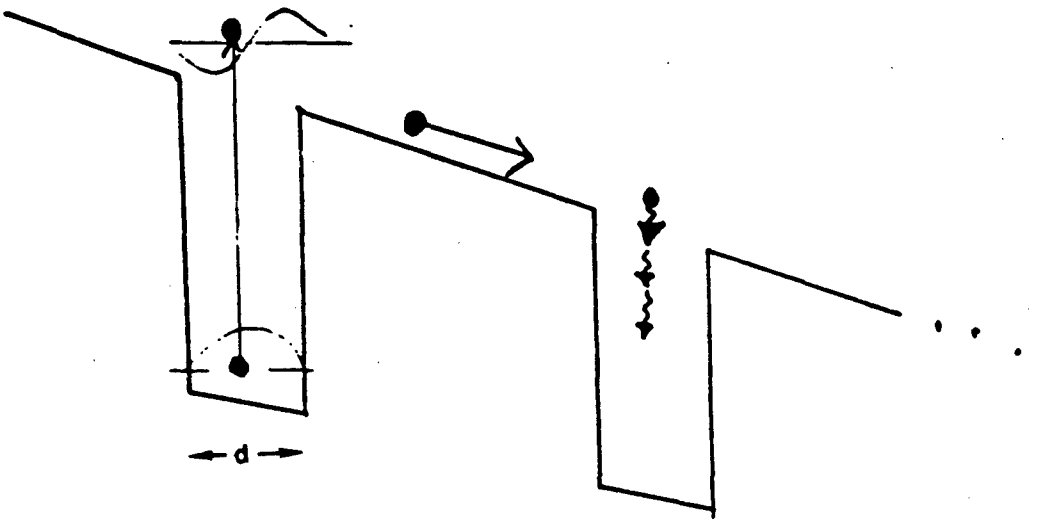


Thermal generation current vs temperature for GaAs/AlGaAs IR superlattices and HgCdTe alloys at $\lambda_c = 8.3$ and $10\,\mu$m. The assumed effective quantum efficiencies are $\eta = 0.125$ and 0.7 for GaAs/AlGaAs and HgCdTe, respectively.

M. A. Kinch and A. Yariv 2094

(APL, Vol. 55, Nov., 1989)


T_B = 300
B = 0.13ν
ν = 3 x 10^{13} Hz
(λ = 10 μm)
(a)
(b)
D^*_λ (cm√Hz/W)
θ_B ($D^*_B = D^*_\lambda$)
θ_B degrees
10^{13}
10^{12}
10^{11}
10^0
10^2
10^1
Z
Y
X
W
40
50
60
70
77
T = K

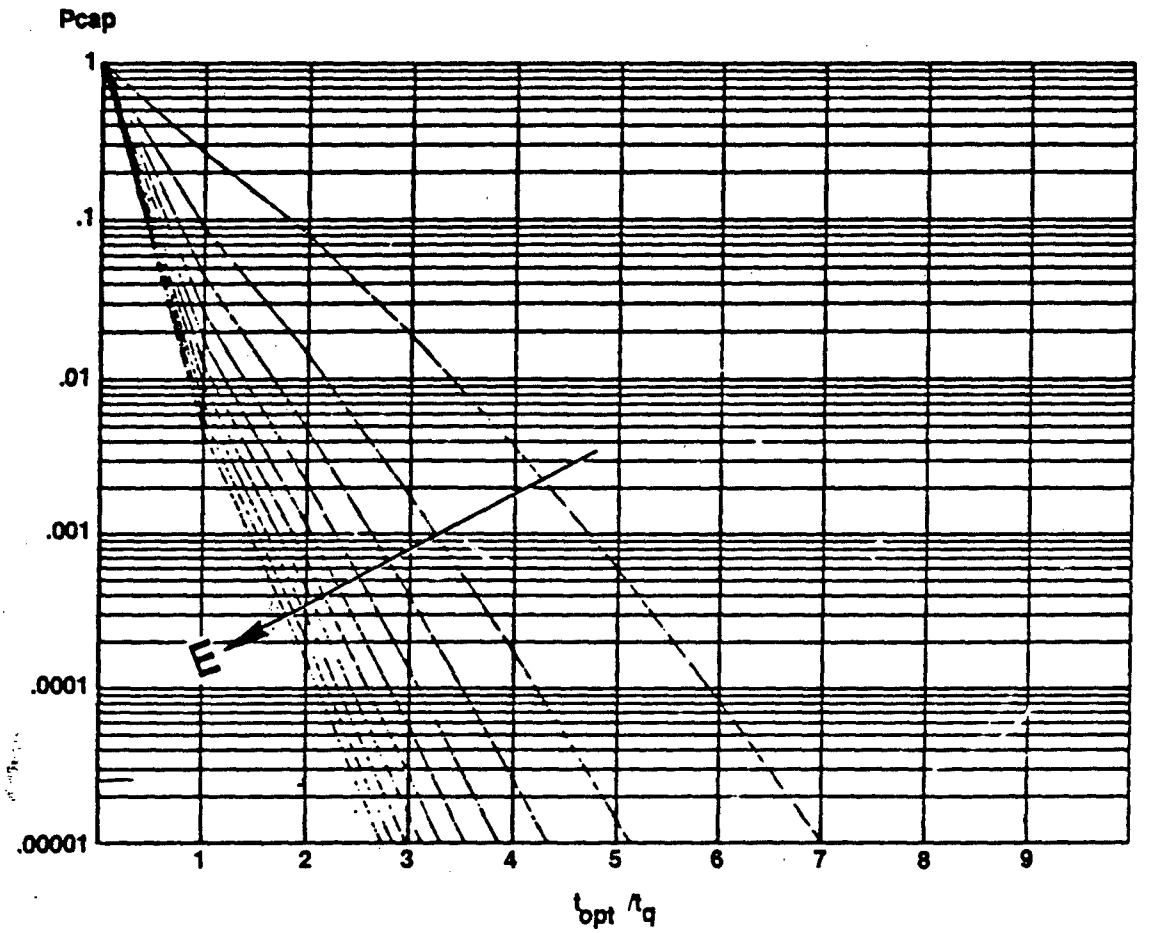


t_q = TIME OVER WELL = $\frac{d}{\mu\varepsilon}$ ~ 5×10^{-14} s

t_{op} = TIME TO EMIT LO PHONON ~ 10^{-13} s

t_{op}/t_q ~ 2 - 5

$$P_{cap}(E) = 1 - \sum_{x=0}^{I_n(E/\hbar\omega_{op})} \frac{(\tau_{opt}/t_q)^x}{X!} e^{-\tau_{opt}/t_q}$$



probability of capture by optical phonon emission as a function of the energy at injection and (τ_{op}/t_q)

(S. Smith, Ph.D. Thesis, Caltech, April, 1986)

N91
14398
UNCLAS

V-7

N91-14398

New Heterojunction LWIR Detector Options*

J. Maserjian
Center for Space Microelectronics Technology
Jet Propulsion Laboratory

We investigate a heterojunction internal photoemission (HIP) approach that potentially offers LWIR photovoltaic detector performance (single pixel) that is competitive with the best of other approaches being considered. Most significantly, our approach offers a relatively simple device technology that promises producible and uniform FPA's. We emphasize an exciting process based on intervalence band absorption. We investigate both III-V and Si-based heterojunctions grown by molecular beam epitaxy (MBE) in which the barrier can be tailored to the desired cutoff wavelength. In addition, MBE allows one to optimize the device structure with precise control of doping profiles and layer thicknesses, and perform band structure engineering by control of composition and heterojunction strain.

We also consider free carrier absorption in heterojunctions. Acceptable absorption coefficients can be achieved in very heavily n^+ doped semiconductor layers ($\approx 10^{20}$ cm^{-3}). However, in this case the appreciable filling of conduction band states leads to a Schottky-like photoresponse with a gradual (quadratic) turn-on above threshold. A more satisfactory approach would be to use p^+ doping so that with the higher density of states in the heavy hole valence band there would be a narrow band of occupied states. This gives the desirable effect of a more rapid (linear) turn-on above threshold. Unfortunately, the higher hole effective mass also reduces (inversely) the free carrier absorption. For this and other reasons, the intervalence band absorption process looks much more promising.

The valence band structure of GaAs (and closely related alloys) is particularly attractive for achieving an optimum effect. The light and heavy hole bands become parallel at values of wave vector k away from the zone center, separated by a constant energy of about 80 meV along the <100> directions. The parallel E-k behavior leads to a large joint density of states and correspondingly, a large absorption coefficient α for photon energy hv equal to this separation (corresponding to wavelengths ≈15 μm). This effect requires heavy doping (>10^{19} cm^{-3}) so that states are occupied to sufficient values of k. Extrapolation of theoretical work of E.O.Kane and published absorption data suggest $\alpha > 10^4$ cm^{-1} for our case of interest. Theoretical calculations are in progress to extend Kane's early work.

Some interesting features are immediately evident. The selection rules for these transitions *prefer normal incidence of light* (giving a $\sin^2\theta$ distribution of k-directions, where θ is the angle from the field vector in the plane of the layer). Furthermore, photoexcitations between the <100> E-k bands generate the dominant k-directions normal to the heterojunction interface of (100) oriented

* This work was sponsored by NASA and SDIO/IST.

material. We have the opportunity of tailoring the interband separation to the desired value of hν and matching with an optimum (slightly smaller) heterojunction barrier ϕ. In this case the conservation of transverse momentum at the interface is satisfied for most k-directions of photoexcited holes. Holes excited in the reverse direction can be redirected in the forward direction by reflection from a higher barrier (e.g., AlGaAs/GaAs). Therefore, inelastic scattering losses can be minimized with an optimum layer thickness to achieve a maximum quantum efficiency η.

In the case of Si-based structures, we can still utilize transitions to the split-off valence band. In this case we lose some of the above advantages, but still retain strong absorption (large matrix element) and favorable selection rules. We can also use band structure engineering through control of composition and interface strain to optimize the intervalence band transition energies relative to the heterojunction barrier (i.e., the cutoff wavelength).

Preliminary results on $Si_{1-x}Ge_x/Si$ heterojunctions are encouraging (see T-L. Lin, next session) and work on $In_xGa_{1-x}As/\ Al_xGa_{1-x}As$ heterojunctions is just getting under way. The opportunity exists for fabricating photovoltaic detector structures designed to achieve maximum η and the limiting thermionic emission dark current at the heterojunction. To minimize inelastic scattering loss of photoexcited holes while still obtaining adequate absorption per layer (e.g.,>1%), the p^+ layers must be of some optimum thickness (e.g.,≈40 nm). The total absorption can be enhanced by multiple passes; for example, two passes with a single reflector or 2N passes in an optical cavity structure (as commonly done with SB detectors). The HIP structures can also be configured as two stacked diodes connected in parallel (straightforwardly with planar technology) to gain another factor of two.

Based on the above considerations, we project η= 0.20 in optimized detector structures. The thermionic emission limited detectivity [$D^* \rightarrow (\eta/h\nu)(2J_o/e)^{-1/2}$, where $J_o = 120(m^*/m)T^2\exp(-\phi/kT)$ A/cm^2] becomes $D^* \equiv 10^9$ cm-$Hz^{1/2}$/W, for 15μm peak response (hν=82 meV), with ϕ=0.9hν and T=65K. This gives a noise equivalent differential temperature NEDT≡0.04K for a background temperature of 300K (assuming f/2 optics, 50μm square pixels and 30Hz bandwidth). Therefore, even with relatively low η, the thermionic emission dark current of HIP detectors provides excellent pixel performance. Most important, the simplicity of the HIP structure offers real promise for producibility and uniformity which often are the limiting factors for FPA performance.

JPL

New Heterojunction Detector Options

Joseph Maserjian
Center for Space Microelectronics Technology
Jet Propulsion Laboratory

Contributors

Theory:	Mark Huberman
	Robert Terhune
Si MBE:	Robert Fathauer
	True-Lon Lin
III-V MBE:	Frank Grunthaner
	Anders Larsson
Readouts:	Eric Fossum

Outline

- Motivation
- Heterojunction Approach
- Theoretical Considerations
- Detector Structure
- Predicted Performance

JPL

Technology Considerations

Detector Performance
- Detectivity (D*)
- Quantum Efficiency (QE)
- Noise Equiv. Diff. Temperature (NEDT)
- Operating Temperature
- Thermal Generation Noise
- Excess Detector Noise (eg. 1/f)

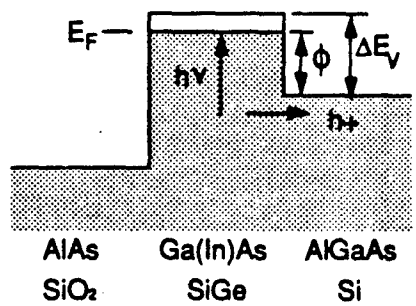
Array Compatibility
- Hybrid or monolithic readout circuits
- Zero or reverse bias resistance
- Dark current / power dissipation
- Detector capacitance
- Fill factor (front vs. backside illum.)
- Detector linearity and stability
- Frame rate and dynamic range
- Array uniformity

Producibility & Robustness
- Material manufacturability
- Material quality and uniformity
- Material stability / surface passivation
- Production yield / cost
- Radiation hardness

Approach

Heterojunction Internal Photoemission (HIP)

- Simple structure / normal incidence radiation
- Emphasis on intervalence band absorption
- Optimized HIP structure using MBE:
  - valence band engineering with control of composition and strain
  - optimize doping and layer thickness for maximum quantum efficiency
  - match heterojunction barrier to cutoff wavelength for minimum dark current
- Configure into high performance PV detector arrays:
  - stacked planar detector structures
  - optical cavities



JPL

Free Carrier Absorption
Classical Theory

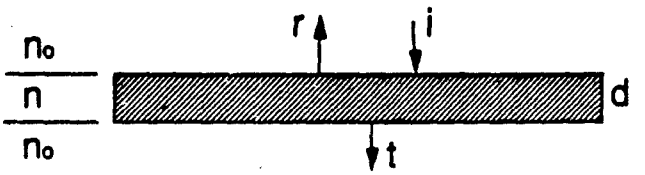
$\varepsilon = \varepsilon_o + 4\pi i\,\sigma/\omega$, $\quad n = \sqrt{\varepsilon}$

$\sigma = \sigma_o/(1 - i\,\omega\tau)$, $\quad \sigma_o = Ne^2\tau/m$

$\mathbf{E} = \hat{x}\, E \exp\{i(nkz - \omega t)\}$

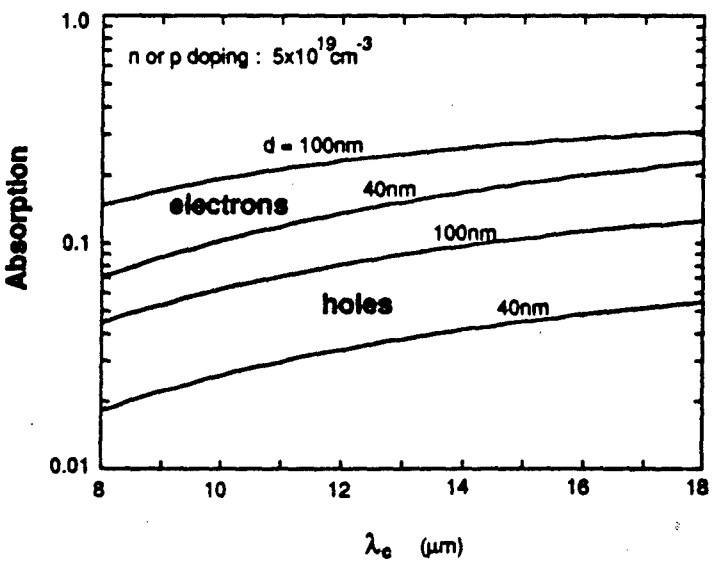
$\mathbf{H} = \hat{y}\, nE \exp\{i(nkz - \omega t)\}$

Match **E** and **B** at boundries of thin layer:



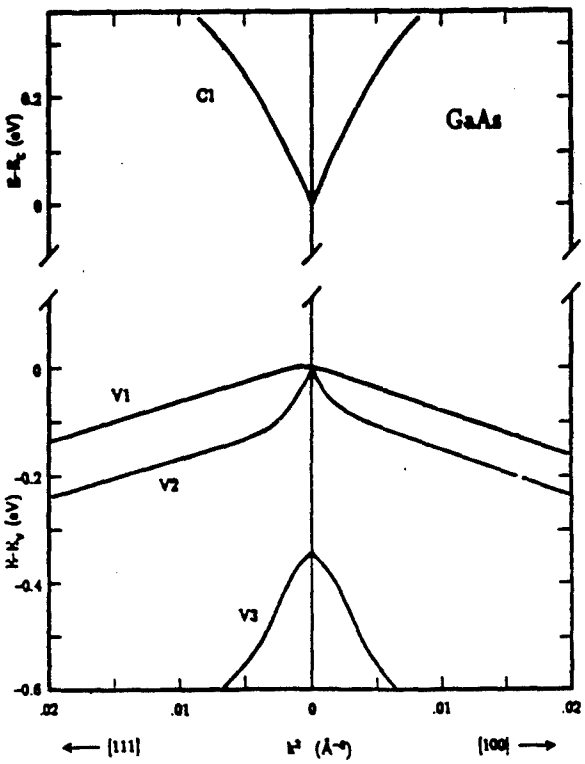
Free Carrier Absorption

(classical theory for finite GaAs layer of thickness d)



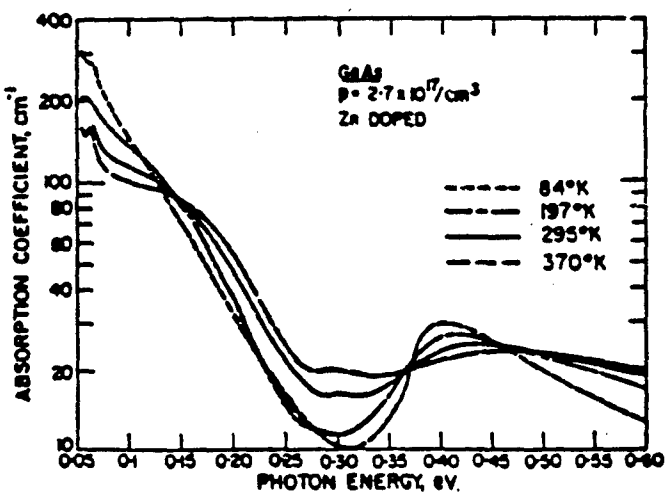
JPL

GaAs Band Structure



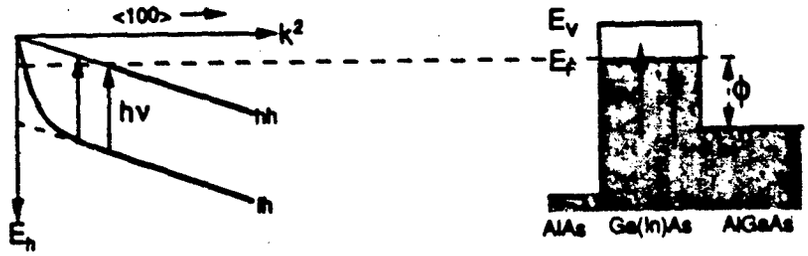
GaAs Absorption Data

R.Braunstein and E.O.Kane (1956)



JPL

Intervalence Band Absorption



Valence Band E - k^2 Diagram

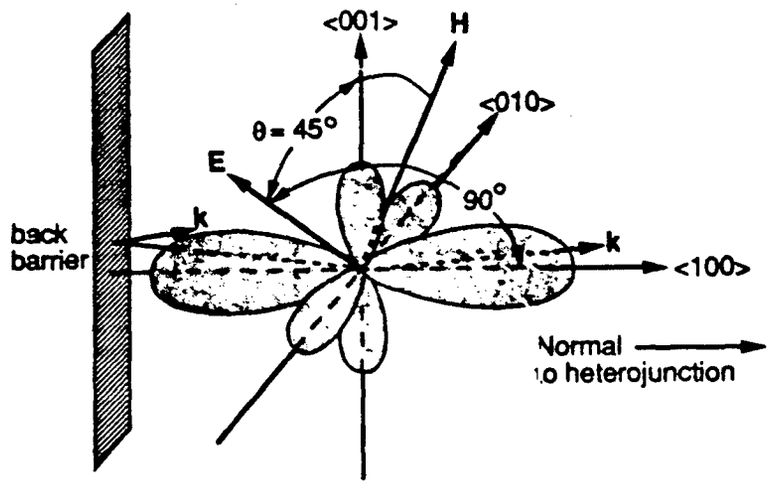
Heterojunction Internal Photoemission

$$\alpha = \frac{4\pi^2 e^2 \hbar^2}{nc\omega m^2} \sum_k |M(k)|^2 \delta\{E_{lh}(k) - E_{hh}(k) - h\nu\}$$

$$|M(k)|^2 = \langle \psi_{lh} | \hat{e} \cdot \nabla | \psi_{hh} \rangle^2$$

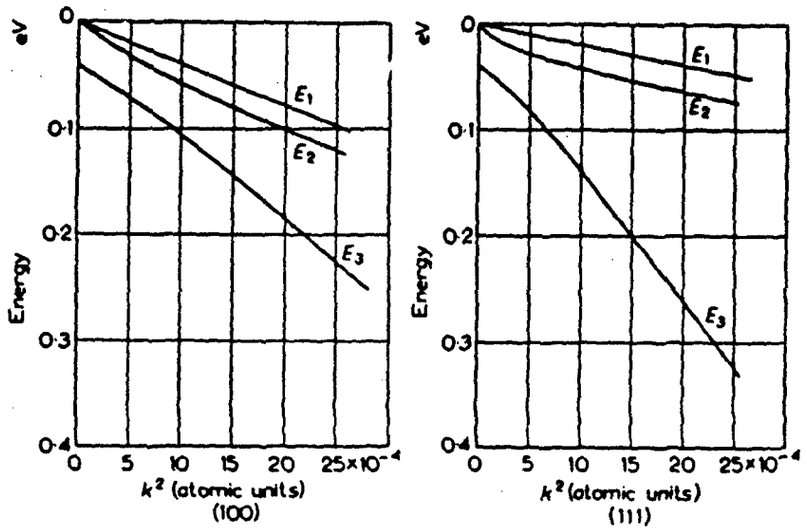
$$\sim \sin^2 \theta$$

Selection Rules for k-Directions



JPL

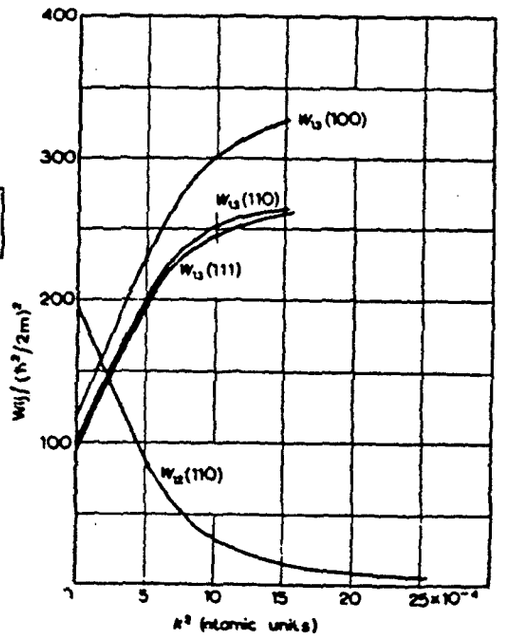
Si Valence Band Structure



Intervalence Band Absorption Matrixes for Ge

(E.O. Kane, 1962)

$$W_{ij} = M_{ij}^2 / K^2$$



JPL

Quantum Efficiency (η)

$$\eta = (1 - e^{-2N\alpha d})\, e^{-d/L_z}$$

$$\equiv 2N\alpha d \cdot e^{-d/L_z}$$

Maximum η when: $d = L_z$

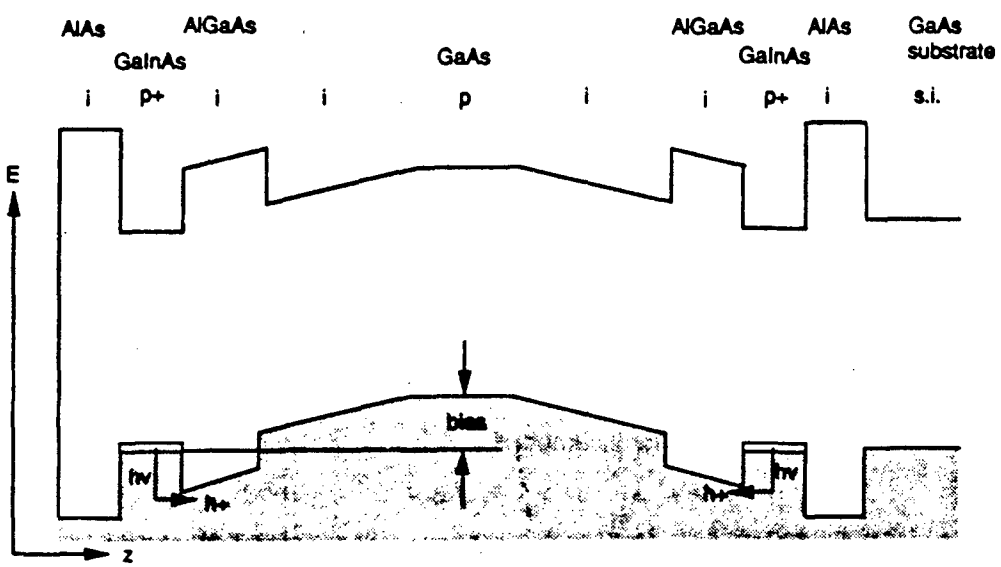
$$\eta_{max} = 2N\alpha L_z e^{-1}$$

Assume: $\langle v_z \rangle \approx 2 \cdot 10^7$ cm/s
$\tau \approx 3 \cdot 10^{-13}$ s
$\alpha \approx 2 \cdot 10^4$ cm^{-1}

Then: $L_z = \langle v_z \rangle \tau$
≈ 60nm
$\eta_{max} \approx .09\ N$

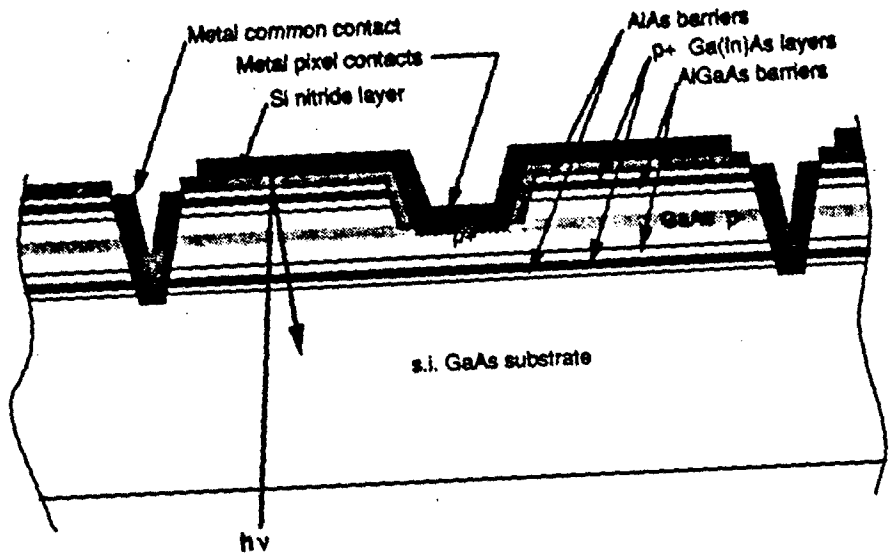
Stacked HIP Diode

Band Diagram



Stacked HIP Diode

Planar Structure



JPL

Detector Relations

(HIP Photovoltaic Diode)

$$D^* \equiv (A\Delta f)^{1/2} / NEP$$

$$= (\eta/\sqrt{2}\, h\nu)\, (r_B + r_T + r_{ex})^{-1/2}$$

Background: $r_B = \int_{\nu 1}^{\nu 2} \eta(\nu)\, [S(\nu,T_B)/h\nu]\, d\nu\,, \qquad S = 2\pi h\nu^3/c^2 \,/\, (e^{h\nu/kT_B}-1)$

Thermal: $r_T = [A^{**}T^2/e]\, \exp(-\phi/kT)\,, \qquad \phi \equiv .9\, h\nu$

$$D^*(\nu,T) \rightarrow (\eta(\nu)/h\nu)\, (2r_T)^{-1/2}$$

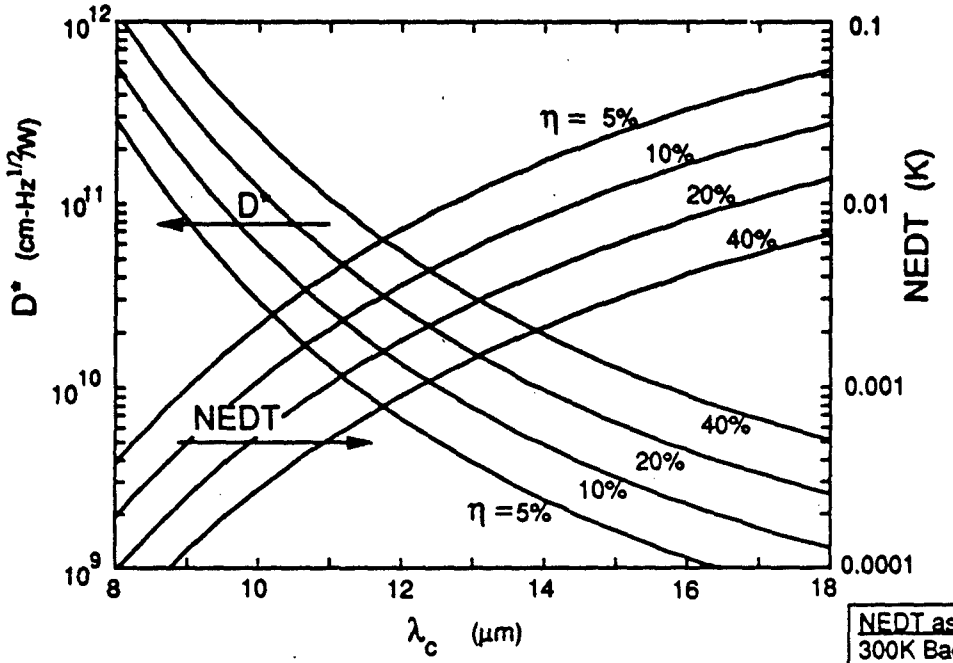
$$NEDT \equiv NEP \,/\, dP/dT_B = (A\Delta f)^{1/2} / D^* dP/dT_B$$

where for f-number F:

$$P = A\int_{\nu 1}^{\nu 2} S(\nu,T_B)\, d\nu \,/\, 4F^2$$

JPL

Predicted Performance of HIP Detector at 65K



NEDT assumes:
300K Background
f / 2 optics
50μm sq. pixels
Δf = 30 Hz

Summary

- HIP detector uses normal incidence radiation
- Intervalence band absorption offers high η
- Band structure / barrier tailoring for optimum response
- Thermionic current gives good performance at 65K
- Simple device structure -- easy to configure into stacked PV diode arrays
- Compatible with monolithic readout circuits
- Potential for low cost uniform arrays

SESSION VI: Si-Based Detectors

VI - 1 Intersubband Absorption in Si_{1-x} Ge_x/Si Superlattices for Long Wavelength Infrared Detectors
Y. Rajakarunanayake, California Institute of Technology

V1-2 Possibilities for LWIR Detectors Using MBE-Grown Si($Si_{1-x}Ge_x$) Structures
R.J. Hauenstein, Hughes Research Laboratories

V1-3 Novel $Si_{1-x}Ge_x$/Si Heterojunction Internal Photoemission Long Wavelength Infrared Detectors
T.L. Lin, Jet Propulsion Laboratory

PRECEDING PAGE BLANK NOT FILMED

N91
14399
UNCLAS

N91-14399

Intersubband absorption in $Si_{1-x}Ge_x/Si$ superlattices for long wavelength infrared detectors

Y. Rajakarunanayake and T. C. McGill

California Institute of Technology

Pasadena, California 91125

ABSTRACT

We have calculated the absorption strengths for intersubband transitions in n-type $Si_{1-x}Ge_x/Si$ superlattices. These transitions can be used for the detection of long-wavelength infrared radiation. A significant advantage in $Si_{1-x}Ge_x/Si$ superlattice detectors is the ability to detect normally incident light; in $Ga_{1-x}Al_xAs/GaAs$ superlattices intersubband absorption is possible only if the incident light contains a polarization component in the growth direction of the superlattice. We present detailed calculations of absorption coefficients, and peak absorption wavelengths for [100], [111] and [110] $Si_{1-x}Ge_x/Si$ superlattices. Peak absorption strengths of about 2000-6000 cm^{-1} were obtained for typical sheet doping concentrations ($\approx 10^{12}$ cm^{-2}). Absorption comparable to that in $Ga_{1-x}Al_xAs/GaAs$ superlattice detectors, compatibility with existing Si technology, and the ability to detect normally incident light make these devices promising for future applications.

PRECEDING PAGE BLANK NOT FILMED

Intersubband Absorption in Si/Ge Superlattices for Long Wavelength Infrared Detectors

Yasantha Rajakarunanayake
T. C. McGill

California Institute of Technology

Si/Ge Multi Quantum Wells for LWIR detection

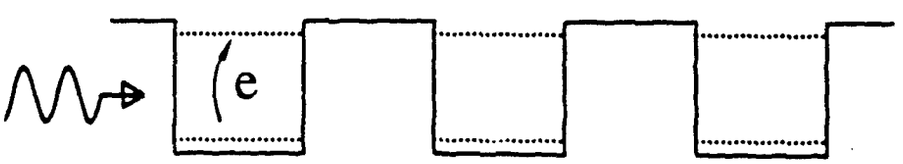
- Similar to extrinsic Si detectors
- Can change wavelength response by varying layer thicknesses
- Possible to achieve absorption at normal incidence
- Can achieve high doping concentrations
- Improved uniformity
- Compatibility with Si readout electronics

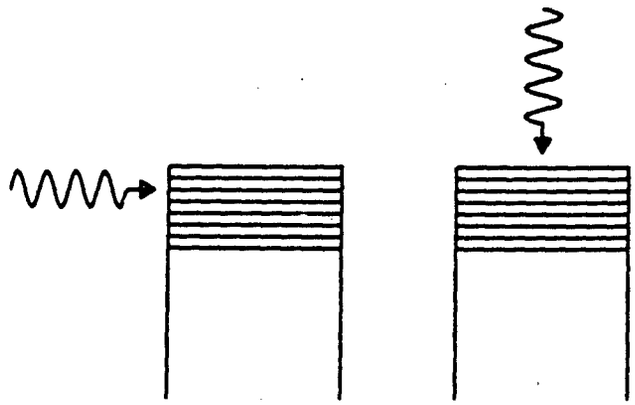
Outline

- Introduction
- Possibilities with [111],[110][1] directions
- Intersubband absorption coefficient
- Si/Ge band offsets
- Strain effects
- Results
- Conclusions

[1]C. L. Yang, D. S. Pan and R. Somoano, J. Appl. Phys. **65**, 3253 (1989).

QW Absorption

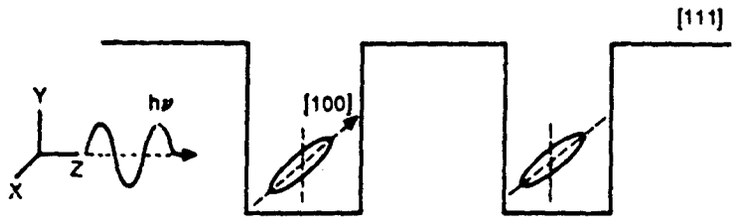




Parallel Incidence

Normal Incidence

Quantum well states of ellipsoidal valley materials



Consider the case where ellipsoids are not oriented in the growth direction

- Effective mass is a tensor; large anisotropy
- Possible to couple orthogonal components of vector potential and electron motion

Optical Matrix Element in Superlattices / Multi Quantum Wells

$$M_{op} = \left(\frac{e}{mc}\right) \langle U_1 F_1 | \vec{A} \cdot \vec{P} | U_2 F_2 \rangle$$

- Interband Case: V $\rightarrow$ C

$$M_{op} \sim \left(\frac{e}{mc}\right) \langle U_C | \vec{A} \cdot \vec{P} | U_V \rangle \langle F_C | F_V \rangle$$

- Intersubband Case: C1 $\rightarrow$ C2

$$M_{op} \sim \left(\frac{e}{mc}\right) \langle F_{C1} | A_i \left(\frac{1}{m^*}\right)_{ij} P_j | F_{C2} \rangle$$

Normal Absorption

$$\alpha(\omega) \approx \left(\frac{e_x}{m^*_{xz}} + \frac{e_y}{m^*_{yz}} + \frac{e_z}{m^*_{zz}}\right)^2$$

- $1/m^*_{xz}$ and $1/m^*_{yz} \neq 0$ necessary
- shearing terms of the reciprocal effective mass tensor are important.
- large eccentricity improves absorption

Si/Ge system

- SiGe alloys; X valleys, Si conc. $x < 0.85$
- SiGe alloys; L valleys, Ge conc. $x > 0.85$

Other systems of interest

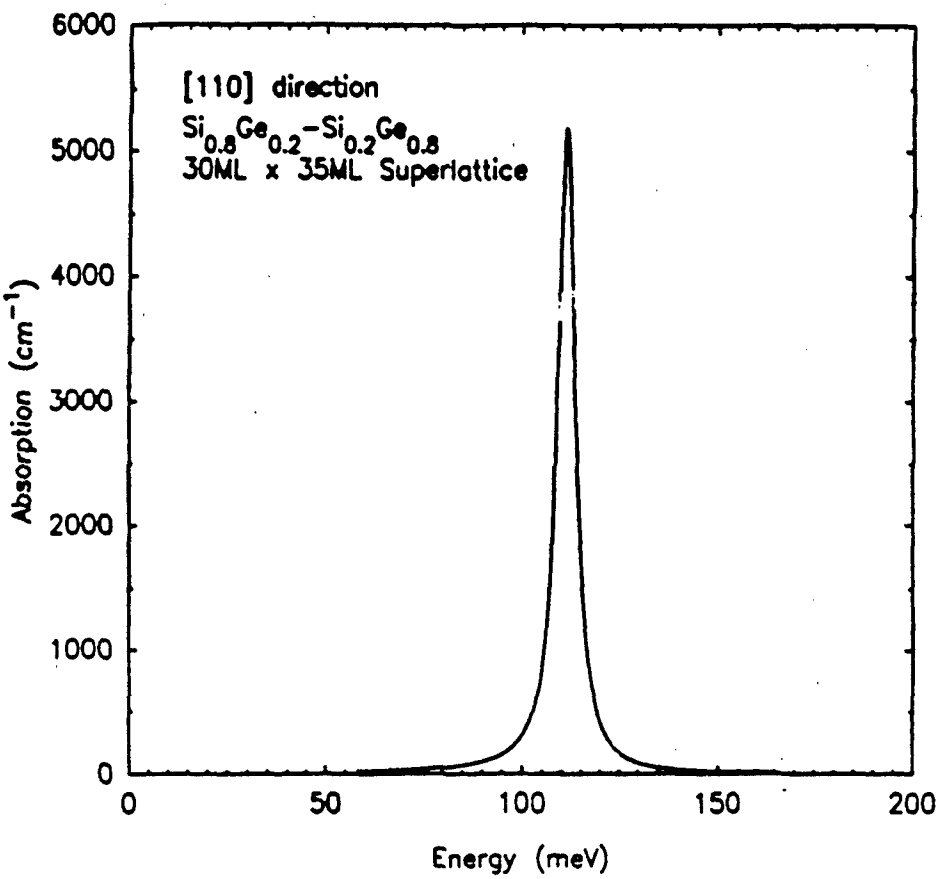
- GaAlAs alloys; X valleys, Al conc. $x > 0.45$
- GaAlSb alloys; L valleys, Al conc. $0.25 < x < 0.55$
- GaAlP, PbSnTe

Absorption

$$\alpha(w) = \frac{4\pi e^2 \pi^2}{nm^2 cw} N_S \left| \langle F_2(z) \nabla_z F_1(z) \rangle \right|^2 \left(\frac{e_x}{m^*_{xz}} + \frac{e_y}{m^*_{yz}} + \frac{e_z}{m^*_{zz}} \right)^2$$

$$\int_0^{\pi/L} \frac{\Gamma/2\pi}{(\hbar w - E(k_z))^2 + \Gamma^2/4} dk_z$$

- Γ is the broadening due to lifetime $\approx$ (5 meV)
- Absorption depends on m*. Shearing terms m^*_{xz} and m^*_{yz} important
- e_j denotes the polarization direction of light
- N_s is the sheet doping concentration
- L is the length of a superlattice unit cell
- $E(k_z)$ is the subband separation energy
- F_1 and F_2 denote envelope functions

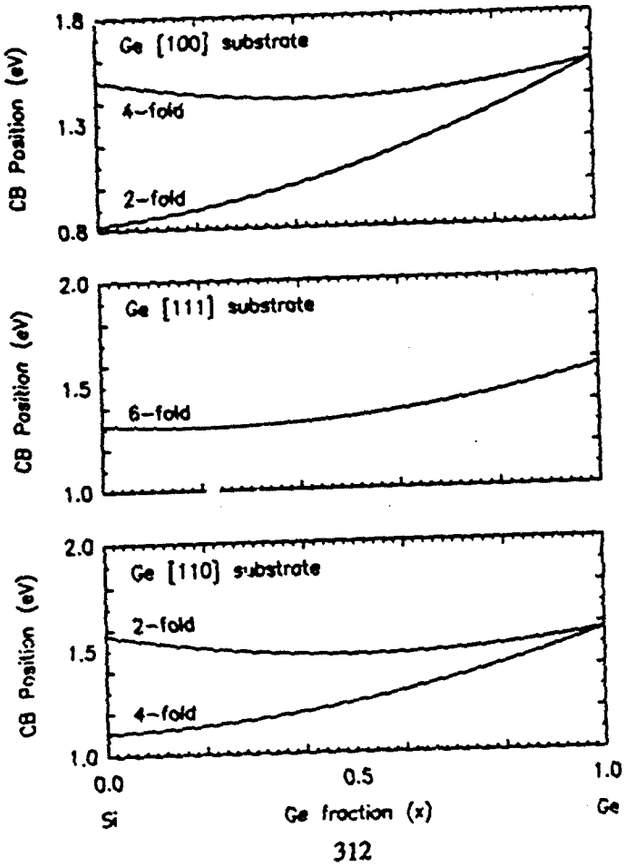


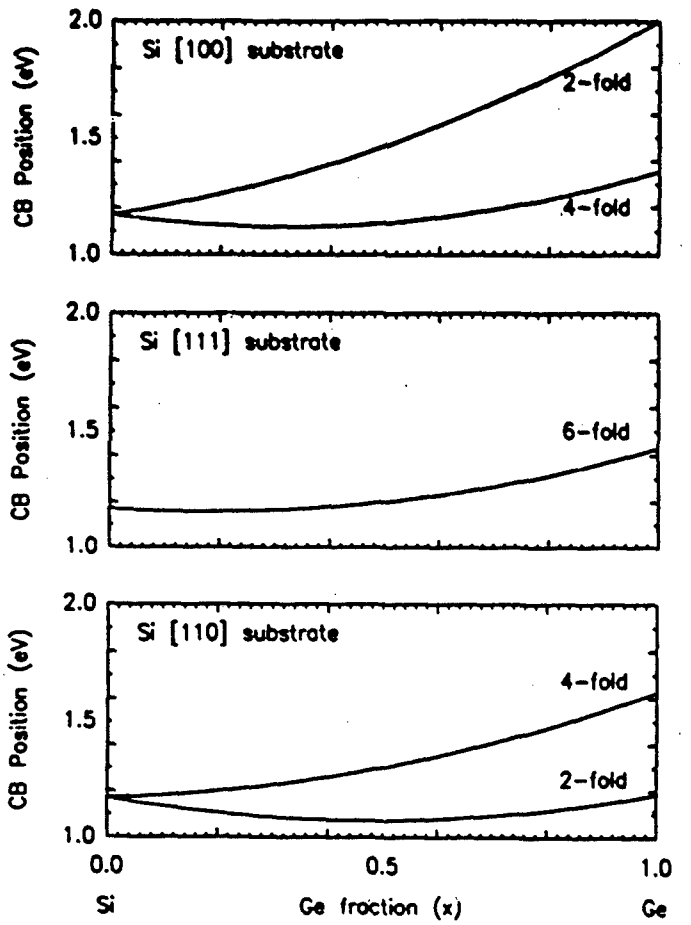
Band Offset

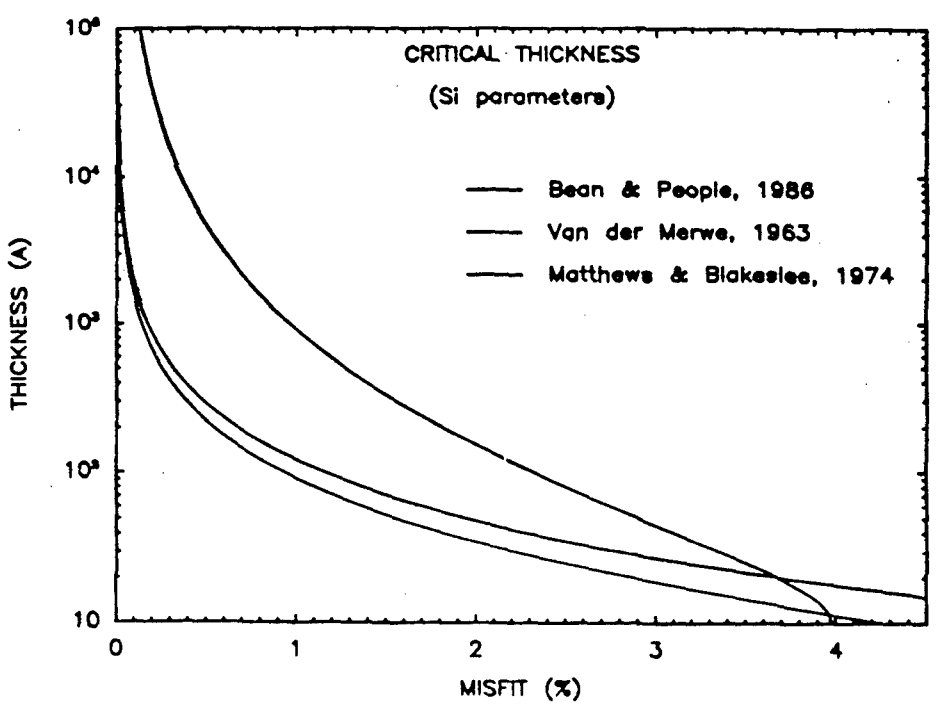
- Si/Ge average VB offset 0.54 eV
- Strain effects important
- CB offsets are small
- VB offsets are large

Strain Effects

- Lattice mismatch
- Splits the valence band degeneracy;
  HH and LH splitting
  * Compression → HH shifts up
  * Tension → LH shifts up
- Splits the conduction band degeneracy
  Six Δ valleys
  * Compression → 4-fold valleys shift down
  * Tension → 2-fold valleys shift down




Si [100] substrate
2-fold
4-fold
Si [111] substrate
6-fold
Si [110] substrate
4-fold
2-fold
CB Position (eV)
2.0
1.5
1.0
0.0
0.5
1.0
Si
Ge fraction (x)
Ge

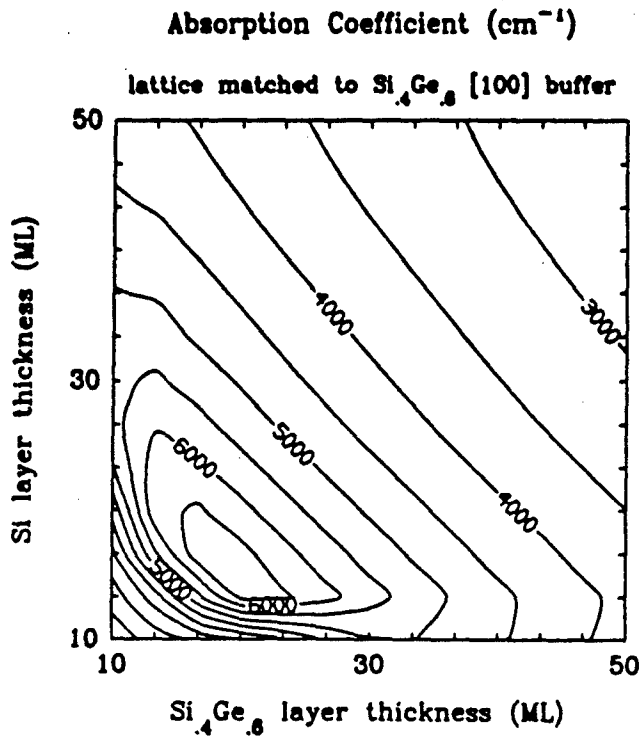

CRITICAL THICKNESS
(Si parameters)
Bean & People, 1986
Van der Merwe, 1963
Matthews & Blakeslee, 1974
THICKNESS (A)
10^6
10^4
10^3
10^2
10
0
1
2
3
4
MISFIT (%)

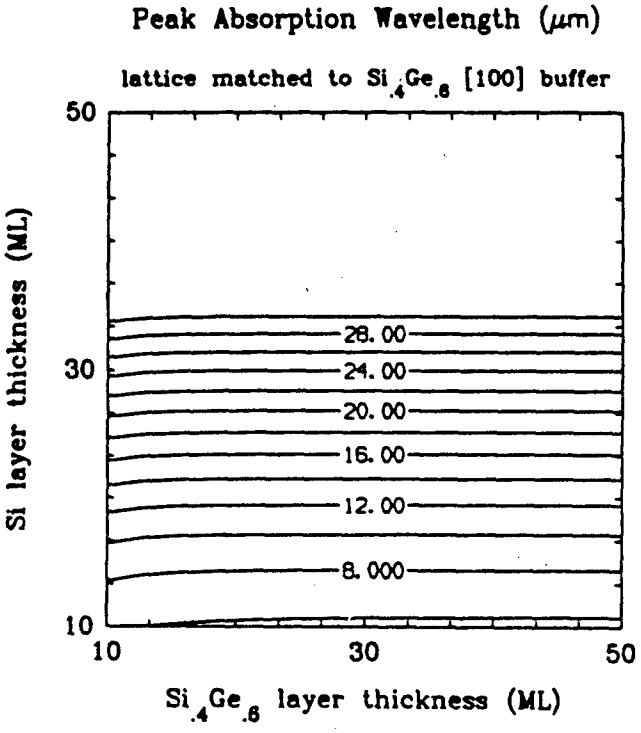
cases:

- [100] 2-fold electrons
- [100] 4-fold electrons
- [111] 6-fold electrons
- [110] 4-fold electrons

[100] direction
parallel incidence
2-fold electrons

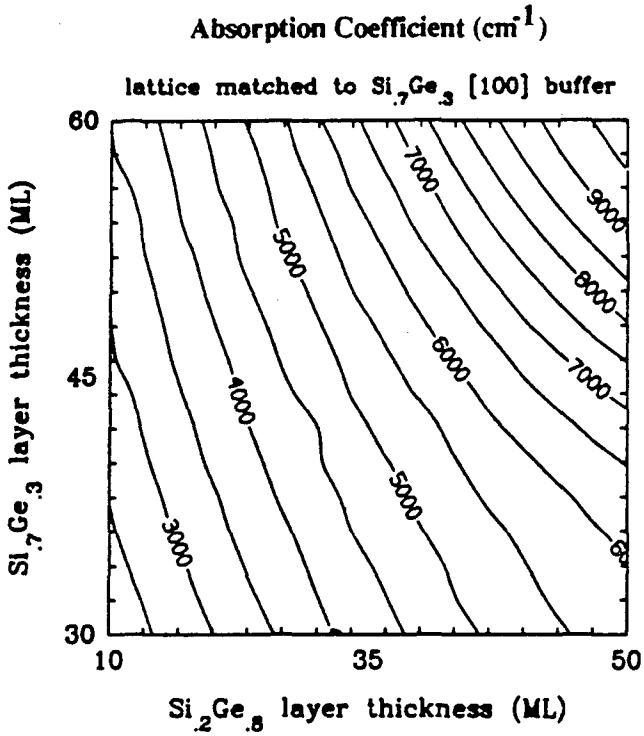
- purpose of study is to compare with GaAs
- effective masses large
- possible to achieve good confinement
- structures:
  * barrier layer, Ge rich: $Si_{0.4}Ge_{0.6}$
  * well layer, Si rich: Si
  * coherently strained to Ge rich $Si_{0.4}Ge_{0.6}$ buffer

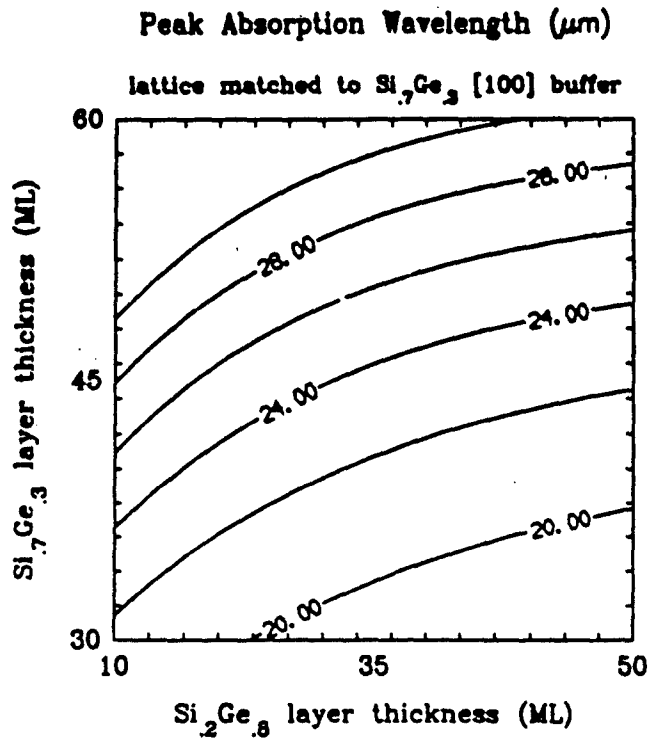

Absorption Coefficient (cm^{-1})
lattice matched to $Si_{.4}Ge_{.6}$ [100] buffer
50
30
10
10
30
50
Si layer thickness (ML)
$Si_{.4}Ge_{.6}$ layer thickness (ML)
1000
3000
5000
6000
4000
5000
15000


Peak Absorption Wavelength (μm)
lattice matched to $Si_{.4}Ge_{.6}$ [100] buffer
50
30
10
10
30
50
Si layer thickness (ML)
$Si_{.4}Ge_{.6}$ layer thickness (ML)
28.00
24.00
20.00
16.00
12.00
8.000

[100] direction
parallel incidence
4-fold electrons

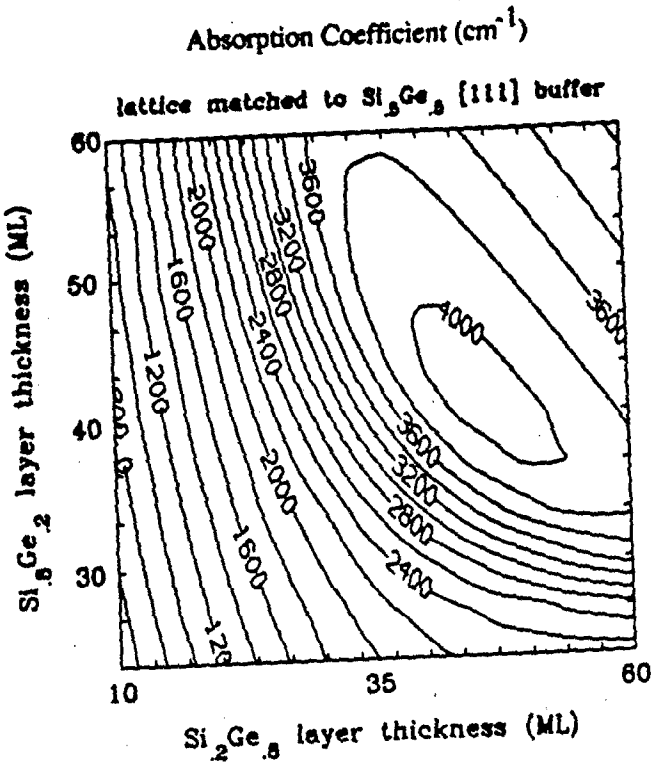
- purpose of study is to compare with GaAs
- effective masses small
- poor confinement
- structures:
  * barrier layer, Ge rich: $Si_{0.2}Ge_{0.8}$
  * well layer, Si rich: $Si_{0.7}Ge_{0.3}$
  * coherently strained to Si rich $Si_{0.7}Ge_{0.3}$ buffer

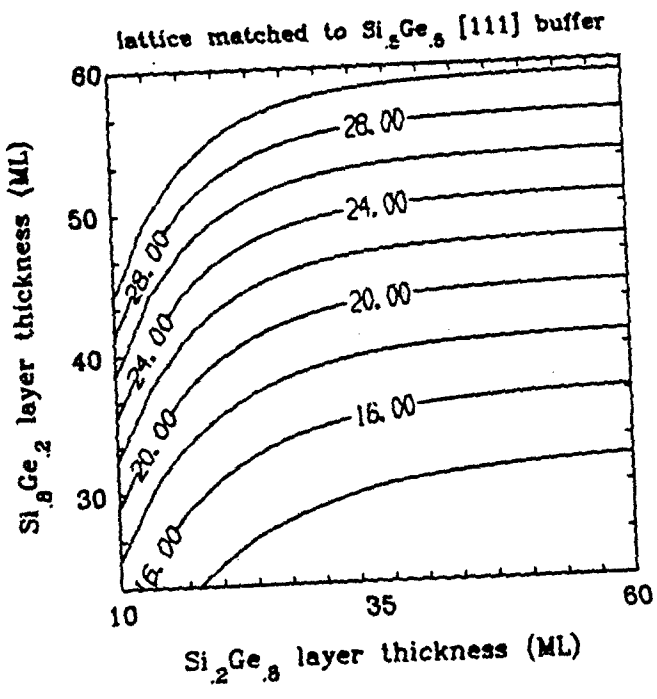




[111] direction
normal incidence
6-fold electrons

- effective masses: medium
- wavefunction confinement: medium
- no preferred azimuthal dependence to absorption
- possible to grow on a buffer layer lattice matched to free standing SL
- structures:
  * barrier layer, Ge rich: $Si_{0.2}Ge_{0.8}$
  * well layer, Si rich: $Si_{0.8}Ge_{0.2}$
  * coherently strained to $Si_{0.5}Ge_{0.5}$ buffer


Absorption Coefficient (cm-1)
lattice matched to Si.5Ge.5 [111] buffer
Si.8Ge.2 layer thickness (ML)
Si.2Ge.8 layer thickness (ML)
60
50
40
30
10
35
60
3600
2000
1600
1200
3200
2800
2400
4000
3600
3200
2800
2400
2000
1600


Peak Absorption Wavelength (μm)
lattice matched to Si.2Ge.8 [111] buffer
Si.8Ge.2 layer thickness (ML)
Si.2Ge.8 layer thickness (ML)
60
50
40
30
10
35
60
28.00
24.00
20.00
16.00
28.00
24.00
20.00
16.00

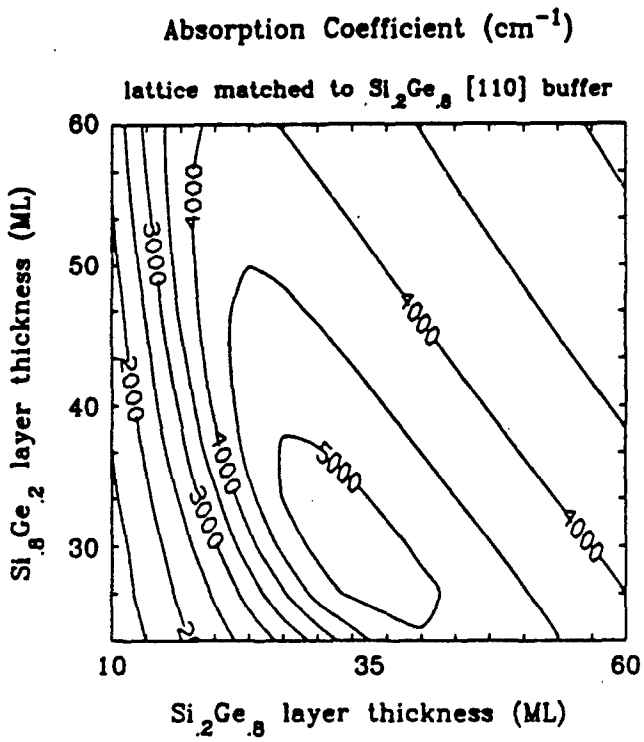
[110] direction
normal incidence
4-fold electrons

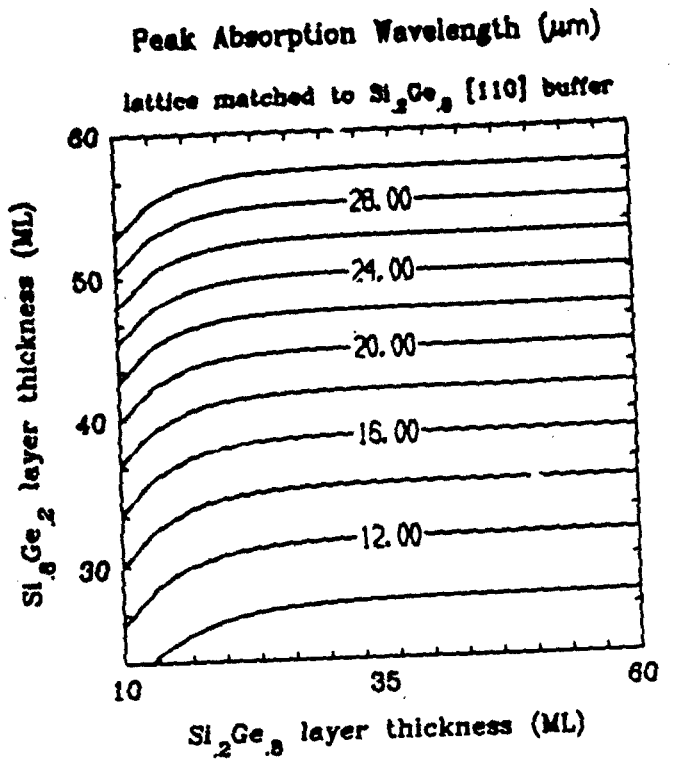
- effective masses: medium
  larger than [111]

- wavefunction confinement: medium
  better than [111]

- preferred azimuthal dependence
  for absorption in [1$\bar{1}$0]
  polarized light

- structures:
  - * barrier layer, Ge rich: $Si_{0.2}Ge_{0.8}$
  - * well layer, Si rich: $Si_{0.8}Ge_{0.2}$
  - * coherently strained to $Si_{0.2}Ge_{0.8}$ buffer





Other major issues

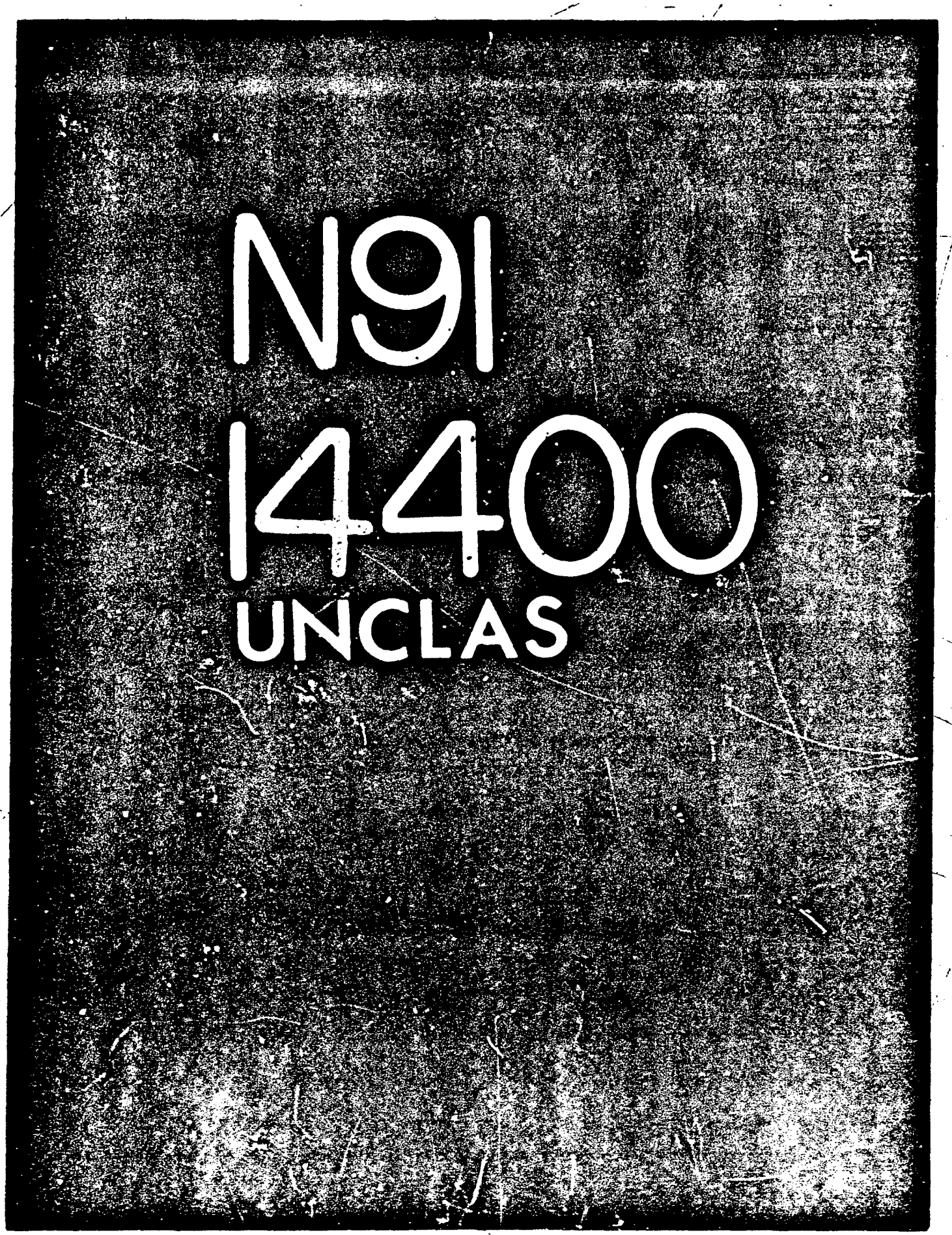
- Role of dislocations
- Excited state lifetime
- Intervalley scattering
- Responsivity, Detectivity

Conclusions

- Absorption of [100] Si/Ge superlattices is comparable to GaAs/AlGaAs (absorption coefficient $\approx 5000\ cm^{-1}$) for $10^{12}\ cm^{-2}$ doping.

- Absorption of [111], and [110] Si/Ge superlattices is superior to GaAs/AlGaAs since normal incidence can be detected

- Similar to extrinsic Si; Can vary absorption wavelength; Large absorption coefficients possible


N91
14400
UNCLAS

N91-14400

Possibilities for LWIR Detectors using MBE-grown Si(/$Si_{1-z}Ge_z$) Structures

R. J. Hauenstein, R. H. Miles, and M. H. Young

Hughes Research Laboratories

Malibu, California 90265

Traditionally, LWIR detection in Si-based structures has involved either extrinsic Si or Si/metal Schottky barrier devices. Molecular beam epitaxially (MBE) grown Si and Si/$Si_{1-z}Ge_z$ heterostructures offer new possibilities for LWIR detection, including sensors based on intersubband transitions as well as improved conventional devices. The improvement in doping profile control of MBE in comparison with conventional chemical vapor deposited (CVD) Si films has resulted in the successful growth of extrinsic Si:Ga, blocked impurity-band conduction detectors. These structures exhibit a highly abrupt step change in dopant profile between detecting and blocking layers which is extremely difficult or impossible to achieve through conventional epitaxial growth techniques. Through alloying Si with Ge, Schottky barrier infrared detectors are possible, with barrier height values between those involving pure Si or Ge semiconducting materials alone. For both *n*-type and *p*-type structures, strain effects can split the band edges, thereby splitting the Schottky threshold and altering the spectral response. Our measurements of photoresponse of *n*-type Au/$Si_{1-z}Ge_z$ Schottky barriers demonstrate this effect. For intersubband multiquantum well (MQW) LWIR detection, $Si_{1-z}Ge_z$/Si detectors grown on Si substrates promise comparable absorption coefficients to that of the Ga(Al)As system while in addition offering the fundamental advantage of response to normally incident light as well as the practical advantage of Si-compatibility. We have grown $Si_{1-z}Ge_z$/Si MQW structures aimed at sensitivity to IR in the 8 to 12 μm region and longer, guided by recent theoretical work.[1] Preliminary measurements of our *n*- and *p*-type $Si_{1-z}Ge_z$/Si MQW structures will be presented.

[1] Y. Rajakarunanayake and T. C. McGill, *Proc. of the 17th Annual Meeting of the Physics and Chemistry of Semiconductor Interfaces*, Clearwater, 1990.

PRECEDING PAGE BLANK NOT FILMED

POSSIBILITIES FOR LWIR DETECTORS USING MBE-GROWN Si(/SiGe) STRUCTURES

R.J. HAUENSTEIN
HUGHES RESEARCH LABORATORIES

OUTLINE

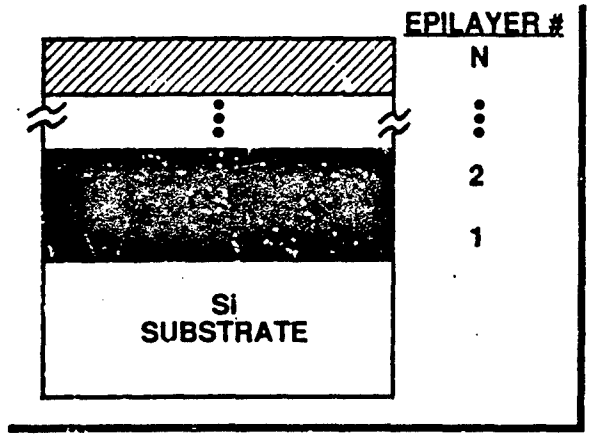
- INTRODUCTION
- EXTRINSIC Si DETECTORS
- $Si_{1-x}Ge_x$ /Si MQW DETECTORS
- SCHOTTKY BARRIERS ON Si_{1-x} Ge_x
- SUMMARY

TRADITIONAL MID TO LONG WAVELENGTH IR DETECTORS IN Si

- EXTRINSIC DETECTORS
  - PC TYPE
  - BLOCKED IBC TYPE
- SCHOTTKY DETECTORS
  - e.g., PtSi/Si

MATERIALS PRODUCED BY Si MBE

HUGHES



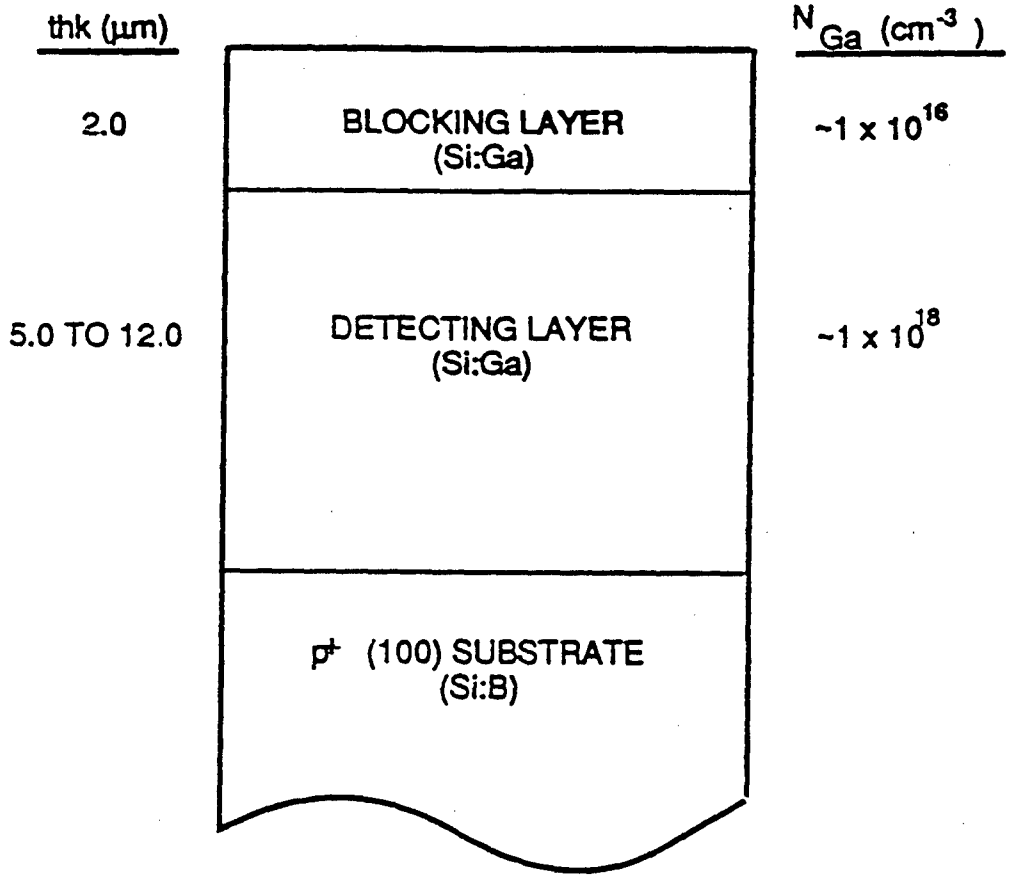
- MANY EPITAXIAL COMBINATIONS POSSIBLE
  - $Si_{1-x}Ge_x$ (COHERENTLY STRAINED)
  - SILICIDES (M_xSi_y)
  - SELECTIVELY DOPED Si
  - OTHER

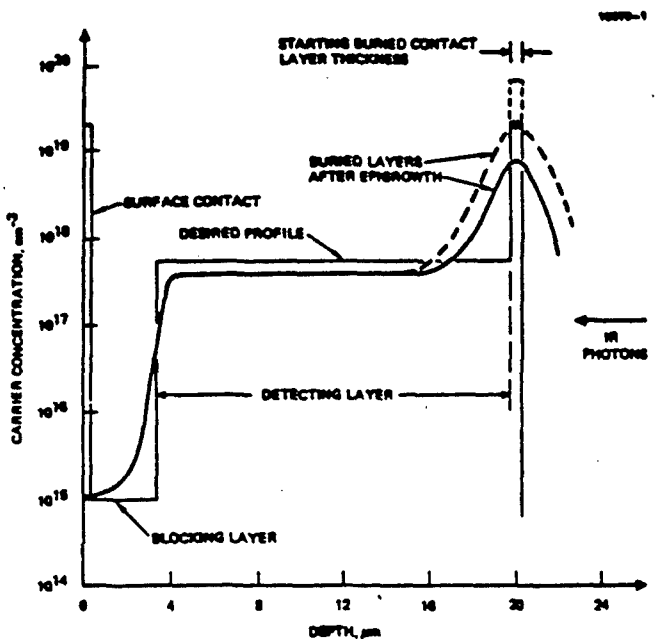
EXTRINSIC Si DETECTORS

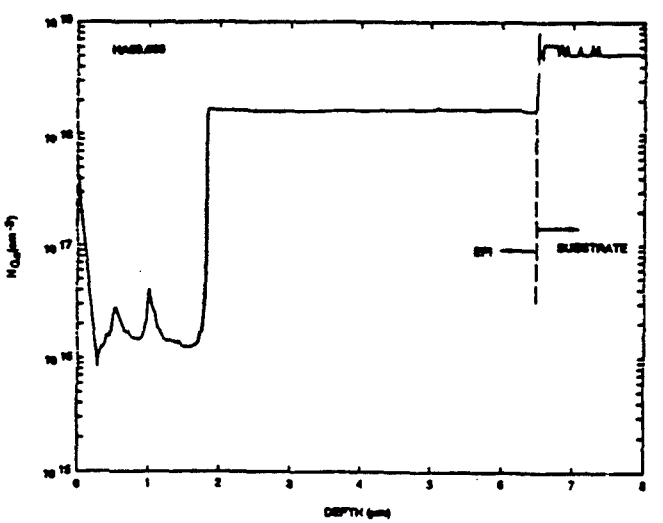
- **MBE ⇒ SUPERIOR DOPANT PROFILE CONTROL FOR FAST DIFFUSERS (e.g., Ga IN Si)**

  CONCENTRATIONS > SOLID SOLUBILITY SOMETIMES POSSIBLE

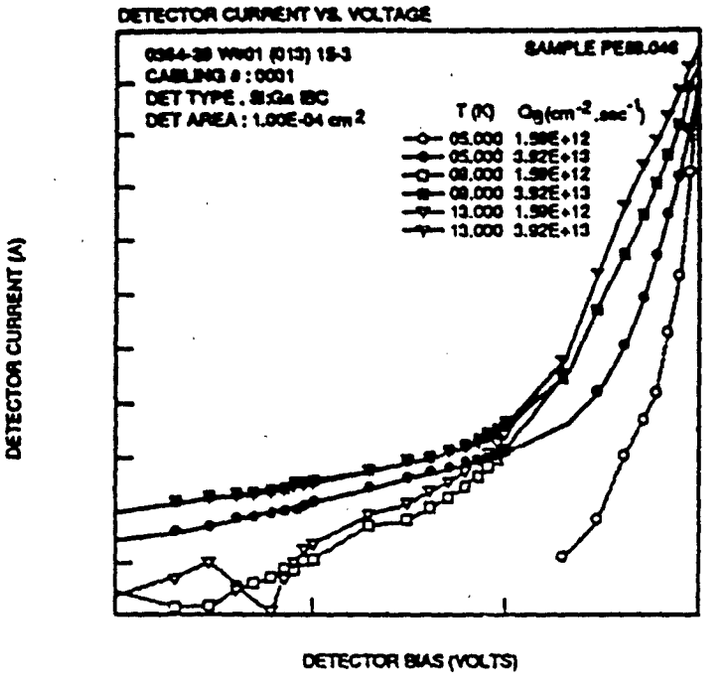
- **MBE + LOW-ENERGY ION IMPLANT PROVIDES GREAT FLEXIBILITY**



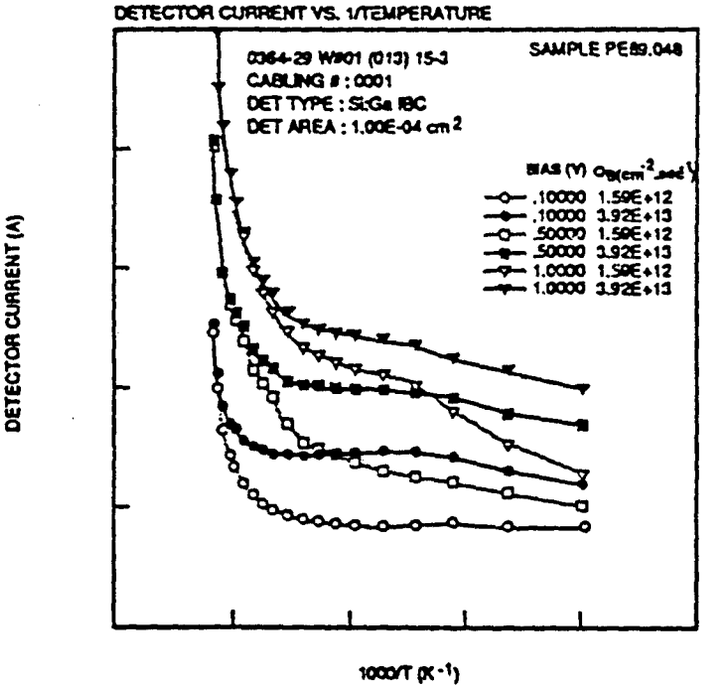




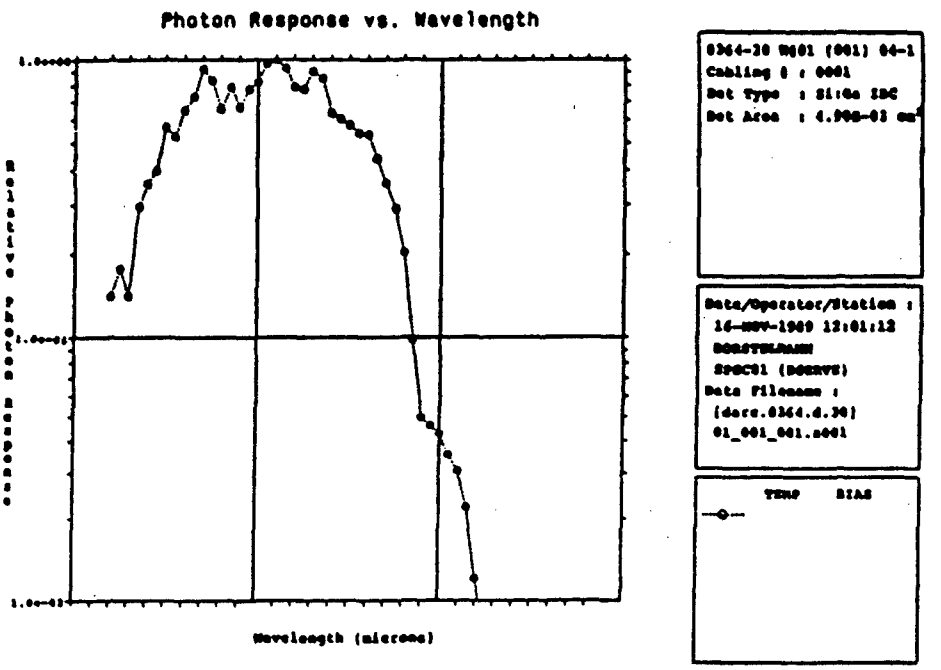
ORIGINAL PAGE IS
OF POOR QUALITY


DETECTOR CURRENT VS. VOLTAGE
0364-29 W#01 (013) 15-3
CABLING # : 0001
DET TYPE : Si:Ga IBC
DET AREA : 1.00E-04 cm 2
SAMPLE PE89.048
T (K) Qg(cm-2 ,sec-1)
05.000 1.59E+12
05.000 3.92E+13
08.000 1.59E+12
08.000 3.92E+13
13.000 1.59E+12
13.000 3.92E+13
DETECTOR CURRENT (A)
DETECTOR BIAS (VOLTS)

a)


DETECTOR CURRENT VS. 1/TEMPERATURE
0364-29 W#01 (013) 15-3
CABLING # : 0001
DET TYPE : Si:Ga IBC
DET AREA : 1.00E-04 cm 2
SAMPLE PE89.048
BIAS (V) Qg(cm-2 ,sec-1)
.10000 1.59E+12
.10000 3.92E+13
.50000 1.59E+12
.50000 3.92E+13
1.0000 1.59E+12
1.0000 3.92E+13
DETECTOR CURRENT (A)
1000/T (K-1)

b)



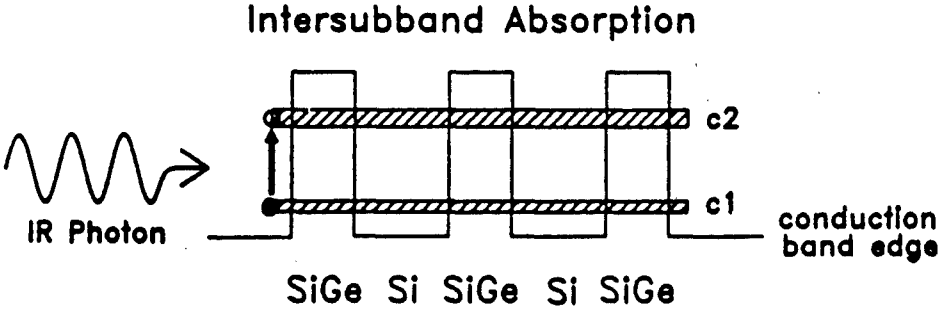
MBE Si:Ga BLOCKED IBC RESULTS

- IBC BEHAVIOR DEMONSTRATED
- WAVELENGTH RESPONSE GOOD (~ 12 μm PEAK)
  HOWEVER: POOR Q.E. DUE TO
  - LIMITED PURITY (NEED ~ 10^{12} CM $^{-3}$!)
  - TOO MANY PARTICULATES

HRL IS DEVELOPING A GAS-SOURCE Si MBE TECHNIQUE TO IMPROVE UPON ABOVE RESULTS

ORIGINAL PAGE IS
OF POOR QUALITY

SiGe/Si MULTI-QUANTUM WELL DETECTOR



- Tunable response throughout infrared
- Normal-incidence absorption
- Predicted absorption stronger than GaAs-based

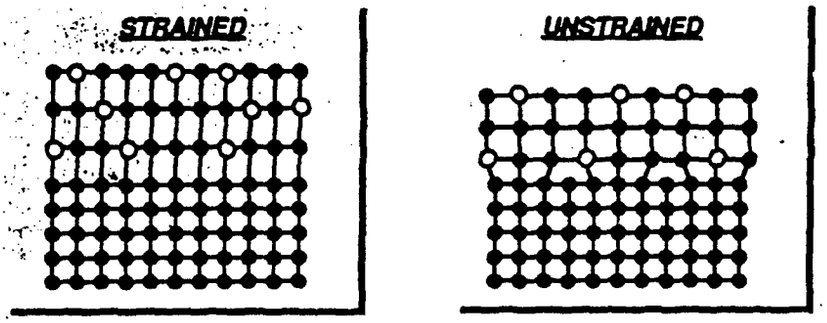
SiGe/Si MQWS – IMPORTANT ISSUES

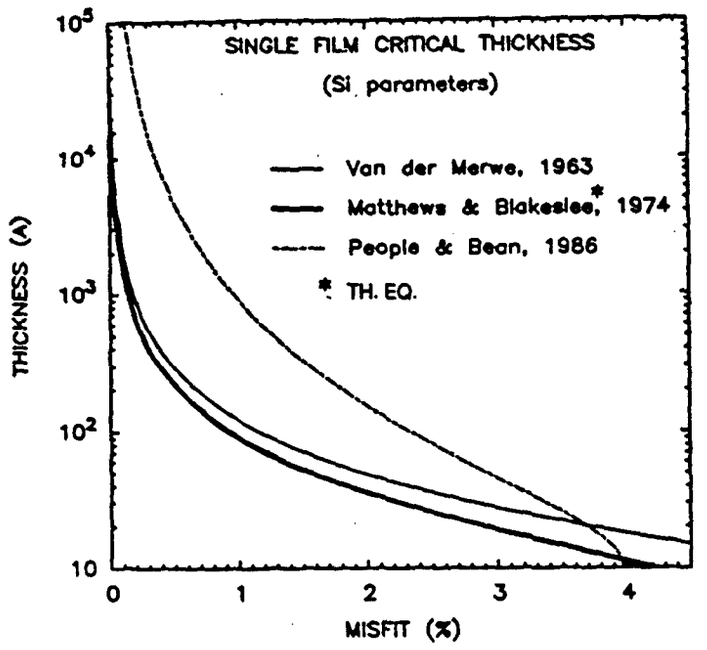
- **STRAIN**
  - **CRITICAL THICKNESS(ES)**
  - **EFFECT ON BAND STRUCTURE**
- **COND. BAND ANISOTROPY**
- **GROWTH ISSUES**
  - **GOOD "RELAXED" LAYER**
  - **n-TYPE DOPING**
  - **UNIFORMITY OF THIN LAYERS**

$Si_{1-x}Ge_x$ ON Si

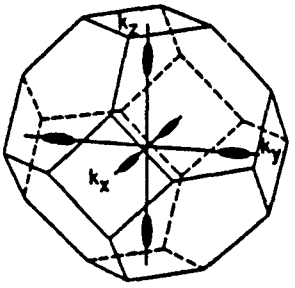
HUGHES

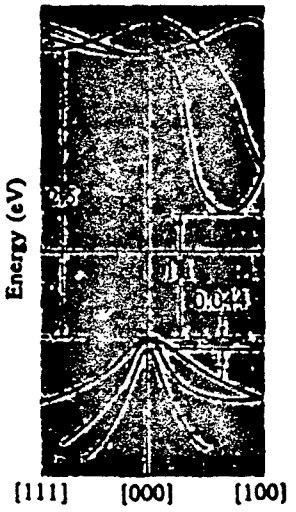
- KEY FEATURE
  - LATTICE CONSTANT MISMATCH (~ 4.2% Ge TO Si)
- EPITAXIAL POSSIBILITIES
  - COHERENTLY STRAINED GROWTH
  - UNSTRAINED (RELAXED) GROWTH





Si(Ge) BAND STRUCTURE

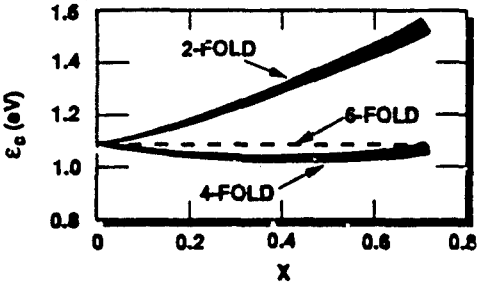




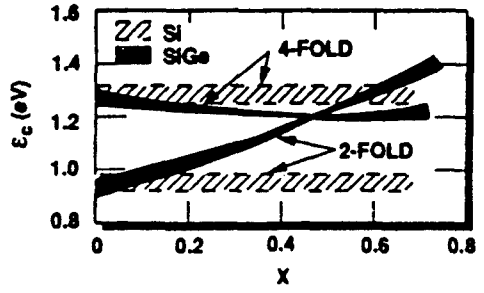
EFFECT OF STRAIN ON $Si_{1-x}Ge_x$ BANDSTRUCTURE

HUGHES

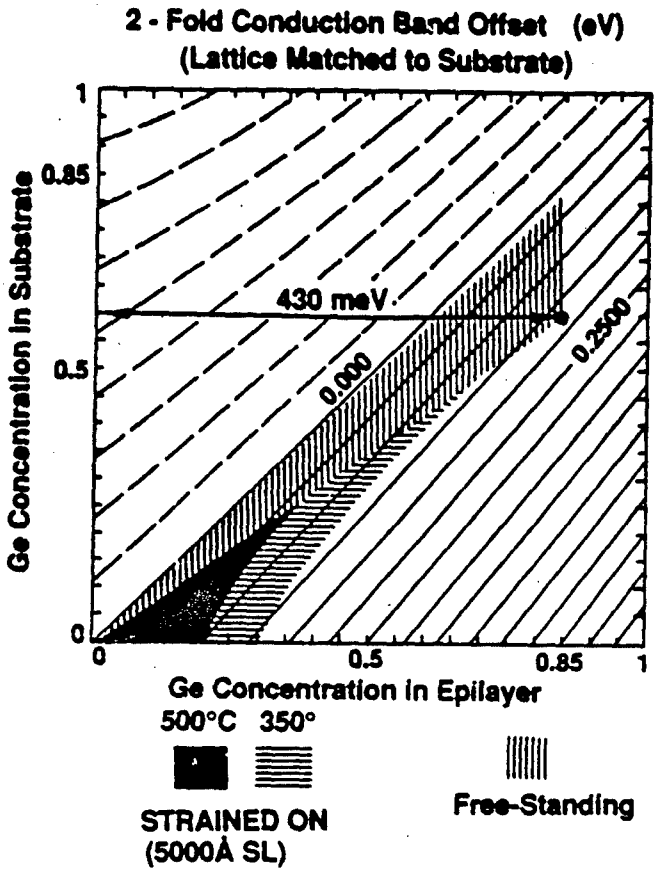
$Si_{1-x}Ge_x$ ON Si (100):

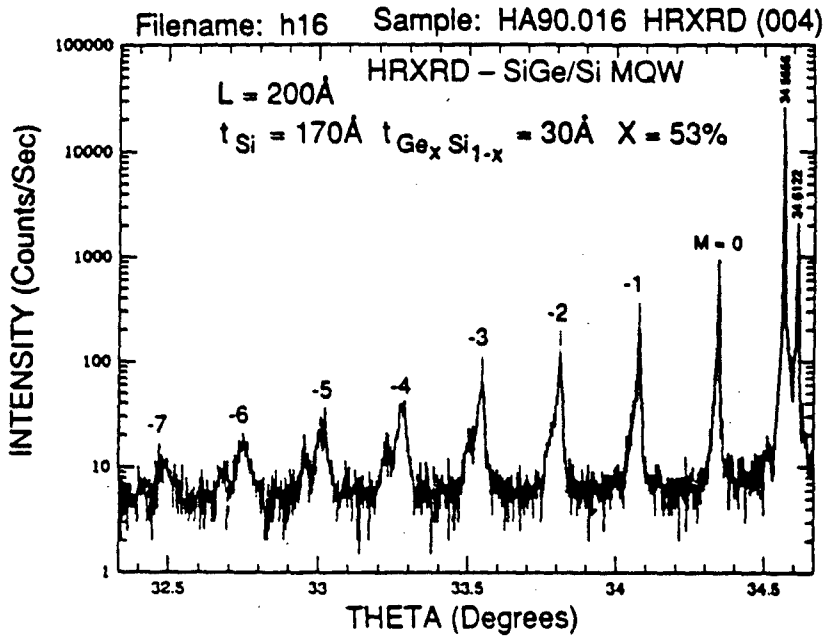


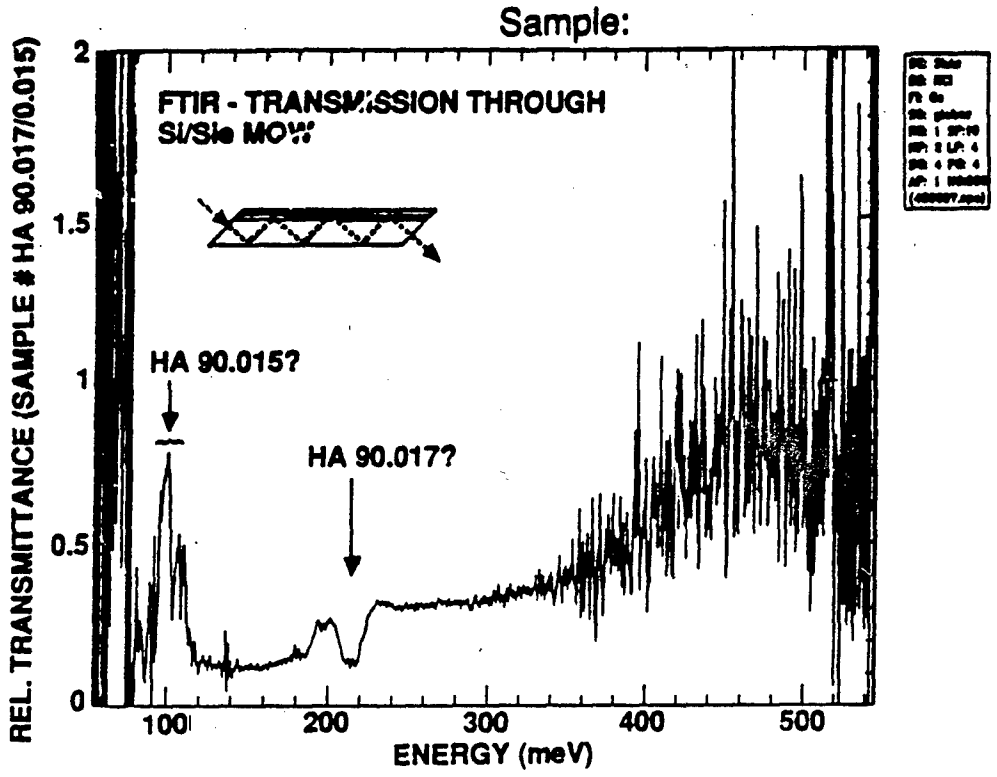
$Si_{1-x}Ge_x$ ON $Si_{0.5}Ge_{0.5}$ (100):



USEFUL GROWTH RANGE







SYNOPSIS - SiGe/Si MQW'S - (100) FILMS

	WELL	BARRIER	BUFFER	NON-PARAB.	MBE GROWTH
n-Type	Si	Si_{1-X} Ge_X	$Si_{1-X}Ge_X$(RLX)	WEAK	HARDER
p-Type	Si_{1-X} Ge_X	Si	Si(COH)	STRONG	EASIER

	DETECTS NORM. ALUM.?	8 - 12mm?	α RAIC(CM^{-1})
n-(100)	NO	YES	~ 6000
n-(110)	YES	YES	~ 5000
n-(111)	YES	NO	~ 4000

SCHOTTKY BARRIERS ON Si AND Ge FOR SELECTED METALS (300K)

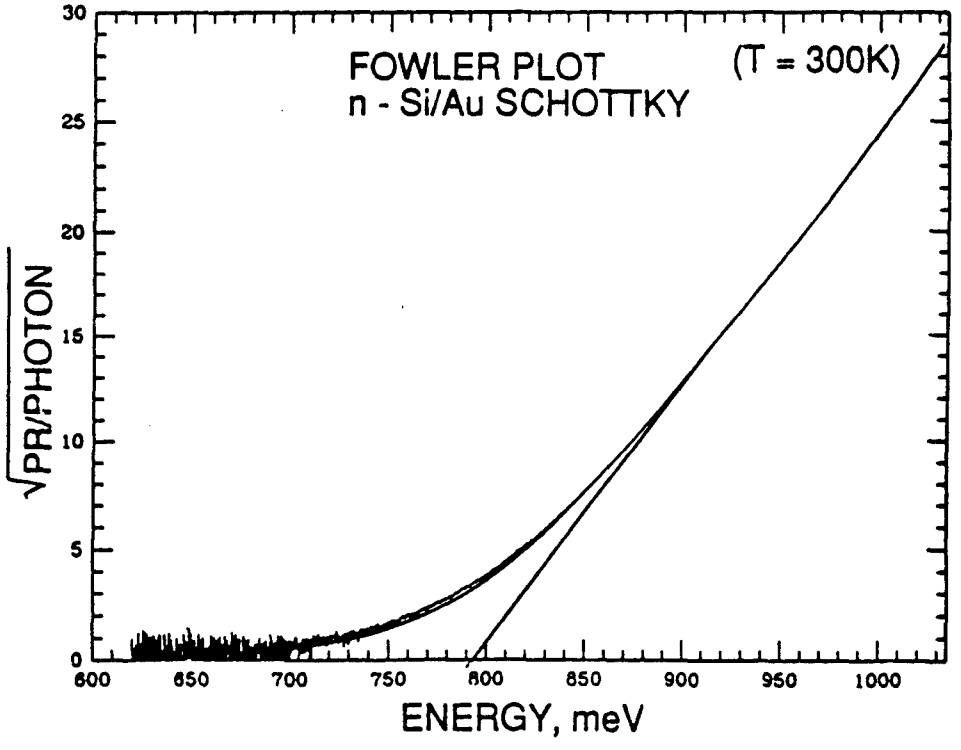
	Ag	Al	Au	Cu	Ni	Pt	W
(n) Si	0.78	0.72	0.80	0.58	0.61	0.90	0.67
(p) Si	0.54	0.58	0.34	0.46	0.51	–	0.45
(n) Gr	0.54	0.48	0.59	0.52	0.49	–	0.48
(p) Ge	0.50	–	0.30	–	–	–	–

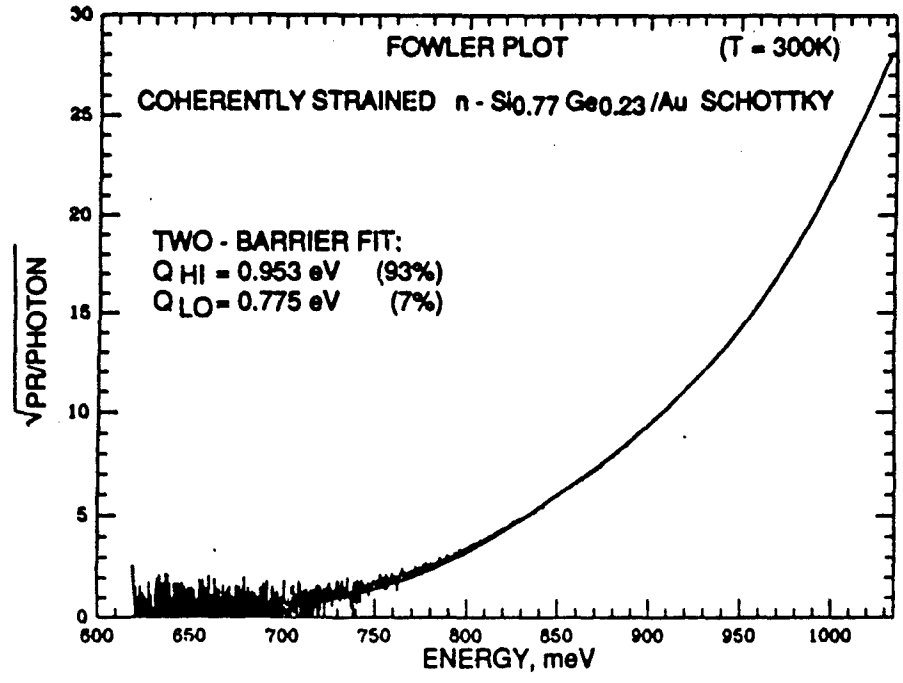
$\Delta Q_n >> \Delta Q_p$ IN MOST CASES

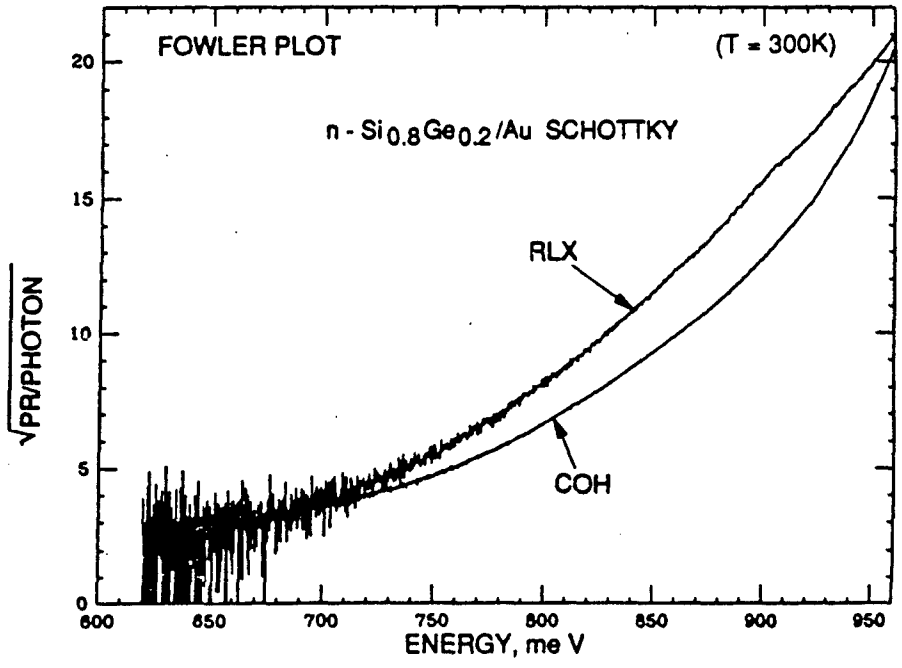
$\Rightarrow E_F^{METAL} \approx$ PINNED TO VALENCE BAND EDGE

INTERPOLATE VALUES FOR UNSTRAINED $Si_{1-x}\ Ge_x$?

FROM S.M. SZE, "PHYSICS OF SEMICONDUCTOR DEVICES," WILEY, 1981, CHAP. 5

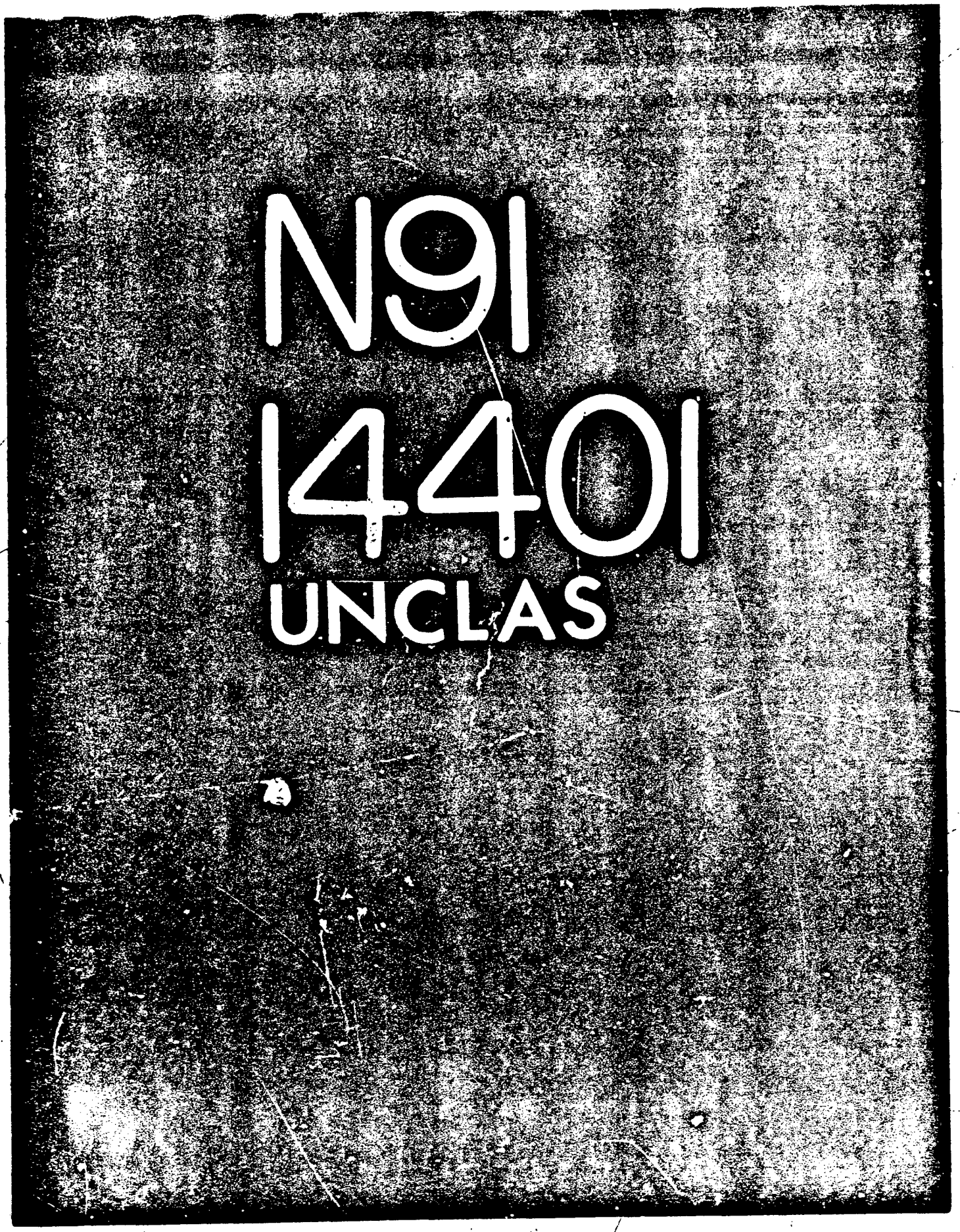



FOWLER PLOT
(T = 300K)
COHERENTLY STRAINED n - Si0.77 Ge0.23 /Au SCHOTTKY
TWO - BARRIER FIT:
Q HI = 0.953 eV (93%)
Q LO = 0.775 eV (7%)
√PR/PHOTON
ENERGY, meV


FOWLER PLOT
(T = 300K)
n - Si0.8 Ge0.2 /Au SCHOTTKY
RLX
COH
√PR/PHOTON
ENERGY, me V

SUMMARY

- Si MBE ⇒ MULTILAYERS IN A Si-PROCESS - COMPATIBLE TECHNOLOGY
- BETTER "CONVENTIONAL" DEVICES POSSIBLE (E.G., Si:Ga IBC)
- NOVEL DEVICES POSSIBLE (MQW)
- SiGe/Si MQW ADVANTAGE: DETECTS NORMALLY INCIDENT LIGHT
- Si(Ge) STRAINED SCHOTTKY BARRIERS: INTERESTING PROSPECTS FOR DEVICES AND PHYSICS


N91
14401
UNCLAS

N91-14401

Novel $Si_{1-x}Ge_x$/Si Heterojunction Internal Photoemission Long Wavelength Infrared Detectors

T. L. Lin, J. Maserjian, T. N. Krabach, A. Ksendzov, M. L. Huberman, and R. Terhune
Center for Space Microelectronics Technology
Jet Propulsion Laboratory
California Institute of Technology

ABSTRACT

There is a major need for long-wavelength-infrared (LWIR) detector arrays in the range of 8 to 16 μm which operate with close cycle cryocoolers above 65 K. In addition, it would be very attractive to have Si-based infrared (IR) detectors that can be easily integrated with Si readout circuitry and have good pixel-to-pixel uniformity, which is critical for focal plane array (FPA) applications. We report here a novel $Si_{1-x}Ge_x$/Si heterojunction internal photoemission (HIP) detector approach with a tailorable LWIR cutoff wavelength, based on internal photoemission over the $Si_{1-x}Ge_x$/Si heterojunction. The HIP detectors were grown by molecular beam epitaxy (MBE), which allows one to optimize the device structure with precise control of doping profiles, layer thickness and composition.

The HIP detector incorporates a degenerately doped p^+-$Si_{1-x}Ge_x$ layer as the photo emitter, and the Si substrate as the collector. The detection mechanism is IR absorption in the p^+-$Si_{1-x}Ge_x$ emitter followed by internal photoemission of photoexcited holes over the $Si_{1-x}Ge_x$/Si heterojunction barrier into the p-Si substrate. The valence band discontinuity between $Si_{1-x}Ge_x$ and Si layers determines the energy barrier, and can be adjusted by varying the Ge composition ratio x. Thus, the cutoff wavelength of the $Si_{1-x}Ge_x$/Si HIP IR detector is tailorable over a wide LWIR range; for example, 8 -16 μm with x ranging from about 0.2 to 0.4. The tailorable cutoff wavelength can be used to optimize the trade-off between the LWIR response and the cooling requirements of the detector.

The $Si_{1-x}Ge_x$/Si HIP detector approach is made possible by the recent advance in MBE growth of degenerately doped p^+-$Si_{1-x}Ge_x$ layers with abrupt boron doping profiles. Doping concentrations to 10^{20} cm^{-3} in the $Si_{1-x}Ge_x$ layers are achieved using boron from an HBO_2 source during MBE growth. The p^+ doping enables adequate IR absorption for photoexcited hole generation in the $Si_{1-x}Ge_x$ layers.

Compared to silicide Schottky-barrier detectors, the HIP detector offers a higher internal quantum efficiency (QE). One reason is the narrow band of hole occupied states in the p^+-$Si_{1-x}Ge_x$ layer due to its semiconductor band structure. In Schottky detectors, photons can excite carriers from states far below the Fermi energy such that they do not gain sufficient energy to overcome the barrier. Near threshold only a small fraction of the photoexcited carriers can exceed

PRECEDING PAGE BLANK NOT FILMED

the barrier energy. Consequently, its QE rises only slowly with energy above the barrier cutoff energy. In contrast, the narrow band of absorbing states in the HIP detector leads to a sharper turn-on, which in turn results in useful sensitivities close to the cutoff. This property avoids a serious weakness of Schottky detectors where the Fowler's dependence provides reasonable QE only at wavelengths well below the cutoff, which requires lower operating temperatures for a given dark current. Another reason is that photoexcited holes traveling over the potential barrier can more easily conserve their lateral momentum because of the more favorable ratio of effective masses across the heterojunction. Furthermore, improvement is expected because of reduced inelastic hole scattering in the $Si_{1-x}Ge_x$ layers compared with the silicides, and the ability to grow $Si_{1-x}Ge_x$ layers with optimal thickness, doping and composition.

Preliminary HIP detectors have been fabricated by MBE growth of $Si_{1-x}Ge_x$ layers with x = 0.2, 0.3 and 0.4 on patterned p-type Si substrates. The detectors incorporate n-type guard-rings defining the periphery of the active device areas to suppress leakage current. The photoresponses of the detectors were measured with front-side illumination using a blackbody source at 940 K. Photoresponses at wavelength 2 to 10 μm are obtained with QE above ~ 1% in these non-optimized structures. The tailorable cutoff wavelength of the proposed HIP detector has also been demonstrated by varying the Ge ratio x in the $Si_{1-x}Ge_x$ layers. The photoresponses of $Si_{1-x}Ge_x$/Si HIP detectors with x = 0.2, 0.3 and 0.4 increase and extend to longer wavelengths as the Ge ratio x reduces from 0.4 to 0.2. Furthermore, the QE of the device can be improved by optimizing the layer thickness and the doping profile of the $Si_{1-x}Ge_x$ layers. By reducing the thickness of $Si_{0.7}Ge_{0.3}$ layers from 400 nm to 40 nm, and increasing the boron doping concentrations from 10^{19} to 10^{20} cm^{-3}, the QE's have been improved by two orders of magnitude (from 0.003 % to ~0.3% at 8 μm).

In conclusion, the feasibility of a novel $Si_{1-x}Ge_x$/Si HIP detector has been demonstrated with tailorable cutoff wavelength in the LWIR region. Photoresponse at wavelengths 2 to 10 μm are obtained with QE above ~ 1% in these non-optimized device structures. It should be possible to significantly improve the QE of the HIP detectors by optimizing the thickness, composition, and doping concentration of the $Si_{1-x}Ge_x$ layers and by configuring the detector for maximum absorption such as the use of a cavity structure. With optimization of the QE and by matching the barrier energy to the desired wavelength cutoff to minimize the thermionic current, we predict near background limited performance in the LWIR region with operating temperatures above 65K. Finally, with mature Si processing, our relatively simple device structure offers potential for low-cost producible arrays with excellent uniformity.

*This work is supported by NASA and SDIO.

JPL

$Si_{1-x}Ge_x$/Si Heterojunction Internal Photoemission Detectors for LWIR Focal Plane Array Applications

True-Lon Lin, T. N. Kraback, S. Dejewski, A. Ksendzov,
J. Maerjian, M. L. Huberman and R. Terhue

Center for Space Microelectronics Technology
Jet Propulsion Laboratory
California Institute of Technology

Supported by NASA/OAET and SDIO/ISTO

OUTLINE

- Introduction
- Advantages of the $Si_{1-x}Ge_x$ HIP detectors
- Growth and Fabrication of the HIP detectors
- Results and Discussion
- Summary

JPL

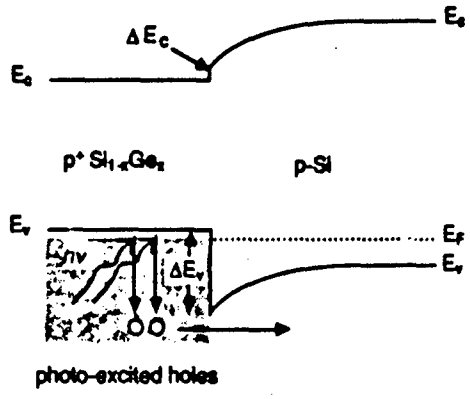
INTRODUCTION

Novelties

- Degenerately doped p^+-$Si_{1-x}Ge_x$ layers for strong IR absorption
- $Si_{1-x}Ge_x$/Si valence band offset as the potential barrier, which is tailorable over a wide LWIR range

Detection mechanism

- IR absorption in the p^+-$Si_{1-x}Ge_x$ layers
- Internal photoemission over the heterojunction barrier



Band Structure of $Si_{1-x}Ge_x$ /Si Heterojunction Internal Photoemission (HIP) IR Detectors

IR Absorption in Degenerately Doped P+ $Si_{1-x}Ge_x$ Layers

- Degenerately doped p^+-$Si_{1-x}Ge_x$ layers are required for strong IR absorption for photoexcited hole generation.
- Two IR absorption mechanisms
  - Free-carrier absorption

$$\alpha_f = \frac{Nq^2\lambda^2}{m^* 8\pi^2 nc^3\tau} \sim N^{1.5}\,\lambda^{1.5\text{-}3.5}$$

  - Intra-valence-band transition

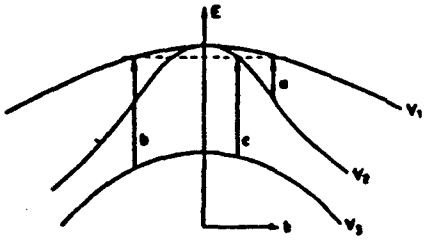
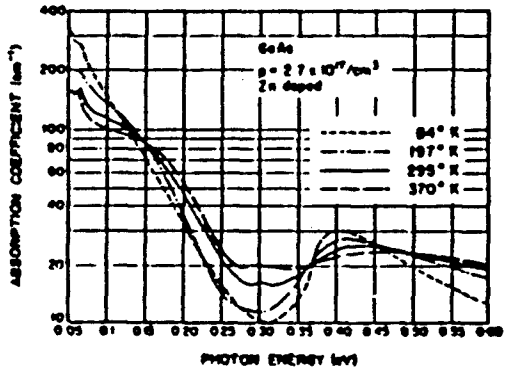


Fig. 3-34 Valence subband structure and intraband transitions.



IR absorption increases with carrier concentration and photon wavelength

JPL

Low Temperature Boron Doping for P+ $Si_{1-x}Ge_x$ Layers

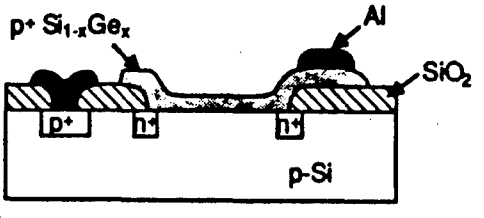
The $Si_{1-x}Ge_x$ /Si HIP detector approach is made possible by utilizing a low temperature boron doping technique developed at JPL.

Low growth temperatures required
- 2-dimensional (planar) $Si_{1-x}Ge_x$ growth
- Abrupt boron doping profiles

$[B] > 10^{20}$ cm^{-3} has been achieved using boron from an HBO_2 source during MBE growth

Advantages of $Si_{1-x}Ge_x$ /Si HIP LWIR Detectors

- Si-based IR detector with similar advantages of Schottky-barrier IR detectors:
  - Integration with Si readout circuitry either monolithically or by In bond bounding
  - Good pixel-to-pixel uniformity
  - Allows normal IR illumination
  - High yield and low cost (cents/pixel)
- Feasible for large focal plane array application as demonstrated by commercially available 512x512 PtSi arrays, but extended to the LWIR regime
- Tailorable LWIR Cutoff
  - can be adjusted to match the desirable cutoff to minimize the dark current
- Relatively good QE's for large array applications



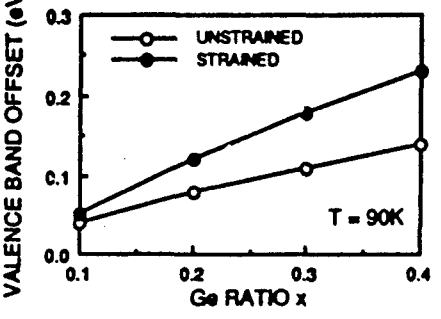
Device structure of $Si_{1-x}Ge_x$/Si HIP LWIR detectors

JPL

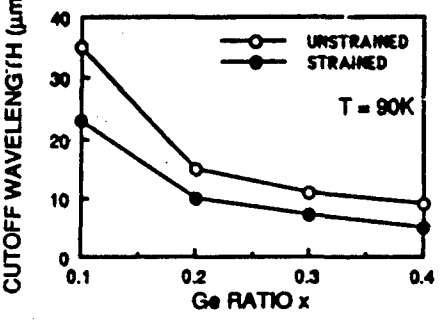
Tailorable Cutoff in LWIR Regime

- The cutoff wavelength λc of the $Si_{1-x}Ge_x$/Si HIP detector is determined by the valence band offset ΔEv between $Si_{1-x}Ge_x$ and Si, which is equal to ~ 90% of the bandgap difference between $Si_{1-x}Ge_x$ and Si. The bandgap of $Si_{1-x}Ge_x$ can be varied by adjusting Ge ratio x and strain. Consequently, the cutoff wavelength of $Si_{1-x}Ge_x$ /Si HIP detector is tailorable in a wide LWIR region.

ΔEv as a function of Ge ratio x

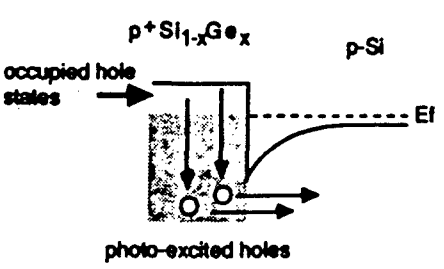


The corresponding cutoff λc

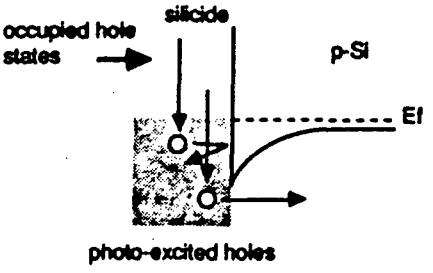


Higher QE (compared with Schottky detectors)

- Narrow band of occupied hole states (due to its semiconductor band structure) in the p^+-$Si_{1-x}Ge_x$ layer of the HIP detector leads to a sharper turn-on, resulting in useful sensitivities close to the cutoff



$Si_{1-x}Ge_x$/Si HIP detectors



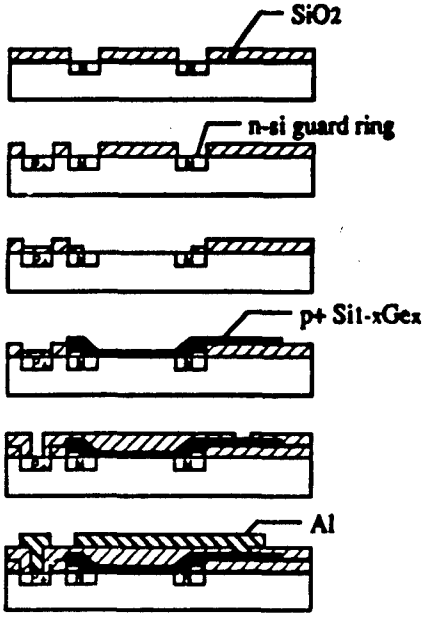
Silicide Schottky detectors

- The more favorable ratio of effective masses across the heterojunction reduces the backscattering of photoexcited holes

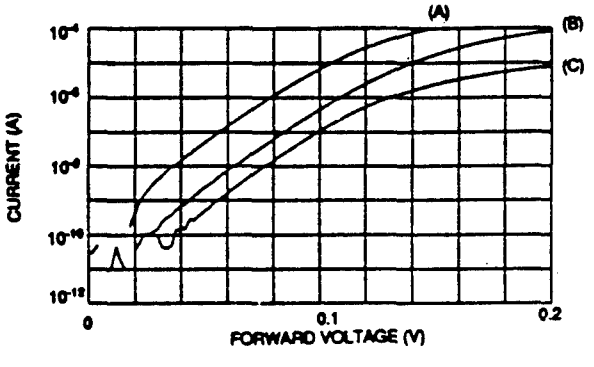
JPL

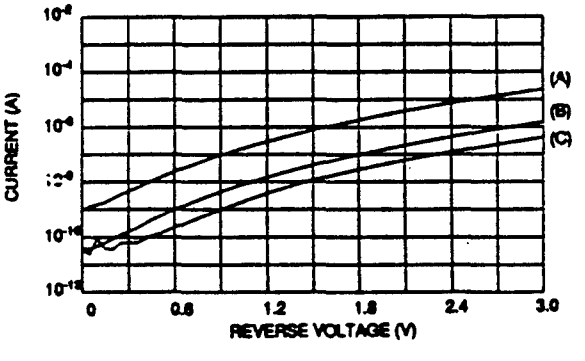
Fabrication of $Si_{1-x}Ge_x$/Si HIP IR Detectors

- Surface preparation : using "spin-clean" technique
- MBE growth of p^+-$Si_{1-x}Ge_x$ layers on patterned p-type Si(100) wafers
  - Growth temperature = 600°C
  - [B] = 10^{19} to 10^{20} cm^{-3}
  - Ge ratio x = 0.2, 0.3 and 0.4
- Device fabrication
  - Six level mask set
  - In-house fabrication



Current-Voltage Characteristic





400 nm thick $Si_{0.72}Ge_{0.28}$ layers, [B] = 10^{19} cm^{-3}

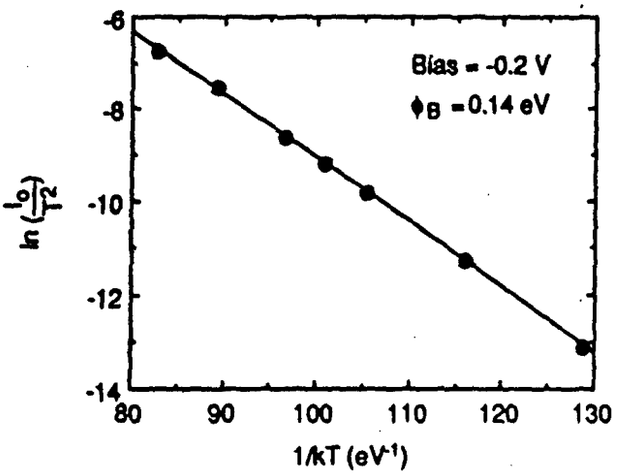
Temp = 77 K

Bias applied to p-Si substrate, with the $Si_{0.72}Ge_{0.28}$ layer grounded

Ideality factor n =1.4, $J_o \sim 2 \times 10^{-6}$ Acm^{-2}

JPL

Activation Energy Measurement



400 nm thick $Si_{0.72}Ge_{0.28}$

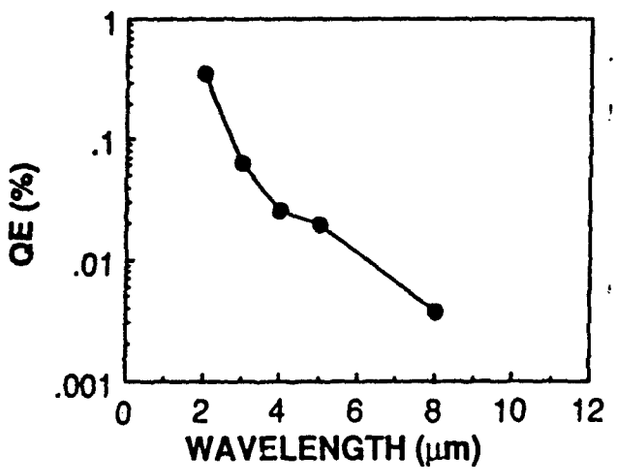
[B] = 10^{19} cm^{-3}

Temp = 90 - 145 K

$$J_o = A^* T^2 \exp\left(-\frac{q\phi_B}{kT}\right)$$

$$\ln\left(\frac{J_o}{T^2}\right) = -\frac{q\phi_B}{kT} + \ln(A^*)$$

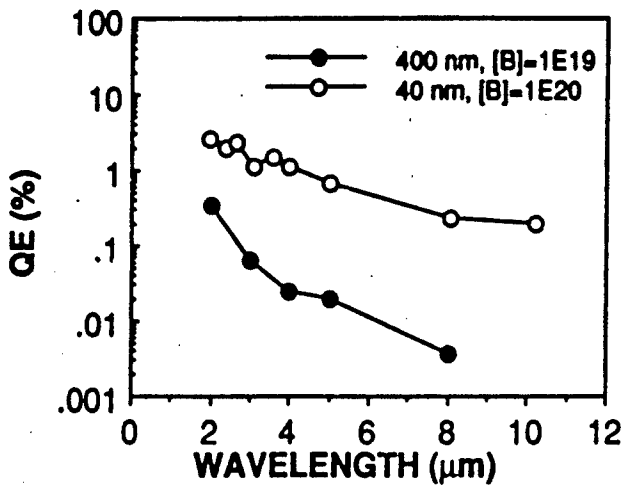
PHOTORESPONSE MEASUREMENTS



- 400 nm thick $Si_{0.72}Ge_{0.28}$
- [B] = 10^{19} cm^{-3}
- -1.5 V bias
- 77K measurement

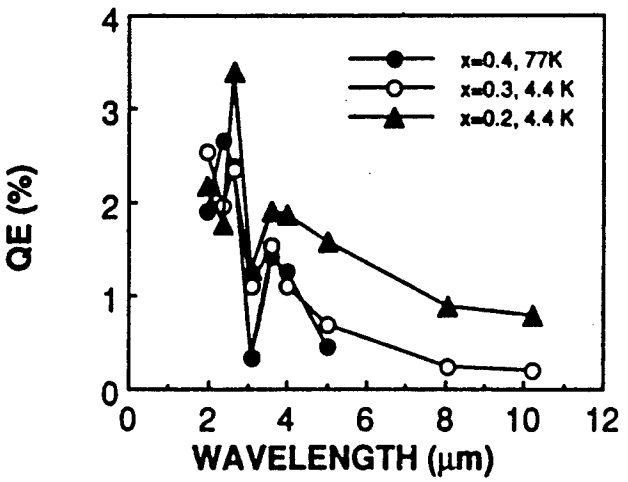
JPL

Optimization of Device Structure



- Two orders of magnitude QE improvement (from 0.003% to 0.3% at 8 μm) by reducing the thickness from 400 to 40 nm, and increasing [B] from 10^{19} to 10^{20} cm^{-3}
- Extended photoresponse as Ef moves further below Ev for degenerately doped p^+-$Si_{1-x}Ge_x$ layers

Tailorable LWIR Cutoff Wavelengths



- 40-nm-thick p^+-$Si_{1-x}Ge_x$ layers
- x = 0.2, 0.3 and 0.4
- [B] = 10^{20} cm^{-3}

- Photoresponse extends to longer wavelengths as Ge ratio x decreases
- QE increases as Ge ratio x decreases
- Demonstrated photoresponse improvement by optimizing the thickness, doping concentration and composition of the $Si_{1-x}Ge_x$ layers

JPL

Discussion

NEΔT: Noise Equivalent Temperature change *NEΔT* (the minimum ΔT required to have S/N=1) is the array figure of merit

- Uniformity-limited NEΔT

$$NE\Delta T_u = 7 \times 10^{-5} T^2 \lambda U$$

NEΔT = 60 mK for U= 0.1%, T= 293 K, and λ= 10 μm

- Single-pixel-limited NEΔT

$$NE\Delta T = \frac{(A\Delta f)^{1/2}}{D^* (dP_B/dT) \sin^2 (\theta/2)}$$

For $D^* = 10^{10}$ cmHz$^{1/2}$/W, NEΔT ≈ 10 mK for 50 μm square pixel, Δf =60 Hz, and f/2 optics.

For NEΔT (pixel) < 60 mK, $D^* > 1.6 \times 10^9$ cmHz$^{1/2}$/W

- Detectivity D* is given by

$$D^* = 0.4 \eta\lambda (qJ_o)^{-0.5}$$

For $Si_{1-x}Ge_x$ /Si HIP detectors with an 11μm cutoff and η = 0.3% at 10 μm operating at 65 K ($J_o = 2 \times 10^{-4}$ Acm^{-2}), $D^* = 2 \times 10^9$ cmHz$^{1/2}$/W

Summary

- A new p^+-$Si_{1-x}Ge_x$/p-Si HIP detector approach has been demonstrated at wavelengths ranging from 2 to 10 μm with > 1% QE's.
- Cutoff is tailorable over a wide LWIR range by varying the Ge ratio x in the $Si_{1-x}Ge_x$ layers.
- Initial improvement of detector performance has been demonstrated by optimizing the thickness, doping concentration and composition of the $Si_{1-x}Ge_x$ layers.
- The potential detector performance ($D^* \sim 2 \times 10^9$ cmHz$^{1/2}$/W, at 65K) allows the fabrication of large LWIR FPA's with uniformity-limited performance (assuming 0.1% uniformity).
- Potential for low cost and producible large focal plane array fabrication with mature silicon processing and our relatively simple device structure.

SESSION VII: Alternate II-VI Detectors

VII-1 MBE HgCdTe Heterostructure Detectors
J.N. Schulman, Hughes Research Laboratories

VII-2 Growth and Properties of Hg-Based Quantum Well Structures and Superlattices
J.F. Schetzina, North Carolina State University

VII-3 HgZnTe-Based Detectors for LWIR NASA Applications
E.A. Patten, Santa Barbara Research Center

N91
14402
UNCLAS

N91-14402

Innovative Long Wavelength Infrared Detector Workshop
Pasadena, April 1990

MBE HgCdTe Heterostructure Detectors

J.N. Schulman and O.K. Wu
Hughes Research Laboratories
3011 Malibu Canyon Road
Malibu, CA 90265

HgCdTe has been the mainstay for medium (3-5μm) and long (10-14μm) wavelength infrared detectors in recent years. Conventional growth and processing techniques are continuing to improve the material. However, the additional ability to tailor composition and placement of doped layers on the tens of angstroms scale using MBE provides the opportunity for new device physics and concepts to be utilized. MBE-based device structures to be discussed here can be grouped into two categories: tailored conventional structures and quantum structures.

The tailored conventional structures are improvements on familiar devices, but make use of the ability to create layers of varying composition and thus band gap at will. The heterostucture junction can be positioned independently of doping p-n junctions. This allows the small band gap region in which the absorption occurs to be separated from a larger band gap region in which the electric field is large and where unwanted tunneling can occur. Data from hybrid MBE/LPE/bulk structures will be shown.

Quantum structures include the HgTe-CdTe superlattice, in which the band gap and transport can be controlled by alternating thin layers (tens of angstroms thick) of HgTe and CdTe. The superlattice has been shown to exhibit behavior which is non-alloy like, including very high hole mobilities, two-dimensional structure in the absorption coefficient, resonant tunneling, and anisotropic transport.

PRECEDING PAGE BLANK NOT FILMED

MBE HgCdTe HETEROSTRUCTURE DETECTORS

J.N. SCHULMAN and O.K. WU

HUGHES RESEARCH LABORATORIES
3011 Malibu Canyon Road
Malibu, CA 90265

HUGHES

QUANTUM / CLASSICAL STRUCTURES

I. Quantum effect structure
Superlattice - New material properties.

A. Layer thickness tailorable band gaps.

B. Enhanced effective masses / reduced tunneling.

C. New physics

1. High hole mobilities

2. 2-D density of states

3. Intrinsic interface states

QUANTUM / CLASSICAL STRUCTURES

II. "Classical Devices"

A. Doping profile control.

B. Composition profile control.

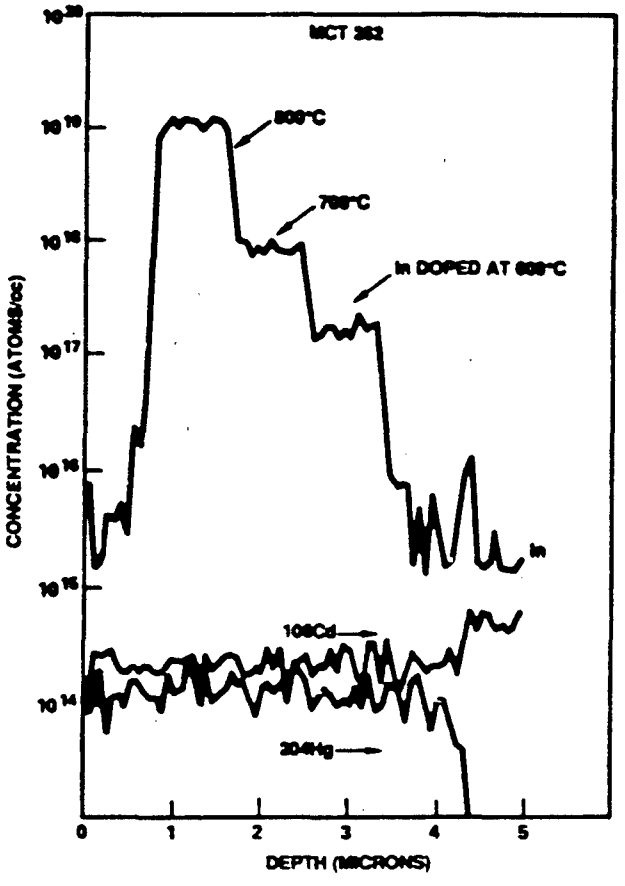
C. Carrier generation / collection regions separated.

D. Hybrid devices - diodes, transistors, signal processing, lasers.

An MBE GROWN MULTILAYER STRUCTURE (In DOPED & UNDOPED)

HUGHES

$Hg_{0.7}Cd_{0.3}Te$ UNDOPED		0.8 μm
$Hg_{0.7}Cd_{0.3}Te$ In DOPED	800°C	0.8 μm
$Hg_{0.7}Cd_{0.3}Te$ In DOPED	700°C	0.8 μm
$Hg_{0.7}Cd_{0.3}Te$ In DOPED	600°C	0.8 μm
$Hg_{0.7}Cd_{0.3}Te$ UNDOPED		0.8 μm
CdTe BUFFER		0.8 μm
CdTe SUBSTRATE		



HUGHES

9023-09-01

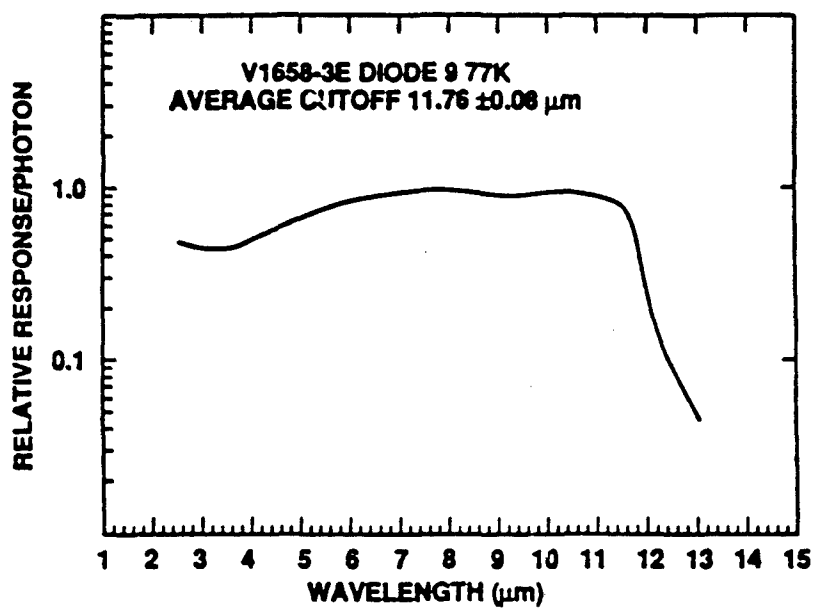
SIMS PROFILE OF AN n TYPE (IN DOPED) MBE GROWN HgCdTe MULTILAYER (5) STRUCTURE

A HYBRID p-on-n HETEROJUNCTION STRUCTURES

$Hg_{0.7}Cd_{0.3}Te$	As DOPED, $5 \times 10^{16}/cm^3$ MBE GROWN, 2 μm
$Hg_{0.8}Cd_{0.2}Te$	In DOPED, $5 \times 10^{14}/cm^3$ BULK GROWN

RELATIVE SPECTRAL RESPONSE OF p-on-n HETEROJUNCTION DIODES

HUGHES



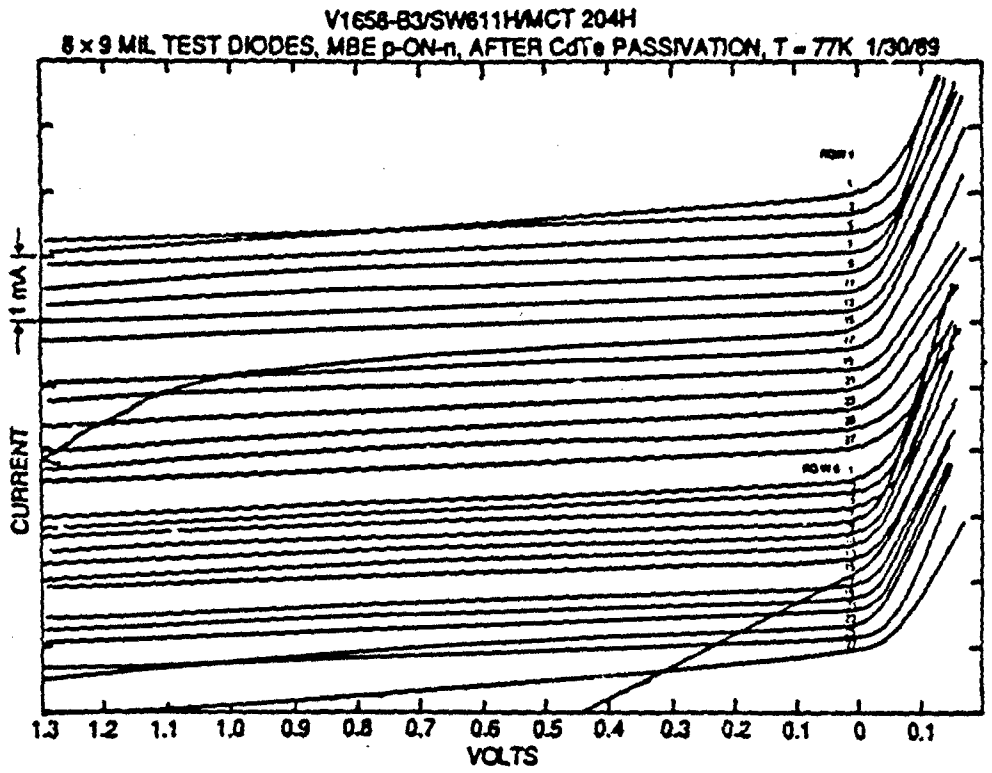
MBE p ON n DLHJ WAFERS

HUGHES

CM

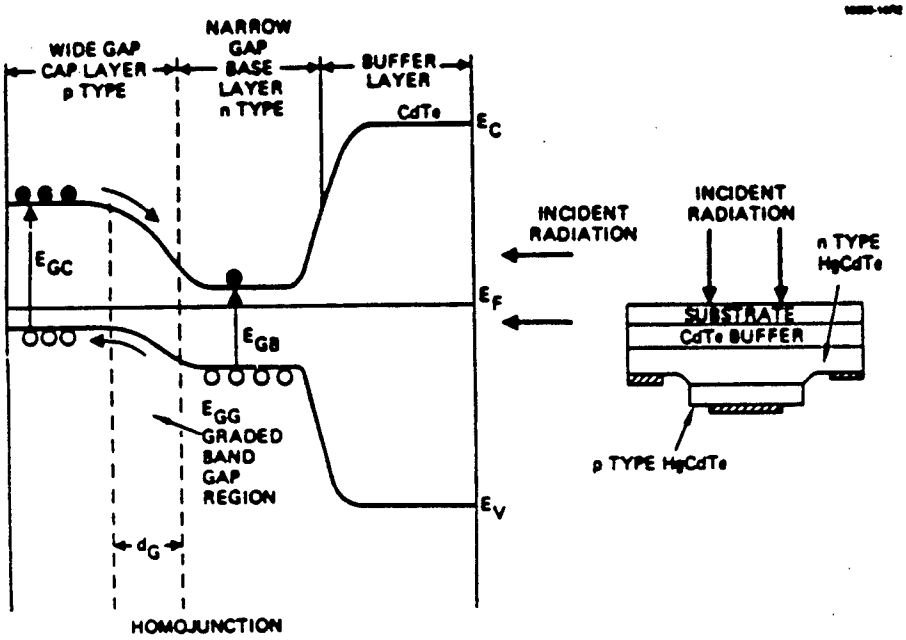
MBE TECHNOLOGY PROVIDES EXCELLENT P+-N HETERO-JUNCTION CHARACTERISTICS

HUGHES



DOUBLE LAYER HETEROJUNCTION STRUCTURE AND ITS BAND DIAGRAM

HUGHES

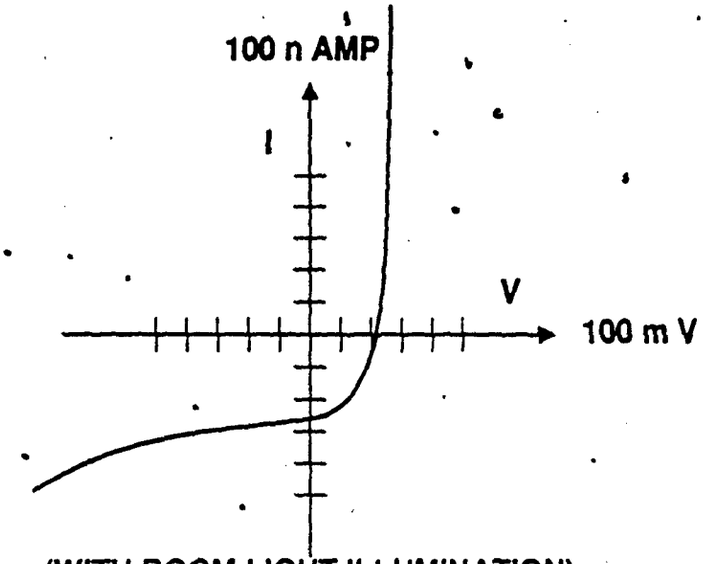


A HYBRID n-on-p HETEROJUNCTION STRUCTURE

HgCdTe	X=0.35, In DOPED, 2 μm MBE GROWN, $5x10^{17}/cm^3$
HgCdTe	X=0.3, As DOPED, 10 μm LPE GROWN, $5x10^{16}/cm^3$
CdTe	SUBSTRATE

I-V CHARACTERISTICS OF A HYBRID n-on-p HETEROJUNCTION DIODE (30 μm x 30 μm)

HUGHES

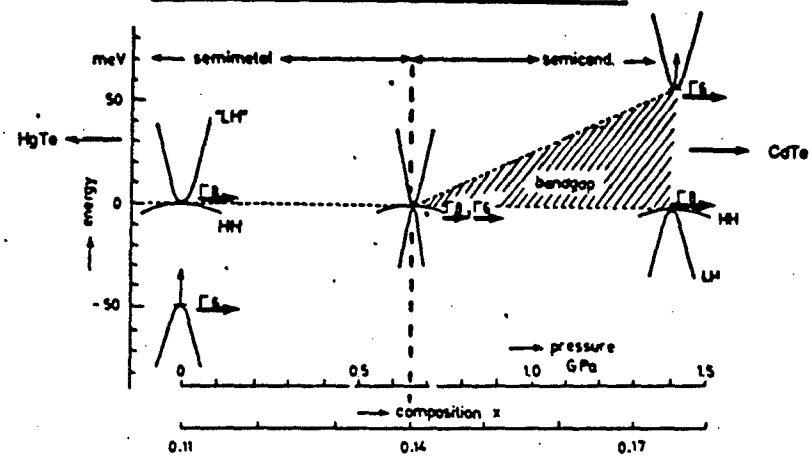


(WITH ROOM LIGHT ILLUMINATION)

An ALL MBE GROWN DOUBLE LAYER HETEROJUNCTION STRUCTURES

HgCdTe (X=0.3) As DOPED 5 x 10^{17} /cm^3, 2 μm
HgCdTe (X=0.2) In DOPED 5 x 10^{15} /cm^3, 8 μm
CdTe BUFFER LAYER
CdTe SUBSTRATE

Hg(1-x)Cd(x) Te Band Gap versus x



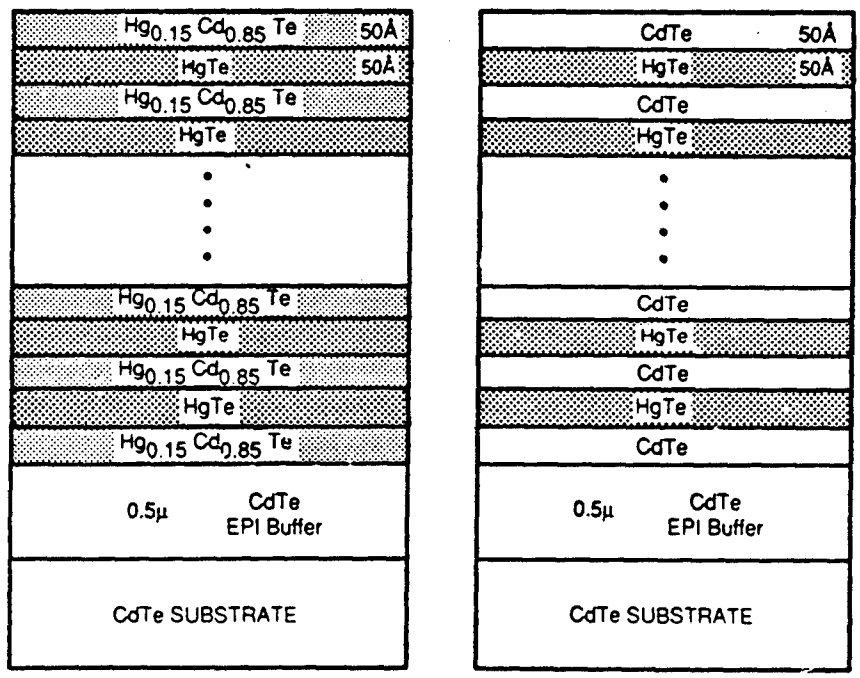
CdTe Band Gap ≈ 1.6 eV

HgTe Band Gap ≈ -0.3 eV

$Hg_{0.15}Cd_{0.85}Te$/HgTe vs HgTe/CdTe SUPERLATTICES

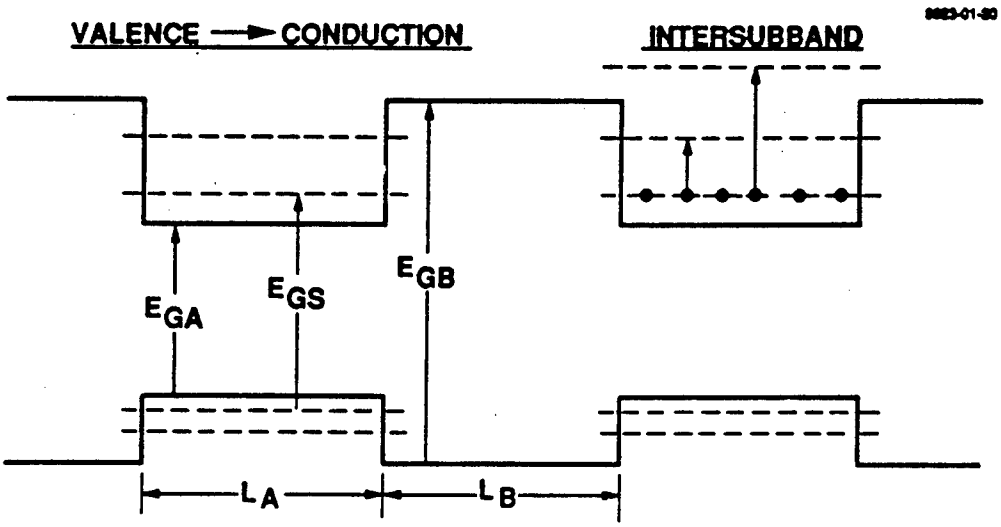
HUGHES

17036-16R2



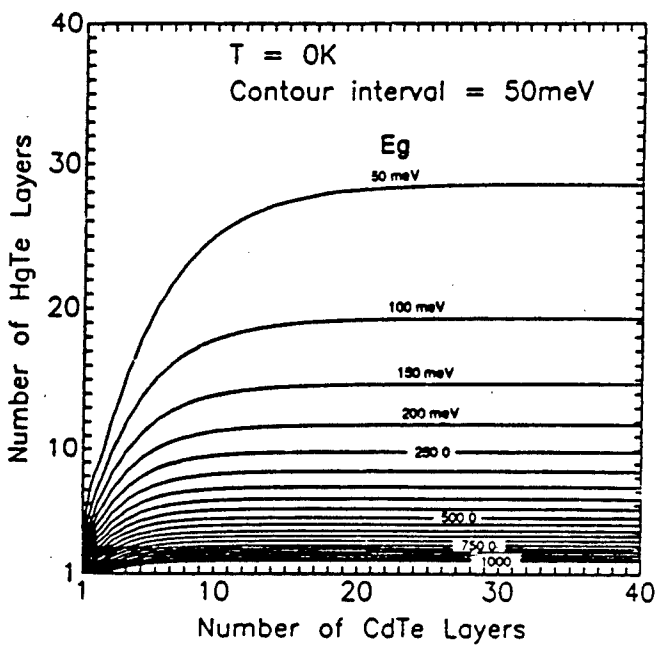
SUPERLATTICE ENERGY LEVELS

HUGHES



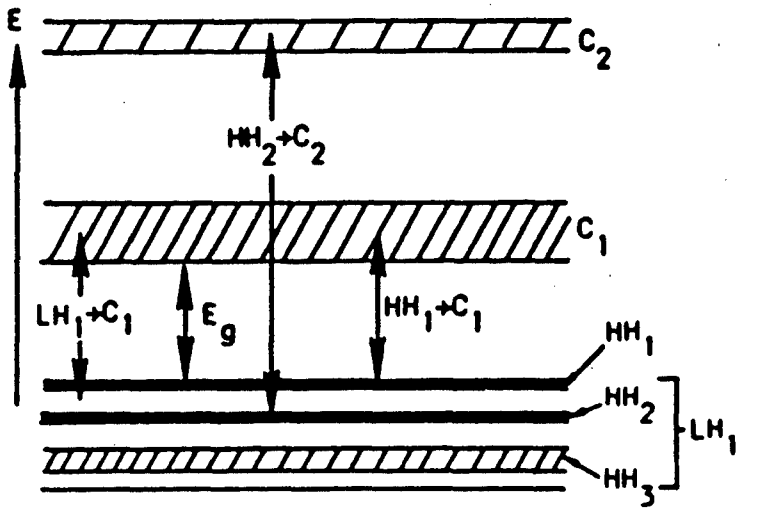
E_{GS} = SUPERLATTICE BAND GAP

HgTe–CdTe SUPERLATTICE BAND GAP



McGill, Wu, Hetzler, J. Vac. Sci. A4, 2091(86)

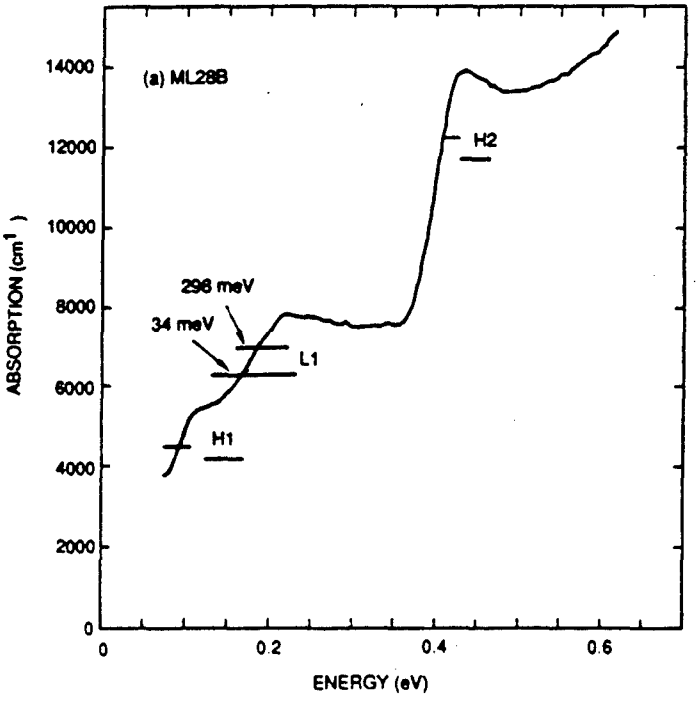
VALENCE TO CONDUCTION SUBBAND ABSORPTION



18246-1R3

HgTe/HgCdTe

Schulman, (+7), APL 53, 2420 (1988)



CONCLUSIONS

I. MBE alloy device-quality composition / doping control available. Much progress for variety of applications soon.

II. Superlattice composition control excellent, doping control in progress. New device structures utilizing new physics needed.

N91
14403
UNCLAS

N91-14403

Growth and Properties of Hg-Based Quantum Well Structures and Superlattices

J.F. Schetzina

Department of Physics, North Carolina State University, Raleigh, NC 27695-8202

An overview of the properties of HgTe-CdTe quantum well structures and superlattices will be presented. These new quantum structures are candidates for use as new LWIR and VLWIR detectors, as well as for other optoelectronic applications. Much as been learned within the past two years about the physics of such structures. The valence band offset has been determined to be ~350 meV, independent of temperature. The occurrence of electron and hole mobilities in excess of 10^5 $cm^2/V{\cdot}s$ is now understood on the basis of SL band structure calculations. The in-plane and out-of-plane electron and hole effective masses have been measured and interpreted theoretically for HgTe-CdTe superlattices. Controlled substitutional doping of superlattices has recently been achieved at NCSU, and modulation-doped SLs have now been succesfully grown and studied. Most recently, a dramatic lowering of the growth temperature of Hg-based quantum well structures and SLs (to~100 C) has been achieved by means of photoassisted MBE at NCSU. A number of new devices have been fabricated from these doped multilayers.

Work supported by NSF grant DMR-88-13525 and NRL contract N00014-89-5-2024.

GROWTH AND PROPERTIES OF Hg-BASED QUANTUM WELL STRUCTURES & SUPERLATTICES

J. F. Schetzina

Department of Physics

North Carolina State University, Raleigh, NC

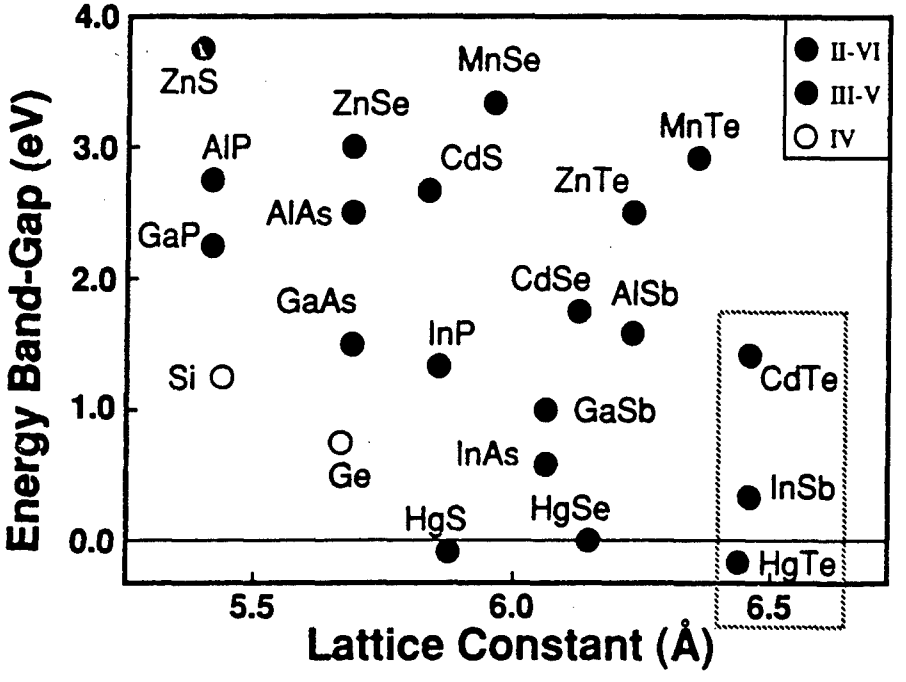
NCSU II-VI SEMICONDUCTOR MBE PROGRAM
Collaborators and Students at NCSU

- Research Associates
  - N.C. Giles
  - S. Hwang
  - Z. Yang
  - J. Yu
- Graduate Students
  - D. Dreifus
  - J. Han
  - Y. Lansari
  - R. Vaudo
  - R. Reed
- Technicians
  - J. Matthews
  - B. Sneed
  - K. Bowers
- Secretary
  - T. Hockenberger
- Undergraduates (4)

OVERVIEW OF PRESENTATION

- **Photoassisted MBE at NCSU**
  - Experimental Procedures
  - Summary of Materials Properties
- **HgTe-CdTe Superlattices**
  - Growth of VLWIR Structures (18 - 22 μm)
  - Controlled Doping Studies
  - Low Temperature Processing at NCSU
- **Applications**
  - Sources & Detectors
  - Amplifiers & Modulators

ENERGY BAND GAP vs LATTICE CONSTANT OF SELECTED SEMICONDUCTORS

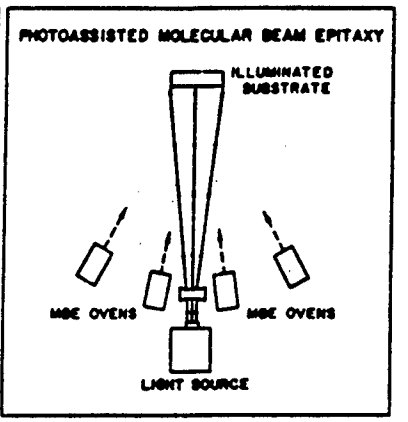


PHOTOASSISTED MOLECULAR BEAM EPITAXY

A New Approach to Controlled Substitutional Doping

R.N. Bicknell, N.C. Giles, and J.F. Schetzina
Appl. Phys. Lett. 49, 1095 (1986)

- A Form of Energy-Assisted Epitaxy
- Growth Temperatures of II-VI Compounds are Low (150 - 350 °C)
- Photons Provide a Source of High Energy, Low Momentum Particles that Bathe the Substrate Surface during Film Growth & Induce Photochemical Reactions
- "Its all done with MIRRORS!!!"



SUBSTITUTIONAL DOPING OF II-VI SEMICONDUCTORS
Major Long-Term Problems

- **Poor Quality Bulk Crystals & Substrates**
- **Large Dislocation Densities**
- **Large Densities of Native Defects**
- **Low Percentage of Dopant Activation**
- **Compensation Effects Often Dominate**
- **Poor Electrical Properties - Low Mobilities**
- **Inferior Optical Properties - Deep Levels**

PHOTOASSISTED MOLECULAR BEAM EPITAXY

Microscopic Mechanisms

- Conversion of Surface Molecules into Atoms
- Photochemical Changes in Atomic Bonding
- Enhancement of Surface Mobility of Atoms
- Photochemical Activation of Dopant Atoms
- Modification of Stoichiometry of Growth Surface

PHOTOASSISTED MOLECULAR BEAM EPITAXY

MBE Film Growth Systems at NCSU

SYSTEMS DESIGNED AND CONSTRUCTED AT NCSU

- Custom Features for II-VI Materials
- Cost Effective

MBE FACILITIES

- Three Hg-Compatible Systems
- One System for Wide Gap II-VIs
- Special Hg Sources (NCSU)
- Two-Zoned Furnaces (NCSU)
- Computer-Controlled Shutters
- Spectra Physics Argon Ion Laser

PHOTOASSISTED MOLECULAR BEAM EPITAXY

WIDE-BAND-GAP & NARROW-BAND-GAP II-VIs

MATERIALS GROWN		PROPERTIES
CdTe:In	CdMnTe:In	• Controlled Doping
CdTe:Sb	CdMnTe:Sb	• High Carrier Mobilities
CdTe:As	HgCdTe	• Narrow Rocking Curves
CdMnTe-CdTe Superlattices		• Bright Photoluminescence
HgTe-CdTe Superlattices		• p-n Junctions Fabricated
Modulation-Doped HgCdTe		• FETs Fabricated

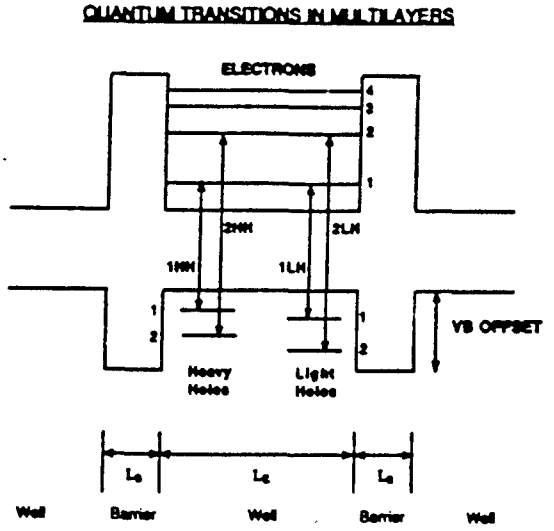
HgTe-CdTe SUPERLATTICES

Growth Parameters

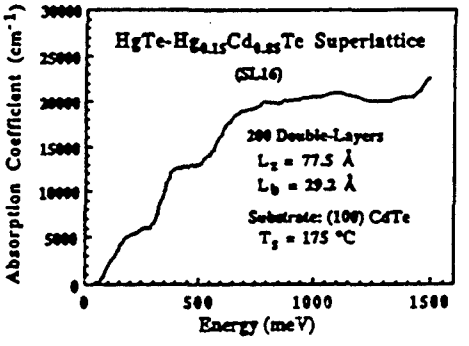
SUBSTRATE:	(100) CdZnTe
SUBSTRATE TEMPERATURE:	150 °C
	140 °C (Photoassisted)
T_{In} :	400-475 °C
T_{As}:	220 °C
Hg FLUX:	1.5 X10^{-4} Torr
DEPOSITION RATE:	1-3 Å/sec
LAYER THICKNESSES:	
HgTe	32-160 Å
CdTe	26-102 Å

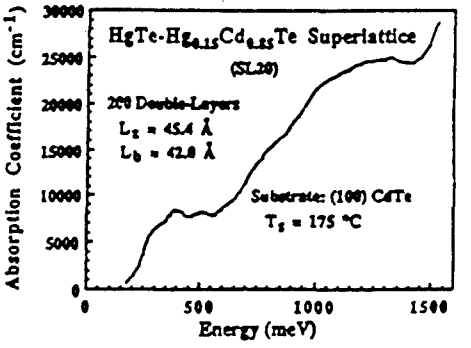
Hg Te-CdTe SUPERLATTICES

Designation of Electronic Transitions



Optical Properties

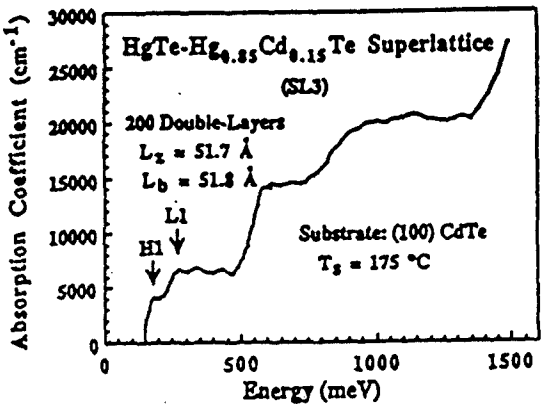


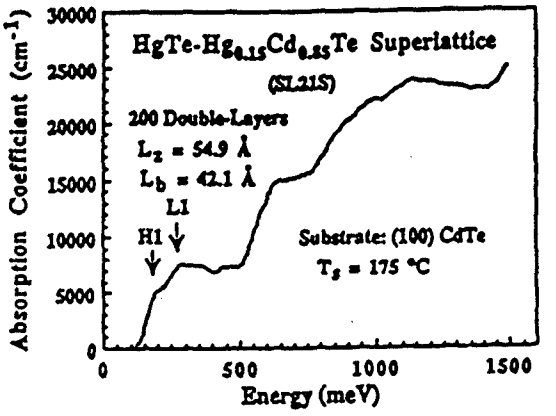


ORIGINAL PAGE IS
OF POOR QUALITY

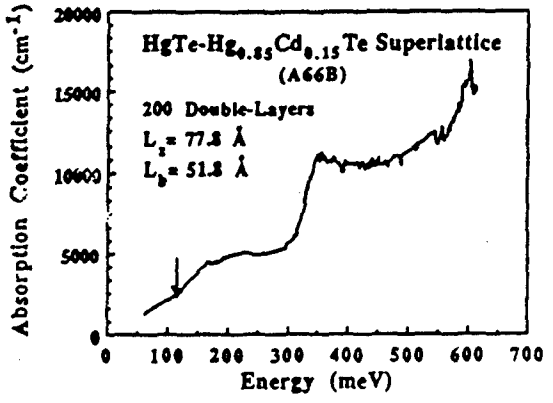
HgTe-CdTe SUPERLATTICES

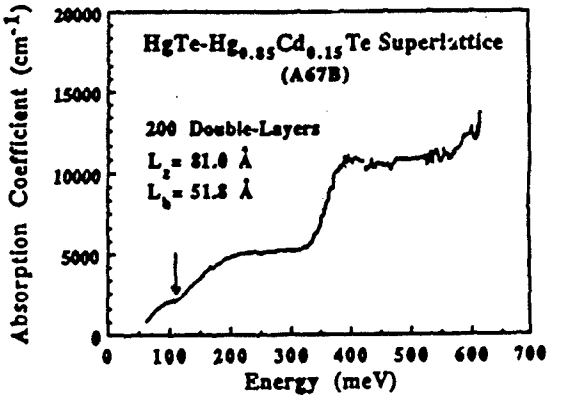
Optical Properties





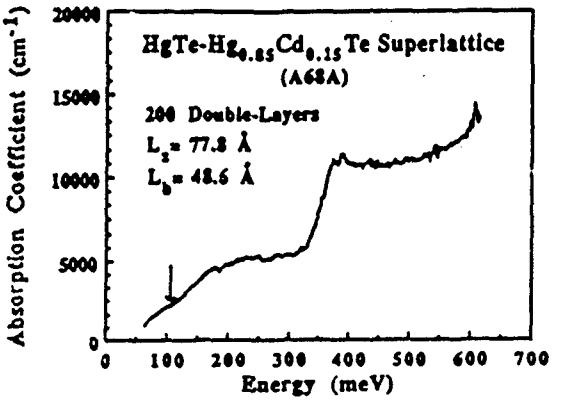
Optical Properties: VLWIR Structures

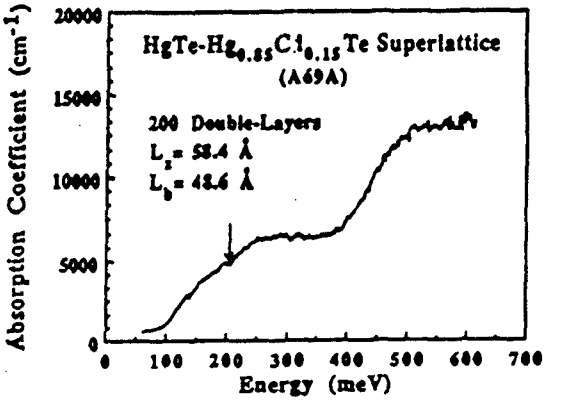


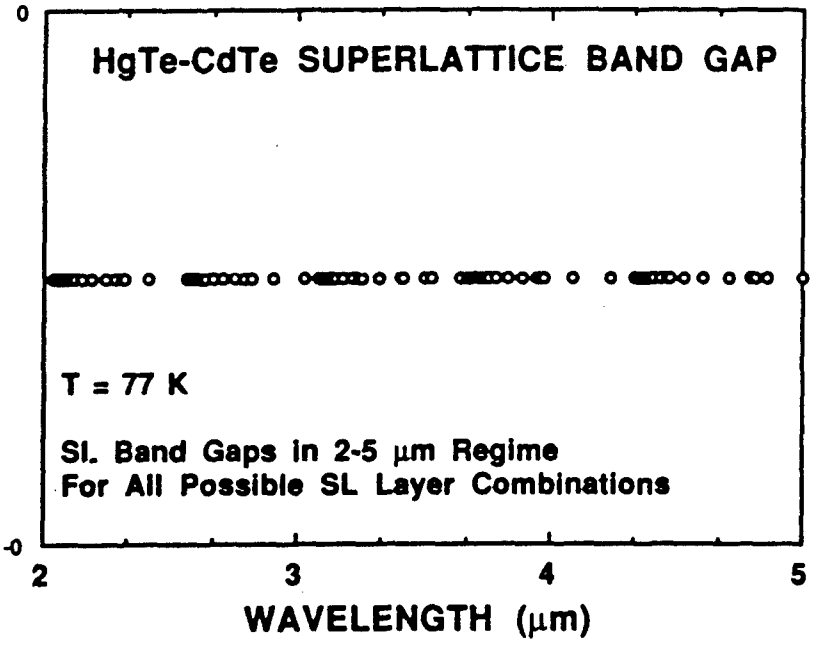


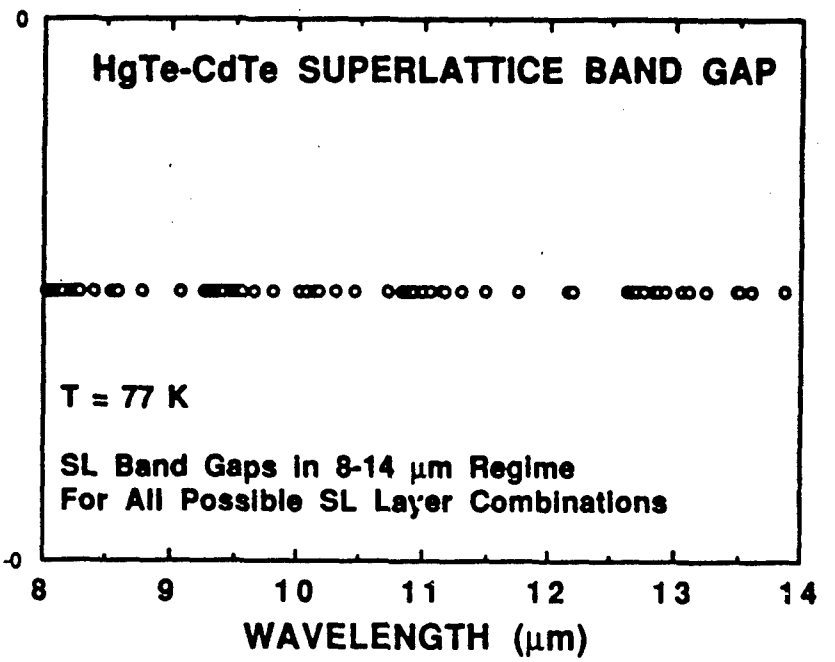
HgTe-CdTe SUPERLATTICES

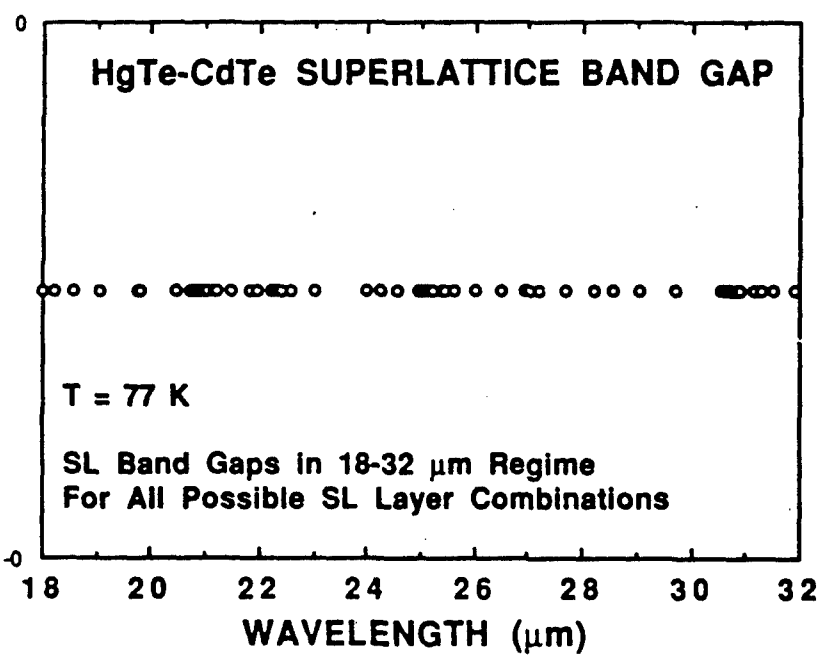
Optical Properties: VLWIR Structures

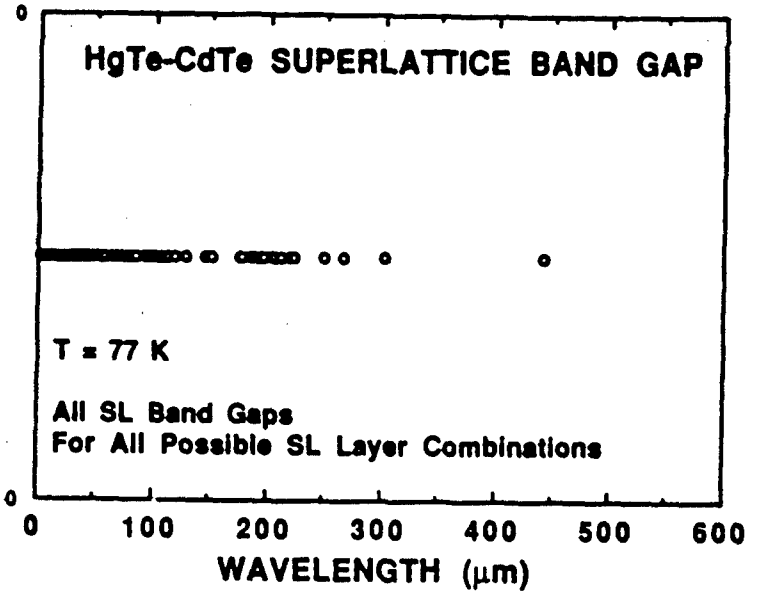




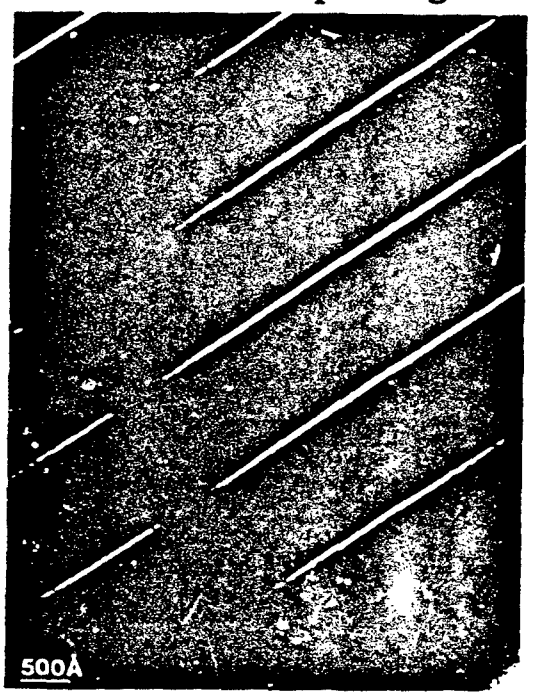



HgTe-CdTe SUPERLATTICE BAND GAP
T = 77 K
SL Band Gaps in 8-14 μm Regime
For All Possible SL Layer Combinations
0
-0
8
9
10
11
12
13
14
WAVELENGTH (μm)


HgTe-CdTe SUPERLATTICE BAND GAP
T = 77 K
SL Band Gaps in 18-32 μm Regime
For All Possible SL Layer Combinations
0
-0
18
20
22
24
26
28
30
32
WAVELENGTH (μm)



Vertical Cross-Section TEM Photo
of Modulation Doped HgCdTe

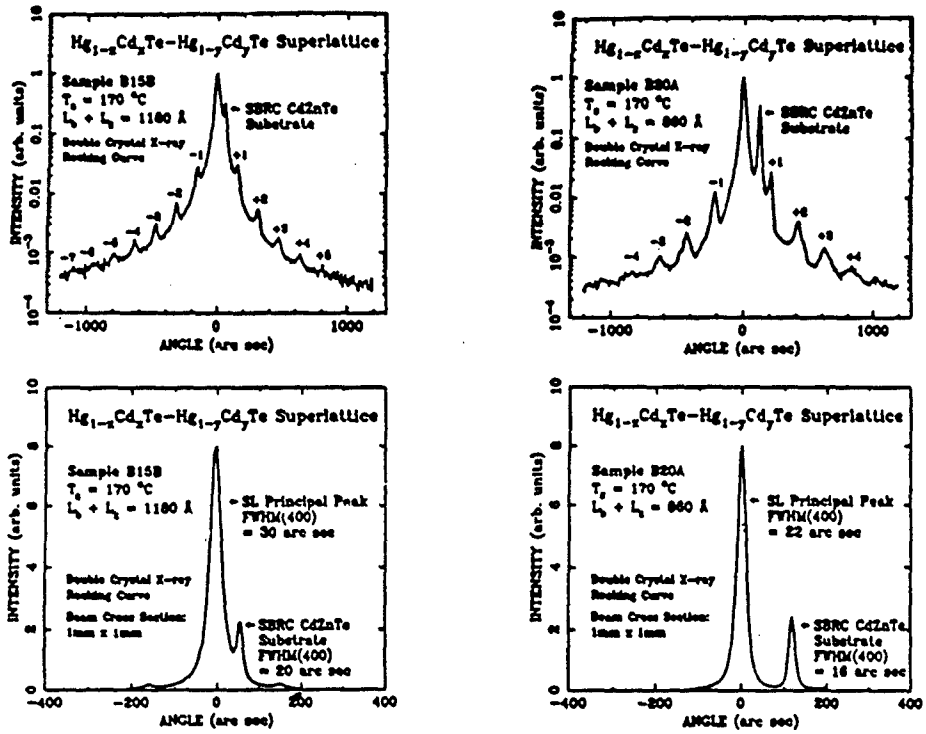


N. Otsuka, Purdue University

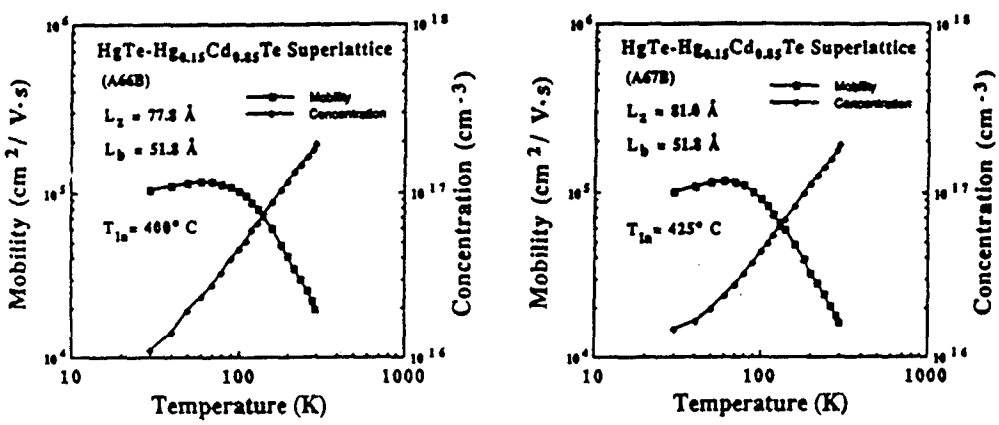
ORIGINAL PAGE IS
OF POOR QUALITY

HgTe-CdTe SUPERLATTICES

Structural Properties: X-Ray Diffraction

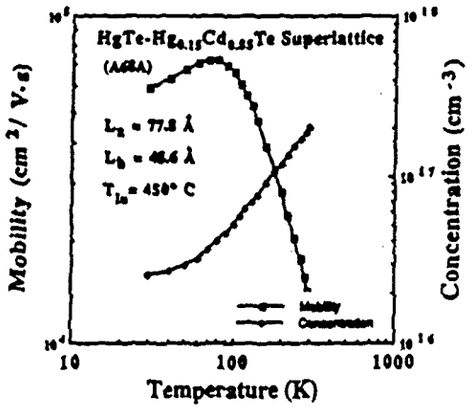


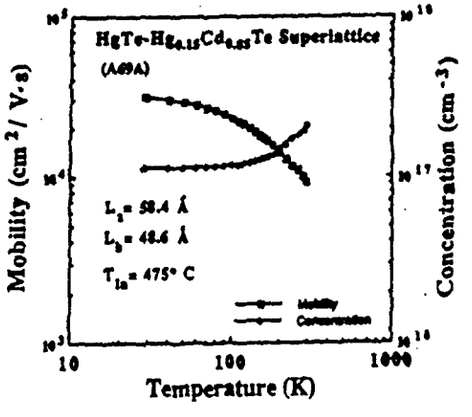
Substitutional Doping: n-Type (Indium)



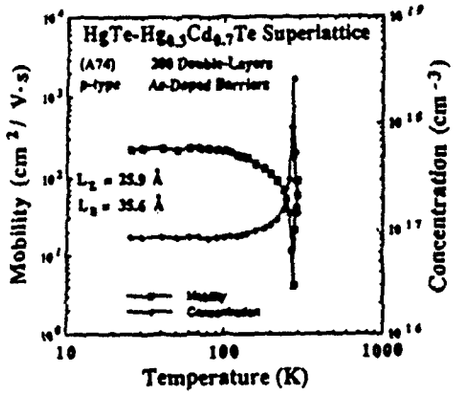
HgTe-CdTe SUPERLATTICES

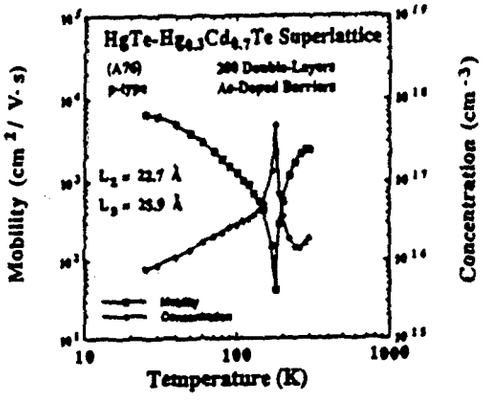
Substitutional Doping: n-Type (Indium)





Substitutional Doping: p-Type (Arsenic)

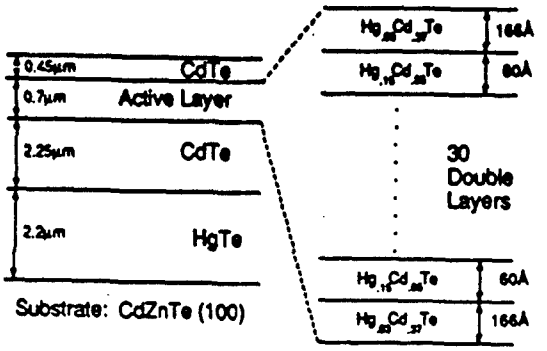


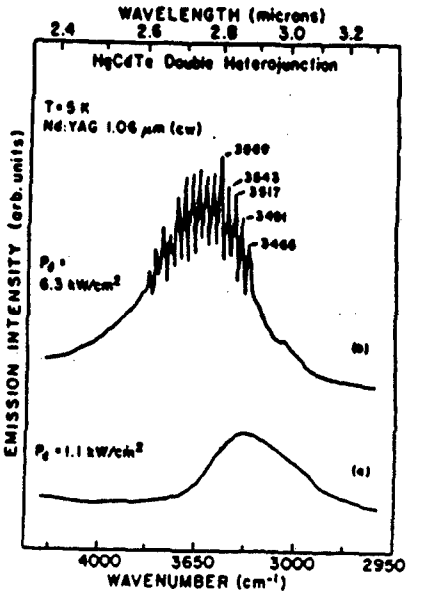


HgCdTe-CdTe SUPERLATTICES

Stimulated Emission

HgCdTe Double Heterojunction

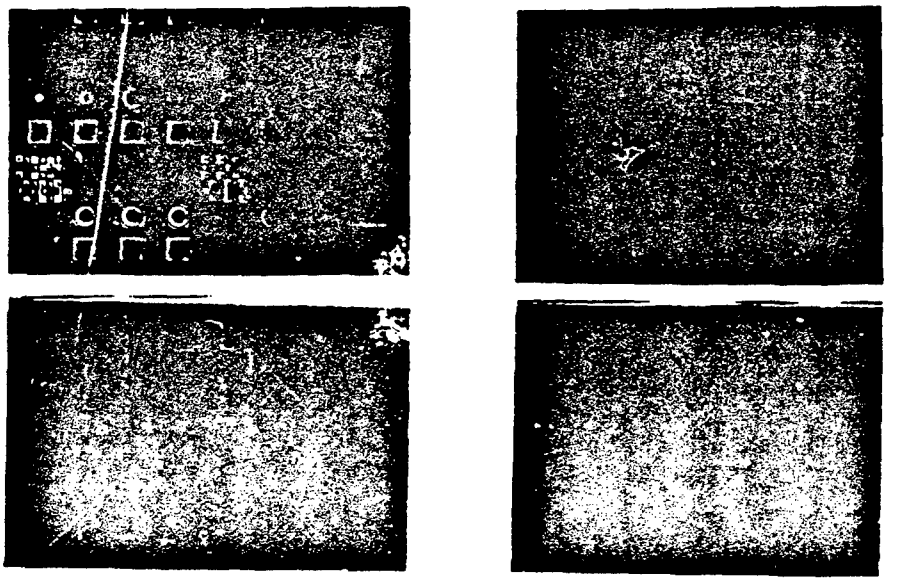




DARPA

Selective-Area Epitaxy of HgTe-CdTe Superlattices

NCSU



ORIGINAL PAGE IS
OF POOR QUALITY

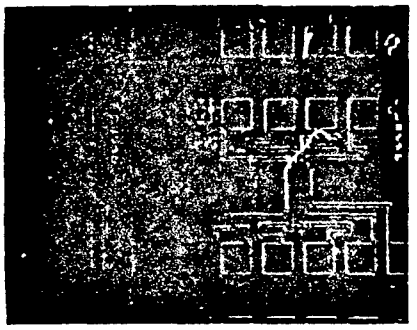
DARPA

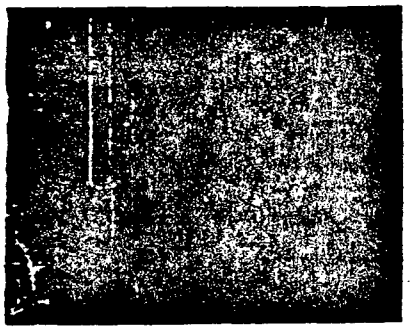
Selective-Area Epitaxy of HgTe-CdTe Superlattices

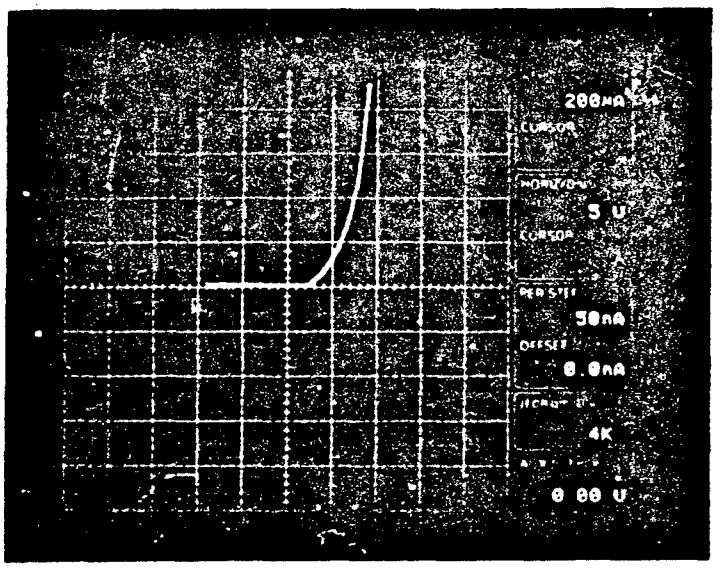
NCSU

Growth Parameters: CdZnTe Substrates, Ts = 150 °C

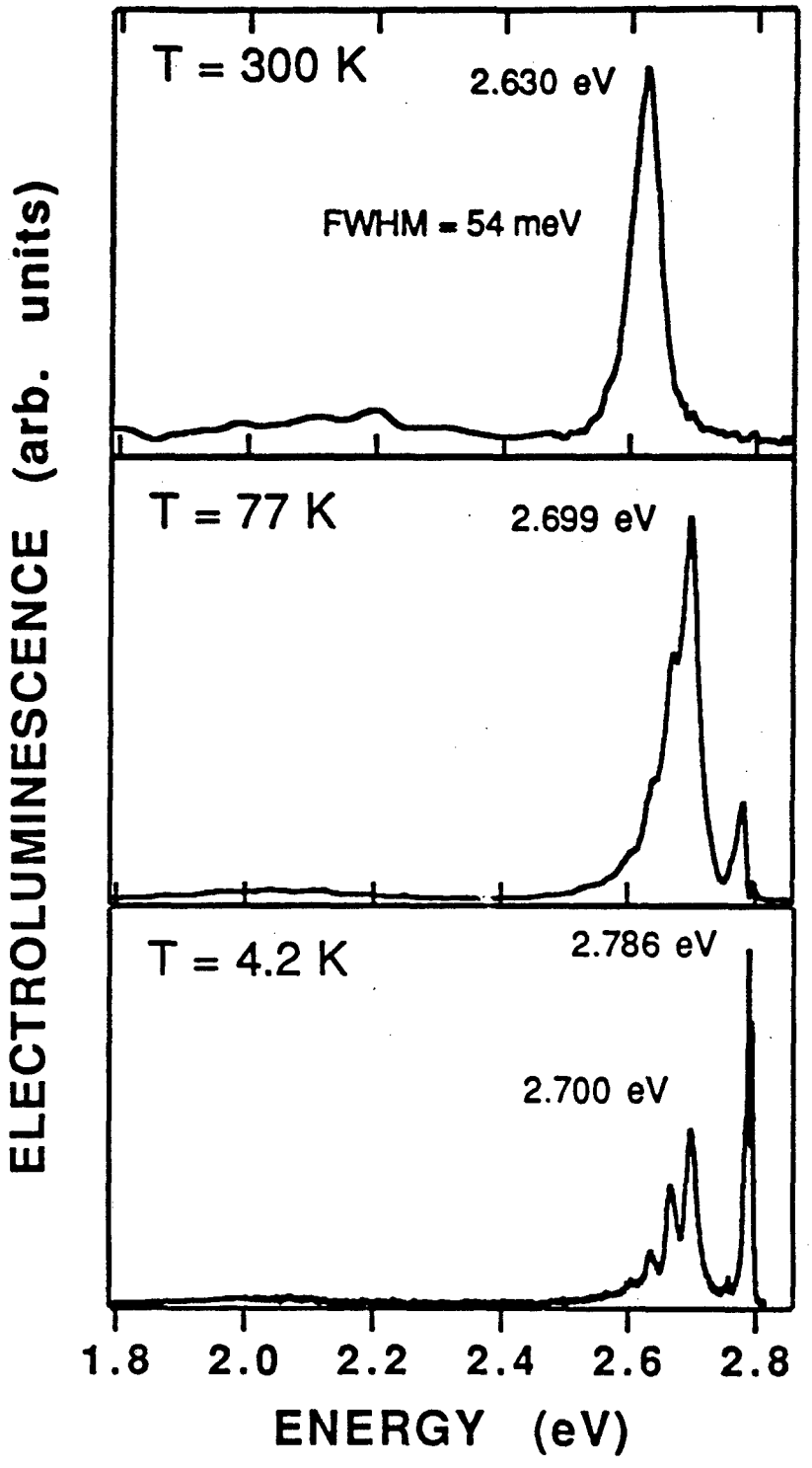
Applications: Multicolored Sources and/or Detectors; Optical Waveguides; Light Modulators

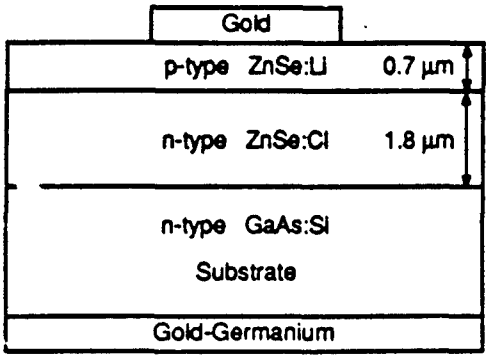


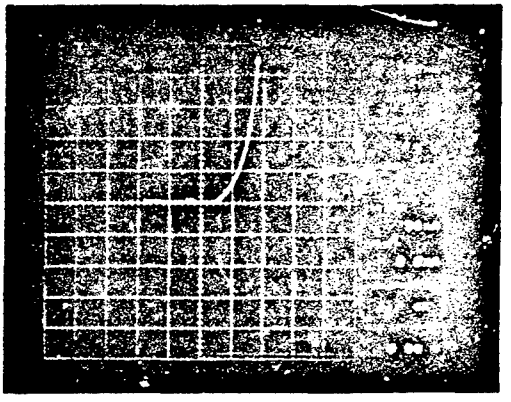




ORIGINAL PAGE IS
OF POOR QUALITY


T = 300 K
2.630 eV
FWHM = 54 meV
T = 77 K
2.699 eV
T = 4.2 K
2.786 eV
2.700 eV
ELECTROLUMINESCENCE (arb. units)
1.8
2.0
2.2
2.4
2.6
2.8
ENERGY (eV)





HgTe-CdTe SUPERLATTICES

Summary of Properties

- AN INTERESTING INFRARED QUANTUM STRUCTURE
- SUPERLATTICE HAS MANY DIFFERENT STATES WHICH EXHIBIT VERY DIFFERENT PROPERTIES
- A VARIABLE BAND GAP STRUCTURE AS PREDICTED
- EXHIBITS LARGE ABSORPTION IN INFRARED REGION
- EXCELLENT ELECTRICAL PROPERTIES
- EXCELLENT STRUCTURAL PROPERTIES
- SHORT MINORITY CARRIER LIFETIMES (10 - 20 ns)
- DETECTOR APPLICATIONS: VLWIR REGION (18 - 24 µm)

ORIGINAL PAGE IS
OF POOR QUALITY

N91
14404
UNCLAS

N91-14404

HgZnTe-based Detectors for LWIR NASA Applications

Elizabeth A. Patten and Murray H. Kalisher
Santa Barbara Research Center, Santa Barbara, CA.

HgZnTe has become of growing interest in recent years for IR detector applications because of the promise of equivalent performance but with greater producibility and reliability than HgCdTe-based detectors. The substitution of Zn for Cd in a dilute alloy with HgTe was predicted by Arden Sher et al (J. Vac. Sci. Technol. A 3(1), Jan/Feb 1985, pp. 105-111) to give a material with greater mechanical hardness along with other advantageous properties for IR detectors. Over the past four years, our group and others have grown and characterized HgZnTe and shown that it indeed has increased microhardness, lower Hg diffusion rates and equivalent crystal quality, electrical and optical properties as compared with HgCdTe. Other advantageous properties including higher Hg vacancy formation energies, sharper exciton line, and reduced Te antisite formation have been predicted and/or measured. Triboulet and coworkers in France have fabricated diodes from bulk-grown HgZnTe and have seen greater bake stability for these devices as compared with their HgCdTe diodes. We report here today on test results on our first lot of VLWIR HgZnTe photoconductors using the HIT approach developed for HgCdTe.

Our initial goal on this program was to grow and characterize HgZnTe and determine if it indeed had the advantageous properties that were predicted. We grew both bulk and liquid phase epitaxial HgZnTe and collaborating with SRI and Stanford we determined that HgZnTe had the following properties: 1) microhardness at least 50% greater than HgCdTe of equivalent bandgap, 2) Hg annealing rates of at least 2 - 4 times longer than HgCdTe, and 3) higher Hg vacancy formation energies. This early work did not focus on one specific composition (x-value) of HgZnTe since NASA was interested in HgZnTe's potential for a variety of applications. Since the beginning of 1989, we have been concentrating, however, on the liquid phase growth of VLWIR HgZnTe (cutoff ~ 17 μm at 65K) to address the requirements of the Earth Observing System (Eos).

Since there are no device models to predict the advantages in reliability one can gain with increased microhardness, surface stability, etc., one must fabricate HgZnTe detectors and assess their relative bake stability (accelerated life test behavior) as compared with HgCdTe devices fabricated in the same manner. Fabrication of HgZnTe devices only became feasible for us in 1989 as we were able to reduce Te melt retention on the surface of our layers and obtain a reasonable yield of device quality layers. We have chosen to fabricate HIT detectors as a development vehicle for this program because high performance in the VLWIR has been demonstrated with HgCdTe HIT detectors and the HgCdTe HIT process should be applicable to HgZnTe. HIT detectors have a significant advantage for satellite applications since these devices dissipate much less power than conventional photoconductors to achieve the same responsivity.

PRECEDING PAGE BLANK NOT FILMED

Our first lot of HgZnTe HIT photoconductors exhibit high performance with cutoffs greater than 18 μm. We have performed initial radiometric testing at 30K and 80K and have achieved peak D* of 6×10^{10} cm√Hz/W at 30K which is within a factor of two of BLIP for the background level used (3×10^{16} ph/cm^2/sec). Peak responsivites at 80K of 3×10^4 V/W have been measured which are comparable with those typically seen for conventional HgCdTe photoconductors. These results are very exciting especially in view of the fact that this is our first lot of HgZnTe devices. Parameters of the starting material which may have limited performance of this first lot will be discussed. Also to be discussed are our plans to continue this year to refine the material parameters (thickness, cutoff, etc.) to achieve higher performance with our second lot to be processed in June.

HgZnTe-Based Detectors for LWIR NASA Applications

Elizabeth A. Patten and Murray H. Kalisher

Innovative LWIR Detector Workshop
April 25, 1990

Sponsored by NASA/Langley (W. E. Miller, Technical Monitor)

HUGHES
SANTA BARBARA RESEARCH CENTER
a subsidiary

Outline

HUGHES
SANTA BARBARA RESEARCH CENTER
a subsidiary

- Why HgZnTe?
- Early Program Results
- 1989 Materials Improvements
- First HgZnTe PC Results

HgZnTe Offers Many Potential Advantages for LWIR Applications

HUGHES
SANTA BARBARA RESEARCH CENTER
a subsidiary

- HgZnTe offers same performance as HgCdTe but potentially with:
  - Greater stability against thermal and mechanical degradation
    - Short ZnTe bond
- Specific advantages predicted and/or measured:
  - HgZnTe mechanically harder (at least 50% for same bandgap)
    - Lattice matches to tougher substrate (20% CdZnTe)
  - Slower Hg diffusion (annealing data)
  - Larger Hg vacancy formation energies predicted
  - Greater bake stability of HgZnTe diodes (French data)
  - Concentration fluctuations suppressed - large binary lattice mismatch
    - Measured uniformity greater for THM HgZnTe vs HgCdTe
    - Exciton line is very sharp
  - Higher m^* for same bandgap (15% for .1 eV)

EARLY PROGRAM RESULTS

NASA Has Funded HgZnTe At SBRC Since 1986

HUGHES
SANTA BARBARA RESEARCH CENTER
a subsidiary

- NASA's main concern is device stability in satellite FPAs
- Began as coordinated program with SRI, Stanford:
  - SRI: Theory
  - Stanford: Hardness, Diffusion Measurements
  - SBRC:
    - Bulk HgZnTe Growth (SSR & ZM)
    - Bulk CdZnTe Growth (20% Zn for lattice matched substrates)
    - HLPE HgZnTe
    - Phase Diagram - Liquidus Measurements
    - Materials Characterization/Device Science
- Current goal is development for VLWIR EOS applications
  - 17 μm at ≥ 65 K
- Other HgZnTe work in France, Israel, Poland, Pittsburgh

Growth of HgZnTe is Difficult

HUGHES
SANTA BARBARA RESEARCH CENTER
a subsidiary

- Initial goals to see if HgZnTe could be grown and had promised properties
- Issues concerning HgZnTe growth:
  - Low Zn solubility in Hg or Te-rich melt - much lower than Cd
    - Lowest in Hg melt
    - Same issues with Te-melt growth as for HCT (melt retention)
  - High segregation coefficient of Zn in Te-rich melt
    - 3.5 times that of Cd
    - Tends to increase layer grading
  - HgTe-ZnTe lattice mismatch large - 6% vs 0.3% for HgTe-CdTe
- Both bulk and epitaxial HgZnTe were goals for the program

All Early Program Goals Met

HUGHES
SANTA BARBARA RESEARCH CENTER
a subsidiary

- Early focus of program on material issues
  - Can we grow HgZnTe?
  - Does it have predicted advantageous properties?
- In first year of program, growth goals achieved:
  - Successful bulk growth of HgZnTe (x = 0.16) of high quality - required for structural characterization
    - Mechanical hardness
    - Photoemission
  - Successful bulk growth of $Cd_{.8}Zn_{.2}Te$ with high crystal quality - required for lattice-matched substrates
  - Successful growth of HLPE HgZnTe ($.11 \leq x \leq .24$)
    - Good compositional uniformity/crystal quality

Many HLPE HgZnTe Properties Similar to LPE HgCdTe

HUGHES
SANTA BARBARA RESEARCH CENTER
a subsidiary

- In first year, demonstrated that compared with LPE HgCdTe, HLPE HgZnTe has comparable:
  - Crystal quality
  - Vertical and lateral compositional uniformity
  - Low impurity densities (in annealed wafers)
- Experimentally and theoretically showed that HLPE HgZnTe has:
  - Comparable carrier lifetime with good lateral uniformity
  - Comparable electron mobility (μ) and predicted factor of two smaller hole μ
- Valence band offest measured in bulk HgZnTe by photoemission
  - Smaller than in HgCdTe (≈ 200 meV vs 350 meV)

First Year Work Shows Advantages of HgZnTe

HUGHES
SANTA BARBARA RESEARCH CENTER
a subsidiary

- Both bulk and epitaxial HgZnTe found at least 50% harder than same E_g HgCdTe
  - Knoop microhardness measurements, nanoindenter
- Hg in-diffusion rate at least 2 - 4 times slower for HgCdTe
  - Annealing experiments
- Larger Hg vacancy formation energies predicted
  - HgZnTe should be more stable against Hg loss
- Larger electron m* predicted
  - Reduced tunneling

HARDENING OF ALLOY DUE TO Zn DEMONSTRATED BY MICROHARDNESS MEASUREMENTS

HUGHES
SANTA BARBARA RESEARCH CENTER
a subsidiary

MATERIAL	KHN	OTHER MATERIALS	KHN
$Hg_{0.80}Zn_{0.10}Te$	45.9	$Cd_{0.80}Zn_{0.20}Te$	78.5
$Hg_{0.90}Zn_{0.10}Te$	38.9	$Cd_{0.96}Zn_{0.04}Te$	46.3
$Hg_{0.80}Cd_{0.20}Te$	31.6	CdTe	36.1

KHN = KNOOP HARDNESS NUMBER

- **THEORETICAL FOUNDATION — SRI**
  - HARDNESS DETERMINED BY ENERGY REQUIRED TO FORM PAIRS OF DISLOCATIONS, E_{PD}
    - $E_{PD} \sim 1/d^{10} \sim d$ = CATION-ANION BOND LENGTH
  - $d_{ZnTe}/d_{CdTe} \simeq 0.94$ ($d_{HgTe}/d_{CdTe} \simeq 1$)
  - SMALLER ZnTe BOND LENGTH INHIBITS DISLOCATION FORMATION AND PROPAGATION

Concentration Fluctuations Probably Suppressed in HgZnTe

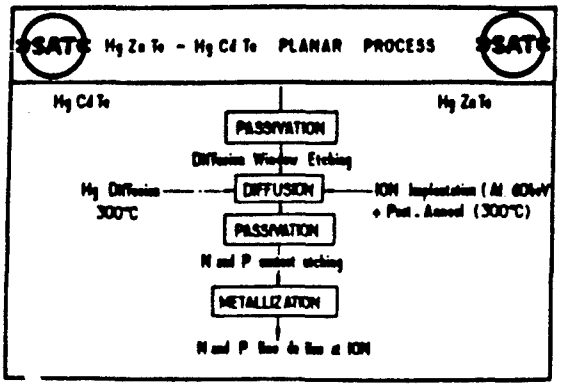
HUGHES
SANTA BARBARA RESEARCH CENTER
a subsidiary

- Large lattice mismatch between HgTe and ZnTe favors uniform composition
  - Negligible mismatch between HgTe and CdTe
- Evidence of greater compositional uniformity in HgZnTe exists (Triboulet):
  - THM ingot uniformity
  - Sharpness of exciton line
  - Excellent diode cutoff uniformity
- Greater compositional uniformity offsets larger dE_g/dx in HgZnTe
  - Bowing in E_g vs x also reduces dE_g/dx at long wavelengths:
    - dE_g/dx = 2.1 eV for HgZnTe ;
      = 1.9 eV for HgCdTe
      (at E_g = 0.1 eV or 12.4 μm)

SAT in France Has Produced LWIR HgZnTe Diodes

HUGHES
SANTA BARBARA RESEARCH CENTER
a subsidiary

- SAT achieved comparable diode performance to HgCdTe with bulk HgZnTe and modified SAT process:
  - 14.35 μm performance was achieved with implanted HgZnTe



French Data Implies Greater HgZnTe Diode Bake Stability

HUGHES
SANTA BARBARA RESEARCH CENTER
a subsidiary

- Maximum temperature of vacuum bake before degradation is higher for HZT
- Evaluation of bake data requires details of separate processes for HCT and HZT

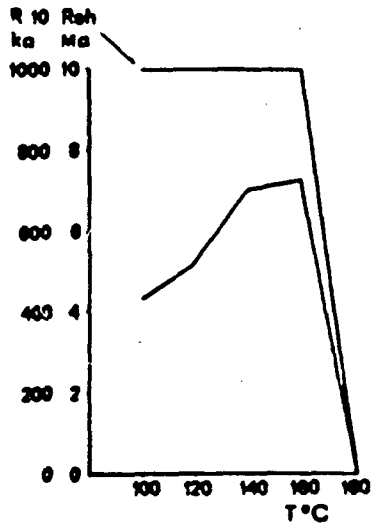


Figure 3. Variation of the shunt (Rsh) and R(- 10 mV) resistances during the thermal test under vacuum.

These performances of MIT are comparable to those of their MCT counterparts.

Over eight hundred elements have been submitted to thermal test to assess their reliability, under the following conditions of vacuum heating :

(100°, 96 h) + (120°, 96 h) + (140°, 96 h) + (160°, 96 h) + (180°, 96 h).

The great majority of the diodes display results as in figure 3. The shunt resistances are limited to 10 MΩ because of the precision of the measurements under automatic points. R (- 10 mV) increases during the first stages of heating before falling, together with Rsh, after the last heating at 180°C. These results express well a very significant improvement in stability compared to MCT diodes of the same cut-off wavelength.

6. CONCLUSIONS

This study demonstrates clearly that the fundamental advantages predicted for MIT over MCT are now confirmed by many relevant experimental results. The reliability of the photodiodes together with their high performances make new MIT the successor designate of MCT for IR detection. The ready ability for MIT to be processed in existing MCT manufacturing facilities can be also considered to be a determining advantage.

Spie Vol. 1106 (1989)

ORIGINAL PAGE IS
OF POOR QUALITY

RECENT PROGRESS

HUGHES
SANTA BARBARA RESEARCH CENTER
a subsidiary

1989 Goal to Achieve/Process Device Quality VLWIR HgZnTe

HUGHES
SANTA BARBARA RESEARCH CENTER
a subsidiary

- Focused on obtaining device quality VLWIR HgZnTe in 1989
  - Shifted to VLWIR ($\lambda_{co} \geq 16\ \mu m$ @ 80K) from LWIR
- Goals were to routinely achieve:
  - Good surface morphology - reduce melt retention
  - Desired electrial properties
  - High optical transmission below gap
  - Good carrier lifetimes
  - Cutoff, thickness in desired range
- Device goal was to process/test one lot of HgZnTe Common Module
- Use Trapping Mode approach demonstrated for VLWIR HCT

CURRENT GROWTH PARAMETERS

HUGHES
SANTA BARBARA RESEARCH CENTER
a subsidiary

- GROWTH TECHNIQUE: Te MELT LPE, HORIZONTAL SLIDER
- TEMPERATURE RANGE: 462 - 455° C
- MELT COMPOSITION: 14 g Te, .07 g ZnTe, SEPARATE Hg SOURCE
- COOLING RATE: 0.1° C / MINUTE
- SUBSTRATES: CdTe, $Cd_{.96}Zn_{.04}Te$, $Cd_{.80}Zn_{.20}Te$ (NOMINAL)
- SIZE: 1 X 1 INCH
- X-VALUE RANGE: X = .12 - .18

HgZnTe LPE Growth Improved Dramatically in 1989

HUGHES
SANTA BARBARA RESEARCH CENTER
a subsidiary

- Layer Yield Historically Lowered by:
  - Te Melt Retention
  - Strong Composition/Thickness Dependence on Temperature
    - High Zn Segregation
- Sources of Recent Improvement (VLWIR HgZnTe, x = 0.14):
  - Reduced O_2 Contamination
  - Substrate Screening
  - Use of Lower Zn% Substrates
  - Improved Temperature Control

HgZnTe PC Lot 1 Testing

HUGHES
SANTA BARBARA RESEARCH CENTER
a subsidiary

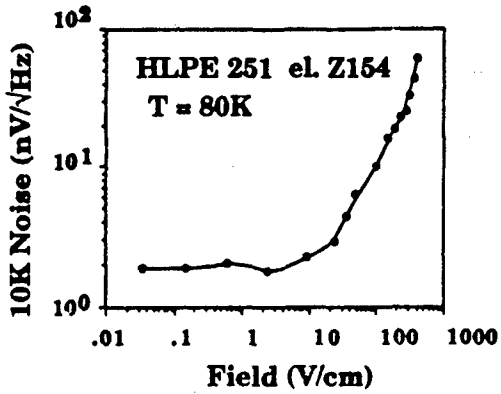
HgZnTe PC Lot 1 Testing Overview

HUGHES
SANTA BARBARA RESEARCH CENTER
a subsidiary

- Several wafers tested at both 80K and 30K with:
  - 800K blackbody, 30° FOV
  - Background Flux = 3×10^{16} photon/cm^2 /sec
- 80K results:
  - Blackbody D* = 5×10^{9} cm√Hz/W
  - Spectral measurements indicate cutoffs as great as 19 μm
- 30K results
  - Blackbody D* = 3×10^{10} cm√Hz/W
  - Peak D* = 6×10^{10} cm√Hz/W (BLIP D* = 1.2×10^{11} cm√Hz/W)
- Initial results show cutoffs are longer than desired

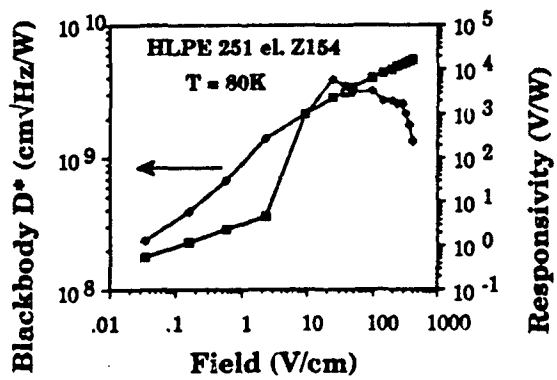
80K Noise Increases as Expected at High Bias

HUGHES
SANTA BARBARA RESEARCH CENTER
a subsidiary



D* at 80K Limited by Noise from Long Cutoff

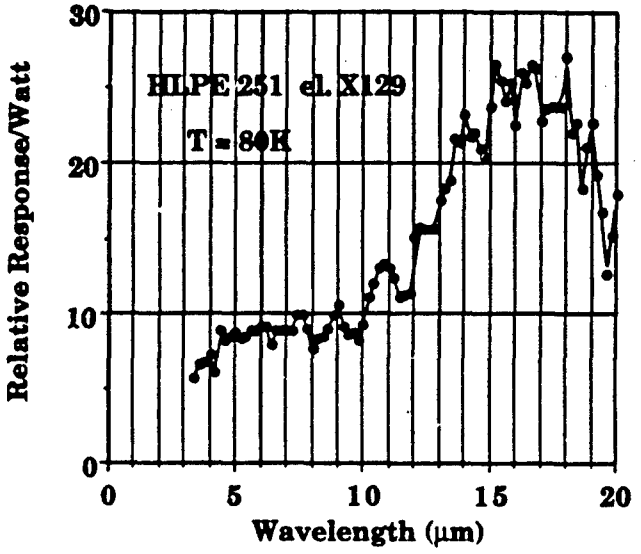
HUGHES
SANTA BARBARA RESEARCH CENTER
a subsidiary



- 80K Blackbody D* ≈ 5 x 10 ^{9} cm√Hz/W

Spectral Cutoffs of 19 μm at 80K Measured for HgZnTe PCs

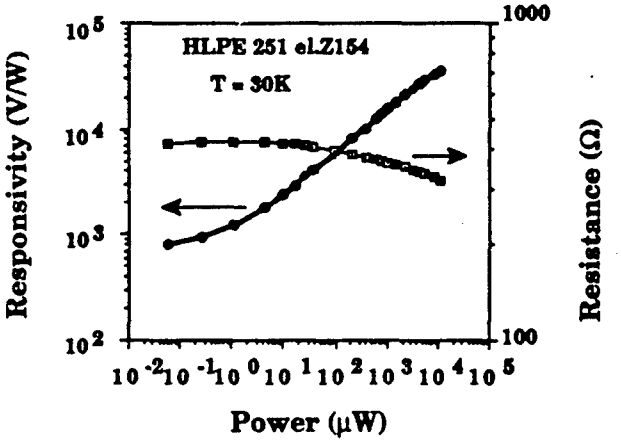
HUGHES
SANTA BARBARA RESEARCH CENTER
a subsidiary



- Initial HgZnTe Devices Longer Than Desired
- Performance Should Improve With Decreased Wavelength

Excellent Blackbody Responsivity for HgZnTe Lot 1 at 30K

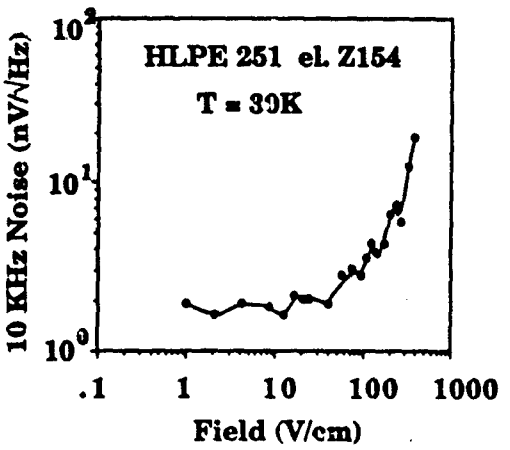
HUGHES
SANTA BARBARA RESEARCH CENTER
a subsidiary



- **Blackbody Responsivities up to 3 x 10^4 V/W at 30K**
  - **Comparable with conventional HgCdTe PC**
- **Responsivity still not saturating at highest bias**

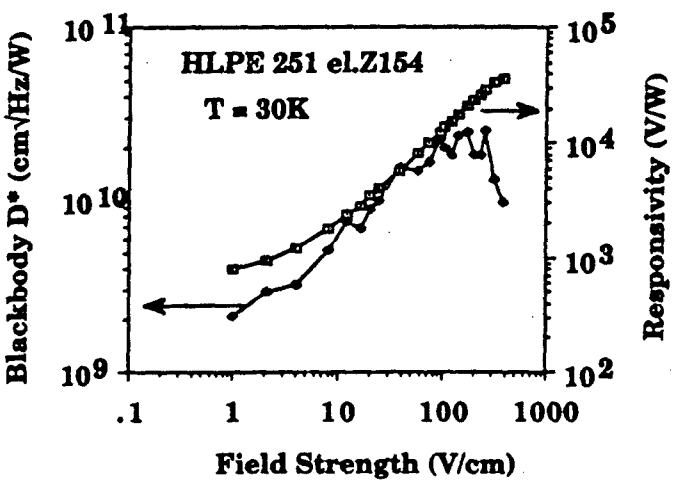
Noise Reduced at 30K for HgZnTe PC Lot 1

HUGHES
SANTA BARBARA RESEARCH CENTER
a subsidiary



Peak D* at 30K Close to BLIP

HUGHES
SANTA BARBARA RESEARCH CENTER
a subsidiary



- Peak D* of 6 x 10^{10} cm√Hz/W

Summary and Future Plans

HUGHES
SANTA BARBARA RESEARCH CENTER
a subsidiary

- Excellent VLWIR performance demonstrated with initial HgZnTe PCs
- Results show that HgCdTe processing largely compatible with HgZnTe
  - Trapping mode PCs should perform as well in HgZnTe as in HgCdTe
- Sources for improving next HgZnTe device lot defined
  - Shorter cutoff
  - Thinner layers
- Ultimate test of HgZnTe's promise will be accelerated life testing

SESSION VIII: III-V Superlattice Detectors

VIII-1 Small Band Gap Superlattices as Intrinsic Long Wavelength Infrared Detector Materials
D.L. Smith, Los Alamos National Laboratory

VIII-2 LWIR Detector Research in InAsSb/InAs
P.S. Peercy, Sandia National Laboratories

VIII-3 InAs/$Ga_{1-x}In_xSb$ Superlattices for Infrared Detector Applications
R.H. Miles, Hughes Research Laboratories

VIII-4 IR Detectors Based on n-i-p-i Superlattices
P.P. Ruden, University of Minnesota

VIII-5 InAs/GaAs and InAs Doping Superlattices
F.J. Grunthaner, Jet Propulsion Laboratory

PRECEDING PAGE BLANK NOT FILMED

N91
14405
UNCLAS

N91-14405

"SMALL BAND GAP SUPERLATTICES AS INTRINSIC LONG WAVELENGTH INFRARED DETECTOR MATERIALS"

D. L. Smith
Los Alamos National Laboratory

Intrinsic long wavelength ($\lambda \geq 10\ \mu m$) infrared (IR) detectors are currently made from the alloy (Hg, Cd) Te. There is one parameter, the alloy composition, which can be varied to control the properties of this material. The parameter is chosen to set the band gap (cut-off wavelength). The (Hg, Cd) Te alloy has the zincblend crystal structure. Consequently, the electron and light-hole effective masses are essentially inversely proportional to the band gap whereas the heavy-hole effective mass is essentially independent of the band gap. As a result, the electron and light-hole effective masses are very small ($M_c^*/M_o \sim M_h/M_o \leq 0.01$) whereas the heavy-hole effective mass is ordinary size ($M_{hh}^*/M_o \sim 0.4$) for the alloy compositions required for intrinsic long wavelength IR detection. This combination of effective masses leads to rather easy tunneling and relatively large Auger transition rates. These are undesirable characteristics, which must be designed around, of an IR detector material. They follow directly from the fact that (Hg, Cd) Te has the zincblend crystal structure and a small band gap.

In small band gap superlattices, such as HgTe/CdTe, In(As, Sb)/InSb and InAs/(Ga,In)Sb, the band gap is determined by the superlattice layer thicknesses as well as by the alloy composition (for superlattices containing an alloy). The effective masses are not directly related to the band gap and can be separately varied. In addition, both strain and quantum confinement can be used to split the light-hole band away from the valence band maximum. These "band structure engineering" options can be used to reduce tunneling probabilities and Auger transition rates compared with a small band gap zincblend structure material. We discuss the different "band structure engineering" options for the various classes of small band gap superlattices.

PRECEDING PAGE BLANK NOT FILMED

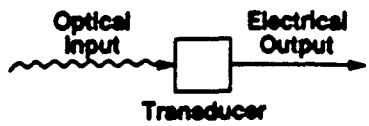
SMALL BAND-GAP SUPERLATTICES AS INTRINSIC IR DETECTOR MATERIALS

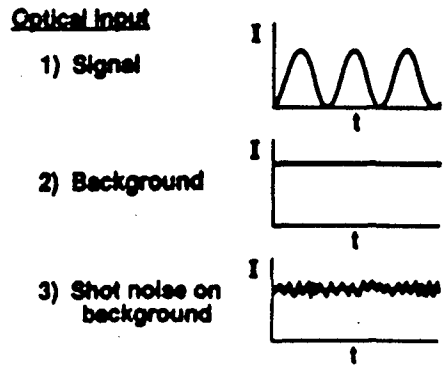
D.L. Smith - Los Alamos
C. Mailhiot - Lawrence Livermore

OUTLINE

1) Introduction
2) Band structure engineering
   a) Zincblende structure materials
   b) Small band-gap superlattices
3) An example InAs/GaInSb
4) Conclusion

IR DETECTORS





$$V_N = \left[V_1^2 + V_2^2 + \cdots \right]^{1/2}$$

BEST TRANSDUCER DOESN'T DEGRADE S/N (BACKGROUND LIMITED)

$$V_N^2 = \text{STUFF} \left[\frac{\eta Q_B \tau}{d} + n_T + \cdots \right]$$

→ SHOT NOISE ON OPTICAL BACKGROUND

IDEAL DEVICE BEHAVIOR
- 1) MINORITY CARRIER DENSITY; INTRINSIC
- 2) THERMALLY IONIZED CARRIER DENSITY; EXTRINSIC

NONIDEAL BEHAVIOR
- DIODE TUNNELING; 1/f ETC.

Want $\frac{\eta Q_B \tau}{d} > n_T$ Min $\frac{n_T}{\alpha \tau}$

$d \sim \alpha^{-1}$ $\sim e^{-E_t / kT}$

BAND STRUCTURE PARAMETERS

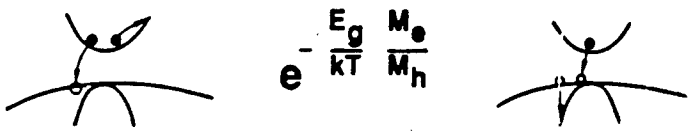


PARAMETERS	PHYSICAL PROCESS
E_g	ABSORPTION THRESHOLD
$M_e^* (M_\perp; M_{11})$	RECOMBINATION TIMES (AUGER; RADIATIVE)
$M_h^* (M_\perp; M_{11})$	ABSORPTION COEFFICIENT
P_{eh}	TRANSPORT (TUNNELING; DIFFUSION)

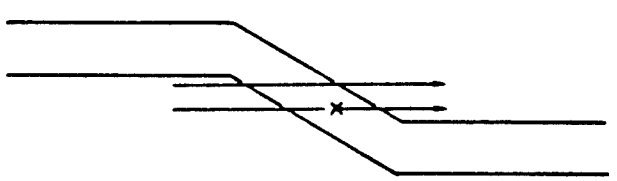
DESIGN PROCESS
1) MATERIAL DESIGN
2) DEVICE DESIGN

AVOIDABLE PROCESSES

AUGER



TUNNELING



K•P THEORY

$$\left[\frac{p^2}{2M} + V\right] \psi = \epsilon \psi$$

$$\psi = e^{ik\cdot r} u^k$$

$$\left[\frac{p^2}{2M} + \frac{\hbar k \cdot P}{M} + \frac{(\hbar k)^2}{2M} + V\right] u^k = \epsilon u^k$$

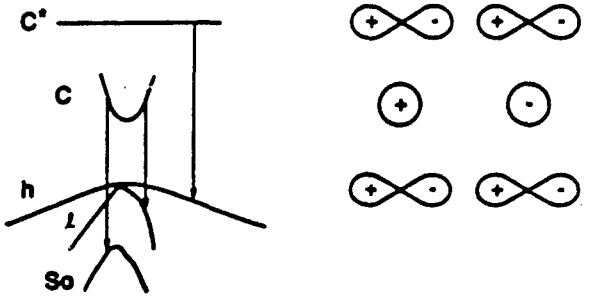
AT ZONE CENTER (k = o)

$$\left[\frac{p^2}{2M} + V\right] u_j^o = \epsilon_j^o u_j^o$$

$$U = \sum_j a_j u_j^o$$

$$0 = \sum_j \left[\left(\epsilon_j^o + \frac{(\hbar k)^2}{2M} - \epsilon\right) \delta_{ij} + \frac{\hbar \vec{k}}{M} \langle U_i | \vec{P} | U_j \rangle\right] a_j$$

ZINCBLENDE STRUCTURE MATERIALS

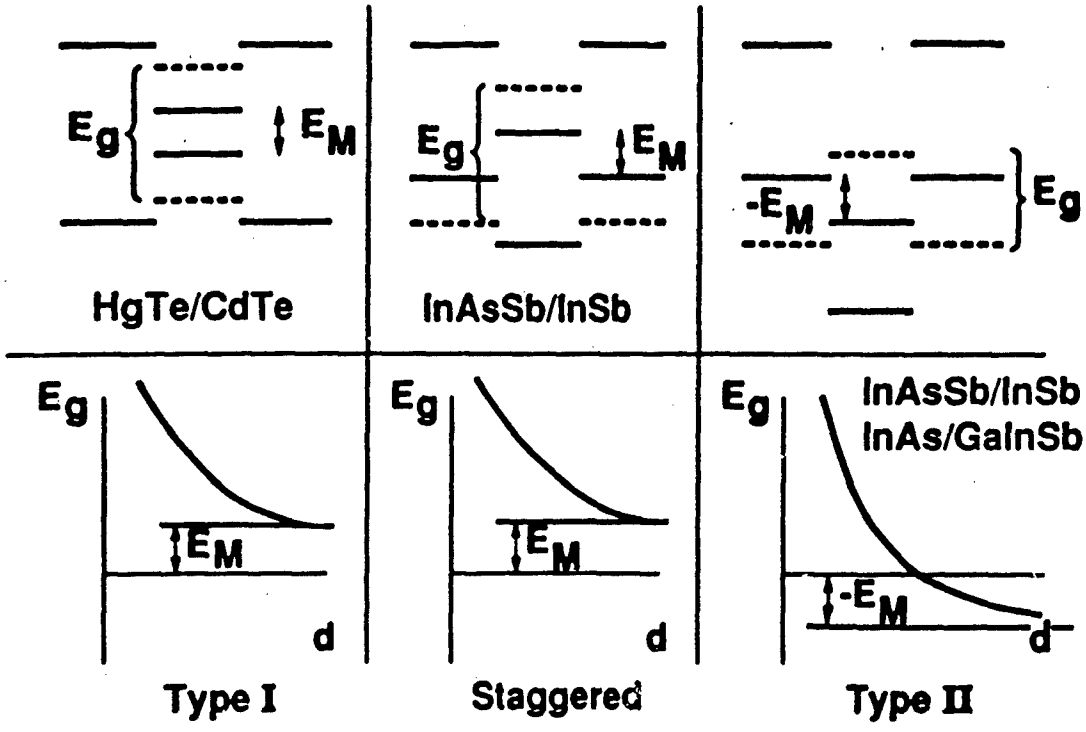


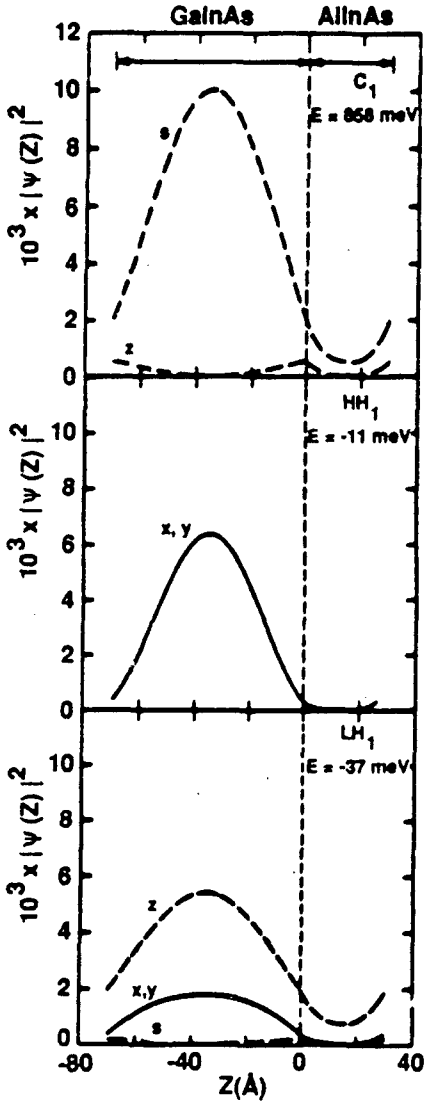
ELECTRON AND LIGHT HOLE (SMALL E_g, LARGE Δ)

$$\begin{vmatrix} \epsilon_c - \epsilon & \alpha \\ \alpha^* & \epsilon_v - \epsilon \end{vmatrix} = 0 \qquad \alpha = \sqrt{\frac{2}{3}}\, |P| k$$

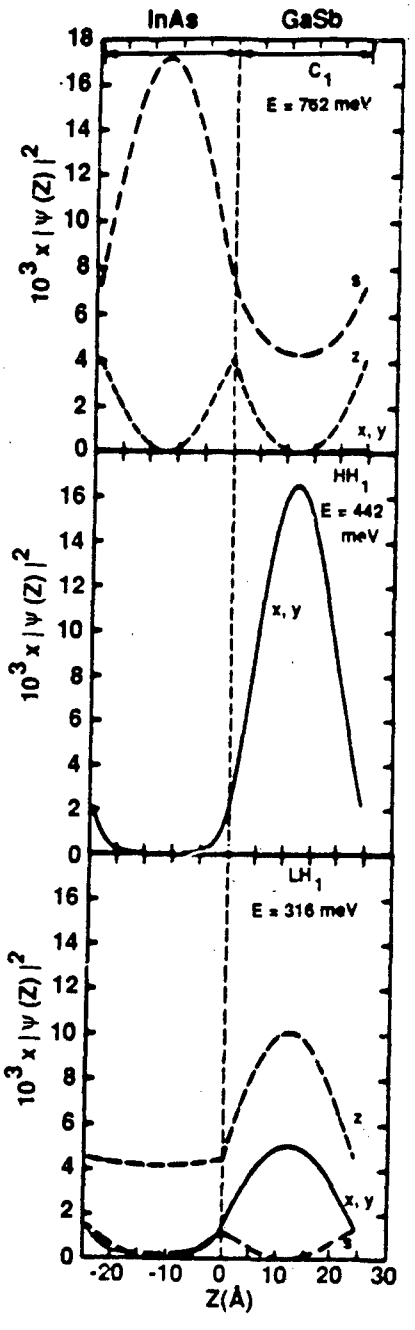
$$\frac{M_o}{M^*} = \pm \frac{2M}{\hbar^2} \quad |P|^2 \quad \left(\frac{2}{3}\left(\frac{1}{E_g}\right)\right)$$

SMALL BANDGAP SUPERLATTICES



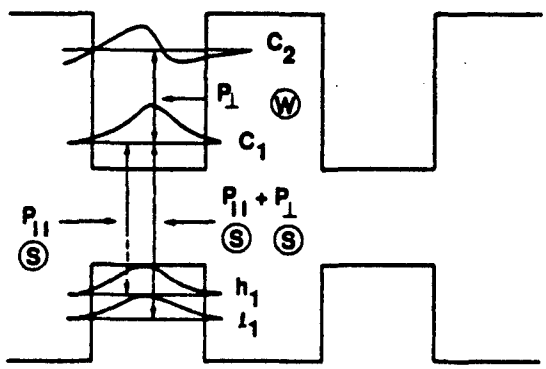


TYPE I



TYPE II

K•P THEORY SUPERLATTICE
SIMPLE CASE



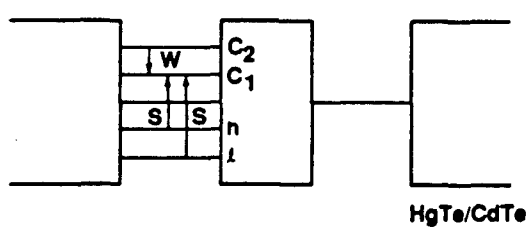
$\Psi = F U$

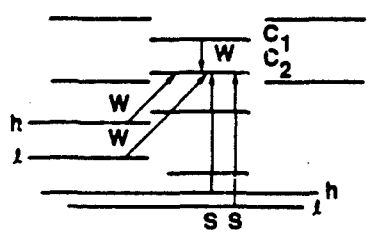
$\langle F_1 U_1 | P | F_2 U_2 \rangle$

$\sim \langle F_1 | F_2 \rangle \langle U_1 | P | U_2 \rangle$ S

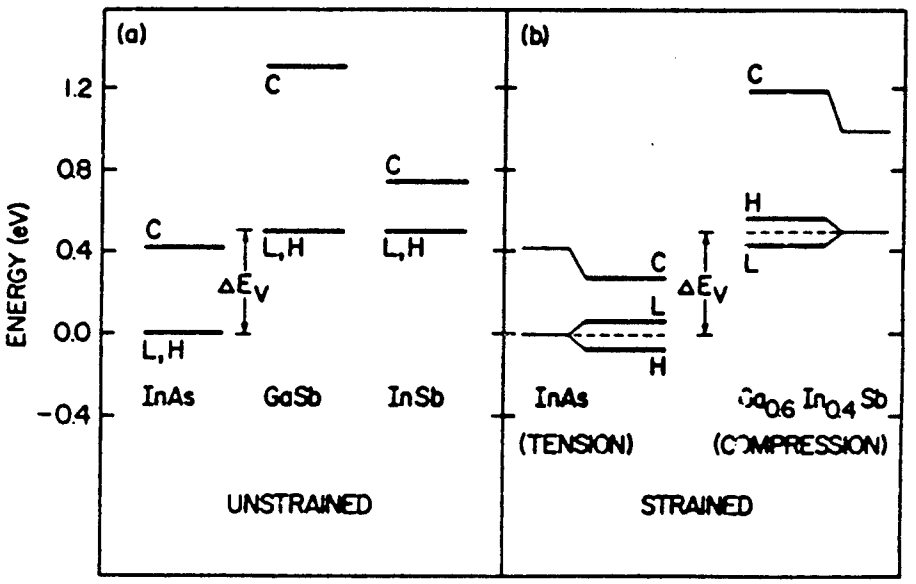
$+ \langle F_1 | P | F_2 \rangle \langle U_1 | U_2 \rangle$ W

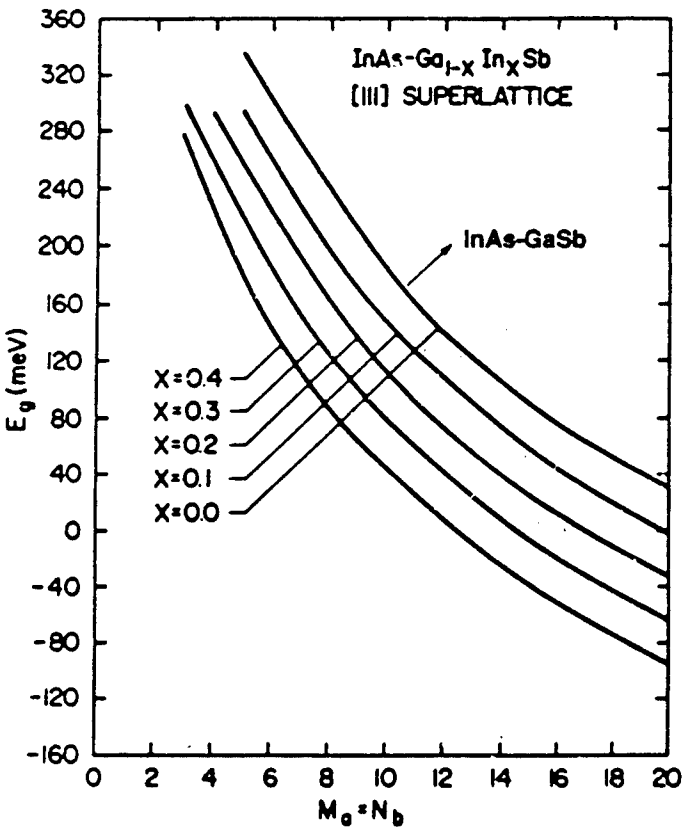
K•P THEORY SUPERLATTICE
SMALL GAP

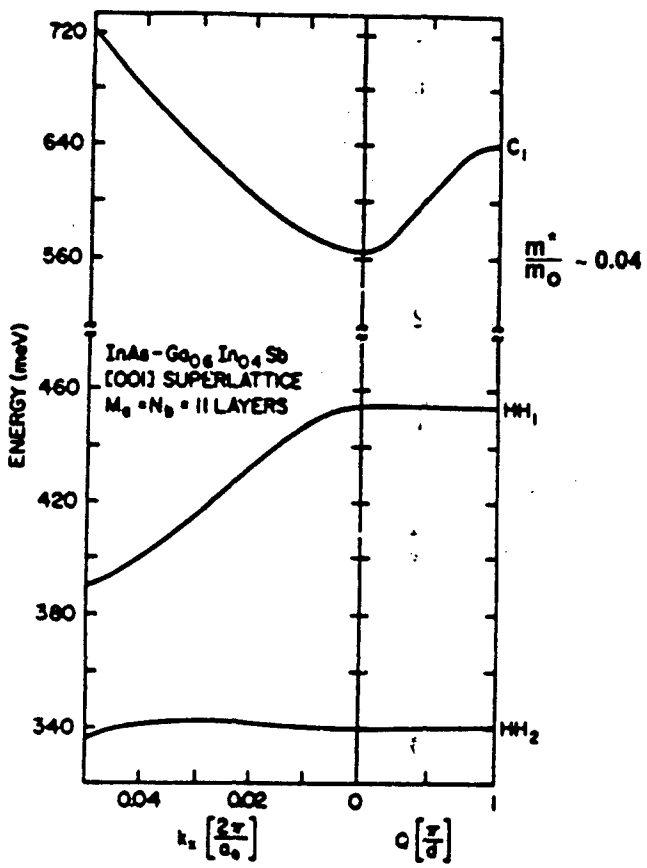


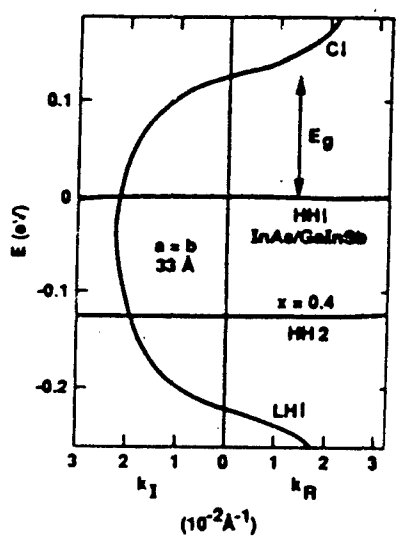


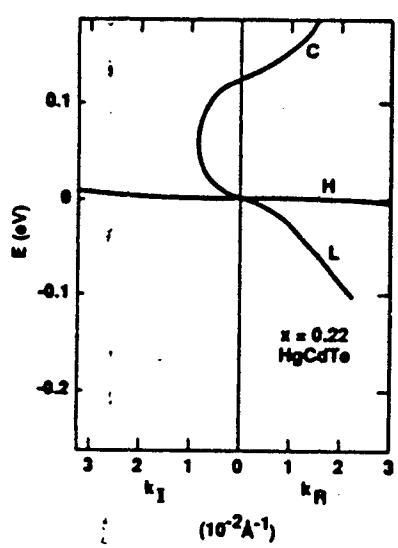
TYPE II

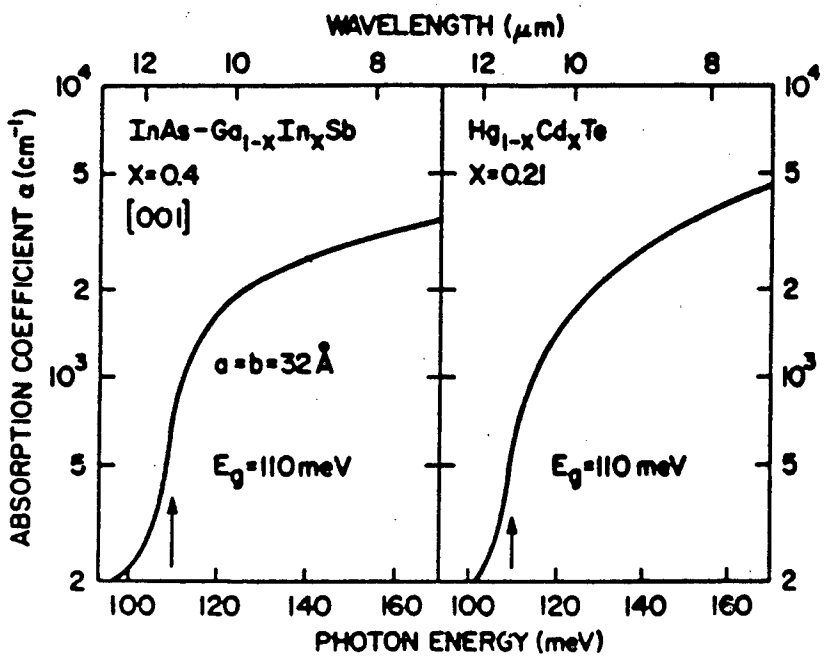

(a)
(b)
1.2
0.8
0.4
0.0
-0.4
ENERGY (eV)
C
C
C
L,H
L,H
L,H
ΔEV
InAs
GaSb
InSb
UNSTRAINED
C
H
L
C
L
H
ΔEV
InAs
(TENSION)
Ga0.6 In0.4 Sb
(COMPRESSION)
STRAINED


InAs-Ga1-X InX Sb
[111] SUPERLATTICE
InAs-GaSb
X=0.4
X=0.3
X=0.2
X=0.1
X=0.0
Eg (meV)
360
320
280
240
200
160
120
80
40
0
-40
-80
-120
-160
0
2
4
6
8
10
12
14
16
18
20
Ma=Nb


720
640
560
460
420
380
340
ENERGY (meV)
InAs-Ga0.6 In0.4 Sb
[001] SUPERLATTICE
Ma = Nb = 11 LAYERS
C1
HH1
HH2
m*/m0 ~ 0.04
0.04
0.02
0
1
kz [2π/a0]
Q [π/d]


CI
Eg
HHI
InAs/GaInSb
a = b
33 Å
x = 0.4
HH2
LHI
E (eV)
0.1
0
-0.1
-0.2
3 2 1 0 1 2 3
kI
kR
(10-2Å-1)


C
H
L
x = 0.22
HgCdTe
E (eV)
0.1
0
-0.1
-0.2
3 2 1 0 1 2 3
kI
kR
(10-2Å-1)



SUMMARY

1) Small band-gap superlattices offer band structure engineering options which make them interesting IR materials

2) Examples of such superlattices include:
   a) HgTe/CdTe
   b) InAsSb/InSb
   c) InAs/GaInSb

3) Predictions on Eg and α in InAs/GaInSb

N91
14406
UNCLAS

N91-14406

LWIR DETECTOR RESEARCH IN InAsSb/InAs

P. S. Peercy

Sandia National Laboratories
Albuquerque, NM 87185-5800

The InAsSb/InSb strained-layer system forms a type-II superlattice in the Sb-rich region of the phase diagram. The band gap of InAsSb/InSb strained-layer superlattices grown on lattice-matched buffers can be varied continuously to produce semiconducting systems with band gaps ranging from that of InSb (0.23 eV with an absorption edge at 5.5 μm at 77 K) to 0. The semiconductor to semimetal transition occurs at As concentrations of approximately 30 %, with the precise value dependent upon the strain and quantum well dimensions. At higher As content, the system is a semimetal. We have fabricated photovoltaic detectors with high D^* at 77 K at wavelengths beyond 10 μm, and both photovoltaic and photoconductive detectors have been demonstrated with response to 15 μm. The photoconductive detectors exhibit gain of up to 100. This talk will discuss details of the materials growth, studies of the band structure and properties, device processing and the detector performance observed to date in these systems.

PRECEDING PAGE BLANK NOT FILMED

LWIR DETECTOR RESEARCH IN InAsSb

P. S. Peercy

Sandia National Laboratories
Albuquerque, New Mexico

(Presented at the Long Wavelength Infrared Detector Workshop, April 24-26, 1990)

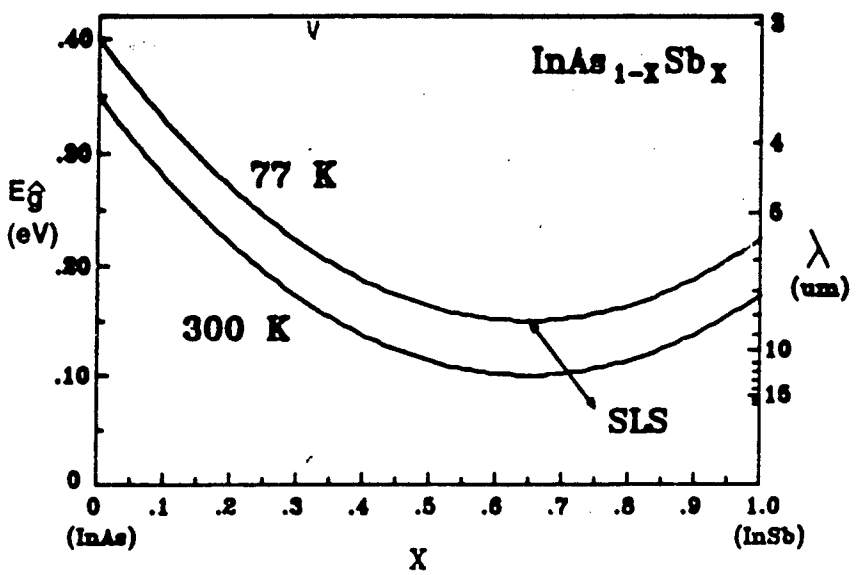
psp04.01.90

OUTLINE

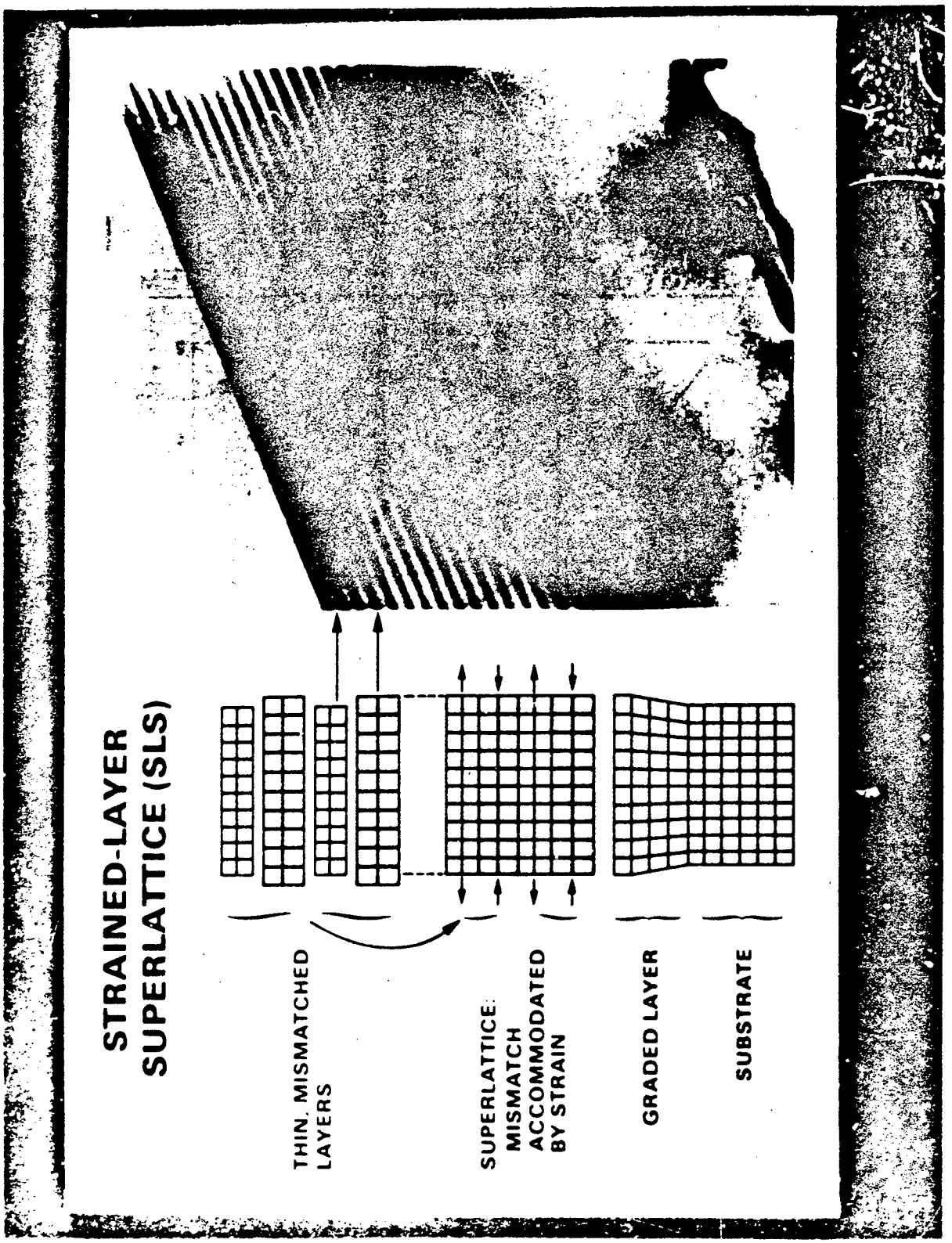
- Summary of InAsSb SLS Properties
  - Band structure
  - Optical properties
- Photoconductive Detectors
  - High gain type II superlattices
- Photovoltaic Detectors
  - Electrical characteristics
  - Detector response
- Extension to wavelengths beyond 10 μm
- Process Monitors and control
  - REMS for on-line growth control
  - PL for monitoring material quality
  - Processing issues
- Summary

psp04.11.90

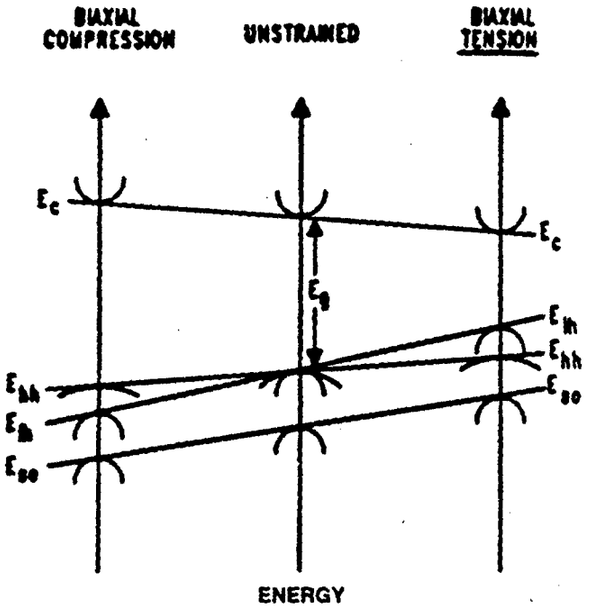
ENERGY GAP IN THE InAsSb ALLOY SYSTEM



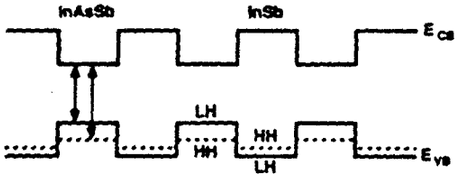
ORIGINAL PAGE
BLACK AND WHITE PHOTOGRAPH



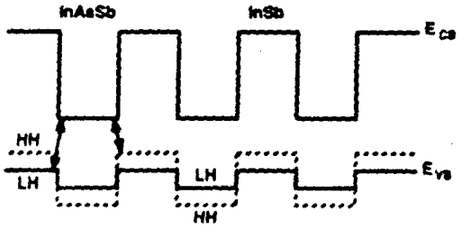
ORIGINAL PAGE IS
OF POOR QUALITY



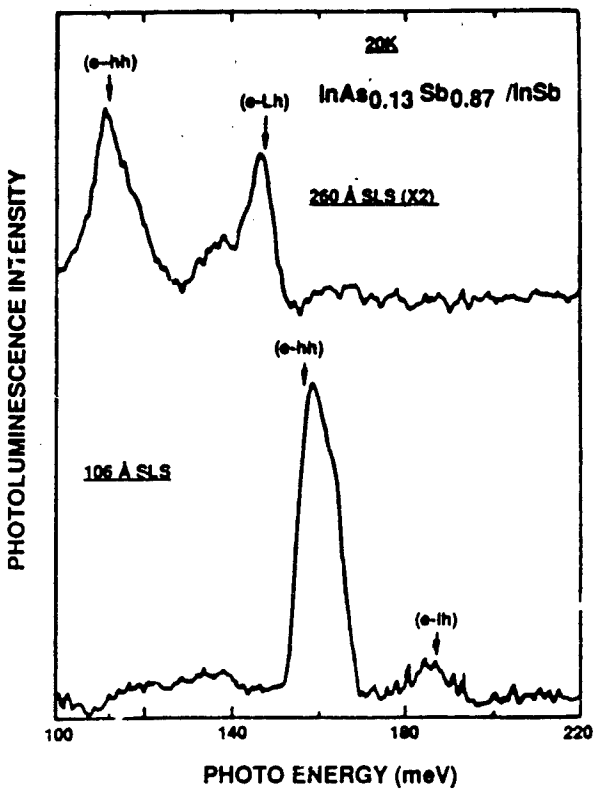
TYPE I OFFSET:
(Spatially "direct", low energy transitions)



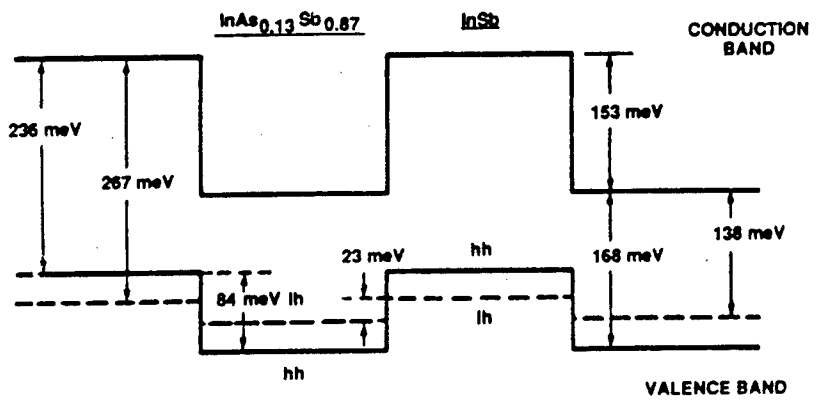
TYPE II OFFSET:
(Lower energy, spatially "indirect" transitions)



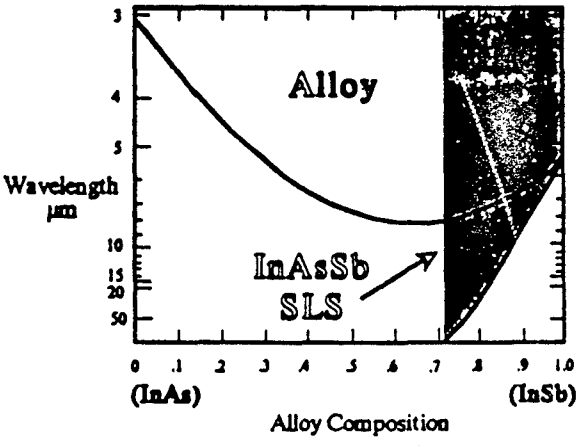
Infrared Photoluminescence (SLS)



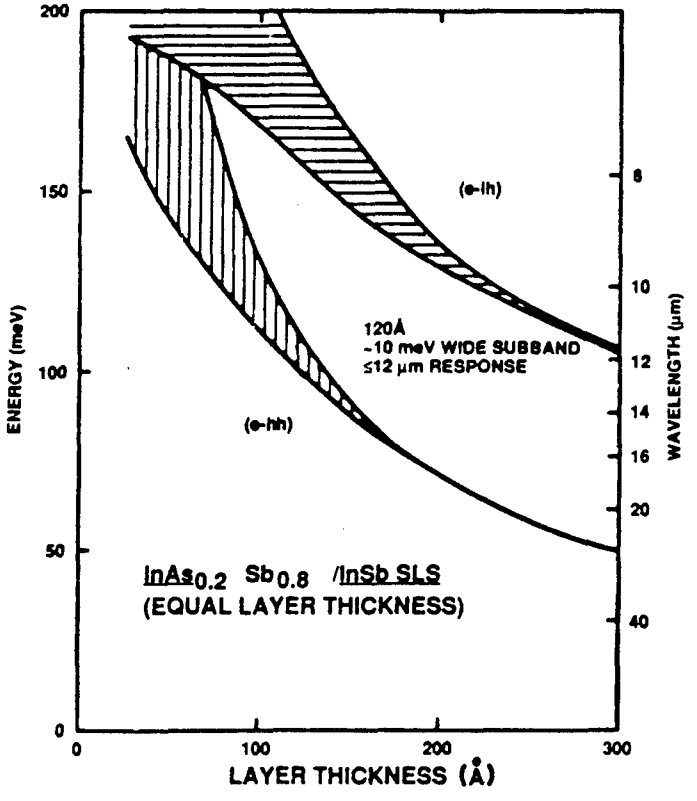
QUANTUM WELL STRUCTURE FROM PL DATA



Far IR Wavelength Accessibility of SLS InAsSb Detectors at 77K

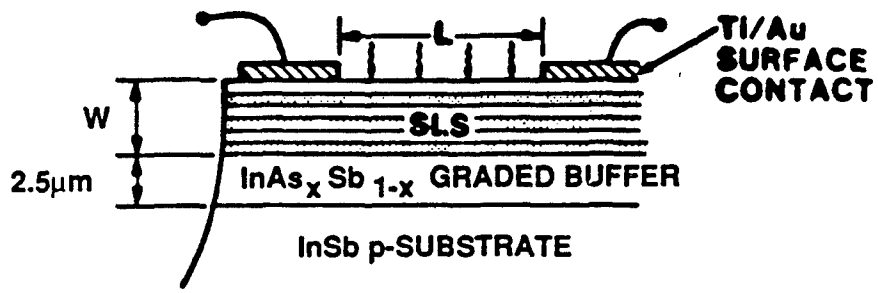


N=1 Transitions For 20% As SLS

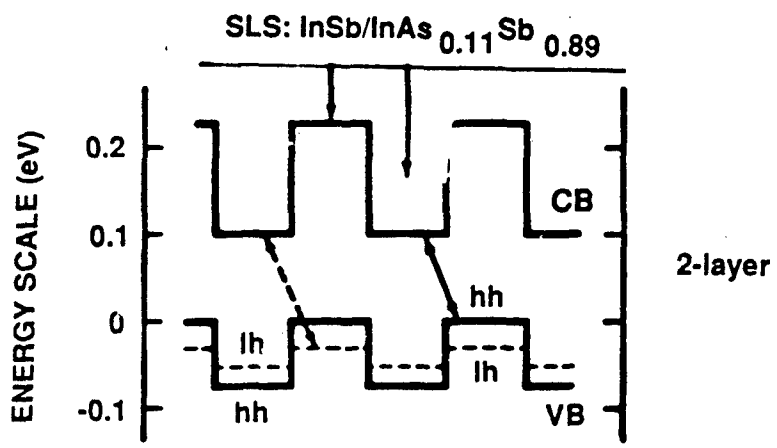


InAsSb SLS Photoconductive Detector

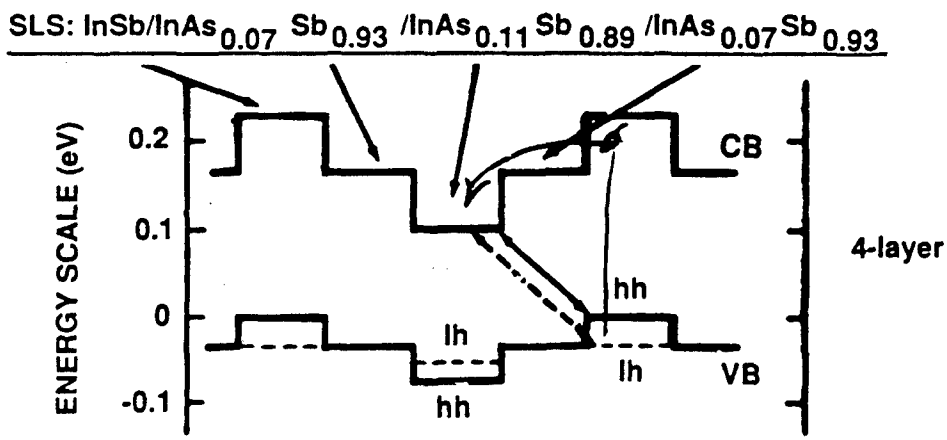
(a)



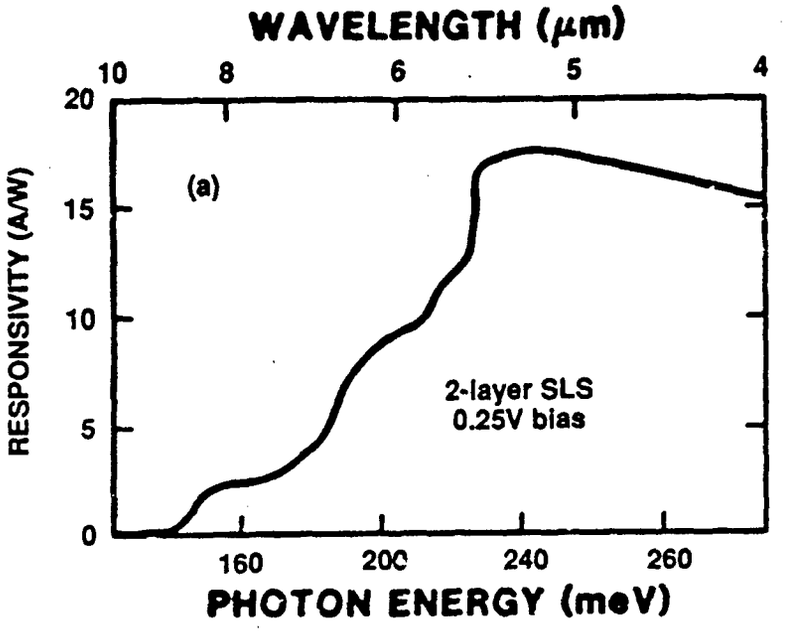
(b)

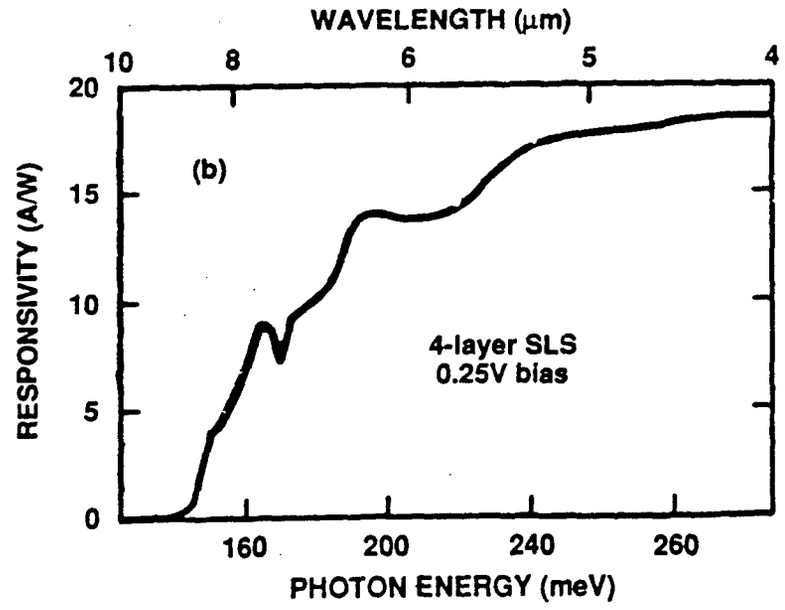


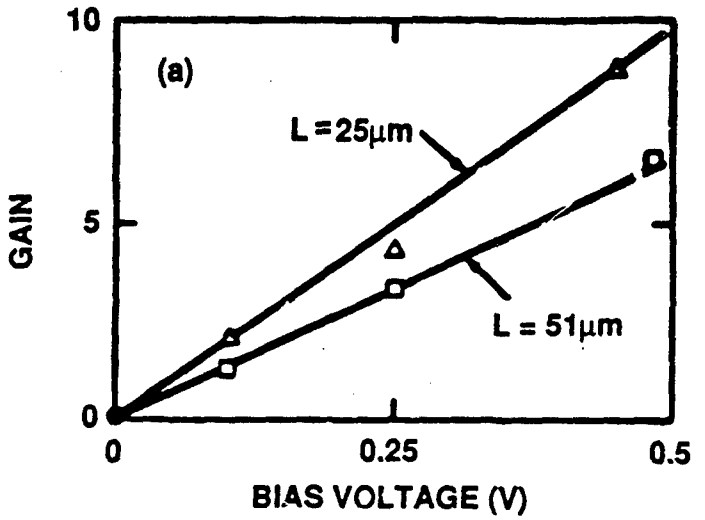
(c)

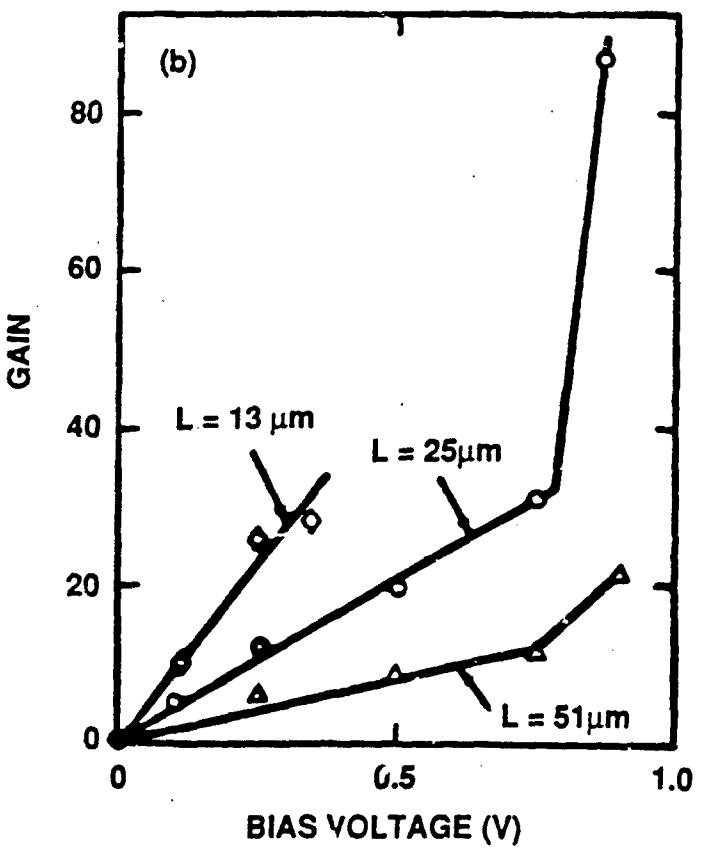


Photoconductive Detector Responsivity

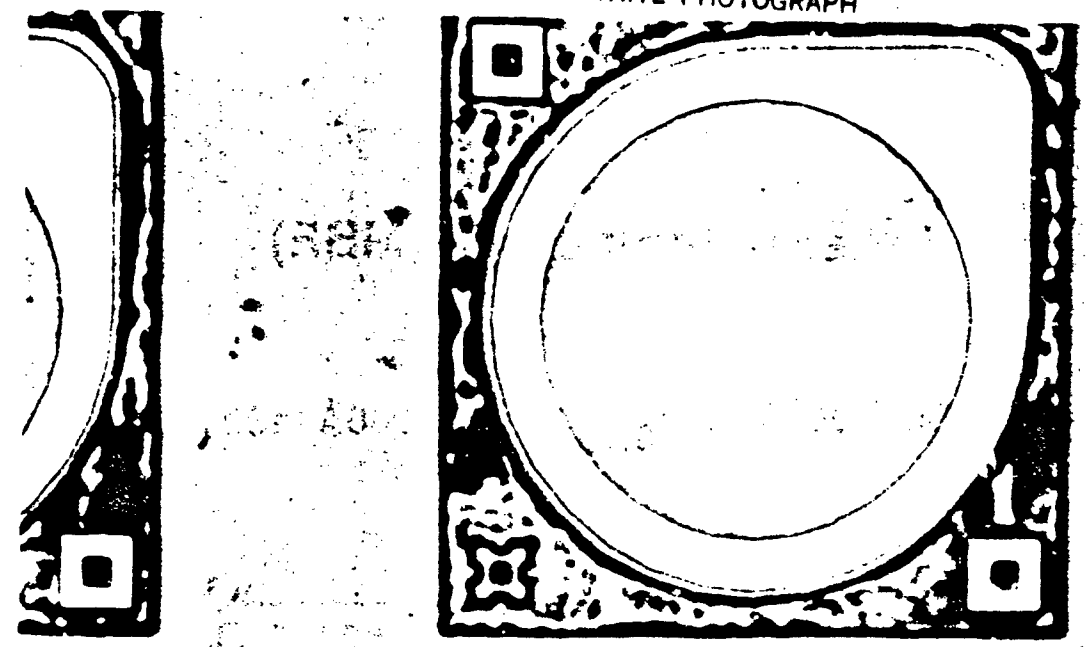


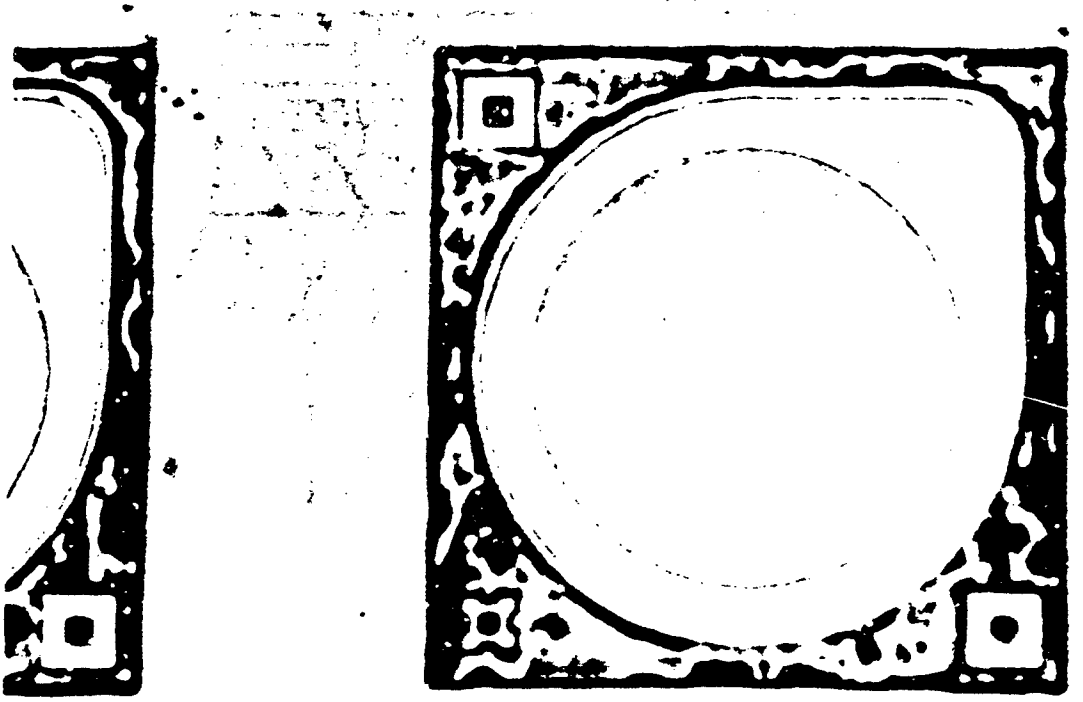



(a)
L = 25μm
L = 51μm
GAIN
10
5
0
0
0.25
0.5
BIAS VOLTAGE (V)


(b)
L = 13 μm
L = 25μm
L = 51μm
GAIN
80
60
40
20
0
0
0.5
1.0
BIAS VOLTAGE (V)

ORIGINAL PAGE
BLACK AND WHITE PHOTOGRAPH

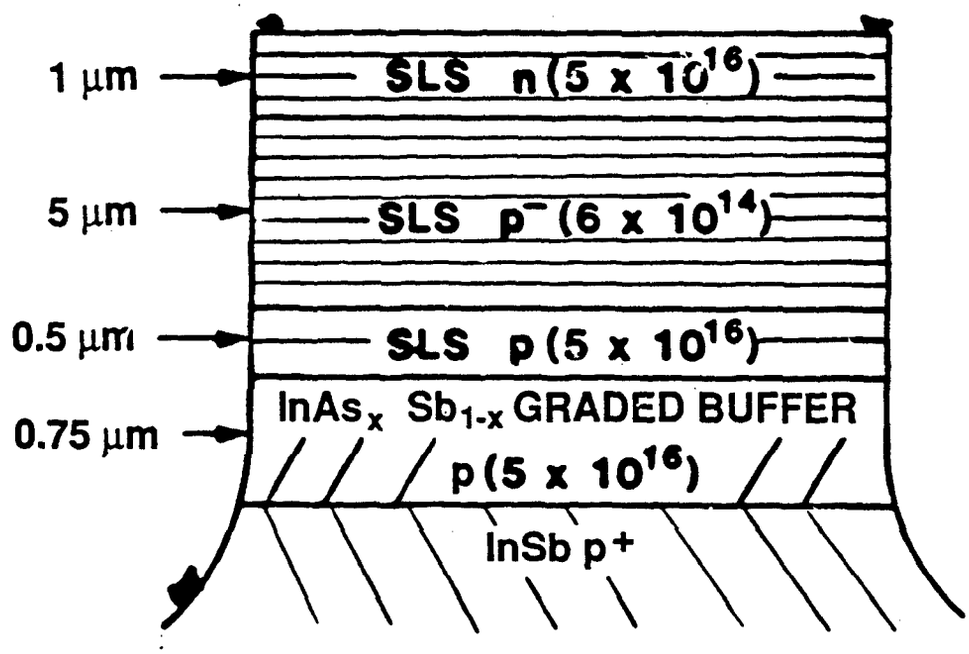


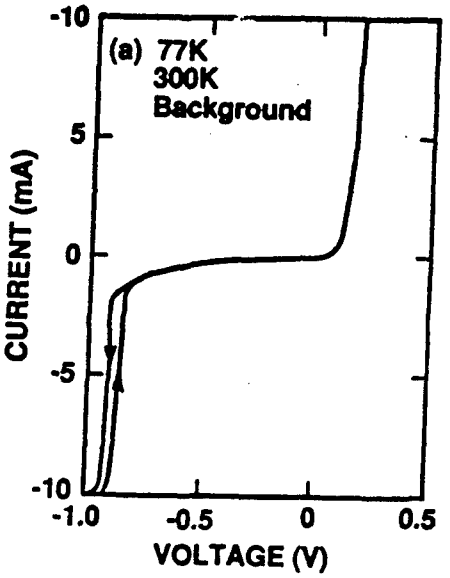


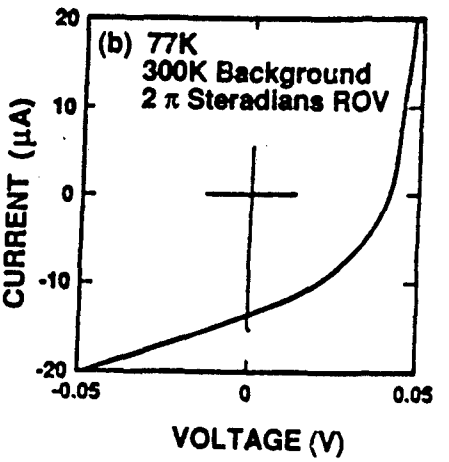
ORIGINAL PAGE IS
OF POOR QUALITY

InAsSb Photodiode (MBE)

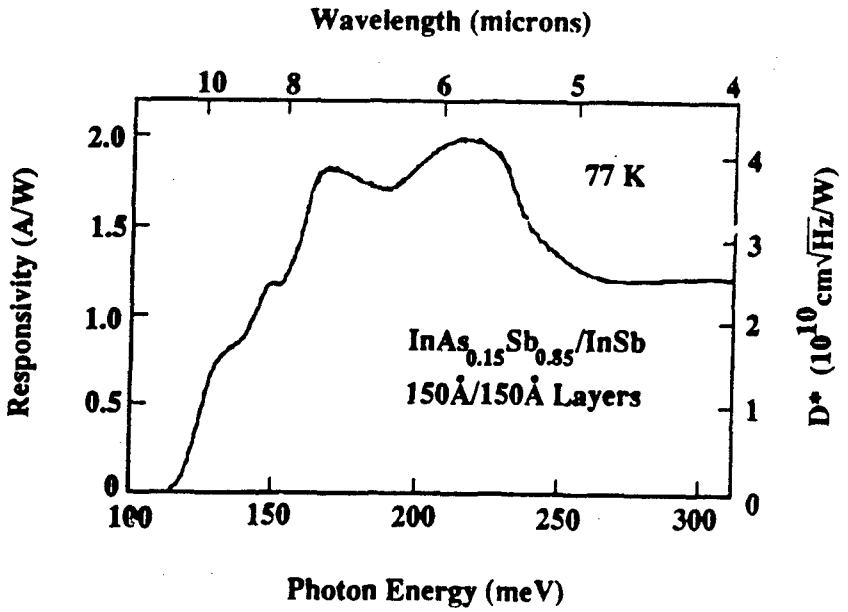
SLS: 200Å $InAs_{0.15}$ $Sb_{0.85}$ /200Å InSb



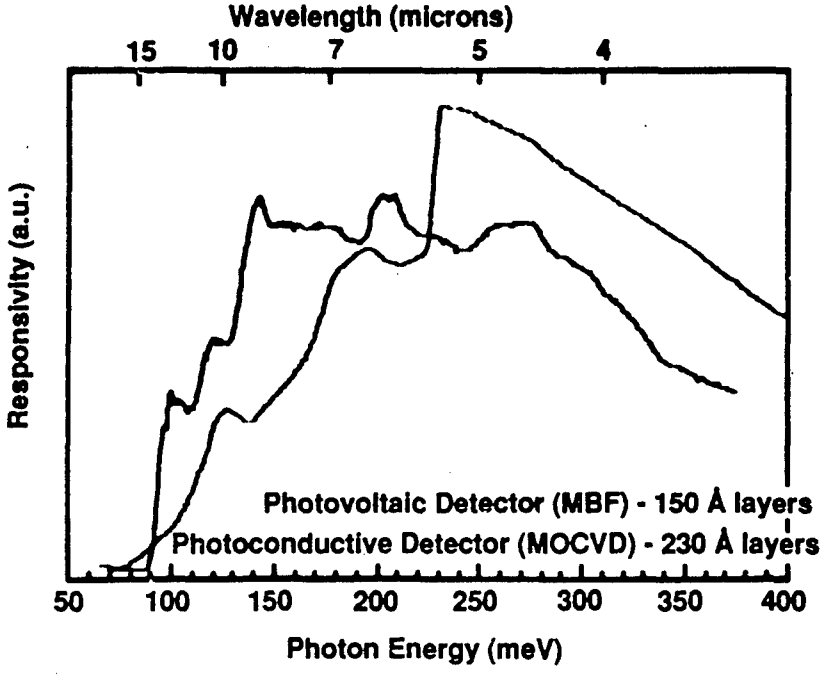

(a) 77K
300K
Background
CURRENT (mA)
VOLTAGE (V)
-10
5
0
-5
-10
-1.0
-0.5
0
0.5


(b) 77K
300K Background
2 π Steradians ROV
CURRENT (μA)
VOLTAGE (V)
20
10
0
-10
-20
-0.05
0
0.05

BLIP (300K)


Wavelength (microns)
10
8
6
5
4
Responsivity (A/W)
D* (10^10 cm√Hz/W)
77 K
InAs0.15Sb0.85/InSb
150Å/150Å Layers
2.0
1.5
1.0
0.5
0
4
3
2
1
0
100
150
200
250
300
Photon Energy (meV)

PHOTOVOLTAIC AND PHOTOCONDUCTIVE SLS DETECTOR PHOTORESPONSE TO 15 μm



PROCESS CONTROLS

- On-line monitors and control during growth

  REMS (MBE)

  UV absorption (MOCVD)

- Monitor of superlattice quality

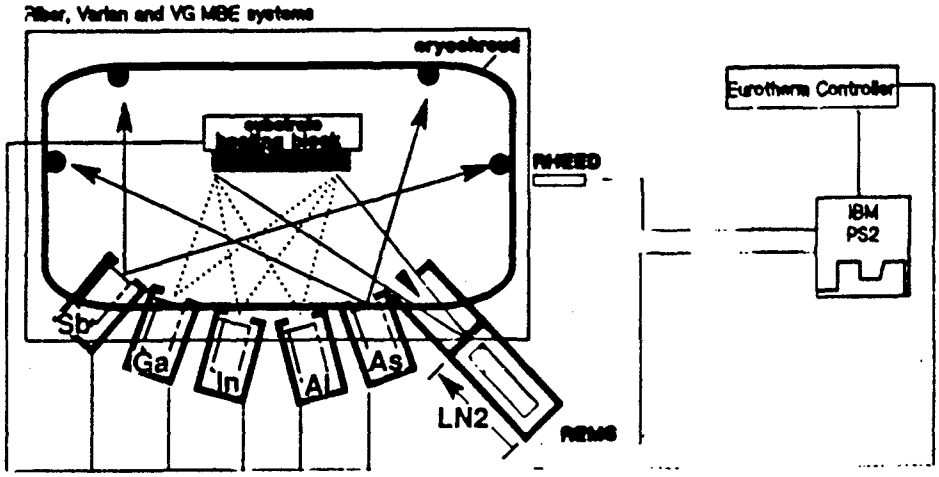
  Photoluminescence

Reflection Mass Spectometry and III/V MBE

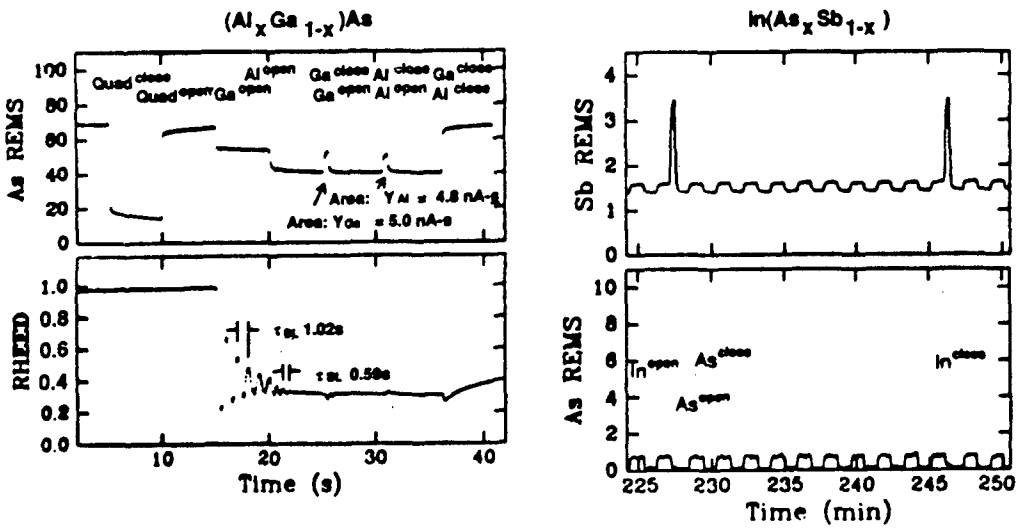
"REMS"

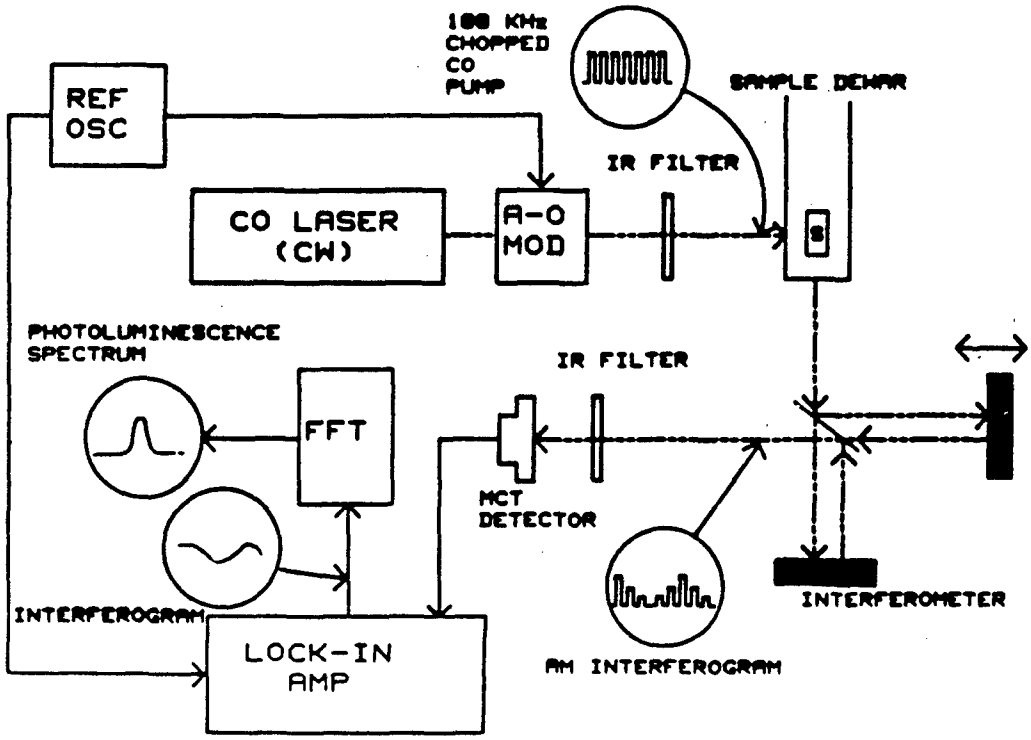
Jeff Tsao, Tom Brennan, Gene Hammons
Ray Hibray, John Klem, Ralph Dawson

Riber, Varian and VG MBE systems

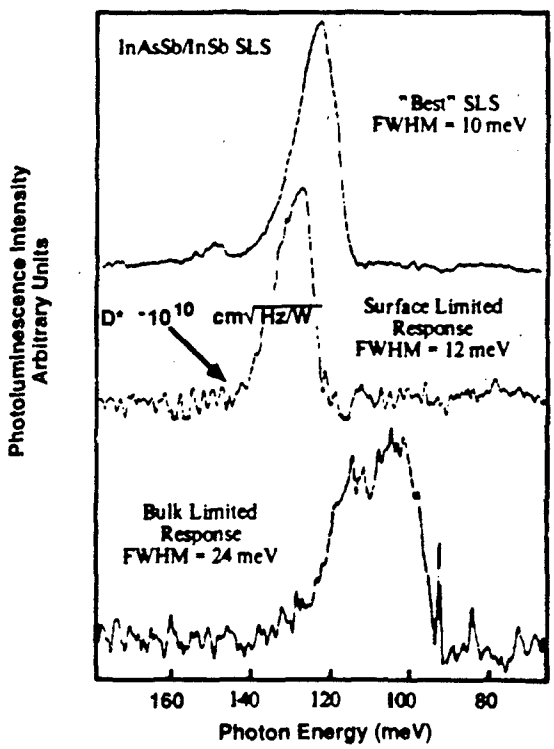


Composition Control using REMS





Photoluminescence Linewidth Characterization of Wafer Quality



PROCESSING TECHNIQUES

ETCHING - STANDARD WET-CHEMICAL TECHNIQUES USING STANDARD PHOTORESIST PROCESSES

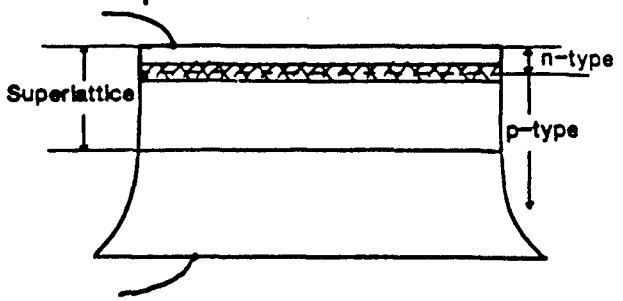
METALLIZATION - NON-ALLOYED Ti/Au OR Cr/Au OHMIC CONTACTS DEFINED BY CONVENTIONAL LIFTOFF TECHNIQUES

PASSIVATION - VARIOUS SCHEMES ARE BEING INVESTIGATED WITH POSITIVE RESULTS

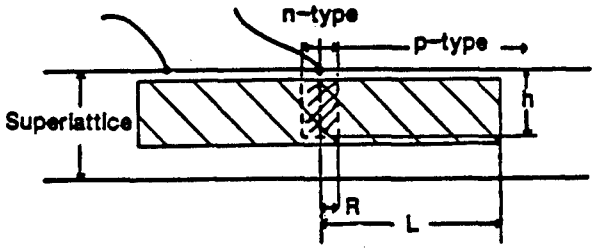
PACKAGING - STANDARD PACKAGES AND ADHESIVES WITH ULTRASONIC LEAD BONDING HAVE BEEN USED SUCCESSFULLY

INTERFACING - ISSUE NOT ADDRESSED YET

Superlattice Mesa Photodiode:



Lateral Superlattice Photodiode:



SUMMARY

- InAsSb SLS detectors can span the 8-15 μm spectral region
- LWIR photovoltaic detectors have been demonstrated with $D^* > 10^{10}$ cm√Hz/W at 10 μm
- LWIR photoconductive detectors with high gain have been demonstrated
- REMS and PL have been demonstrated to be valuable growth and process monitors

N91
14407
UNCLAS

N91-14407

InAs/$Ga_{1-x}In_xSb$ Superlattices for Infrared Detector Applications

R. H. Miles

Hughes Research Laboratories
Malibu, California 90265

D. H. Chow and T. C. McGill

California Institute of Technology
Pasadena, California 91125

InAs/$Ga_{1-x}In_xSb$ superlattices have been proposed as possible alternatives to $Hg_{1-x}Cd_xTe$ for infrared detector applications, particularly in the $8-12\,\mu m$ region and beyond.[1,2] Long wavelength response has been predicted based on the strongly misaligned (type-II) band alignment of the superlattice. Semimetallic behavior consistent with this band alignment has been demonstrated in InAs/GaSb superlattices ($\Delta E_v \simeq 510$meV), but only for comparatively thick layers ($\simeq 100$ Å).[3] As type-II structures confine electrons and holes in different layers, electron-hole overlap is poor for layers this thick, and as a consequence the optical absorption coefficients are small. It was proposed that long wavelength response could be achieved for substantially thinner layers by replacing the GaSb layers with $Ga_{1-x}In_xSb$, further misaligning the bands through strain effects and reducing the antimonide band gap.[1,2] Calculated absorption coefficients for these structures are comparable to those of $Hg_{1-x}Cd_xTe$.

We report the successful growth of InAs/$Ga_{1-x}In_xSb$ superlattices and their optical and structural characterization. Samples were grown by molecular beam epitaxy at fairly low substrate temperatures ($< 400\,°C$). Structural quality was assessed by reflection high energy electron diffraction, transmission electron microscopy, and x-ray diffraction. Excellent structures were achieved for growth on thick, strain relaxed GaSb buffer layers on GaAs substrates, despite a residual threading dislocation density of $10^9 cm^{-2}$ originating at the GaSb/GaAs interface. Despite a lattice mismatch of 1.7%, InAs/$Ga_{0.75}In_{0.25}Sb$ superlattices are observed to be free of misfit dislocations at the thicknesses examined here, owing to the close lattice match between the superlattice and GaSb, which evenly distributes compressive and tensile stresses between the InAs and $Ga_{0.75}In_{0.25}Sb$ layers.

Photoluminescence and photoconductivity measurements indicate that the energy gaps of the strained-layer superlattices are smaller than those of InAs/GaSb superlattices with the same layer thicknesses, and are in agreement with the theoretical predictions of Smith and Mailhiot. Energy gaps of 80-250meV ($15-5\,\mu m$) have been measured for InAs/$Ga_{0.75}In_{0.25}Sb$ superlattices with $45-25$ Å/25 Å layer thicknesses. Our results demonstrate that far-infrared cutoff wavelengths are compatible with the thin superlattice layers required for strong optical absorption in type-II superlattices.

[1] D. L. Smith and C. Mailhiot, *J. Appl. Phys.* **62**, 2545 (1987).

[2] C. Mailhiot and D. L. Smith, *J. Vac. Sci. Technol. A* **7**, 445 (1989).

[3] G. A. Sai-Halasz, L. L. Chang, J.-M. Welter, C.-A. Chang, and L. Esaki, *Solid State Commun.* **27**, 935 (1978).

InAs/$Ga_{1-x}In_xSb$ SUPERLATTICES FOR INFRARED APPLICATIONS

R. H. Miles & J. N. Schulman, HRL
D. H. Chow & T. C. McGill, Caltech

OUTLINE

HUGHES

- Motivation
- Growth & structural properties
  - TEM
  - x-ray diffraction
- Optical properties
  - photoconductivity
  - photoluminescence
  - absorption
- Conclusion, comparison with theory

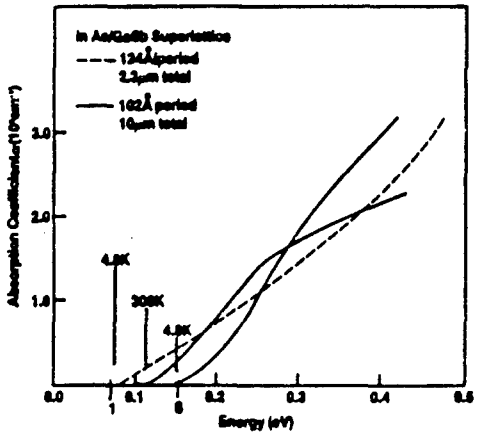
InAs/$Ga_{1-x}In_xSb$ SUPERLATTICES

HUGHES

- Proposed as IR detectors by D. L. Smith and C. Mailhiot (J. Appl. Phys. 62, 2545 (1987)).
  - IR energy gaps tunable over entire spectrum
  - large absorption coefficients
  - favorable transport properties ($m^*_{e,\perp}/m_e \simeq 0.04$)
  - III-V processing

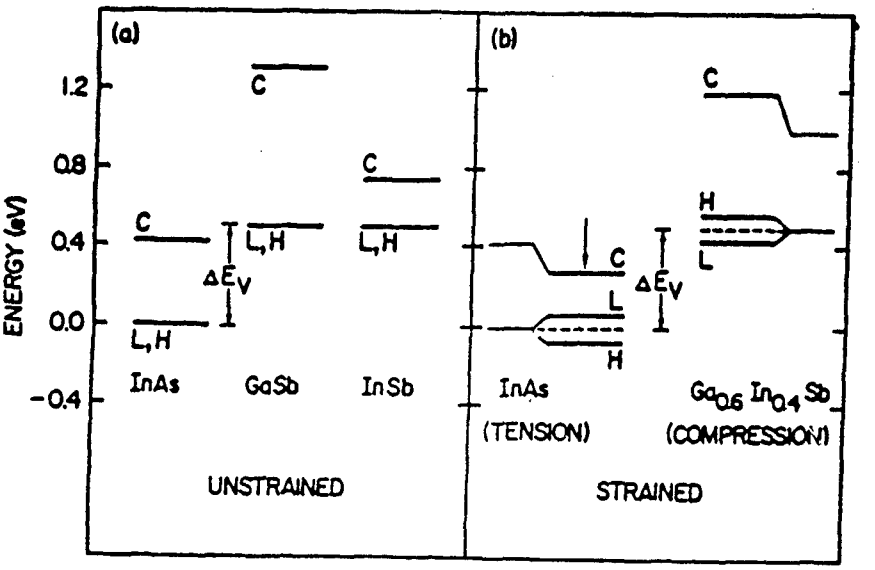
InAs/GaSb SUPERLATTICE ABSORPTION

HUGHES



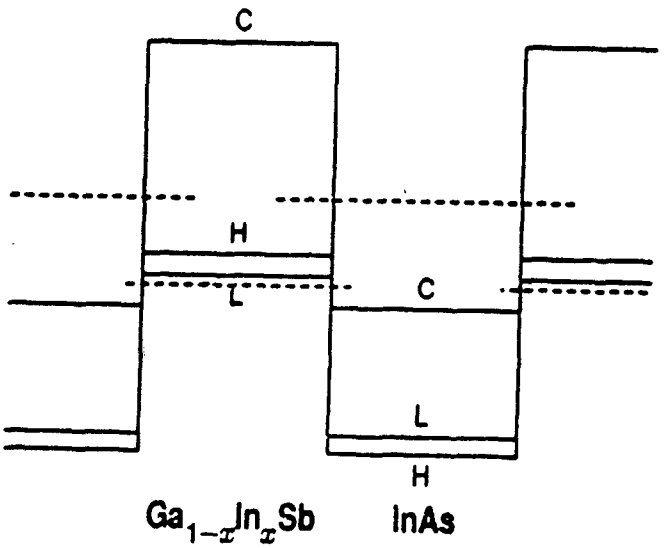
- D. K. Arch *et al.*, *J. Appl. Phys.* 58, 3934 (1985).

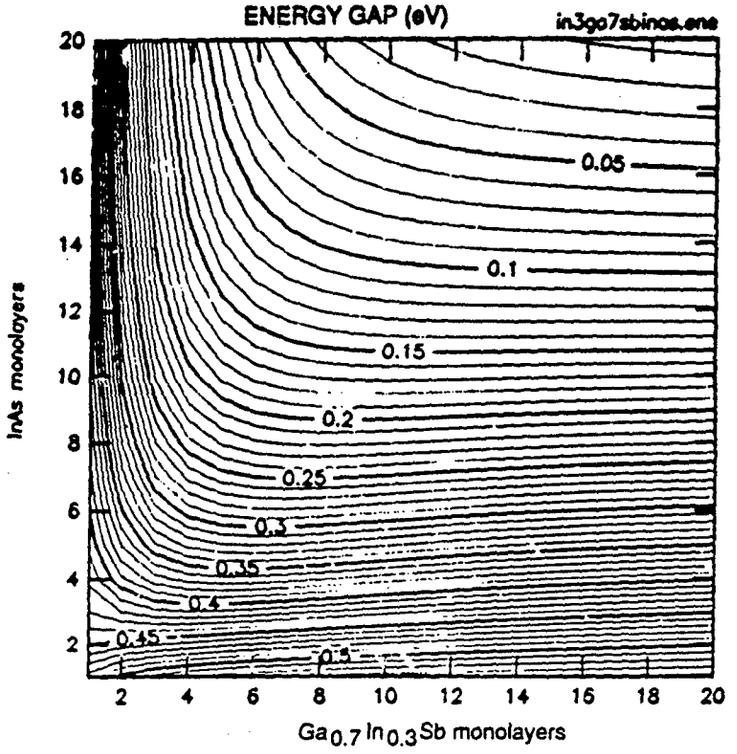
ALIGNMENT OF ENERGY BAND EDGES

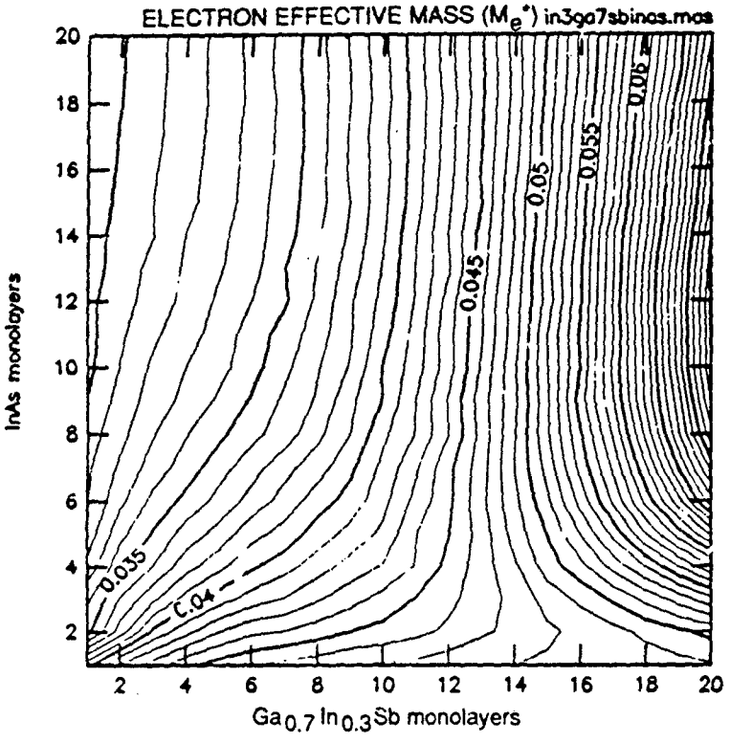


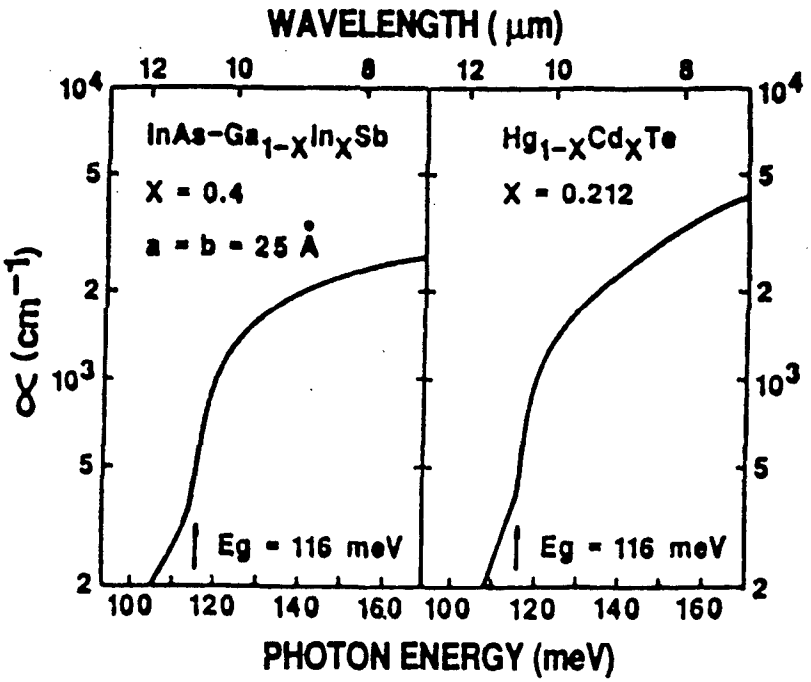
(Smith and Mailhiot)

InAs/$Ga_{1-x}In_xSb$ SUPERLATTICE BAND EDGES




ENERGY GAP (eV)
in3ga7sbinas.ene
0.05
0.1
0.15
0.2
0.25
0.3
0.35
0.4
0.45
0.5
InAs monolayers
Ga0.7 In0.3Sb monolayers


ELECTRON EFFECTIVE MASS (Me*) in3ga7sbinas.mas
0.035
0.04
0.045
0.05
0.055
0.06
InAs monolayers
Ga0.7 In0.3Sb monolayers



InAs/Ga_{1-x} In_xSb Superlattices

Growth and Structural Characterization

A. Growth

- PHI 430 MBE system
- As_2 and Sb_2 (cracker) sources
- (100) GaAs substrates
- Substrate temperature monitoring

B. Structural Characterization Techniques

- Surface Morphology
- *in situ* Reflection High Energy Electron Diffraction (RHEED)
- X-ray diffraction
- Transmission Electron Microscopy (TEM)

As-incorporation in InGaSb Layers

I. Experimental

- Grew 2500 Å GaSb(As) Layer on InAs Buffer
- X-ray diffraction to determine As-incorporation

II. Growth Parameters Varied

- Substrate Temperature
- As background pressure
- Sb flux

III. Results

- Virtually no Sb incorporated in InAs layers
- Up to 30% As found in GaSb(As) layers
- Reduced As incorporation at lower substrate temperatures, reduced As background (< 7%)
- Sb flux has no effect on As incorporation in GaSb(As)

InAs/Ga_{1-x} In_xSb Superlattice

Growth Conditions

I. Substrate Temperature

- Poor surface morphology, x-ray diffraction for $T > 400°C$
- Excellent surfaces, x-ray diffraction for $370 < T < 400°C$

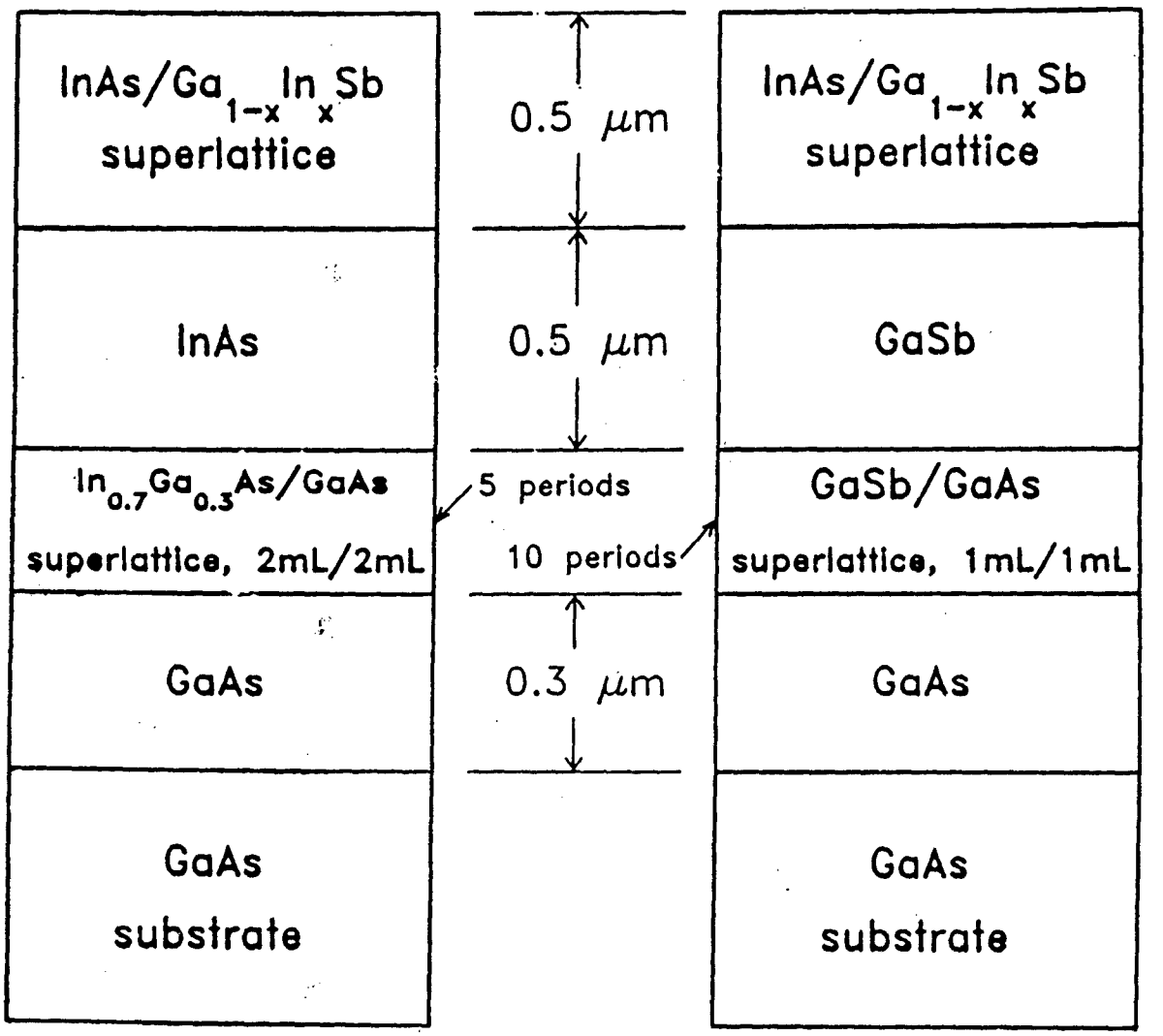
II. Growth Fluxes

- InAs growth rate = 0.5 Å/sec
- Ga_{1-x} In_xSb growth rate = 2.0 Å/sec
- Sb_2 flux >> As_2 flux

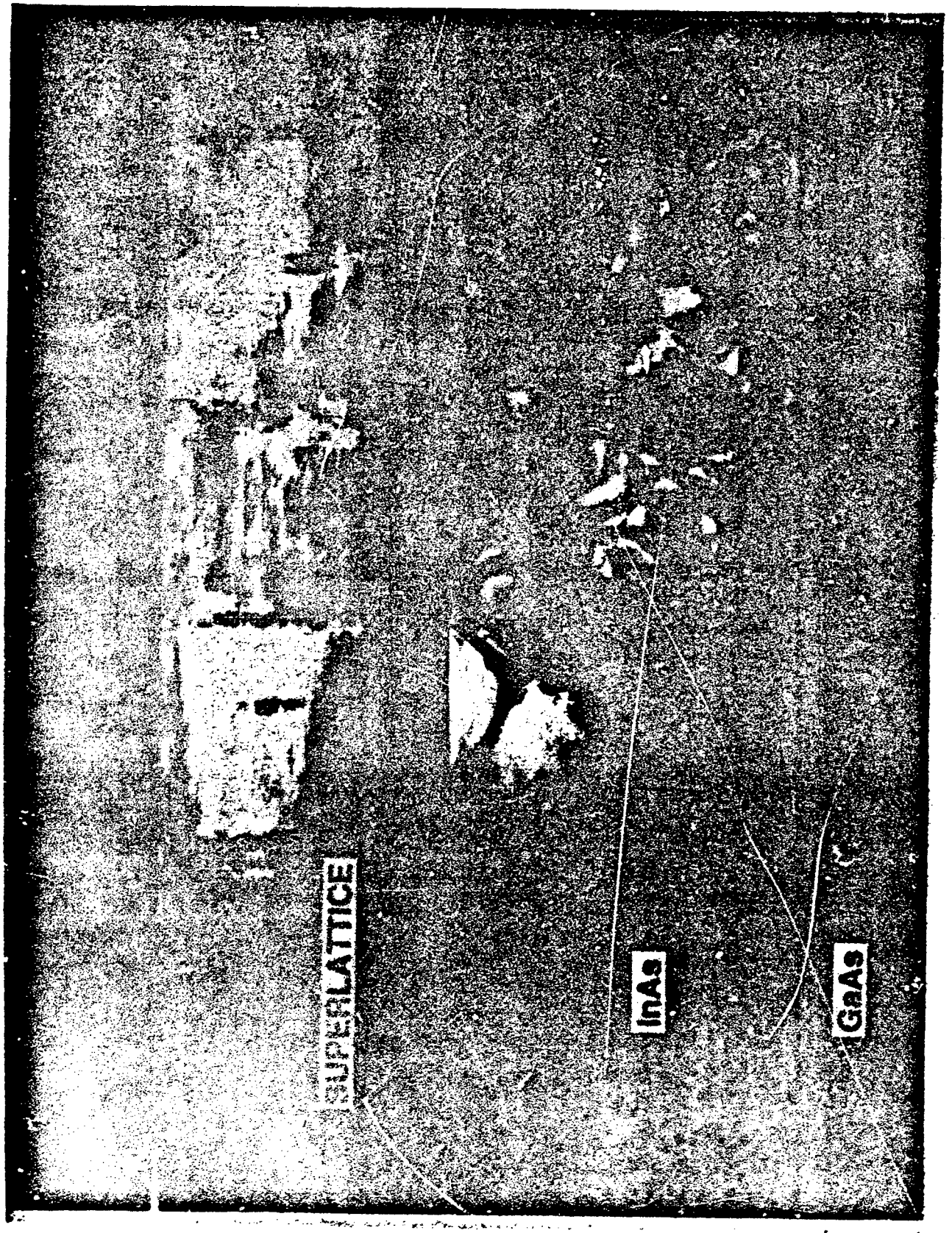
III. Surface Reconstruction

- 1 x 3 for Ga_{1-x} In_xSb
- 1 x 2 for InAs

SCHEMATIC LAYER DIAGRAM



ORIGINAL PAGE
BLACK AND WHITE PHOTOGRAPH

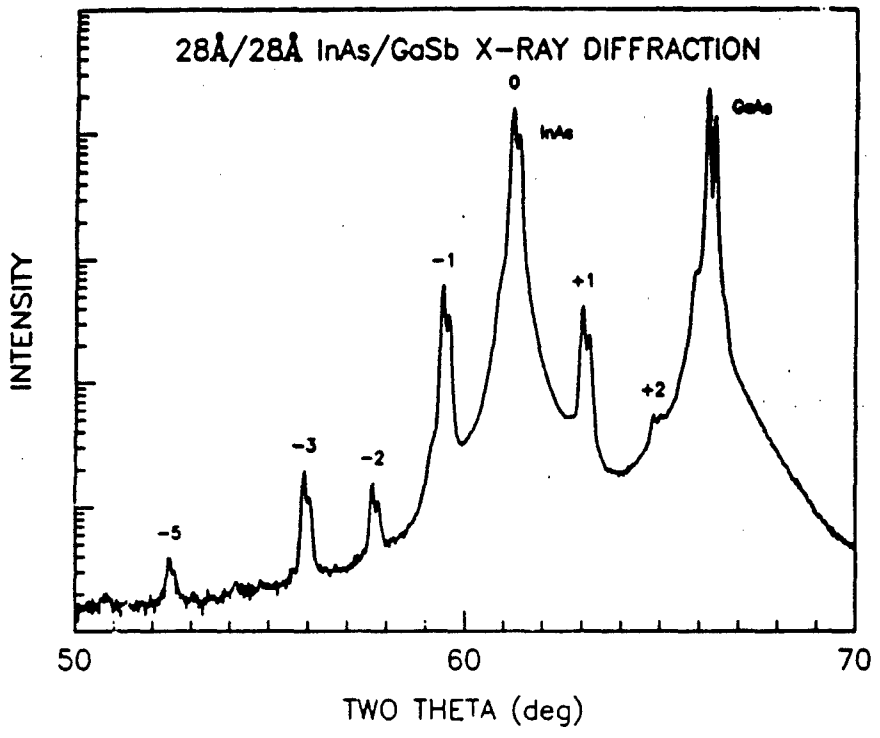


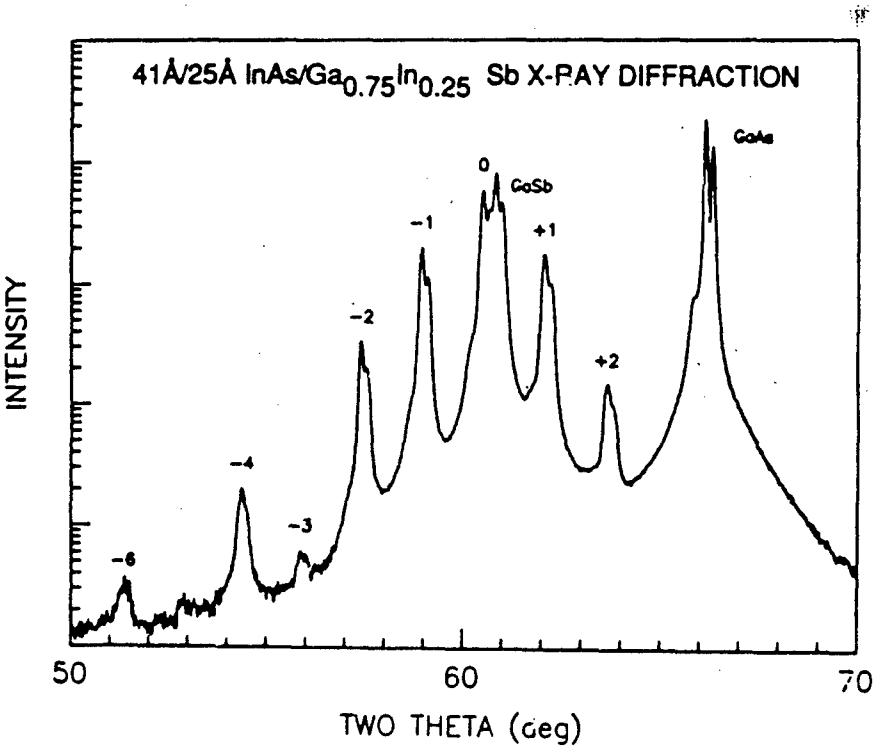
ORIGINAL PAGE IS
OF POOR QUALITY

ORIGINAL PAGE
BLACK AND WHITE PHOTOGRAPH



ORIGINAL PAGE IS
OF POOR QUALITY

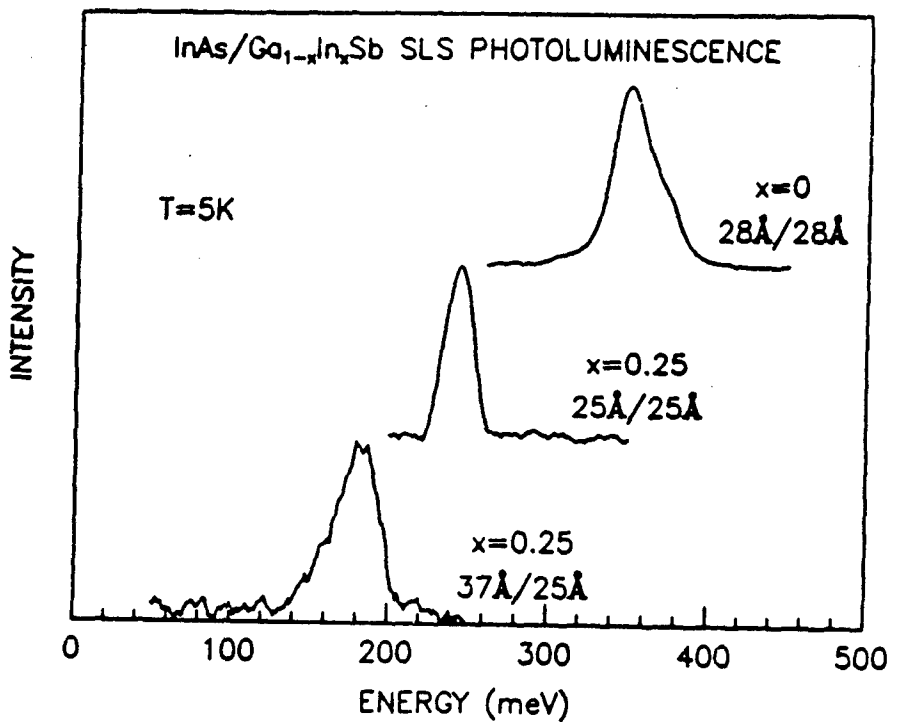

28Å/28Å InAs/GaSb X-RAY DIFFRACTION
INTENSITY
0
InAs
GaAs
-1
+1
+2
-3
-2
-5
50
60
70
TWO THETA (deg)


41Å/25Å InAs/Ga0.75In0.25 Sb X-RAY DIFFRACTION
INTENSITY
GaAs
0
GaSb
-1
+1
-2
+2
-4
-3
-6
50
60
70
TWO THETA (deg)

PHOTOLUMINESCENCE

HUGHES

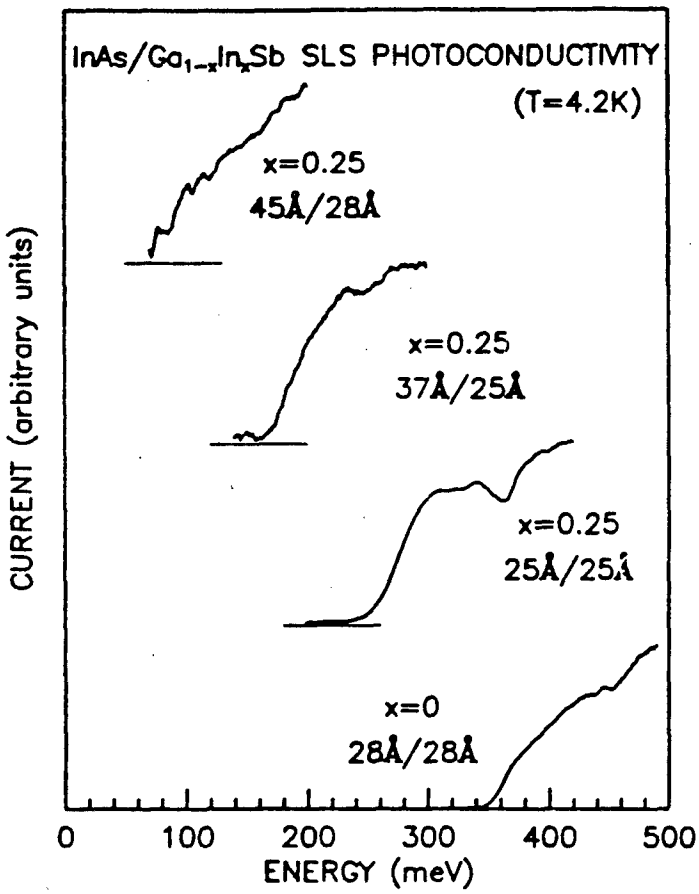
- OPTICAL EXCITATION
  - AlGaAs laser diode
  - Ar ion laser
  - 40 kHz modulation
- DETECTION OF LUMINESCENCE
  - Bomem Fourier Transform Infrared Spectrometer (FTIR)
  - lock-in amplifier
  - InSb or Si:As detector



PHOTOCONDUCTIVITY

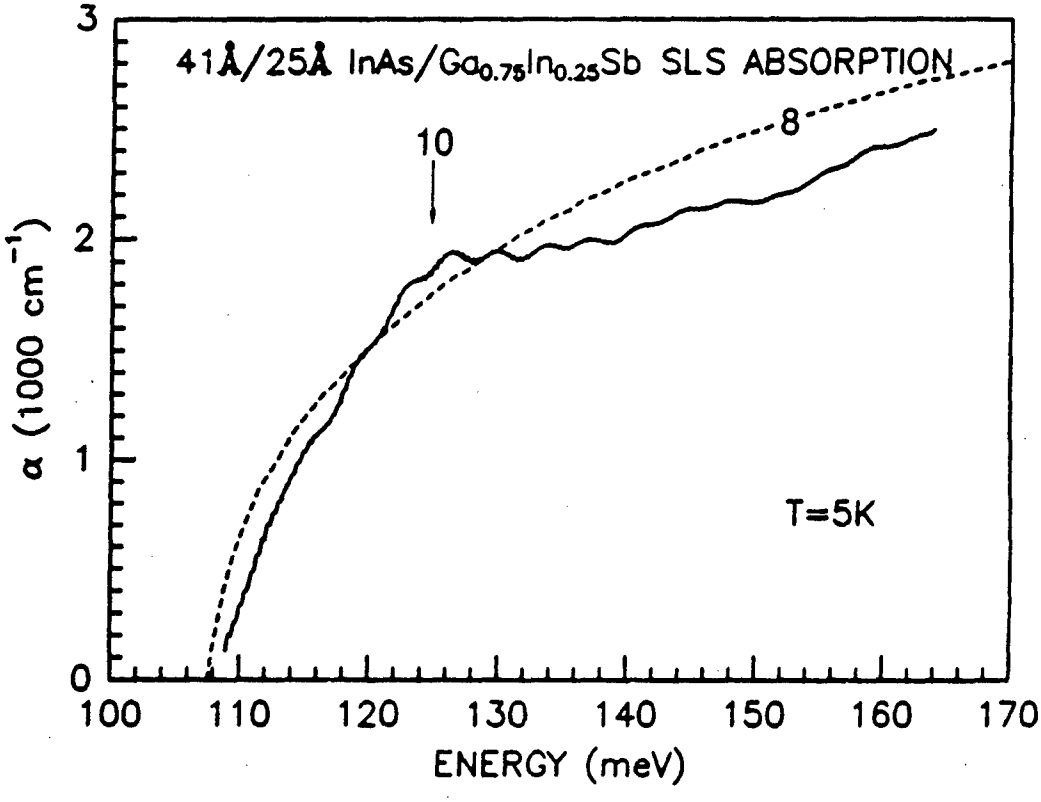
HUGHES

- SAMPLE PREPARATION
  - conventional photolithography
  - 60 x 160 μm mesas etched with Br_2:HBr:H_2O
  - Al contacts to mesas and etched surface
- MEASUREMENT
  - blackbody illumination from back (substrate) side of device
  - sample cooled over 5-300K range
  - sample used as detector in FTIR



LAYER THICKNESS (Å)				ENERGY GAP (meV)		
InAs	$Ga_{1-x}In_xSb_{1-y}As_y$	x	y	PL	PC	Theory
28	28	0	0.07	330±10	350±10	320
25	25	0.25	0.08	240±10	250±10	280
37	25	0.25	0.05	150±10	170±10	180
41	25	0.25	0	*	110±10	110
45	28	0.25	0	*	80±10	100

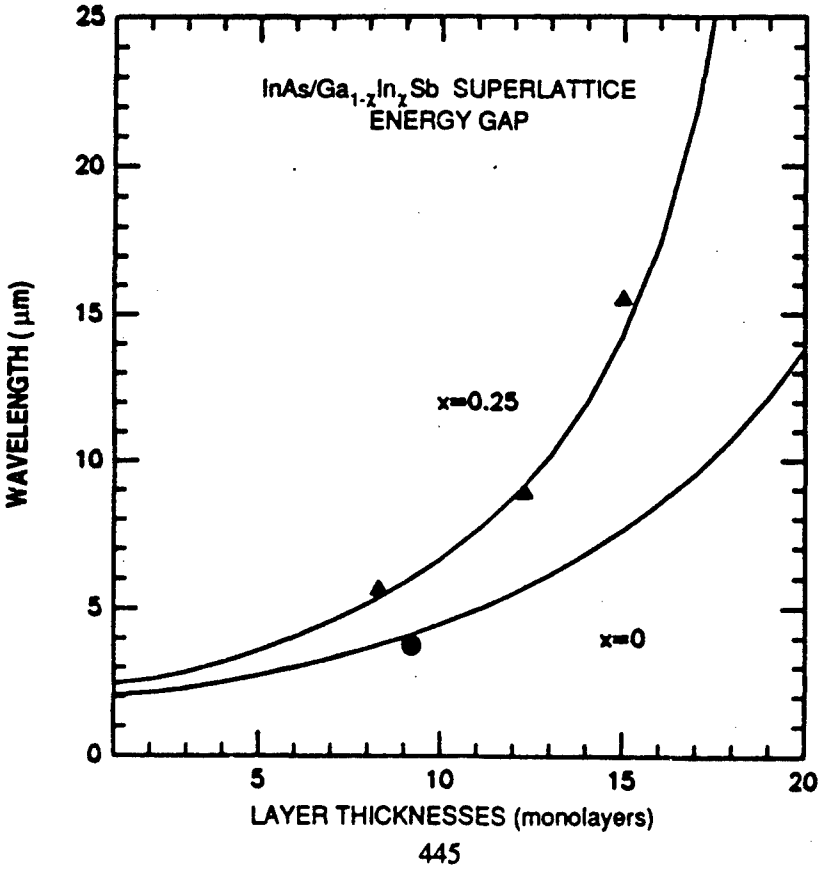
TABLE I. Comparison of energy band gaps derived from photoluminescence, photoconductivity, and theory for the $InAs/Ga_{1-x}In_xSb$ superlattices examined here.



InAs/$Ga_{1-\chi}In_{\chi}Sb$ SUPERLATTICES: CONCLUSIONS

HUGHES

- GROWTH & STRUCTURAL PROPERTIES
  - GaAs substrates
  - $x = 0, 0.25, 0.35$
  - no misfit dislocations, $10^9 cm^{-2}$ threading dislocations
  - best structure for $370 < T < 400°C$
- OPTICAL CHARACTERIZATION
  - infrared photoluminescence observed
  - photoconductive response beyond 15 μm
  - energy gaps shift with strain as predicted
  - thin layers (¡75 Å period) yield far-infrared energy gaps
  - 10 μm absorption comparable to bulk $Hg_{1-x}Cd_xTe$



N91
14408
UNCLAS

N91-14408

IR Detectors based on n-i-p-i Superlattices

P. Paul Ruden

Department of Electrical Engineering
University of Minnesota
Minneapolis, Minnesota 55455

It has been demonstrated that the internal electric fields present in n-i-p-i doped semiconductor superlattices give rise to interband photo absorption well below the bandgap of the host semiconductor material. In addition, the internal fields separate the photo generated electrons and holes resulting in large non-equilibrium charge carrier lifetimes and, consequently, in large photoconductive gain. Experimental results on GaAs n-i-p-i superlattices have confirmed these expectations for photon wavelengths in the near infrared ($\lambda < 1.5$ μm). For an extension of the wavelength range to the mid and far infrared, semiconductors with smaller bandgaps are more suitable than GaAs as n-i-p-i superlattice host materials. Strong candidate materials are InAs and InSb because of their favorable growth and doping properties.

In this paper the principles of operation of n-i-p-i photodetectors will be discussed. Special consideration is given to issues that are relevant to the performance of IR detectors such as noise, dark current, and surface effects. In addition, we will discuss a novel IR detector that promises to provide information about the spectral distribution of the infrared radiation emitted from an object and, consequently, about its temperature, independent of the distance between detector and object. This detector makes use of the possibility to modulate the internal electric fields of an n-i-p-i superlattice with an applied voltage. By this technique the spectral responsivity of the detector may be controlled electrically and some information about the shape of the emission spectrum may be obtained.

PRECEDING PAGE BLANK NOT FILMED

IR DETECTORS BASED ON DOPING SUPERLATTICES

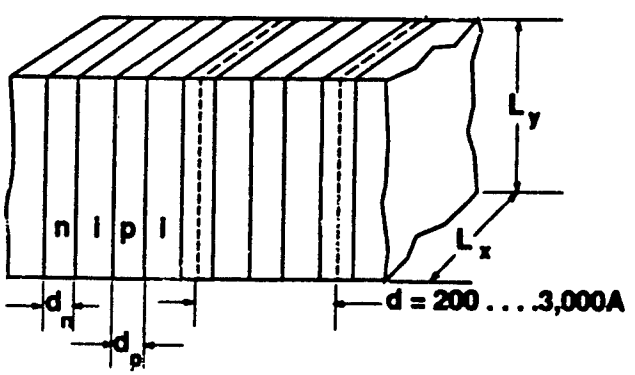
P. Paul Ruden

University of Minnesota
Department of Electrical Engineering

Outline

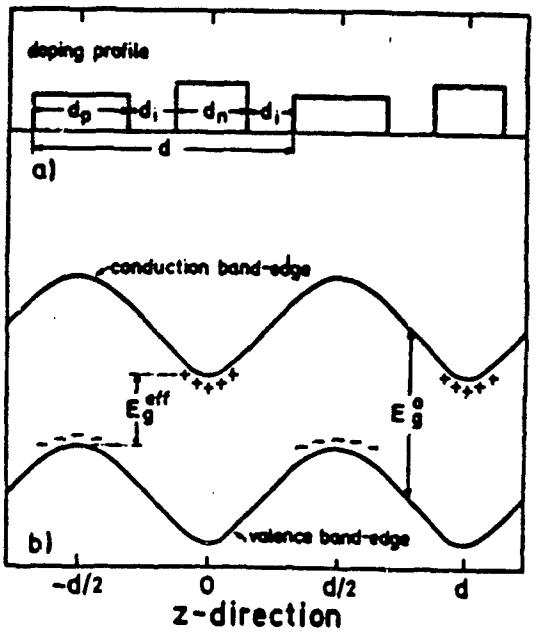
- Introduction, optical absorption in nipi SL
- Electroabsorption GaAs, InAs, InSb
- Noise in nipi detectors
- Spectrally agile detector
- Inhomogeneous excitation and surface effects
- Summary

Doping Superlattice (n-i-p-i)

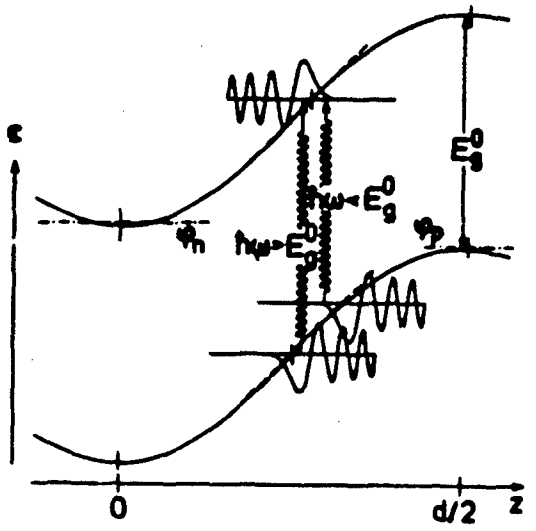


Materials: GaAs, AlGaAs, InP, GaP, InAs, InSb, InGaAs, PbTe, Si,...?

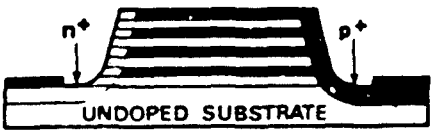
Schematic Doping Profile and Band Diagram of NIPI Superlattice

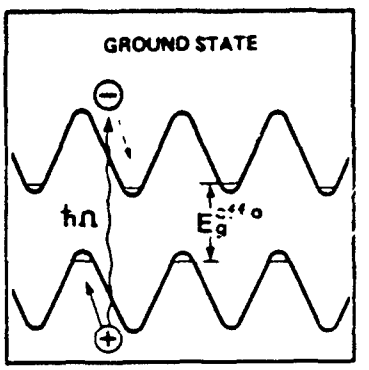


Photon Absorption in Doping Superlattice



DOPING SUPERLATTICE PHOTODETECTOR





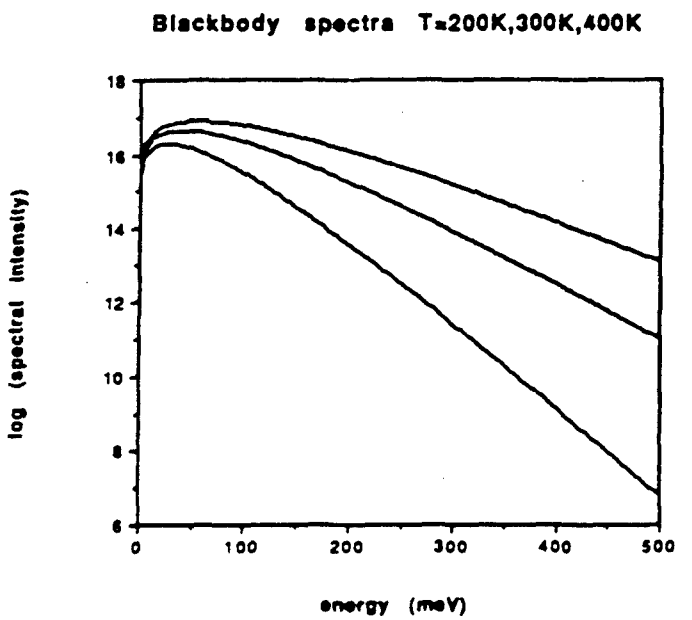
Two modes of operation:

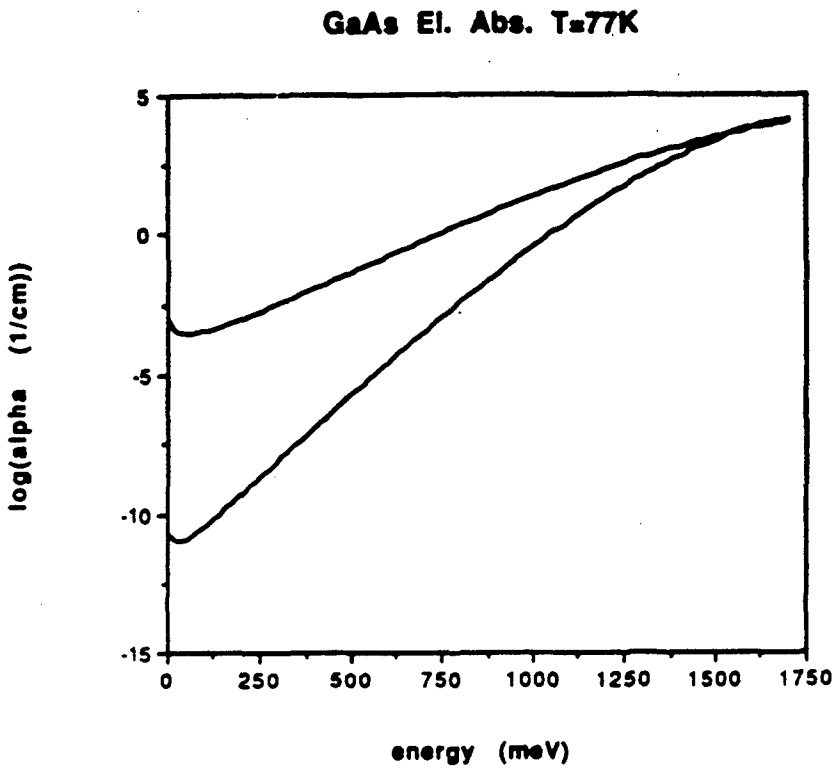
1) Photovoltaic mode:

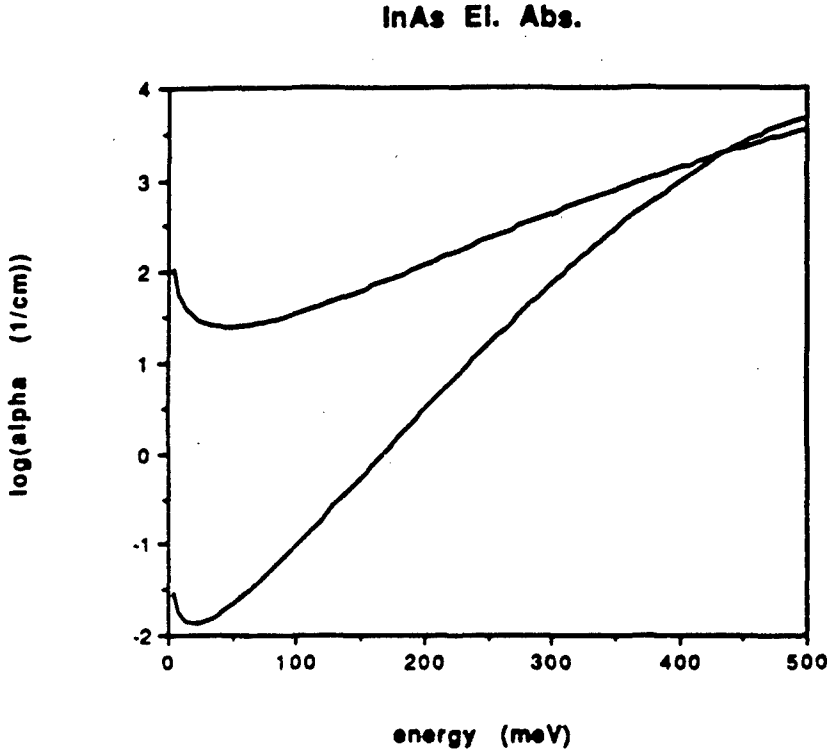
δI_{np}

2) Photoconductive mode:

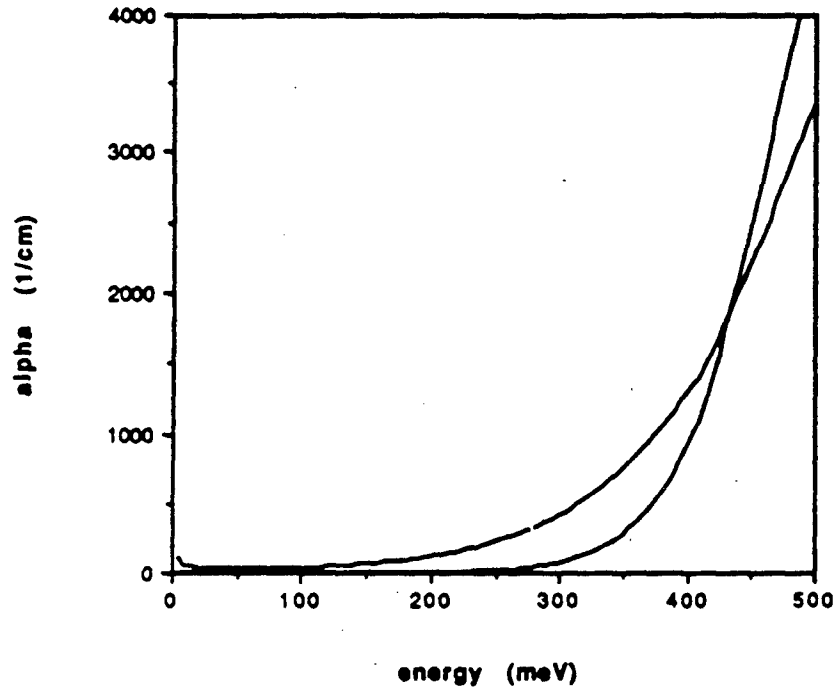
δI_{nn} or δI_{pp}



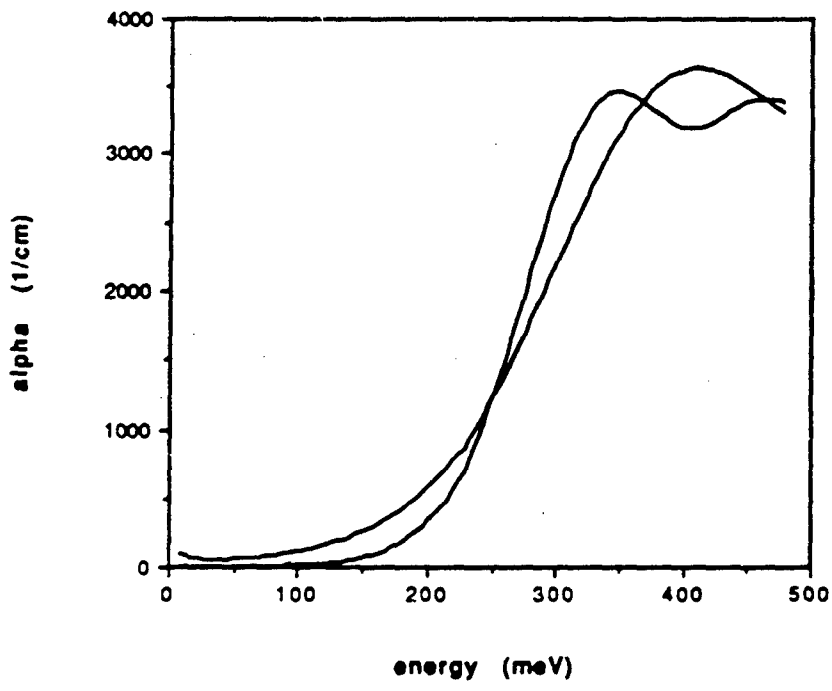

GaAs El. Abs. T=77K
log(alpha (1/cm))
5
0
-5
-10
-15
0
250
500
750
1000
1250
1500
1750
energy (meV)

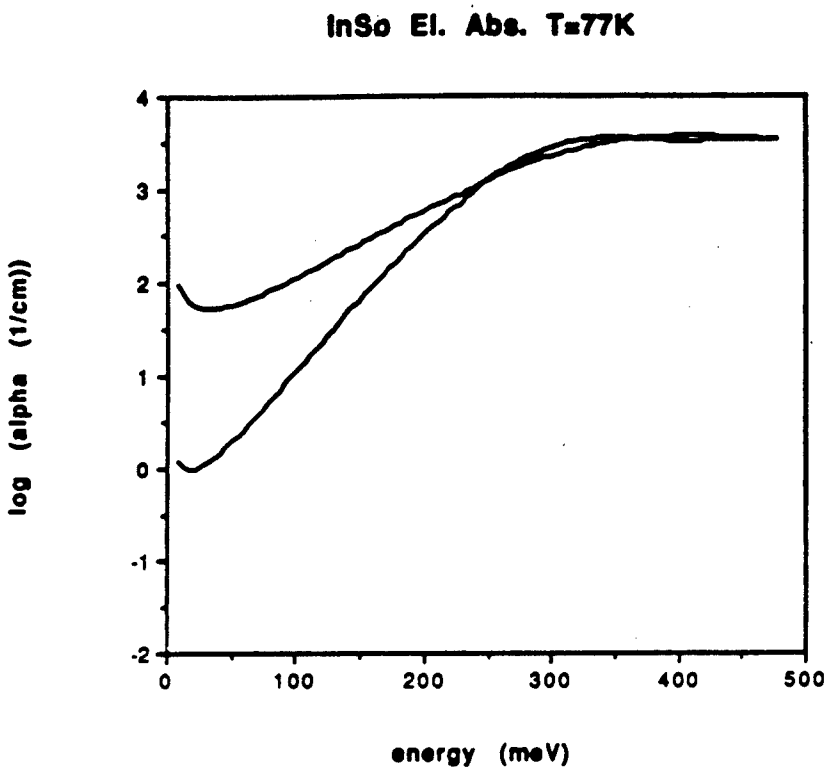

InAs El. Abs.
log(alpha (1/cm))
4
3
2
1
0
-1
-2
0
100
200
300
400
500
energy (meV)

InAs El. Abs.



InSb El. Abs. T=77K





Example

InSb nipi BLIP $n_D^{(2)} = 3.5\times10^{12}$ cm^{-2}

$d_i = 100$ A

$\rightarrow F_{bi}d_i \sim E_g^o$

$\hbar\omega_o = 108$ meV $\triangleq \lambda_o = 11.5$ μm , $T_B = 300$K

$\alpha(\hbar\omega_o) = 130$ cm^{-1}

$\bar{\alpha} = 51$ cm^{-1} with cut-off $\hbar\omega_c = 100$ meV $D^* = 2.6\times10^8 \sqrt{N_{SL}}$ cm $\sqrt{Hz}$ /W

$\bar{\alpha} = 107$ cm^{-1} without cut-off $D^* = 1.8\times10^8 \sqrt{N_{SL}}$ cm $\sqrt{Hz}$ /W

$N_{SL} = 1750 \rightarrow D^* = 1.1\times10^{10}$ cm $\sqrt{Hz}$ /W

compared to BLIP with $\eta = 1$ $\lambda_c = 11$ μm $D^* = 3.4\times10^{10}$ cm $\sqrt{Hz}$ /W

Noise Sources in nipi IR Detectors

Detectivity

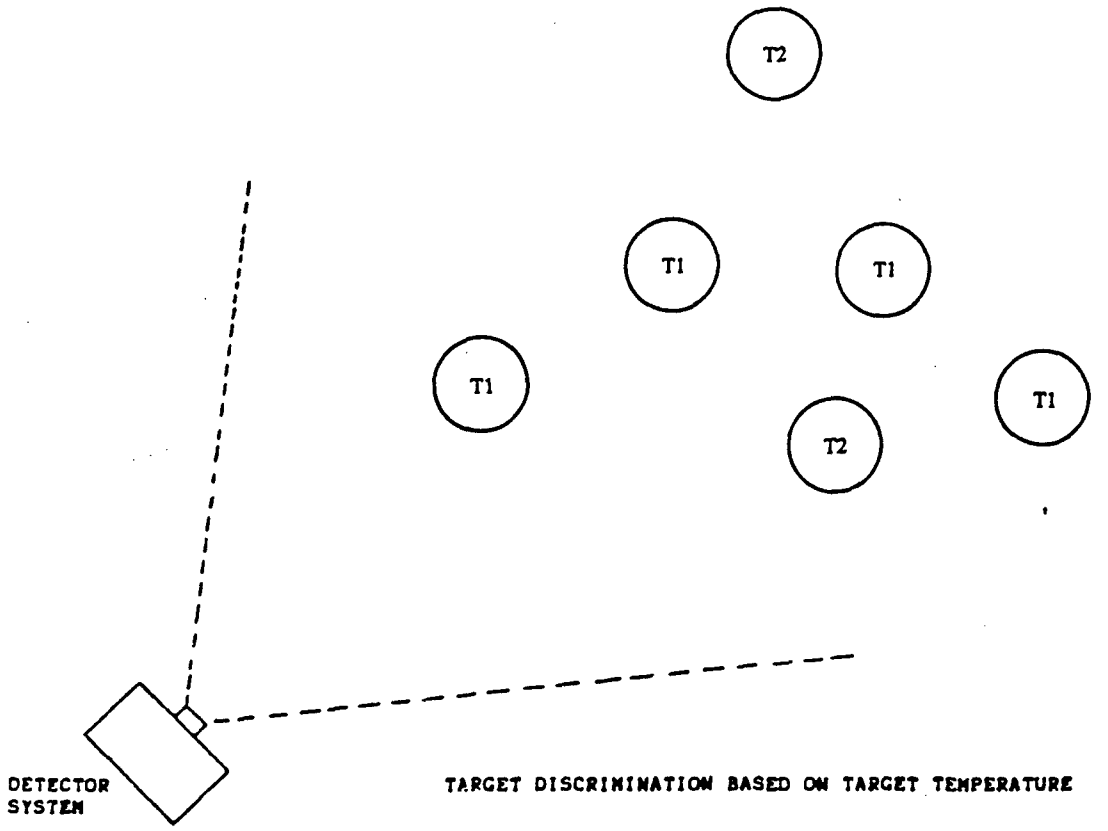
$$D^* = \sqrt{A}\,\frac{R}{I_{noise}}\,\sqrt{\Delta f}$$

Thermal g-r noise limited : $$D^* = \frac{1}{2h\omega}\,\frac{\alpha(\omega)d_i}{\sqrt{p^{(2)}}}\,\sqrt{\tau}\,\sqrt{N_{SL}}$$

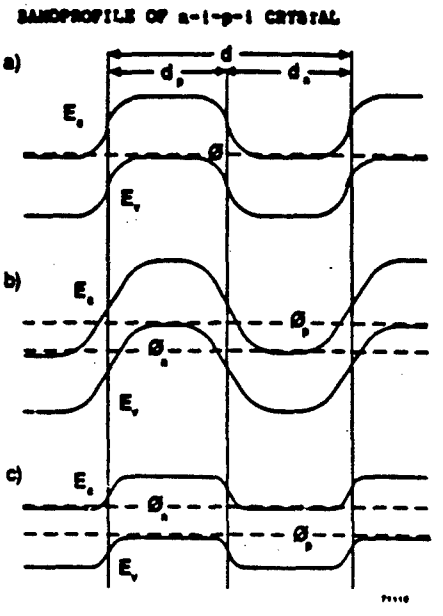
$\bar{\alpha}\, d_i\, \sigma_\rho T_B^3 < p^{(2)}/\tau$

Background g-r noise limited : $$D^* = \frac{1}{2h\omega}\,\frac{\alpha(\omega)}{(\bar{\alpha}\,\sigma_\rho T_B^3)^{1/2}}\,\sqrt{d_i}\,\sqrt{N_{SL}}$$

$\bar{\alpha}\, d_i\, \sigma_\rho T_B^3 > p^{(2)}/\tau$ $$\bar{\alpha} = \frac{\int dE\, \alpha(E) M_p(E,T_B)}{\sigma_\rho T_B^3}$$



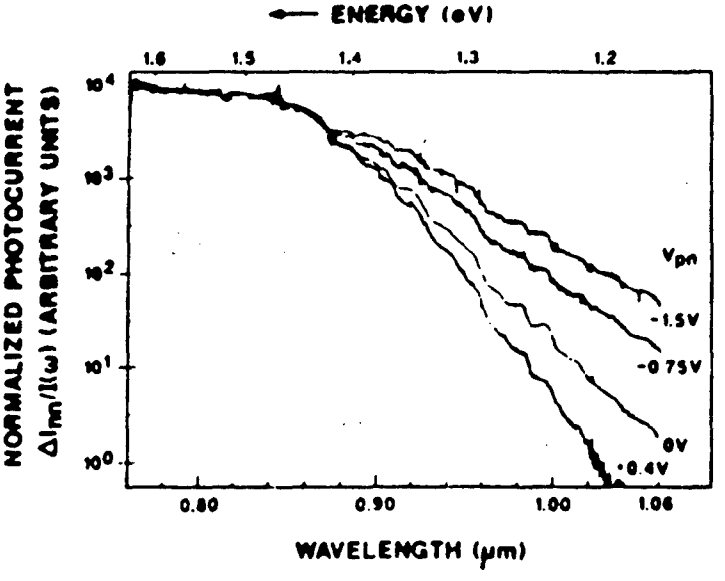
TARGET DISCRIMINATION BASED ON TARGET TEMPERATURE



a) Ground State

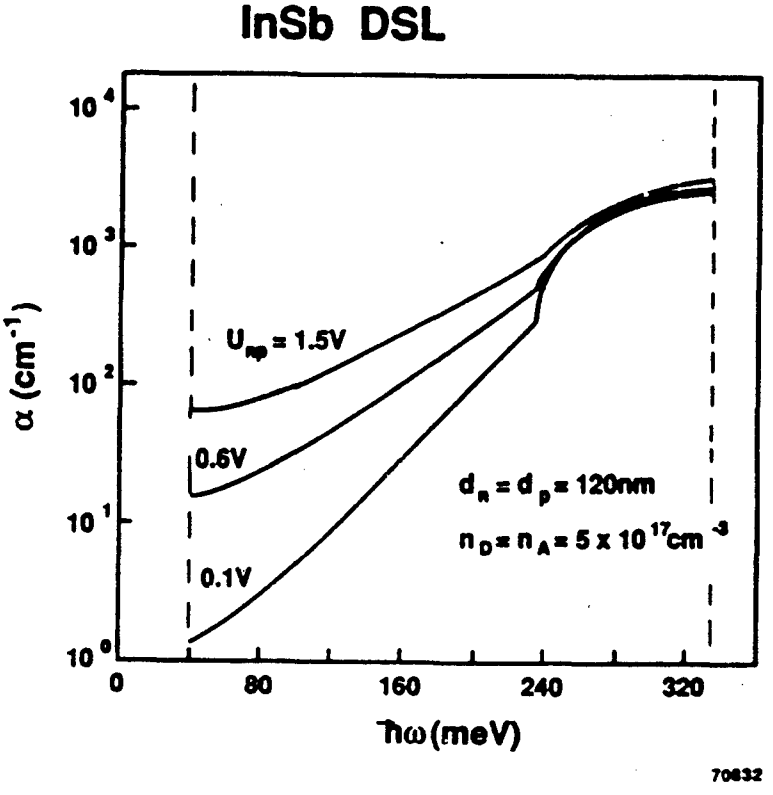
b) Reverse Bias U_{ap}

c) Forward Bias U_{ap}



C.J. Chang-Hasnain, et al. (1986)

ORIGINAL PAGE IS
OF POOR QUALITY



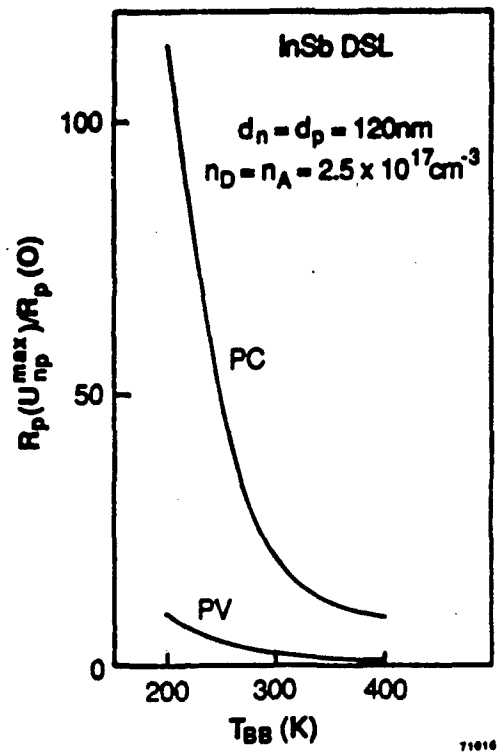
Spectrally Agile nipi Detector

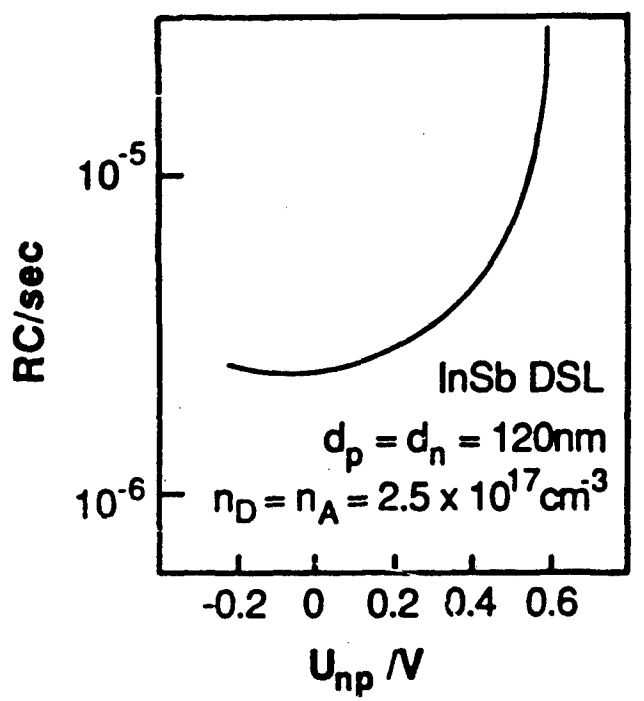
incident spectrum: $\phi_o M_p(E,T_T)$

$$I_{ph}(U_{np}) = \frac{q\mu\tau(U_{np})V_a}{L}\,\phi_o \int dE\, \eta(U_{np},E)\, M_p(E,T_T)$$

$$= \frac{q\mu\tau(U_{np})Va}{L}\,\phi_o \bar{\eta}\,(U_{np},T_T)$$

$$\frac{I_{ph}(U_{np1})}{I_{ph}(U_{np2})} = \frac{\tau(U_{np1})}{\tau(U_{np2})}\,\frac{\bar{\eta}(U_{np1},T_T)}{\bar{\eta}(U_{np2},T_T)} \quad \rightarrow \quad T_T$$

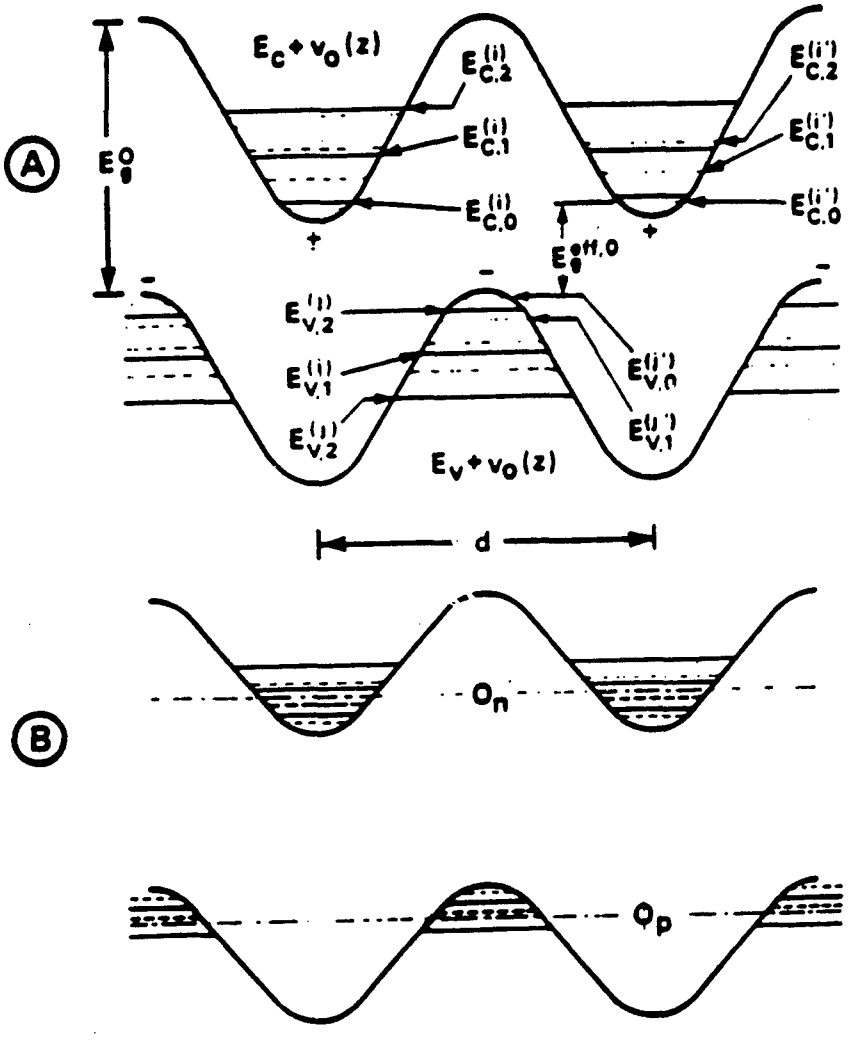

InSb DSL
$d_n = d_p = 120nm$
$n_D = n_A = 2.5 \times 10^{17} cm^{-3}$
100
50
0
$R_p(U_{np}^{max})/R_p$ (O)
PC
PV
200
300
400
T_{BB} (K)
71016


10^{-5}
10^{-6}
RC/sec
InSb DSL
$d_p = d_n = 120nm$
$n_D = n_A = 2.5 \times 10^{17} cm^{-3}$
-0.2
0
0.2
0.4
0.6
U_{np} /V
71017

Schematic Band Diagram
for Doping Superlattice

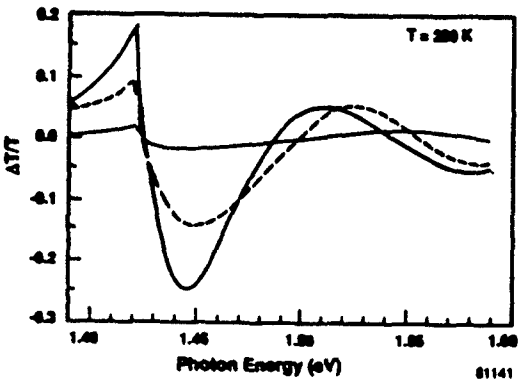
A: Ground state

B: Excited state

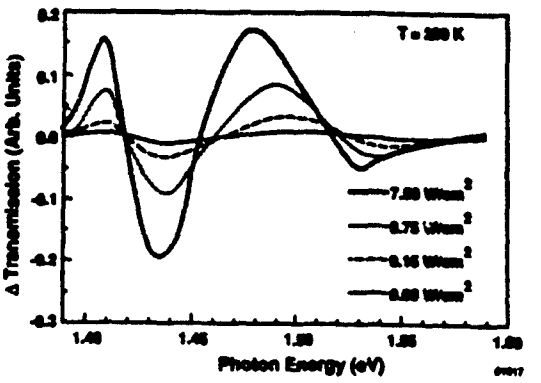


Comparison of Theoretical and Experimental Results for Doping SL Transmission Nonlinearity

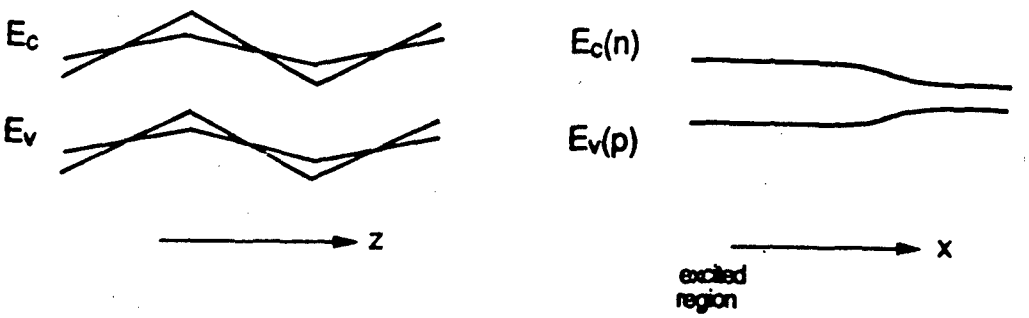
Theoretical Calculation of Optically Modulated Transmission
(GaAs Doping SL for Different Excitation Levels)



Optically Modulated Transmission
(GaAs Doping SL for Different Excitation Levels)



Lateral Charge Carrier Distribution

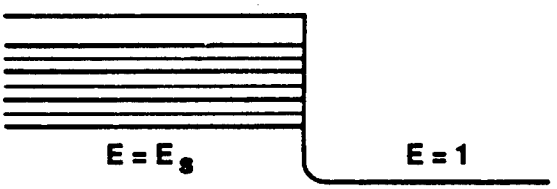


$$j_n \alpha [(V(n^{(2)})-V_o) + kT] (dn^{(2)}/dx)$$

$$R(n^{(2)}) \alpha n^{(2)}p^{(2)} \exp(-V(n^{(2)})/kT)$$

$$n^{(2)}(x) \approx n_o^{(2)} \exp(-x/L(n^{(2)}))$$

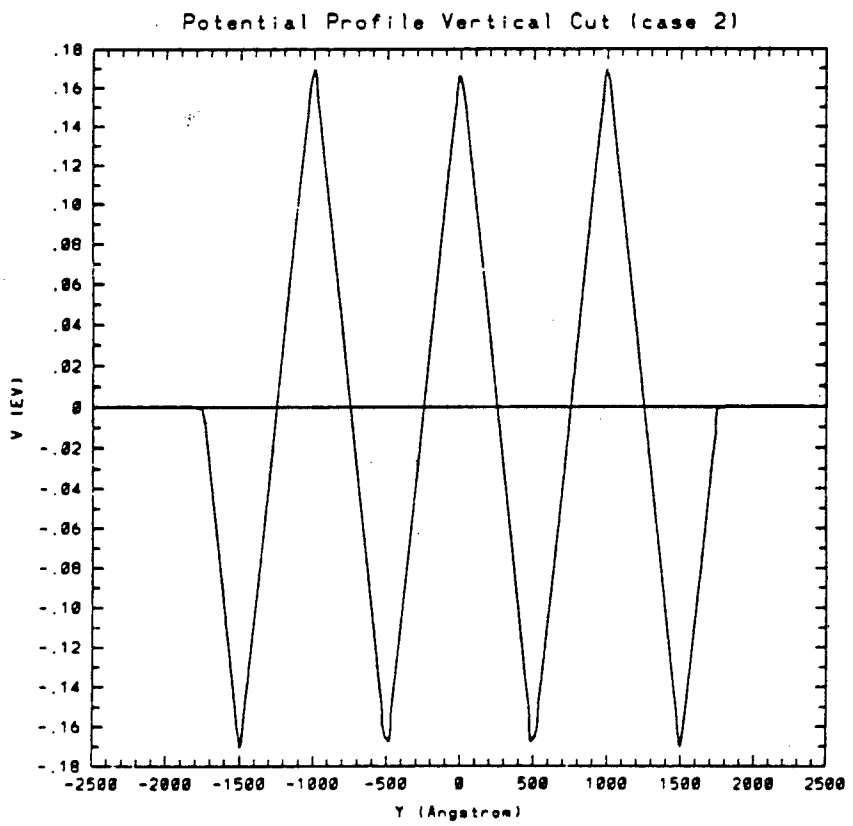
Potential At Surface

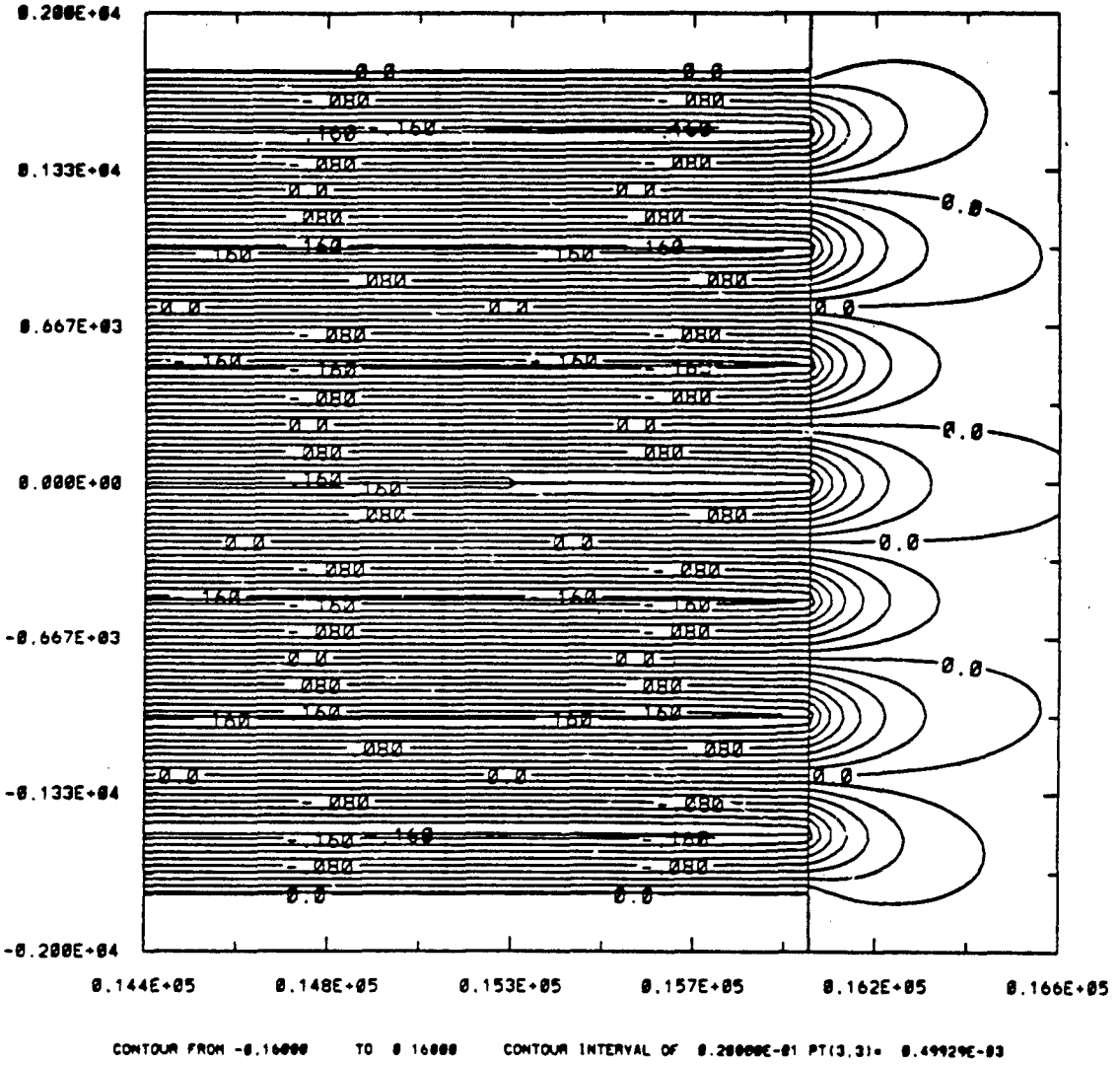


Surface Recombination May Reduce Effective Lifetime
→ Reduce Photoconductive Gain

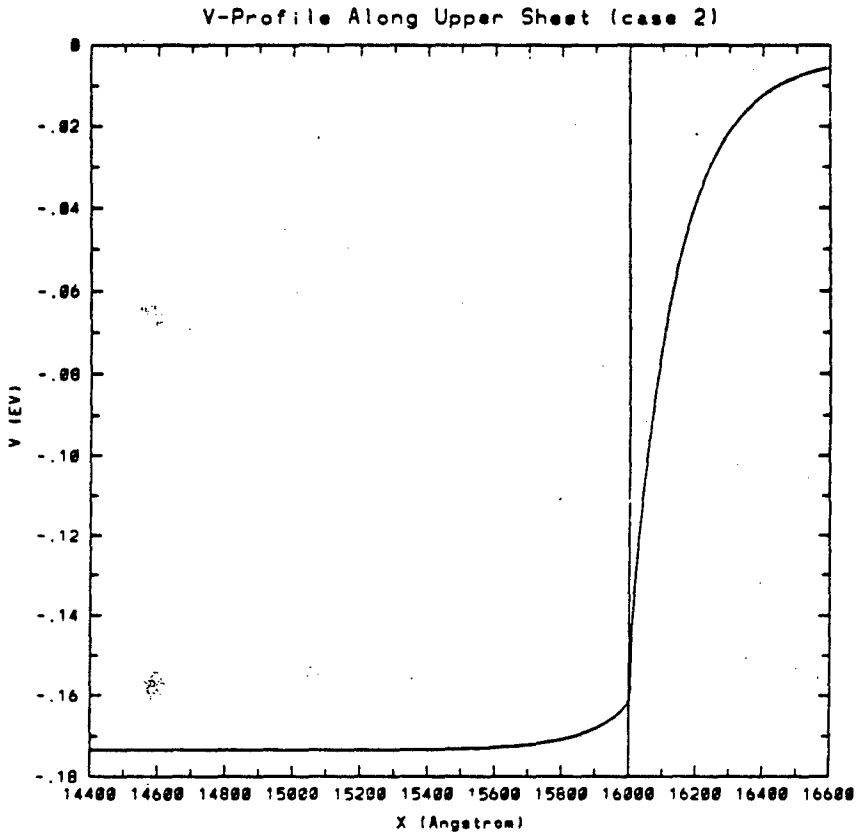
Surface Potential Barrier

$$\sigma V_s \sim \frac{2V_o}{2E_s}$$





ORIGINAL PAGE IS
OF POOR QUALITY



Summary

- IR detection with nipi SL based on InAs or InSb is feasible.
- Detector performance can be competitive.
- Spectrally agile detectors may be practical.
- Non-uniform excitation, su face and contact effects are critical.
- Optical nonlinearity can be useful.

N91-14409
UNCLAS

N91-14409

InAs/GaAs and InAs Doping Superlattices*

F.J. Grunthaner, B.R. Hancock and J. Maserjian
Center for Space Microelectronics Technology
Jet Propulsion Laboratory
California Institute of Technology
Pasadena, California 91109

The extension of the optical response of narrow band gap III-V semiconductors into the LWIR regime for high sensitivity sensor applications is a challenging problem. Recent advances in nipi doped GaAs superlattices, lattice mismatched epitaxy and the heteroepitaxial growth of III-V compound semiconductors on silicon substrates offer a number of opportunities. In this paper, we describe two different device approaches based on the MBE growth of superlattice materials which are directed to LWIR focal plane array technology. The first of these uses nipi superlattices fabricated in bulk InAs which has been grown on either GaAs or Si substrates. The second is based on the growth of a new pseudomorphic tetragonal phase of InAs on GaAs to create a semimetal/semiconductor superlattice material.

Considerable progress has been made in recent years in the design, fabrication, and characterization of nipi superlattices in GaAs. The key property of the nipi doping superlattice is the incorporation of alternating planes of dopant atoms in the z-direction as the crystal is grown. This results in an undulating or sawtooth potential superimposed on the existing conduction and valence band electronic structure. At sufficiently high doping levels, the effective gap of the host crystal can be reduced to that of a semimetal. Because of the spatial separation of electron and hole wave functions, the anticipated quantum efficiency of a doping superlattice detector is relatively low. Recent calculations have shown that by shortening the nipi period and by using high doping levels one can achieve practical values for the absorption coefficient at extended wavelengths beyond that corresponding to the bulk bandgap. These calculations indicate that the low effective mass and the intrinsic gap of InAs can be used to create a high quantum efficiency (QE) detector with tailored response over the range 3 - 17 μm. In this device concept, we propose to grow high quality InAs epitaxially on Si substrates, and fabricate InAs nipi photodetectors on this substrate. Although the lattice mismatch between InAs and Si is slightly greater than 11%, heteroepitaxy of high structural quality material has already been achieved. In the final implementation of the concept, the Si substrate would be the backside of a fully processed multiplexer and carriers collected in the InAs would be injected into the Si device for areal image processing.

In this paper, we report the growth of high performance InAs pin photodiode arrays on GaAs substrates. These structures were grown at JPL using RHEED controlled MBE

*This work was sponsored by NASA

growth techniques, and were processed into photodiode arrays by Cincinnati Electronics. Performance results show quantum efficiencies, dark currents, reverse bias breakdown, and component-to-component variation in characteristics equal to or better than the corresponding performance of CE's benchmark material which is based on InAs bulk wafers. The device yield was greater than 85%. Esaki InAs tunnel diodes grown by MBE at a doping level of mid 10^{18} cm^{-3} on GaAs (100) substrates show a peak to valley ratio of 14:1 at 77 K. This compares to values of 7 to 10 obtained for InAs epi on InAs bulk substrates at 4 K. These results demonstrate the high electronic quality of heteroepitaxial InAs grown on GaAs. We will also present cross-sectional TEM data and RHEED surface lattice constant measurements to show defect control in InAs growth on GaAs and silicon substrates. IR absorption spectral measurements are currently ongoing.

In the second device concept, we propose to grow superlattices with the pseudomorphic tetragonal high pressure phase of InAs interleaved with GaAs to create a semimetal/semiconductor system. Recent data characterizing high pressure phases of InAs have shown the existence of a β-Sn and a rock salt crystal structure, both of which are semimetals. As demonstrated in the HgTe/CdTe system, choosing different thicknesses of the component layers of the superlattice should give a material with selectable small bandgaps in the range from 0.7 to 0.070 eV. This would correspond to cutoff wavelengths of up to 20 μm. This material will then be fabricated into photovoltaic arrays on GaAs substrates. In the mature concept, the detector structure could be grown on a preprocessed GaAs wafer which could include CCD structures or other control functions for intelligent sensors.

Using specialized MBE growth techniques specifically engineered for lattice mismatched epitaxy, we have succeeded in growing InAs films on GaAs substrates which are lattice matched to GaAs in the growth plane. This represents a 7.4% compression in the x and y axes of the InAs film on the 100 surface. RHEED surface lattice constant data are consistent with a tetragonal symmetry for the InAs layer. Recent data characterizing high pressure phases of InAs have shown that the β-Sn crystal structure exists for pressures greater than 7 GPa. The calculated equivalent hydrostatic pressure exerted on the pseudomorphic InAs phase which has been grown lattice matched to GaAs by MBE is greater than 70 GPa. The in plane lattice constant on the 100 surface of the high pressure phase of InAs is lattice matched to GaAs within 1.2%.

In this paper, we will report recent results on the growth and characterization of pseudomorphic InAs grown on GaAs (100) surfaces. In a systematic study of growth by RHEED, electronic structure and composition by x-ray photoemission, coordination geometry by EELFS, and defect structure by Transmission Electron Microscopy, we demonstrate the existence of new phases of InAs in single quantum structures.

InAs/GaAs and InAs Doping Superlattices

F. J. Grunthaner, B. Hancock, and J. Maserjian,

Center for Space Microelectronics Technology
Jet Propulsion Laboratory
California Institute of Technology
Pasadena, California 91109

Collaborators: K. Delgadillo, J. K. Liu*, A. Ksendzov, F. D. Schowengerdt#, M. E. Greiner^

* TRW, Los Angeles, California
Colorado School of Mines, Golden, Colorado
^Cincinnati Electronics Corporation, Cincinnati, Ohio

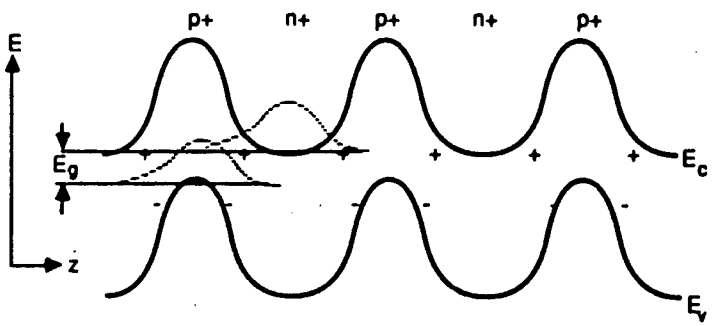
Outline

- Objectives
- Doping Superlattices
- InAs (bulk) / GaAs Material Growth
- Tunnel Diode Results
- InAs / GaAs Strained-Layer Epitaxy
- Future Directions
- Summary

Objectives

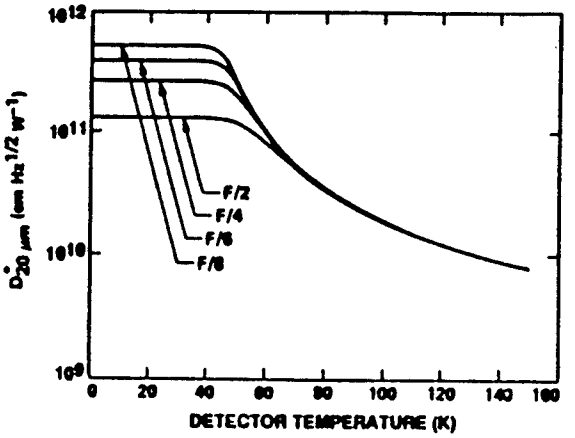
- Investigate new quantum engineering device concepts with III-V MBE for LWIR detectors.
- Achieve near background limited performance at 16μm and at operating temperatures above 65K.
- Demonstrate detector arrays integrated with multiplexers.
- Develop with industry LWIR (6-17μm) focal plane arrays (64x64).
- Explore Doping Superlattice Concepts.
- Apply Strained Layer Epitaxy To LWIR Detector Problem.

Doping Superlattice Concept



Band Diagram of Hole-Impeded-Doping-Superlattice (HIDS)

D* Estimates



Calculated detectivity of *nipi* detector at 20 μm wavelength. F is optics F-number. Other assumed parameters are described in the text.

nipi Design Parameters

Table I. Determination of P

Material	ϵ/ϵ_0	m_e/m	m_{hh}/m	E_g°(77 K) (eV)	N_D, N_A (cm^{-3})	N_s (cm^{-2})	a (Å)	b (Å)	P
InSb	17.7	0.015	0.40	0.23	—	2×10^{12}	—	113	1.2×10^{-2}
					6×10^{16}	—	122	—	1.1×10^{-2}
InAs	14.6	0.023	0.40	0.41	—	2×10^{12}	—	166	2.3×10^{-3}
					—	5×10^{12}	—	66	1.4×10^{-2}
					6×10^{16}	—	149	—	1.2×10^{-4}
					3×10^{19}	—	67	—	1.7×10^{-2}
GaAs	13.1	0.067	0.48	1.51	—	2×10^{12}	—	547	4.8×10^{-49}
					6×10^{16}	—	270	—	3.5×10^{-23}

Hole- Impeded Doping Superlattice

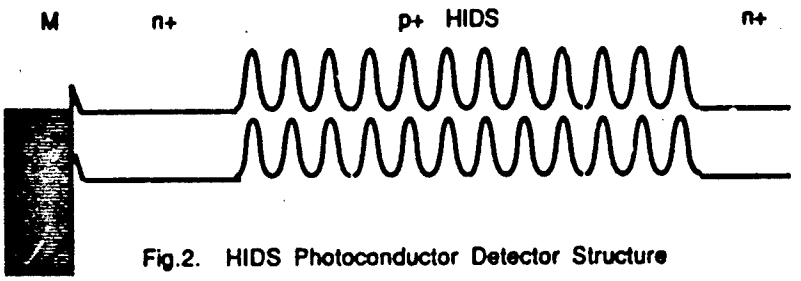
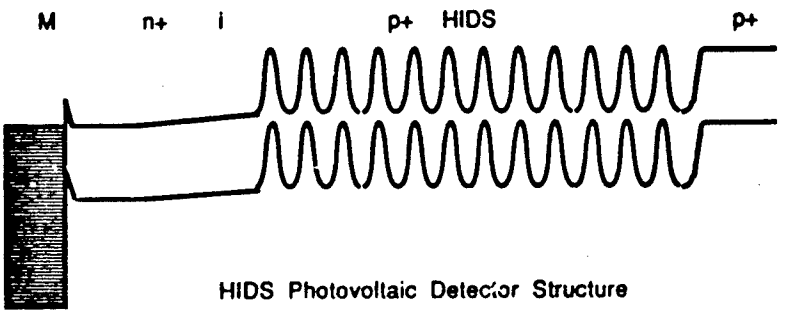
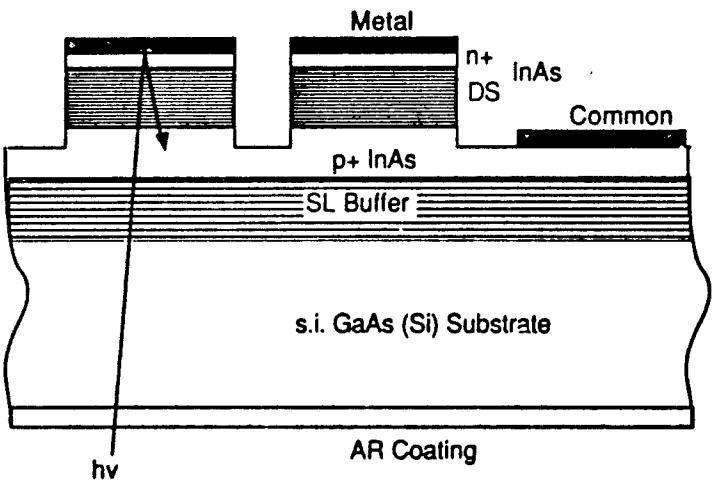
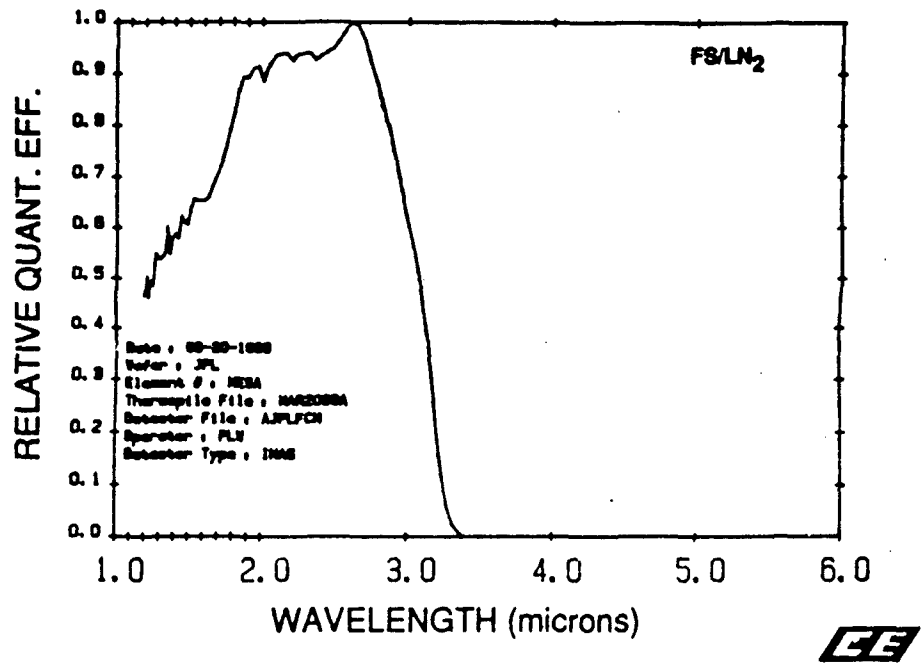


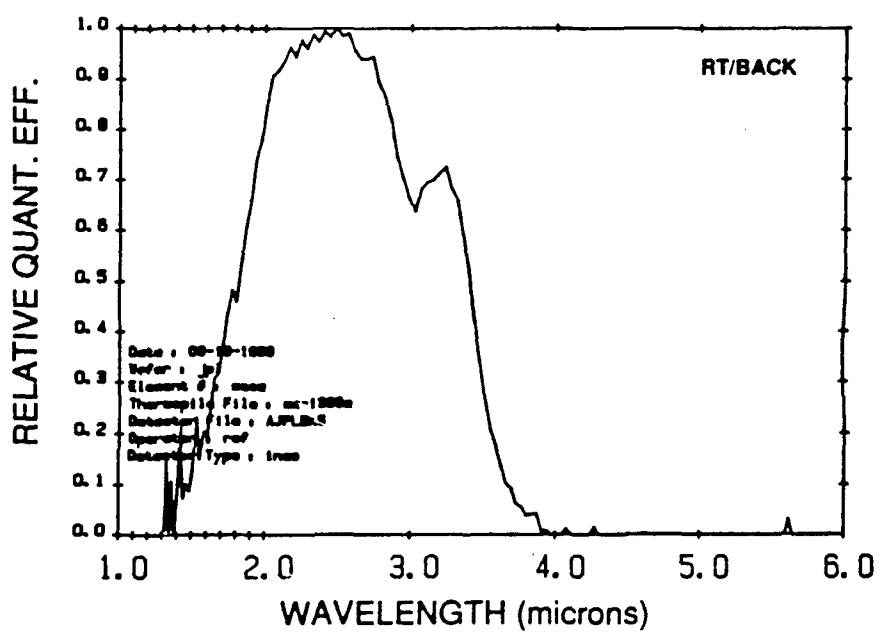
Fig.2. HIDS Photoconductor Detector Structure

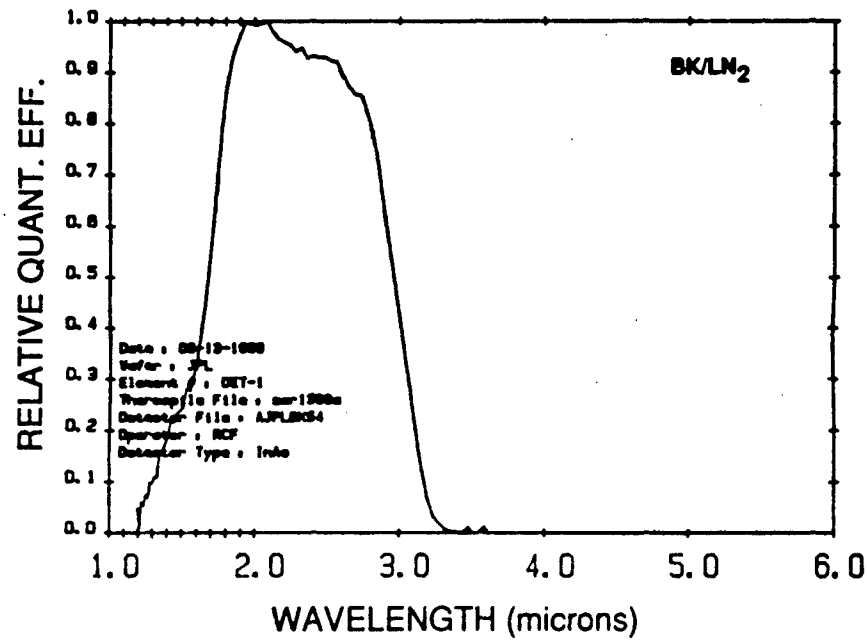


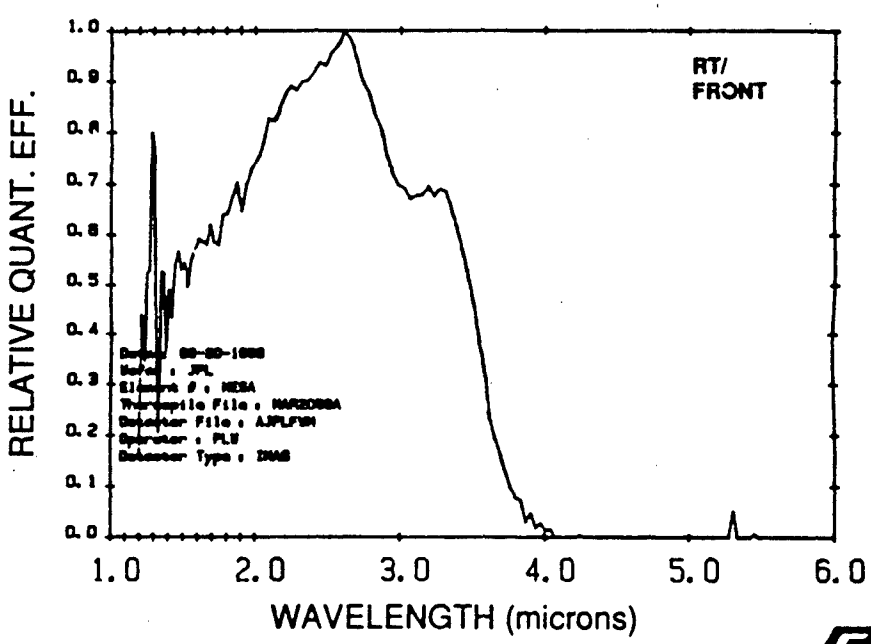
HIDS Photovoltaic Detector Structure




FS/LN2
RELATIVE QUANT. EFF.
1.0
0.9
0.8
0.7
0.6
0.5
0.4
0.3
0.2
0.1
0.0
1.0
2.0
3.0
4.0
5.0
6.0
WAVELENGTH (microns)


RT/BACK
RELATIVE QUANT. EFF.
1.0
0.9
0.8
0.7
0.6
0.5
0.4
0.3
0.2
0.1
0.0
1.0
2.0
3.0
4.0
5.0
6.0
WAVELENGTH (microns)

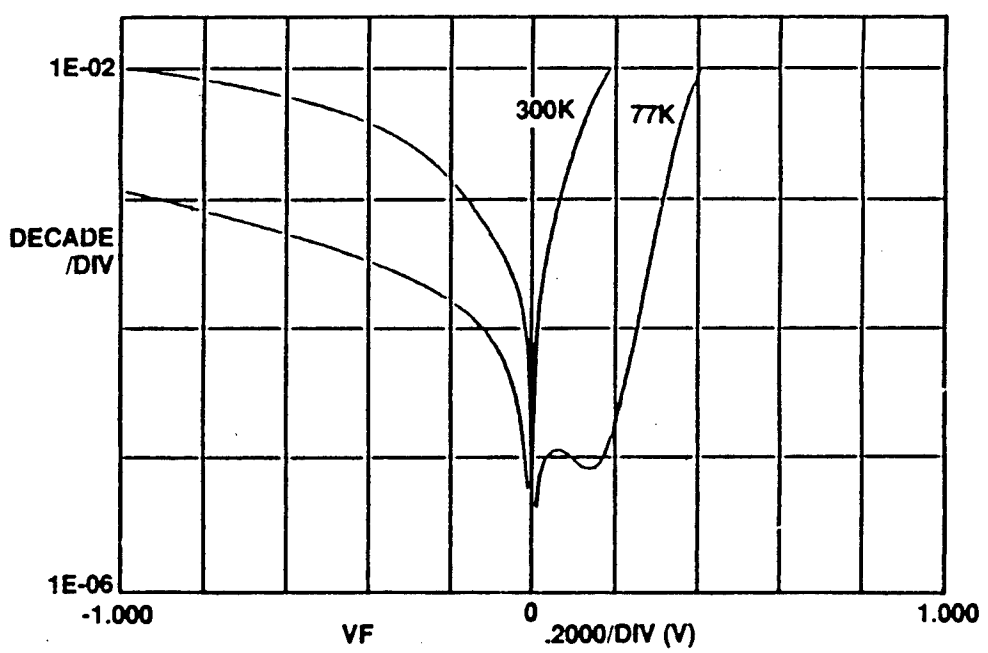

RELATIVE QUANT. EFF.
1.0
0.9
0.8
0.7
0.6
0.5
0.4
0.3
0.2
0.1
0.0
BK/LN2
1.0
2.0
3.0
4.0
5.0
6.0
WAVELENGTH (microns)

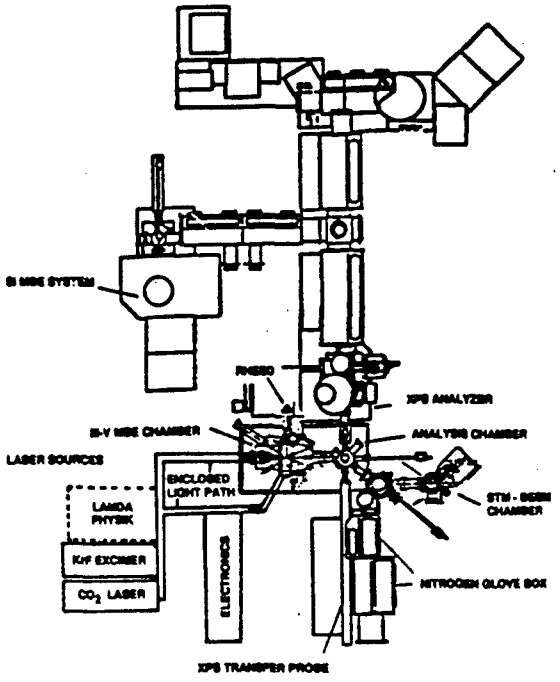

RELATIVE QUANT. EFF.
1.0
0.9
0.8
0.7
0.6
0.5
0.4
0.3
0.2
0.1
0.0
RT/
FRONT
1.0
2.0
3.0
4.0
5.0
6.0
WAVELENGTH (microns)

p/n Diode Result Summary

- 1.5 - 3.0 μm response, high η (70% at 77K, 20% at 298K)
- Low dark current --good R0A
- Compares with best bulk InAs
- Higher yield (85%), uniformity
- Transparent GaAs substrate
  --backside illumination for arrays
- Compatible with MUX integration
  --monolithic InAs/GaAs or hybrid

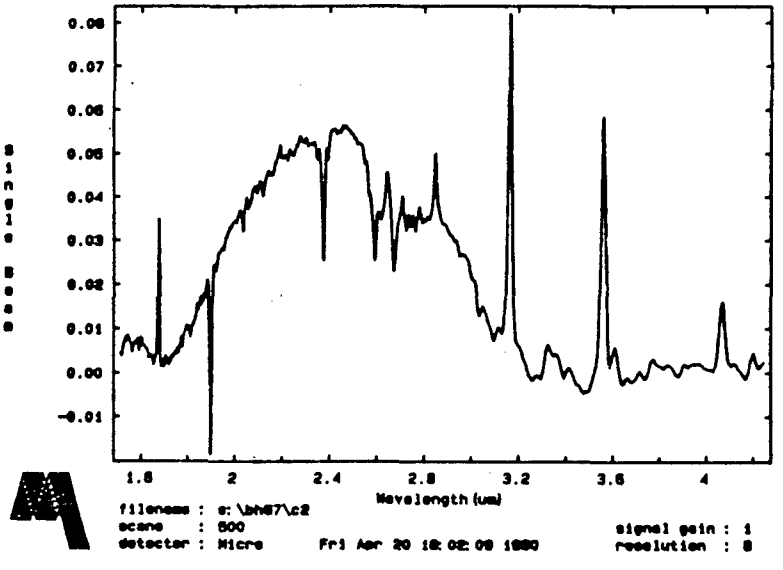
Electrical Properties of InAs on GaAs



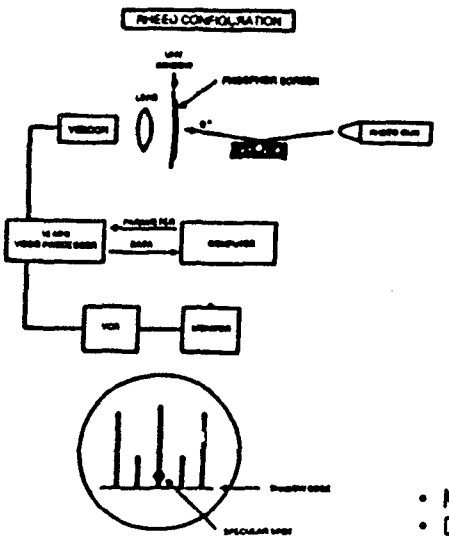


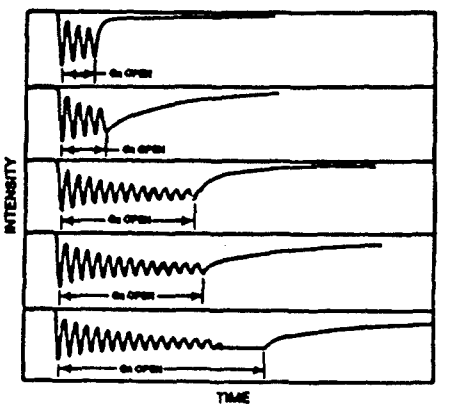
Schematic drawing of the in vacuo growth and characterization facilities. The lower left hand portion shows the laser sources; the pre-insertion sample preparation glove boxes are shown on the lower right; the analysis chamber and the hemispherical XPS analyzer are shown in ascending order

InAs pn structure photocurrent at 77 K



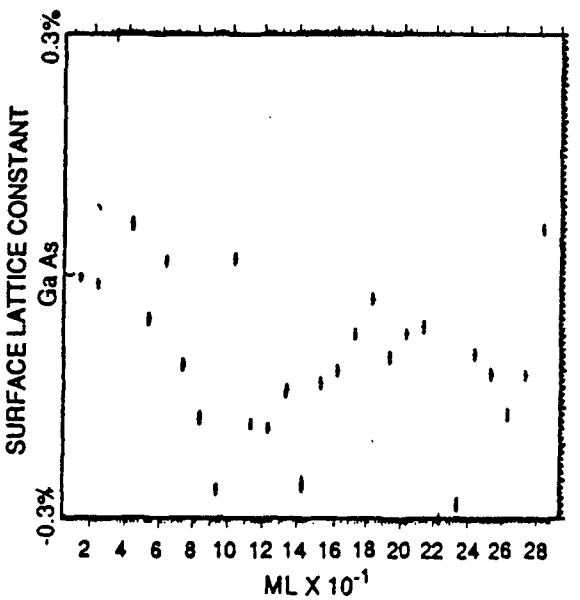
InAs on GaAs RHEED

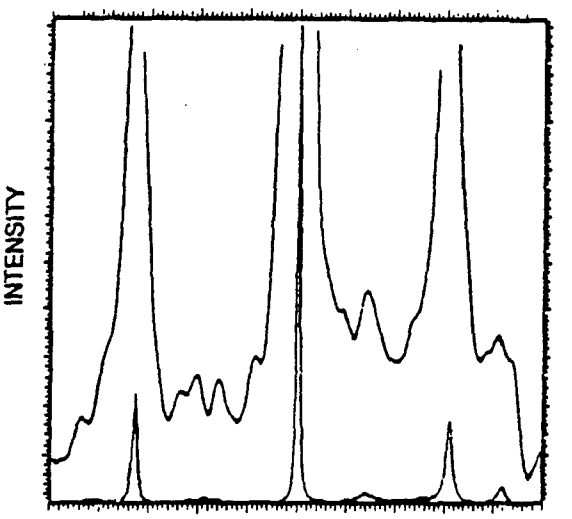




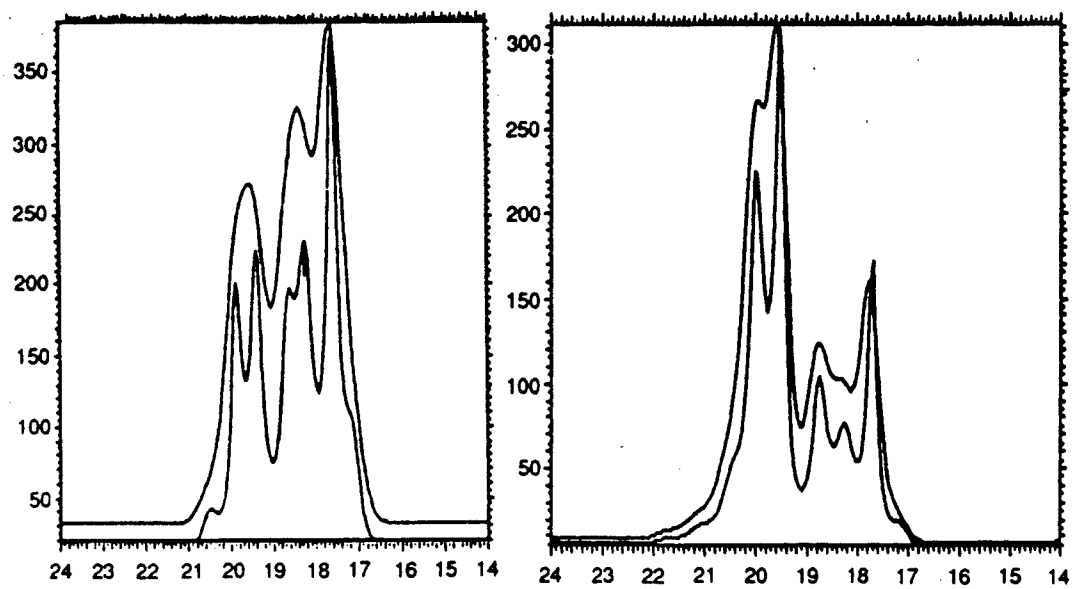
- MEASURE GROWTH RATE TO 0.01 ML
- DETERMINE FILM/SURFACE QUALITY
- FOLLOW AND CONTROL SURFACE DYNAMICS

RHEED Surface Lattice Constant

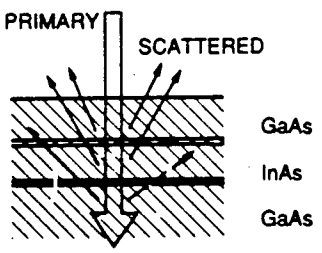


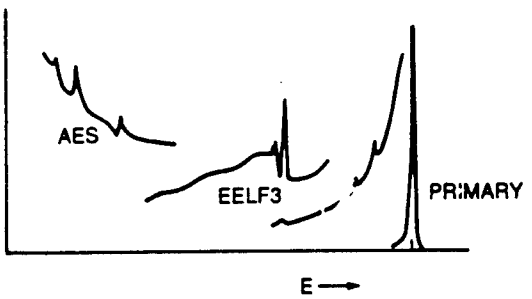


High Resolution XPS Data for InAs Quantum Well on GaAs

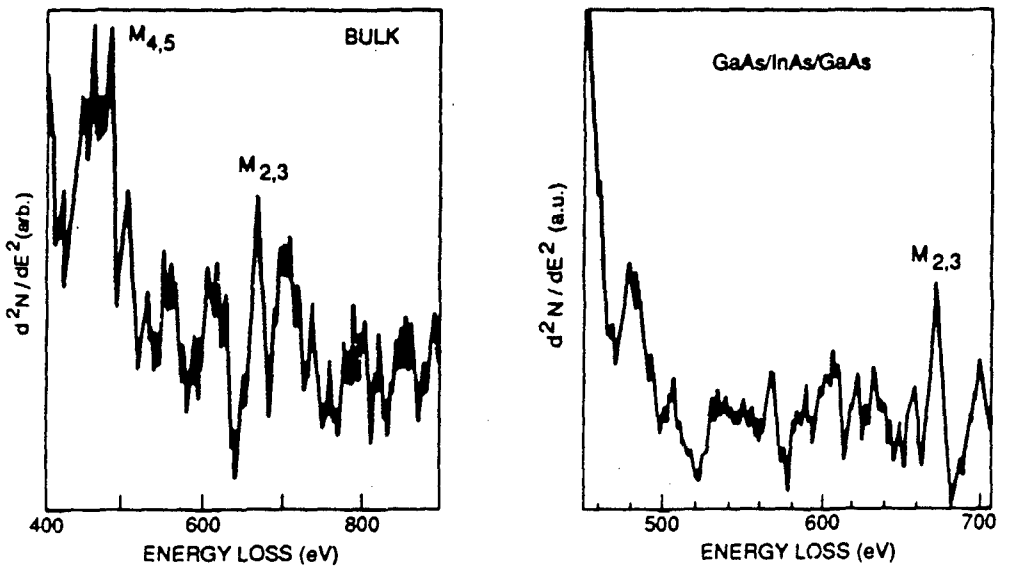


REFLECTED-ELECTRON ANALOG OF EXAFS

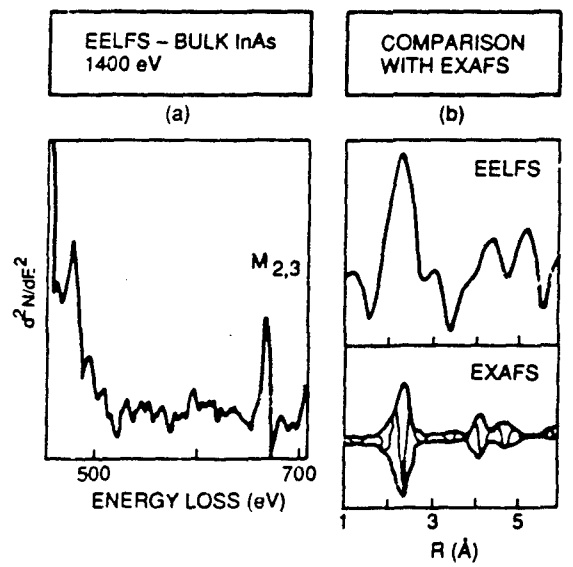




EELFS Spectrum

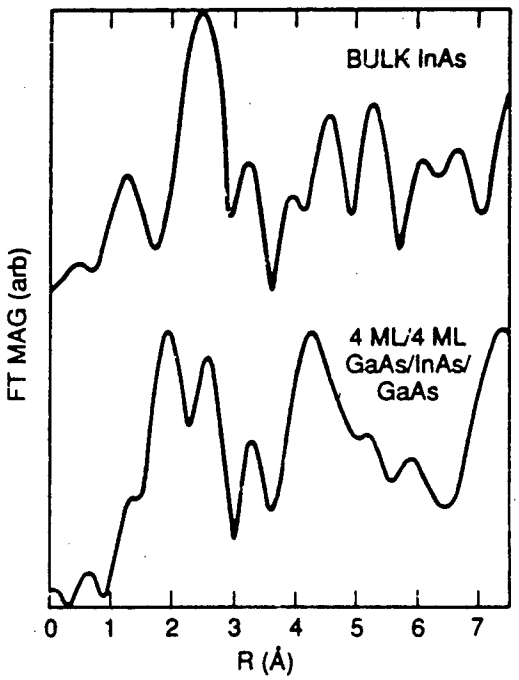


Radial Distribution Function For Bulk InAs



SUMMARY OF EELFS RESULTS
ON BULK InAs STANDARD:
R_{NN} = 2.40 ± 0.04 Å

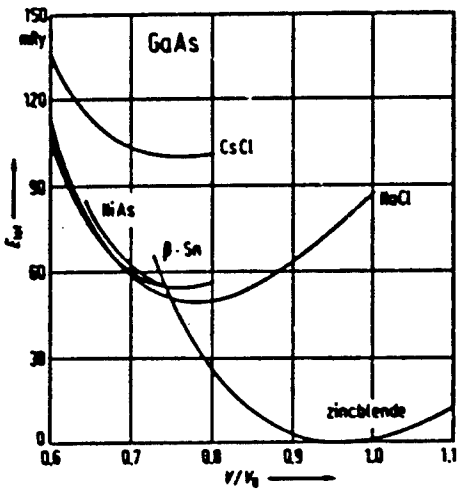
EELFS Distribution Function for 4 ml InAs QW



EELFS Result Summary

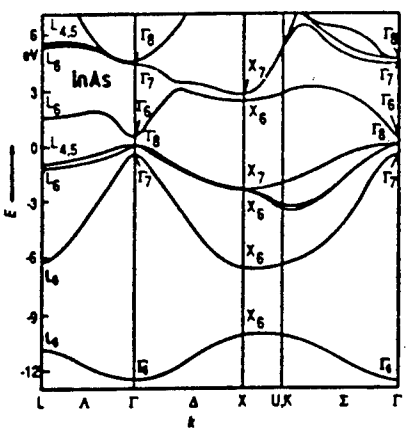
- Bulk Data Agrees with EXAFS Results
- Uncapped Strained Layers Show One First Nearest Neighbor Distance
- Capped Quantum Wells Give Two Nearest Neighbor Distances with 0.32 Å Difference
- Distances in ß-Sn Phase 0.15 Å

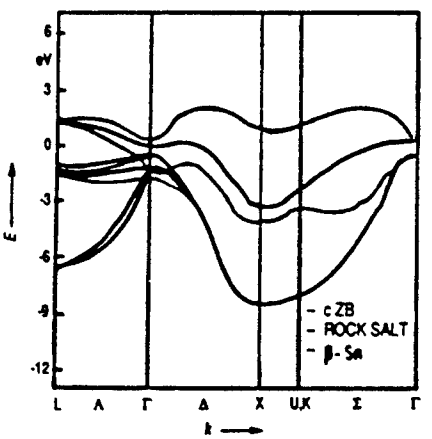
High Pressure Bulk Phases



GaAs. Calculated total energy per molecule vs. reduced volume (volume relative to experimental equilibrium volume) for five possible structures [83F].

Band Structure of High Pressure Phases





Conclusions

- High Quality InAs grown on GaAs Substrates
- Epitaxial Approach Compatible with Si Substrates
- nipi Concept Requires High Doping Level - Delta Doping Experiments Under Way
- Demonstrated First Structural Results Suggesting Tetragonal Phase of InAs
- Optical Response and Characterization

SESSION IX: New Materials Systems

IX-1 InAsSbBi, A Direct Band-Gap, III-V, LWIR Material
G.B. Stringfellow, University of Utah

IX-2 AlSb/InAs/AlSb Quantum Wells
H. Kroemer, University of California, Santa Barbara

N91
14410
UNCLAS

N91-14410

InAsSbBi, A Direct Band-gap, III-V, LWIR Material

G. B. Stringfellow
Dept. of Materials Science and Engineering, University of Utah
Salt Lake City, Utah 84112

Colin E. Jones
Santa Barbara Focalplane
Goleta, CA 93117
and

John Frodsham
Space Systems Engineering
Logan, Utah 84321

ABSTRACT

There has been extensive progress in the last twenty years in the growth of device quality III-V mixed alloys. Most of this work has centered around the wider band-gap alloys like AlGaAs and InP. In the last several years some of this effort has been extended to the narrower band-gap InAsSb system. This ternary has a direct band gap ranging from 145meV for $InAs_{(0.35)}Sb_{(0.65)}$ to 415meV for InAs with the other end point being at 235meV for InSb. It is possible to lower the band gap even further by adding bismuth. Bismuth is a large atom and its equilibrium solubility is estimated to be only 0.02 % in InAs and 2 % in InSb. Several attempts at adding 1 to 2 % Bi to III-V alloys by LPE or MBE have shown poor quality material with phase separations and precipitates.

In the last several years Dr. Stringfellow's group at the University of Utah has reported success in incorporating over 3 % Bi in InAs and 1.5 % in InAsSb using OMVPE growth techniques. For InAs the lattice constant increase is linear with $a=6.058+0.966x$ ($InAs_{(1-x)}Bi_{(x)}$), and a decrease in band gap energy of $dEg / dx = -55meV$ / at % Bi. (1) Extrapolating this to the ternary minimum band gap at $InAs_{(0.35)}Sb_{(0.65)}$ an addition of 1 to 2 % Bi should drop the band gap to the 0.1 to 0.05eV range (10 to 20 microns). These alloys are direct band gap semiconductors making them candidates for far IR detectors. The end points InAs and InSb are used extensively as MWIR detectors now.

The current status of the InAsSbBi alloys is that good crystal morphology and X-Ray diffraction data has been obtained for up to 3.4 % Bi. The Bi is metastable at these concentrations but the OMVPE grown material has been able to withstand the 400 C growth temperature for several hours without phase separation.

PRECEDING PAGE BLANK NOT FILMED

The electrical evaluation of the material has only just started. Hall data on OMVPE InSb has shown an n-type mobility of greater than 20,000 cm2 / V-sec at 200 K and carrier concentrations in the low E14 range. The ability of these alloys to show luminescence implies reasonable electrical quality over the range of alloy studied. (2) Both luminescence and transmission have been used to determine the change in band gap with Bi concentration. Some increase in the luminescence band width is seen with increasing Bi suggesting some compositional variation. Alloys have been grown near the InAs end with up to 30 % Sb. InSb has also been grown by OMVPE but the low band gap region has not yet been explored. At present there is no optical detector data on these alloys.

This effort is to continue with Dr. Stringfellow's group at the University of Utah growing material and with Santa Barbara Focalplane extending the material characterization and starting the processing of test detectors and arrays.

REFERENCES

1. "Organometallic Vapor Phase Epitaxial Growth and Characterization of InAsBi and InAsSbBi", K. Y. Ma, Z. M. Fang, D.H. Jaw, R. M. Cohen and G. B. Stringfellow, Appl. Phys. Lett. 55(23), 2420 (1989).

2. "Photoluminescence of InAsBi and InAsSbBi Grown by Organometallic Vapor Phase Epitaxy", Z. M. Fang, K. Y. Ma, R. M. Cohen, and G. B. Stringfellow, To be Published, J. Applied Phys. (1990).

InAsSbBi, A DIRECT BAND-GAP, III-V, LWIR MATERIAL

G.B. Stringfellow
University of Utah

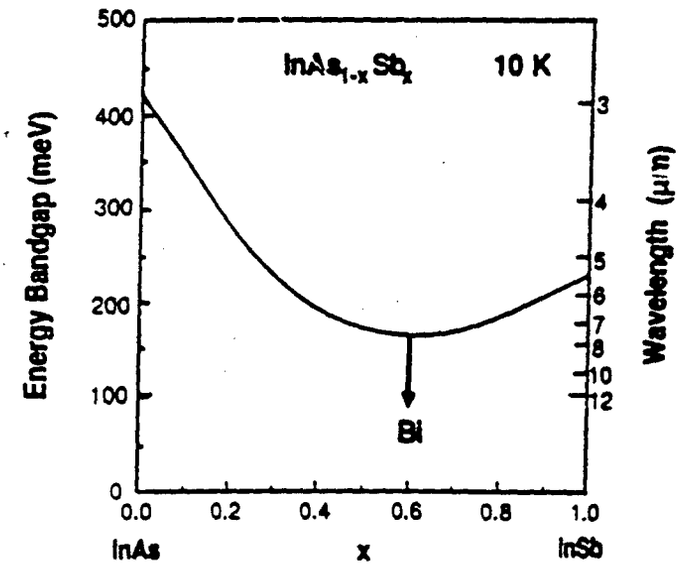
Colin E. Jones
Santa Barbara Focalplane

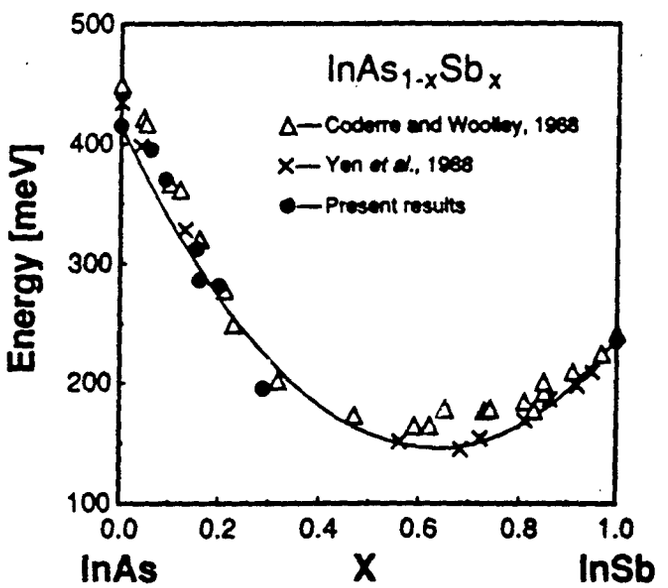
John Frodsham
Space Systems Engineering

REASONS FOR INTEREST IN InAsSbBi

1. DIRECT BAND-GAP SEMICONDUCTOR
2. GAP TUNABLE FROM <0.05eV TO 0.415eV
3. EXTENSION OF CURRENT OMVPE III-V MATERIALS GROWTH TECHNOLOGY PRODUCING DEVICES IN GaAs, AlGaAs, InP .....

Energy Bandgap vs. Composition x





- **SOLUBILITY OF Bi IS LOW**

  2.1% IN InSb, 0.02% IN InAs

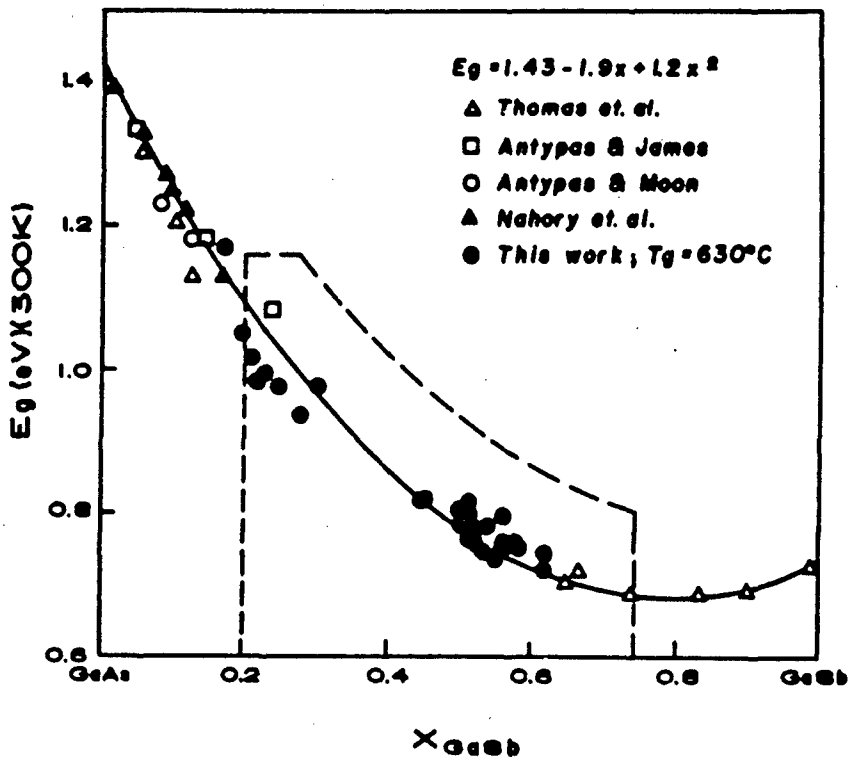
- **OMVPE GROWTH HAS BEEN ABLE**

  TO GROW METASTABLE COMPOSITIONS

  OF MANY ALLOYS AND OF Bi IN InAsSb

METASTABLE III/V ALLOYS GROWN BY OMVPE

Alloy	T_c(°C)	Range of Immiscibility	Reference
GaAsSb	750	0.2-0.8 (600°C)	Cherng et al (1984) Univ of Utah
GaInAsSb	1467	90% of Phase Field (600°C)	Cherng et al(1986) Univ of Utah
InPSb	1046	0.03-0.98(460°C)	Jou et al (1988) Univ of Utah
GaPSb	1723	0.01-0.99(540°C)	Jou et al (1988) Univ of Utah

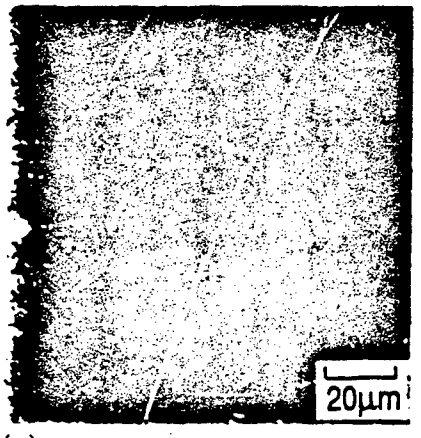


SANTA BARBARA FOCALPLANE

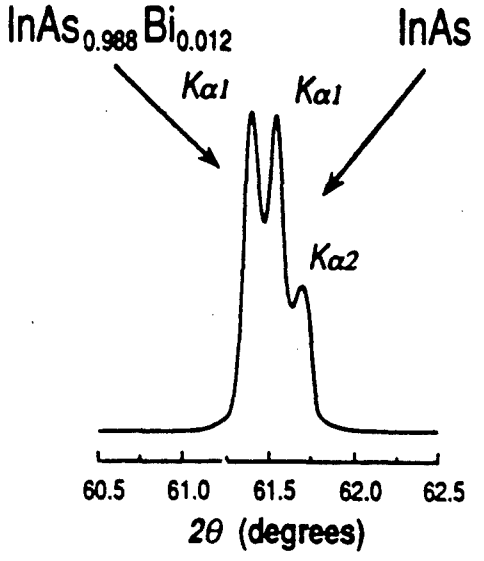
A NUMBER OF GROWTHS HAVE BEEN MADE FOR

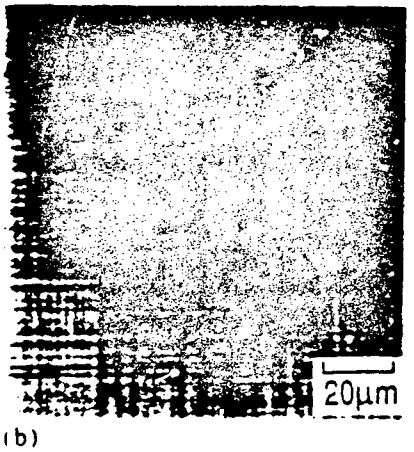
InAsBi AND InAsSbBi

TO UP TO 3% Bi AND 30% Sb

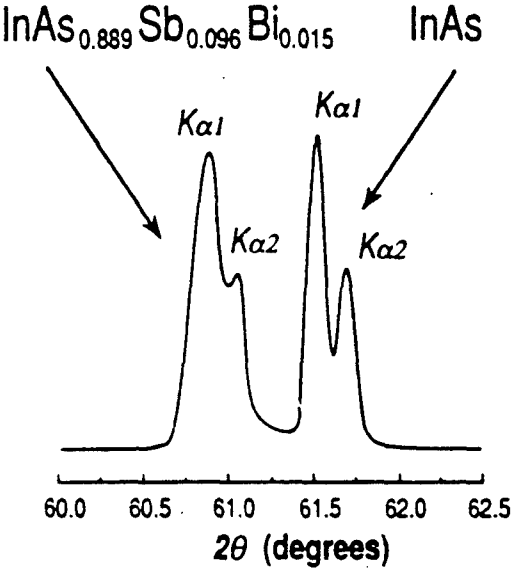


(a)





(b)



ORIGINAL PAGE IS
OF POOR QUALITY

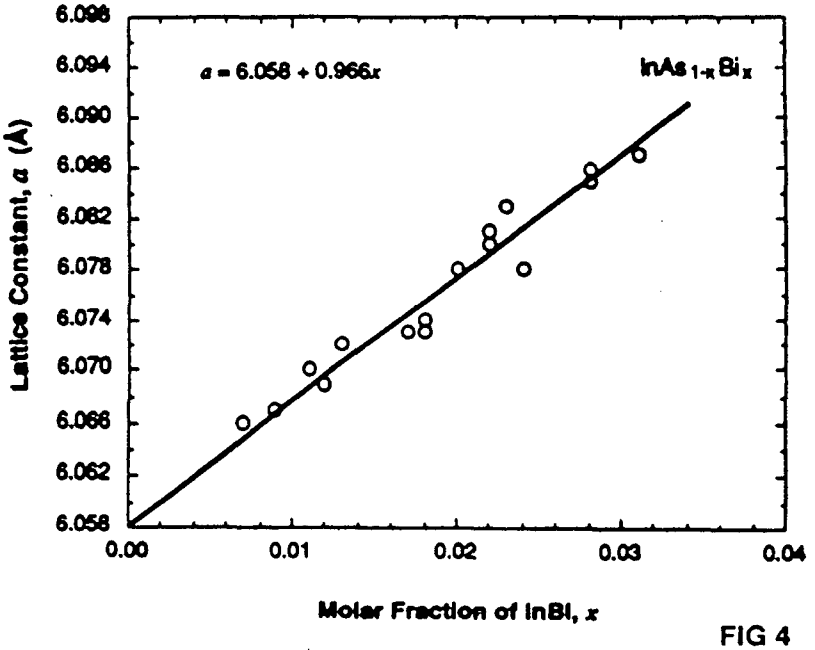
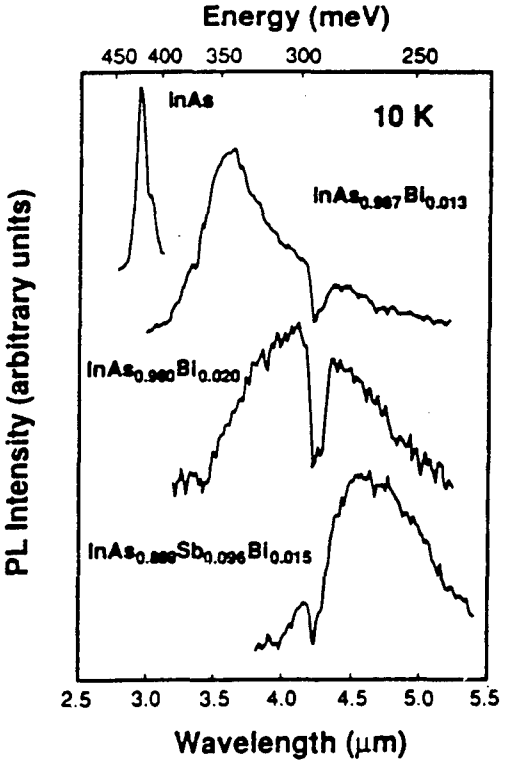
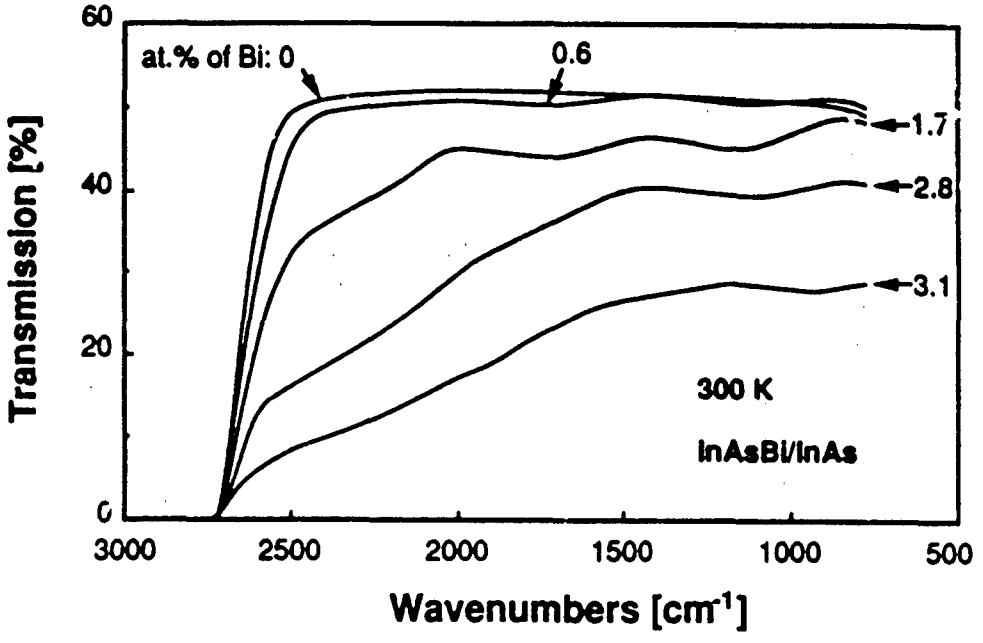
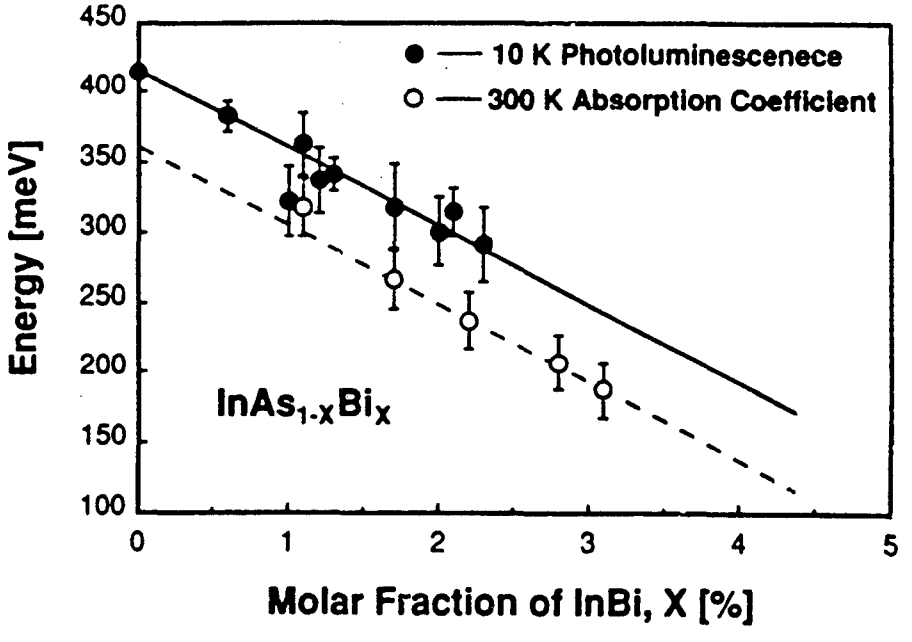

a = 6.058 + 0.966x
InAs1-xBix
Lattice Constant, a (Å)
6.098
6.094
6.090
6.086
6.082
6.078
6.074
6.070
6.066
6.062
6.058
0.00
0.01
0.02
0.03
0.04
Molar Fraction of InBi, x

FIG 4


Energy (meV)
450 400 350 300 250
InAs
10 K
InAs0.987Bi0.013
InAs0.980Bi0.020
InAs0.889Sb0.096Bi0.015
PL Intensity (arbitrary units)
2.5 3.0 3.5 4.0 4.5 5.0 5.5
Wavelength (μm)


60
40
20
0
Transmission [%]
at.% of Bi: 0
0.6
1.7
2.8
3.1
300 K
InAsBi/InAs
3000
2500
2000
1500
1000
500
Wavenumbers [cm-1]

Fang Fig.5


450
400
350
300
250
200
150
100
Energy [meV]
10 K Photoluminescenece
300 K Absorption Coefficient
InAs1-XBiX
0
1
2
3
4
5
Molar Fraction of InBi, X [%]

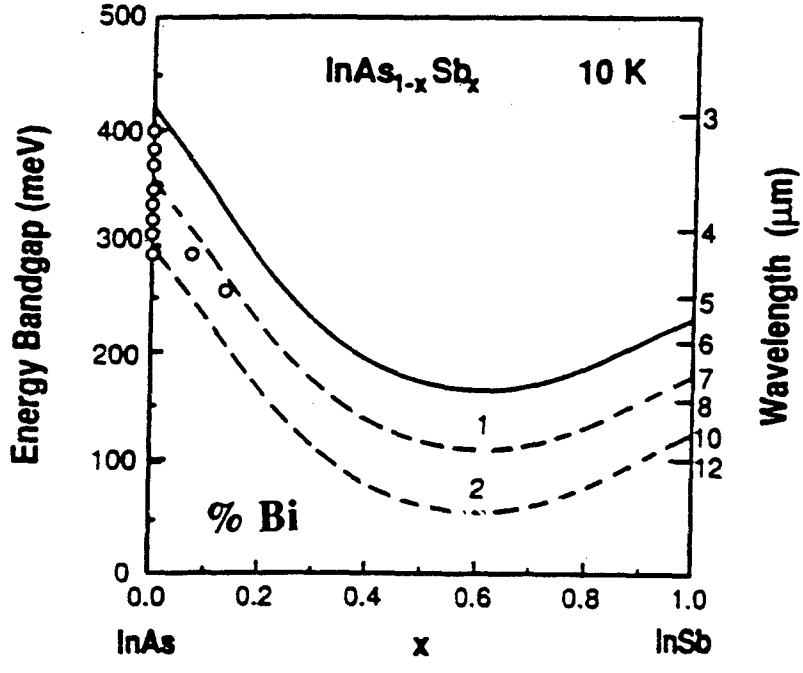
- EXTRAPOLATION OF DATA TO $InAs_{0.35}Sb_{0.65}$

  SUGGESTS THAT 2% Bi WOULD YIELD

  GAP EN. ≈ 0.034 eV (36 microns)

  MAKING A DIRECT BAND-GAP VLWIR MATERIAL

Energy Bandgap vs. Composition x



STATUS

- OMVPE GROWTHS HAVE BEEN MADE WITH UP TO 3.4% Bi AND UP TO 30% Sb
- Bi SEEMS TO BE SUBSTITUTIONAL

  LATTICE INCREASE IS LINEAR,
  BAND GAP SHIFT IS LINEAR,
  X-RAY DATA IS SHARP,
  NO SIGN OF TWO PHASES,
  MORPHOLOGY IS GOOD

STATUS CONTINUED

- ENERGY DECREASES BY 55meV per % Bi
- $a = 6.058 + 0.966\,x$ FOR $InAs_{(1-x)}Bi_{(x)}$
- LUMINESCENCE SEEN
  - IMPLIES LIFETIME AND ELECTRICAL QUALITY TO BE AT LEAST GOOD
  - BROADENING IMPLIES SOME COMPOSITIONAL VARIATION
- THICKNESS - 8 micron THICK InSb GROWN p-TYPE, $5 E 14$

- **PROGRAM FUTURE DIRECTION**
  - OMVPE GROWTH NEAR $InAs_{0.34}Sb_{0.64}Bi_{0.02}$
  - EXTENDED ELECTRICAL AND OPTICAL TESTING TO OPTIMIZE THE GROWTH AND PROVIDE INITIAL OPTICAL DETECTOR DATA

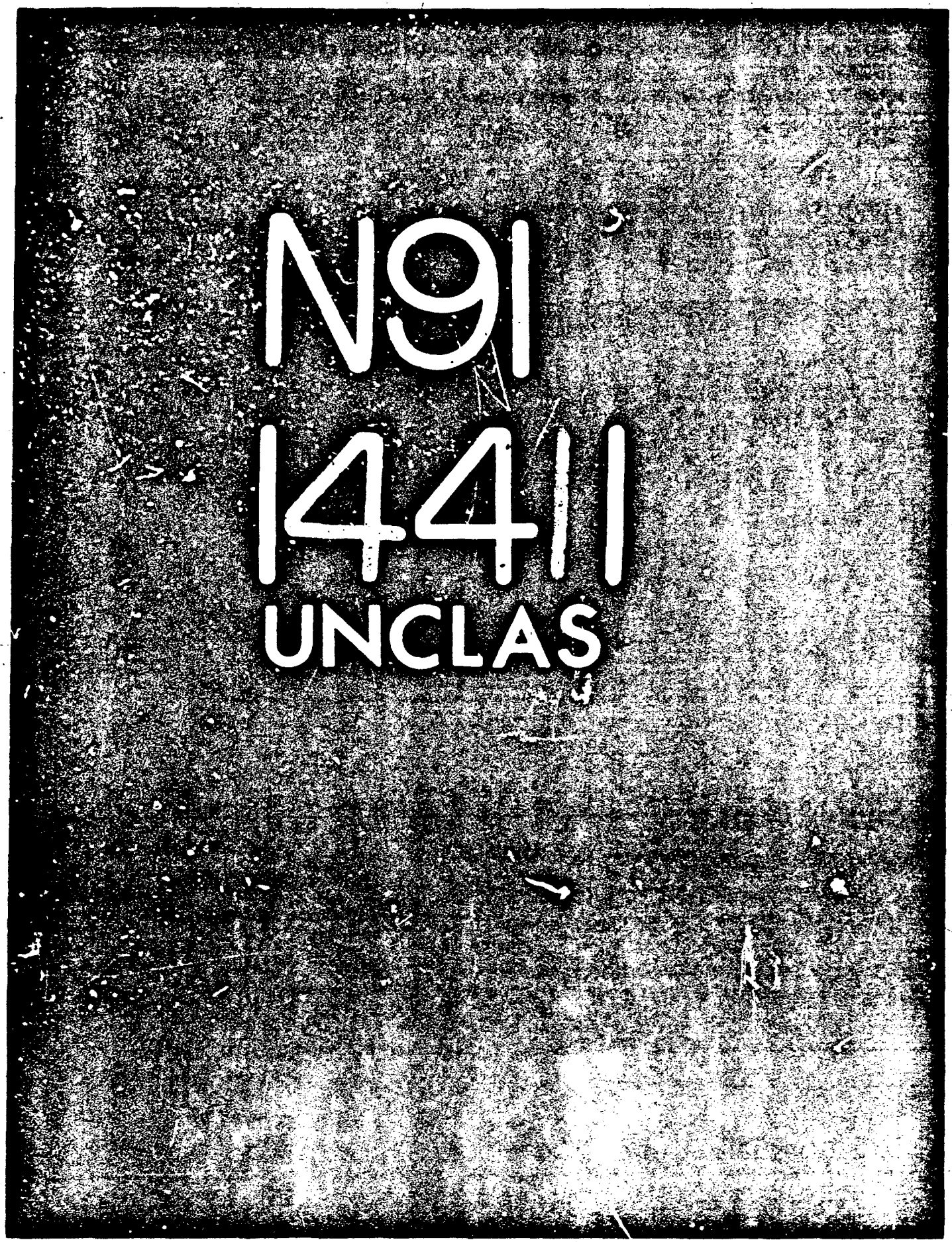
THE LATTER IS A JOINT PROJECT BETWEEN UNIVERSITY OF UTAH AND SANTA BARBARA FOCALPLANE, A COMPANY THAT PROCESSES AND TESTS IR ARRAYS AND MATERIALS

SBF MATERIALS CHARACTERIZATION

PROPERTY	CHARACTERIZATION
BAND-GAP	IR TRANSMISSION
CARRIERS	HALL, CV
EL. TRAPPING	DLTS
CRYSTAL QUALITY	ELECTROREFLECTION
MORPHOLOGY	OPTICAL MIC., SEM
LIFETIME	PC DECAY
SURFACE	MULTI-WAVELENGTH ELLIPSOMETRY

DEVICE AND ARRAY TESTING

DEVICES	TEST
DIODES, VARIABLE AREA VARIABLE PERIMETER GATED, UNGATED	IV, LEAKAGE, RoA, SRV, V BREAKDOWN NOISE, 1/F EL. TRAPPING DLTS
CAPACITORS	CV, GV, Nss, ZERBST, Tgen, Qss, Vfb, Vh
FETS	SURFACE MOBILITY
HALL	MOBILITY, RESISTIVITY, CARRIER CONC.
ARRAYS	RESPONSIVITY VS. WAVELENGTH D*, QUANTUM EFFICIENCY, UNIFORMITY, YIELD


N91
14411
UNCLAS

N91-14411

AlSb/InAs/AlSb Quantum Wells

Herbert Kroemer
Department of Electrical and Computer Engineering
University of California
Santa Barbara, CA 93106

Much heterostructure and quantum well work is now devoted to materials combinations other than GaAs/(Al,Ga)As. One of the most interesting is the InAs/(Al,Ga)Sb system. In the InAs/GaSb limit, it exhibits a broken gap, which offers a number of interesting possibilities for new kinds of physical phenomena, most of which remain unexplored.

In the InAs/AlSb limit, it offers quantum wells of exceptional depth (1.35 eV), combined with the low effective mass (0.023 m_0) and high mobilities of InAs, a combination of interest for several potential device applications. The lattice mismatch (1.3%), while not negligible, is sufficiently small that in quantum well structures with well widths of practical interest ($\leq$ 10 nm) the growth should be pseudomorphic, with the mismatch taken up by elastic strain, rather than leading to disastrous misfit dislocation formation.

We have been exploring the InAs/AlSb system recently, obtaining 12nm wide quantum wells with room temperature mobilities up to 28,000 $cm^2/V \cdot s$ and low-temperature mobilities up to 325,000 $cm^2/V \cdot s$, both at high electron sheet concentrations in the $10^{12}/cm^2$ range (corresponding to *volume* concentrations in the $10^{18}/cm^2$ range). These wells were not intentionally doped; the combination of high carrier concentrations and high mobilities suggest that the electrons are due to not-intentional "modulation doping" by an unknown donor in the AlSb barriers, presumably a stoichiometric defect, like an antisite donor. Inasmuch as not intentionally doped *bulk* AlSb is semi-insulating, the donor must be a deep one, being ionized only by draining into the even deeper InAs quantum well.

The excellent transport properties are confirmed by other observations, like excellent quantum Hall effect data, and the successful use of the quantum wells as superconductive weak links between Nb electrodes, with unprecedentedly high critical current densities. The system is promising for future FETs, but many processing problems must first be solved. Although

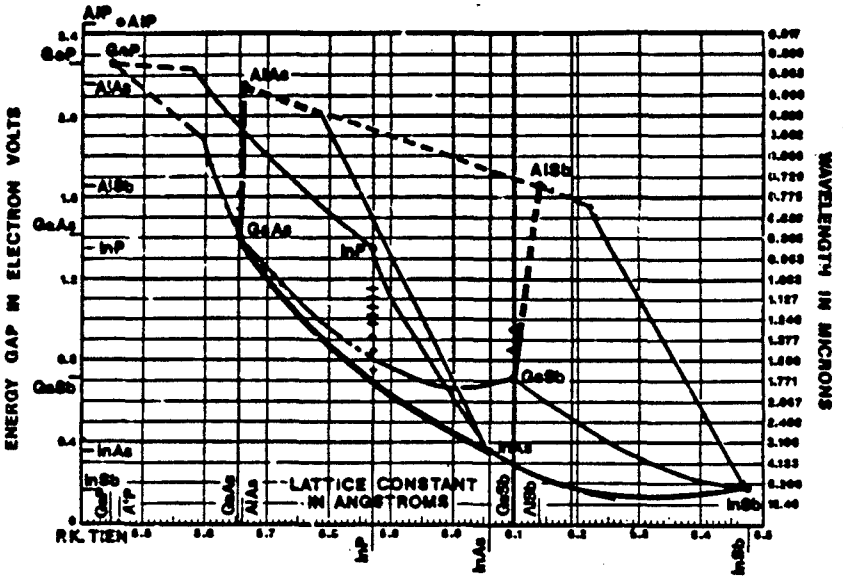
PRECEDING PAGE BLANK NOT FILMED

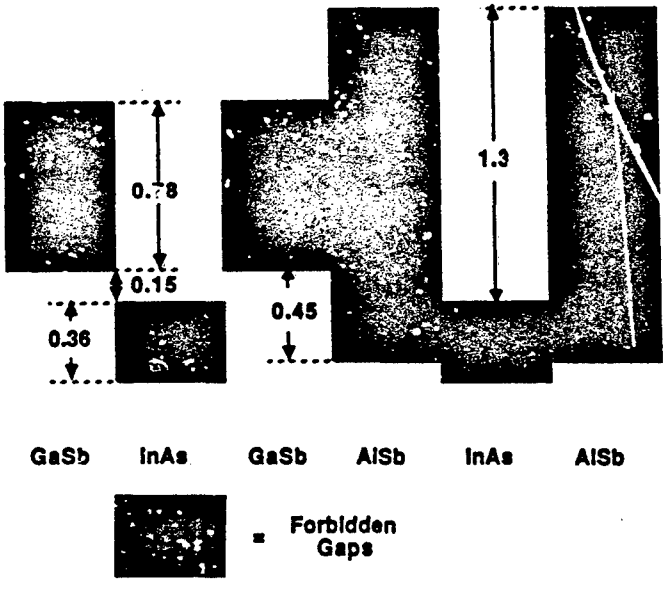
we have achieved FETs, the results so far have not been competitive with GaAs FETs.

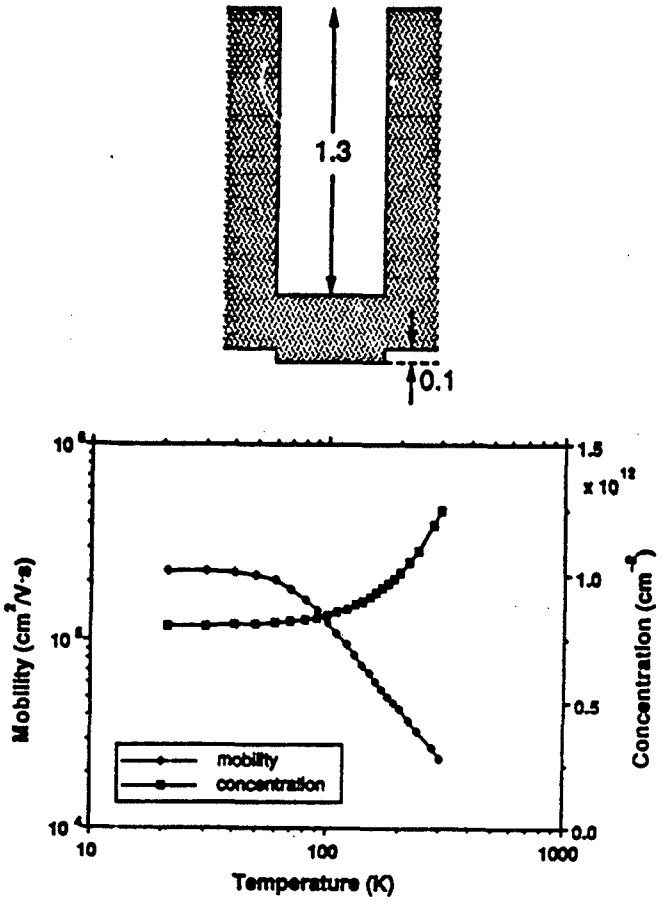
Although most of our work until recently has stressed the transport properties of the system, its optical properties should also be interesting. The large well depths should make the system promising for superlattices with exceedingly short periods. The latter presumably have interesting optical properties, such as strong inter-sub-band absorption effects, of potential use for detector applications. Work exploring the optical properties has been initiated, but we do not have any results to report yet.

Any superlattice applications require particular attention to the quality of the hetero-interfaces, and in this regard the InAs/AlSb system differs *fundamentally* from the GaAs/(Al,Ga)As and (Ga,In)As/(Al,In)As systems: Because both the cation and anion change across an InAs/AlSb (or InAs/GaSb) interface, two distinctly different interface structures may occur. In one case, the InAs would be terminated with a final layer of In, and the adjoining AlSb would start with a layer of Sb, leading to InSb bonds across the interface. We call this the "InSb-like" interface. The complement to this is the "AlAs-like" interface, in which Al atoms from the AlSb side are bonded to As atoms on the InAs side. Experiments show that different kinds of interfaces can indeed be generated by choosing suitable MBE growth parameters, yielding drastically different quantum well properties. All our high-mobility wells were grown under conditions presumably leading to InSb-like interfaces.

A systematic study of the effect of differently grown interfaces showed that wells having AlAs-like *bottom* (i.e. first) interfaces had properties quite different from wells with InSb-like bottom interfaces, while nature of the *upper* (i.e. second) interfaces played little role in determining the properties of the quantum well. More specifically, wells with AlAs-like interfaces at the bottom (but not at the top!) yield a higher electron concentration but much lower mobilities, indicating the presence of a charged defect at those interfaces, believed to be a (deep) As antisite donor on Al sites. Several observations strongly support this interpretation: The magnitude of the effect correlates strongly with the length of exposure of the Al-stabilized AlSb surface to the As flux prior to turning on the In beam. Furthermore, by interrupting the growth of the AlSb barrier some distance away (~10 nm) from the InAs/AlSb interface, and exposing the stagnant AlSb surface to an As flux, we were able to "modulation-dope" the quantum well, with results very similarly to conventional modulation doping with Te donors.


ENERGY GAP IN ELECTRON VOLTS
WAVELENGTH IN MICRONS
AlP
GaP
AlAs
AlSb
GaAs
InP
GaSb
InAs
InSb
AlSb
GaAs
InP
GaSb
InSb
LATTICE CONSTANT
IN ANGSTROMS
R.K. TIEN


0.78
0.15
0.36
0.45
1.3
GaSb
InAs
GaSb
AlSb
InAs
AlSb
= Forbidden Gaps

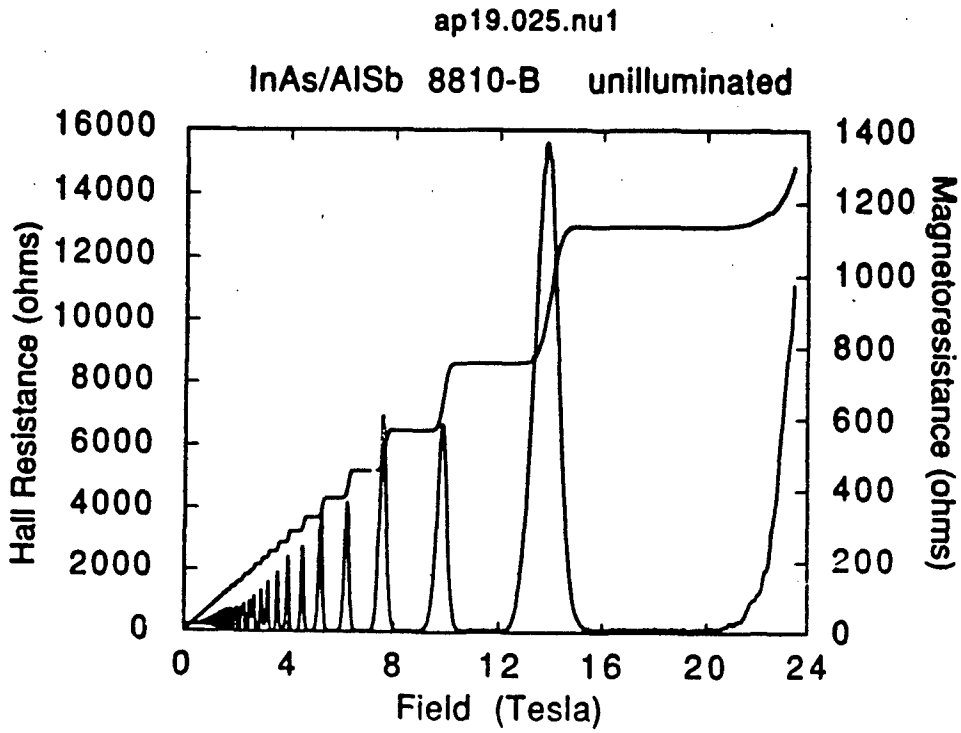


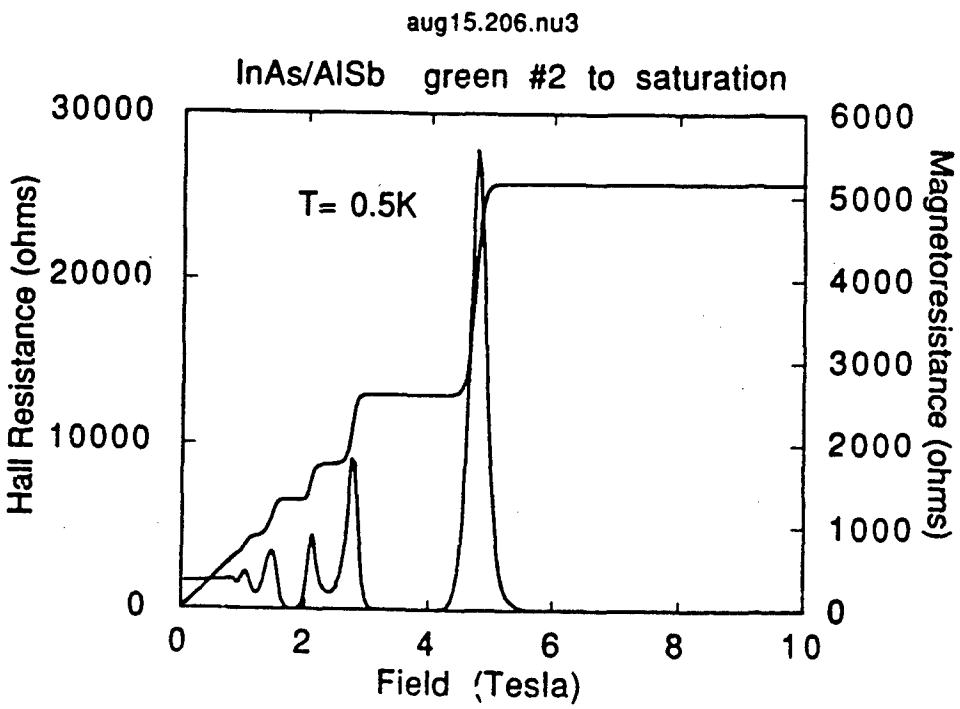
Quantization Energy in an Infinitely Deep Quantum Well of Width L:

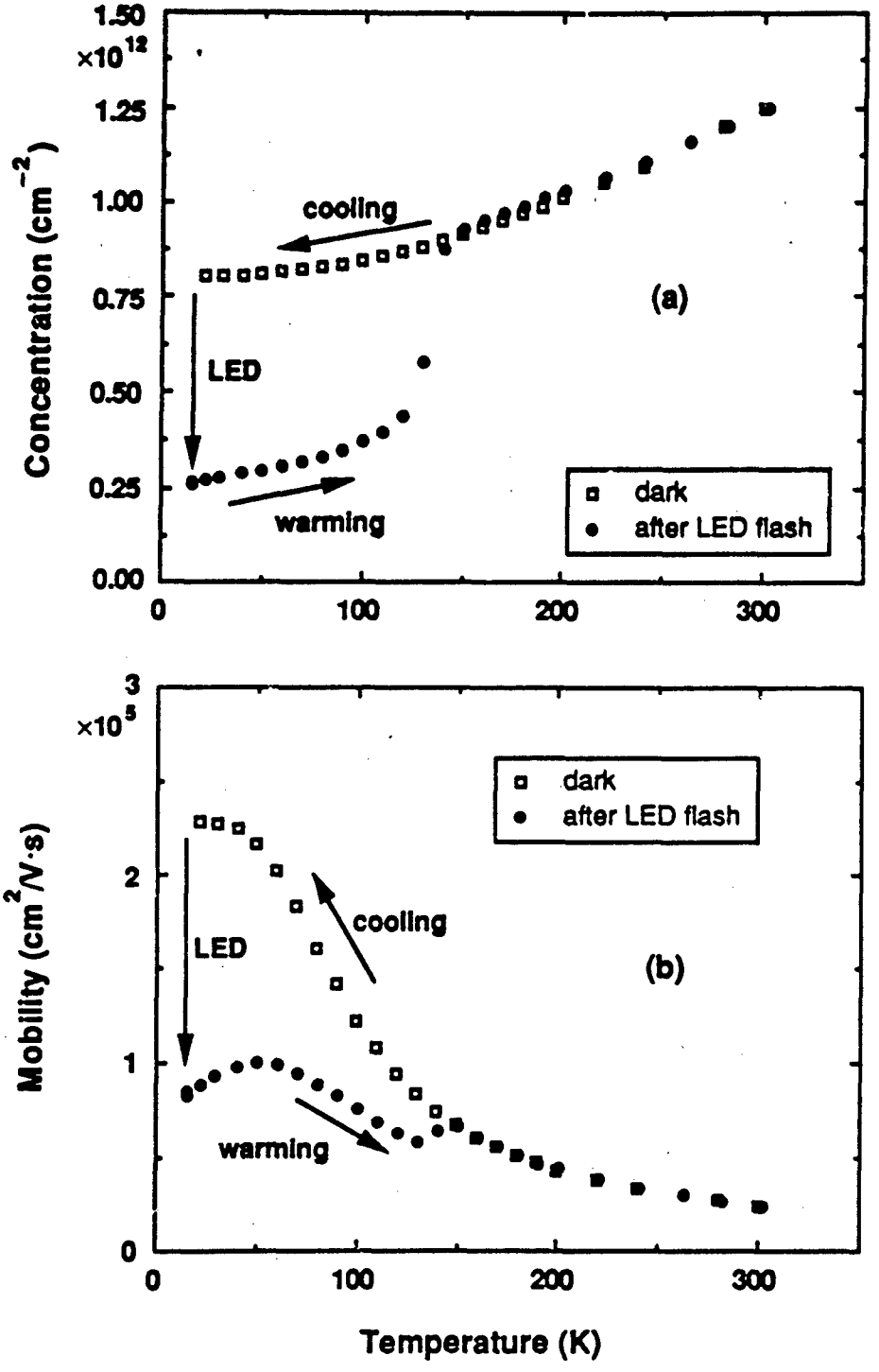
$$\Delta E = \frac{\hbar^2 \pi^2}{2m^* L^2}$$

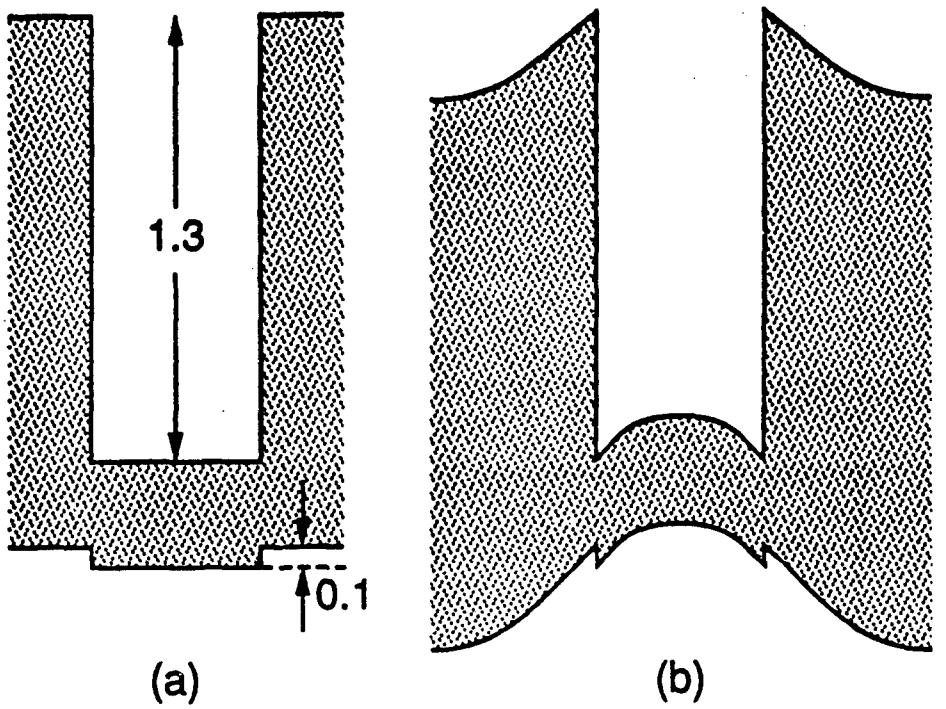
For $m^* = 0.026\, m_0$ and L = 100Å:

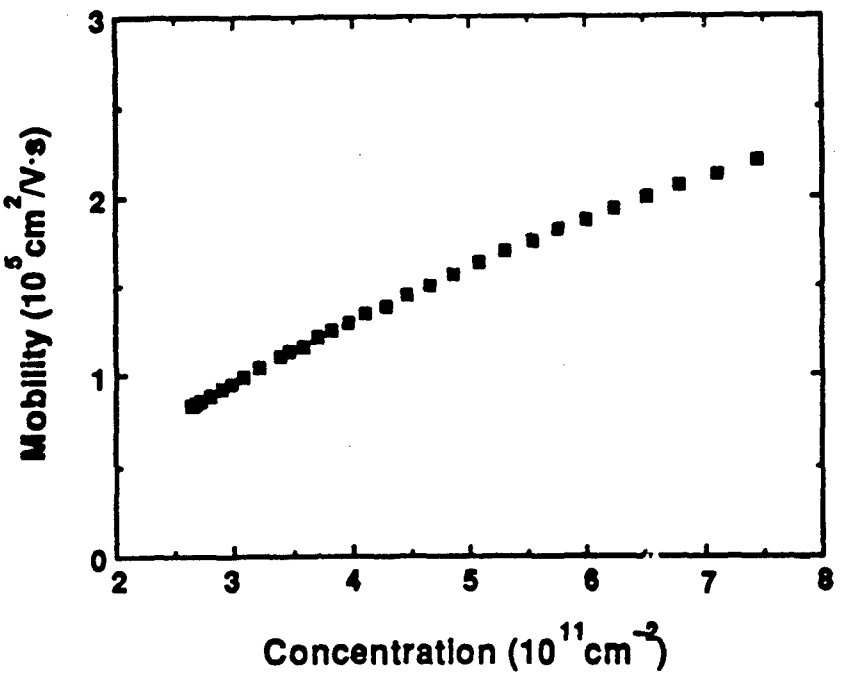
$\Delta E = 0.145$ eV

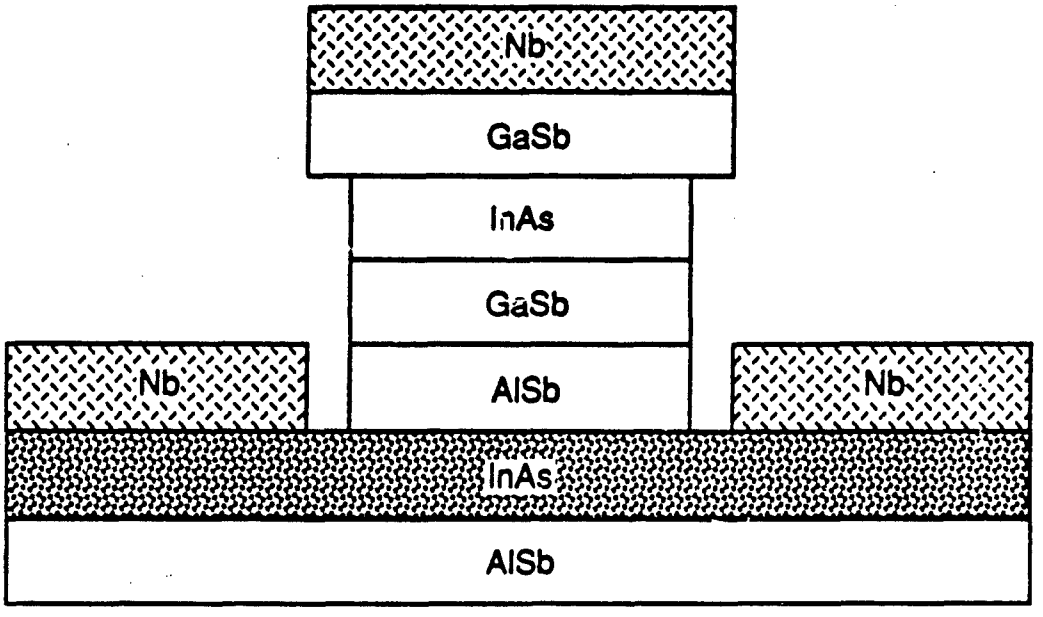

ap19.025.nu1
InAs/AlSb 8810-B unilluminated
Hall Resistance (ohms)
Magnetoresistance (ohms)
Field (Tesla)
16000
14000
12000
10000
8000
6000
4000
2000
0
1400
1200
1000
800
600
400
200
0
0
4
8
12
16
20
24

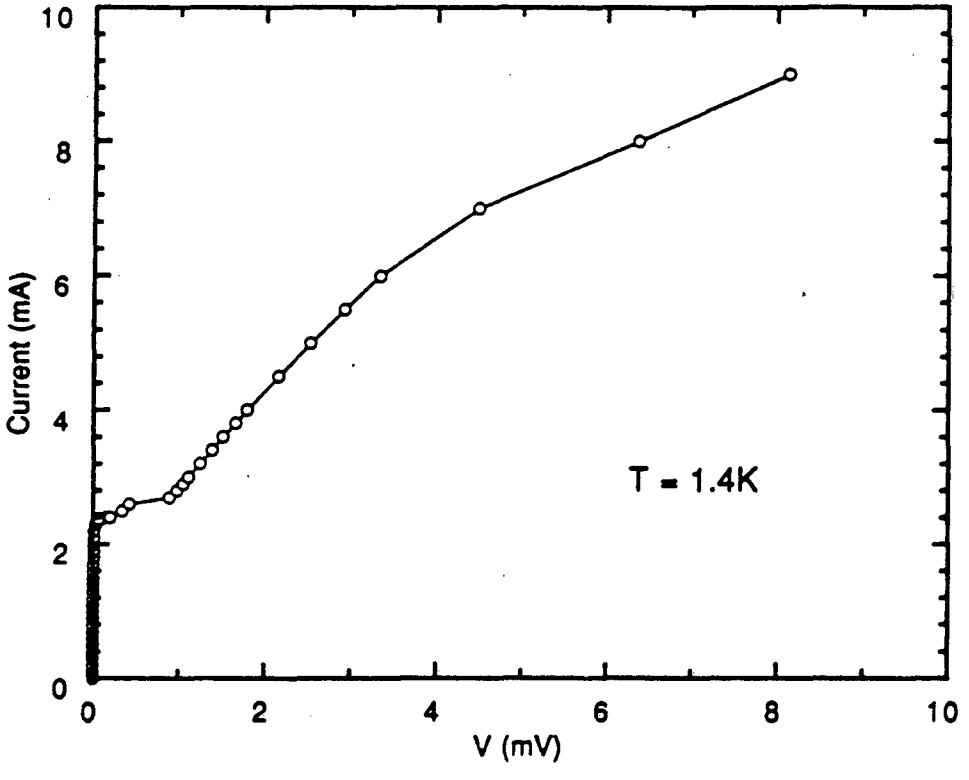

aug15.206.nu3
InAs/AlSb green #2 to saturation
T= 0.5K
Hall Resistance (ohms)
Magnetoresistance (ohms)
Field (Tesla)
30000
20000
10000
0
6000
5000
4000
3000
2000
1000
0
0
2
4
6
8
10

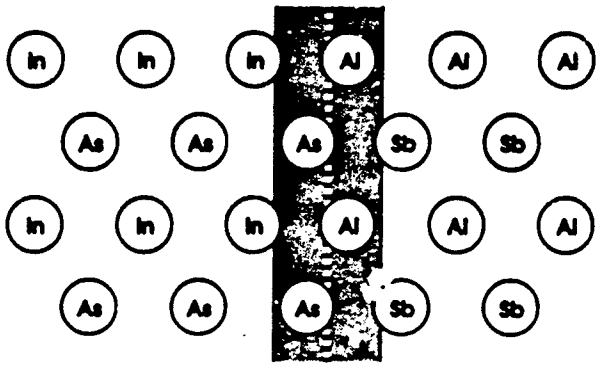

1.50
×10^12
1.25
1.00
0.75
0.50
0.25
0.00
Concentration (cm^-2)
cooling
LED
warming
(a)
dark
after LED flash
0
100
200
300
3
×10^5
2
1
0
Mobility (cm^2/V·s)
dark
after LED flash
cooling
LED
warming
(b)
0
100
200
300
Temperature (K)


1.3
0.1
(a)
(b)

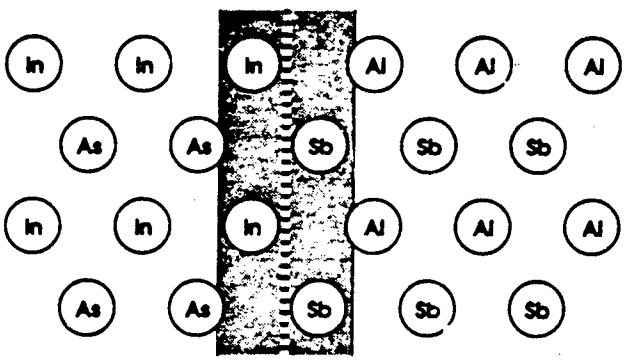

Mobility (10^5 cm^2/V·s)
Concentration (10^{11} cm^{-2})
0
1
2
3
2
3
4
5
6
7
8


Nb
GaSb
InAs
GaSb
AlSb
Nb
Nb
InAs
AlSb

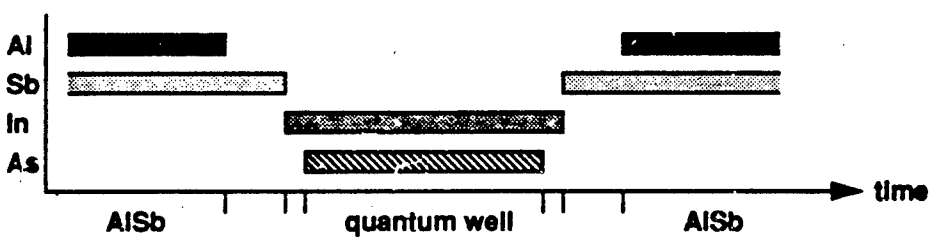

10
8
6
4
2
0
Current (mA)
0
2
4
6
8
10
V (mV)
T = 1.4K


In
In
In
Al
Al
Al
As
As
As
Sb
Sb
In
In
In
Al
Al
Al
As
As
As
Sb
Sb

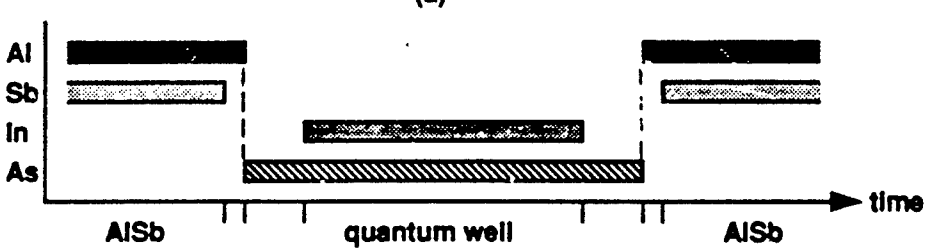
(a)


In
In
In
Al
Al
Al
As
As
Sb
Sb
Sb
In
In
In
Al
Al
Al
As
As
Sb
Sb
Sb

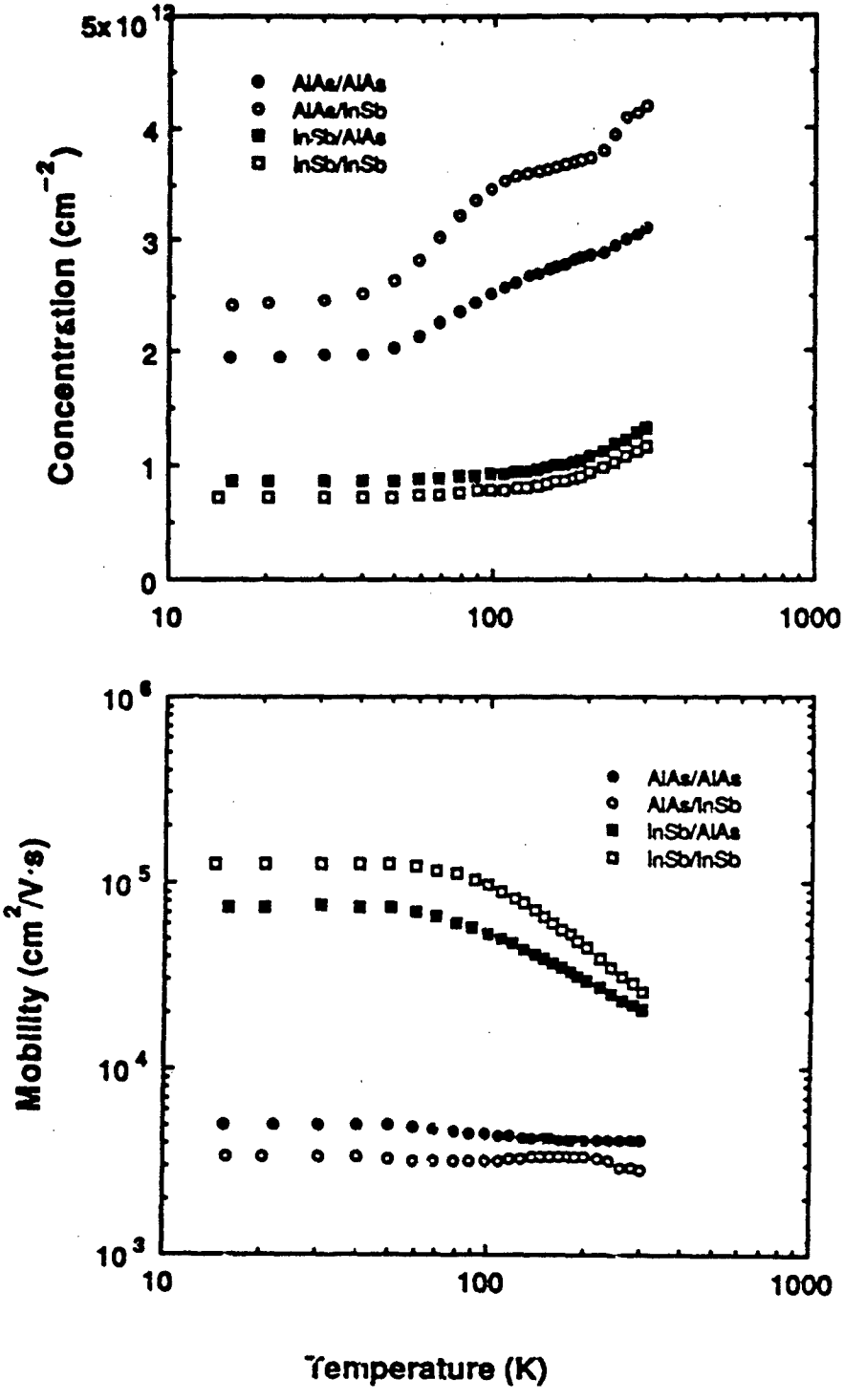
(b)

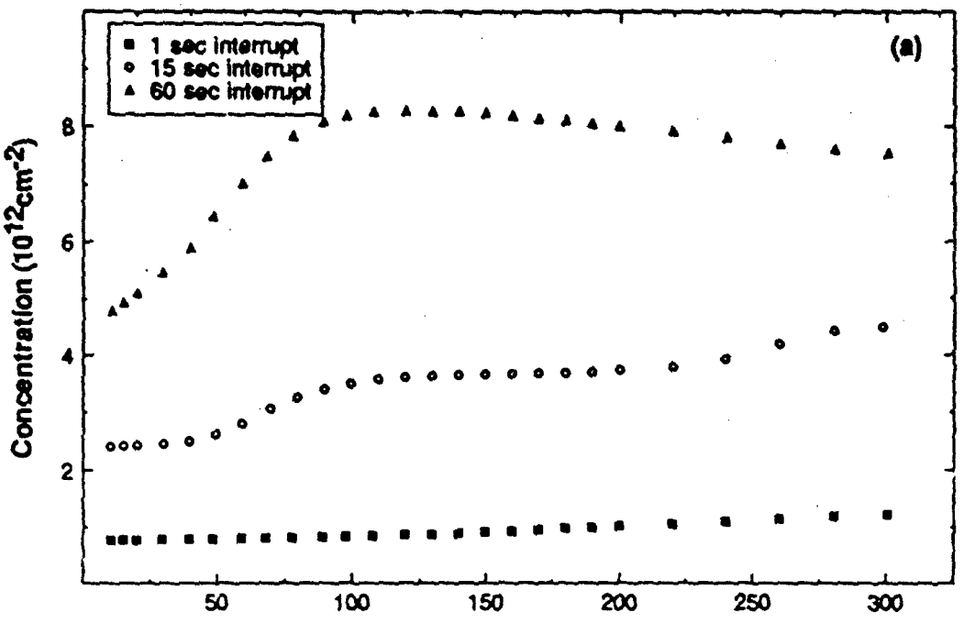

Al
Sb
In
As
time
AlSb
quantum well
AlSb

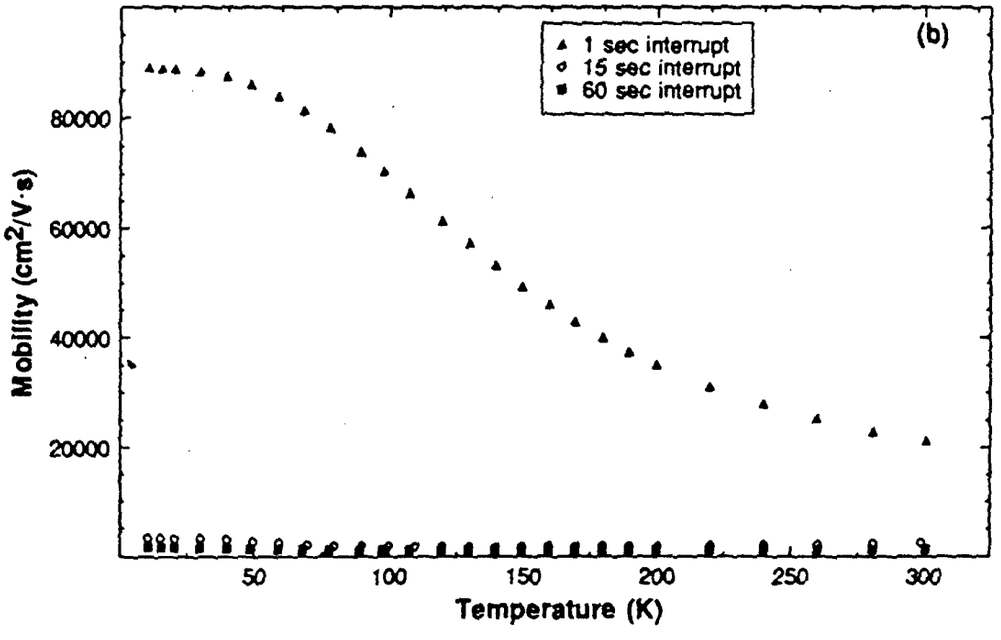
(a)

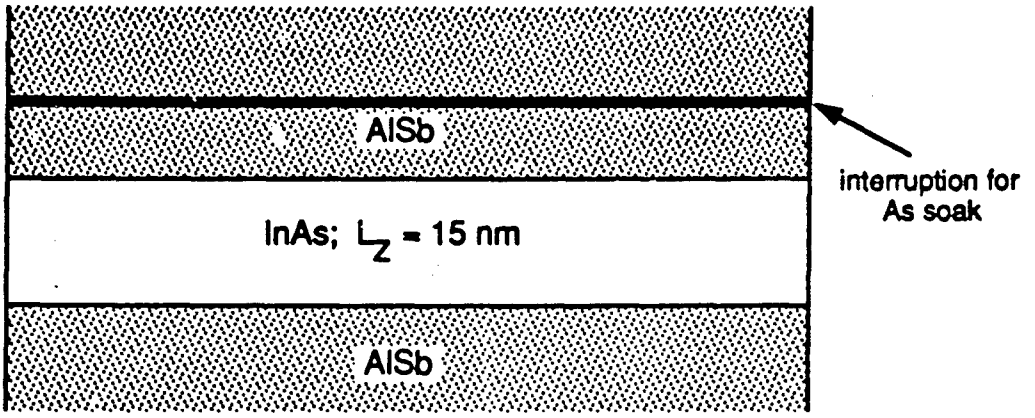

Al
Sb
In
As
time
AlSb
quantum well
AlSb

(b)

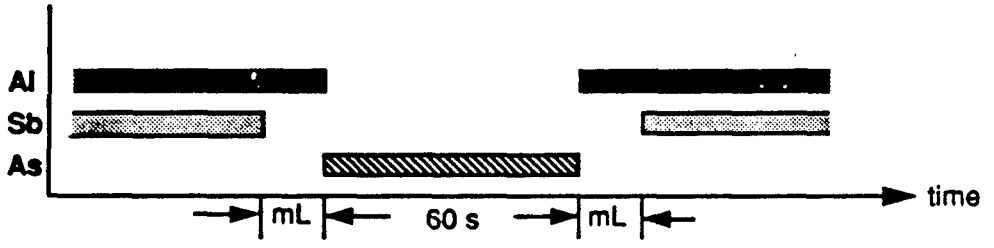

5x10^12
4
3
2
1
0
Concentration (cm^-2)
AlAs/AlAs
AlAs/InSb
InSb/AlAs
InSb/InSb
10
100
1000
10^6
10^5
10^4
10^3
Mobility (cm^2/V·s)
AlAs/AlAs
AlAs/InSb
InSb/AlAs
InSb/InSb
10
100
1000
Temperature (K)


1 sec interrupt
15 sec interrupt
60 sec interrupt
(a)
Concentration ($10^{12}cm^{-2}$)
2
4
6
8
50
100
150
200
250
300

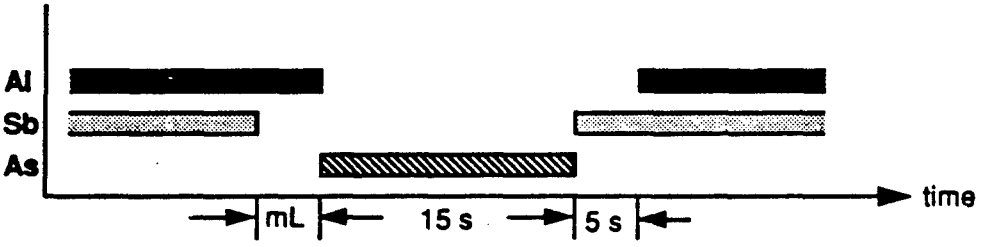

1 sec interrupt
15 sec interrupt
60 sec interrupt
(b)
Mobility ($cm^2/V \cdot s$)
20000
40000
60000
80000
50
100
150
200
250
300
Temperature (K)


AlSb
InAs; L_z = 15 nm
AlSb
interruption for
As soak

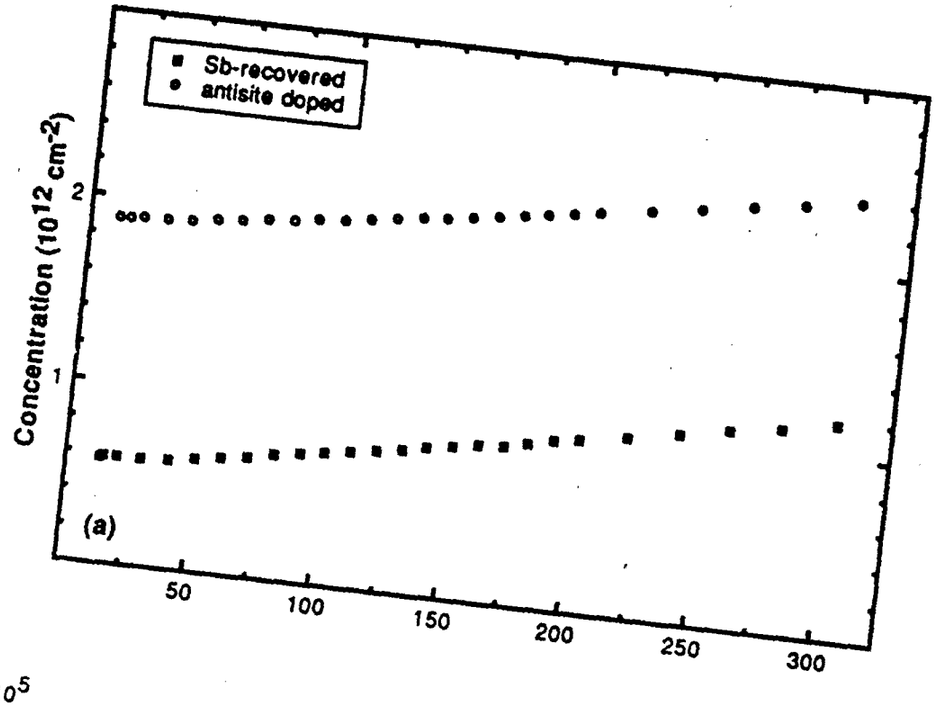
(a)

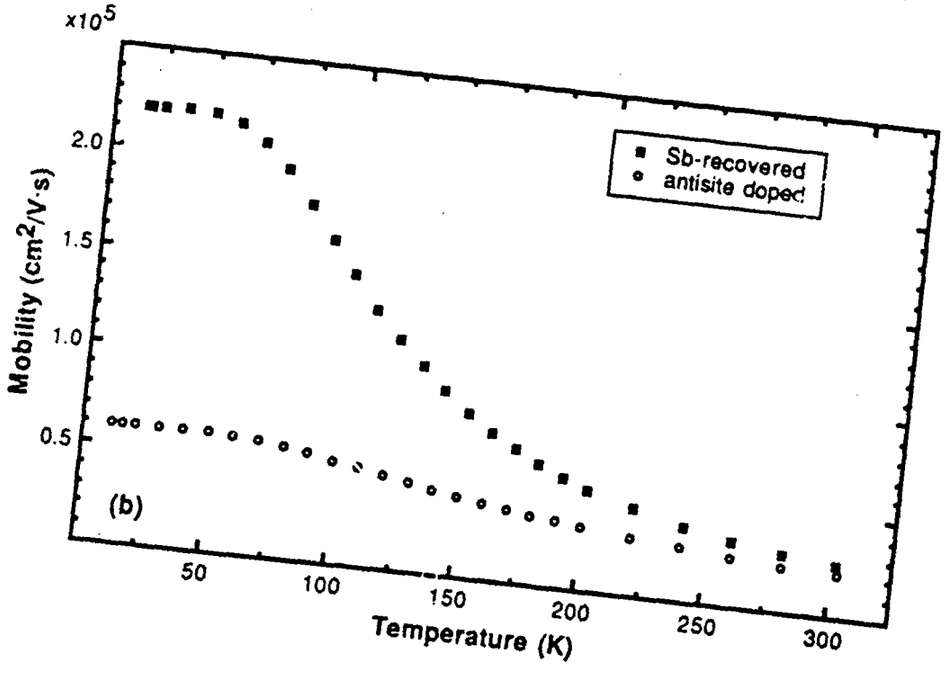

Al
Sb
As
time
mL
60 s
mL

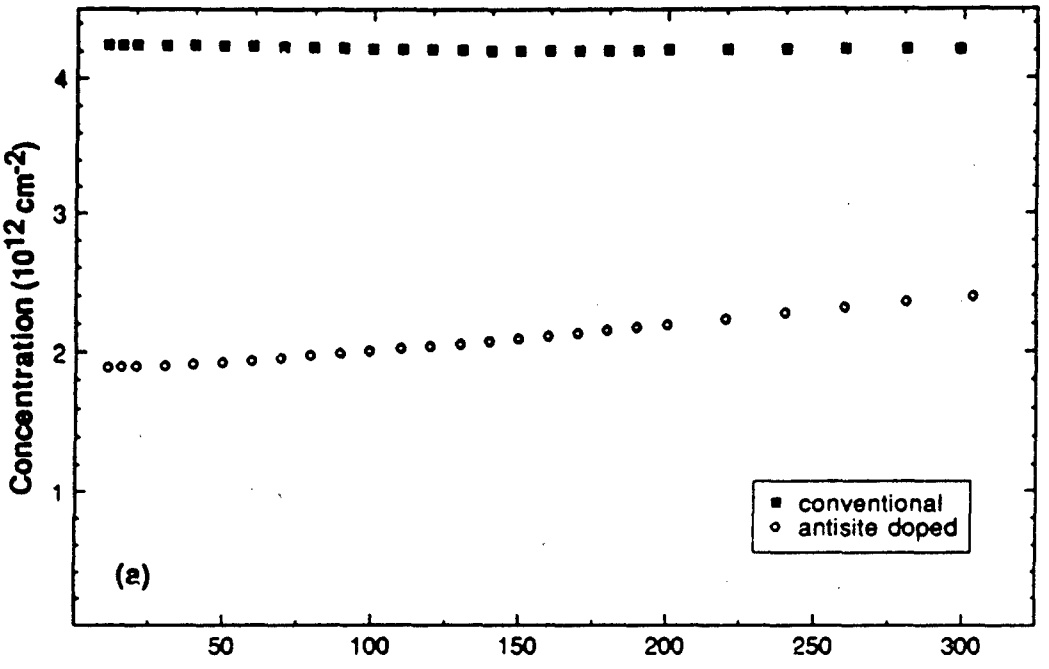
(b)

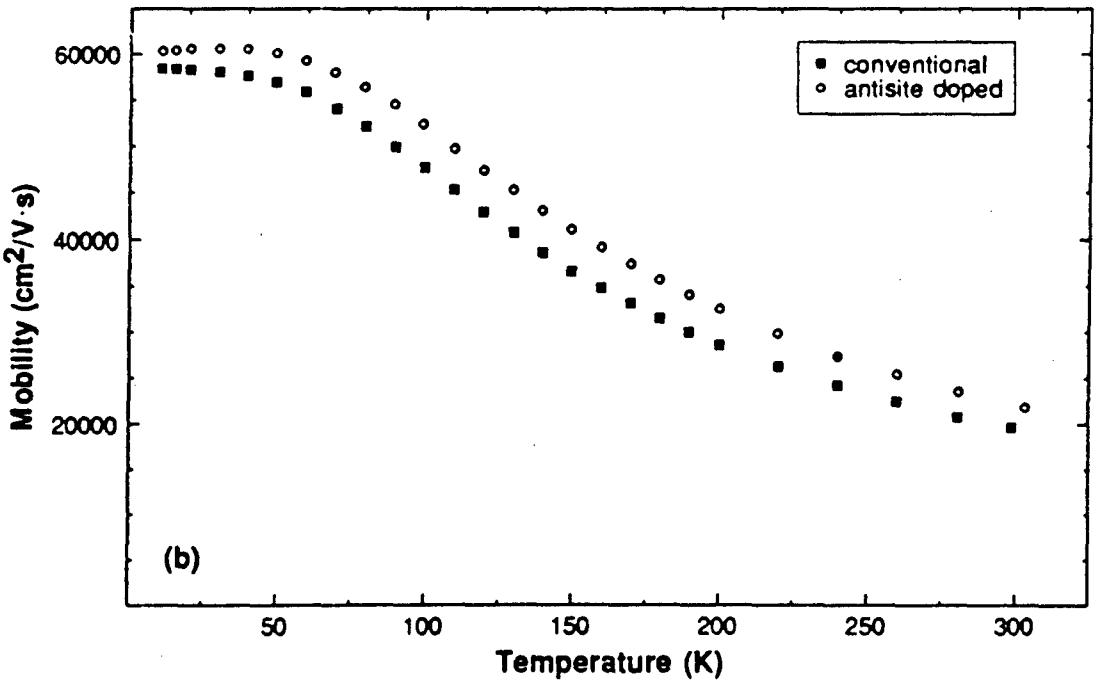

Al
Sb
As
time
mL
15 s
5 s

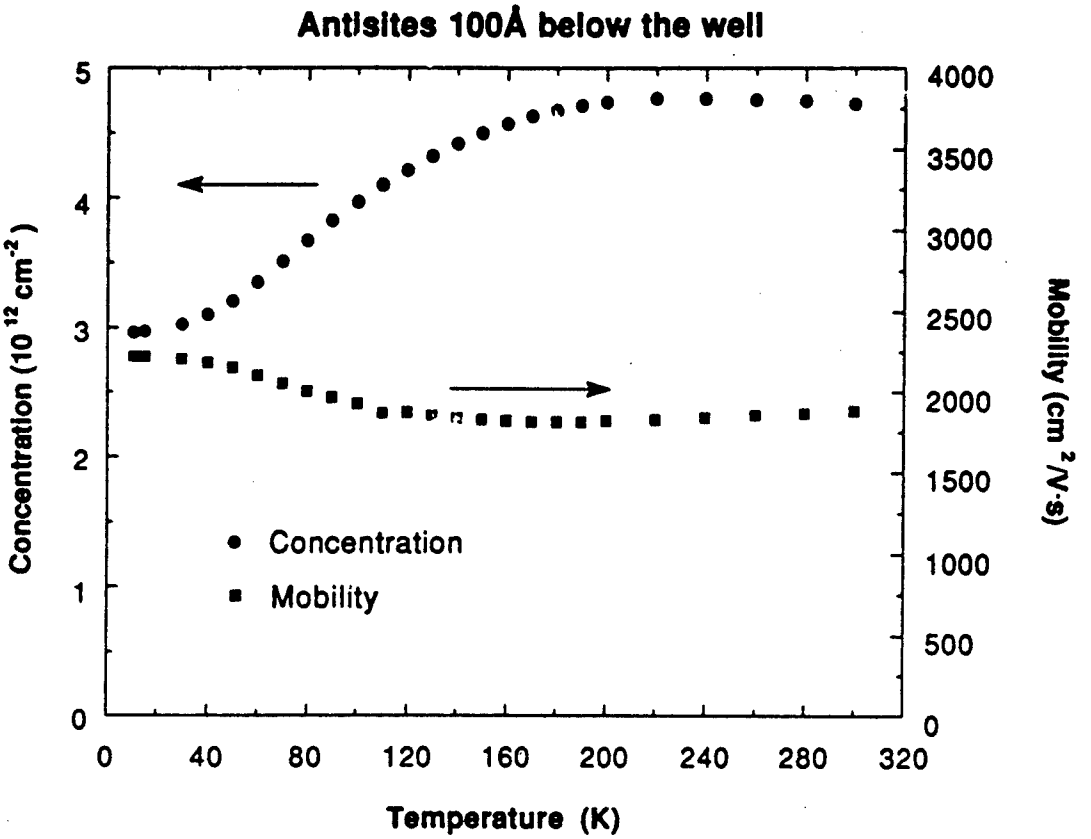
(c)


Sb-recovered
antisite doped
Concentration (10^{12} cm^{-2})
2
1
(a)
50
100
150
200
250
300


x10^5
2.0
1.5
1.0
0.5
Mobility (cm^2/V·s)
Sb-recovered
antisite doped
(b)
50
100
150
200
250
300
Temperature (K)


Concentration (10^{12} cm^{-2})
4
3
2
1
50
100
150
200
250
300
conventional
antisite doped
(a)


Mobility (cm^2/V·s)
60000
40000
20000
50
100
150
200
250
300
Temperature (K)
conventional
antisite doped
(b)


Antisites 100Å below the well
Concentration (10^{12} cm^{-2})
Mobility ($cm^2/V \cdot s$)
Temperature (K)
Concentration
Mobility
0
1
2
3
4
5
0
500
1000
1500
2000
2500
3000
3500
4000
0
40
80
120
160
200
240
280
320

APPENDIX: Attendance List

INNOVATIVE LONG WAVELENGTH INFRARED DETECTOR WORKSHOP

Jet Propulsion Laboratory
April 24 - 26, 1990

PRECEDING PAGE BLANK NOT FILMED

Adams, F.W.
Lockheed Missiles & Space Co.
3251 Hanover St.
Palo Alto, CA 94304-1191
(415)424-2227

Allario, F.
NASA/Langley Research Center
MS 117
Hampton, VA 23665-5225
(804)864-6027

Bahraman, A.
Northrop Electronics Systems Div.
One Research Park
Palos Verdes, CA 90274
(213)544-5336

Balcerak, R.
DARPA
1400 Wilson Blvd.
Arlington, VA
(202)693-4278

Bandara, Sumith
Microtronics Assoc.
4516 Henry St., Ste. 403
Pittsburgh, PA 15213-3728
(412)681-0888

Baron, Robert
Hughes Research Labs
3011 Malibu Canyon Rd.
Malibu, CA 90265
(213)317-5392

Barton, Jeffrey
Amber Engineering
5756 Thornwood Dr.
Goleta, CA 93117
(805)683-6621

Beck, William
Martin Marietta Lab
1450 S. Rolling Rd.
Baltimore, MD 21227
(301)247-2291

Beeman, Jeffrey
Lawrence Berkeley Laboratory
s-200
Berkeley, CA
(415)486-4439

Berding, Marcy
SRI International
333 Ravenswood Ave. LOC 410-33
Menlo Park, CA 94025
(415)859-4267

Bharat, R.
Rockwell International Corp.
3370 Miraloma Ave.,031-BC16
Anaheim, CA 92803
(714)762-1460

Bickel, Thomas
Sandia National Laboratory
PO Box 5800, Dept. 6220
Albuquerque, NM 87185
(505)844-2392

Bloss, Walter
The Aerospace Corp.
PO Box 92957, MS M2-244
Los Angeles, CA 90009
(213)336-9269

Bly, Vincent
US Army
Infrared Technology Division
Fort Belvoir, VA 22060-5677
(703)664-1585

Boisrert, Joseph
S-CUBED
3020 Callan Rd.
San Diego, CA 92121-1095
(619)450-2404

Borenstain, Shmuel
Jet Propulsion Laboratory
MS 302-306, 4800 Oak Grove Dr.
Pasadena, CA 91109
(818)354-5046

Boyle, Jack
Charles Stark Draper Lab
555 Technology Dr.
Cambridge, MA 02139
(617)258-3238

Braun, Robert
AT & T Bell Laboratories
600 Mountain Ave.
Murray Hill, NJ 07974-2070
(201)582-2996

Brown, Duncan
Advanced Technology Materials
520-B Danbury Rd.
New Milford, CT 06776
(203)355-2691

Brown, Gail
Air Force Materials Laboratory
WRDC/MLPO
WrightPatterson AFB,OH 45433
(513)255-4098

Brown, Kenneth
The Aerospace Corporation
2nd & B Sts., PO Box 9045
Albuquerque, NM 87119
(505)844-0113

Brown, Lyn
US Air Force
WRDC/MLPO
Wright Patterson AFB, OH 45433
(513)255-4098

Capps, Richard
Jet Propulsion Laboratory
MS 303-210, 4800 Oak Grove Dr.
Pasadena, CA 91109
(818)354-6305

Casselman, Tom
Santa Barbara Research Center
75Coromar Dr.
Santa Barbara, CA 93117
(805)562-2981

Chahine, Moustafa
Jet Propulsion Laboratory
MS 180-904, 4800 Oak Grove Dr.
Pasadena, CA 91109
(818)354-6057

Chang, Nien Chich
The Aerospace Corp.
PO Box 92957
Los Angeles, CA 90009-2957
(213)336-7186

Cheung, Derek
Rockwell International Science Cntr
1409 Camino Dos Rios
Thousand Oaks, CA 91360
(805)373-4269

Choi, Kwong-kit
US Army Elect. Tech & Devices Lab
ATTN: SLCET-ED
Fort Monmouth, NJ 07703-5000
(201)544-3806

Clouse, Larry
TRW
12610 Venice Blvd., Apt. A
Los Angeles, CA
(213)812-0182

Cole, Terry
Jet Propulsion Laboratory
MS 180-500, 4800 Oak Grove Dr.
Pasadena, CA 91109
(818)354-5458

Collins, Stewart
Jet Propulsion Laboratory
MS 168-222, 4800 Oak Grove Dr.
Pasadena, CA 91109
(818)354-7734

Correa, Craig
Booz Allen & Hamilton
1725 Jefferson Davis Hwy.
Arlington, VA 22202
(703)271-1654

Crowe, Thomas
University of Virginia
Thornton Hall
Charlottesville, VA 22903-2442
(804)924-7693

Dafesh, Philip
The Aerospace Corp.
PO Box 92957
El Segundo, CA 90009-2957
(213)336-8733

Davidson, Richard
Jet Propulsion Laboratory
MS 300-315, 4800 Oak Grove Dr.
Pasadena, CA 91109
(818)354-7812

De Luccia, Frank
The Aerospace Corp.
2350 E. El Segundo Blvd.
El Segundo, CA 90245
(213)336-9312

DePaula, Ramon
NASA Headquarters
Code R
Washington, DC 20546
(202)453-2748

DeVaux, Lloyd
DeVaux Associates
466 Camino Talavera
Goleta, CA 93117
(805)964-3384

Dejewski, Susan
Jet Propulsion Laboratory
MS 303-210, 4800 Oak Grove Dr.
Pasadena, CA 91109
(818)354-1292

Denison, Robert
Wright Rsch. & Devlp. Center
WRDC/MLPO
Wright-Patterson AFB,OH 45433
(513)255-4474

Dereniak, E.
University of Arizona

Devine, Michael
Kirtland AFB
HQ AFSTC/SWS
Kirtland AFB, NM 87117-6008
(505)846-5788

Dickerman, Ronald
Army Space Tech & Rsch Office
2902 Adams St.
Dale City, VA 22193
(703)355-2709

Duston, Dwight
SDIO/TNI
Washington, DC
(202)693-1527

Eaton, Larry
TRW
One Space Park
Redondo Beach, CA 90278
(213)812-0155

Empson, Kevin
DOD/IAO
9733 Evergreen Knoll Ct.
Alexandria, VA 22303
(703)351-2143

Fathouer, Robert
Jet Propulsion Laboratory
MS 302-231, 4800 Oak Grove Dr.
Pasadena, CA 91109
(818)354-4962

Fischler, Fred
Texas Instruments Inc.
13532 N. Central Expway, MS 28
Dallas, TX 75265
(214)995-1089

Forrest, Kate
NASA/Goddard Space Flight Center
Bldg. 5 Rm. 324
Greenbelt, MD 20771
(301)286-7138

Fossum, Eric
Columbia University
Dept. EE, 1312 S.W. Mudd Bldg.
New York, NY 10027
(212)854-3107

Goldberg, Arnold
Martin Marietta Laboratories
1450 S. Rolling Road
Baltimore, MD 21227
(301)247-0700

Golding, Terry
University of Houston
Science & Research 1
Houston, TX 77204-3507
(713)749-1641

Grave, Ilan
Caltech
Pasadena, CA 91125
(818)356-4823

Greiner, Mark
Cincinnati Electronics Corp.
7500 Innovation Way
Mason, OH 45040-9699
(513)573-6151

Grunthaner, Frank
Jet Propulsion Laboratory
MS 302-306, 4800 Oak Grove Dr.
Pasadena, CA 91109
(818)354-5564

Grunthaner, Paula
Jet Propulsion Laboratory
MS 302-231, 4800 Oak Grove Dr.
Pasadena, CA 91109
(818)354-0360

Gulkis, Samuel
Jet Propulsion Laboratory
MS 169-506, 4800 Oak Grove Dr.
Pasadena, CA 91109
(818)354-5708

Haas, T.W.
US Air Force
WRDC/MLBM
Wright Patterson AFB, OH 45433
(513)255-5892

Haller, Eugene
Lawrence Berkeley Laboratory
1 Cyclotron Rd., MS 2-200
Berkeley, CA 94720
(415)486-5294

Hancock, Bruce
Jet Propulsion Laboratory
MS 302-306, 4800 Oak Grove Dr.
Pasadena, CA 91109
(818)354-8801

Hansen, William
Lawrence Berkeley Laboratory
1 Cyclotron Rd., MS 2-200
Berkeley, CA 94720
(415)486-5632

Herring, Mark
Jet Propulsion Laboratory
MS 11/116, 4800 Oak Grove Dr.
Pasadena, CA 91109
(818)354-6817

Hubbard, G. Scott
NASA/Ames Research Center
MS 244-14
Moffett Field, CA 94035
(415)604)5697

Huffman, James
Rockwell Scince Center
3370 Miraloma Ave., MS BC18
Anaheim, CA 92803
(714)762-4011

Jack, Michael
Santa Barbara Research Center
75 Coromar Dr.
Santa Barbara, CA 93117
(805)562-2981

Jindal, Bal
XACTON Corp.
PO Box 3129
Tempe, AZ 85280
(602)966-8765

Jones, Richard
Charles Stark Draper Lab
555 Technology Dr.
Cambridge, MA 02139
(617)258-3238

Kahn, Cynthia
Jet Propulsion Laboratory
MS 168-222, 4800 Oak Grove Dr.
Pasadena, CA 91109
(818)354-4101

Kenny, T.
Jet Propulsion Laboratory
4800 Oak Grove Dr.
Pasadena, CA 91109

Kohn, Stanley
The Aerospace Corp.
PO Box 92957
El Segundo, CA 90009-2957
(213)336-8871

Hauenstein, Robert
Hughes Research Laboratories
3011 Malibu Canyon Rd.,MS RL63
Malibu, CA 90265
(213)317-5819

Hinkley, David
TRW
One Space Park
Redondo Beach, CA 90278
(213)814-0295

Huberman, Mark
Jet Propulsion Laboratory
MS 302-306, 4800 Oak Grove Dr.
Pasadena, CA 91109
(818)354-7452

Ito, Chris
Ford Microelectronics Inc.
9965 Federal Dr.
Colorado Springs, CO 80921
(719)528-7727

Janousek, Bruce
The Aerospace Corporation
M 2/244, PO Box 92957
Los Angeles, CA 90009
(213)336-1820

Jones, Colin
Santa Barbara Focalplane
69 Santa Felicia Dr.
Goleta, CA 93117
(805)562-8777

Jost, Steven
General Electric Company
EP3-223, PO Box 4840
Syracuse, NY 13221
(315)456-2934

Kalma, Arne
Mission Research Corporation
4935 North 30th Street
Colorado Springs, CO 80919
(719)528-8080

Khanna, Satish
Jet Propulsion Laboratory
MS 302-205, 4800 Oak Grove Dr.
Pasadena, CA 91109
(818)354-4489

Koliwad, Kris
Jet Propulsion Laboratory
MS 302-205, 4800 Oak Grove Dr.
Pasadena, CA 91109
(818)354-5197

Krabach, Timothy
Jet Propulsion Laboratory
MS 303-210, 4800 Oak Grove Dr.
Pasadena, CA 91109
(818)354-9654

Kroemer, H.
UC Santa Barbara
Santa Barbara, CA

Larsson, Anders
Jet Propulsion Laboratory
4800 Oak Grove Dr.
Pasadena, CA 91109
(818)354-7496

Lee, T.H.
Eastman Kodak Company
Eastman Kodak
Rochester, NY 14580-2008
(716)477-7468

Levine, B.F.
AT & T Bell Laboratories

Lin, T.L.
Jet Propulsion Laboratory
4800 Oak Grove Dr.
Pasadena, CA 91109

Macurda, Hayden
Nichols Research Corp.
1901 Dove St.
Newport Beach, CA 92660
(714)476-0800

McCreight, Craig
NASA/Ames Research Center
MS 244-10
Moffett Field, CA 94035-1000
(415)604-6549

McMurray, Jr., Robert
NASA/Ames Research Center
MS 244-10
Moffett Field, CA 94035
(415)604-3179

Merz, James
UC Santa Barbara
Elec. & Computer Eng. Dept.
Santa Barbara, CA 93106
(805)961-4446

Krikorian, Esther
Aerospace Corp.
PO Box 92967- M4/978
Los Angeles, CA 90009-2957
(213)336-7527

Kukkonen, Carl
Jet Propulsion Laboratory
4800 Oak Grove Dr.
Pasadena, CA 91109
(818)354-4814

Laurich, Bernhard
Los Alamos National Laboratory
MS D429
Los ALamos, NM 87545
(505)665-0333

Lemons, Ross
Los Alamos National Laboratory
MS D429
Los Alamos, NM 87545
(505)667-6832

Lichtmann, Lawrence
Aerojet ElectroSystems
1100 W. Hollyvale St.
Azusa, CA 91702
(818)812-1008

Lyon, Steve
Princeton University
Electrical Engineering Dept.
Princeton, NJ 08544
(609)258-4635

Maserjian, Joe
Jet Propulsion Laboratory
MS 302-306, 4800 Oak Grove Dr.
Pasadena, CA 911098
(818)354-3801

McGill, Tom
Caltech
MS 128-95, Applied Physics
Pasadena, CA 91125
(818)356-4849

Meginniss, James
SUMMA Technology Inc.
125 W. Park Loop, Ste. 102
Huntsville, AL 35806
(205)430-4310

Miles, Richard
Hughes Research LAboratories
3011 Malibu Canyon Rd.,MS RL63
Malibu, CA 90265
(213)317-5986

Miller, William
NASA/Langley Research Center
MS 474
Hampton, VA 23665-5225
(804)864-1720

Milnes, A.G.
Carnegie Mellon University
ECE Dept., 5000 Forbes Ave.
Pittsburgh, PA 15213
(412)268-2463

Mink, J.
US Army Research Office
PO Box 12211
Research Triangle Pk, NC
(919)549-0641

Mitchel, William
Wright Research & Development Cntr
WRDC/MLPO
Wright-Patterson, OH 45433
(513)255-4474

Moldovan, Anton
Ford Aerospace
Ford Road, PO Box A
Newport Beach, CA 92658-8900
(714)720-4246

Nahum, Michael
UC Berkeley
Dept. of Physics
Berkeley, CA 94720
(415)642-1247

Nelms, Richard
NASA/Langley Research Center
MS 186
Hampton, VA 23665-5225
(804)864-1726

Nelson, Edward
Eastman Kodak Company
Bldg. 81, Fl. 6, RL
Rochester, NY 14650-2008
(716)722-0245

Nelson, Richard
Ford Aerospace
Ford Road
Newport Beach, CA 92660
(714)720-6417

Nelson, Snadra
TRW
601 Anderson
Manhatten Beach, CA 90266
(213)814-1303

Norton, Paul
Santa Barbara Research Center
75 Coromar Dr.
Goleta, CA 93117
(805)562-2746

Nouhi, Akbar
Jet Propulsion Laboratory
MS 302-306, 4800 Oak Grove Dr.
Pasadena, CA 91109
(818)354-7135

Odenwald, Sten
SFA, Inc.
Code 4033.6
Washington, DC 20375
(202)767-3010

Patten, Elizabeth
Santa Barbara Research Center
75 Coromar Drive, B2/8
Goleta, CA 93117
(805)562-2168

Pawlik, Eugene
Jet Propulsion Labvoratory
MS 186-133, 4800 Oak Grove Dr.
Pasadena, CA 91109
(818)354-4263

Peercy, Paul
Sandia National Labs
Organization 1140
Albuquerque, NM 87185
(505)844-4309

Petroff, Michael
Rockwell International Science Cntr
Miraloma Ave.
Anaheim, CA
(714)762-4513

Pham, Le Thanh
Hughes Micro Electronics
6155 El Camino Real, MS 115
Carlsbad, CA 92009
(619)931-5087

Pirich, Ronald
Grumman Corp. Research Center
MS A02-26
Bethpage, NY 11714
(516)575-0612

Plotkin, Henry
NASA/Goddard Space Flight Center
NASA/GSFC
Greenbelt, MD 20771
(301)286-6185

Proffitt, Shellba
US Army Strategic Defense Command
Huntsville, AL.
(205)895-4820

Rajakarunanayake, Y.
Caltech
Pasadena, CA 91125

Reine, M.
Loral Infrared & Imaging Systems
MS 146, 2 Forbes Rd.
Lexington, MA 02173
(617)863-3043

Richards, P.
UC Berkeley
Berkeley, CA

Ritchie, Donald
Jet Propulsion Laaboratory
MS 303-210, 4800 Oak Grove Dr.
Pasadena, CA 91109
(818)354-6305

Ruden, P. Paul
University of Minnesota
Dept. of EE, 200 Union Street
Minneaapolis, MN 55455
(612)624-6350

Sarohia, Virendra
Jet Propulsion Laboratory
MS 180-606, 4800 Oak Grove Dr.
Pasadena, CA 91109
(818)354-6758

Scheihing, John
Air Force Electronic Tech. Lab
WRDC/ELOD
Aright-Patterson AFB,OH 45433
(513)255-5147

Schnitzler, Alvin
BDM International Inc.
1300 N. 17th Street, Ste. 950
Arlington, VA 22209
(703)247-0376

Schueler, Donald
Sandia National Laboratory
PO Box 5800, Dept. 6220
Albuquerque, NM 87185
(505)844-4041

Quelle, Fred
ONR Boston
495 Summer St.
Boston, MA 02210
(617)451-3171

Randall, Rick
Aerojet ElectroSystems
1100 W. Hollyvale St.
Azusa, CA 91702
(818)812-2952

Reitz, Larry
AF Electronic Technology Lab
MS WRDC/ELOD
Wright Patterson AFB,OH 45433
(513)255-5147

Riffee, Lyle
US Air Force
WRDC/MLPO
Wright Patterson AFB,OH 45433
(513)255-4474

Rodgers, Richard
USASDC
106 Wynn Dr. (POB1500)
Huntsville, AL 35807
(205)895-3771

Sachtjen, Scott
Conductus, Inc.
969 W. Maude Ave.
Sunnyvale, CA 94086
(408)732-3181

Sato, Robert
RNS Electronics & Technology
50 Montemalaga Plaza
Palos Verdes Estates, CA 90274
(213)373-1832

Schetzina, J.
N. Carolina State University

Schoolar, Richard
Aerospace Corp.
MS M4-978, PO Box 92957
Los Angeles, CA 90009
(213)336-6676

Schulman, Joel
Hughes Research Laboratories
3011 Malibu Canyon Rd.
Malibu, CA 90265
(213)317-5085

Shu, Peter
NASA/Goddard Space Flight Center
NASA/GSFC
Greenbelt, MD 20771
(301)286-7606

Silver, Arnold
TRW
One Space Park
Redondo Beach, CA 90278
(213)812-0155

Song, J.J.
Oklahoma State University
Dept. of Physics
Stillwater, OK 74078-0444
(405)744-9877

Spears, David
MIT Lincoln Laboratory
240 Wood St.
Lexington, MA 01720
(617)981-7855

Stapelbroek, M.G.
Rockwell International
3370 Miraloma Ave.,MS D/781
Anaheim, CA 92803
(714)762-4528

Stevens, Christopher
Jet Propulsion Laboratory
MS 168-227, 4800 Oak Grove Dr.
Pasadena, CA 91109
(818)354-3545

Swenson, H.R.
SDIO/TNS
7601 Sweet Hours
Columbia, MD
(301)381-6302

Taylor, Mark
Institute for Defense Analysis
1801 N. Beauregard St.
Alexandria, VA 22311-1772
(703)578-2986

Thompson, Les
NASA/Goddard Space Flight Center
Code 925
Greenbelt, MD 20771
(301)286-8382

Vydyanath, H.R.
Aerojet ElectroSYstems
1100 W. Hollyvale St.
Azusa, CA 91702
(818)812-2892

Silberstein, Robert
Grumman Corp. Research Center
MS A02-26
Bethpage, NY 11714-3580
(516)575-8196

Smith, Darryl
Los Alamos National Laboratory
MEE-11, D429
Los Alamos, NM 87545
(505)667-2036

Song, Jong-In
Columbia University
Dept. of Electrical Engineering
New York, NY 10027
(212)854-6588

Staller, Craig
Jet Propulsion Laboratory
MS 303-210, 4800 Oak Grove Dr.
Pasadena, CA 91109
(818)354-9143

Starr, Ron
Ford Aerospace
Ford Road., MS 2/59
Newport Beach, CA 92658-8900
(714)720-6538

Swanson, Paul
Jet Propulsion Laboratory
4800 Oak Grove Dr.
Pasadena, CA 91109
(818)354-6707

Takei, William
Westinghouse Electric Corp.
STC, 1310 Beulah Rd.
Pittsburgh, PA 15235
(412)256-1992

Tennant, William
Rockwell Intl. Science Center
1049 Camino Dos Rios
Thousand Oaks, CA 91360
(805)373-4247

Turner, Gary
Rockwell International
M/S D/781, 031-BC17
Anaheim, CA 92803-3105
(714)762-2969

Wagner, Robert
Naval Research Laboratory
4555 Overlook Ave., SW
Washington, DC 20375-5000
(202)767-3665

Wen, Chang
Hughes
3100 W. Lomita
Torrance, CA 90509
(213)517-6997

Wigdor, Marc
Nichols Research COrp.
8618 Westwood Center Dr.
Vienna, VA 22182-2222
(703)893-9720

Wilkenfeld, Jason
S-CUBED
3020 Callan Rd.
San Diego, CA 92121
(619)450-2435

Wilson, Barbara
Jet Propulsion Laboratory
MS 302-306, 4800 Oak Grove Dr.
Pasadena, CA 91109
(818)354-2969

Winston, Jan
Aerojet ElectroSystems
1100 W. Hollyvale St.
Azusa, NCA 91702
(818)812-1454

Witteles, Eleonora
WIT
4714 Browndeer Lane
Palos Verdes, CA 90274
(213)541-9934

Woodall, J.M.
IBM

Wu, C.S.
Hughes Aircraft Co.

Wu, Owen
Hughes Research Laboratories
3011 Malibu Canyon Rd.
Malibu, CA 90265
(213)317-5749

Yariv, Amnon
Caltech
EE & Applied Physics
Pasadena, CA 91125
(818)356-4821

Young, Mary
Hughes Research Lab
3011 MAlibu Canyon Rd.
Malibu, CA 90265
(213)317-5465

NTIS does not permit return of items for credit or refund. A replacement will be provided if an error is made in filling your order, if the item was received in damaged condition, or if the item is defective.

Reproduced by NTIS
National Technical Information Service
U.S. Department of Commerce
Springfield, VA 22161

This report was printed specifically for your order from our collection of more than 2 million technical reports.

For economy and efficiency, NTIS does not maintain stock of its vast collection of technical reports. Rather, most documents are printed for each order. Your copy is the best possible reproduction available from our master archive. If you have any questions concerning this document or any order you placed with NTIS, please call our Customer Services Department at (703)487-4660.

Always think of NTIS when you want:
• Access to the technical, scientific, and engineering results generated by the ongoing multibillion dollar R&D program of the U.S. Government.
• R&D results from Japan, West Germany, Great Britain, and some 20 other countries, most of it reported in English.

NTIS also operates two centers that can provide you with valuable information:
• The Federal Computer Products Center - offers software and datafiles produced by Federal agencies.
• The Center for the Utilization of Federal Technology - gives you access to the best of Federal technologies and laboratory resources.

For more information about NTIS, send for our FREE *NTIS Products and Services Catalog* which describes how you can access this U.S. and foreign Government technology. Call (703)487-4650 or send this sheet to NTIS, U.S. Department of Commerce, Springfield, VA 22161. Ask for catalog, PR-827.

Name _____
Address _____
_____
_____
Telephone _____

- Your Source to U.S. and Foreign Government Research and Technology.